HEARING LOSS: FROM PATHOGENESIS TO TREATMENT

EDITED BY: Zuhong He, Hai Huang, Wei-Jia Kong and Su-Hua Sha

PUBLISHED IN: Frontiers in Cellular Neuroscience

frontiers Research Topics

frontiers

ISSN 1664-8714
ISBN 978-2-88976-500-3
DOI 10.3389/978-2-88976-500-3

About Frontiers

Frontiers is more than just an open-access publisher of scholarly articles: it is a pioneering approach to the world of academia, radically improving the way scholarly research is managed. The grand vision of Frontiers is a world where all people have an equal opportunity to seek, share and generate knowledge. Frontiers provides immediate and permanent online open access to all its publications, but this alone is not enough to realize our grand goals.

Frontiers Journal Series

The Frontiers Journal Series is a multi-tier and interdisciplinary set of open-access, online journals, promising a paradigm shift from the current review, selection and dissemination processes in academic publishing. All Frontiers journals are driven by researchers for researchers; therefore, they constitute a service to the scholarly community. At the same time, the Frontiers Journal Series operates on a revolutionary invention, the tiered publishing system, initially addressing specific communities of scholars, and gradually climbing up to broader public understanding, thus serving the interests of the lay society, too.

Dedication to Quality

Each Frontiers article is a landmark of the highest quality, thanks to genuinely collaborative interactions between authors and review editors, who include some of the world's best academicians. Research must be certified by peers before entering a stream of knowledge that may eventually reach the public - and shape society; therefore, Frontiers only applies the most rigorous and unbiased reviews.
Frontiers revolutionizes research publishing by freely delivering the most outstanding research, evaluated with no bias from both the academic and social point of view. By applying the most advanced information technologies, Frontiers is catapulting scholarly publishing into a new generation.

What are Frontiers Research Topics?

Frontiers Research Topics are very popular trademarks of the Frontiers Journals Series: they are collections of at least ten articles, all centered on a particular subject. With their unique mix of varied contributions from Original Research to Review Articles, Frontiers Research Topics unify the most influential researchers, the latest key findings and historical advances in a hot research area! Find out more on how to host your own Frontiers Research Topic or contribute to one as an author by contacting the Frontiers Editorial Office: frontiersin.org/about/contact

HEARING LOSS: FROM PATHOGENESIS TO TREATMENT

Topic Editors:
Zuhong He, Wuhan University, China
Hai Huang, Tulane University, United States
Wei-Jia Kong, Huazhong University of Science and Technology, China
Su-Hua Sha, Medical University of South Carolina, United States

Citation: He, Z., Huang, H., Kong, W.-J., Sha, S.-H., eds. (2022). Hearing Loss: From Pathogenesis to Treatment. Lausanne: Frontiers Media SA. doi: 10.3389/978-2-88976-500-3

Table of Contents

frontiers | Frontiers in Cellular Neuroscience

EDITORIAL
published: 10 June 2022
doi: 10.3389/fncel.2022.907483

Editorial: Hearing Loss: From Pathogenesis to Treatment

Zuhong He[1]*, *Weijia Kong*[2], *Shengyu Zou*[1], *Hai Huang*[3] and *Suhua Sha*[4]

[1] Department of Otorhinolaryngology-Head and Neck Surgery, Zhongnan Hospital of Wuhan University, Wuhan, China, [2] Department of Otorhinolaryngology, Union Hospital, Tongji Medical College, Huazhong University of Science and Technology, Wuhan, China, [3] Department of Cell and Molecular Biology, Brain Institute, Tulane University, New Orleans, LA, United States, [4] Department of Pathology and Laboratory Medicine, Medical University of South Carolina, Charleston, SC, United States

Keywords: sensorineural deafness, hearing loss, hair cell, neuron, auditory organ

Editorial on the Research Topic

Hearing Loss: From Pathogenesis to Treatment

Damage to the auditory system is associated with many factors, including genetic deficiency, aging, ototoxic drugs, noise, infection, and many other environmental factors. The mammalian inner ear is a highly differentiated organ, particularly the hair cells that cannot regenerate. Therefore, excessive damage to the inner ear cells will lead to permanent hearing loss. At present, there are limited clinical approaches to prevent and treat hearing loss due to the unique nature of the inner ear structure and cells. With the advance of new technologies and methods, including gene therapy, stem cell therapy, biomaterials, and tissue engineering, we hope that future studies will provide theoretical and experimental bases for the prevention and treatment of sensorineural hearing loss and that these basic research findings can be translated into therapeutic applications. This Frontiers Research Topic, entitled *Hearing Loss: From Pathogenesis to Treatment*, encompasses 18 contributions about the mechanisms and prevention of auditory organ injury, new technologies and biomaterials to recover hearing loss in animals and patients, and a range of promising approaches for hearing loss treatment.

The regeneration of inner ear hair cells is a hot topic arousing general interest in otology research. In this review, some important regeneration-related signal pathways have been discussed by Xu and Yang. They introduced some reports about the role of adeno-associated virus (AAV) vectors in improving hearing and summarized the role of transcription factors and epigenetic regulation in hair cell regeneration. Chai et al. have investigated the role of the super elongation complex (SEC) and its three key components in the regulation of inner ear progenitor cell differentiation. The three key components of the SEC can be detected in cochlear hair cells and supporting cells in neonatal mice, and inhibiting the activity of the SEC affects the proliferation ability of $Lgr5^{+}$ progenitors but not the differentiation ability. Qian et al. have used zebrafish to study dual-specificity phosphatase 14 (DUSP14)-regulated hair cell fate. They found that *dusp14* knockdown will reduce the number of hair cells, neuromasts, and supporting cells, eventually causing hearing defects. RNA sequencing was performed to explore the molecular mechanism responsible for regulating the *dusp14* gene on hearing function. They found that the p38 signaling pathway plays a vital role in *dusp14* knockdown-related hearing defects, and p38 inhibitor treatment could reverse *dusp14* knockdown-induced absence of supporting cells and proliferation disability.

As commonly used antibacterial drugs, the relationship between aminoglycoside antibiotics and hearing loss has not been fully elucidated. Gao et al. have explored the protective role of monosialote trahexosylganglioside (GM1) in aminoglycoside-induced hair cell injury. They found that GM1 could reduce the ROS level by regulating the expression balance of oxidative and antioxidant genes.

OPEN ACCESS

Edited and reviewed by:
Dirk M. Hermann, University of Duisburg-Essen, Germany

***Correspondence:**
Zuhong He
hezuhong@163.com

Specialty section:
This article was submitted to Cellular Neuropathology, a section of the journal Frontiers in Cellular Neuroscience

Received: *29 March 2022*
Accepted: *06 May 2022*
Published: *10 June 2022*

Citation:
He Z, Kong W, Zou S, Huang H and Sha S (2022) Editorial: Hearing Loss: From Pathogenesis to Treatment. Front. Cell. Neurosci. 16:907483. doi: 10.3389/fncel.2022.907483

GM1 also reduces the rate of apoptosis and hair cell death caused by aminoglycoside antibiotics.

The role of autophagy in the auditory system has received much attention in recent years. Zheng et al. have found that otitis media (OM) can impair the autophagy pathway in middle ear (ME) tissues. The initial stage of autophagy in OM mice was activated, but downregulation of Rab7 and Syntaxin 17 disrupts the fusion of autophagosomes and lysosomes in OM mice, thereby blocking autophagic flux. Rapamycin treatment was found to protect hearing by inhibiting the activity of mTOR1 and activating autophagy flux to reduce the inflammatory infiltrates and TNF-α expression. Yang et al. have reviewed the role of autophagy in sensorineural hearing loss (SNHL), including noise, ototoxic drugs, and age-related hearing loss. They also introduced the pro-apoptotic effect of autophagy in cisplatin-induced HEI-OC1 cell death. This review concluded the role of TFEB, PTEN, FoxG1, and STAT proteins and miRNAs in the pathogenesis of SNHL by regulating the autophagy pathway.

Xu et al. have reviewed current developments in promising nanocarrier systems for inner ear disease therapy. Hydrogel delivery systems have the advantage of enabling a higher residence time for drugs so that they reach equilibrium in the inner ear and easy degradation with good biocompatibility. As a novel drug delivery system, nanoparticle-based systems, such as nanosized polymers, peptides, silicas, and metal–organic frameworks, have been widely employed as drug delivery systems for inner ear disease therapy. Those nanoparticles could prolong the half-life of drugs and increase the solubility of drugs for ease of crossing physiological barriers. Tang et al. have discussed the role of superparamagnetic iron oxide nanoparticles (SPIOs), a biomaterial with excellent biocompatibility, in neural stem cell (NSC) proliferation. They found that SPIOs could promote NSC proliferation in the absence of a static magnetic field (SMF). However, when the SMF intensity (over 100 ± 10 mT) and SPIO concentration (more than 500 μg/ml) increased, the proliferation of NSC was suppressed. Uncovering the underlying mechanism could have profound significance for tissue engineering and regenerative medicine for SPIO applications. Ding et al. have reviewed novel materials for auditory disease treatment, including conductive and sensorineural hearing loss and auditory-related conditions. New materials used in clinical otologic surgery have the advantages of excellent biocompatibility, lower incidence of postoperative complications, and shorter postoperative recovery time. Novel drug delivery systems exhibit stable and sustained drug release, capable of transporting the drug into target cells with high selectivity.

Lu et al. have found that the systemic administration of mitochondria-target antioxidant mito-TEMPO (MT) mitigated oxidative stress in the cochlea after noise exposure, reduced the hair cell and ribbon synapse loss induced by acoustic trauma, and overall exhibited a protective effect on hearing. MT treatment could restore mtDNA and ATP levels to improve mitochondrial function during noise exposure. Furthermore, they found that MT treatment attenuated TFAM and SOD2 expression reduction after noise exposure independent of the PGC-1α/NRF-1/TFAM pathway. In addition, MT treatment partially recovered the TFAM–mtDNA interaction and reduced the amount of naked mtDNA in the cytoplasm of outer hair cells. Zhang et al. used desmopressin injections to generate an endolymphatic hydrops (EH) model to mimic Meniere's disease. They observed the cochlear structure and hearing changes in the EH model. The increased hearing loss and reduced round window membrane vibration were found to correlate positively with the severity of EH. Then, a mannitol–saline solution was used as a dehydration treatment to recover hearing in the EH model, showing that rehydration can recover the early hearing loss in ER but not after a long duration.

Yang et al. have focused on the role of histidyl-tRNA synthetase HARS2 in cochlear hair cell development. They found that *Hars2* conditional knockout mice exhibited gradual hearing loss at P30 and complete hearing loss at P60. The abnormal mitochondria began to appear in HCs at P14 of the *Hars2* CKO mice, which indicated reduced inner membrane surface and low-density mitochondrial mass. As a result, the expression of the antioxidant genes xCT, Nqo1, Sod2, and Gsr significantly decreased, and apoptosis HCs gradually appeared at P45. They confirmed that *Hars2* is a critical gene for hair cell survival and maintaining the normal function of mitochondria. *GJB2* gene mutations were the predominant cause of hereditary deafness. However, current research focuses on the role of the *GJB2* gene in the morphological development of the organ of Corti. Yang et al. have reported the role of *GJB2* in Kölliker's organ. $Gjb2^{loxP/loxP}$ and $ROSA26^{CreER}$ mice were used in this study, and TUNNEL-positive cells were detected in Kölliker's organ at P1. Meanwhile, autophagy flux was also blocked in Cx26-cKD mice. The Cx26 knockdown will reduce the ATP level in lysosomal vesicles and affect the ATP-dependent Ca^{2+} signaling pathway in Kölliker's organ, which is crucial for hearing acquisition. Yang et al. also used CRISPR/Cas9 technology to generate connexin 30 (Cx30) knockout mice and confirmed the important role of Cx30 in hearing development. Compared with WT mice, Cx30-deficient mice exhibited mild hearing loss from 4 to 16 kHz at 6 months. The expression of the Cx26 protein was decreased in the cochlea of Cx30 knockout mice. The structure of the stria vascularis, endocochlear potential, and ATP release were affected in Cx30 knockout mice.

Li et al. have established a "trinomial forced-choice method" to match tinnitus pitch with 16 frequency measurement points from 250 Hz to 16 kHz. They found that clinical patients with normal hearing were almost within the high-frequency range of tinnitus pitch. They have demonstrated a more direct correspondence between tinnitus pitch and hearing frequency deficits.

In hearing protection-related research, the damage mechanism of cochlear hair cells has always been the focus of attention. Sun et al. have reviewed the damage mechanism of spiral ganglion neurons (SGNs) in different hearing injury models. They have also introduced some potential therapies to reduce SGN damage. Adenovirus (Ad)-based and AAV-based vectors mediated exogenous NT (BDNF, GDNF, NT3, CNTF, and others) and provided good results in SGN protection. Transplanted embryonic stem cells were successfully engrafted into the modiolus and formed ectopic ganglia with differentiated neuronal-type cells. However, many challenges must be

overcome before applications can be made for humans. Liu et al. have explored the function of glutathione peroxidase 1 (GPX1) on cochlear SGNs in *gpx1* knockout mice ($gpx1^{-/-}$) after peroxynitrite treatment. They found that after culturing with peroxynitrite, GPX1 expression significantly decreased in cochlear SGNs. In $gpx1^{-/-}$ mice, the cell-counting results showed that SGNs experienced severe damage after peroxynitrite treatment compared with WT mice. Ebselen pretreatment, a GPX1 mimic, can reverse peroxynitrite-induced SGN apoptosis and cell loss. Furthermore, they found that NF-κB pathway activation plays an important role in peroxynitrite-induced SGN damage. NF-κB inhibitors and upregulating GPX1 expression can block NF-κB pathway activation through downstream pro-apoptosis–related gene expression.

Sun et al. have performed a cross-sectional population-based study to analyze the link between hearing impairment and air pollution. After adjusting for confounding factors, they found that exposure to PM_{10}, NO_X, and NO_2 was linked to hearing impairment. However, $PM_{2.5}$ and $PM_{2.5}$ absorbance showed no association with hearing loss. They proposed that oxidative stress and pro-inflammatory pathways may be involved in the association between air pollution and hearing loss.

In conclusion, the research articles and reviews collected in this Research Topic provide a comprehensive set of information on the damage mechanisms and protection methods of hair cells and SGN, hair cell regeneration, and the application of new materials and approaches in the treatment of hearing diseases. Together, the achievements included in this Research Topic contribute to further understanding of the pathogenesis of hearing loss, attracting the interest of readers in hearing-related research, and providing a reference for the development of novel hearing loss therapies.

AUTHOR CONTRIBUTIONS

WK, SZ, and ZH participated in writing the manuscript. ZH, SZ, WK, HH, and SS participated in reviewing the manuscript. All authors contributed to the article and approved the submitted version.

Conflict of Interest: The authors declare that the research was conducted in the absence of any commercial or financial relationships that could be construed as a potential conflict of interest.

Publisher's Note: All claims expressed in this article are solely those of the authors and do not necessarily represent those of their affiliated organizations, or those of the publisher, the editors and the reviewers. Any product that may be evaluated in this article, or claim that may be made by its manufacturer, is not guaranteed or endorsed by the publisher.

frontiers in Cellular Neuroscience

REVIEW
published: 20 August 2021
doi: 10.3389/fncel.2021.732507

Research Progress on the Mechanism of Cochlear Hair Cell Regeneration

*Shan Xu and Ning Yang**

Department of Otolaryngology, The First Hospital of China Medical University, Shenyang, China

Mammalian inner ear hair cells do not have the ability to spontaneously regenerate, so their irreversible damage is the main cause of sensorineural hearing loss. The damage and loss of hair cells are mainly caused by factors such as aging, infection, genetic factors, hypoxia, autoimmune diseases, ototoxic drugs, or noise exposure. In recent years, research on the regeneration and functional recovery of mammalian auditory hair cells has attracted more and more attention in the field of auditory research. How to regenerate and protect hair cells or auditory neurons through biological methods and rebuild auditory circuits and functions are key scientific issues that need to be resolved in this field. This review mainly summarizes and discusses the recent research progress in gene therapy and molecular mechanisms related to hair cell regeneration in the field of sensorineural hearing loss.

Keywords: inner ear, stem cell, hair cell, regeneration, sensorineural hearing loss

OPEN ACCESS

Edited by:
Zuhong He,
Wuhan University, China

Reviewed by:
Yuhua Zhang,
Southeast University, China
Wenwen Liu,
Shandong University, China

****Correspondence:***
Ning Yang
ningyang0312@sina.com

Specialty section:
This article was submitted to Cellular Neuropathology, a section of the journal Frontiers in Cellular Neuroscience

Received: *29 June 2021*
Accepted: *28 July 2021*
Published: *20 August 2021*

Citation:
Xu S and Yang N (2021) Research Progress on the Mechanism of Cochlear Hair Cell Regeneration. Front. Cell. Neurosci. 15:732507. doi: 10.3389/fncel.2021.732507

INTRODUCTION

Neural stem cells have the ability to self-renew and differentiate into various types of nerve cells and have been used as a potential treatment for various diseases. Some supporting cells with proliferation ability in the inner ear are also called sensory precursor cells (Monzack and Cunningham, 2013). Stem cell therapy refers to a treatment that uses the diversity of stem cells to induce differentiation into the same structure as the original shape and function when the normal structure of the organism is damaged or changed. This treatment can supplement the defective and damaged inner ear hair cells. The differentiation mechanism of inner ear stem cells is a complex regulatory network system. In addition to the expression sequence of genes playing an important role in the regulation of their differentiation, the secretion and interaction of various cytokines are also closely related to it. At present, the molecular regulation mechanism of inner ear stem cells is still unclear. With the increase of related research and the development of molecular biology technology, the molecular regulation mechanism of neural stem cell differentiation has gradually been elucidated. In recent years, the inner ear sensory precursor cells or stem cells are induced to re-enter the cell cycle by activating the inner ear-related signal pathways, and proliferate and differentiate into hair cells, and finally restore hearing or vestibular function, which have gradually become a research hotspot (Monzack and Cunningham, 2013). The proliferation and differentiation of sensory precursor cells are regulated by various related signal pathways, including

Abbreviations: AAV, adeno-associated virus; AAV-ie, AAV-inner ear; CDK, cycl-dependent protein kinase; BMP4, bone morphogenetic protein 4; DKK, Dickkopf; mTORC1, Akt-mTOR complex 1; Dnmt, DNA methyltransferase.

WNT, Notch, BMP/Smad, FGF, IGF, and Shh signal pathways (Schimmang, 2007; Munnamalai and Fekete, 2016; Waqas et al., 2016; Wu et al., 2016). The regulation of these signal pathways and related factors is very important for the induction of inner ear stem cells and sensory precursor cells to differentiate into mature inner ear hair cells.

In recent years, with the in-depth research on the pathogenesis of deafness, more and more researchers are trying to treat hearing diseases through stem cell therapy. At present, there are two main ways to regenerate hair cells in the inner ear: one is that the supporting cells will re-enter the cell cycle and differentiate into hair cells after mitosis. Another way is that supporting cells will directly transdifferentiate into hair cells. In addition to Sox2$^+$ cells, Lgr5$^+$ cells, and Axin2$^+$ cells that are often used for stem cell research, Chai et al. (2012) found that the cell population of Fzd9$^+$ cells is much smaller than Lgr5$^+$ progenitor cells in the cochlea of newborn Fzd9-CreER/Rosa26-tdTomato mice (Zhang et al., 2019). They also found that Fzd9$^+$ cells have the ability to generate hair cells *in vivo*. In addition, the proliferation, differentiation, and hair cell generation capabilities of Fzd9$^+$ cells cultured *in vitro* are similar to those of Lgr5$^+$ progenitor cells. Therefore, Fzd9$^+$ cells may be the main functional progenitor cell type in Lgr5$^+$ cells (Zhang et al., 2019). Therefore, Fzd9 can be used as a marker for hair cell progenitor, which is more specific than Lgr5 in hair cell progenitor.

APPLICATION OF AAV VECTORS IN INNER EAR

The method of regulating the differentiation and development of stem cells through gene editing to promote the regeneration of inner ear hair cells has gradually become a research hotspot in the field of hearing. The ideal vector for gene editing needs to accurately deliver the nucleic acid fragments into the inner ear and target cells and express them efficiently. In addition, the vector needs to have high transfection efficiency, controllable intensity and time, and high safety. Traditional viral vectors are toxic and carry limited gene capacity. In recent years, researchers have discovered some ideal adeno-associated virus (AAV) vectors that can be transfected in the inner ear (Iizuka et al., 2008; Giannelli et al., 2018; Gu et al., 2019; Tan et al., 2019). AAV vector-mediated gene therapy has been approved in the United States and can be used to treat rare hereditary eye diseases (Tan et al., 2019). Omar Akil et al. have used the AAV virus vector to deliver the *VGLUT3* gene to VGLUT3 knockout mice and achieved significant improvement in hearing (Akil et al., 2012). In order to avoid the shortcomings of low efficiency of traditional AAVs infecting outer hair cells, Zinn et al. made the vector AAV2/Anc80L65 based on the original sequence of the AAV capsid (Zinn et al., 2015). This vector can efficiently target the inner hair cells and outer hair cells of the cochlea, which indicates an important breakthrough in the research of AAV vectors in cochlear cell targeting. Kevin and colleagues found that AAV2.7m8 can also efficiently infect inner hair cells and outer hair cells in the cochlea, and the efficiency of infecting outer hair cells is even higher than that of Anc80L65 (Gu et al., 2019; Isgrig et al., 2019). In addition, AAV2.7m8 not only preferentially targets cochlear hair cells, but it can also efficiently infect Lgr5$^+$ supporting cells. Tan et al. constructed the AAV mutant AAV-inner ear (AAV-ie) by inserting the polypeptide DGTLAVPFK, which can increase the infection efficiency by generating a transmembrane structure (Tan et al., 2019). AAV-ie can efficiently infect cochlear hair cells and vestibular hair cells. In the cochlea, since GFAP protein is expressed in supporting cells but not in hair cells, the GFAP promoter can be used to achieve specific expression of AAV-ie genes in supporting cells. In addition, studies have found that AAV-ie does not affect the function of hair cells and the auditory system (Tan et al., 2019).

SIGNAL PATHWAYS RELATED TO HAIR CELL REGENERATION

In recent years, researchers have discovered through the study of related pathways in the inner ear that WNTs, FGFs, BMP, Shh, Notch, and other signaling molecules play different roles in the process of hair cell regeneration (**Figure 1**). Therefore, hair cell regeneration does not depend on the activation of one signal pathway but is coordinated by multiple signal pathways.

The Role of Wnt Signaling Pathway in Hair Cell Regeneration

The WNT/β-catenin signaling pathway plays an important regulatory role in cell proliferation, cell fate determination, and hair cell differentiation (Jacques et al., 2014). When the WNT/β-catenin signal is inhibited, the proliferation ability of sensory cells is reduced, and the activation of the WNT/β-catenin signal promotes the increase of hair cells (Jacques et al., 2012; Shi et al., 2014). The target genes *Lgr5* and *Lgr6* of the WNT pathway are expressed in embryonic and neonatal cochlear progenitor cells (Chai et al., 2011; Samarajeewa et al., 2019). Lgr5$^+$ cells have the characteristics of hair cell progenitor cells, such as proliferation, self-renewal, and regeneration into hair cells (Chai et al., 2012; Shi et al., 2012; Cox et al., 2014; Wang et al., 2015). After WNT agonist treatment, the proliferation ability of the Lgr5$^+$ progenitor cells of the neonatal mouse cochlea and their ability to differentiate into hair cells were enhanced (Romero-Carvajal et al., 2015; Samarajeewa et al., 2019). WNT agonists or overexpression of β-catenin can increase the proliferation of Lgr5$^+$ progenitor cells and promote the formation of hair cells, while WNT antagonists inhibit the proliferation of Lgr5$^+$ cells and the ability to regenerate hair cells (Chai et al., 2012; Shi et al., 2012, 2013). In newborn mice, the activation of WNT signaling can also cause Axin2-positive cells to proliferate and differentiate into hair cells and supporting cells (Jan et al., 2013). When the expression of β-catenin and Atoh1 are activated simultaneously, the proliferation ability and the directed differentiation ability of Lgr5$^+$ cells into hair cells and the survival ability of newly regenerated hair cells are enhanced (Kuo et al., 2015; Mittal et al., 2017). In addition, the combination of WNT signal activation and Notch signal inhibition in the cochlea of newborn mice has also been

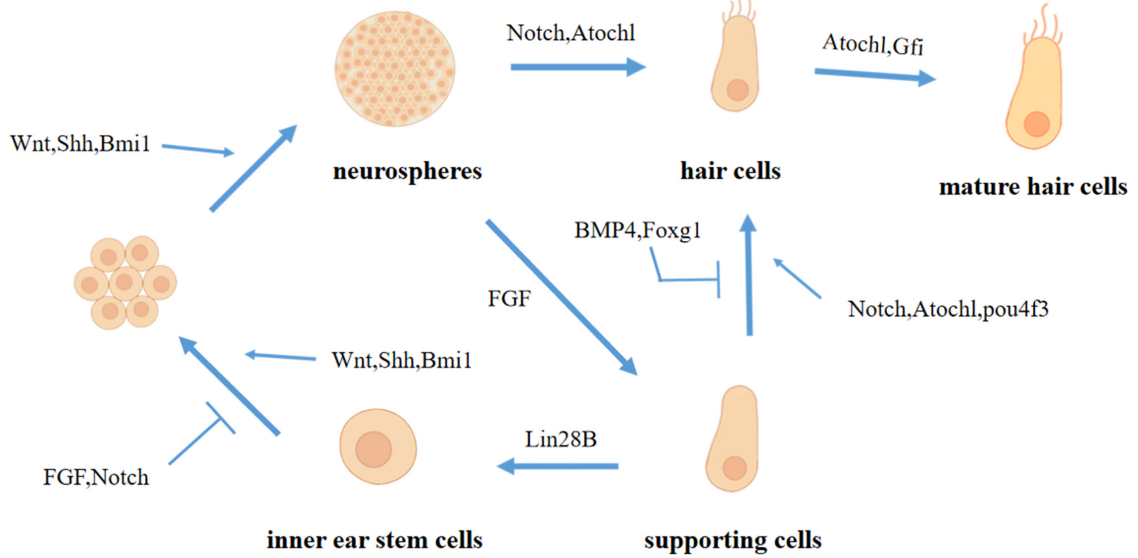

FIGURE 1 | The role of various signal pathways and related factors in the process of hair cell regeneration.

shown to promote the proliferation of supporting cells and the regeneration of hair cells (Ni et al., 2016).

The Role of Notch Signaling Pathway in Hair Cell Regeneration

The Notch signaling pathway plays an important role in the development and regeneration of hair cells. Supporting cells are induced to transdifferentiate into hair cells when Notch signaling in the cochlea of newborn mice is suppressed (Yamamoto et al., 2006; Mizutari et al., 2013; Bramhall et al., 2014). Researchers found that activating the Notch pathway in supporting cells puts them in a quiescent state and inhibits hair cell regeneration (Ma et al., 2008; Daudet et al., 2009). Previous studies found that in the cochlea of neonatal mammals, the expression of Atoh1 was up-regulated after γ-secretase inhibitor blocked the Notch signal, and caused the adjacent supporting cells to transdifferentiate into hair cells. However, this newly generated hair cell does not have the characteristics of a mature hair cell (Korrapati et al., 2013; Mizutari et al., 2013). In addition, knocking out Hes1 and Hes5 members of the Hes family with siRNA can also up-regulate the expression of Atoh1, leading to an increase in the number of hair cells in the cochlea of newborn and adult mice (Du et al., 2018). Conditional inhibition of Notch signal can accelerate $Lgr5^+$ cells in supporting cells to become new hair cells (Mittal et al., 2017). Co-activating the cell cycle activator Myc and Notch1 in the inner ear can induce the proliferation of different types of cochlear sensory epithelial cells. After the cochlear supporting cells are reprogrammed by regulating the activity of MYC/NICD, Atoh1 can induce the supporting cells *in vivo* and *in vitro* to effectively transdifferentiate into hair cell-like cells (Shu et al., 2019). Li et al. (2015) found that the combined inhibition of WNT and Notch signals can reduce the generation of hair cells, indicating that the progenitor cell proliferation phenomenon that occurs after Notch inhibition is mainly regulated by the WNT pathway (Li et al., 2015).

The Role of Hedgehog Signaling Pathway in Hair Cell Regeneration

The Hedgehog pathway is a highly conserved signaling pathway, which plays an important role in regulating the proliferation and cell fate determination and differentiation of progenitor cells in the early developmental stage of the inner ear (Zarei et al., 2017). Previous studies have found that inactivation of Hedgehog signaling causes abnormal proliferation and differentiation of mammalian cochlear cells, leading to abnormal development of cochlear structure and function (Brown and Epstein, 2011; Bok et al., 2013; Son et al., 2015). Lu et al. (2013) found that after neomycin damage, Shh signaling may inhibit the function of pRb to promote sensory epithelial cells in the cochlea of newborn mice to re-enter the cell cycle and regenerate into new hair cells. Chen et al. (2017) found that recombinant Shh protein can effectively promote the proliferation and differentiation of $Lgr5^+$ progenitor cells in the cochlea of newborn mice. In addition, after R26-SmoM2 mouse cochlear explants are treated with neomycin, Hedgehog signal activation can significantly promote cochlear epithelial cell proliferation and hair cell regeneration (Chen et al., 2017).

The Role of FGF Signaling Pathway in Hair Cell Regeneration

The FGF signaling pathway activates the gene regulatory network of the early development of the inner ear and induces the formation of the pre-placodal region and the auditory placode (Padanad et al., 2012; Ornitz and Itoh, 2015). In addition, the FGF signaling pathway plays a key role in the spontaneous

regeneration of lower vertebrate hair cells and the induction and differentiation of stem cells into hair cells. Ku et al. found that when the chicken utricle was damaged by ototoxic drugs, the decrease of FGF expression level promoted the proliferation of supporting cells (Ku et al., 2014). Jiang et al. found that the inhibition of the FGF and Notch pathway in the process of supporting cell proliferation is consistent with the down-regulation of the cycl-dependent protein kinase (CDK) inhibitor CDKN1b (p27/kip1; Jiang et al., 2014). Therefore, the inhibition of FGF and Notch signaling pathway is the triggering factor for supporting cell proliferation. Piotrowski et al. found through scRNA-seq that the deletion of *Fgf3* expression in zebrafish supporting cells resulted in enhanced hair cell regeneration and increased the number of cells in neuromast (Lush et al., 2019). Lee et al. (2016) used drugs and genes to block FGF signaling and found that inhibiting FGF signaling can significantly inhibit the regeneration of hair cells in neuromast. Tang et al. found that the FGF signaling pathway and WNT signaling pathway have a coordinated regulatory effect on the proliferation of zebrafish lateral line cells (Tang et al., 2019). When the FGF signal is inhibited, the WNT pathway-mediated cell proliferation will also be inhibited. In the absence of WNT activity, activating the FGF signal with bFGF will restore part of supporting cell proliferation and hair cell regeneration.

TRANSCRIPTION FACTORS RELATED TO HAIR CELL REGENERATION

Atoh1 is a transcription factor with a helix-loop-helix structure, which is essential for the differentiation of hair cells during the development of the inner ear (Bermingham et al., 1999). In animal experiments, it was found that the sensory epithelium of the cochlea of Atoh1 knockout mice differentiated into supporting cells, but not cochlear hair cells and vestibular hair cells (Chen et al., 2002). Therefore, Atoh1 gene is an essential transcription factor in the process of hair cell generation. In *in vitro* experiments, researchers found that activating the expression of Atoh1 in the cochlea or vestibular sensory epithelium can induce hair cell regeneration (Bermingham et al., 1999; Izumikawa et al., 2005; Gubbels et al., 2008; Liu et al., 2012). In damaged mouse utricle, overexpression of Atoh1 can induce the proliferation of supporting cells and promote them transdifferentiate into hair cell-like cells (Jen et al., 2019). In addition, the overexpression of Atoh1 also caused the up-regulation of many hair cell-related genes but did not include the hair cell maturation-related genes. Cheng found that the expression of Atoh1 in prenatal rats can induce supporting cells to differentiate into sensory hair cells, but the regenerated hair cells are immature, which may be due to the absence of Atoh1 down-regulation during hair cell development (Cheng, 2019). Therefore, hair cell regeneration and maturation are not only regulated by Atoh1, but also coordinated by other transcription factors.

Gfi1 is one of the GPS (Gfi1/pag3/SENS) family transcription factors with a zinc finger domain. During the development of the inner ear, Gfi1 plays an important role in the normal differentiation, survival, and maturation of hair cells (Wallis et al., 2003). Gfi1 expression-deficient mice showed abnormal hair cell development, such as cochlear outer hair cells and inner hair cells degenerating from the basal turn to the apex turn until they were completely absent (Wallis et al., 2003; Li and Doetzlhofer, 2020). Matern et al. found that when Gfi1 expression is absent, the maturation of hair cells in the cochlea and vestibule is blocked, and the expression of hair cell maturation markers, such as Strc, Tmc1, and Ocm, is inhibited (Matern et al., 2020). Lee et al. found that Gfi1 and upstream Atoh1 coordinately regulate the regeneration of cochlear hair cells in newborn mice (Lee et al., 2020).

The secreted protein bone morphogenetic protein 4 (BMP4) can regulate inner ear morphogenesis and hair cell development. Lewis et al. found that when the cochlea cultured *in vitro* is damaged, the addition of BMP4 can inhibit the expression of Atoh1 in supporting cells, thereby inhibiting supporting cell mitosis and hair cell regeneration (Lewis et al., 2018). After treatment with the BMP4 inhibitor noggin, the number of regenerated hair cells increased (Lewis et al., 2018).

Bmi1 is a member of the Polycomb protein family and plays a regulatory role in the proliferation of progenitor cells and stem cells in multiple organs (Bruggeman et al., 2007; López-Arribillaga et al., 2015; Lu et al., 2017). Recently, researchers have discovered that Bmi1 activates WNT signaling by inhibiting the Dickkopf (DKK) family with WNT inhibitor functions (Cho et al., 2013). Lu et al. (2017) demonstrated in *in vitro* experiments that knocking out Bmi1 can significantly inhibit the proliferation of $Lgr5^+$ progenitor cells in the cochlea of neonatal mice after neomycin damage. Compared with wild-type mice, the expression of DKK1 in $Bmi1^{-/-}$ neonatal mice was significantly up-regulated, while the expression of β-catenin and Lgr5 was significantly down-regulated. In addition, the WNT agonist BIO inhibited the decline of the proliferation ability of $Bmi1^{-/-}$ mouse supporting cells, indicating that Bmi1 affects the proliferation of supporting cells and $Lgr5^+$ progenitor cells through the regulation of WNT signaling pathway. Therefore, Bmi1 may be a new therapeutic target for hair cell regeneration.

The POU domain transcription factor Pou4f3 plays an important role in the development of inner ear hair cells (Masuda et al., 2011). Recent studies have found that in the adult mouse cochlea, the ectopic expression of Pou4f3 can promote the transdifferentiation of supporting cells into hair cells together with Atoh1 (Walters et al., 2017). The activation of downstream target genes by Pou4f3 can promote Atoh1-mediated hair cell development and survival (Walters et al., 2017). Pou4f3 not only regulates the expression of Gfi1 and Nr2f2 related to hair cell regeneration (Zhong et al., 2019) but also is the direct target gene of Atoh1 during hair cell development (Lee et al., 2020). Atoh1-Pou4f3-target gene (such as Gfi1) is not only an important molecular pathway for regulating the fate and differentiation of hair cells but also an important molecular pathway for hair cell maturation and survival. Therefore, POU4f3 as a therapeutic target, activating its activity alone or coordinating with Atoh1 may promote the regeneration of auditory hair cells.

Foxg1 is one of the forkhead box genes involved in morphogenesis, cell fate determination, and proliferation. Previous studies reported that Foxg1 is necessary for the morphogenesis of the inner ear in mammals (Pauley et al., 2006; Hwang et al., 2009; He et al., 2018). Pauley et al. found that in Foxg1 knockout mice, the cochlear duct became shorter, the number of hair cells increased, the vestibule shrank, the growth of axons, and the distribution of vestibular neurons were abnormal (Pauley et al., 2006). Chai et al. (2012) found that conditionally knocking out *Foxg1* in $Sox2^+$ supporting cells and $Lgr5^+$ progenitor cells of newborn mice induced these cells to transdifferentiate into hair cells, resulting in a significant increase in the number of hair cells and a significant decrease in supporting cells (Zhang et al., 2020). In addition, they also found that knocking out Foxg1 expression down-regulated the expression of several Notch signaling pathway factors such as Hes1, Hes5, and Hey1. At the same time, the expression of cell cycle-dependent kinase (Cdk2) was also down-regulated, while the expression of cell cycle repressors Cdkn1c, Cdkn2a, and Gadd45g were up-regulated, indicating that Foxg1 knockout may cause cell cycle and Notch signaling pathway to be inhibited, which led to the increase of hair cells (Zhang et al., 2020). Chai et al. (2012) also found that knocking out Foxg1 in $Sox9^+$ supporting cells can promote the transdifferentiation of supporting cells into hair cells in neonatal mouse utricle (Zhang et al., 2020). The above studies provide evidence for the role of Foxg1 in the regeneration of cochlear hair cells in newborn mice.

The Lin28 gene encodes an evolutionarily highly conserved RNA binding protein, which is known to regulate the larval development time of Caenorhabditis elegans (Moss and Tang, 2003). In humans and mice, Lin28a and its homolog Lin28b are key regulators of organ growth, metabolism, tumorigenesis, and tissue repair (Ambros and Horvitz, 1984; Shyh-Chang and Daley, 2013). Doetzlhofer and colleagues found that the pathway composed of *Lin28b* and *let-7* miRNAs regulates the generation of new hair cells in P2 mouse cochlear explants (Golden et al., 2015). The role of *Lin28b* is mainly to promote the generation of new hair cells, while the role of *let-7* miRNAs is to inhibit the generation of new hair cells. *Lin28b* functional defect or overexpression of *let-7g* miRNAs leads to the inhibition of the activity of Akt-mTOR complex 1 (mTORC1) so that immature supporting cells cannot be transdifferentiated into hair cells (Li and Doetzlhofer, 2020). On the contrary, overexpression of Lin28b increased the activity of Akt-mTORC1, and dedifferentiated the maturing supporting cells into progenitor-like cells, and generated hair cells through mitotic and non-mitotic mechanisms (Li and Doetzlhofer, 2020). These findings may provide new strategies for future hair cell regeneration treatments.

In addition, Menendez et al. (2020) found that the combination of four transcription factors (Six1, Atoh1, Pou4f3, and Gfi1) can transdifferentiate neonatal mouse supporting cells (P8), mouse embryonic fibroblasts, and adult mouse tail fibroblasts into induced hair cells (IHCs). IHCs have various characteristics of hair cells, such as morphology, transcriptome and epigenetic characteristics, electrophysiological characteristics, mechanosensory channel expression, and ototoxin susceptibility. Therefore, IHCs can be used as an ideal *in vitro* model for studying hair cell function, maturation, regeneration, and ototoxin sensitivity.

THE ROLE OF EPIGENETIC REGULATION OF HAIR CELL REGENERATION

Epigenetic modification plays an important role in the development of the inner ear, and recent studies have found that it also has an important regulatory role in hair cell regeneration. During the development of zebrafish larvae, the inhibition of LSD1 by 2-PCPA decreased the expression of WNT/β-catenin and FGF signaling pathways, thereby significantly inhibiting the regeneration of supporting cells and hair cells after neomycin damage (He et al., 2016). The inhibition of G9a/GLP by BIX01294 significantly reduced the dimethylation of H3K9 in the zebrafish lateral line (Tang et al., 2016). The defect of H3K9me2 significantly inhibited the WNT/β-catenin and FGF signaling pathways, which significantly reduced the proliferation of supporting cells after neomycin damage, and ultimately lead to the reduction of mitotic regeneration of hair cells in the zebrafish lateral line (Tang et al., 2016). Previous studies have found that when 5-azacytidine, a DNA methyltransferase (Dnmt) inhibitor, is injected into the cochlea of mature mice that are chemically deafened, DNA demethylation may promote the regeneration of hair cells in the cochlea of mature mice (Deng and Hu, 2020). The advantage of this epigenetic method is that the DNA sequence remains unchanged during the process without integrating the exogenous DNA sequence.

CONCLUSION

There are various ways and mechanisms that cause sensorineural hearing loss, among which irreversible damage to inner ear hair cells is the main cause of sensorineural hearing loss. Although the commonly used hearing aids and cochlear implants in clinical practice also improve the hearing of patients, their effect depends on the quantity and quality of residual hair cells and spiral neurons. Therefore, the ideal way to treat sensorineural hearing loss is to regenerate hair cells through stem cells to repair the structure and function of the cochlea so as to fundamentally restore hearing. Stem cell therapy in the auditory field has been a research hotspot in recent years. Although some progress has been made, almost all are results at the animal level, and there is still a long way to go before clinical transformation. The microenvironment of inner ear stem cells and the interaction with neighboring cells are very important for inner ear stem cells or sensory precursor cells to induce differentiation into mature inner ear hair cells. In the reported studies, the efficiency of differentiation of inner ear stem cells or sensory precursor cells into hair cells is still low. An insufficient number of new hair cells, immature new hair cells without the function of mature hair cells, and long–term survival of new hair cells are all key

problems and difficulties that need to be solved urgently. All these indicate that it is more difficult to regulate a single signal pathway to regenerate functional hair cells, and it may require coordinated regulation of multiple genes to effectively promote hair cell regeneration and the functional maturity and survival of new hair cells. At present, inducing the committed differentiation of stem cells into hair cells or nerve cells, the exploration of the methods of stem cell transplantation into the inner ear, and the safety research of stem cell transplantation have laid the foundation for the transplantation of stem cells *in vivo*.

AUTHOR CONTRIBUTIONS

SX and NY wrote the article. All authors contributed to the article and approved the submitted version.

REFERENCES

Akil, O., Seal, R. P., Burke, K., Wang, C., Alemi, A., During, M., et al. (2012). Restoration of hearing in the VGLUT3 knockout mouse using virally mediated gene therapy. *Neuron* 75, 283–293. doi: 10.1016/j.neuron.2012.05.019

Ambros, V., and Horvitz, H. R. (1984). Heterochronic mutants of the nematode *Caenorhabditis elegans*. *Science* 226, 409–416. doi: 10.1126/science.6494891

Bermingham, N. A., Hassan, B. A., Price, S. D., Vollrath, M. A., Ben-Arie, N., Eatock, R. A., et al. (1999). Math1: an essential gene for the generation of inner ear hair cells. *Science* 284, 1837–1841. doi: 10.1126/science.284.5421.1837

Bok, J., Zenczak, C., Hwang, C. H., and Wu, D. K. (2013). Auditory ganglion source of Sonic hedgehog regulates timing of cell cycle exit and differentiation of mammalian cochlear hair cells. *Proc. Natl. Acad. Sci. U S A* 110, 13869–13874. doi: 10.1073/pnas.1222341110

Bramhall, N. F., Shi, F., Arnold, K., Hochedlinger, K., and Edge, A. S. B. (2014). Lgr5-positive supporting cells generate new hair cells in the postnatal cochlea. *Stem Cell Rep.* 2, 311–322. doi: 10.1016/j.stemcr.2014.01.008

Brown, A. S., and Epstein, D. J. (2011). Otic ablation of smoothened reveals direct and indirect requirements for Hedgehog signaling in inner ear development. *Development (Cambridge, England)* 138, 3967–3976. doi: 10.1242/dev.066126

Bruggeman, S. W. M., Hulsman, D., Tanger, E., Buckle, T., Blom, M., Zevenhoven, J., et al. (2007). Bmi1 controls tumor development in an Ink4a/Arf-independent manner in a mouse model for glioma. *Cancer Cell* 12, 328–341. doi: 10.1016/j.ccr.2007.08.032

Chai, R., Kuo, B., Wang, T., Liaw, E. J., Xia, A., Jan, T. A., et al. (2012). Wnt signaling induces proliferation of sensory precursors in the postnatal mouse cochlea. *Proc. Natl. Acad. Sci. U S A* 109, 8167–8172. doi: 10.1073/pnas.1202774109

Chai, R., Xia, A., Wang, T., Jan, T. A., Hayashi, T., Bermingham-McDonogh, O., et al. (2011). Dynamic expression of Lgr5, a Wnt target gene, in the developing and mature mouse cochlea. *J. Assoc. Res. Otolaryngol.* 12, 455–469. doi: 10.1007/s10162-011-0267-2

Chen, P., Johnson, J. E., Zoghbi, H. Y., and Segil, N. (2002). The role of Math1 in inner ear development: uncoupling the establishment of the sensory primordium from hair cell fate determination. *Development* 129, 2495–2505. doi: 10.3410/f.1006295.78812

Chen, Y., Lu, X., Guo, L., Ni, W., Zhang, Y., Zhao, L., et al. (2017). Hedgehog signaling promotes the proliferation and subsequent hair cell formation of progenitor cells in the neonatal mouse cochlea. *Front. Mol. Neurosci.* 10:426. doi: 10.3389/fnmol.2017.00426

Cheng, Y.-F. (2019). Atoh1 regulation in the cochlea: more than just transcription. *J. Zhejiang Univ. Sci. B.* 20, 146–155. doi: 10.1631/jzus.B1600438

Cho, J.-H., Dimri, M., and Dimri, G. P. (2013). A positive feedback loop regulates the expression of polycomb group protein BMI1 via WNT signaling pathway. *J. Biol. Chem.* 288, 3406–3418. doi: 10.1074/jbc.M112.422931

Cox, B. C., Chai, R., Lenoir, A., Liu, Z., Zhang, L., Nguyen, D.-H., et al. (2014). Spontaneous hair cell regeneration in the neonatal mouse cochlea *in vivo*. *Development* 141, 816–829. doi: 10.1242/dev.103036

Daudet, N., Gibson, R., Shang, J., Bernard, A., Lewis, J., and Stone, J. (2009). Notch regulation of progenitor cell behavior in quiescent and regenerating auditory epithelium of mature birds. *Dev. Biol.* 326, 86–100. doi: 10.1016/j.ydbio.2008.10.033

Deng, X., and Hu, Z. (2020). Generation of cochlear hair cells from Sox2 positive supporting cells via DNA demethylation. *Int. J. Mol. Sci.* 21:8649. doi: 10.3390/ijms21228649

Du, X., Cai, Q., West, M. B., Youm, I., Huang, X., Li, W., et al. (2018). Regeneration of cochlear hair cells and hearing recovery through Hes1 modulation with siRNA nanoparticles in adult guinea pigs. *Mol. Ther.* 26, 1313–1326. doi: 10.1016/j.ymthe.2018.03.004

Giannelli, S. G., Luoni, M., Castoldi, V., Massimino, L., Cabassi, T., Angeloni, D., et al. (2018). Cas9/sgRNA selective targeting of the P23H Rhodopsin mutant allele for treating retinitis pigmentosa by intravitreal AAV9.PHP.B-based delivery. *Hum. Mol. Genet.* 27, 761–779. doi: 10.1093/hmg/ddx438

Golden, E. J., Benito-Gonzalez, A., and Doetzlhofer, A. (2015). The RNA-binding protein LIN28B regulates developmental timing in the mammalian cochlea. *Proc. Natl. Acad. Sci. U S A* 112, E3864–E3873. doi: 10.1073/pnas.1501077112

Gu, X., Chai, R., Guo, L., Dong, B., Li, W., Shu, Y., et al. (2019). Transduction of adeno-associated virus vectors targeting hair cells and supporting cells in the neonatal mouse cochlea. *Front. Cell. Neurosci.* 13:8. doi: 10.3389/fncel.2019.00008

Gubbels, S. P., Woessner, D. W., Mitchell, J. C., Ricci, A. J., and Brigande, J. V. (2008). Functional auditory hair cells produced in the mammalian cochlea by *in utero* gene transfer. *Nature* 455, 537–541. doi: 10.1038/nature07265

He, Y., Tang, D., Cai, C., Chai, R., and Li, H. (2016). LSD1 is required for hair cell regeneration in zebrafish. *Mol. Neurobiol.* 53, 2421–2434. doi: 10.1007/s12035-015-9206-2

He, Z., Fang, Q., Li, H., Buwei, S., Zhang, Y., Zhang, Y., et al. (2018). The role of FOXG1 in the postnatal development and survival of mouse cochlear hair cells. *Neuropharmacology* 144, 43–57. doi: 10.1016/j.neuropharm.2018.10.021

Hwang, C. H., Simeone, A., Lai, E., and Wu, D. K. (2009). Foxg1 is required for proper separation and formation of sensory cristae during inner ear development. *Dev. Dyn.* 238, 2725–2734. doi: 10.1002/dvdy.22111

Iizuka, T., Kanzaki, S., Mochizuki, H., Inoshita, A., Narui, Y., Furukawa, M., et al. (2008). Noninvasive *in vivo* delivery of transgene via adeno-associated virus into supporting cells of the neonatal mouse cochlea. *Hum. Gene Ther.* 19, 384–390. doi: 10.1089/hum.2007.167

Isgrig, K., McDougald, D. S., Zhu, J., Wang, H. J., Bennett, J., and Chien, W. W. (2019). AAV2.7m8 is a powerful viral vector for inner ear gene therapy. *Nat. Commun.* 10:427. doi: 10.1038/s41467-018-08243-1

Izumikawa, M. R., Minoda, K., Kawamoto, K. A., Abrashkin, D. L., Swiderski, D. F., Dolan, D. E., et al. (2005). Auditory hair cell replacement and hearing improvement by Atoh1 gene therapy in deaf mammals. *Nat. Med.* 11, 271–276. doi: 10.1038/nm1193

Jacques, B. E., Montgomery Iv, W. H., Uribe, P. M., Yatteau, A., Asuncion, J. D., Resendiz, G., et al. (2014). The role of Wnt/β-catenin signaling in proliferation and regeneration of the developing basilar papilla and lateral line. *Dev. Neurobiol.* 74, 438–456. doi: 10.1002/dneu.22134

Jacques, B. E., Puligilla, C., Weichert, R. M., Ferrer-Vaquer, A., Hadjantonakis, A.-K., Kelley, M. W., et al. (2012). A dual function for canonical Wnt/β-catenin signaling in the developing mammalian cochlea. *Development* 139, 4395–4404. doi: 10.1242/dev.080358

Jan, T. A., Chai, R., Sayyid, Z. N., van Amerongen, R., Xia, A., Wang, T., et al. (2013). Tympanic border cells are Wnt-responsive and can act as progenitors for postnatal mouse cochlear cells. *Development* 140, 1196–1206. doi: 10.1242/dev.087528

Jen, H.-I., Hill, M. C., Tao, L., Sheng, K., Cao, W., Zhang, H., et al. (2019). Transcriptomic and epigenetic regulation of hair cell regeneration in the mouse utricle and its potentiation by Atoh1. *eLife* 8:e44328. doi: 10.7554/eLife.44328

Jiang, L., Romero-Carvajal, A., Haug, J. S., Seidel, C. W., and Piotrowski, T. (2014). Gene-expression analysis of hair cell regeneration in the zebrafish lateral line. *Proc. Natl. Acad. Sci. U S A* 111, E1383–E1392. doi: 10.1073/pnas.1402898111

Korrapati, S., Roux, I., Glowatzki, E., and Doetzlhofer, A. (2013). Notch signaling limits supporting cell plasticity in the hair cell-damaged early postnatal murine cochlea. *PLoS One* 8:e73276. doi: 10.1371/journal.pone.0073276

Ku, Y.-C., Renaud, N. A., Veile, R. A., Helms, C., Voelker, C. C. J., Warchol, M. E., et al. (2014). The transcriptome of utricle hair cell regeneration in the avian inner ear. *J. Neurosci.* 34, 3523–3535. doi: 10.1523/JNEUROSCI.2606-13.2014

Kuo, B. R., Baldwin, E. M., Layman, W. S., Taketo, M. M., and Zuo, J. (2015). *In vivo* cochlear hair cell generation and survival by coactivation of β-catenin and Atoh1. *J. Neurosci.* 35, 10786–10798. doi: 10.1523/JNEUROSCI.0967-15.2015

López-Arribillaga, E., Rodilla, V., Pellegrinet, L., Guiu, J., Iglesias, M., Roman, A. C., et al. (2015). Bmi1 regulates murine intestinal stem cell proliferation and self-renewal downstream of Notch. *Development* 142, 41–50. doi: 10.1242/dev.107714

Lee, S. G., Huang, M., Obholzer, N. D., Sun, S., Li, W., Petrillo, M., et al. (2016). Myc and Fgf are required for zebrafish neuromast hair cell regeneration. *PLoS One* 11:e0157768. doi: 10.1371/journal.pone.0157768

Lee, S., Song, J. -J., Beyer, L. A., Swiderski, D. L., Prieskorn, D. M., Acar, M., et al. (2020). Combinatorial Atoh1 and Gfi1 induction enhances hair cell regeneration in the adult cochlea. *Sci. Rep.* 10:21397. doi: 10.1038/s41598-020-78167-8

Lewis, R. M., Keller, J. J., Wan, L., and Stone, J. S. (2018). Bone morphogenetic protein 4 antagonizes hair cell regeneration in the avian auditory epithelium. *Hear. Res.* 364, 1–11. doi: 10.1016/j.heares.2018.04.008

Li, W., Wu, J., Yang, J., Sun, S., Chai, R., Chen, Z.-Y., et al. (2015). Notch inhibition induces mitotically generated hair cells in mammalian cochleae via activating the Wnt pathway. *Proc. Natl. Acad. Sci. U S A* 112, 166–171. doi: 10.1073/pnas.1415901112

Li, X.-J., and Doetzlhofer, A. (2020). LIN28B/let-7 control the ability of neonatal murine auditory supporting cells to generate hair cells through mTOR signaling. *Proc. Natl. Acad. Sci. U S A* 117, 22225–22236. doi: 10.1073/pnas.2000417117

Liu, Z., Dearman, J. A., Cox, B. C., Walters, B. J., Zhang, L., Ayrault, O., et al. (2012). Age-dependent *in vivo* conversion of mouse cochlear pillar and Deiters' cells to immature hair cells by Atoh1 ectopic expression. *J. Neurosci.* 32, 6600–6610. doi: 10.1523/JNEUROSCI.0818-12.2012

Lu, N., Chen, Y., Wang, Z., Chen, G., Lin, Q., Chen, Z.-Y., et al. (2013). Sonic hedgehog initiates cochlear hair cell regeneration through downregulation of retinoblastoma protein. *Biochem. Biophys. Res. Commun.* 430, 700–705. doi: 10.1016/j.bbrc.2012.11.088

Lu, X., Sun, S., Qi, J., Li, W., Liu, L., Zhang, Y., et al. (2017). Bmi1 regulates the proliferation of cochlear supporting cells via the canonical Wnt signaling pathway. *Mol. Neurobiol.* 54, 1326–1339. doi: 10.1007/s12035-016-9686-8

Lush, M. E., Diaz, D. C., Koenecke, N., Baek, S., Boldt, H., St Peter, M. K., et al. (2019). scRNA-Seq reveals distinct stem cell populations that drive hair cell regeneration after loss of Fgf and Notch signaling. *eLife* 8:e44431. doi: 10.7554/eLife.44431

Ma, E. Y., Rubel, E. W., and Raible, D. W. (2008). Notch signaling regulates the extent of hair cell regeneration in the zebrafish lateral line. *J. Neurosci.* 28, 2261–2273. doi: 10.1523/JNEUROSCI.4372-07.2008

Masuda, M., Dulon, D., Pak, K., Mullen, L. M., Li, Y., Erkman, L., et al. (2011). Regulation of POU4F3 gene expression in hair cells by 5′ DNA in mice. *Neuroscience* 197, 48–64. doi: 10.1016/j.neuroscience.2011.09.033

Matern, M. S., Milon, B., Lipford, E. L., McMurray, M., Ogawa, Y., Tkaczuk, A., et al. (2020). GFI1 functions to repress neuronal gene expression in the developing inner ear hair cells. *Development* 147:dev186015. doi: 10.1242/dev.186015

Menendez, L., Trecek, T., Gopalakrishnan, S., Tao, L., Markowitz, A. L., Yu, H. V., et al. (2020). Generation of inner ear hair cells by direct lineage conversion of primary somatic cells. *eLife* 9:e55249. doi: 10.7554/eLife.55249

Mittal, R., Nguyen, D., Patel, A. P., Debs, L. H., Mittal, J., Yan, D., et al. (2017). Recent advancements in the regeneration of auditory hair cells and hearing restoration. *Front. Mol. Neurosci.* 10:236. doi: 10.3389/fnmol.2017.00236

Mizutari, K., Fujioka, M., Hosoya, M., Bramhall, N., Okano, H. J., Okano, H., et al. (2013). Notch inhibition induces cochlear hair cell regeneration and recovery of hearing after acoustic trauma. *Neuron* 77, 58–69. doi: 10.1016/j.neuron.2012.10.032

Monzack, E. L., and Cunningham, L. L. (2013). Lead roles for supporting actors: critical functions of inner ear supporting cells. *Hear. Res.* 303, 20–29. doi: 10.1016/j.heares.2013.01.008

Moss, E. G., and Tang, L. (2003). Conservation of the heterochronic regulator Lin-28, its developmental expression and microRNA complementary sites. *Dev. Biol.* 258, 432–442. doi: 10.1016/s0012-1606(03)00126-x

Munnamalai, V., and Fekete, D. M. (2016). Notch-Wnt-Bmp crosstalk regulates radial patterning in the mouse cochlea in a spatiotemporal manner. *Development* 143, 4003–4015. doi: 10.1242/dev.139469

Ni, W., Lin, C., Guo, L., Wu, J., Chen, Y., Chai, R., et al. (2016). Extensive supporting cell proliferation and mitotic hair cell generation by *in vivo* genetic reprogramming in the neonatal mouse cochlea. *J. Neurosci.* 36, 8734–8745. doi: 10.1523/JNEUROSCI.0060-16.2016

Ornitz, D. M., and Itoh, N. (2015). The fibroblast growth factor signaling pathway. *Wiley Interdiscip. Rev. Dev. Biol.* 4, 215–266. doi: 10.1002/wdev.176

Padanad, M. S., Bhat, N., Guo, B., and Riley, B. B. (2012). Conditions that influence the response to Fgf during otic placode induction. *Dev. Biol.* 364, 1–10. doi: 10.1016/j.ydbio.2012.01.022

Pauley, S., Lai, E., and Fritzsch, B. (2006). Foxg1 is required for morphogenesis and histogenesis of the mammalian inner ear. *Dev. Dyn.* 235, 2470–2482. doi: 10.1002/dvdy.20839

Romero-Carvajal, A., Acedo, J. N., Jiang, L., Kozlovskaja-Gumbrienė, A., Alexander, R., Li, H., et al. (2015). Regeneration of sensory hair cells requires localized interactions between the Notch and Wnt pathways. *Dev. Cell* 34, 267–282. doi: 10.1016/j.devcel.2015.05.025

Samarajeewa, A., Jacques, B. E., and Dabdoub, A. (2019). Therapeutic potential of wnt and notch signaling and epigenetic regulation in mammalian sensory hair cell regeneration. *Mol. Ther.* 27, 904–911. doi: 10.1016/j.ymthe.2019.03.017

Schimmang, T. (2007). Expression and functions of FGF ligands during early otic development. *Int. J. Dev. Biol.* 51, 473–481. doi: 10.1387/ijdb.072334ts

Shi, F., Hu, L., and Edge, A. S. B. (2013). Generation of hair cells in neonatal mice by β-catenin overexpression in Lgr5-positive cochlear progenitors. *Proc. Nat. Acad. Sci. U. S. A.* 110, 13851–13856. doi: 10.1073/pnas.1219952110

Shi, F., Hu, L., Jacques, B. E., Mulvaney, J. F., Dabdoub, A., and Edge, A. S. B. (2014). β-Catenin is required for hair-cell differentiation in the cochlea. *J. Neurosci.* 34, 6470–6479. doi: 10.1523/JNEUROSCI.4305-13.2014

Shi, F., Kempfle, J. S., and Edge, A. S. B. (2012). Wnt-responsive Lgr5-expressing stem cells are hair cell progenitors in the cochlea. *J. Neurosci.* 32, 9639–9648. doi: 10.1523/JNEUROSCI.1064-12.2012

Shu, Y., Li, W., Huang, M., Quan, Y. -Z., Scheffer, D., Tian, C., et al. (2019). Renewed proliferation in adult mouse cochlea and regeneration of hair cells. *Nat. Commun.* 10:5530. doi: 10.1038/s41467-019-13157-7

Shyh-Chang, N., and Daley, G. Q. (2013). Lin28: primal regulator of growth and metabolism in stem cells. *Cell Stem Cell* 12, 395–406. doi: 10.1016/j.stem.2013.03.005

Son, E. J., Ma, J.-H., Ankamreddy, H., Shin, J.-O., Choi, J. Y., Wu, D. K., et al. (2015). Conserved role of sonic Hedgehog in tonotopic organization of the avian basilar papilla and mammalian cochlea. *Proc. Nat. Acad. Sci. U S A* 112, 3746–3751. doi: 10.1073/pnas.1417856112

Tan, F., Chu, C., Qi, J., Li, W., You, D., Li, K., et al. (2019). AAV-ie enables safe and efficient gene transfer to inner ear cells. *Nat. Commun.* 10:3733. doi: 10.1038/s41467-019-11687-8

Tang, D., He, Y., Li, W., and Li, H. (2019). Wnt/β-catenin interacts with the FGF pathway to promote proliferation and regenerative cell proliferation in the zebrafish lateral line neuromast. *Exp. Mol. Med.* 51, 1–16. doi: 10.1038/s12276-019-0247-x.

Tang, D., Lin, Q., He, Y., Chai, R., and Li, H. (2016). Inhibition of H3K9me2 reduces hair cell regeneration after hair cell loss in the zebrafish lateral line by down-regulating the Wnt and Fgf signaling pathways. *Front. Mol. Neurosci.* 9:39. doi: 10.3389/fnmol.2016.00039

Wallis, D., Hamblen, M., Zhou, Y., Venken, K. J. T., Schumacher, A., Grimes, H. L., et al. (2003). The zinc finger transcription factor Gfi1, implicated in lymphomagenesis, is required for inner ear hair cell differentiation and survival. *Development* 130, 221–232. doi: 10.1242/dev.00190

Walters, B. J., Coak, E., Dearman, J., Bailey, G., Yamashita, T., Kuo, B., et al. (2017). *In vivo* interplay between p27(Kip1), GATA3, ATOH1 and POU4F3 converts non-sensory cells to hair cells in adult mice. *Cell Rep.* 19, 307–320. doi: 10.1016/j.celrep.2017.03.044

Wang, T., Chai, R., Kim, G. S., Pham, N., Jansson, L., Nguyen, D. -H., et al. (2015). Lgr5+ cells regenerate hair cells via proliferation and direct transdifferentiation in damaged neonatal mouse utricle. *Nat. Commun.* 6:6613. doi: 10.1038/ncomms7613

Waqas, M., Zhang, S., He, Z., Tang, M., and Chai, R. (2016). Role of Wnt and Notch signaling in regulating hair cell regeneration in the cochlea. *Front. Med.* 10, 237–249. doi: 10.1007/s11684-016-0464-9

Wu, J., Li, W., Lin, C., Chen, Y., Cheng, C., Sun, S., et al. (2016). Co-regulation of the Notch and Wnt signaling pathways promotes supporting cell proliferation and hair cell regeneration in mouse utricles. *Sci. Rep.* 6:29418. doi: 10.1038/srep29418

Yamamoto, N., Tanigaki, K., Tsuji, M., Yabe, D., Ito, J., and Honjo, T. (2006). Inhibition of Notch/RBP-J signaling induces hair cell formation in neonate mouse cochleas. *J. Mol. Med. (Berl)* 84, 37–45. doi: 10.1007/s00109-005-0706-9

Zarei, S., Zarei, K., Fritzsch, B., and Elliott, K. L. (2017). Sonic hedgehog antagonists reduce size and alter patterning of the frog inner ear. *Dev. Neurobiol.* 77, 1385–1400. doi: 10.1002/dneu.22544

Zhang, S., Liu, D., Dong, Y., Zhang, Z., Zhang, Y., Zhou, H., et al. (2019). Frizzled-9 + supporting cells are progenitors for the generation of hair cells in the postnatal mouse cochlea. *Front. Mol. Neurosci.* 12:184. doi: 10.3389/fnmol.2019.00184

Zhang, S., Zhang, Y., Dong, Y., Guo, L., Zhang, Z., Shao, B., et al. (2020). Knockdown of Foxg1 in supporting cells increases the trans-differentiation of supporting cells into hair cells in the neonatal mouse cochlea. *Cell. Mol. Life Sci.* 77, 1401–1419. doi: 10.1007/s00018-019-03291-2

Zhang, Y., Zhang, S., Zhang, Z., Dong, Y., Ma, X., Qiang, R., et al. (2020). Knockdown of Foxg1 in Sox9+ supporting cells increases the trans-differentiation of supporting cells into hair cells in the neonatal mouse utricle. *Aging (Albany NY)* 12, 19834–19851. doi: 10.18632/aging.104009

Zhong, C., Fu, Y., Pan, W., Yu, J., and Wang, J. (2019). Atoh1 and other related key regulators in the development of auditory sensory epithelium in the mammalian inner ear: function and interplay. *Dev. Biol.* 446, 133–141. doi: 10.1016/j.ydbio.2018.12.025

Zinn, E., Pacouret, S., Khaychuk, V., Turunen, H. T., Carvalho, L. S., Andres-Mateos, E., et al. (2015). *In silico* reconstruction of the viral evolutionary lineage yields a potent gene therapy vector. *Cell Rep.* 12, 1056–1068. doi: 10.1016/j.celrep.2015.07.019

Conflict of Interest: The authors declare that the research was conducted in the absence of any commercial or financial relationships that could be construed as a potential conflict of interest.

Publisher's Note: All claims expressed in this article are solely those of the authors and do not necessarily represent those of their affiliated organizations, or those of the publisher, the editors and the reviewers. Any product that may be evaluated in this article, or claim that may be made by its manufacturer, is not guaranteed or endorsed by the publisher.

frontiers in Cellular Neuroscience

ORIGINAL RESEARCH
published: 27 September 2021
doi: 10.3389/fncel.2021.751867

The Ganglioside Monosialotetrahexosylganglioside Protects Auditory Hair Cells Against Neomycin-Induced Cytotoxicity Through Mitochondrial Antioxidation: An *in vitro* Study

Yujin Li[1,2†], Ao Li[1,3,4†], Chao Wang[5], Xin Jin[2], Yaoting Zhang[2], Ling Lu[1,3,4], Shou-Lin Wang[5*] and Xia Gao[1,3,4*]*

[1] Department of Otolaryngology-Head and Neck Surgery, Nanjing Drum Tower Clinical College of Nanjing Medical University, Nanjing, China, [2] Department of Otolaryngology-Head and Neck Surgery, The Affiliated Huaian No. 1 People's Hospital of Nanjing Medical University, Huai'an, China, [3] Research Institute of Otolaryngology, Nanjing, China, [4] Jiangsu Provincial Key Medical Discipline (Laboratory), Department of Otolaryngology-Head and Neck Surgery, Affiliated Drum Tower Hospital of Nanjing University Medical School, Nanjing, China, [5] School of Public Health, Nanjing Medical University, Nanjing, China

OPEN ACCESS

Edited by:
Zuhong He,
Wuhan University, China

Reviewed by:
Gaoying Sun,
Shandong University, China
Wenwen Liu,
Shandong University, China

***Correspondence:**
Ling Lu
entluling60@126.com
Shou-Lin Wang
wangshl@njmu.edu.cn
Xia Gao
xiagaogao@hotmail.com

[†] These authors have contributed equally to this work and share first authorship

Specialty section:
This article was submitted to Cellular Neuropathology, a section of the journal Frontiers in Cellular Neuroscience

Received: 02 August 2021
Accepted: 06 September 2021
Published: 27 September 2021

Citation:
Li Y, Li A, Wang C, Jin X, Zhang Y, Lu L, Wang S-L and Gao X (2021) The Ganglioside Monosialotetrahexosylganglioside Protects Auditory Hair Cells Against Neomycin-Induced Cytotoxicity Through Mitochondrial Antioxidation: An in vitro Study. Front. Cell. Neurosci. 15:751867. doi: 10.3389/fncel.2021.751867

Neomycin is a common ototoxic aminoglycoside antibiotic that causes sensory hearing disorders worldwide, and monosialotetrahexosylganglioside (GM1) is reported to have antioxidant effects that protect various cells. However, little is known about the effect of GM1 on neomycin-induced hair cell (HC) ototoxic damage and related mechanism. In this study, cochlear HC-like HEI-OC-1 cells along with whole-organ explant cultures were used to establish an *in vitro* neomycin-induced HC damage model, and then the apoptosis rate, the balance of oxidative and antioxidant gene expression, reactive oxygen species (ROS) levels and mitochondrial membrane potential (MMP) were measured. GM1 could maintain the balance of oxidative and antioxidant gene expression, inhibit the accumulation of ROS and proapoptotic gene expression, promoted antioxidant gene expression, and reduce apoptosis after neomycin exposure in HEI-OC-1 cells and cultured cochlear HCs. These results suggested that GM1 could reduce ROS aggregation, maintain mitochondrial function, and improve HC viability in the presence of neomycin, possibly through mitochondrial antioxidation. Hence, GM1 may have potential clinical value in protecting against aminoglycoside-induced HC injury.

Keywords: monosialotetrahexosylganglioside, neomycin, hair cell, cytotoxicity, reactive oxygen species

INTRODUCTION

Sensorineural hearing loss is a common sensory disorder in humans. Many factors, including viral infections, noise, and exposure to ototoxic drugs, can cause hair cell (HC) damage and induce hearing impairment (Sotoudeh, 2021). Adult mammalian HCs cannot regenerate, and once these cells are damaged, the effects are often permanent (Zhang et al., 2020). Aminoglycoside

antibiotics are antibacterial drugs commonly used in clinical treatment and are also the most commonly encountered ototoxic drugs. It is estimated that approximately one-quarter of people who are treated with aminoglycoside antibiotics will develop ototoxicity (Lopez-Novoa et al., 2011). However, these drugs still play a crucial role in the treatment of severe gram-negative bacterial infections and multidrug-resistant tuberculosis and are becoming more irreplaceable as microbial resistance to conventional antimicrobial agents increases (Germovsek et al., 2017). Therefore, exploring the mechanism through which they exert ototoxicity and identifying effective treatment measures is of great significance (Guo et al., 2019). The ototoxic mechanism of aminoglycoside drugs has not been fully elucidated. Recent studies have found that it may be related to oxidative stress (Jiang et al., 2016), apoptosis (Jiang et al., 2017), and mitochondrial dysfunction (Jiang et al., 2017). Previous studies have found that aminoglycoside drugs accumulate in mitochondria after entering HCs and that this can lead to disorders of mitochondrial metabolism, imbalanced expression of prooxidants (ALOX15) and antioxidants (GSR, SOD1, NQO1, GLRX), and the production of excessive reactive oxygen species (ROS) such as hydrogen peroxide (H_2O_2) and hydroxyl radicals (•OH) in cells. Aminoglycosides also disrupt the normal synthesis of mitochondrial proteins and reduce the mitochondrial membrane potential (MMP), leading to increased mitochondrial permeability and release of cytochrome C and ultimately to cell apoptosis (He et al., 2020; Yao et al., 2020). It has been reported that some antioxidants exert protective effects against the ototoxicity of aminoglycosides *in vitro* and *in vivo* (Li et al., 2018; Pham et al., 2020). However, no ideal drug that is protective against ototoxicity has been identified for use in clinical practice (Guo et al., 2019).

Gangliosides are sphingolipid cell membrane components containing sialic acid (Magistretti et al., 2019) that are widely present in the cell membranes of vertebrate tissues. Monosialotetrahexosylganglioside (GM1) is the most extensively studied of the gangliosides to date. GM1 plays a protective role in the nervous system by regulating the expression of BCL-2 protein, reducing the damage caused by free radicals (Rao et al., 2019), increasing mitochondrial activity and stabilizing mitochondrial function (Fazzari et al., 2020). GM1 has also been found to have a cytoprotective effect outside of the nervous system. Franco et al. (2016) found that GM1-containing nanoliposomes protect against light chain protein (LC)-induced human microvascular dysfunction by increasing nitric oxide bioavailability and reducing oxidative and nitrative stress mediated by the Nrf-2-dependent antioxidant stress response. Guo et al. (2021) reported that treatment with GM1 ganglioside (40 μM) significantly decreased α-synuclein accumulation, alleviated mitochondrial dysfunction and oxidative stress, and played an anti-PD role in doxycycline-treated PC12α-Syn A53T cells. In addition, GM-1 treatment was found to significantly decrease auditory brainstem response (ABR) threshold shifts and HC loss after acoustic overexposure, and immunostaining for 4-hydroxynonenal (4-HNE) was found to be reduced by GM-1 treatment, suggesting that GM-1 protects the cochlea against acoustic injury by inhibiting lipid peroxidation (Tanaka et al., 2010) and indicating that GM1 has an antioxidant effect on cochlear HCs.

GM1 has been used as a neuroprotective drug in some countries for the treatment of Alzheimer's disease, stroke, peripheral nerve damage, and Parkinson's disease (Magistretti et al., 2019), and some physicians in China are attempting to use GM1 in the clinical treatment of sudden deafness (Diao and Dong, 2012). However, the protective effect of GM1 against cochlear HC damage and the possible mechanism of this effect are still unclear. Therefore, clarification of the protective effect and mechanism of GM1 on cochlear and HC injury is of practical significance.

Neomycin is a representative ototoxic aminoglycoside drug and is often used in ototoxicity studies. We established a mature neomycin HC injury model in previous experiments (Gao et al., 2019). In the present study, we used neomycin to damage cochlear HC-like HEI-OC-1 cells and used whole-organ explant cultures to establish an *in vitro* model of neomycin-induced HC damage with the aim of investigating the potential protective effect of GM1 on ototoxic HC damage and attempting to provide evidence for the potential clinical use of GM1 in protecting against HC injury caused by aminoglycosides.

MATERIALS AND METHODS

Chemicals and Reagents

GM1 (Macklin, Shanghai, China, G873919), penicillin (CSPC, Shijiazhuang, China, h20033291), CCK-8 Kits (Beyotime, Shanghai, China, C0038), BeyoRT^{TM} II First-Strand cDNA Synthesis Kits with gDNA Eraser (Beyotime, D7170 M), TUNEL Apoptosis Assay Kits (Beyotime, C1086), DMSO (Sigma-Aldrich, Saint Louis, MO, United States, D8371), neomycin (Sigma-Aldrich, N6386-5G), paraformaldehyde (Sigma-Aldrich, 158127), TRIzol reagent (Sangon Biotech, Shanghai, China, B610409-0100), SYBR Green (Roche, Basel, Switzerland, 4913914001), MitoSOX Red (Life Technologies, Carlsbad, CA, United States, M36008), TMRE Mitochondrial Membrane Potential Assay Kits (Abcam, Cambridge, United Kingdom, ab113852), Triton X-100 (Solarbio, Beijing, China, T8260), DAPI (Solarbio, C0060), antibodies against cleaved CASPASE-3 (Thermo Fisher Scientific, Carlsbad, CA, United States, Cat# 43-7800, RRID:AB_2533540), antibody against MYOSIN 7a (Santa Cruz Biotechnology, Santa Cruz, United States, Cat# sc-74516, RRID:AB_2148626), Alexa Fluor 488 goat anti-rabbit IgG (Abcam, Cat# ab150077, RRID:AB_2630356), Alexa Fluor 555 donkey anti-rabbit IgG (Abcam, Cat# ab150062, RRID:AB_2801638), Alexa Fluor 555 goat anti-mouse IgG (Abcam, Cat# ab150118, RRID:AB_2714033), and Alexa Fluor 647 donkey anti-rabbit IgG (Abcam, Cat# ab150077, RRID:AB_2630356) were used in this study.

Cell Culture and Treatment

The House Ear Institute Organ of Corti 1 cell line (HEI-OC-1, RRID: CVCL_D899), which is used as an HC-like model system, expresses Atoh1, Prestin, Myosin7a and other cellular markers specific for auditory and sensory HCs. The cells were cultured

in DMEM/F12 containing 10% fetal bovine serum (FBS) and 100 IU/mL penicillin at 37°C in a 5% CO_2 atmosphere. In this study, we exposed cells in FBS-free culture medium to 2 mM neomycin for 24 h to establish an HEI-OC-1 cell injury model, as reported previously (Gao et al., 2019). For the establishment of the HEI-OC-1 cell injury protection model, we plated the cells, cultured them for 12 h, replaced the medium with FBS-free culture medium, and treated the cells with 10–100 μM GM1 or with the corresponding volume of DMSO for 12 h. After 24 h treatment with 2 mM neomycin, the medium was replaced with complete culture medium lacking neomycin and GM1, and the cells were cultured for an additional 12 h before subsequent evaluation (**Figure 1A**).

Whole-Organ Explant Culture

On postnatal day 3 (P3), wild-type FVB mice were placed under deep anesthesia and sacrificed, and the animals' heads were removed and placed in 75% alcohol. The temporal bone cochlea was removed using scissors and placed in a sterile culture dish containing precooled HBSS buffer. Under microscopic view, the volute covering was peeled off, and the spiral ganglia and vascular stripes were separated to obtain a complete basilar membrane, which was then placed face up in the center of a sterile cover glass coated with Cell-tak tissue glue. The cover glass was placed in a 4-well plate and cultured in 120 μL of DMEM/F12 medium containing 2% B27, 1% N-2 and 100 IU/mL penicillin at 37°C in a 5% CO_2 atmosphere. The cochlear HC damage condition was 0.5 mM neomycin for 12 h, as reported previously (Gao et al., 2019). The explants in the GM1 group were cultured in medium to which 20 μM GM1 had been added; after 12 h, 0.5 mM neomycin was added, and the explant was cultured for an additional 12 h. The medium containing GM1 and neomycin was then removed, and the explants were cultured in fresh medium for an additional 12 h for recovery. The control group and the neomycin group were treated with the same volume of DMSO. All procedures involving FVB mice were performed in accordance with the procedures approved by the Animal Care and Use Committee of Nanjing Medical University, and all efforts were made to use the minimum number of animals necessary and to minimize their suffering.

Cell Viability and Number Analysis

Cell viability was measured using a CCK-8 kit. HEI-OC-1 cells were seeded in 96-well plates at 2,000 cells/well. After the treatment described above, 10 μL of CCK-8 was added to each well, and the plates were incubated at 37°C for 30 min. The absorbance at 450 nm was measured using a microtiter plate reader (Bio-Rad). In addition, the HCs of explant-cultured cochleae were immunolabeled using antibodies against MYOSIN 7a and counted by fluorescence labeling

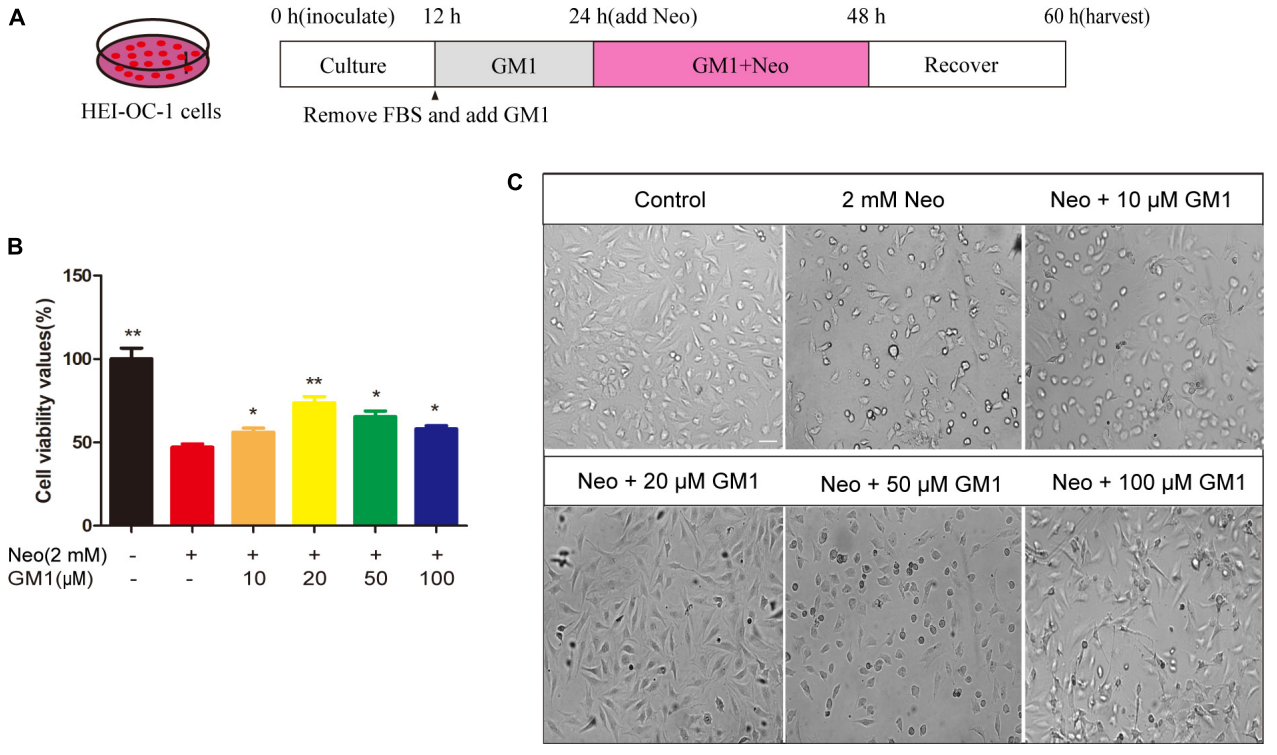

FIGURE 1 | GM1 enhanced HEI-OC-1 cell survival after neomycin exposure. **(A)** Schematic diagram illustrating GM1 and neomycin addition in cell culture. **(B)** Effects of GM1 on the viability of HEI-CO-1 cells after exposure to neomycin. Viability was measured using the CCK-8 assay, and the data are expressed as the mean ± SD of triplicate determinations obtained in three independent experiments. *$p < 0.05$, **$p < 0.01$ compared with neomycin treatment alone. **(C)** Morphology of HC-like HEI-OC-1 cells observed under a live-cell imaging system. Scale bars = 20 μm.

microscopy. The MYOSIN 7a-positive cells in three regions of equal length (160 μm) selected from the apical to the basal turns of the cochlea were viewed under fluorescence microscopy and counted.

Quantitative Real-Time PCR

TRIzol reagent was used to extract total RNA from HEI-OC-1 cells. The concentration and quality of RNA in the samples were measured by NanoDrop spectroscopy (Thermo NanoDrop 2000, United States). A BeyoRT^{TM} II First-Strand cDNA Synthesis Kit with gDNA Eraser was used for reverse transcription according to the instructions supplied by the manufacturer. SYBR Green was used to perform quantitative polymerase chain reaction (qPCR) on a real-time PCR instrument (cfx96, Bio-Rad). *Gapdh* was used as the internal reference gene. The primers were synthesized by Sangon Biotech (Shanghai, China). The primer sequences for the candidate genes are shown in **Table 1**.

Immunofluorescence Assay

An antibody against cleaved CASPASE-3, the TUNEL Apoptosis Assay Kit, MitoSOX Red, the TMRE Mitochondrial Membrane Potential Assay Kit, an antibody against MYOSIN 7a (1:500 dilution), and DAPI (1:1,000 dilution) were used to analyze apoptotic cells, measure ROS, measure MMP, and stain HCs and nuclei. Briefly, after fixation with 4% paraformaldehyde at room temperature for 1 h, the cells and tissues were washed three times with PBST (1 × PBS containing 0.1% Triton X-100) and incubated in blocking medium (PBS containing 10% heat-inactivated donkey serum, 1% Triton X-100, 1% BSA, and 0.02% sodium azide, pH 7.2) at room temperature for 1 h. The samples were then incubated with primary antibodies against cleaved CASPASE-3 or MYOSIN 7a at 4°C for 8 h. After 3 washes with PBST, the samples were labeled with a secondary antibody for 1 h, washed again 3 times with PBST, mounted with a fluorescent blocking agent, and imaged with laser scanning confocal microscopy (Zeiss LSM700, Germany). TUNEL, MitoSox Red, and TMRE signals were measured according to the manufacturer's instructions.

TABLE 1 | Primer sequences for qRT-PCR.

Gene	Sequence (5′ → 3′)	
Gapdh	F:	AGGTCGGTGTGAACGGATTTG
	R:	TGTAGACCATGTAGTTGPAGGTCA
Caspase-3	F:	ATGGAGAACAACAAAACCTCAGT
	R:	TTGCTCCCATGTATGGTCTTTAC
Bax	F:	TGAAGACAGGGGCCTTTTTG
	R:	AATTCGCCGGAGACACTCG
Bcl-2	F:	ATGCTTTGTGGAACTATATGGC
	R:	GGTATGCACCCAGAGTGATGC
Alox15	F:	GGCTCCAACAACGAGGTCTAC
	R:	AGGTATTCTGACACATCCACCTT
Sod1	F:	AACCAGTTGTGTTGTCAGGAC
	R:	CCACCATGTTTCTTAGAGTGAGG
Caspase-9	F:	CCTAGTGAGCGAGCTGCAAG
	R:	ACCGCTTTGCAAGAGTGAAG
Gsr	F:	TGCACTTCCCGGTAGGAAAC
	R:	GATCGCAACTGGGGTGAGAA
Sirt1	F:	TGTGGTGAAGATCTATGGAGGC
	R:	TGTACTTGCTGCAGACGTGGTA

F, forward; R, reverse.

Flow Cytometry Assay

We used DAPI and propidium iodide (PI) to distinguish dead cells from living cells. HEI-OC-1 cells were treated with neomycin in the presence or absence of GM1 and were then treated with trypsin and collected. The cells were washed twice, resuspended in PBS, and diluted to a concentration of 1×10^6 cells/mL in PBS. DAPI and PI were added; the cells were then incubated in the dark at room temperature for 10–20 min and analyzed by flow cytometry (FACSCanto, BD) within 1 h. In addition, MitoSOX Red was used to determine the level of mitochondrial ROS.

Statistical Analysis

All data are expressed as mean ± SD. All statistical analyses were performed using GraphPad Prism 7 software. Two-tailed and unpaired Student's *t*-tests were used to assess the statistical significance of differences between the two groups. One-way ANOVA and Dunnett's multiple comparison tests were used to compare multiple groups. $P < 0.05$ indicated a significant difference.

RESULTS

Monosialotetrahexosylganglioside Protects HEI-OC-1 Cells From Neomycin-Induced Cytotoxicity

As shown in **Figure 1**, exposure to 2 mM neomycin decreased cell viability by approximately half in comparison with the control cells, and GM1 at 10–100 μM exhibited a certain degree of protection; 20 μM GM1 gave the strongest protection. At GM1 concentrations higher than 20 μM, the viability of HEI-OC-1 cells began to decrease (**Figure 1B**). To confirm this finding, we used a live-cell imaging system to observe HEI-OC-1 cells and found that the morphology of living cells in the 20 μM GM1 group was most similar to that of the cells in the control group (**Figure 1C**). Therefore, 20 μM GM1 was used as the treatment concentration in the follow-up experiments in this study.

Monosialotetrahexosylganglioside Decreased Neomycin-Induced Apoptosis in HEI-OC-1 Cells

To confirm the protective effect of GM1 against apoptosis of HEI-OC-1 cells, HEI-OC-1 cells were stained using TUNEL and antibodies against cleaved CASPASE-3. The percentages of TUNEL-positive and cleaved CASPASE-3-positive cells in the neomycin group were significantly higher than those in the control group, and pretreatment with 20 μM GM1 significantly reduced the percentages of TUNEL-positive and

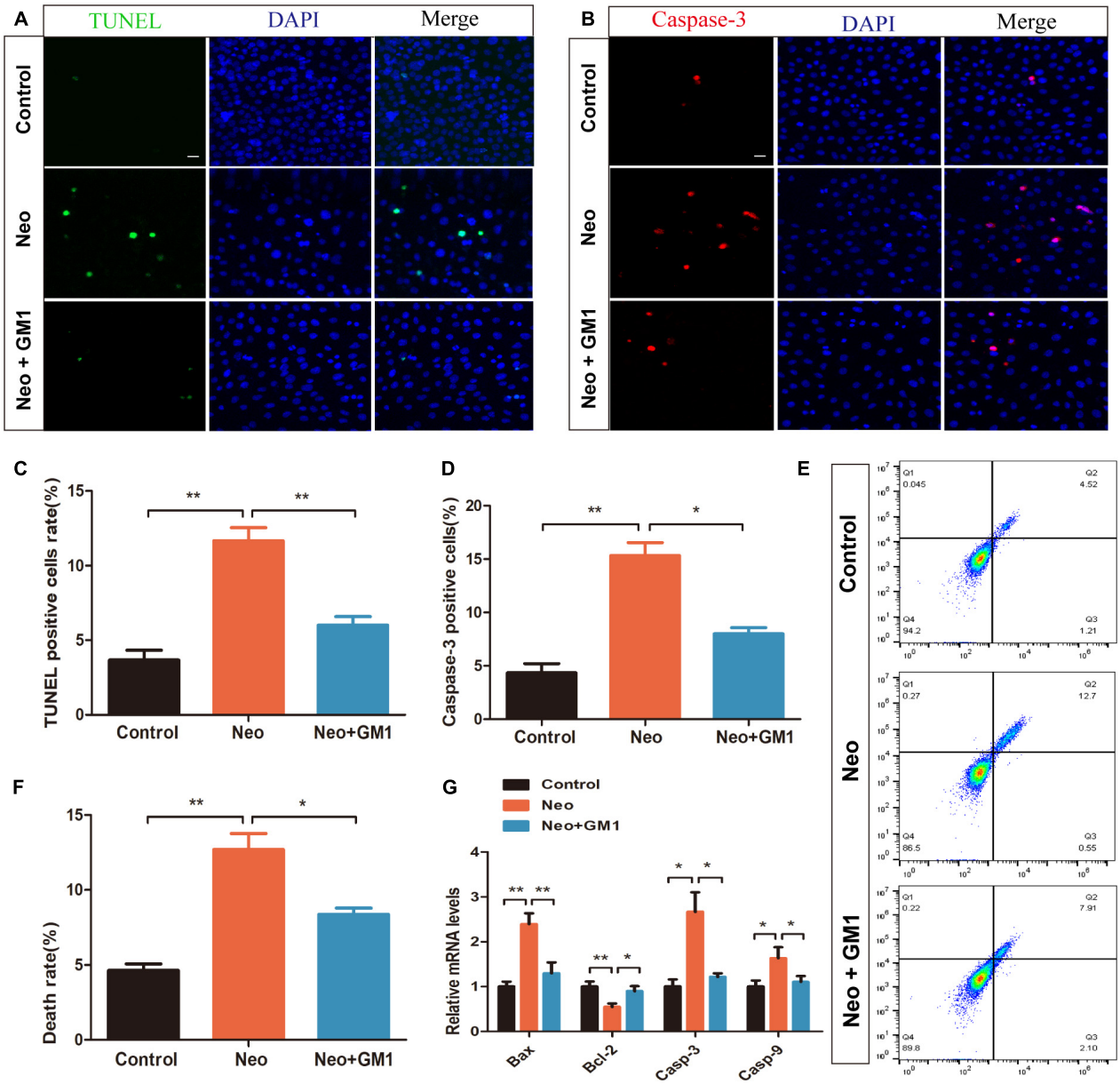

FIGURE 2 | GM1 reduced neomycin-induced apoptosis in HEI-OC-1 cells. **(A)** Immunofluorescence images of apoptotic HEI-OC-1 cells with TUNEL and DAPI double staining. **(B)** Immunofluorescence images of apoptotic HEI-OC-1 cells with cleaved CASPASE-3 and DAPI double staining. **(C,D)** Quantification of the number of apoptotic cells in **(A,B)**. **(E,F)** Survival and percentage of HEI-OC-1 cells determined by DAPI/PI staining flow cytometry. **(G)** Expression of proapoptotic and antiapoptotic genes in HEI-OC-1 cells treated with neomycin and/or GM1 determined by qRT-PCR; the values were normalized to *Gapdh* as an internal control. The data are expressed as the mean ± SD of triplicate samples. $^{*}p < 0.05$, $^{**}p < 0.01$. Scale bars = 20 μm.

cleaved CASPASE-3-positive cells after neomycin exposure (**Figures 2A–D**). Similarly, flow cytometry showed that 20 μM GM1 significantly reduced the death of HEI-OC-1 cells induced by neomycin (**Figures 2E,F**). The qRT-PCR results also showed that the mRNA expression of *Caspase-3, Bax,* and *Caspase-9* decreased significantly, while *Bcl-2* expression increased significantly, in the GM1 group compared with the neomycin group (**Figure 2G**). Taken together, our results suggest that GM1 protects HEI-OC-1 cells from neomycin-induced apoptosis.

Monosialotetrahexosylganglioside Reduced Neomycin-Induced Apoptosis of Hair Cells in Explant-Cultured Cochleae

To explore the protective effect of GM1 on explant-cultured cochleae, TUNEL and antibody staining for cleaved CASPASE-3 were used to measure apoptosis of the cells in the explants after treatment. We found that the percentages of TUNEL-positive

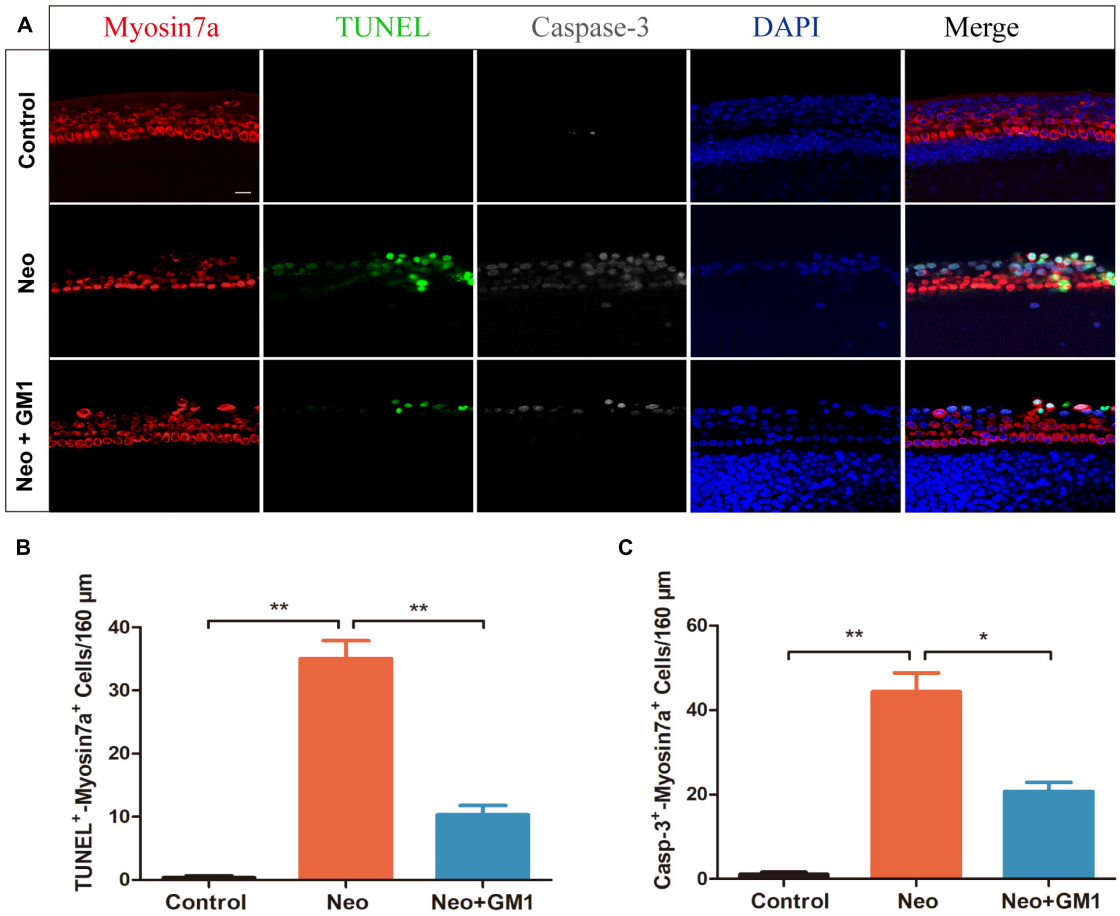

FIGURE 3 | GM1 decreased neomycin-induced HC apoptosis in cochleae. **(A)** Immunofluorescence staining for TUNEL, cleaved CASPASE-3, and MYOSIN 7a in the basal turn of the cochlea in different treatment groups. **(B,C)** Quantification of the number of TUNEL/MYOSIN 7a and cleaved CASPASE-3/MYOSIN 7a double-positive cells per 160 μm of cochlea in **(A)**. The data are expressed as the mean ± SD of triplicate samples. $^{**}p < 0.01$. Scale bars = 16 μm.

and cleaved CASPASE-3-positive cells in the neomycin group were significantly higher than those in the control group and that pretreatment with 20 μM GM1 significantly reduced the percentage of TUNEL-positive and cleaved CASPASE-3-positive cells after neomycin exposure (**Figures 3A–C**), consistent with the results obtained for HEI-OC-1 cells.

Monosialotetrahexosylganglioside Protects Against Neomycin-Induced Hair Cell Loss in Explant-Cultured Cochleae

The procedures used to process the samples in the explant-cultured cochlea experiment are described in **Figure 4A**. MYOSIN 7a and DAPI staining were used to observe the changes in the number of HCs in the apical, middle and basal turns of the cochlea. We found that the number of HCs in the apical turn did not change significantly after neomycin exposure (**Figure 4B**). In contrast, the number of HCs in the middle and basal turns of the cochlea decreased significantly, and GM1 treatment successfully reduced HC loss in the middle and basal turns after neomycin exposure (**Figures 4C–E**).

Monosialotetrahexosylganglioside Attenuates Oxidative Stress in Explant-Cultured Cochleae and HEI-OC-1 Cells After Neomycin Treatment

In this study, MitoSox Red immunofluorescence staining showed that the levels of ROS were significantly increased in the neomycin group compared with the control group and that pretreatment with 20 μM GM1 significantly reduced ROS levels compared with the neomycin group both in explant-cultured cochleae (**Figures 5A,B**) and in HEI-OC-1 cells (**Figures 6A,B**). MitoSOX flow cytometry of HEI-OC-1 cells yielded similar results (**Figure 6C**). qRT-PCR showed that the mRNA expression of *Gsr, Sod1,* and *Sirt1* was significantly upregulated in the GM1 pretreatment group compared with the neomycin group (**Figure 6D**). This suggests that GM1 alleviates the neomycin-induced imbalance in antioxidant-prooxidant gene expression. However, the mRNA expression of *Alox15* did not change significantly after GM pretreatment. We also found that the MMP decreased in the neomycin group but significantly increased

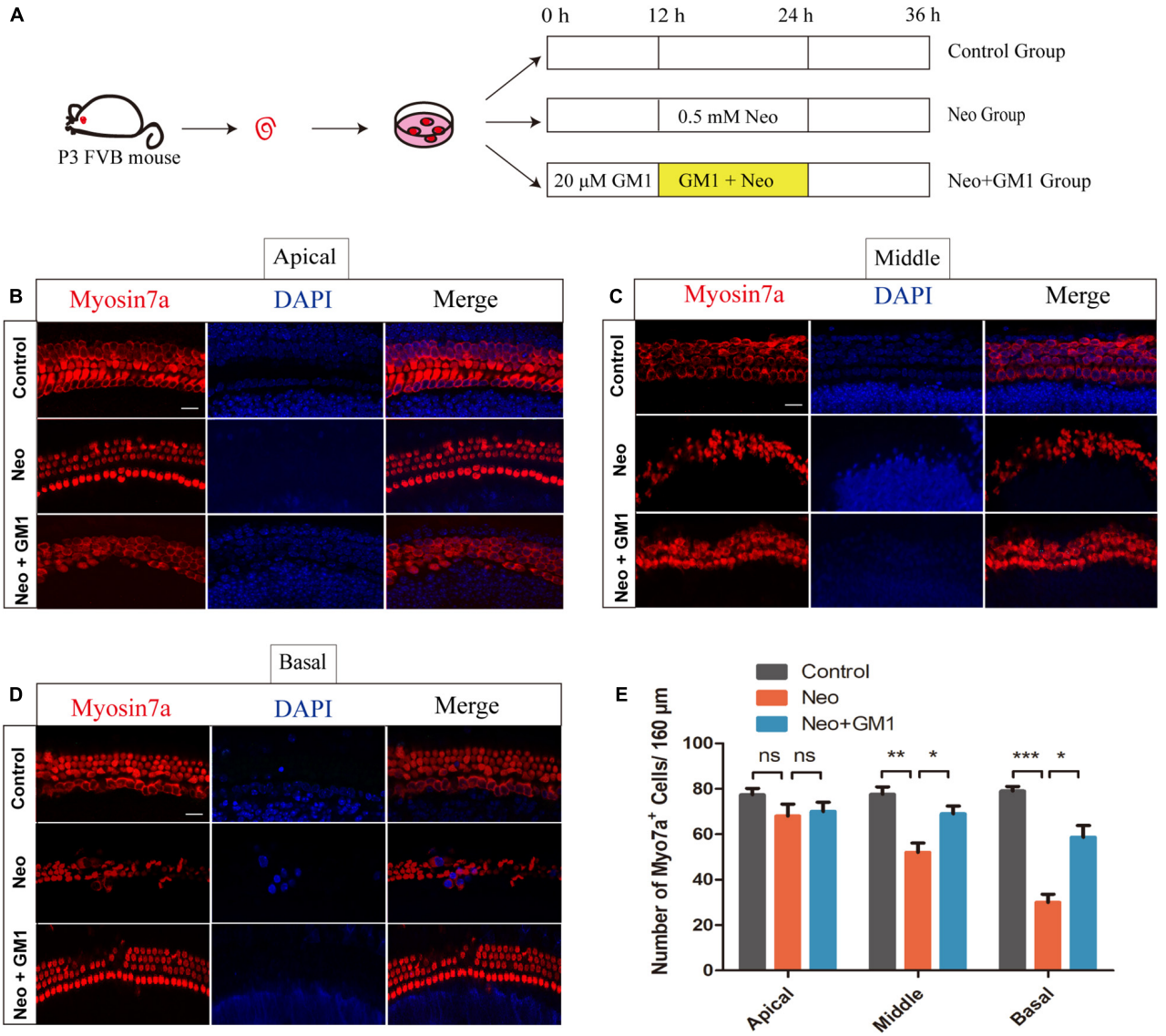

FIGURE 4 | GM1 promoted the survival of cochlear HCs in explant cultures after neomycin exposure. **(A)** Schematic diagram illustrating GM1 and neomycin addition to explant-cultured cochleae. **(B,D)** Immunofluorescence staining of MYOSIN 7a/DAPI in the apical turns **(B)**, middle turns **(C)**, and basal turns **(D)** of explant-cultured cochleae in the different treatment groups. **(E)** Quantification of the number of MYOSIN 7a-positive cells per 160 μm of cochlea in **(B–D)**. The data are expressed as the mean ± SD of triplicate samples $^{*}p < 0.05$, $^{**}p < 0.01$, $^{***}p < 0.001$. Scale bars = 16 μm.

in the GM1 group compared to that in the neomycin group, indicating that 20 μM GM1 treatment can prevent the MMP decrease induced by neomycin exposure in HEI-OC-1 cells (**Figures 7A,B**).

DISCUSSION

Gangliosides are mainly composed of hydrophobic ceramide and hydrophilic oligosaccharide chains containing sialic acid, which are fat-soluble and water-soluble, respectively. Ceramide is composed of long basic hydrophobic chains attached to fatty acids that are embedded in the lipid bilayer of the cell membrane and enhance the stability of the cell membrane structure. Oligosaccharides are linked to the serine residue of ceramide, and the sialic acid in oligosaccharides binds to peripheral calcium ions to maintain normal cellular physiological functions (Schnaar, 2016; Ledeen and Wu, 2018). Recent studies have reported that GM1 exerts antioxidant effects through its regulation of intracellular calcium levels in the hippocampus (She et al., 2009) and its activation of tyrosine kinase Trk receptors (Vlasova Iu et al., 2009) and that it has a protective effect on a variety of cells when applied as an intervention (Nikolaeva et al., 2015; Zhao et al., 2015). In this study, we used the HEI-OC-1 cell line and whole-organ explant cultures to investigate the protective effect of GM1 on neomycin-induced

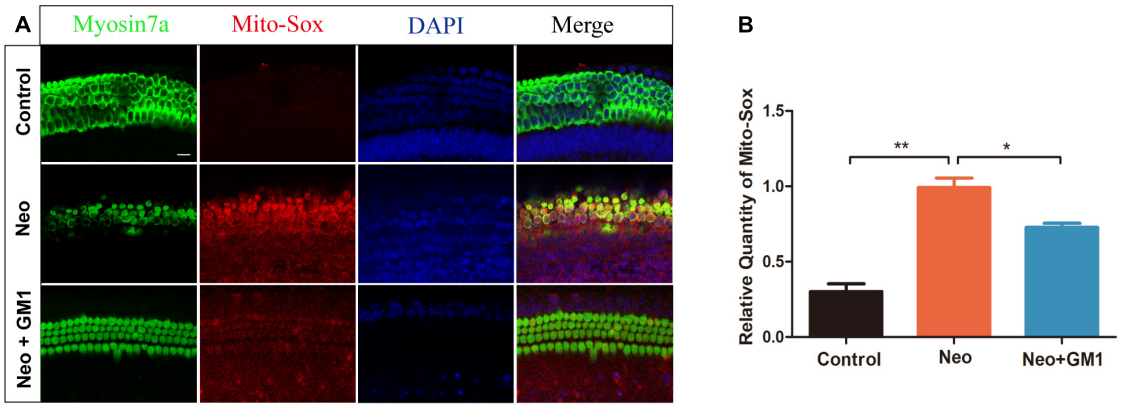

FIGURE 5 | GM1 decreased ROS levels in explant-cultured cochlear HCs after neomycin exposure. **(A)** Immunofluorescence due to MitoSox, MYOSIN 7a and DAPI in the middle turns of explant-cultured cochleae in the different treatment groups. **(B)** Relative MitoSox immunofluorescence intensity. The data are expressed as the mean ± SD of triplicate samples. $^{*}p < 0.05$, $^{**}p < 0.01$. Scale bars = 16 μm.

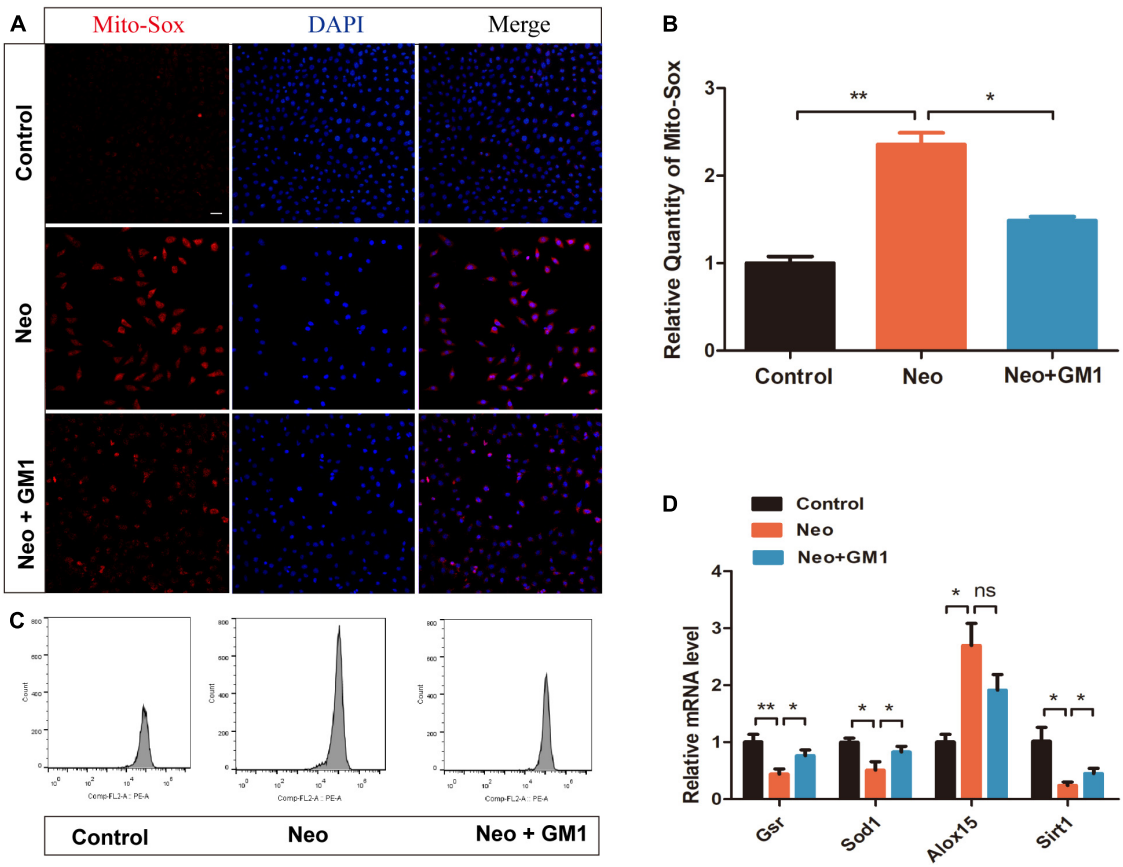

FIGURE 6 | GM1 decreased ROS levels in HEI-OC-1 cells after neomycin exposure. **(A,B)** Immunofluorescence of MitoSox/DAPI in different treatment groups. **(C)** MitoSox levels of HEI-OC-1 cells in different treatment groups determined by flow cytometry. **(D)** mRNA expression levels of redox-related genes in HEI-OC-1 cells determined by qRT-PCR and normalized to *Gapdh*. The data are expressed as the mean ± SD of triplicate samples. $^{*}p < 0.05$, $^{**}p < 0.01$. Scale bars = 20 μm.

HC injury *in vitro*. Our results showed that a protective effect of GM1 on HEI-OC-1 cells is observed when GM1 is applied at concentrations between 10 and 100 μM and that 20 μM is the optimal concentration; beyond this, the protective effect begins to decline, suggesting that GM1 can protect HCs when applied at an appropriate concentration.

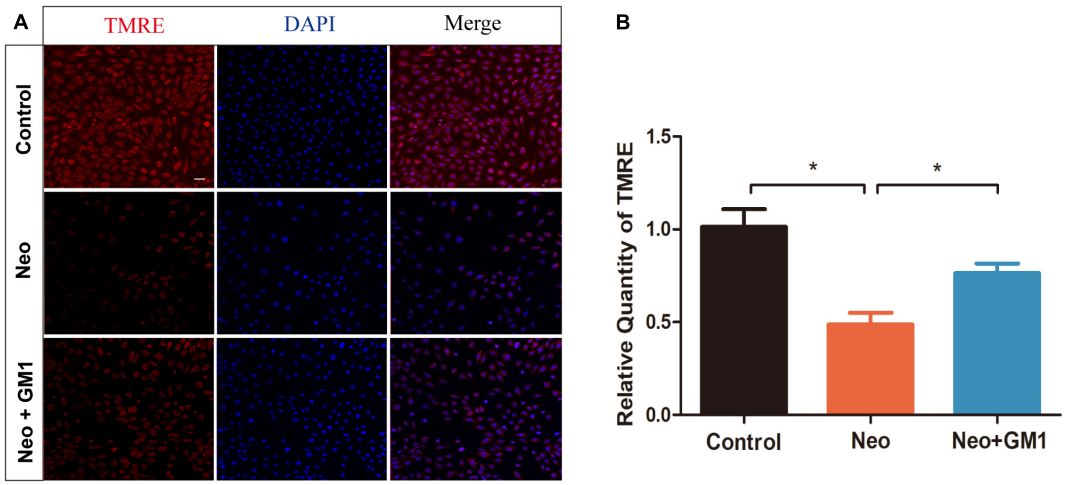

FIGURE 7 | GM1 increases the mitochondrial membrane potential (MMP) after neomycin exposure. **(A)** Immunofluorescence of HEI-OC-1 cells in different treatment groups after labeling using a TMRE staining kit and DAPI. **(B)** Relative immunofluorescence intensities of the cells in **(A)**. The data are expressed as the mean ± SD of triplicate samples. *$p < 0.05$. Scale bars = 20 μm.

Previous studies have suggested that aminoglycoside drugs induce HEI-OC-1 cell apoptosis by promoting the release of proapoptotic factors (Leis et al., 2015). Our previous research also showed that after exposure of HEI-OC-1 cells to neomycin, the expression of proapoptotic genes such as *Caspase 3* and *Bax* increased significantly, while that of the antiapoptotic genes *Bcl-2* and *Nf-kb* decreased significantly (Gao et al., 2019). In the current study, we found that treatment with GM1 decreases the death and apoptosis induced by neomycin. Moreover, our results also showed that exposure of cochlear explant cultures to GM1 protected HC cells in the middle and basal turns of the cochlea from damage; since the damage caused by aminoglycoside drugs shows a decreasing trend from the basal turn to the apical turn of the cochlea (Zhang et al., 2019) and high-frequency hearing loss is the first and most severe impairment in patients with ototoxic hearing loss (Guo et al., 2019), the protective effect of GM1 on high-frequency hearing may have potential clinical significance.

BCL-2 family proteins play a key role in the apoptosis process. Proapoptotic proteins such as BAX change their molecular conformations when they encounter apoptosis signals; they then translocate and insert into the outer mitochondrial membrane, eventually leading to increased permeability of the outer mitochondrial membrane, the release of cytochrome c (Cyt C), and the activation of multiple caspases. BCL-2 can prevent this process (Verma and Syed Mohammed, 2019; Tian et al., 2020; Zeng et al., 2020). Our study found that the mRNA expression of *Bcl-2* was upregulated and that that of *Bax* was downregulated, indicating that GM1 can relieve neomycin-induced HC damage by regulating the mRNA expression of *Bax* and *Bcl-2*. This is consistent with the report by Chen et al. (2019) that GM1 increases *Bcl-2* expression and reduces *Bax* expression, thereby protecting against lead-induced neurological damage in developing rats.

Many studies have found that aminoglycoside antibiotics aggregate in inner ear HCs, where they affect normal metabolism and produce a large number of highly toxic ROS (Han et al., 2020). ROS include hydroxyl radicals (OH•), hydrogen peroxide, superoxide and other free radicals, all of which exhibit great oxygen toxicity. ROS can affect various signaling pathways and physiological activities of cells, including cell growth, division, differentiation and apoptosis. Excessive ROS levels can lead to a variety of diseases (Zhang et al., 2016). Studies have found that aminoglycosides bind to calreticulin, which is highly expressed in cochlear marginal cells and HCs. and disrupt chaperone activity. This binding in turn elevates mitochondrial Ca^{2+} levels, and this leads to elevated levels of both mitochondrial oxidation and cytoplasmic ROS and to an imbalance in the redox state (Jiang et al., 2017). The high reactivity of oxygen free radicals can damage cell components and structures such as nucleic acids and cell membranes. ROS accumulation can also cause mitochondrial depolarization and change mitochondrial membrane permeability. The resulting impairment of mitochondrial function leads to the further accumulation of oxygen free radicals and eventually to apoptosis (He et al., 2020; Zhong et al., 2020). In this study, we found that GM1 significantly decreased ROS levels in HEI-OC-1 cells and explant-cultured cochlear HCs, suggesting that GM1 can alleviate mitochondrial dysfunction after exposure to neomycin. Redox balance plays an important role in the generation and elimination of ROS. In this study, the mRNA expression levels of *Gsr, Sod1,* and *Sirt1* decreased and that of *Alox15* increased significantly after neomycin exposure, and GM1 pretreatment significantly improved the imbalance in the mRNA expression of *Gsr, Sod1,* and *Sirt1* induced by neomycin. These results suggest that exposure of cells to GM1 can correct the imbalance in the expression of prooxidant and antioxidant genes observed after neomycin exposure, thereby reducing the ROS level and preventing HC mitochondrial dysfunction and apoptosis. However, it must be noted that the use of high GM1 concentrations will reduce

the protective effect and may cause additional damage to HCs. Drug dosage must be considered in future animal and clinical studies.

In conclusion, our results suggest that GM1 can maintain the normal balance between oxidative and antioxidant gene expression, reduce the accumulation of ROS, and reduce apoptosis after exposure of HEI-OC-1 cells and cultured cochlear HCs to neomycin. These results indicate that GM1 may have potential clinical value in protecting against hearing impairment in individuals treated with aminoglycoside drugs.

DATA AVAILABILITY STATEMENT

The original contributions presented in the study are included in the article/supplementary material, further inquiries can be directed to the corresponding author/s.

ETHICS STATEMENT

The animal study was reviewed and approved by the Animal Care and Use Committee of Nanjing Medical University.

AUTHOR CONTRIBUTIONS

YL, AL, and CW performed the experiments, analyzed the data, and wrote the manuscript. LL, S-LW, and XG designed the experiments and provided critical revision. XJ and YZ reviewed the experimental data and conducted the statistical analysis. All authors contributed to the article and approved the submitted version.

FUNDING

This work was supported by the National Natural Science Foundation of China (81771019, 81970884, and 82071059), the Jiangsu Provincial Key Research and Development (BE2018605), and the Fellowship of China Postdoctoral Science Foundation (2020M681561).

ACKNOWLEDGMENTS

We would like to express our sincere appreciation to the Project of Invigorating Health Care through Science, Technology and Education ZDXKB2016015.

REFERENCES

Chen, C., Wang, S., and Liu, P. (2019). Deferoxamine enhanced mitochondrial iron accumulation and promoted cell migration in triple-negative MDA-MB-231 breast cancer cells via a ROS-dependent mechanism. *Int. J. Mol. Sci.* 20:4952. doi: 10.3390/ijms20194952

Diao, Y., and Dong, M. (2012). The observation on curative effect of 90 cases of sudden hearing loss. *Lin chuang er bi yan hou tou jing wai ke za zhi* 36, 306–308.

Fazzari, M., Audano, M., Lunghi, G., Di Biase, E., Loberto, N., Mauri, L., et al. (2020). The oligosaccharide portion of ganglioside GM1 regulates mitochondrial function in neuroblastoma cells. *Glycoconj J.* 37, 293–306. doi: 10.1007/s10719-020-09920-4

Franco, D. A., Truran, S., Weissig, V., Guzman-Villanueva, D., Karamanova, N., Senapati, S., et al. (2016). Monosialoganglioside-containing nanoliposomes restore endothelial function impaired by AL amyloidosis light chain proteins. *J. Am. Heart Assoc.* 5:e003318. doi: 10.1161/JAHA.116.003318

Gao, S., Cheng, C., Wang, M., Jiang, P., Zhang, L., Wang, Y., et al. (2019). Blebbistatin inhibits neomycin-induced apoptosis in hair cell-like HEI-OC-1 cells and in cochlear hair cells. *Front. Cell. Neurosci.* 13:590. doi: 10.3389/fncel.2019.00590

Germovsek, E., Barker, C. I., and Sharland, M. (2017). What do I need to know about aminoglycoside antibiotics? *Arch. Dis. Child Educ. Pract. Ed.* 102, 89–93. doi: 10.1136/archdischild-2015-309069

Guo, J., Chai, R., Li, H., and Sun, S. (2019). Protection of hair cells from ototoxic drug-induced hearing loss. *Adv. Exp. Med. Biol.* 1130, 17–36. doi: 10.1007/978-981-13-6123-4_2

Guo, Y. L., Duan, W. J., Lu, D. H., Ma, X. H., Li, X. X., Li, Z., et al. (2021). Autophagy-dependent removal of α-synuclein: a novel mechanism of GM1 ganglioside neuroprotection against Parkinson's disease. *Acta Pharmacol. Sin.* 42, 518–528. doi: 10.1038/s41401-020-0454-y

Han, H., Dong, Y., and Ma, X. (2020). Dihydromyricetin protects against gentamicin-induced ototoxicity via PGC-1α/SIRT3 Signaling in vitro. *Front. Cell. Dev. Biol.* 8:702. doi: 10.3389/fcell.2020.00702

He, Y., Li, W., Zheng, Z., Zhao, L., Li, W., Wang, Y., et al. (2020). Inhibition of Protein arginine methyltransferase 6 reduces reactive oxygen species production and attenuates aminoglycoside- and cisplatin-induced hair cell death. *Theranostics* 10, 133–150. doi: 10.7150/thno.37362

Jiang, M., Karasawa, T., and Steyger, P. S. (2017). Aminoglycoside-Induced cochleotoxicity: A review. *Front. Cell Neurosci.* 11:308. doi: 10.3389/fncel.2017.00308

Jiang, P., Ray, A., Rybak, L. P., and Brenner, M. J. (2016). Role of STAT1 and oxidative stress in gentamicin-induced hair cell death in organ of corti. *Otol. Neurotol.* 37, 1449–1456. doi: 10.1097/MAO.0000000000001192

Ledeen, R., and Wu, G. (2018). Gangliosides of the nervous system. *Methods Mol. Biol.* 1804, 19–55. doi: 10.1007/978-1-4939-8552-4_2

Leis, J. A., Rutka, J. A., and Gold, W. L. (2015). Aminoglycoside-induced ototoxicity. *Curr. Pharm. Des.* 187:E52. doi: 10.1503/cmaj.140339

Li, A., You, D., Li, W., Cui, Y., He, Y., Li, W., et al. (2018). Novel compounds protect auditory hair cells against gentamycin-induced apoptosis by maintaining the expression level of H3K4me2. *Drug Deliv.* 25, 1033–1043. doi: 10.1080/10717544.2018.1461277

Lopez-Novoa, J. M., Quiros, Y., Vicente, L., Morales, A. I., and Lopez-Hernandez, F. J. (2011). New insights into the mechanism of aminoglycoside nephrotoxicity: an integrative point of view. *Kidney Int.* 79, 33–45. doi: 10.1038/ki.2010.337

Magistretti, P. J., Geisler, F. H., Schneider, J. S., Li, P. A., Fiumelli, H., and Sipione, S. (2019). Gangliosides: treatment avenues in neurodegenerative disease. *Front. Neurol.* 10:859. doi: 10.3389/fneur.2019.00859

Nikolaeva, S., Bayunova, L., Sokolova, T., Vlasova, Y., Bachteeva, V., Avrova, N., et al. (2015). GM1 and GD1a gangliosides modulate toxic and inflammatory effects of E. coli lipopolysaccharide by preventing TLR4 translocation into lipid rafts. *Biochim. Biophys. Acta* 1851, 239–247.

Pham, T. N. M., Jeong, S. Y., Kim, D. H., Park, Y. H., Lee, J. S., Lee, K. W., et al. (2020). Protective mechanisms of avocado oil extract against ototoxicity. *Nutrients* 12:947.

Rao, S., Lin, Y., Du, Y., He, L., Huang, G., Chen, B., et al. (2019). Designing multifunctionalized selenium nanoparticles to reverse oxidative stress-induced spinal cord injury by attenuating ROS overproduction and mitochondria dysfunction. *J. Mater Chem. B* 7, 2648–2656. doi: 10.1039/c8tb02520g

Schnaar, R. L. (2016). Gangliosides of the vertebrate nervous system. *J. Mol. Biol.* 428, 3325–3336. doi: 10.1016/j.jmb.2016.05.020

She, J. Q., Wang, M., Zhu, D. M., Tang, M., Chen, J. T., Wang, L., et al. (2009). Monosialoanglioside (GM1) prevents lead-induced neurotoxicity on long-term potentiation, SOD activity, MDA levels, and intracellular calcium levels of

hippocampus in rats. *Naunyn Schmiedebergs Arch. Pharmacol.* 379, 517–524. doi: 10.1007/s00210-008-0379-3

Sotoudeh, H. (2021). Hearing loss prevalence and years lived with disability, 1990–2019: findings from the Global Burden of Disease Study 2019. *Lancet* 397, 996–1009.

Tanaka, S., Tabuchi, K., Hoshino, T., Murashita, H., Tsuji, S., and Hara, A. (2010). Protective effects of exogenous GM-1 ganglioside on acoustic injury of the mouse cochlea. *Neurosci. Lett.* 473, 237–241. doi: 10.1016/j.neulet.2010.02.057

Tian, J., Mo, J., Xu, L., Zhang, R., Qiao, Y., Liu, B., et al. (2020). Scoulerine promotes cell viability reduction and apoptosis by activating ROS-dependent endoplasmic reticulum stress in colorectal cancer cells. *Chem. Biol. Interact* 327:109184.

Verma, J., and Syed Mohammed, T. (2019). Evaluating hearing loss in patients undergoing second line anti tubercular treatment. *Indian J. Otolaryngol. Head Neck Surg.* 71, 1202–1206. doi: 10.1007/s12070-018-1266-y

Vlasova Iu, A., Zakharova, I. O., Sokolova, T. V., Furaev, V. V., Rychkova, M. P., and Avrova, N. F. (2009). Role of tyrosine kinase of Trk-receptors in realization of antioxidant effect of ganglioside GM1 in PC12 cells. *Zh. Evol. Biokhim. Fiziol.* 45, 465–471.

Yao, L., Zhang, J. W., Chen, B., Cai, M. M., Feng, D., Wang, Q. Z., et al. (2020). Mechanisms and pharmacokinetic/pharmacodynamic profiles underlying the low nephrotoxicity and ototoxicity of etimicin. *Acta Pharmacol. Sin.* 41, 866–878.

Zeng, H., Kong, X., Zhang, H., Chen, Y., Cai, S., Luo, H., et al. (2020). Inhibiting DNA methylation alleviates cigarette smoke extract-induced dysregulation of Bcl-2 and endothelial apoptosis. *Tob. Induc. Dis.* 18:51. doi: 10.18332/tid/119163

Zhang, J., Wang, X., Vikash, V., Ye, Q., Wu, D., Liu, Y., et al. (2016). ROS and ROS-mediated cellular signaling. *Oxid Med. Cell Longev.* 2016:4350965. doi: 10.1155/2016/4350965

Zhang, S., Qiang, R., Dong, Y., Zhang, Y., Chen, Y., Zhou, H., et al. (2020). Hair cell regeneration from inner ear progenitors in the mammalian cochlea. *Am. J. Stem Cells* 9, 25–35.

Zhang, Y., Li, W., He, Z., Wang, Y., Shao, B., Cheng, C., et al. (2019). Pre-treatment with fasudil prevents neomycin-induced hair cell damage by reducing the accumulation of reactive oxygen species. *Front. Mol. Neurosci.* 12:264. doi: 10.3389/fnmol.2019.00264

Zhao, H., Li, X., Li, G., Sun, B. O., Ren, L., and Zhao, C. (2015). Protective effects of monosialotetrahexosylganglioside sodium on H2O2-induced human vascular endothelial cells. *Exp. Ther. Med.* 10, 947–953. doi: 10.3892/etm.2015.2603

Zhong, Z., Fu, X., Li, H., Chen, J., Wang, M., Gao, S., et al. (2020). Citicoline protects auditory hair cells against neomycin-induced damage. *Front. Cell. Dev. Biol.* 8:712. doi: 10.3389/fcell.2020.00712

Conflict of Interest: The authors declare that the research was conducted in the absence of any commercial or financial relationships that could be construed as a potential conflict of interest.

Publisher's Note: All claims expressed in this article are solely those of the authors and do not necessarily represent those of their affiliated organizations, or those of the publisher, the editors and the reviewers. Any product that may be evaluated in this article, or claim that may be made by its manufacturer, is not guaranteed or endorsed by the publisher.

frontiers in Cellular Neuroscience

ORIGINAL RESEARCH
published: 01 October 2021
doi: 10.3389/fncel.2021.735723

The Expression and Roles of the Super Elongation Complex in Mouse Cochlear Lgr5+ Progenitor Cells

Yin Chen[1†], Ruiying Qiang[2†], Yuan Zhang[2†], Wei Cao[3†], Leilei Wu[2], Pei Jiang[2], Jingru Ai[2], Xiangyu Ma[2], Ying Dong[2], Xia Gao[1], He Li[4], Ling Lu[1]*, Shasha Zhang[2]* and Renjie Chai[2,5,6,7]**

[1] Jiangsu Provincial Key Medical Discipline (Laboratory), Department of Otolaryngology Head and Neck Surgery, Drum Tower Hospital Clinical College of Nanjing Medical University, Nanjing, China, [2] State Key Laboratory of Bioelectronics, Jiangsu Province High-Tech Key Laboratory for Bio-Medical Research, School of Life Sciences and Technology, Southeast University, Nanjing, China, [3] Department of Otorhinolaryngology, Head and Neck Surgery, The Second Hospital of Anhui Medical University, Hefei, China, [4] Department of Otolaryngology, The First Affiliated Hospital of Wenzhou Medical University, Wenzhou, China, [5] Co-innovation Center of Neuroregeneration, Nantong University, Nantong, China, [6] Institute for Stem Cell and Regeneration, Chinese Academy of Sciences, Beijing, China, [7] Beijing Key Laboratory of Neural Regeneration and Repair, Capital Medical University, Beijing, China

The super elongation complex (SEC) has been reported to play a key role in the proliferation and differentiation of mouse embryonic stem cells. However, the expression pattern and function of the SEC in the inner ear has not been investigated. Here, we studied the inner ear expression pattern of three key SEC components, AFF1, AFF4, and ELL3, and found that these three proteins are all expressed in both cochlear hair cells (HCs)and supporting cells (SCs). We also cultured Lgr5+ inner ear progenitors *in vitro* for sphere-forming assays and differentiation assays in the presence of the SEC inhibitor flavopiridol. We found that flavopiridol treatment decreased the proliferation ability of Lgr5+ progenitors, while the differentiation ability of Lgr5+ progenitors was not affected. Our results suggest that the SEC might play important roles in regulating inner ear progenitors and thus regulating HC regeneration. Therefore, it will be very meaningful to further investigate the detailed roles of the SEC signaling pathway in the inner ear *in vivo* in order to develop effective treatments for sensorineural hearing loss.

Keywords: super elongation complex (SEC), inner ear, expression, proliferation, differentiation

OPEN ACCESS

Edited by:
Zuhong He,
Wuhan University, China

Reviewed by:
Elaine Y. M. Wong,
Ear Science Institute Australia, Australia
Tihua Zheng,
Binzhou Medical University, China
Huizhan Liu,
Creighton University, United States
Le Xie,
Huazhong University of Science and Technology, China

****Correspondence:***
Renjie Chai
renjiec@seu.EdU.cn
Shasha Zhang
zhangss5576@163.com
Ling Lu
entluling60@126.com
He Li
lihewuyao@163.com

[†] These authors have contributed equally to this work

Specialty section:
This article was submitted to Cellular Neuropathology, a section of the journal Frontiers in Cellular Neuroscience

Received: *03 July 2021*
Accepted: *14 September 2021*
Published: *01 October 2021*

Citation:
Chen Y, Qiang R, Zhang Y, Cao W, Wu L, Jiang P, Ai J, Ma X, Dong Y, Gao X, Li H, Lu L, Zhang S and Chai R (2021) The Expression and Roles of the Super Elongation Complex in Mouse Cochlear Lgr5+ Progenitor Cells. Front. Cell. Neurosci. 15:735723. doi: 10.3389/fncel.2021.735723

INTRODUCTION

Hearing loss occurs mainly due to noise exposure, aging, ototoxic drugs, and genetic factors (Sun et al., 2017). There were around 466 million people worldwide with disabling hearing loss in 2020, and the World Health Organization [WHO] (2019) estimates that by 2050 over 900 million people will have disabling hearing loss. Deafness has become a major global health problem, and sensorineural hearing loss is the most common type of hearing impairment (Youm and Li, 2018). However, due to the lack of effective drugs and a non-invasive method for targeted delivery of drugs to the inner ear, the treatment options for sensorineural hearing loss are

limited (Mittal et al., 2019). Cochlear hair cells (HCs) in adult mammals lose the ability to regenerate, thus hearing deficits caused by HC loss are permanent (Warchol et al., 1993; Ryan, 2003; Cox et al., 2014; Xu et al., 2017; Chen et al., 2019). Therefore, induction of HC regeneration after injury by stimulating quiescent inner ear progenitor cells has been a main focus of auditory research in recent years.

The super elongation complex (SEC) is extremely important in the transcriptional elongation checkpoint control stage of transcription and is composed mainly of P-TEFb (positive transcription elongation factor), ELL (11–19 lysine-rich leukemia gene) family proteins, AFF (AF4/FMR2) family proteins, ENL (11–19 leukemia), AF9 (ALL1-fused gene from chromosome 9), and many other transcription factors (Luo et al., 2012b). P-TEFb and ELL are RNA polymerase II (Pol II)-related elongation factors (Shilatifard et al., 2003). AFF family proteins act as transcriptional activators with a positive action on RNA elongation (Melko et al., 2011). ENL and AF9 are homologous, and they can connect the SEC to RNA Pol II-related factors (He et al., 2011). P-TEFb is composed of cyclin-dependent kinase 9 (CDK9) and cyclin T (CycT), and it promotes the transition into productive elongation by phosphorylating RNA polymerase II (Peng et al., 1998). It has been reported that the SEC plays an important role in regulating mouse embryonic stem cell proliferation and differentiation (Lin et al., 2011), and mis-regulation of the SEC leads to the uncontrolled regulation of gene expression during the differentiation of embryonic stem cells, which results in a variety of diseases such as acute lymphoblastic leukemia, cerebellar ataxia, and diffuse midline glioma (Lin et al., 2011; Dahl et al., 2020). ELL3, one of the key factors of the SEC, can protect differentiated cells from apoptosis by promoting the degradation of p53, enhancing the differentiation of mouse embryonic stem cells, and regulating the proliferation and survival of embryonic stem cells (Ahn et al., 2012). However, the roles of the SEC in the inner ear remain unclear.

Flavopiridol is a semi-synthetic flavonoid that has been used in the treatment of acute myeloid leukemia (Zeidner and Karp, 2015), chronic lymphocytic leukemia (Wiernik, 2016), and other chronic diseases. Flavopiridol binds directly to CDK9, which is a component of P-TEFb, and inhibits its kinase activity (Chao et al., 2000). In turn, P-TEFb, as an important component of the SEC, can activate RNA polymerase II and transcriptional elongation (Hnisz et al., 2013). Thus, the most common method for blocking SEC function is to directly inhibit CDK9 with flavopiridol (Morales and Giordano, 2016), and we used flavopiridol to inhibit the function of the SEC as previously reported (Lin et al., 2011).

Recent studies have shown that Lgr5+ supporting cells (SCs) are inner ear progenitors and that they have the ability to regenerate new HCs in the neonatal stage (Shi et al., 2012). The activation of Wnt/β-catenin signaling and inhibition of Notch signaling can induce Lgr5+ progenitors to regenerate Myo7a+ HCs (Chai et al., 2012; Korrapati et al., 2013; Mizutari et al., 2013), and several recent studies have also shown that Lgr5+ progenitors can be regulated by many other factors and signaling pathways such as Shh, Foxg1, and Hippo (Gregorieff et al., 2015; Chen et al., 2017; Zhang et al., 2020). However, the regeneration efficiency of Lgr5+ progenitors is still very limited, which suggests that there are other factors or signaling pathways involved in the HC regeneration process. Because the transcription extension stage is the main stage of gene expression regulation, transcriptional regulation of developmental regulatory genes is the core link between embryonic stem cell differentiation and organ formation (Smith and Shilatifard, 2010; Levine, 2011). Therefore, we speculate that the SEC may also play important roles in cochlear progenitor cells.

Here we measured the expression of the key SEC factors AFF1, AFF4, and ELL3 in the neonatal mouse cochlea, the function of SEC inhibitor flavopiridol in House Ear Institute-Organ of Corti 1 (HEI-OC1) cell line, and we assessed the proliferation and differentiation ability of Lgr5+ progenitors after treatment with the SEC inhibitor flavopiridol. Our results suggest important roles for the SEC in Lgr5+ progenitors *in vitro*, and further *in vivo* studies need to be done to elucidate the roles of the SEC in the inner ear. These studies will form the experimental basis for using cochlear progenitors to regenerate functional HCs in order to treat patients with sensorineural hearing loss.

MATERIALS AND METHODS

Experimental Animals

Lgr5-EGFP-Ires-CreERT2 (Lgr5-EGFP) mice (Barker et al., 2007) (Jackson Laboratory, Stock No. 00887) and FVB mice used as wide-type mice were raised in a comfortable environment with suitable temperature and light and fed with standard laboratory food and water *ad libitum*. We are approved by the Animal Care and Use Committee of Southeast University and were consistent with the National Institutes of Health Guide for the Care and Use of Laboratory Animals. All the operations were carried out in accordance with the procedures.

RNA Extraction and Reverse Transcription-Polymerase Chain Reaction

About 20 wild-type mouse cochleae were dissected to extract total RNA, which was reverse transcribed into cDNA with the cDNA Synthesis Kit (Thermo Fisher Scientific, K1622). Gene expression was measured by reverse transcription-polymerase chain reaction (RT-PCR) with GAPDH as the endogenous reference gene. The RT-PCR conditions were as follow for a total of 35 cycles: initial denaturation at 95°C for 15 s, denaturation at 95°C for 15 s, annealing at 60°C for 60 s, and extension at 72°C. The primers were as follows: GAPDH: (F) 5′-AGG TCG GTG TGA ACG GAT TTG-3′; (R) 5′-TGT AGA CCA TGT AGT TGA GGT CA-3′; AFF1: (F) 5′-GAA GGA AAG ACG CAA CCA AGA-3′; (R) 5′-TAG CTC ATC GCC TTT TGC AGT-3′; AFF4: (F) 5′-ATG AAC CGT GAA GAC CGG AAT-3′; (R) 5′-TGC TAG TGA CTT TGT ATG GCT CA-3′; ELL3: (F) 5′-GAC CAG CCT CCT GAT GCT AAG-3′; (R) 5′-GCC ACC ATT AGT GCC CTC TTG-3′.

Western Blotting

About 10 cochleae from postnatal day (P)3 mice were dissected in order to extract proteins. GAPDH was used as the reference protein. The primary antibodies were anti-AFF1 (Sigma-Aldrich,

#SAB2106246), anti-AFF4 (Santa Cruz, #sc135337), and anti-ELL3 (Abcam, #ab67415). Peroxidase-conjugated goat anti-rabbit (Life, A-31572) and goat anti-mouse (Invitrogen, A21202) were used as the secondary antibodies. The gray levels were measured by Image-J.

Cell Culture

HEI-OC1 cells were cultured in Dulbecco's modified Eagle's medium (DMEM) with 10% fetal bovine serum and 1% ampicillin at 37°C and 5% CO_2. The cells were divided into two groups. The experimental group was treated with flavopiridol (AbMole M1710) at the concentration of 10 μM. Control cells were treated with dimethyl sulfoxide (DMSO) in the same culture medium. After 12-h culture, cells were treated with 0.25% trypsin/ethylene diamine tetraacetic acid (EDTA) and then ultrasonicated (Bioruptor^{TM} UCD-200) for CDK9 kinase detection.

Cyclin-Dependent Kinase 9 Kinase Assay

HEI-OC1 cells with or without flavopiridol treatment were used after ultrasonication to detect the CDK9 activity by using CDK9 Cyclin K Kinase Assay kit (Promega, V4104) and ADP-Glo Kinase Assay kit (Promega, V6930). To initiate the CDK9 reaction, CDK9 substrate PDKtides and adenosine triphosphate (ATP) were added into each group for 120 min at room temperature to produce adenosine diphosphate (ADP) according to the manufacturer's instruction (Promega, #TM313). And then ADP-Glo Reagent was added for 40 min at room temperature to deplete the remaining ATP. The Kinase Detection Reagent was added to convert the ADP produced at the first step to ATP with luminescence. Finally, the luminescence was recorded by BioTek CYTATION 5 (Integration time 1 s) to determine the CDK9 activity in each sample. The relative light units were calculated to represent the activity of CDK9.

Isolation of Lgr5+ Progenitors *via* Flow Cytometry

About 50–60 cochleae were isolated from P0 to P3 Lgr5-EGFP mice and then treated with 0.125% trypsin/EDTA (Invitrogen, 25200114) at 37°C. Trypsin inhibitor (10 mg/ml, Worthington Biochem) was added after 10 min to terminate the reaction. The trypsinized cochleae were pipetted up and down 80–100 times to obtain single cells, and the cells were then filtered through a 40 μM cell strainer (BD Biosciences, 352340). Dissociated cells were sorted on a flow cell sorter (BD FACS Aria III). The EGFP+ cells were collected as Lgr5+ progenitors for further *in vitro* cell culture experiments.

Sphere-Forming Assay and Differentiation Assay

Sorted Lgr5+ cells were cultured in DMEM/F12 medium at a density of 2 cells/μl (200 cells per well) for 5 days for sphere forming. The formula of DMEM/F12 medium was the same in previous study (Zhang et al., 2020). Spheres were identified with the Live Cell Imaging System and quantified using Image J. For differentiation, cells were cultured in the DMEM/F12 medium described above at a density of 20 cells/μl (2,000 cells per well) for 10 days. EdU [10 μM (Invitrogen, C10420)] was added to label proliferating cells from day 4 to day 7. Flavopiridol (AbMole, M1710) was added to the experimental group from day 1 to day 10 at a concentration of 10 μM, while DMSO was added to the control group. Differentiated neurospheres were analyzed by immunofluorescent staining.

Immunofluorescent Staining

The cochleae were dissected in cold Hanks Balanced Salt Solution (HBSS) in order to prevent protein degradation and then fixed with 4% paraformaldehyde (PFA) for 1 h at room temperature. *In vitro* cultured neurospheres were also fixed with 4% PFA for 1 h at room temperature. After washing with phosphate buffered saline with tween (PBST) three times, the cochleae or neurospheres were blocked with blocking solution for 1 h at room temperature and then incubated overnight at 4°C with primary antibodies. The primary antibodies used were anti-Myosin7a (Myo7a; Proteus Bioscience, #25-6790; 1:1,000 dilution), anti-Sox2 (1:400 dilution), anti-AFF1 (1:400 dilution), anti-AFF4 (1:50 dilution), and anti-ELL3 (1:400 dilution). After washing again three times, the cochleae or neurospheres were further incubated with secondary antibodies (Invitrogen, A21131, A21124) diluted 1:400 in PBT2 for 1 h at room temperature. After washing three times, the cochleae or neurospheres were mounted on slides with anti-fade fluorescence mounting medium (DAKO, S3023). Images were captured by Zeiss LSM 710 confocal microscope and analyzed by Image J software.

Tissue Embedment

The P40 temporal bones were dissected and put in 4% PFA to be shaken for 1–2 h and sit overnight at 4°C. Later, the temporal bones were put in 0.5 M EDTA for decalcification for 2 days. After washing with PBST three times, the temporal bones were transferred into 15% sucrose solution, vacuum for 1 h, 4°C overnight. Afterward, the temporal bones were put in 20% sucrose solution, vacuum for 1 h, then transferred to 30% sucrose solution, vacuum 1 h, 4°C overnight. Then, the temporal bones were put into a 1:1 solution of 30% sucrose in optimum cutting temperature (OCT) medium (Sakura 4583), vacuum for 1 h, overnight at 4°C. The following day, temporal bones were put in a 3:7 solution of 30% sucrose in OCT medium, vacuum for 1 h, then the 3:17 solution of 30% sucrose in OCT medium, vacuum for 1 h, and lastly the 100% OCT medium (adjust position as round window and ellipse window are toward on the ground), vacuum for 1 h, 4°C overnight. For the last step, the temporal bones were put in 100% OCT into vacuum for 1 h adjust position, then in cryostat (Microm HM525) for a 20-min quick-freeze, and restored in −80°C. For slicing, adjust the cryostat half an hour in advance; secondly, adjust the blade temperature and internal temperature to −20°C. The selected sections were stained using the method described above.

Statistical Analysis

All the data in this research are presented as means ± SEM, and all experiments were repeated at least three times. All statistical analyses were performed in GraphPad Prism 5. *P*-values were calculated using a two-tailed, unpaired Student's *t*-test, and a p-value < 0.05 was considered statistically significant.

RESULTS

AFF1, AFF4, and ELL3 Are Expressed in the Cochlea

We first measured the expression of the three key SEC subunits AFF1, AFF4, and ELL3 by RT-PCR (**Figure 1A**) and Western blotting analysis (**Figures 1B,C**), and we found that AFF1, AFF4, and ELL3 were all highly expressed in the cochlea. Moreover, we measured the expression of AFF1, AFF4, and ELL3 in Lgr5+ cells (**Figure 1D**), and we found those three expressions in both cochlea and Lgr5+ cells were similar. We further studied the expression pattern from both the obverse and lateral sides of AFF1, AFF4, and ELL3 in the cochlea of P3 and P40 mice and found that AFF1, AFF4, and ELL3 were all expressed in the cochlear HCs and SCs (**Figures 2A–D**). However, the immunostaining intensities of these three subunits in the SCs were weaker than in the HCs.

Flavopiridol Treatment Inhibited the Activity of Cyclin-Dependent Kinase 9 in House Ear Institute-Organ of Corti 1 Cells

Flavopiridol has been reported to be an inhibitor of CDK9 which is an indispensable part of SEC and the low level of its kinase activity prevents the recruitment of other elongation factors in

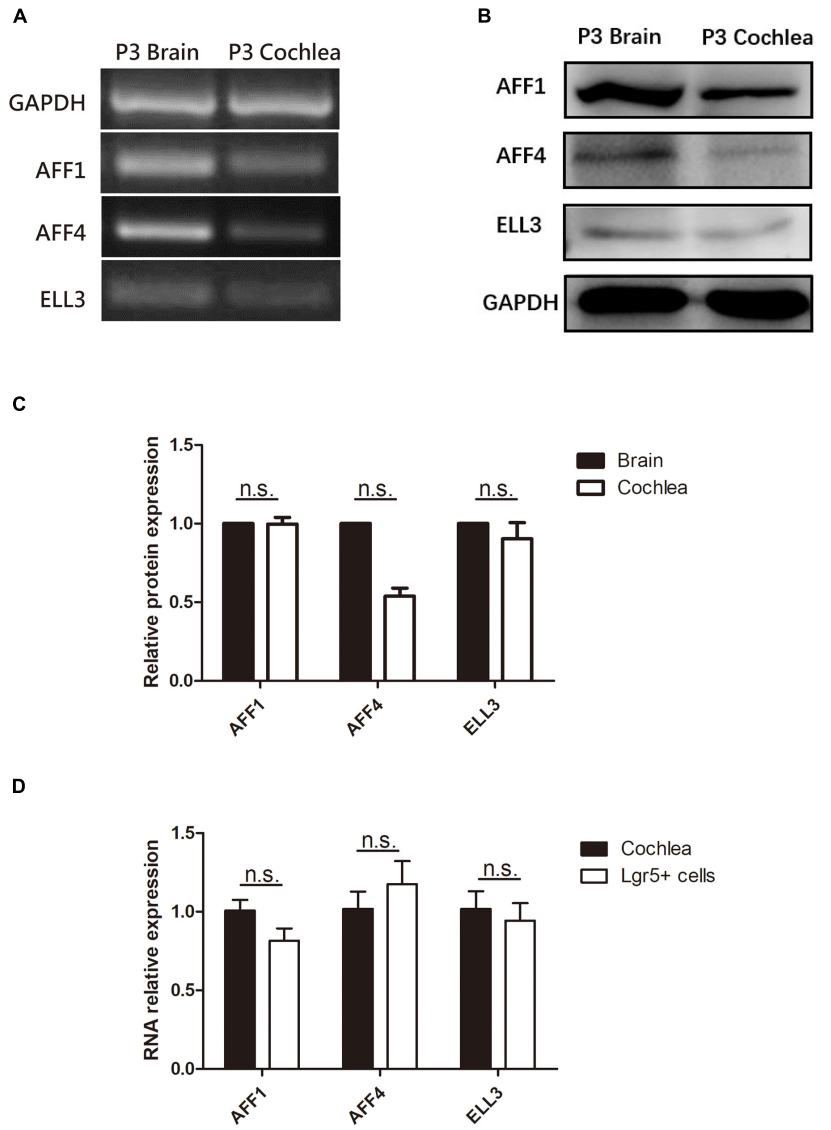

FIGURE 1 | The expression of AFF1, AFF4, and ELL3 in the neonatal mouse cochlea. **(A,B)** The mRNA and protein expression of AFF1, AFF4, and ELL3 in P3 mouse cochleae were detected by RT-PCR **(A)** and western blotting **(B)**, respectively. **(C)** The gray levels comparison of western blot. **(D)** The mRNA expression of AFF1, AFF4, and ELL3 in Lgr5+ cells. Brain samples of P3 mice were used as the positive control, and GAPDH was used as the internal reference. n.s., not significant.

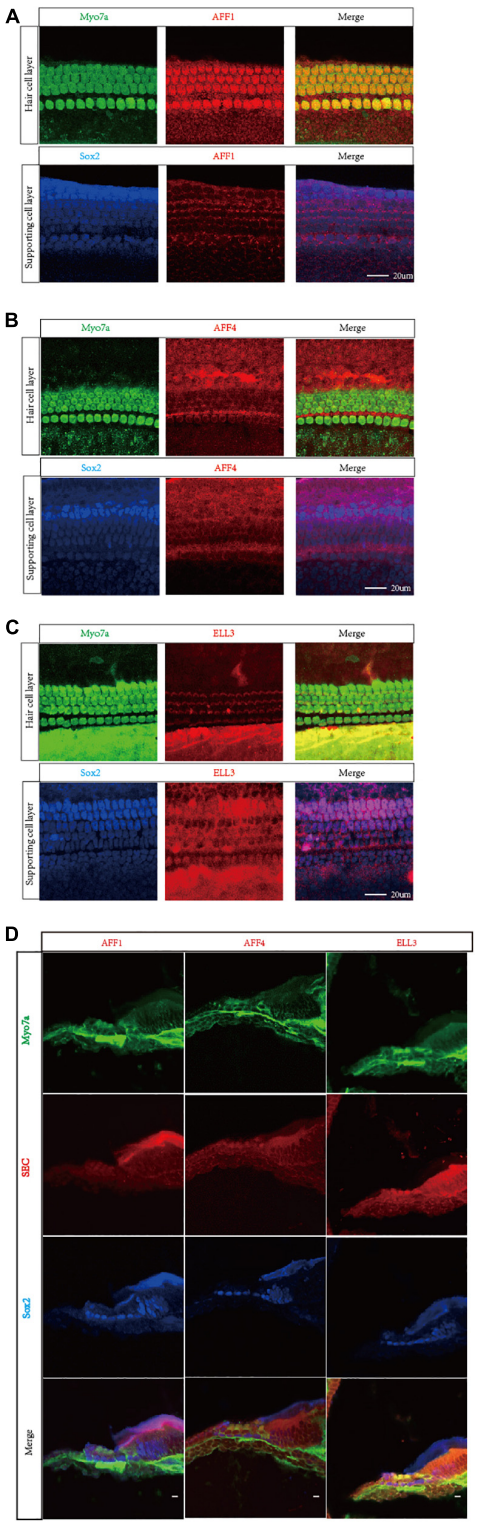

FIGURE 2 | Immunofluorescent staining of AFF1, AFF4, and ELL3 in the mouse cochlea. **(A–C)** The whole-mount basilar membrane of P3 was immunostained by antibodies against AFF1 **(A)**, AFF4 **(B)**, and ELL3 **(C)**. **(D)** Frozen sections of P40 were immunostained by antibodies against AFF1, AFF4, and ELL3. Myo7a and Sox2 were used to label hair cells (HCs) and supporting cells (SCs), respectively. Scale bar = 20 μM.

SEC (Peng et al., 1998). However, the function of flavopiridol has not been verified in inner ear. Here, we used ADP-Glo Kinase Assay to detect the activity of CDK9. After the kinase reaction, the remaining ATP was depleted and the ADP was converted to luminescent ATP (**Figure 3A**). HEI-OC1 cells were cultured for 3 days, and then treated by 10 μM flavopiridol which was diluted in the culture medium for 12 h. Images of cells were taken before and after flavopiridol treatment (**Figure 3B**). After flavopiridol treatment, the number and diameter of cells visually decrease in comparison with the control group with no change in shapes. The luminescent ATP was recorded and the relative light units was calculated to represent the activity of CDK9 (**Figure 3C**). The results showed that flavopiridol could also function as the CDK9 inhibitor to inhibit SEC activity in HEI-OC1 cells.

Flavopiridol Treatment Decreased the Sphere-Forming Ability of Lgr5+ Progenitors *in vitro*

Flavopiridol was previously used to inhibit SEC transcription activity (Lin et al., 2011). Here we also used flavopiridol to inhibit SEC activity in Lgr5+ progenitors in order to determine whether the SEC plays roles in the proliferation and differentiation ability of Lgr5+ progenitors. In order to determine the effect of the SEC on the sphere-forming ability of Lgr5+ progenitors, Lgr5+ cells were isolated from Lgr5-EGFP mice by flow cytometry and then cultured *in vitro* for 5 days to form spheres with or without 10 μM flavopiridol treatment (**Figures 4A,B**). The flavopiridol treatment decreased both the number (**Figure 4C**) and diameter of the spheres (**Figure 4D**), which suggested that inhibition of the SEC could decrease the sphere-forming ability and proliferation ability of Lgr5+ progenitors *in vitro*.

No Difference Was Observed in the Differentiation Assay After Flavopiridol Treatment

In order to further evaluate the effect of the SEC on the differentiation ability of Lgr5+ progenitors, we isolated Lgr5+ cells by flow cytometry and cultured them *in vitro* for the differentiation assay with or without 10 μM flavopiridol treatment (**Figure 5A**). The cells were immunostained with Myo7a, EdU, and DAPI (**Figure 5B**), and the Myo7a+ cells and EdU+ cells inside and outside the colonies were quantified. There were more EdU+ cells in the flavopiridol treatment group than in the control group (**Figure 5C**), while the numbers of Myo7a+ cells were almost the same in the flavopiridol treatment group and the control group (**Figure 5D**). These results suggested that inhibition of the SEC did not affect the differentiation ability of Lgr5+ cells *in vitro*.

In summary, our results showed that the key SEC factors AFF1, AFF4, and ELL3 are all highly expressed in the cochlea. And we verified that flavopiridol could inhibit SEC by inhibiting CDK9 activity in HEI-OC1 cell line. We used flavopiridol as an SEC inhibitor to investigate the effect of the SEC on the proliferation and differentiation ability of Lgr5+ progenitors and found that the number and diameter of spheres of Lgr5+ progenitors were both decreased after SEC inhibitor treatment,

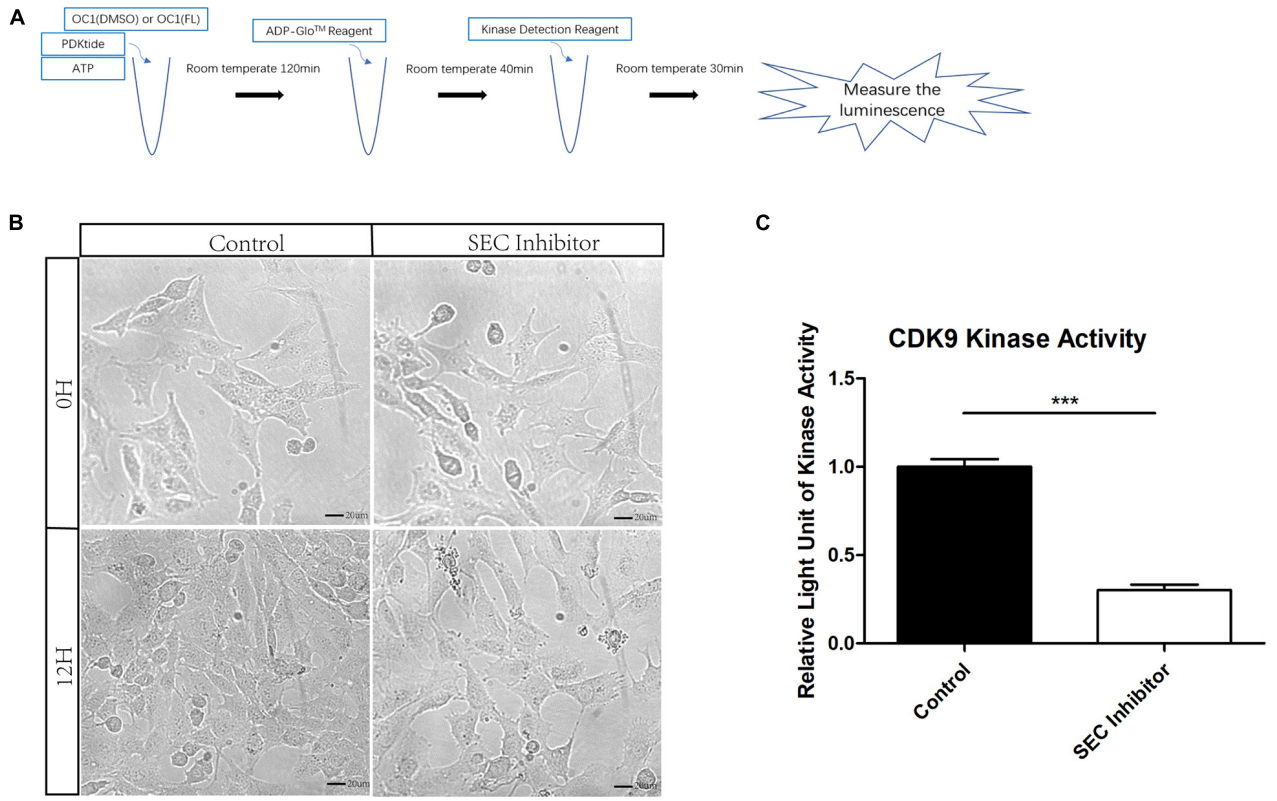

FIGURE 3 | The activity of cyclin-dependent kinase 9 (CDK9) in HEI-OC1 cells before and after Flavopiridol treatment. **(A)** HEI-OC1 cells after ultrasonication were incubated with CDK9 substrate PDKtides and ATP for 120 min at room temperature. The ADP which was consumed during CDK9 kinase assay was converted to ATP and could be quantitated by luciferase assay. **(B)** Images of HEI-OC1 cells before and after 10 μM Flavopiridol treatment. DMSO was added as control treatment in the Control group. Scale bar = 20 μM. **(C)** Fold change of CDK9 kinase activity in HEI-OC1 cells with or without Flavopiridol treatment. $n = 3$, $^{***}p < 0.001$.

while the differentiation ability of Lgr5+ progenitors was not affected. Therefore, the SEC appears to promote the proliferation ability of Lgr5+ progenitors, but not their differentiation ability.

DISCUSSION

Irreversible damage to HCs in the mammalian cochlea is the main cause of sensorineural hearing loss. Previous studies have reported that Lgr5+ cells are cochlear progenitors with the ability to regenerate HCs (Shi et al., 2012), and it has been documented that the SEC plays an important role in the process of gene transcription and extension and that it is necessary for the differentiation of mouse embryonic stem cells (Lin et al., 2011). Therefore, we speculated that the SEC also plays an important role in the proliferation and differentiation of mouse cochlear progenitors. Besides, it has also been reported that AFF proteins and ELL proteins increase the diversity and regulatory potential of the SEC family in mammals (Luo et al., 2012a). Furthermore, AFF1 and AFF4 are the backbones of the SEC (Mück et al., 2016) and ELL3 has the ability to associate with other translocation partners of the SEC (Lin et al., 2011). Thus we chose to investigate the expression of AFF1, AFF4, and ELL3 in the inner ear. Our results showed that AFF1, AFF4, and ELL3, were all highly expressed in the cochlea and that the SEC inhibitor flavopiridol could induce the proliferation of Lgr5+ progenitors *in vitro*, but not their differentiation. This study thus provides an experimental foundation for the clinical application of HC regeneration for treating hearing loss.

The SEC is known to be widely expressed in most tissues, and it plays important roles during development (Kapushesky et al., 2010). However, its expression in the inner ear has not been studied. We found that AFF1, AFF4, and ELL3 were highly expressed in the cochlea, and this suggests that the SEC functions in the inner ear. Furthermore, we found that AFF1, AFF4, and ELL3 were all expressed in the cochlear HCs and SCs by immunostaining, but the expression of SEC proteins in SCs was lower than that in HCs. In addition to its role in Lgr5+ progenitors studied in our research, the SEC likely plays an essential role in cochlear HCs. However, due to the lack of studies of the SEC in the inner ear and the lack of mouse models, the specific role of the SEC in HCs awaits further study.

Flavopiridol, a potent inhibitor of CDK9, is reported to inhibit transcription (Blagosklonny, 2004; Lee and Zeidner, 2019). CDKs combine with cyclins to play important roles in transcription and stem cell self-renewal (Lim and Kaldis, 2013), and P-TEFb (composed of CDK9 and CycT) is an indispensable part of the SEC that phosphorylates RNA polymerase II and thus

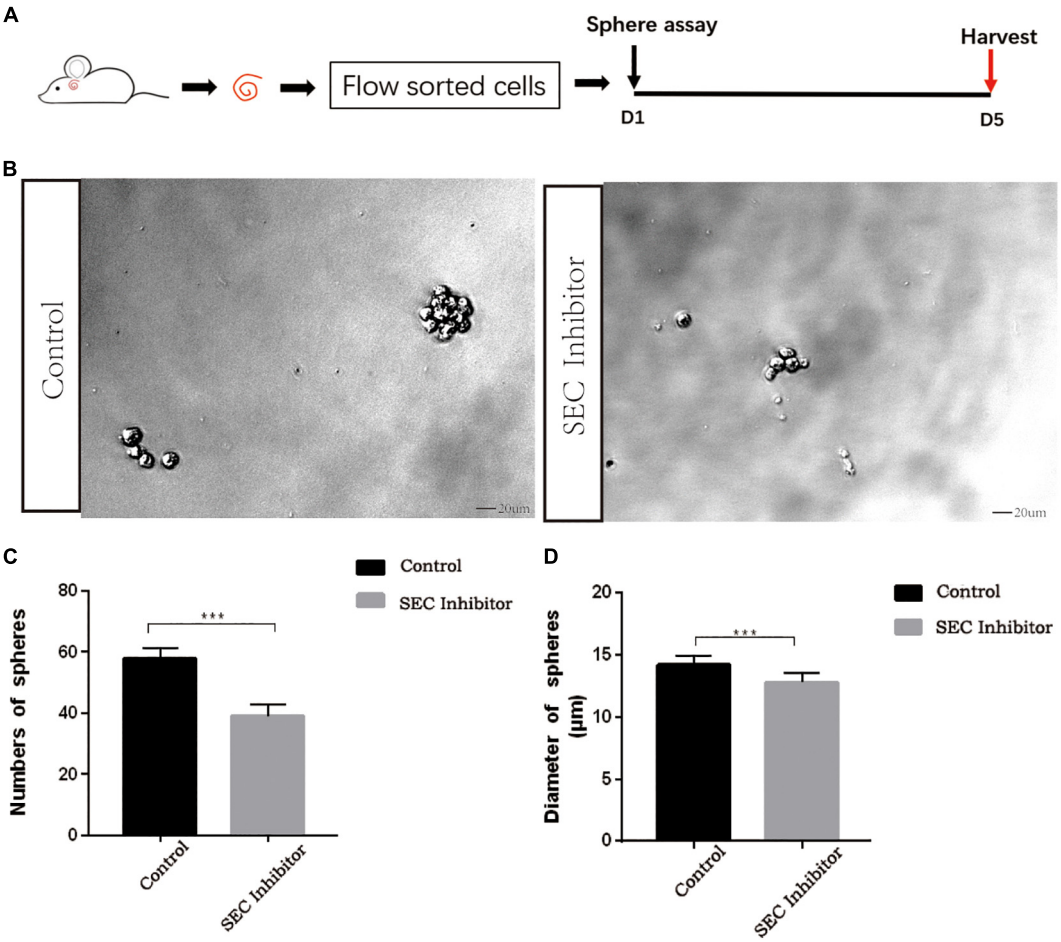

FIGURE 4 | The sphere-forming assay of Lgr5+ progenitors after inhibition of the super elongation complex (SEC). **(A)** Schematic of the sphere-forming assay. The cochleae of neonatal Lgr5-EGFP-CreER mice were trypsinized for FAC sorting, and the sorted Lgr5+ progenitors were cultured *in vitro* for 5 days to form spheres with or without 10 μM flavopiridol treatment. **(B)** The spheres (indicated by black arrows) formed by Lgr5+ progenitors with 10 μM flavopiridol added as the SEC inhibitor. DMSO was added as control treatment in the Control group. Scale bar = 20 μM. **(C,D)** Quantification of the sphere number per well **(C)** and the sphere diameter **(D)**. $n = 3$. $^{***}P < 0.001$.

activates transcription elongation of important genes involved in cell proliferation and survival (Zhu et al., 1997; Zeidner and Karp, 2015). Flavopiridol can inhibit the function of the SEC by inactivating CDK9 (Chao and Price, 2001), and thus we chose flavopiridol as the SEC inhibitor as previously reported (Lin et al., 2011).

In addition, our results suggest that inhibition of the SEC by flavopiridol could reduce the sphere-forming ability and proliferating cell number of Lgr5+ progenitors in the differentiation assay, which is consistent with previous reports that AFF1 promotes leukemia cell proliferation (Fioretti et al., 2019), that AFF4 enhances the sphere-forming capacity and tumor-initiation capacity in head and neck squamous cell carcinoma (Deng et al., 2018), and that ELL3 stimulates the proliferation and stem cell properties of breast cancer cells (Ahn et al., 2013).

ELL3 has also been shown to promote the differentiation of mouse embryonic stem cells by regulating the epithelial-mesenchymal transition and apoptosis (Ahn et al., 2012), and the overexpression of AFF1 impairs the differentiation of mesenchymal stem cells, while overexpression of AFF4 enhances their differentiation (Zhou et al., 2017). In our results, inhibition of the SEC did not affect the differentiation ability of Lgr5+ progenitors *in vitro*, which might be because of the different regulatory roles of these three proteins in cell differentiation.

The different roles of SEC in the proliferation and differentiation ability of Lgr5 progenitors might have been expected. SEC was first systematically studied for being associated with infant acute lymphoblastic and mixed lineage leukemia (Lin et al., 2010). Then it has since been studied in other neoplastic models (Hashizume et al., 2014; Narita et al., 2017; Liang et al., 2018). While transcriptional regulation is a complex process, it has been sure that the role of SEC is essential in transcriptional elongation. The SEC incorporates the CDK9 to promote rapid transcriptional elongation facilitates cell growth

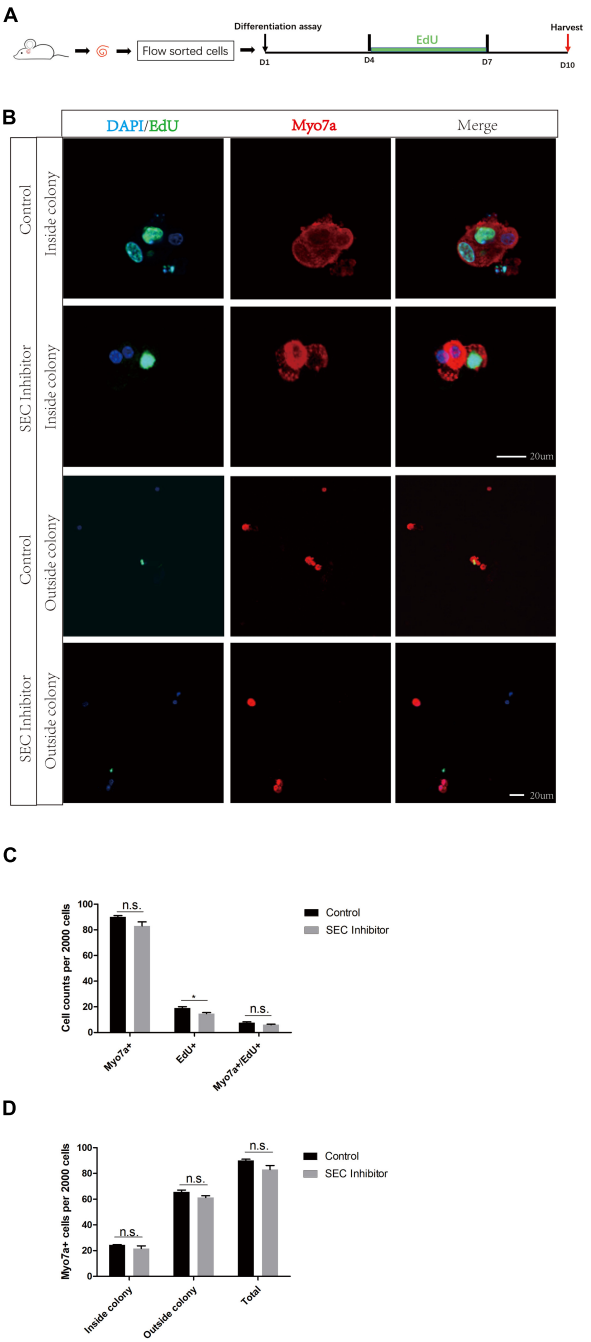

FIGURE 5 | The differentiation assay of Lgr5+ cells after inhibition of the super elongation complex (SEC). **(A)** Schematic of the differentiation assay. The cochleae of neonatal Lgr5-EGFP-CreER mice were trypsinized for FAC sorting, and the sorted Lgr5+ progenitors were cultured *in vitro* for 10 days with or without 10 μM flavopiridol. EdU was added during day 4–7 to label proliferating cells. **(B)** Immunofluorescence images of colonies and single cells formed from Lgr5+ progenitors with 10 μM flavopiridol added as the SEC inhibitor. DMSO was used as the control treatment in the Control group. Myo7a and Sox2 were used to label hair cells (HCs) and supporting cells (SCs), respectively, and EdU was used to label proliferating cells. Scale bar = 20 μM. **(C,D)** Quantification of the total numbers of Myo7a+ and EdU+ cells **(C)** and the number of Myo7a+ cells inside and outside the colonies **(D)**. $n = 3$. n.s., not significant. $^*P < 0.05$.

(Dahl et al., 2020). However, speaking of the differentiation ability of SEC, totally different results were found concerning the different components of this complex. Our paper first studied the differentiation ability of the total complex and found that the whole SEC cannot change the differentiation in Lgr5 progenitors. There is a certain possibility that this finding may also apply to other stem cells. The detailed mechanisms behind this need further exploration.

CONCLUSION

In conclusion, we show here that the SEC is expressed in cochlear HCs and SCs in neonatal mice and that the SEC can induce the proliferation ability of Lgr5+ progenitors but not their differentiation. Our study thus provides new candidates for regulating inner ear progenitor cells as a step toward HC regeneration.

DATA AVAILABILITY STATEMENT

The raw data supporting the conclusions of this article will be made available by the authors, without undue reservation.

ETHICS STATEMENT

The animal study was reviewed and approved by the Animal Care and Use Committee of Southeast University, the National Institutes of Health, and the Guide for the Care and Use of Laboratory Animals.

AUTHOR CONTRIBUTIONS

YC, HL, LL, SZ, and RC conceived and designed the experiments and wrote the manuscript. YC, RQ, YZ, WC, YD, LW, PJ, JA, and XM performed the experiments. YC, RQ, YZ, WC, XG, LL, SZ, and RC analyzed the data. All authors read and approved the final manuscript.

FUNDING

This work was supported by grants from the National Key R&D Program of China (No. 2017YFA0103903), the Strategic Priority Research Program of the Chinese Academy of Sciences (XDA16010303), the National Natural Science Foundation of China (Nos. 82171149, 81970882, 81970892, and 81700913), the Natural Science Foundation of Jiangsu Province (BE2019711, BE2018605, and BK20190062), the Jiangsu Provincial Medical Youth Talent of the Project of Invigorating Health Care through Science, Technology and Education (QNRC2016002), the Fundamental Research Funds for the Central Universities for the Support Program of Zhishan Youth Scholars of Southeast University (2242021R41136), and the Zhejiang Provincial Natural Science Foundation of China (LY19H130004).

REFERENCES

Ahn, H.-J., Cha, Y., Moon, S.-H., Jung, J.-E., and Park, K.-S. (2012). Ell3 enhances differentiation of mouse embryonic stem cells by regulating epithelial-mesenchymal transition and apoptosis. *PLoS One* 7:e40293. doi: 10.1371/journal.pone.0040293

Ahn, H.-J., Kim, G., and Park, K.-S. (2013). Ell3 stimulates proliferation, drug resistance, and cancer stem cell properties of breast cancer cells *via* a MEK/ERK-dependent signaling pathway. *Biochem. Biophys. Res. Commun.* 437, 557–564. doi: 10.1016/j.bbrc.2013.06.114

Barker, N., van Es, J. H., Kuipers, J., Kujala, P., van den Born, M., Cozijnsen, M., et al. (2007). Identification of stem cells in small intestine and colon by marker gene Lgr5. *Nature* 449, 1003–1007.

Blagosklonny, M. V. (2004). Flavopiridol, an inhibitor of transcription: implications, problems and solutions. *Cell Cycle* 3, 1537–1542. doi: 10.4161/cc.3.12.1278

Chai, R., Kuo, B., Wang, T., Liaw, E. J., Xia, A., Jan, T. A., et al. (2012). Wnt signaling induces proliferation of sensory precursors in the postnatal mouse cochlea. *Proc. Natl. Acad. Sci. U.S.A.* 109, 8167–8172. doi: 10.1073/pnas.1202774109

Chao, S. H., Fujinaga, K., Marion, J. E., Taube, R., Sausville, E. A., Senderowicz, A. M., et al. (2000). Flavopiridol inhibits P-TEFb and blocks HIV-1 replication. *J. Biol. Chem.* 275, 28345–28348. doi: 10.1074/jbc.C000446200

Chao, S. H., and Price, D. H. (2001). Flavopiridol inactivates P-TEFb and blocks most RNA polymerase II transcription *in vivo*. *J. Biol. Chem.* 276, 31793–31799. doi: 10.1074/jbc.M102306200

Chen, Y., Lu, X., Guo, L., Ni, W., Zhang, Y., Zhao, L., et al. (2017). Hedgehog signaling promotes the proliferation and subsequent hair cell formation of progenitor cells in the neonatal mouse cochlea. *Front. Mol. Neurosci.* 10:426. doi: 10.3389/fnmol.2017.00426

Chen, Y., Zhang, S., Chai, R., and Li, H. (2019). Hair cell regeneration. *Adv. Exper. Med. Biol.* 1130, 1–16. doi: 10.1007/978-981-13-6123-4_1

Cox, B. C., Chai, R., Lenoir, A., Liu, Z., Zhang, L., Nguyen, D.-H., et al. (2014). Spontaneous hair cell regeneration in the neonatal mouse cochlea *in vivo*. *Development* 141, 816–829. doi: 10.1242/dev.103036

Dahl, N. A., Danis, E., Balakrishnan, I., Wang, D., Pierce, A., Walker, F. M., et al. (2020). Super elongation complex as a targetable dependency in diffuse midline glioma. *Cell Rep.* 31:107485. doi: 10.1016/j.celrep.2020.03.049

Deng, P., Wang, J., Zhang, X., Wu, X., Ji, N., Li, J., et al. (2018). AFF4 promotes tumorigenesis and tumor-initiation capacity of head and neck squamous cell carcinoma cells by regulating SOX2. *Carcinogenesis* 39, 937–947. doi: 10.1093/carcin/bgy046

Fioretti, T., Cevenini, A., Zanobio, M., Raia, M., Sarnataro, D., Salvatore, F., et al. (2019). Crosstalk between 14-3-3θ and AF4 enhances MLL-AF4 activity and promotes leukemia cell proliferation. *Cell Oncol.* 42, 829–845. doi: 10.1007/s13402-019-00468-6

Gregorieff, A., Liu, Y., Inanlou, M. R., Khomchuk, Y., and Wrana, J. L. (2015). Yap-dependent reprogramming of Lgr5(+) stem cells drives intestinal regeneration and cancer. *Nature* 526, 715–718. doi: 10.1038/nature15382

Hashizume, R., Andor, N., Ihara, Y., Lerner, R., Gan, H., Chen, X., et al. (2014). Pharmacologic inhibition of histone demethylation as a therapy for pediatric brainstem glioma. *Nat. Med.* 20, 1394–1396. doi: 10.1038/nm.3716

He, N., Chan, C. K., Sobhian, B., Chou, S., Xue, Y., Liu, M., et al. (2011). Human Polymerase-Associated Factor complex (PAFc) connects the Super Elongation Complex (SEC) to RNA polymerase II on chromatin. *Proc. Natl. Acad. Sci. U.S.A.* 108, E636–E645. doi: 10.1073/pnas.1107107108

Hnisz, D., Abraham, B. J., Lee, T. I., Lau, A., Saint-André, V., Sigova, A. A., et al. (2013). Super-enhancers in the control of cell identity and disease. *Cell* 155, 934–947. doi: 10.1016/j.cell.2013.09.053

Kapushesky, M., Emam, I., Holloway, E., Kurnosov, P., Zorin, A., Malone, J., et al. (2010). Gene expression atlas at the European bioinformatics institute. *Nucleic Acids Res.* 38, D690–D698. doi: 10.1093/nar/gkp936

Korrapati, S., Roux, I., Glowatzki, E., and Doetzlhofer, A. (2013). Notch signaling limits supporting cell plasticity in the hair cell-damaged early postnatal murine cochlea. *PLoS One* 8:e73276. doi: 10.1371/journal.pone.0073276

Lee, D. J., and Zeidner, J. F. (2019). Cyclin-dependent kinase (CDK) 9 and 4/6 inhibitors in acute myeloid leukemia (AML): a promising therapeutic approach. *Expert Opin. Investig. Drugs* 28, 989–1001. doi: 10.1080/13543784.2019.1678583

Levine, M. (2011). Paused RNA polymerase II as a developmental checkpoint. *Cell* 145, 502–511. doi: 10.1016/j.cell.2011.04.021

Liang, K., Smith, E. R., Aoi, Y., Stoltz, K. L., Katagi, H., Woodfin, A. R., et al. (2018). Targeting processive transcription elongation *via* SEC disruption for MYC-induced cancer therapy. *Cell* 175, 766–779.e717. doi: 10.1016/j.cell.2018.09.027

Lim, S., and Kaldis, P. (2013). Cdks, cyclins and CKIs: roles beyond cell cycle regulation. *Development* 140, 3079–3093. doi: 10.1242/dev.091744

Lin, C., Garrett, A. S., De Kumar, B., Smith, E. R., Gogol, M., Seidel, C., et al. (2011). Dynamic transcriptional events in embryonic stem cells mediated by the super elongation complex (SEC). *Genes Dev.* 25, 1486–1498. doi: 10.1101/gad.2059211

Lin, C., Smith, E. R., Takahashi, H., Lai, K. C., Martin-Brown, S., Florens, L., et al. (2010). AFF4, a component of the ELL/P-TEFb elongation complex and a shared subunit of MLL chimeras, can link transcription elongation to leukemia. *Mol. Cell* 37, 429–437. doi: 10.1016/j.molcel.2010.01.026

Luo, Z., Lin, C., and Shilatifard, A. (2012b). The super elongation complex (SEC) family in transcriptional control. *Nat. Rev. Mol. Cell Biol.* 13, 543–547. doi: 10.1038/nrm3417

Luo, Z., Lin, C., Guest, E., Garrett, A. S., Mohaghegh, N., Swanson, S., et al. (2012a). The super elongation complex family of RNA polymerase II elongation factors: gene target specificity and transcriptional output. *Mol. Cell Biol.* 32, 2608–2617. doi: 10.1128/mcb.00182-12

Melko, M., Douguet, D., Bensaid, M., Zongaro, S., Verheggen, C., Gecz, J., et al. (2011). Functional characterization of the AFF (AF4/FMR2) family of RNA-binding proteins: insights into the molecular pathology of FRAXE intellectual disability. *Hum. Mol. Genet.* 20, 1873–1885. doi: 10.1093/hmg/ddr069

Mittal, R., Pena, S. A., Zhu, A., Eshraghi, N., Fesharaki, A., Horesh, E. J., et al. (2019). Nanoparticle-based drug delivery in the inner ear: current challenges, limitations and opportunities. *Artific. Cells Nanomed. Biotechnol.* 47, 1312–1320. doi: 10.1080/21691401.2019.1573182

Mizutari, K., Fujioka, M., Hosoya, M., Bramhall, N., Okano, H. J., Okano, H., et al. (2013). Notch inhibition induces cochlear hair cell regeneration and recovery of hearing after acoustic trauma. *Neuron* 77, 58–69. doi: 10.1016/j.neuron.2012.10.032

Morales, F., and Giordano, A. (2016). Overview of CDK9 as a target in cancer research. *Cell Cycle* 15, 519–527. doi: 10.1080/15384101.2016.1138186

Mück, F., Bracharz, S., and Marschalek, R. (2016). DDX6 transfers P-TEFb kinase to the AF4/AF4N (AFF1) super elongation complex. *Am. J. Blood Res.* 6, 28–45.

Narita, T., Ishida, T., Ito, A., Masaki, A., Kinoshita, S., Suzuki, S., et al. (2017). Cyclin-dependent kinase 9 is a novel specific molecular target in adult T-cell leukemia/lymphoma. *Blood* 130, 1114–1124. doi: 10.1182/blood-2016-09-741983

Peng, J., Zhu, Y., Milton, J. T., and Price, D. H. (1998). Identification of multiple cyclin subunits of human P-TEFb. *Genes Dev.* 12, 755–762. doi: 10.1101/gad.12.5.755

Ryan, A. F. (2003). The cell cycle and the development and regeneration of hair cells. *Curr. Top. Dev. Biol.* 57, 449–466.

Shi, F., Kempfle, J. S., and Edge, A. S. B. (2012). Wnt-responsive Lgr5-expressing stem cells are hair cell progenitors in the cochlea. *J. Neurosci.* 32, 9639–9648. doi: 10.1523/JNEUROSCI.1064-12.2012

Shilatifard, A., Conaway, R. C., and Conaway, J. W. (2003). The RNA polymerase II elongation complex. *Annu. Rev. Biochem.* 72, 693–715. doi: 10.1146/annurev.biochem.72.121801.161551

Smith, E., and Shilatifard, A. (2010). The chromatin signaling pathway: diverse mechanisms of recruitment of histone-modifying enzymes and varied biological outcomes. *Mol. Cell* 40, 689–701. doi: 10.1016/j.molcel.2010.11.031

Sun, W., Yang, S., Liu, K., and Salvi, R. J. (2017). Hearing loss and auditory plasticity. *Hear. Res.* 347, 1–2. doi: 10.1016/j.heares.2017.03.010

Warchol, M. E., Lambert, P. R., Goldstein, B. J., Forge, A., and Corwin, J. T. (1993). Regenerative proliferation in inner ear sensory epithelia from adult guinea pigs and humans. *Science* 259, 1619–1622.

Wiernik, P. H. (2016). Alvocidib (flavopiridol) for the treatment of chronic lymphocytic leukemia. *Expert Opin. Investig. Drugs* 25, 729–734. doi: 10.1517/13543784.2016.1169273

World Health Organization [WHO] (2019). *Fact Sheet. Deafness and Hearing Impairment*. Available online at http://www.who.int/mediacentre/factsheets/fs300/en/index.html (accessed March 20, 2019).

Xu, J., Ueno, H., Xu, C. Y., Chen, B., Weissman, I. L., and Xu, P.-X. (2017). Identification of mouse cochlear progenitors that develop hair and supporting cells in the organ of Corti. *Nat. Commun.* 8:15046. doi: 10.1038/ncomms15046

Youm, I., and Li, W. (2018). Cochlear hair cell regeneration: an emerging opportunity to cure noise-induced sensorineural hearing loss. *Drug Discov. Today* 23, 1564–1569. doi: 10.1016/j.drudis.2018.05.001

Zeidner, J. F., and Karp, J. E. (2015). Clinical activity of alvocidib (flavopiridol) in acute myeloid leukemia. *Leuk. Res.* 39, 1312–1318. doi: 10.1016/j.leukres.2015.10.010

Zhang, S., Zhang, Y., Dong, Y., Guo, L., Zhang, Z., Shao, B., et al. (2020). Knockdown of Foxg1 in supporting cells increases the trans-differentiation of supporting cells into hair cells in the neonatal mouse cochlea. *Cell Mol. Life Sci.* 77, 1401–1419. doi: 10.1007/s00018-019-03291-2

Zhou, C.-C., Xiong, Q.-C., Zhu, X.-X., Du, W., Deng, P., Li, X.-B., et al. (2017). AFF1 and AFF4 differentially regulate the osteogenic differentiation of human MSCs. *Bone Res.* 5:17044. doi: 10.1038/boneres.2017.44

Zhu, Y., Pe'ery, T., Peng, J., Ramanathan, Y., Marshall, N., Marshall, T., et al. (1997). Transcription elongation factor P-TEFb is required for HIV-1 tat transactivation *in vitro*. *Genes Dev.* 11, 2622–2632. doi: 10.1101/gad.11.20.2622

Conflict of Interest: The authors declare that the research was conducted in the absence of any commercial or financial relationships that could be construed as a potential conflict of interest.

Publisher's Note: All claims expressed in this article are solely those of the authors and do not necessarily represent those of their affiliated organizations, or those of the publisher, the editors and the reviewers. Any product that may be evaluated in this article, or claim that may be made by its manufacturer, is not guaranteed or endorsed by the publisher.

frontiers in Cellular Neuroscience

REVIEW
published: 13 October 2021
doi: 10.3389/fncel.2021.760422

Autophagy Regulates the Survival of Hair Cells and Spiral Ganglion Neurons in Cases of Noise, Ototoxic Drug, and Age-Induced Sensorineural Hearing Loss

Lingna Guo[1,2†], Wei Cao[2†], Yuguang Niu[3†], Shuangba He[4], Renjie Chai[1,5,6,7*] and Jianming Yang[2*]*

[1] State Key Laboratory of Bioelectronics, School of Life Sciences and Technology, Jiangsu Province High-Tech Key Laboratory for Bio-Medical Research, Southeast University, Nanjing, China, [2] Department of Otolaryngology Head and Neck Surgery, The Second Affiliated Hospital of Anhui Medical University, Hefei, China, [3] Department of Ambulatory Medicine, The First Medical Center of PLA General Hospital, Beijing, China, [4] Department of Otolaryngology Head and Neck Surgery, Nanjing Tongren Hospital, School of Medicine, Southeast University, Nanjing, China, [5] Co-Innovation Center of Neuroregeneration, Nantong University, Nantong, China, [6] Institute for Stem Cell and Regeneration, Chinese Academy of Sciences, Beijing, China, [7] Beijing Key Laboratory of Neural Regeneration and Repair, Capital Medical University, Beijing, China

Inner ear hair cells (HCs) and spiral ganglion neurons (SGNs) are the core components of the auditory system. However, they are vulnerable to genetic defects, noise exposure, ototoxic drugs and aging, and loss or damage of HCs and SGNs results in permanent hearing loss due to their limited capacity for spontaneous regeneration in mammals. Many efforts have been made to combat hearing loss including cochlear implants, HC regeneration, gene therapy, and antioxidant drugs. Here we review the role of autophagy in sensorineural hearing loss and the potential targets related to autophagy for the treatment of hearing loss.

Keywords: hearing loss, hair cells, spiral ganglion neurons, autophagy, mechanism

OPEN ACCESS

Edited by:
Zuhong He,
Wuhan University, China

Reviewed by:
Haiying Sun,
Huazhong University of Science and Technology, China
Yu Sun,
Huazhong University of Science and Technology, China

****Correspondence:***
Shuangba He
hesb@njtrh.org
Renjie Chai
renjiec@seu.edu.cn
Jianming Yang
Jmyang88@163.com

† These authors have contributed equally to this work

Specialty section:
This article was submitted to Cellular Neuropathology, a section of the journal Frontiers in Cellular Neuroscience

Received: *18 August 2021*
Accepted: *15 September 2021*
Published: *13 October 2021*

Citation:
Guo L, Cao W, Niu Y, He S, Chai R and Yang J (2021) Autophagy Regulates the Survival of Hair Cells and Spiral Ganglion Neurons in Cases of Noise, Ototoxic Drug, and Age-Induced Sensorineural Hearing Loss. Front. Cell. Neurosci. 15:760422. doi: 10.3389/fncel.2021.760422

INTRODUCTION

According to the World Health Organization (WHO, 2021), about 5% of the world's population (or 430 million people) suffer from hearing impairment, and it is expected that the number of people with disabling hearing loss will be around 700 million by 2050. Hearing loss is not only a physical and financial burden in social life, but also causes psychological problems and psychiatric disorders, including cognitive decline and depression (Strawbridge et al., 2000; Steffens et al., 2006; Lin et al., 2013). Indeed, hearing loss has become a serious threat to global population health and economic development.

Genetic alterations, noise, ototoxic drugs, and aging can all contribute to hearing loss. Although the causes vary, the most common causes of deafness are damage or loss of hair cells (HCs) and degeneration of spiral ganglion neurons (SGNs). HCs are responsible for converting external sound signals into electrical signals that are transmitted to the brainstem through SGNs (Groves and Fekete, 2012). Recent studies have shown that these sensory

cells cannot spontaneously regenerate in adult mammals (Stone et al., 1998; Brigande and Heller, 2009; Cox et al., 2014), so damage or loss of HCs and degeneration of SGNs can result in permanent deafness.

Cochlear implants offer strategies to mitigate hearing loss, but their effectiveness has been reported to be highly correlated with the remaining HCs and SGNs in the cochlea. Efforts have been made to protect HCs and SGNs against noise or ototoxic drugs-induced death, and N-acetylcysteine and neurotrophins have been shown to prevent HC death and SGN degeneration to some extent (Aladag et al., 2016; Chen et al., 2018; Wu et al., 2020). Recently, autophagy has been reported to play an antioxidative role in preventing sensorineural hearing loss (SNHL) (Ye et al., 2019a). In this review, we present the role of autophagy in hearing loss induced by noise exposure, ototoxic drugs and aging, and describe the molecules and signaling pathways involved in autophagy in the inner ear.

THE MECHANISM AND PROCESS OF AUTOPHAGY

Autophagy is a highly conserved degradation system in eukaryotic cells that maintains cellular homeostasis, and autophagy can be induced by nutrient deficiency and reactive oxygen species (ROS) accumulation (Mizushima, 2007; Eskelinen, 2019). Through the autophagy pathway, damaged cytoplasmic components are absorbed and transferred to lysosomes, where they are degraded and recycled. There are three main types of autophagy, the most common form being macroautophagy, which is the form generally being referred to by the term "autophagy." In this process, bilayer organelles called autophagosomes carry cytoplasmic products to lysosomes for degradation (Mizushima, 2007; Mizushima and Komatsu, 2011). This dynamic process generally comprises the following four steps: first is the initiation of autophagy through the envelopment of the cytosolic contents within phagophores; second is the formation of the autophagosome, which is a double-membrane vesicle; third is the fusion of autophagosomes with lysosomes to form autolysosomes; and fourth is the degradation of the contents of the autolysosomes (Feng et al., 2014). The second form is microautophagy, in which the cytoplasmic contents enter the lysosome through direct invagination or through deformation of the lysosomal membrane (Li et al., 2012). The third form is molecular chaperone-mediated autophagy, which is a highly specific process in which proteins containing a KFERQ motif are recognized and transported to the lysosomal membrane (Kaushik and Cuervo, 2018; Yang et al., 2019).

The biogenesis of autophagy requires many autophagy-related (ATG) proteins. So far more than 30 ATGs have been shown to be involved in the initiation and maturation of autophagy (Klionsky et al., 2003; Xie and Klionsky, 2007; Mizushima et al., 2011; Wesselborg and Stork, 2015), and the ATGs that are required for autophagosome formation are divided into several functional units. The autophagy-related 2 (ATG1)–Unc51-like kinase (ULK) complex (ULK1) plays a vital role during the initiation stage, and because this complex is negatively regulated by mammalian target of rapamycin complex 1 (mTORC1) (Noda and Ohsumi, 1998; Kamada et al., 2010), the inactivation of mTORC1 by rapamycin stimulates autophagy. Alternatively, the activation of autophagy can also be regulated by AMP-activated protein kinase (AMPK) (Kim et al., 2011; Li and Chen, 2019). The phosphatidylinositol 3-kinase complex (PI3KC), which is activated by ULK1, participates in the formation of autophagic vesicle membranes. ATG9 is the only known transmembrane protein shown to be involved in the delivery of membrane particles to form autophagosomes (Noda et al., 2000; Webber and Tooze, 2010). During the maturation stage, two ubiquitin-like conjugation systems, the ATG5-ATG12 system and the LC3-PE system, play vital roles in the elongation of autophagosomes (Geng and Klionsky, 2008). After the autophagosome is encapsulated, the autophagosome and lysosome fuse to form the autolysosome through the function of proteins such as SNARE (Itakura et al., 2012).

THE PROTECTIVE EFFECT OF AUTOPHAGY AGAINST SNHL

Autophagy is responsible for normal cell survival and homeostasis. A variety of human conditions, such as neurodegenerative diseases, cancer, and inflammation, have been reported to be associated with dysregulated autophagic processes (Levine et al., 2011; White, 2012; Kochergin and Zakharova, 2016). In the inner ear, many studies have shown that autophagy played an important role in cell development, differentiation, and survival (Fujimoto et al., 2017; Magarinos et al., 2017), and recently there has been renewed interest in regulating autophagy to prevent SNHL.

Noise and ototoxic drugs increased the levels of oxidative stress in HCs, which contributed to cell death (Warchol, 2010; Tabuchi et al., 2011; Sheth et al., 2017; Wu et al., 2020), and in a mouse model that was exposed to noise, the level of autophagy was increased in HCs (Xu et al., 2021). It is worth noting that the oxidative stress level in response to noise was dose dependent, and moderate noise induced temporary threshold shifts and increased the level of autophagy in outer hair cells, while severe noise produced excess ROS that induced permanent threshold shifts (Yuan et al., 2015). Increasing autophagy with rapamycin can reduce the accumulation of ROS and prevent cell death from noise exposure. In contrast, blocking autophagy through the autophagy inhibitor 3-methyladenine (3-MA) or knocking down LC3 can increase the accumulation of ROS and promote cell death (Yuan et al., 2015). More recently, a study reported that treatment with FK506 (tacrolimus), a calcineurin inhibitor, increased autophagy and inhibited ROS and alleviated moderate noise-induced HC damage and hearing loss (He et al., 2021b).

Ototoxic drugs such as aminoglycoside antibiotics and cisplatin can also result in HC damage and hearing loss. He et al. (2017) found that autophagy activity was increased in neomycin or gentamicin-treated HCs and HEI-OC1 cells. Treatment with rapamycin increased autophagy activity and decreased ROS accumulation and apoptosis, while treatment with 3-MA or knockdown of ATG5 resulted in reduced autophagy activity and increased ROS levels and apoptosis. Other

studies also showed that upregulation of autophagy alleviated cisplatin-induced ototoxicity in HCs (Fang and Xiao, 2014; Liu et al., 2019;Liang et al., 2021).

Presbycusis (age-related hearing loss) is a common sensory disorder associated with aging. The level of autophagy decreased with age, and the upregulation of autophagy can promote aging HC survival and slow the degeneration of auditory cells (Yuan et al., 2018; He et al., 2021a).

Autophagy also exerts a protective effect in SGNs against ototoxic drug-induced damage. Administration of kanamycin and furosemide induced HC loss and subsequent SGN degeneration by impairing autophagic flux and lysosomal biogenesis, and restoration of autophagy by promoting transcription factor EB (TFEB) translocation into the nucleus attenuated SGN degeneration (Ye et al., 2019b). In cisplatin-induced SGN damage, activation of autophagy by rapamycin alleviated SGN apoptosis and hearing loss, and inhibition of autophagy by 3-MA aggravated the degeneration of SGNs (Liu et al., 2021). Thus, autophagy has a protective effect against HC loss, SGN degeneration and subsequent hearing impairment.

THE PRO-APOPTOTIC EFFECT OF AUTOPHAGY IN SNHL

Autophagy has a dual function of pro-survival and pro-apoptotic, which has been demonstrated in many diseases, especially cancers, and the role of autophagy depends on the developmental stage and tumor type (Singh et al., 2018). Several reports have demonstrated the pro-apoptotic role of autophagy in SNHL. In a model of cisplatin-induced HC damage, exposure to 15 μM cisplatin for 48 h induced excessive autophagy, while co-treatment of cisplatin with meclofenamic acid, a highly selective inhibitor of fatmass and obesity-associated enzyme, inhibited the cisplatin-induced excessive autophagy in HEI-OC1 cells and reduced oxidative stress and cell apoptosis (Li et al., 2018). Another study indicated that pretreatment with U0126, an inhibitor of the ERK1/2 signaling pathway, can reduce the level of cisplatin-induced autophagy in HEI-OC1 cells and HCs and can reduce cisplatin-induced ROS and apoptosis (Wang et al., 2021). Interestingly, a study showed that in cisplatin-treated HEI-OC1 cells, autophagy promoted cell survival in the early phase (during the first 8 h) of cisplatin treatment, while autophagy induced cell death in the late phase (Youn et al., 2015).

MITOPHAGY IN SNHL

Autophagy is considered to be a non-selective process in the degradation of a large number of cytoplasmic components. However, recent studies have shown that there are many types of selective autophagy. Some types of selective autophagy have recently been found in the inner ear, for example, mitophagy and pexophagy. Defective, excessive, and aged mitochondria produce toxic byproducts, particularly ROS, and mitophagy is a specific autophagic process that selectively removes these redundant or damaged mitochondria in order to reduce ROS levels and to maintain the normal function of the mitochondria (Kroemer et al., 2007; Novak, 2012). Mitophagy has been linked to neurodegenerative diseases, cancer, and aging (Bernardini et al., 2017; Chu, 2019; Tran and Reddy, 2021). Recent studies have indicated potential associations between mitophagy and age-related hearing loss, and in the cochlea of aged mice, mitophagy was reduced along with decreased expression of mitophagy-related genes and proteins (Oh et al., 2020; Youn et al., 2020). Damaged mitochondria were increased in HCs and SGNs in aged mice, and activation of mitophagy alleviated cellular senescence by promoting mitochondrial protein degradation (Kim et al., 2021). The same phenomenon was observed in carbonyl cyanide m-chlorophenyl hydrazone-induced cytotoxicity in HEI-OC1 cells and in the organ of Corti, and the protein level of mitochondrial cytochrome c oxidase subunit 4 was downregulated (Setz et al., 2018). However, in aminoglycoside-induced HC loss, neither neomycin nor gentamicin exposure had an impact on the level of mitophagy, thus suggesting a mitophagy-independent pathway of aminoglycoside ototoxicity (He et al., 2017; Setz et al., 2018).

PEXOPHAGY IN SNHL

Pexophagy is another selective autophagy pathway, in which peroxisomes are selectively degraded in vacuoles in response to environmental stimuli (Farre et al., 2009; Germain and Kim, 2020). It has been reported that pexophagy was related to inflammation induced by lipopolysaccharide exposure, and impaired pexophagy resulted in the accumulation of impaired peroxisomes and redox disequilibrium (Vasko et al., 2013). Pexophagy was associated with noise-induced HC damage, overexposure to noise led to an increased level of peroxisome in HCs and SGNs, and defective pexophagy led to noise-induced hearing loss (Delmaghani et al., 2015; Defourny et al., 2019). Pejvakin was a peroxisome-associated protein that directly recruited LC3B to promote pexophagy in order to protect cochlear HCs against noise-induced damage (Defourny et al., 2019).

PROTEINS THAT MODULATE AUTOPHAGY IN SNHL

A number of molecules have been reported to respond to cell damage by regulating autophagy. TFEB is a major regulator of autophagy and lysosomal biogenesis, and phosphorylated TFEB is inactive and remains in the cytoplasm, while dephosphorylated TFEB is translocated to the nucleus where it promotes the transcription of its target genes (Martina et al., 2012; Settembre et al., 2012). In kanamycin-induced degenerated SGNs, TFEB remained in the cytoplasm and the autophagic flux was impaired, while the mTOR inhibitor temsirolimus (CCI-779) promoted the translocation of TFEB to the nucleus thus restoring autophagic flux and ameliorating SGN degeneration (Ye et al., 2019b). Phosphatase and tensin homolog (PTEN)-induced putative kinase 1 (PINK1) also shown a protective effect against

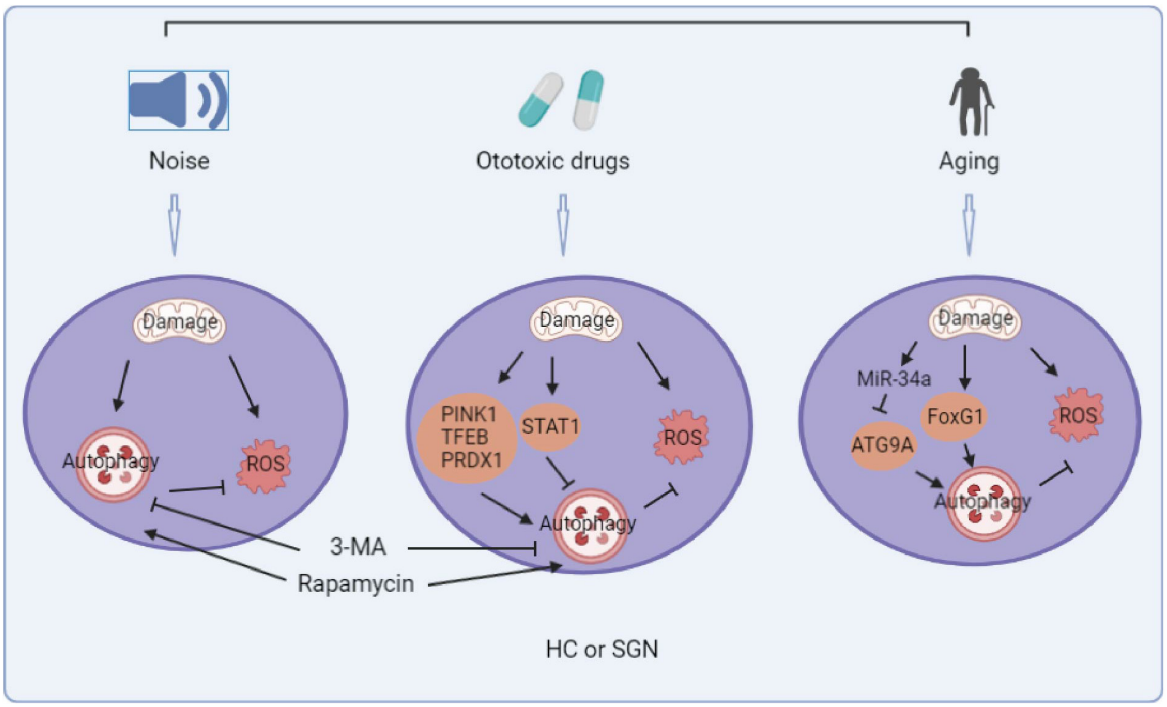

FIGURE 1 | Summary diagram of the role of autophagy in noise, ototoxic drug, and age-induced sensorineural hearing loss. (The picture is created in BioRender.com).

gentamicin and cisplatin-induced ototoxicity. PINK1 promoted autophagy and inhibited the P53 pathway in gentamicin-induced HC damage (Yang et al., 2018b), while in response to cisplatin-induced HC and SGN damage, PINK1 induced autophagy and inhibited the JNK signaling pathway (Yang et al., 2018a). Peroxiredoxin 1 (PRDX1) also played a protective role in cisplatin-induced SGN damage by activating autophagy through the activation of the PTEN-AKT signaling pathway (Liu et al., 2021). FoxG1 protected HC and delayed age-related hearing loss via autophagy making it be used as a strategy to delay age-related hearing loss (He et al., 2021a).

In addition, some proteins have detrimental effects regarding ototoxicity. For example, STAT1 is a regulator of cell death and has been reported to participate in cisplatin-induced HC damage. Knockdown of STAT1 by siRNA reduced cisplatin-induced ototoxicity (Kaur et al., 2011), and Levano et al. found that STAT1 played a role in modulating the autophagy pathway, with higher levels of autophagy seen in STAT1−/− explants in response to gentamicin and cisplatin (Levano and Bodmer, 2015). Thus, different molecules and pathways regulate the occurrence and development of SNHL in different contexts.

miRNAs RELATED TO AUTOPHAGY IN SNHL

miRNAs are a class of small endogenous RNAs with a length of about 21–23 nucleotides, and they play a variety of important regulatory roles in cells (Rupaimoole and Slack, 2017). miRNAs are potential therapeutic targets for treating cancer and other diseases, and miRNAs are also involved in SNHL (Chen et al., 2019). miR-34a was shown to be associated with age-related hearing loss in mice and humans (Pang et al., 2016, 2017), and miR-34a was activated with aging and overexpression of miR-34a significantly decreased the level of ATG9A thus inhibiting autophagic flux and inducing cell death (Pang et al., 2017). A considerable number of miRNAs have been found to be involved in autophagy cascades, such as miR-204, miR-216a, and miR-375 etc. (Su et al., 2015), but the roles of these miRNAs are poorly studied in relation to SNHL (**Figure 1**).

CONCLUSION

There is no doubt that autophagy plays an important role in SNHL. Although excessive autophagy can lead to cell death under some conditions, activation of autophagy protects HCs and SGNs against oxidative stress-induced death. It is important to be clear that the mechanisms of autophagy are complex and that different stimuli may lead to activation of different pathways. Though we have known that some proteins and miRNAs participate in the autophagic pathways involved in SNHL making them potential targets for treatment of SNHL, however, the specific signaling pathways they participate in remain unclear, let alone the known connections between these proteins and miRNAs. Furthermore, there are potential proteins and miRNAs whose functions in SNHL have not yet been identified. Future studies should thus

further clarify the mechanism of autophagy in response to different stimuli in order to develop ways to regulate autophagy and thus protect HCs and SGNs. However, the application of autophagy as a treatment for deafness is still a long way off. Current research has been limited to cell lines, explants and animals, and few clinical trials have examined the role of autophagy. Given the complexity of mechanisms and functions of autophagy, the safest and most effective strategies must be studied in future research.

AUTHOR CONTRIBUTIONS

All authors listed have made a substantial, direct and intellectual contribution to the work, and approved it for publication.

FUNDING

This work was supported by the Strategic Priority Research Program of the Chinese Academy of Sciences (XDA16010303), National Key R&D Program of China (No. 2017YFA0103903), the National Natural Science Foundation of China (Nos. 82030029, 81970882, and 82071055), Natural Science Foundation from Jiangsu Province (BE2019711), and the Shenzhen Fundamental Research Program (JCYJ20190814093401920).

ACKNOWLEDGMENTS

We are grateful to Matthew Hogg for revising the manuscript. We are thankful to the reviewers for their insightful comments.

REFERENCES

Aladag, I., Guven, M., and Songu, M. (2016). Prevention of gentamicin ototoxicity with N-acetylcysteine and vitamin A. *J. Laryngol. Otol.* 130, 440–446. doi: 10.1017/S0022215116000992

Bernardini, P., Lazarou, M., and Dewson, G. (2017). Parkin and mitophagy in cancer. *Oncogene* 36, 1315–1327. doi: 10.1038/onc.2016.302

Brigande, J. V., and Heller, S. (2009). Quo vadis, hair cell regeneration? *Nat. Neurosci.* 12, 679–685. doi: 10.1038/nn.2311

Chen, H. R., Wijesinghe, P., and Nunez, D. A. (2019). MicroRNAs in acquired sensorineural hearing loss. *J. Laryngol. Otol.* 133, 650–657. doi: 10.1017/S0022215119001439

Chen, Y., Xing, L. Xia, Chen, Z., Yin, S., and Wang, J. (2018). AAV-mediated NT-3 overexpression protects cochleae against noise-induced synaptopathy. *Gene Ther.* 25, 251–259. doi: 10.1038/s41434-018-0012-0

Chu, C. T. (2019). Mechanisms of selective autophagy and mitophagy: implications for neurodegenerative diseases. *Neurobiol. Dis.* 122, 23–34. doi: 10.1016/j.nbd.2018.07.015

Cox, B. C., Chai, R. J., Lenoir, A., Liu, Z. Y., Zhang, L. L., Nguyen, D. H., et al. (2014). Spontaneous hair cell regeneration in the neonatal mouse cochlea in vivo. *Development* 141, 816–829. doi: 10.1242/dev.109421

Defourny, J., Aghaie, A., Perfettini, I., Avan, P., Delmaghani, S., and Petit, C. (2019). Pejvakin-mediated pexophagy protects auditory hair cells against noise-induced damage. *Proc. Natl. Acad. Sci. U.S.A.* 116, 8010–8017. doi: 10.1073/pnas.1821844116

Delmaghani, S., Defourny, J., Aghaie, A., Beurg, M., Dulon, D., Thelen, N., et al. (2015). Hypervulnerability to sound exposure through impaired adaptive proliferation of peroxisomes. *Cell* 163, 894–906. doi: 10.1016/j.cell.2015.10.023

Eskelinen, E. L. (2019). Autophagy: supporting cellular and organismal homeostasis by self-eating. *Int. J. Biochem. Cell Biol.* 111, 1–10. doi: 10.1016/j.biocel.2019.03.010

Fang, B., and Xiao, H. J. (2014). Rapamycin alleviates cisplatin-induced ototoxicity in vivo. *Biochem. Biophys. Res. Commun.* 448, 443–447. doi: 10.1016/j.bbrc.2014.04.123

Farre, J. C., Krick, R., Subramani, S., and Thumm, M. (2009). Turnover of organelles by autophagy in yeast. *Curr. Opin. Cell Biol.* 21, 522–530. doi: 10.1016/j.ceb.2009.04.015

Feng, Y. C., He, D., Yao, Z. Y., and Klionsky, D. J. (2014). The machinery of macroautophagy. *Cell Res.* 24, 24–41. doi: 10.1038/cr.2013.168

Fujimoto, C., Iwasaki, S., Urata, S., Morishita, H., Sakamaki, Y., Fujioka, M., et al. (2017). Autophagy is essential for hearing in mice. *Cell Death Dis.* 8:e2780. doi: 10.1038/cddis.2017.194

Geng, J., and Klionsky, D. J. (2008). The Atg8 and Atg12 ubiquitin-like conjugation systems in macroautophagy. 'Protein modifications: beyond the usual suspects' review series. *EMBO Rep.* 9, 859–864. doi: 10.1038/embor.2008.163

Germain, K., and Kim, P. K. (2020). Pexophagy: a model for selective autophagy. *Int. J. Mol. Sci.* 21:578.

Groves, K., and Fekete, D. M. (2012). Shaping sound in space: the regulation of inner ear patterning. *Development* 139, 245–257. doi: 10.1242/dev.078257

He, Z. H., Guo, L. N., Shu, Y. L., Fang, Q. J., Zhou, H., Liu, Y. Z., et al. (2017). Autophagy protects auditory hair cells against neomycin-induced damage. *Autophagy* 13, 1884–1904. doi: 10.1080/15548627.2017.1359449

He, Z. H., Pan, S., Zheng, H. W., Fang, Q. J., Hill, K., and Sha, S. H. (2021b). Treatment with calcineurin inhibitor FK506 attenuates noise-induced hearing loss. *Front. Cell Dev. Biol.* 9:648461. doi: 10.3389/fcell.2021.648461

He, Z. H., Li, M., Fang, Q. J., Liao, F. L., Zou, S. Y., Wu, X., et al. (2021a). FOXG1 promotes aging inner ear hair cell survival through activation of the autophagy pathway. *Autophagy*. doi: 10.1080/15548627.2021.1916194 [Epub ahead of print].

Itakura, E., Kishi-Itakura, C., and Mizushima, N. (2012). The hairpin-type tail-anchored SNARE syntaxin 17 targets to autophagosomes for fusion with endosomes/lysosomes. *Cell* 151, 1256–1269. doi: 10.1016/j.cell.2012.11.001

Kamada, Y., Yoshino, K., Kondo, C., Kawamata, T., Oshiro, N., Yonezawa, K., et al. (2010). Tor directly controls the Atg1 kinase complex to regulate autophagy. *Mol. Cell. Biol.* 30, 1049–1058. doi: 10.1128/Mcb.01344-09

Kaur, T., Mukherjea, D., Sheehan, K., Jajoo, S., Rybak, L. P., and Ramkumar, V. (2011). Short interfering RNA against STAT1 attenuates cisplatin-induced ototoxicity in the rat by suppressing inflammation. *Cell Death Dis.* 2:e180.

Kaushik, S., and Cuervo, A. M. (2018). The coming of age of chaperone-mediated autophagy. *Nat. Rev. Mol. Cell Biol.* 19, 365–381. doi: 10.1038/s41580-018-0001-6

Kim, J., Kundu, M., Viollet, B., and Guan, K. L. (2011). AMPK and mTOR regulate autophagy through direct phosphorylation of Ulk1. *Nat. Cell Biol.* 13, 132–141. doi: 10.1038/ncb2152

Kim, Y. J., Choo, O. S., Lee, J. S., Jang, J. H., Woo, H. G., and Choung, Y. H. (2021). BCL2 interacting protein 3-like/NIX-mediated mitophagy plays an important role in the process of age-related hearing loss. *Neuroscience* 455, 39–51. doi: 10.1016/j.neuroscience.2020.12.005

Klionsky, D. J., Cregg, J. M., Dunn, W. A., Emr, S. D., Sakai, Y., . Sandoval, I. V., et al. (2003). A unified nomenclature for yeast autophagy-related genes. *Dev. Cell* 5, 539–545. doi: 10.1016/S1534-5807(03)00296-X

Kochergin, J. A., and Zakharova, M. N. (2016). The role of autophagy in neurodegenerative diseases. *Neurochem. J.* 10, 7–18. doi: 10.1134/S1819712416010098

Kroemer, G., Galluzzi, L., and Brenner, C. (2007). Mitochondrial membrane permeabilization in cell death. *Physiol. Rev.* 87, 99–163. doi: 10.1152/physrev.00013.2006

Levano, S., and Bodmer, D. (2015). Loss of STAT1 protects hair cells from ototoxicity through modulation of STAT3, c-Jun, Akt, and autophagy factors. *Cell Death Dis.* 6:e2019.

Levine, B., Mizushima, N., and Virgin, H. W. (2011). Autophagy in immunity and inflammation. *Nature* 469, 323–335. doi: 10.1038/nature09782

Li, H., Song, Y. D., He, Z. H., Chen, X. Y., Wu, X. M., Li, X. F., et al. (2018). Meclofenamic acid reduces reactive oxygen species accumulation and apoptosis, inhibits excessive autophagy, and protects hair cell-like HEI-OC1 cells from cisplatin-induced damage. *Front. Cell. Neurosci.* 12:139. doi: 10.3389/fncel.2018.00139

Li, J., and Chen, Y. Y. (2019). AMPK and autophagy. autophagy: biology and diseases. *Basic Sci.* 1206, 85–108. doi: 10.1007/978-981-15-0602-4_4

Li, W. W., Li, J., and Bao, J. K. (2012). Microautophagy: lesser-known self-eating. *Cell. Mol. Life Sci.* 69, 1125–1136. doi: 10.1007/s00018-011-0865-5

Liang, Z. R., Zhang, T., Zhan, T., Cheng, G., Zhang, W. J., Jia, H. Y., et al. (2021). Metformin alleviates cisplatin-induced ototoxicity by autophagy induction possibly via the AMPK/FOXO3a pathway. *J. Neurophysiol.* 125, 1202–1212. doi: 10.1152/jn.00417.2020

Lin, F. R., Yaffe, K., Xia, J., Xue, Q. L., Harris, T. B., Purchase-Helzner, E., et al. (2013). Hearing loss and cognitive decline in older adults. *JAMA Int. Med.* 173, 293–299.

Liu, T. Y., Zong, S. M., Luo, P., Qu, Y. J., Wen, Y. Y., Du, P. Y., et al. (2019). Enhancing autophagy by down-regulating GSK-3 beta alleviates cisplatin-induced ototoxicity in vivo and in vitro. *Toxicol. Lett.* 313, 11–18. doi: 10.1016/j.toxlet.2019.05.025

Liu, W. W., Xu, L., Wang, X., Zhang, D. G., Sun, G. Y., Wang, M., et al. (2021). PRDX1 activates autophagy via the PTEN-AKT signaling pathway to protect against cisplatin-induced spiral ganglion neuron damage. *Autophagy*. doi: 10.1080/15548627.2021.1905466 [Epub ahead of print].

Magarinos, M., Pulido, S., Aburto, M. R., Rodriguez, R. D., and Varela-Nieto, I. (2017). Autophagy in the vertebrate inner ear. *Front. Cell Dev. Biol.* 5:56. doi: 10.3389/fcell.2017.00056

Martina, J. A., Chen, Y., Gucek, M., and Puertollano, R. (2012). MTORC1 functions as a transcriptional regulator of autophagy by preventing nuclear transport of TFEB. *Autophagy* 8, 903–914. doi: 10.4161/auto.19653

Mizushima, N. (2007). Autophagy: process and function. *Genes Dev.* 21, 2861–2873. doi: 10.1101/gad.1599207

Mizushima, N., and Komatsu, M. (2011). Autophagy: renovation of cells and tissues. *Cell* 147, 728–741. doi: 10.1016/j.cell.2011.10.026

Mizushima, N., Yoshimori, T., and Ohsumi, Y. (2011). The role of Atg proteins in autophagosome formation. *Ann. Rev. Cell Dev. Biol.* 27, 107–132. doi: 10.1146/annurev-cellbio-092910-154005

Noda, T., and Ohsumi, Y. (1998). Tor, a phosphatidylinositol kinase homologue, controls autophagy in yeast. *J. Biol. Chem.* 273, 3963–3966. doi: 10.1074/jbc.273.7.3963

Noda, T., Kim, J., Huang, W. P., Baba, M., Tokunaga, C., Ohsumi, Y., et al. (2000). Apg9p/Cvt7p is an integral membrane protein required for transport vesicle formation in the Cvt and autophagy pathways. *J. Cell Biol.* 148, 465–479. doi: 10.1083/jcb.148.3.465

Novak, I. (2012). Mitophagy: a complex mechanism of mitochondrial removal. *Antioxid. Redox Signal.* 17, 794–802. doi: 10.1089/ars.2011.4407

Oh, J., Youn, C. K., Jun, Y., Jo, E. R., and Cho, S. I. (2020). Reduced mitophagy in the cochlea of aged C57BL/6J mice. *Exp. Gerontol.* 137:110946. doi: 10.1016/j.exger.2020.110946

Pang, J. Q., Xiong, H., Lin, P. L., Lai, L., Yang, H. D., Liu, Y. M., et al. (2017). Activation of miR-34a impairs autophagic flux and promotes cochlear cell death via repressing ATG9A: implications for age-related hearing loss. *Cell Death Dis.* 8:e3079.

Pang, J. Q., Xiong, H., Yang, H. D., Ou, Y. K., Xu, Y. D., Huang, Q. H., et al. (2016). Circulating miR-34a levels correlate with age-related hearing loss in mice and humans. *Exp. Gerontol.* 76, 58–67. doi: 10.1016/j.exger.2016.01.009

Rupaimoole, R., and Slack, F. J. (2017). MicroRNA therapeutics: towards a new era for the management of cancer and other diseases. *Nat. Rev. Drug Discov.* 16, 203–221. doi: 10.1038/nrd.2016.246

Settembre, C., Zoncu, R., Medina, D. L., Vetrini, F., Erdin, S., Erdin, S., et al. (2012). A lysosome-to-nucleus signalling mechanism senses and regulates the lysosome via mTOR and TFEB. *Embo J.* 31, 1095–1108. doi: 10.1038/emboj.2012.32

Setz, C., Benischke, A. S., Bento, A. C. P. F., Brand, Y., Levano, S., Paech, F., et al. (2018). Induction of mitophagy in the HEI-OC1 auditory cell line and activation of the Atg12/LC3 pathway in the organ of Corti. *Hear. Res.* 361, 52–65. doi: 10.1016/j.heares.2018.01.003

Sheth, S., Mukherjea, D., Rybak, L. P., and Ramkumar, V. (2017). Mechanisms of cisplatin-induced ototoxicity and otoprotection. *Front. Cell. Neurosci.* 11:338. doi: 10.3389/fncel.2017.00338

Singh, S. S., Vats, S., Chia, A. Y. Q., Tan, T. Z., Deng, S., Ong, M. S., et al. (2018). Dual role of autophagy in hallmarks of cancer. *Oncogene* 37, 1142–1158. doi: 10.1038/s41388-017-0046-6

Steffens, D. C., Otey, E., Alexopoulos, G. S., Butters, M. A., Cuthbert, B., Ganguli, M., et al. (2006). Perspectives on depression, mild cognitive impairment, and cognitive decline. *Arch. Gen. Psychiatry* 63, 130–138. doi: 10.1001/archpsyc.63.2.130

Stone, J. S., Oesterle, E. C., and Rubel, E. W. (1998). Recent insights into regeneration of auditory and vestibular hair cells. *Curr. Opin. Neurol.* 11, 17–24. doi: 10.1097/00019052-199802000-00004

Strawbridge, W. J., Wallhagen, M. I., Shema, S. J., and Kaplan, G. A. (2000). Negative consequences of hearing impairment in old age: a longitudinal analysis. *Gerontologist* 40, 320–326. doi: 10.1093/geront/40.3.320

Su, Z. Y., Yang, Z. Z., Xu, Y. Q., Chen, Y. B., and Yu, Q. (2015). MicroRNAs in apoptosis, autophagy and necroptosis. *Oncotarget* 6, 8474–8490. doi: 10.18632/oncotarget.3523

Tabuchi, K., Nishimura, B., Nakamagoe, M., Hayashi, K., Nakayama, M., and Hara, A. (2011). Ototoxicity: mechanisms of cochlear impairment and its prevention. *Curr. Med. Chem.* 18, 4866–4871. doi: 10.2174/092986711797535254

Tran, M., and Reddy, P. H. (2021). Defective autophagy and mitophagy in aging and Alzheimer's disease. *Front. Neurosci.* 14:612757. doi: 10.3389/fnins.2020.612757

Vasko, R., Ratliff, B. B., Bohr, S., Nadel, E., Chen, J., Xavier, S., et al. (2013). Endothelial peroxisomal dysfunction and impaired pexophagy promotes oxidative damage in lipopolysaccharide-induced acute kidney injury. *Antioxid. Redox Signal.* 19, 211–230. doi: 10.1089/ars.2012.4768

Wang, D., Shi, S. M., Zhang, Y. P., Guo, P., Wang, J. L., and Wang, W. Q. (2021). U0126 pretreatment inhibits cisplatin-induced apoptosis and autophagy in HEI-OC1 cells and cochlear hair cells. *Toxicol. Appl. Pharmacol.* 415:115447.

Warchol, M. E. (2010). Cellular mechanisms of aminoglycoside ototoxicity. *Curr. Opin. Otolaryngol. Head and Neck Surg.* 18, 454–458. doi: 10.1097/MOO.0b013e32833e05ec

Webber, L., and Tooze, S. A. (2010). New insights into the function of Atg9. *Febs Lett.* 584, 1319–1326. doi: 10.1016/j.febslet.2010.01.020

Wesselborg, S., and Stork, B. (2015). Autophagy signal transduction by ATG proteins: from hierarchies to networks. *Cell. Mol. Life Sci.* 72, 4721–4757. doi: 10.1007/s00018-015-2034-8

White, E. (2012). Deconvoluting the context-dependent role for autophagy in cancer. *Nat. Rev. Cancer* 12, 401–410. doi: 10.1038/nrc3262

WHO (2021). *Deafness and Hearing Loss*. Available online at: https://www.who.int/news-room/fact-sheets/detail/deafness-and-hearing-loss (accessed April 1, 2021).

Wu, F., Xiong, H., and Sha, S. H. (2020). Noise-induced loss of sensory hair cells is mediated by ROS/AMPK alpha pathway. *Redox Biol.* 29:101406.

Xie, Z. P., and Klionsky, D. J. (2007). Autophagosome formation: core machinery and adaptations. *Nat. Cell Biol.* 9, 1102–1109. doi: 10.1038/ncb1007-1102

Xu, L., Cheng, Y. J., and Yan, W. Y. (2021). Up-regulation of autophagy and apoptosis of cochlear hair cells in mouse models for deafness. *Arch. Med. Sci.* 17, 535–541.

Yang, Q. Q., Zhou, Y. W., Yin, H. Y., Li, H. R., Zhou, M. J., Sun, G. Y., et al. (2018b). PINK1 protects against gentamicin-induced sensory hair cell damage: possible relation to induction of autophagy and inhibition of p53 signal pathway. *Front. Mol. Neurosci.* 11:403. doi: 10.3389/fnmol.2018.00403

Yang, Q. Q., Sun, G. Y., Yin, H. Y., Li, H. R., Cao, Z. X., Wang, J. H., et al. (2018a). PINK1 protects auditory hair cells and spiral ganglion neurons from cisplatin-induced ototoxicity via inducing autophagy and inhibiting JNK signaling pathway. *Free Radic. Biol. Med.* 120, 342–355. doi: 10.1016/j.freeradbiomed.2018.02.025

Yang, R., Wang, L., and Zhu, L. (2019). Chaperone mediated autophagy. autophagy: biology and diseases. *Basic Sci.* 1206, 435–452. doi: 10.1007/978-981-15-0602-4_20

Ye, B., Fan, C., Shen, Y. L., Wang, Q., Hu, H. X., and Xiang, M. L. (2019a). The antioxidative role of autophagy in hearing loss. *Front. Neurosci.* 12:1010. doi: 10.3389/fnins.2018.01010

Ye, B., Wang, Q., Hu, H. X., Shen, Y. L., Fan, C., Chen, P. H., et al. (2019b). Restoring autophagic flux attenuates cochlear spiral ganglion neuron degeneration by promoting TFEB nuclear translocation via inhibiting

MTOR. *Autophagy* 15, 998–1016. doi: 10.1080/15548627.2019.1569926

Youn, C. K., Jun, Y., Jo, E. R., and Cho, S. I. (2020). Age related hearing loss in C57BL/6J mice is associated with mitophagy impairment in the central auditory system. *Int. J. Mol. Sci.* 21:7202.

Youn, C. K., Kim, J., Park, J. H., Do, N. Y., and Cho, S. I. (2015). Role of autophagy in cisplatin-induced ototoxicity. *Int. J. Pediatr. Otorhinolaryngol.* 79, 1814–1819. doi: 10.1016/j.ijporl.2015.08.012

Yuan, H., Wang, X. R., Hill, K., Chen, J., Lemasters, J., Yang, S. M., et al. (2015). Autophagy attenuates noise induced hearing loss by reducing oxidative stress. *Antioxid. Redox Signal.* 22, 1308–1324. doi: 10.1089/ars.2014.6004

Yuan, J., Zhao, X. Y., Hu, Y. J., Sun, H. Y., Gong, G. Q., Huang, X., et al. (2018). Autophagy regulates the degeneration of the auditory cortex through the AMPK-mTOR-ULK1 signaling pathway. *Int. J. Mol. Med.* 41, 2086–2098. doi: 10.3892/ijmm.2018.3393

Conflict of Interest: The authors declare that the research was conducted in the absence of any commercial or financial relationships that could be construed as a potential conflict of interest.

Publisher's Note: All claims expressed in this article are solely those of the authors and do not necessarily represent those of their affiliated organizations, or those of the publisher, the editors and the reviewers. Any product that may be evaluated in this article, or claim that may be made by its manufacturer, is not guaranteed or endorsed by the publisher.

frontiers in Cellular Neuroscience

REVIEW
published: 03 December 2021
doi: 10.3389/fncel.2021.791573

Nanocarriers for Inner Ear Disease Therapy

Xiaoxiang Xu[1,2†], Jianwei Zheng[3†], Yanze He[2†], Kun Lin[1], Shuang Li[1], Ya Zhang[1], Peng Song[1], Yuye Zhou[4,5] and Xiong Chen[1*]*

[1] Department of Otorhinolaryngology-Head and Neck Surgery, Zhongnan Hospital of Wuhan University, Wuhan, China, [2] Department of Otorhinolaryngology, Dawu County People's Hospital, Xiaogan, China, [3] Department of Biliary Pancreatic Surgery, Tongji Hospital, Tongji Medical College, Huazhong University of Science and Technology, Wuhan, China, [4] Division of Applied Physical Chemistry, Analytical Chemistry, Department of Chemistry, School of Engineering Sciences in Chemistry, Biotechnology and Health, Kungliga Tekniska Högskolan (KTH) Royal Institute of Technology, Stockholm, Sweden, [5] Key Laboratory of Applied Surface and Colloid Chemistry, Ministry of Education, School of Chemistry and Chemical Engineering, Shaanxi Normal University, Xi'an, China

Hearing loss is a common disease due to sensory loss caused by the diseases in the inner ear. The development of delivery systems for inner ear disease therapy is important to achieve high efficiency and reduce side effects. Currently, traditional drug delivery systems exhibit the potential to be used for inner ear disease therapy, but there are still some drawbacks. As nanotechnology is developing these years, one of the solutions is to develop nanoparticle-based delivery systems for inner ear disease therapy. Various nanoparticles, such as soft material and inorganic-based nanoparticles, have been designed, tested, and showed controlled delivery of drugs, improved targeting property to specific cells, and reduced systemic side effects. In this review, we summarized recent progress in nanocarriers for inner ear disease therapy. This review provides useful information on developing promising nanocarriers for the efficient treatment of inner ear diseases and for further clinical applications for inner ear disease therapy.

Keywords: nanocarrier, drug delivery system, inner ear disease therapy, soft material nanoparticle, inorganic nanoparticle

OPEN ACCESS

Edited by:
Hai Huang,
Tulane University, United States

Reviewed by:
Mingliang Tang,
Southeast University, China
Lei Xing,
China Pharmaceutical University, China
Jieyu Qi,
Southeast University, China

***Correspondence:**
Yuye Zhou
yuye@kth.se
Xiong Chen
zn_chenxiong@126.com

† These authors have contributed equally to this work

Specialty section:
This article was submitted to Cellular Neuropathology, a section of the journal Frontiers in Cellular Neuroscience

Received: *08 October 2021*
Accepted: *28 October 2021*
Published: *03 December 2021*

Citation:
Xu X, Zheng J, He Y, Lin K, Li S, Zhang Y, Song P, Zhou Y and Chen X (2021) Nanocarriers for Inner Ear Disease Therapy. Front. Cell. Neurosci. 15:791573. doi: 10.3389/fncel.2021.791573

INTRODUCTION

Hearing loss is a common disease due to sensory loss that affects human health and life. According to World Health Organization (WHO) data, about 250 million patients suffered from hearing loss in 2005. By 2050, over 5% of the people in the world will suffer from hearing loss (World Health Organization). The production of hearing begins with the collection of sound waves by the outer ear. Then, the sound is transmitted to the hair cells of the inner ear through the middle ear. The inner ear of mammals consists of the vestibule, the semicircular canals, and the cochlea, which is responsible for hearing (**Figure 1**). The environmental factors, such as excessive acoustic stimulation, aging, infection, autoimmune inner ear diseases, and application of ototoxic drugs, will cause hearing disfunction in the inner ear, directly or indirectly resulting in damage to the cochlear sensory cells and/or related peripheral neurons (Staecker et al., 2001; Ross et al., 2016; Schilder et al., 2019).

The ways to deliver drugs into the inner ear include systemic circulation, from which drugs enter the inner ear through the labyrinth artery, and the round window membrane (RWM). However, current administering drugs have drawbacks, such as disorders, limited labyrinth artery supply, and difficulty in accessing RWM. For example, anti-inflammatory drugs are widely used for inner ear

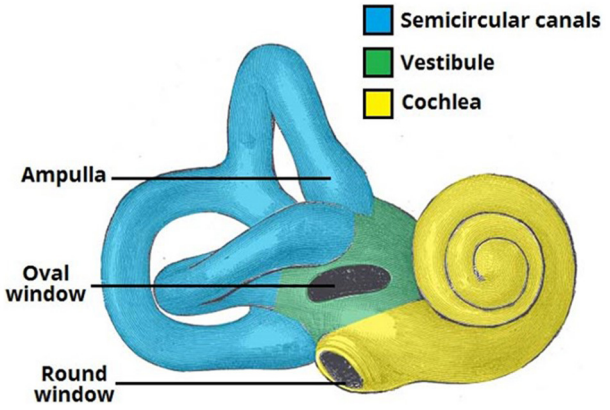

FIGURE 1 | Structure of the inner ear of humans.

disease therapy; however, the short half-time of drugs in the cochlea that causes rapid elimination is the main problem. Scientists have tried different delivery systems, such as systemic drug delivery systems, intratympanic drug delivery systems, and hydrogel delivery systems, to deliver drugs into the inner ear to treat various inner ear diseases, such as Meniere's disease, autoimmune inner ear disease, and sudden sensorineural hearing loss (SHL) (Havia et al., 2002; Salt, 2005; Nakashima et al., 2016; Rathnam et al., 2019). However, there are drawbacks for each system. It is urgent to develop a new delivery system for high efficiency of inner ear disease therapy, high stability of the drugs before they reach the target cells (outer hair cells as OHC and inner hair cells as IHC) in the inner ear, and the ability to target delivery to the inner ear. Very recently, nanoparticle-based drug delivery systems appeared and attracted the attention of many scientists. Although these systems provide opportunities to solve current problems, there are many things that are unclear and need further investigation. Therefore, a review to summarize recent developments and drawbacks of current nanocarriers for inner ear disease therapy is needed.

In this review, we will summarize the nanocarrier systems for inner ear disease therapy, such as systemic systems, intratympanic systems, hydrogel systems, and nanocarrier systems. Then, we will summarize the soft materials and inorganic nanoparticles that can be used for inner ear disease therapy. Finally, we will conclude the advantages and current challenges of nanocarriers for inner ear disease therapy. This review will provide useful information on nanocarrier drug delivery systems for inner ear disease therapy, and these drug delivery systems could also be further used for other diseases.

CURRENT DRUG DELIVERY SYSTEMS FOR INNER EAR DISEASE THERAPY

Delivery systems, including systemic drug delivery, intratympanic injection, hydrogel drug delivery, and nanocarrier drug delivery systems, have been used for inner ear disease therapy (Li et al., 2017; Kayyali et al., 2018; Hao and Li, 2019; Mittal et al., 2019; Rathnam et al., 2019; Gheorghe et al., 2021; Jaudoin et al., 2021). Among all current inner ear therapies, the intratympanic injection of liquid drugs is most widely used. Other delivery systems, such as hydrogel delivery systems and nanocarrier delivery systems, are also available. At present, we still need to overcome some barriers.

Systemic Drug Delivery

Inner ear diseases have been treated by systemic drug delivery systems via the oral route, intramuscular, or intravenous (Ruckenstein, 2004; Alexander et al., 2009; Buniel et al., 2009; McCall et al., 2010; Li et al., 2017). For example, corticosteroids are widely used to treat sudden SHL and have been found to be efficient with a recovery rate of 61%, which is much higher than using a placebo (recovery rate of 32%) demonstrated by Li and Ding (2020). Recently, it was reported that the recovery rates of SHL could reach up to 57–66% with oral corticosteroid (Filipo et al., 2014; Chen et al., 2015). But the limitations of these studies are the small number of patients and the relatively short term for investigation. A long-term course was found when treating autoimmune inner ear disease occurring over weeks to months (Buniel et al., 2009). Nevertheless, when using systemic administration, subtherapeutic local concentrations occur due to the limited blood supply in the inner ear and poor ability to cross the inner ear barrier. However, large doses lead to severe toxicities and undesirable side effects. For example, when aminoglycosides were used, they caused vestibulotoxicity and damage of cochlear, and SHL occurred due to high doses (Graham et al., 1984; Erol, 2007).

Intratympanic Drug Delivery

Intratympanic systems have also been widely used for inner ear disease therapy. The tympanic membrane is a thin membrane between the external and middle ear. For most of the substances, it is difficult to permeate the tympanic membrane, which is considered a barrier. However, the tympanic membrane is easy to be broken during injection of drugs into the middle ear. Taking steroids as an example, inner ear disease therapy was first treated by intratympanic delivery of steroids in the 1990s (Itoh and Sakata, 1991). At present, intratympanic delivery systems are used for the treatment of sudden sensorineural hearing loss (SHL), Meniere's disease, and vertigo (Chandrasekhar, 2001; Doyle et al., 2004). By using intratympanic delivery systems, the bony structure of the tympanic membrane could be prevented. Moreover, physical barriers, such as the round window membrane, and cellular barriers need to be overcome, when delivering drugs into the inner ear. Small molecules enter the inner ear through the RWM by passive diffusion, which will lead to different concentrations related to the location of the cochlea (Salt and Plontke, 2009). In addition, treatment efficacy during intratympanic injections for inner ear disease therapy will be strongly affected by the parameters, such as cone angle and depth of the tympanic membrane of the patients, and various biological, anatomical, and protocol effects (Volandri et al., 2011).

Hydrogel Delivery System

To overcome some drawbacks in intratympanic drug delivery systems, such as short residence time and difficulty in sustained release of drugs, hydrogel delivery systems, such as hydrophilic polymeric networks, have been developed for inner ear disease therapy. Chitosan-glycerophosphate hydrogel was developed for the first time to achieve sustained drug release and reduce the variation (Paulson et al., 2008). Chitosan-glycerophosphate hydrogel was a porous matrix and could be degraded by lysozymes to achieve the sustained release of drugs into the inner ear. This hydrogel delivery system showed a low risk of hearing loss and longer vestibular suppression (Xu et al., 2010). In hydrogel delivery systems, drugs are loaded in the hydrogel and located in a certain region, where the drugs can diffuse across the RWM and are released at meaningful concentrations (El Kechai et al., 2015). In contrast, hydrogels exhibit high viscosity and enable a higher residence time of drugs to reach equilibrium in the inner ear. Hydrogel systems could be designed by controlling the chemical composition of monomers and formed by both natural and synthetic products (Li and Mooney, 2016). Therefore, hydrogel delivery systems are potential for inner ear disease therapy due to good biocompatibility, easy functionality, high drug loading, and easy degradation (Ahmed, 2015).

NANOPARTICLE-BASED DRUG DELIVERY SYSTEMS FOR INNER EAR DISEASE THERAPY

Although the delivery systems mentioned earlier could deliver regulated drugs into the inner ear, they face problems for the delivery of new types of drugs, such as biomolecules. Compared to the regulated drugs, these new types of drugs are less stable within the extracellular compartments. Therefore, it is difficult to deliver new types of drugs to the targeted locations or cells in the inner ear using the delivery systems discussed earlier. Novel drug delivery systems that could overcome these drawbacks are highly demanded in the treatment of inner ear diseases. Recently, various types of nanoparticles, such as nanosized polymer, peptides, silicas, and metal-organic frameworks (MOFs), have been widely employed as drug delivery systems for different kinds of therapies, such as anticancer therapies, anti-inflammatory, and antibacterial therapies. These nanocarriers have a particle size in the nano range, and the particle size could be controlled during the synthesis. For efficient drug delivery, a particle size of $<$300 nm is usually required to avoid opsonization and elimination (Ulbrich et al., 2016). They also possess a tunable surface with modifiable physicochemical properties for different applications. The nanoparticle-based drug delivery systems could increase the solubility of the drugs, protect the drugs from degradation, prolong the half-life of the drugs during circulation, and allow low passage of the loaded drugs across physiological barriers. Furthermore, these nanocarriers could protect drug properties from degradation, increase the solubility of drugs, difficulty in crossing physiological barriers. Nanoparticle-based delivery systems could also deliver a sustained release of drugs and provide targeted delivery to certain cells. Therefore, nanoparticle-based delivery systems have a great potential for inner ear disease therapy. Nanocarriers for inner ear disease therapy will be discussed in detail in the following section.

Soft Material Nanoparticle-Based Delivery System

Among different nanocarrier delivery systems that can be used for inner ear disease therapy, soft materials, such as polymeric, liposome, micelles, and lipid nanoparticle-based delivery systems, are widely used to load different kinds of drugs (**Figure 2**; Lu et al., 2011). These soft material nanoparticle-based delivery systems could increase the half-life of drugs and achieve sustained or targeted release of drugs. As demonstrated by Food and Drug Administration (FDA), poly(lactic-*co*-glycolic acid) (PLGA) was a biodegradable polymer and can be easily functionalized for target delivery. When being conjugated with rhodamine, the rhodamine-conjugated PLGA nanoparticles were observed in the cochlea of guinea pigs and long-term residence in the liver due to tissue-specific barriers and fast degradation of PLGA nanoparticles (**Figure 3**; Palao-Suay et al., 2015; Cai et al., 2017; Szeto et al., 2019). Then, scientists tried to decrease the particle size of the nanocarriers to the range of 150–300 nm, which would enhance the entry of nanoparticles into the inner ear. Further functionalization of the surface with pluronic F127 (PEO_{106}-PPO_{70}-PEO_{106}) increased the accumulation of particles (Zou et al., 2010; Leso et al., 2019). PEGylated polymers could increase the half-life, biocompatibility, and solubility of the loaded drugs and decrease the side effects, as well as the immune reactions, to drugs (Veronese and Mero, 2008). The selected location of nanoparticles in the inner ear was also achieved by modifying the nanoparticles with chitosan, which changed the surface charge and hydrophilicity of the nanoparticles. These modifications could help nanoparticles reach the inner ear before endocytosis. Other types of polymeric nanoparticles, such as dendriplexes and chitosan-based nanoparticles, poly(L-lactic acid) (PLLA), PLLA-PEG, polycaprolactone (PCL), and polyethylene glycol (PEG), have also been used for inner ear disease therapy to encapsulate drugs via electrostatic interaction or hydrophobic-hydrophobic interaction (Dash et al., 2011; Wang et al., 2011; El Kechai et al., 2015; Lajud et al., 2015; Vigani et al., 2019).

Micelles and liposomes are formed by molecules with both hydrophobic and hydrophilic parts. Micelles have a hydrophobic environment inside micelles and enable the loading and delivery of hydrophobic drugs encapsulated inside, while the hydrophilic property of the outer surface of micelles increases their solubilization in aqueous solutions. Furthermore, micelle-based delivery systems could also protect unstable drugs from biological attacks during circulation. When liposome nanoparticles are used as delivery systems for inner ear disease therapy, both the external and internal surface of the liposome are hydrophilic with the same structure as the phospholipid bilayer (Panahi et al., 2017; Zylberberg et al., 2017). Amphiphilic liposomes can carry them across the RWM and deliver them into the cells (Uri et al., 2003; Meyer et al., 2012). Liposomes degrade readily in cells, resulting in low toxicity of liposomal drugs. Multifunctional liposome

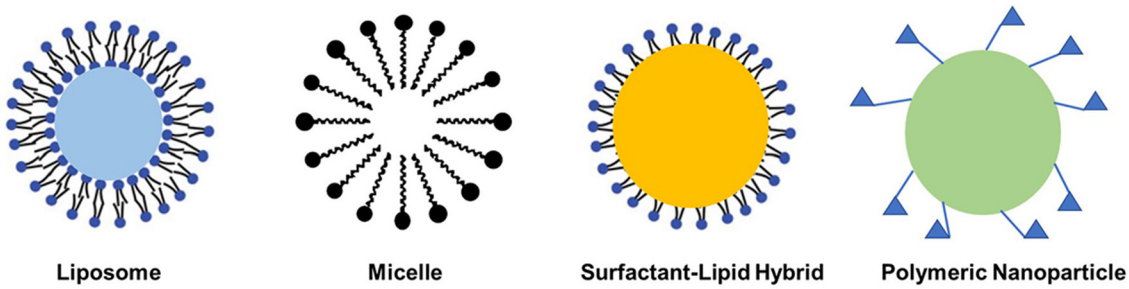

FIGURE 2 | Types of soft material nanoparticle-based delivery systems for inner ear drug delivery.

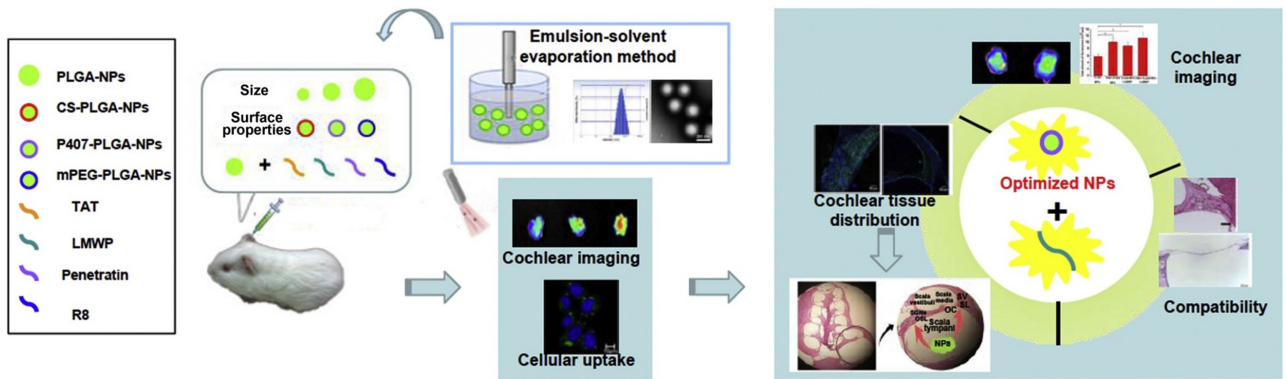

FIGURE 3 | Poly(lactic-*co*-glycolic acid) **(PLGA)** nano-based systems with cell-penetrating peptides for cochlear drug delivery. Reprinted with permission from Cai et al. (2017). Copyright 2017 Published by Elsevier B.V.

nanoparticles could be prepared by modifying the surface with polyethylene glycol, carbohydrates, and folic acid.

There are many other soft materials of nanometer size that could also be used for inner ear disease therapy. Cubosomes formed by a lipid core with a single lipid bilayer and a polymeric shell were very efficient for loading drugs (Barriga et al., 2019). Solid lipid nanoparticles and lipid nanocapsules have also been reported (Gao et al., 2015; Yang et al., 2018). Protein nanoparticles are another option to increase the delivery to the tissue and reduce the toxicity of compounds (Lohcharoenkal et al., 2014).

Inorganic Nanoparticle-Based Delivery System

Compared to soft materials, inorganic nanoparticle-based delivery systems are still in the developing stage. Inorganic nanoparticle-based delivery systems could provide unique properties, such as antimicrobial and magnetic properties (**Figure 4**). Although inorganic nanoparticles provide opportunities for inner ear disease therapy due to some useful qualities, there are many drawbacks, such as high price and limited biological stability.

Superparamagnetic Fe_3O_4 nanoparticles are a kind of inorganic material. These materials could pass the round window by magnetic force and arrive at the inner ear (Guigou et al., 2021). Superparamagnetic iron oxide nanoparticles are easy to synthesize and exhibit low toxicity and intrinsic antimicrobial activity for effective delivery systems (Rodrigues et al., 2019). Superparamagnetic iron oxide nanoparticles have no pores to encapsulate drug molecules, while in combination with polymers, such as PLGA and chitosan, superparamagnetic iron oxide nanoparticles could adsorb drugs via the electrostatic/hydrophobic interaction for inner ear drug delivery (Grumezescu et al., 2013; Sangaiya and Jayaprakash, 2018). Other metal-oxide-based nanoparticles have shown effective inner ear disease therapy-related infectious diseases. For example, TiO_2 nanoparticles are photosensitive and show activity against fungi and bacteria (Luksiene, 2017). Zinc oxide, copper oxide, calcium oxide, silver oxide, aluminum oxide, and zirconium oxide have also been widely investigated as carriers for biomedical applications (Narayanan et al., 2012; Karimiyan et al., 2015; Swaminathan and Sharma, 2019). However, the particle size of these metal oxides is still difficult to control, and the target delivery systems using these metal oxides are needed to be designed to specifically locate nanoparticles in the inner ear.

Porous nanoparticles, such as mesoporous silica nanoparticles, and MOF nanoparticles possess pores for the encapsulation of both hydrophobic and hydrophilic drugs. These materials are usually easy to prepare, have large pore

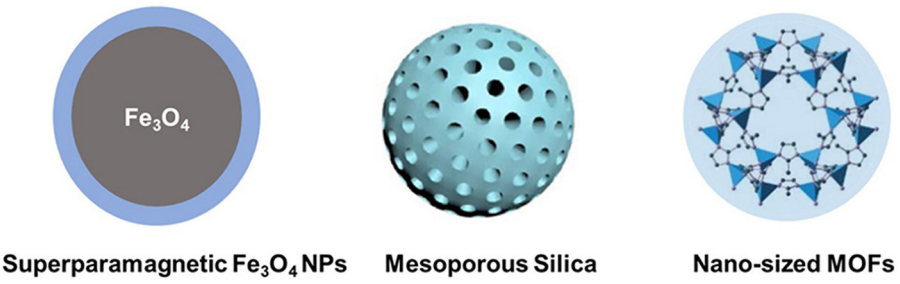

FIGURE 4 | Types of inorganic nanoparticle-based delivery systems for inner ear drug delivery.

volumes, and can be easily functionalized. Mesoporous silica nanoparticles are biocompatible and could slowly degrade under physiological conditions (Zheng et al., 2011, 2013; Bernardos et al., 2019). These materials can be used to construct "smart" delivery systems, which are sensitive to changes in the environment, including changes to the pH, thermal, and magnetic fields. Recently, mesoporous silica nanoparticles could be used to control the encapsulation and release of antibiotics (Selvarajan et al., 2020). Furthermore, the surface of porous silica nanoparticles could be functionalized to target the designed tissues and used for inner ear disease therapy (Tang et al., 2012). When loaded with a brain-derived neurotrophic factor, porous silica nanoparticles could target the spiral ganglion neurons and release drugs for a long time period (Schmidt et al., 2018). More recently, MOFs have been designed and studied for many applications, including biomedical applications (Zheng et al., 2016; Kaneti et al., 2017; Wu and Yang, 2017; Lu et al., 2018). Recently, Xu et al. (2020) encapsulated methylprednisolone (MP) in ZIF-90 nanoparticles for the treatment of inner ear disease for the first time. ZIF-90 prevents the degradation of drugs during circulation after intraperitoneal injection and delivers MP into the inner ear. These MOF nanoparticles exhibit good protection from noise, low damage to the inner ear structure, and low nephrotoxicity during therapy.

Metallic and metal oxide nanoparticles are one group of the most promising inorganic materials for inner ear disease therapy (Paladini et al., 2015). Silver (Ag) nanoparticles could interact with the surface of bacterial cells and break the cell membranes to achieve permeability (Hamad et al., 2020). Ag nanoparticles could enter the inner ear after intraperitoneal injection and break pathogens with antibiotic formulations, which could overcome the drawbacks and achieve high efficacy in the ear therapy (Muhsin and Hachim, 2014; Zou et al., 2015). Similar situation happens to gold (Au) nanoparticles, which are used for loading drugs and imaging applications. Au nanoparticles have shown potential to be used as inner ear contrast agents and are located in cochlear cells (Kayyali et al., 2017). However, at present, Ag and Au nanoparticles have not yet been used for inner ear disease therapy. Quantum dots, such as semiconductor nanocrystals, show unique optical properties and are considered another option (Liu et al., 2010). Due to their advantages of good biocompatibility, biodistribution, stability, and long half-life, metallic and metal oxide nanoparticles and their combinations with polymers and/or proteins are highly potential for inner ear disease therapy in the near future.

Targeting Modification of Nanoparticle-Based Delivery System

Nanoparticles could increase circulation time and prevent the degradation of drugs. Moreover, a specific surface modification could further enable the nanoparticle-based drug delivery systems with target properties to reach a specific type of cell, which is ideal for inner ear therapies to deliver the drugs to a specific type of inner ear cell. Ligands have a specific interaction with certain cells and, thus, could be used for cell-specific targeting of nanoparticles for inner ear disease therapy (Frutos et al., 2018; Valero et al., 2018). For example, in an *in vitro* model prepared from the mouse cochleae, peptide-based nanoparticles could interact with spiral ganglion cells through tyrosine kinase and p75 neurotrophin receptors (Roy et al., 2010). Cy3-labeled silica nanoparticles were demonstrated to be located within the inner ear of RWM of mice compared to the control group of mice (Praetorius et al., 2007). Cy3-labeled silica nanoparticles could also reach central auditory nuclei and superior olive through retrograde axon transport. To target OHCs, prestin was connected to peptides and coupled to nanoparticles. The cellular uptake of these nanoparticles in the OHCs of rat cochleae was achieved (Surovtseva et al., 2012). Using a similar method, nanoparticles were found to be taken up by OHCs *in vivo* (Wang et al., 2018). Using this method, the nanoparticles were located into designed cells, and the uptake efficiency could also be improved.

Moreover, a deep understanding of a suitable ligand for targeting delivery is needed. The interaction between ligand-loaded nanoparticles, and the receptor in the inner ear should be further investigated. The targeting delivery system is also interesting and with high potential to be developed for inner ear disease therapy (Li et al., 2017).

CONCLUSION AND PROSPECTS

In this review, we summarized the currently used systems for inner ear disease therapy, including the most widely used delivery systems (i.e., systemic, intratympanic, and hydrogel delivery systems) and nanotechnology-based systems. To overcome the barriers of these systems in overcoming barriers in the inner

ear, nanoparticle-based drug delivery systems, which have shown many advantages in the treatment of various diseases, have gained increasing attention in inner ear diseases during the past years. Several soft materials and inorganic-based nanoparticles have been investigated and shown to improve the efficiency of drugs, enhance antimicrobial performance, and reduce the side effects of inner ear disease therapy. Nanoparticles could cross the barrier in the inner ear, deliver drugs into the inner ear with low side effects, and remain harmless for healthy tissues. Furthermore, we discussed the targeting drug delivery systems using nanoparticles by modifying the surface with ligands, proteins, and so on. Developing multifunctional nanoparticles that could target specific cells and release drugs in a controlled manner is the way for the future.

Although nanocarriers have been used for inner ear disease therapy, there are still many works that need to be carried out in the future. First, the information on the interaction between nanoparticles and ear toxicity, such as effects on organs, is still unclear. The long-term investigation of health effects could be studied in the future. Second, the critical physicochemical characteristics that affect their biodistribution and the way to overcome physical and cellular barriers are not well-defined. The rational design of nanoparticles to achieve target delivery to the inner ear needs more effort. In summary, nanoparticle-based delivery systems have brought potential solutions and paved a novel way for inner ear disease therapy, but it still has a long way to go for real clinical applications.

AUTHOR CONTRIBUTIONS

XX, JZ, YH, KL, SL, YZha, PS, YZho, and XC prepared this manuscript. YZho and XC guided all aspects of this work. All authors contributed to the article and approved the submitted version.

FUNDING

This work was supported by Swedish Research Council (2021-00295).

REFERENCES

Ahmed, E. M. (2015). Hydrogel: preparation, characterization, and applications: a review. *J. Adv. Res.* 6, 105–121. doi: 10.1016/j.jare.2013.07.006

Alexander, T. H., Weisman, M. H., Derebery, J. M., Espeland, M. A., Gantz, B. J., Gulya, A. J., et al. (2009). Safety of high-dose corticosteroids for the treatment of autoimmune inner ear disease. *Otol. Neurotol.* 30, 443–448. doi: 10.1097/MAO.0b013e3181a52773

Barriga, H. M. G., Holme, M. N., and Stevens, M. M. (2019). Cubosomes: the next generation of smart lipid nanoparticles? *Angew. Chem. Int. Ed.* 58, 2958–2978. doi: 10.1002/anie.201804067

Bernardos, A., Piacenza, E., Sancenón, F., Hamidi, M., Maleki, A., Turner, R. J., et al. (2019). Mesoporous silica-based materials with bactericidal properties. *Small* 15:1900669. doi: 10.1002/smll.201900669

Buniel, M. C., Geelan-Hansen, K., Weber, P. C., and Tuohy, V. K. (2009). Immunosuppressive therapy for autoimmune inner ear disease. *Immunotherapy* 1, 425–434. doi: 10.2217/imt.09.12

Cai, H., Liang, Z., Huang, W., Wen, L., and Chen, G. (2017). Engineering PLGA nano-based systems through understanding the influence of nanoparticle properties and cell-penetrating peptides for cochlear drug delivery. *Int. J. Pharm.* 532, 55–65. doi: 10.1016/j.ijpharm.2017.08.084

Chandrasekhar, S. S. (2001). Intratympanic dexamethasone for sudden sensorineural hearing loss: clinical and laboratory evaluation. *Otol. Neurotol.* 22, 18–23. doi: 10.1097/00129492-200101000-00005

Chen, W. T., Lee, J. W., Yuan, C. H., and Chen, R. F. (2015). Oral steroid treatment for idiopathic sudden sensorineural hearing loss. *Saudi Med. J.* 36, 291–296. doi: 10.15537/smj.2015.3.9940

Dash, M., Chiellini, F., Ottenbrite, R. M., and Chiellini, E. (2011). Chitosan—a versatile semi-synthetic polymer in biomedical applications. *Prog. Polym. Sci.* 36, 981–1014. doi: 10.1016/j.progpolymsci.2011.02.001

Doyle, K. J., Bauch, C., Battista, R., Beatty, C., Hughes, G. B., Mason, J., et al. (2004). Intratympanic steroid treatment: a review. *Otol. Neurotol.* 25, 1034–1039. doi: 10.1097/00129492-200411000-00031

El Kechai, N., Agnely, F., Mamelle, E., Nguyen, Y., Ferrary, E., and Bochot, A. (2015). Recent advances in local drug delivery to the inner ear. *Int. J. Pharm.* 494, 83–101. doi: 10.1016/j.ijpharm.2015.08.015

Erol, S. (2007). Aminoglycoside-induced ototoxicity. *Curr. Pharm. Des.* 13, 119–126. doi: 10.2174/138161207779313731

Filipo, R., Attanasio, G., Russo, F. Y., Cartocci, G., Musacchio, A., De Carlo, A., et al. (2014). Oral versus short-term intratympanic prednisolone therapy for idiopathic sudden hearing loss. *Audiol. Neurotol.* 19, 225–233. doi: 10.1159/000360069

Frutos, S., Hernández, J. L., Otero, A., Calvis, C., Adan, J., Mitjans, F., et al. (2018). Site-specific antibody drug conjugates using streamlined expressed protein ligation. *Bioconjugate Chem.* 29, 3503–3508. doi: 10.1021/acs.bioconjchem.8b00630

Gao, G., Liu, Y., Zhou, C.-H., Jiang, P., and Sun, J.-J. (2015). Solid lipid nanoparticles loaded with edaravone for inner ear protection after noise exposure. *Chin. Med. J.* 128, 203–209. doi: 10.4103/0366-6999.149202

Gheorghe, D. C., Niculescu, A.-G., Bîrcă, A. C., and Grumezescu, A. M. (2021). Nanoparticles for the treatment of inner ear infections. *Nanomaterials* 11:1311. doi: 10.3390/nano11051311

Graham, M. D., Sataloff, R. T., and Kemink, J. L. (1984). Titration streptomycin therapy for bilateral Meniere's disease: a preliminary report. *Otolaryngol. Head Neck Surg.* 92, 440–447. doi: 10.1177/019459988409200413

Grumezescu, A. M., Andronescu, E., Holban, A. M., Ficai, A., Ficai, D., Voicu, G., et al. (2013). Water dispersible cross-linked magnetic chitosan beads for increasing the antimicrobial efficiency of aminoglycoside antibiotics. *Int. J. Pharm.* 454, 233–240. doi: 10.1016/j.ijpharm.2013.06.054

Guigou, C., Lalande, A., Millot, N., Belharet, K., and Bozorg Grayeli, A. (2021). Use of super paramagnetic iron oxide nanoparticles as drug carriers in brain and ear: state of the art and challenges. *Brain Sci.* 11:358. doi: 10.3390/brainsci11030358

Hamad, A., Khashan, K. S., and Hadi, A. (2020). Silver nanoparticles and silver ions as potential antibacterial agents. *J. Inorg. Organomet. Polym. Mater.* 30, 4811–4828. doi: 10.1007/s10904-020-01744-x

Hao, J., and Li, S. K. (2019). Inner ear drug delivery: recent advances, challenges, and perspective. *Eur. J. Pharm. Sci.* 126, 82–92. doi: 10.1016/j.ejps.2018.05.020

Havia, M., Kentala, E., and Pyykkö, I. (2002). Hearing loss and tinnitus in Meniere's disease. *Auris Nasus Larynx* 29, 115–119. doi: 10.1016/S0385-8146(01)00142-0

Itoh, A., and Sakata, E. (1991). Treatment of vestibular disorders. *Acta Otolaryngol.* 111, 617–623. doi: 10.3109/00016489109131486

Jaudoin, C., Agnely, F., Nguyen, Y., Ferrary, E., and Bochot, A. (2021). Nanocarriers for drug delivery to the inner ear: physicochemical key parameters, biodistribution, safety and efficacy. *Int. J. Pharm.* 592:120038. doi: 10.1016/j.ijpharm.2020.120038

Kaneti, Y. V., Dutta, S., Hossain, M. S. A., Shiddiky, M. J. A., Tung, K.-L., Shieh, F.-K., et al. (2017). Strategies for improving the functionality of zeolitic imidazolate frameworks: tailoring nanoarchitectures for functional applications. *Adv. Mater.* 29:1700213. doi: 10.1002/adma.201700213

Karimiyan, A., Najafzadeh, H., Ghorbanpour, M., and Hekmati-Moghaddam, S. H. (2015). Antifungal effect of magnesium oxide, zinc oxide, silicon oxide and copper oxide nanoparticles against *Candida albicans*. *Zahedan J. Res. Med. Sci.* 17:e2179. doi: 10.17795/zjrms-2179

Kayyali, M. N., Brake, L., Ramsey, A. J., Wright, A. C., O'Malley, B. W., and Li, D. D. (2017). A novel nano-approach for targeted inner ear imaging. *J. Nanomed. Nanotechnol.* 8:456. doi: 10.4172/2157-7439.1000456

Kayyali, M. N., Wooltorton, J. R. A., Ramsey, A. J., Lin, M., Chao, T. N., Tsourkas, A., et al. (2018). A novel nanoparticle delivery system for targeted therapy of noise-induced hearing loss. *J. Controlled Release* 279, 243–250. doi: 10.1016/j.jconrel.2018.04.028

Lajud, S. A., Nagda, D. A., Qiao, P., Tanaka, N., Civantos, A., Gu, R., et al. (2015). A novel chitosan-hydrogel-based nanoparticle delivery system for local inner ear application. *Otol. Neurotol.* 36, 341–347. doi: 10.1097/MAO.0000000000000445

Leso, V., Fontana, L., Ercolano, M. L., Romano, R., and Iavicoli, I. (2019). Opportunities and challenging issues of nanomaterials in otological fields: an occupational health perspective. *Nanomedicine* 14, 2613–2629. doi: 10.2217/nnm-2019-0114

Li, J., and Ding, L. (2020). Effectiveness of steroid treatment for sudden sensorineural hearing loss: a meta-analysis of randomized controlled trials. *Ann. Pharmacother.* 54, 949–957. doi: 10.1177/1060028020908067

Li, J., and Mooney, D. J. (2016). Designing hydrogels for controlled drug delivery. *Nat. Rev. Mater.* 1:16071. doi: 10.1038/natrevmats.2016.71

Li, L., Chao, T., Brant, J., O'Malley, B., Tsourkas, A., and Li, D. (2017). Advances in nano-based inner ear delivery systems for the treatment of sensorineural hearing loss. *Adv. Drug Del. Rev.* 108, 2–12. doi: 10.1016/j.addr.2016.01.004

Liu, J., Lau, S. K., Varma, V. A., Moffitt, R. A., Caldwell, M., Liu, T., et al. (2010). Molecular mapping of tumor heterogeneity on clinical tissue specimens with multiplexed quantum dots. *ACS Nano* 4, 2755–2765. doi: 10.1021/nn100213v

Lohcharoenkal, W., Wang, L., Chen, Y. C., and Rojanasakul, Y. (2014). Protein nanoparticles as drug delivery carriers for cancer therapy. *Biomed Res. Int.* 2014:180549. doi: 10.1155/2014/180549

Lu, K., Aung, T., Guo, N., Weichselbaum, R., and Lin, W. (2018). Nanoscale metal–organic frameworks for therapeutic, imaging, and sensing applications. *Adv. Mater.* 30:1707634. doi: 10.1002/adma.201707634

Lu, X.-Y., Wu, D.-C., Li, Z.-J., and Chen, G.-Q. (2011). "Chpater 7: Polymer nanoparticles," in *Progress in Molecular Biology and Translational Science, Vol. 104*, ed A. Villaverde (Academic Press), 299–323. doi: 10.1016/B978-0-12-416020-0.00007-3

Luksiene, Z. (2017). "Chpater 16: Nanoparticles and their potential application as antimicrobials in the food industry," in *Food Preservation,* ed A. M. Grumezescu (Academic Press), 567–601. doi: 10.1016/B978-0-12-804303-5.00016-X

McCall, A. A., Swan, E. E. L., Borenstein, J. T., Sewell, W. F., Kujawa, S. G., and McKenna, M. J. (2010). Drug delivery for treatment of inner ear disease: current state of knowledge. *Ear Hear.* 31, 156–165. doi: 10.1097/AUD.0b013e3181c351f2

Meyer, H., Stöver, T., Fouchet, F., Bastiat, G., Saulnier, P., Bäumer, W., et al. (2012). Lipidic nanocapsule drug delivery: neuronal protection for cochlear implant optimization. *Int. J. Nanomedicine* 7, 2449–2464. doi: 10.2147/IJN.S29712

Mittal, R., Pena, S. A., Zhu, A., Eshraghi, N., Fesharaki, A., Horesh, E. J., et al. (2019). Nanoparticle-based drug delivery in the inner ear: current challenges, limitations and opportunities. *Artif. Cell. Nanomed. B* 47, 1312–1320. doi: 10.1080/21691401.2019.1573182

Muhsin, T. M., and Hachim, A. K. (2014). Mycosynthesis and characterization of silver nanoparticles and their activity against some human pathogenic bacteria. *World J. Microbiol. Biotechnol.* 30, 2081–2090. doi: 10.1007/s11274-014-1634-z

Nakashima, T., Pyykkö, I., Arroll, M. A., Casselbrant, M. L., Foster, C. A., Manzoor, N. F., et al. (2016). Meniere's disease. *Nat. Rev. Dis. Primers* 2:16028. doi: 10.1038/nrdp.2016.28

Narayanan, P. M., Wilson, W. S., Abraham, A. T., and Sevanan, M. (2012). Synthesis, characterization, and antimicrobial activity of zinc oxide nanoparticles against human pathogens. *BioNanoScience* 2, 329–335. doi: 10.1007/s12668-012-0061-6

Paladini, F., Pollini, M., Sannino, A., and Ambrosio, L. (2015). Metal-based antibacterial substrates for biomedical applications. *Biomacromolecules* 16, 1873–1885. doi: 10.1021/acs.biomac.5b00773

Palao-Suay, R., Aguilar, M. R., Parra-Ruiz, F. J., Fernández-Gutiérrez, M., Parra, J., Sánchez-Rodríguez, C., et al. (2015). Anticancer and antiangiogenic activity of surfactant-free nanoparticles based on self-assembled polymeric derivatives of vitamin E: structure–activity relationship. *Biomacromolecules* 16, 1566–1581. doi: 10.1021/acs.biomac.5b00130

Panahi, Y., Farshbaf, M., Mohammadhosseini, M., Mirahadi, M., Khalilov, R., Saghfi, S., et al. (2017). Recent advances on liposomal nanoparticles: synthesis, characterization and biomedical applications. *Artif. Cell. Nanomed. B* 45, 788–799. doi: 10.1080/21691401.2017.1282496

Paulson, D. P., Abuzeid, W., Jiang, H., Oe, T., O'Malley, B. W., and Li, D. (2008). A novel controlled local drug delivery system for inner ear disease. *Laryngoscope* 118, 706–711. doi: 10.1097/MLG.0b013e31815f8e41

Praetorius, M., Brunner, C., Lehnert, B., Klingmann, C., Schmidt, H., Staecker, H., et al. (2007). Transsynaptic delivery of nanoparticles to the central auditory nervous system. *Acta Otolaryngol.* 127, 486–490. doi: 10.1080/00016480600895102

Rathnam, C., Chueng, S.-T. D., Ying, Y.-L. M., Lee, K.-B., and Kwan, K. (2019). Developments in bio-inspired nanomaterials for therapeutic delivery to treat hearing loss. *Front. Cell. Neurosci.* 13:493. doi: 10.3389/fncel.2019.00493

Rodrigues, G. R., López-Abarrategui, C., de la Serna Gómez, I., Dias, S. C., Otero-González, A. J., and Franco, O. L. (2019). Antimicrobial magnetic nanoparticles based-therapies for controlling infectious diseases. *Int. J. Pharm.* 555, 356–367. doi: 10.1016/j.ijpharm.2018.11.043

Ross, A. M., Rahmani, S., Prieskorn, D. M., Dishman, A. F., Miller, J. M., Lahann, J., et al. (2016). Persistence, distribution, and impact of distinctly segmented microparticles on cochlear health following *in vivo* infusion. *J. Biomed. Mater. Res. A* 104, 1510–1522. doi: 10.1002/jbm.a.35675

Roy, S., Johnston, A. H., Newman, T. A., Glueckert, R., Dudas, J., Bitsche, M., et al. (2010). Cell-specific targeting in the mouse inner ear using nanoparticles conjugated with a neurotrophin-derived peptide ligand: potential tool for drug delivery. *Int. J. Pharm.* 390, 214–224. doi: 10.1016/j.ijpharm.2010.02.003

Ruckenstein, M. J. (2004). Autoimmune inner ear disease. *Curr. Opin. Otolaryngol. Head Neck Surg.* 12, 426–430. doi: 10.1097/01.moo.0000136101.95662.aa

Salt, A. N. (2005). Pharmacokinetics of drug entry into cochlear fluids. *Volta Rev.* 105, 277–298.

Salt, A. N., and Plontke, S. K. (2009). Principles of local drug delivery to the inner ear. *Audiol. Neurootol.* 14, 350–360. doi: 10.1159/000241892

Sangaiya, P., and Jayaprakash, R. (2018). A review on iron oxide nanoparticles and their biomedical applications. *J. Supercond. Nov. Magn.* 31, 3397–3413. doi: 10.1007/s10948-018-4841-2

Schilder, A. G. M., Su, M. P., Blackshaw, H., Lustig, L., Staecker, H., Lenarz, T., et al. (2019). Hearing protection, restoration, and regeneration: an overview of emerging therapeutics for inner ear and central hearing disorders. *Otol. Neurotol.* 40, 559–570. doi: 10.1097/MAO.0000000000002194

Schmidt, N., Schulze, J., Warwas, D. P., Ehlert, N., Lenarz, T., Warnecke, A., et al. (2018). Long-term delivery of brain-derived neurotrophic factor (BDNF) from nanoporous silica nanoparticles improves the survival of spiral ganglion neurons *in vitro*. *PLoS ONE* 13:e0194778. doi: 10.1371/journal.pone.0194778

Selvarajan, V., Obuobi, S., and Ee, P. L. R. (2020). Silica nanoparticles—a versatile tool for the treatment of bacterial infections. *Front. Chem.* 8:602. doi: 10.3389/fchem.2020.00602

Staecker, H., Li, D., O'Malley, B. W. Jr., and Van De Water, T. R. (2001). Gene expression in the mammalian cochlea: a study of multiple vector systems. *Acta Otolaryngol.* 121, 157–163. doi: 10.1080/000164801300043307

Surovtseva, E. V., Johnston, A. H., Zhang, W., Zhang, Y., Kim, A., Murakoshi, M., et al. (2012). Prestin binding peptides as ligands for targeted polymersome mediated drug delivery to outer hair cells in the inner ear. *Int. J. Pharm.* 424, 121–127. doi: 10.1016/j.ijpharm.2011.12.042

Swaminathan, M., and Sharma, N. K. (2019). "Antimicrobial activity of the engineered nanoparticles used as coating agents," in *Handbook of Ecomaterials,* eds L. M. T. Martínez, O. V. Kharissova, and B. I. Kharisov (Cham: Springer International Publishing), 549–563. doi: 10.1007/978-3-319-68255-6_1

Szeto, B., Chiang, H., Valentini, C., Yu, M., Kysar, J. W., and Lalwani, A. K. (2019). Inner ear delivery: challenges and opportunities. *Laryngoscope Investig. Otolaryngol.* 5, 122–131. doi: 10.1002/lio2.336

Tang, F., Li, L., and Chen, D. (2012). Mesoporous silica nanoparticles: synthesis, biocompatibility and drug delivery. *Adv. Mater.* 24, 1504–1534. doi: 10.1002/adma.201104763

Ulbrich, K., Holá, K., Šubr, V., Bakandritsos, A., Tuček, J., and Zboril, R. (2016). Targeted drug delivery with polymers and magnetic nanoparticles: covalent and

noncovalent approaches, release control, and clinical studies. *Chem. Rev*. 116, 5338–5431. doi: 10.1021/acs.chemrev.5b00589

Uri, N., Doweck, I., Cohen-Kerem, R., and Greenberg, E. (2003). Acyclovir in the treatment of idiopathic sudden sensorineural hearing loss. *Otolaryngol. Head Neck Surg*. 128, 544–549. doi: 10.1016/S0194-5998(03)00004-4

Valero, T., Delgado-González, A., Unciti-Broceta, J. D., Cano-Cortés, V., Pérez-López, A. M., Unciti-Broceta, A., et al. (2018). Drug "clicking" on cell-penetrating fluorescent nanoparticles for in cellulo chemical proteomics. *Bioconjugate Chem*. 29, 3154–3160. doi: 10.1021/acs.bioconjchem.8b00481

Veronese, F. M., and Mero, A. (2008). The impact of PEGylation on biological therapies. *Biodrugs* 22, 315–329. doi: 10.2165/00063030-200822050-00004

Vigani, B., Rossi, S., Sandri, G., Bonferoni, M. C., Caramella, C. M., and Ferrari, F. (2019). Hyaluronic acid and chitosan-based nanosystems: a new dressing generation for wound care. *Expert Opin. Drug Deliv*. 16, 715–740. doi: 10.1080/17425247.2019.1634051

Volandri, G., Di Puccio, F., Forte, P., and Carmignani, C. (2011). Biomechanics of the tympanic membrane. *J. Biomech*. 44, 1219–1236. doi: 10.1016/j.jbiomech.2010.12.023

Wang, H., Shi, H.-B., and Yin, S.-K. (2011). Polyamidoamine dendrimers as gene delivery carriers in the inner ear: how to improve transfection efficiency. *Exp. Ther. Med*. 2, 777–781. doi: 10.3892/etm.2011.296

Wang, X., Chen, Y., Tao, Y., Gao, Y., Yu, D., and Wu, H. (2018). A666-conjugated nanoparticles target prestin of outer hair cells preventing cisplatin-induced hearing loss. *Int. J. Nanomedicine* 13, 7517–7531. doi: 10.2147/IJN.S170130

World Health Organization. Available online at: https://www.who.int/news-room/fact-sheets/detail/deafness-and-hearing-loss (accessed April 1, 2021).

Wu, M.-X., and Yang, Y.-W. (2017). Metal–organic framework (MOF)-based drug/cargo delivery and cancer therapy. *Adv. Mater*. 29:1606134. doi: 10.1002/adma.201606134

Xu, L., Heldrich, J., Wang, H., Yamashita, T., Miyamoto, S., Li, A., et al. (2010). A controlled and sustained local gentamicin delivery system for inner ear applications. *Otol. Neurotol*. 31, 1115–1121. doi: 10.1097/MAO.0b013e3181eb32d1

Xu, X., Lin, K., Wang, Y., Xu, K., Sun, Y., Yang, X., et al. (2020). A metal–organic framework based inner ear delivery system for the treatment of noise-induced hearing loss. *Nanoscale* 12, 16359–16365. doi: 10.1039/D0NR04860G

Yang, K.-J., Son, J., Jung, S. Y., Yi, G., Yoo, J., Kim, D.-K., et al. (2018). Optimized phospholipid-based nanoparticles for inner ear drug delivery and therapy. *Biomaterials* 171, 133–143. doi: 10.1016/j.biomaterials.2018.04.038

Zheng, H., Gao, C., Peng, B., Shu, M., and Che, S. (2011). pH-responsive drug delivery system based on coordination bonding in a mesostructured surfactant/silica hybrid. *J. Phys. Chem. C* 115, 7230–7237. doi: 10.1021/jp110808f

Zheng, H., Xing, L., Cao, Y., and Che, S. (2013). Coordination bonding based pH-responsive drug delivery systems. *Coord. Chem. Rev*. 257, 1933–1944. doi: 10.1016/j.ccr.2013.03.007

Zheng, H., Zhang, Y., Liu, L., Wan, W., Guo, P., Nyström, A. M., et al. (2016). One-pot synthesis of metal–organic frameworks with encapsulated target molecules and their applications for controlled drug delivery. *J. Am. Chem. Soc*. 138, 962–968. doi: 10.1021/jacs.5b11720

Zou, J., Hannula, M., Misra, S., Feng, H., Labrador, R. H., Aula, A. S., et al. (2015). Micro CT visualization of silver nanoparticles in the middle and inner ear of rat and transportation pathway after transtympanic injection. *J. Nanobiotechnol*. 13:5. doi: 10.1186/s12951-015-0065-9

Zou, J., Zhang, W., Poe, D., Qin, J., Fornara, A., Zhang, Y., et al. (2010). MRI manifestation of novel superparamagnetic iron oxide nanoparticles in the rat inner ear. *Nanomedicine* 5, 739–754. doi: 10.2217/nnm.10.45

Zylberberg, C., Gaskill, K., Pasley, S., and Matosevic, S. (2017). Engineering liposomal nanoparticles for targeted gene therapy. *Gene Ther*. 24, 441–452. doi: 10.1038/gt.2017.41

Conflict of Interest: The authors declare that the research was conducted in the absence of any commercial or financial relationships that could be construed as a potential conflict of interest.

Publisher's Note: All claims expressed in this article are solely those of the authors and do not necessarily represent those of their affiliated organizations, or those of the publisher, the editors and the reviewers. Any product that may be evaluated in this article, or claim that may be made by its manufacturer, is not guaranteed or endorsed by the publisher.

frontiers in Cellular Neuroscience

ORIGINAL RESEARCH
published: 15 December 2021
doi: 10.3389/fncel.2021.804345

Disruption of *Hars2* in Cochlear Hair Cells Causes Progressive Mitochondrial Dysfunction and Hearing Loss in Mice

Pengcheng Xu[1,2,3†], Longhao Wang[1,2,3†], Hu Peng[4], Huihui Liu[1,2,3], Hongchao Liu[1,2,3], Qingyue Yuan[1,2,3], Yun Lin[1,2,3], Jun Xu[1,2,3], Xiuhong Pang[5], Hao Wu[1,2,3*] and Tao Yang[1,2,3*]*

[1] Department of Otolaryngology-Head and Neck Surgery, Shanghai Ninth People's Hospital, Shanghai Jiao Tong University School of Medicine, Shanghai, China, [2] Ear Institute, Shanghai Jiao Tong University School of Medicine, Shanghai, China, [3] Shanghai Key Laboratory of Translational Medicine on Ear and Nose Diseases, Shanghai, China, [4] Department of Otolaryngology-Head and Neck Surgery, Changzheng Hospital, Second Military Medical University, Shanghai, China, [5] Department of Otolaryngology-Head and Neck Surgery, Taizhou People's Hospital, The Fifth Affiliated Hospital of Nantong University, Taizhou, China

OPEN ACCESS

Edited by:
Wei-Jia Kong,
Huazhong University of Science and Technology, China

Reviewed by:
Renjie Chai,
Southeast University, China
Guoqiang Wan,
Nanjing University, China
Ke Liu,
Capital Medical University, China

***Correspondence:**
Tao Yang
yangtfxl@sina.com
Hao Wu
wuhao@shsmu.edu.cn
Xiuhong Pang
pxhzxy@163.com

[†]These authors have contributed equally to this work

Specialty section:
This article was submitted to Cellular Neuropathology, a section of the journal Frontiers in Cellular Neuroscience

Received: *29 October 2021*
Accepted: *29 November 2021*
Published: *15 December 2021*

Citation:
Xu P, Wang L, Peng H, Liu H, Liu H, Yuan Q, Lin Y, Xu J, Pang X, Wu H and Yang T (2021) Disruption of Hars2 in Cochlear Hair Cells Causes Progressive Mitochondrial Dysfunction and Hearing Loss in Mice. Front. Cell. Neurosci. 15:804345. doi: 10.3389/fncel.2021.804345

Mutations in a number of genes encoding mitochondrial aminoacyl-tRNA synthetases lead to non-syndromic and/or syndromic sensorineural hearing loss in humans, while their cellular and physiological pathology in cochlea has rarely been investigated *in vivo*. In this study, we showed that histidyl-tRNA synthetase HARS2, whose deficiency is associated with Perrault syndrome 2 (PRLTS2), is robustly expressed in postnatal mouse cochlea including the outer and inner hair cells. Targeted knockout of *Hars2* in mouse hair cells resulted in delayed onset (P30), rapidly progressive hearing loss similar to the PRLTS2 hearing phenotype. Significant hair cell loss was observed starting from P45 following elevated reactive oxygen species (ROS) level and activated mitochondrial apoptotic pathway. Despite of normal ribbon synapse formation, whole-cell patch clamp of the inner hair cells revealed reduced calcium influx and compromised sustained synaptic exocytosis prior to the hair cell loss at P30, consistent with the decreased supra-threshold wave I amplitudes of the auditory brainstem response. Starting from P14, increasing proportion of morphologically abnormal mitochondria was observed by transmission electron microscope, exhibiting swelling, deformation, loss of cristae and emergence of large intrinsic vacuoles that are associated with mitochondrial dysfunction. Though the mitochondrial abnormalities are more prominent in inner hair cells, it is the outer hair cells suffering more severe cell loss. Taken together, our results suggest that conditional knockout of *Hars2* in mouse cochlear hair cells leads to accumulating mitochondrial dysfunction and ROS stress, triggers progressive hearing loss highlighted by hair cell synaptopathy and apoptosis, and is differentially perceived by inner and outer hair cells.

Keywords: *HARS2*, mitochondrial, apoptosis, hair cells, hearing loss

INTRODUCTION

Hearing loss is the most common sensory disorder affecting approximately 6.1% of the world population (Davis and Hoffman, 2019), which can be caused by excessive noise exposure (Guo L. et al., 2021), ototoxic drugs (He et al., 2017; Li et al., 2018; Liu et al., 2019c, 2021; Zhong et al., 2020), aging (Cheng et al., 2019; Zhou et al., 2020; He et al., 2021), genetic factors (Qian et al., 2020;

Cheng et al., 2021; Fu et al., 2021a; Lv et al., 2021; Zhang S. et al., 2021), and infections (Han et al., 2020; He et al., 2020; Zhang Y. et al., 2021). To date, more than 100 genes have been identified associating with genetic hearing loss (Hereditary Hearing Loss Homepage; https://hereditaryhearingloss.org/, updated in September 2021), which contribute to more than 50% of congenital hearing loss as well as a significant portion of pediatric-onset hearing loss (Sheffield and Smith, 2019). Autosomal recessive mutations in a number of genes encoding Aminoacyl-tRNA synthetases (ARSs), including *HARS2* (Perrault syndrome 2), *LARS2* (Perrault syndrome 4), *NARS2* (DFNB94), *IARS2* (Cataracts, growth hormone deficiency, sensory neuropathy, sensorineural hearing loss, and skeletal dysplasia), *PARS2* (Developmental and epileptic encephalopathy 75 including deafness), and *KARS* (DFNB89) may lead to a variety of syndromic and non-syndromic hearing loss (Konovalova and Tyynismaa, 2013; Oprescu et al., 2017; Wang et al., 2020). ARSs are a group of nuclear-encoded enzymes that ensure correct translation of the genetic code by conjugating each of the 20 amino acids to their cognate tRNA molecule in the cytoplasm and mitochondria (Oprescu et al., 2017). Deficiency of ARSs, especially the mitochondrial ARSs (mtARSs) often affect tissues with high metabolic demands such as the brain, muscle, and inner ear (Fine et al., 2019). Clinical features associated with mutations in mtARS-encoding genes typically include encephalopathy, leukodystrophy, cardiomyopathy, ovarian dysgenesis, and deafness (Figuccia et al., 2021).

Characterized by enzyme kinetic assays, yeast complementation assays and studies of patient-derived cell cultures, most of the mtARS mutations have been shown to disrupt its aminoacylation activity (Oprescu et al., 2017; Figuccia et al., 2021). Previous study on a *Dars2* conditional knockout mouse showed that DARS2 depletion in heart and skeletal muscle causes severe dysfunction of mitochondrial protein synthesis in both tissues, which activates various stress responses predominantly in the cardiomyocytes (Dogan et al., 2014). In another *Dars2* neuron-specific knockout mouse, the immune and cell stress pathways have been shown to be initiated prior to behavioral dysfunction and cerebral deficits (Nemeth et al., 2020). Studies in zebrafish and rat have shown that inhibition of WARS2 leads to cardiac angiogenesis defects and impaired heart function (Wang et al., 2016). A mouse line harboring hypomorphic p.V117L mutation in *Wars2* displays various pathologies including progressive hearing loss, adipose dysfunction and hypertrophic cardiomyopathy (Agnew et al., 2018). The homozygous mutant mice have been shown to gradually lose their outer hair cells and spiral ganglion neurons, but the cellular pathogenesis associated with the hearing loss has not been studied in depth.

Numerous studies have shown that mitochondrial dysfunction is an important step toward a broad spectrum of sensorineural hearing loss associated with noise, ototoxic-drug, and aging (Fischel-Ghodsian et al., 2004; Zhang L. et al., 2021). For example, it has been reported that noise exposure leads to mitochondrial swollen and cristae disruption in outer hair cells and stria vascularis in guinea pig and rat (Spoendlin, 1971; Yu et al., 2014), administration of gentamicin induces opening of the mitochondrial permeability transition pore and reduction of mitochondrial membrane potential (Dehne et al., 2002), and accumulation of mitochondrial DNA common deletion contributes to development of age-related hearing loss (Du et al., 2012; Natarajan et al., 2020). As a major source of reactive oxygen species (ROS) production, mitochondrial dysfunction often leads to ROS formation and accumulation after noise (Wu et al., 2020) or ototoxic drug exposure (Fu et al., 2021b), and ultimately lead to death of hair cells and spiral ganglion neurons (Bock and Tait, 2020).

Though mutations in many mtARS-encoding genes are associated with sensorineural hearing loss, their cellular and physiological pathology in inner ear has rarely been investigated *in vivo*. In this study, we established a hair cell specific knockout mouse model for the mitochondrial histidyl-tRNA synthetase encoding gene *Hars2*, whose recessive mutations lead to decreased levels of aminoacylated $tRNA^{His}$ and sensorineural hearing loss with female ovarian dysgenesis (Perrault syndrome 2) in humans (Pierce et al., 2011), and whose overexpression restores mitochondrial dysfunction caused by a deafness-associated m.12201T > C mutation in $tRNA^{His}$ (Gong et al., 2020). Morphological and electrophysiological studies of this conditional knockout (CKO) mouse model furthered our understanding of the pathogenic mechanism underlying the mtARS-associated hearing loss.

MATERIALS AND METHODS

Generation and Genotyping of the *Hars2* Conditional Knockout Mice

The $Hars2^{Loxp/+}$ mice were generated using the CRISPR/Cas9 system (GemPharmatech, China). Briefly, Cas9 mRNA, single guide RNAs and donor were co-injected into the zygotes, directing Cas9 endonuclease cleavage and Loxp site insertion in intron 1 and intron 8 of mouse *Har2* (NM_080636.2, **Figure 1C**). As the $Hars2^{Loxp/Loxp}$; $ACTB^{Cre/+}$ full-body knockout (KO) mice die perinatally, the $Hars2^{Loxp/Loxp}$;$Gfi1^{Cre/+}$ mice (*Hars2* CKO mice) were used to specifically knockout *Hars2* in hair cells (Yang et al., 2010; He et al., 2019). Considering the $Gfi1^{Cre/+}$ mice have been previously reported to have early-onset, progressive hearing loss (Matern et al., 2017), we used littermates of the *Hars2* CKO and wild-type (WT) control mice under the same $Gfi1^{Cre/+}$ background. All animal procedures were approved by the Committee of Laboratory Animals of the Ninth People's Hospital, Shanghai Jiao Tong University School of Medicine. All efforts were practiced to minimize the number of animals used and to prevent their suffering.

For genotyping of the *Hars2* CKO mice, DNA was extracted from mouse tails and PCR amplified using the primers listed in **Supplementary Table 1**. The PCR products of 351, 256, and 672 bp represent the *Hars2* CKO, wild-type, and $Gfi1^{Cre}$ alleles, respectively (**Figure 1D**).

Auditory Brainstem Response

Auditory brainstem response (ABR) analysis was performed in anesthetized mice at P21, P30, P45, and P60. Following a

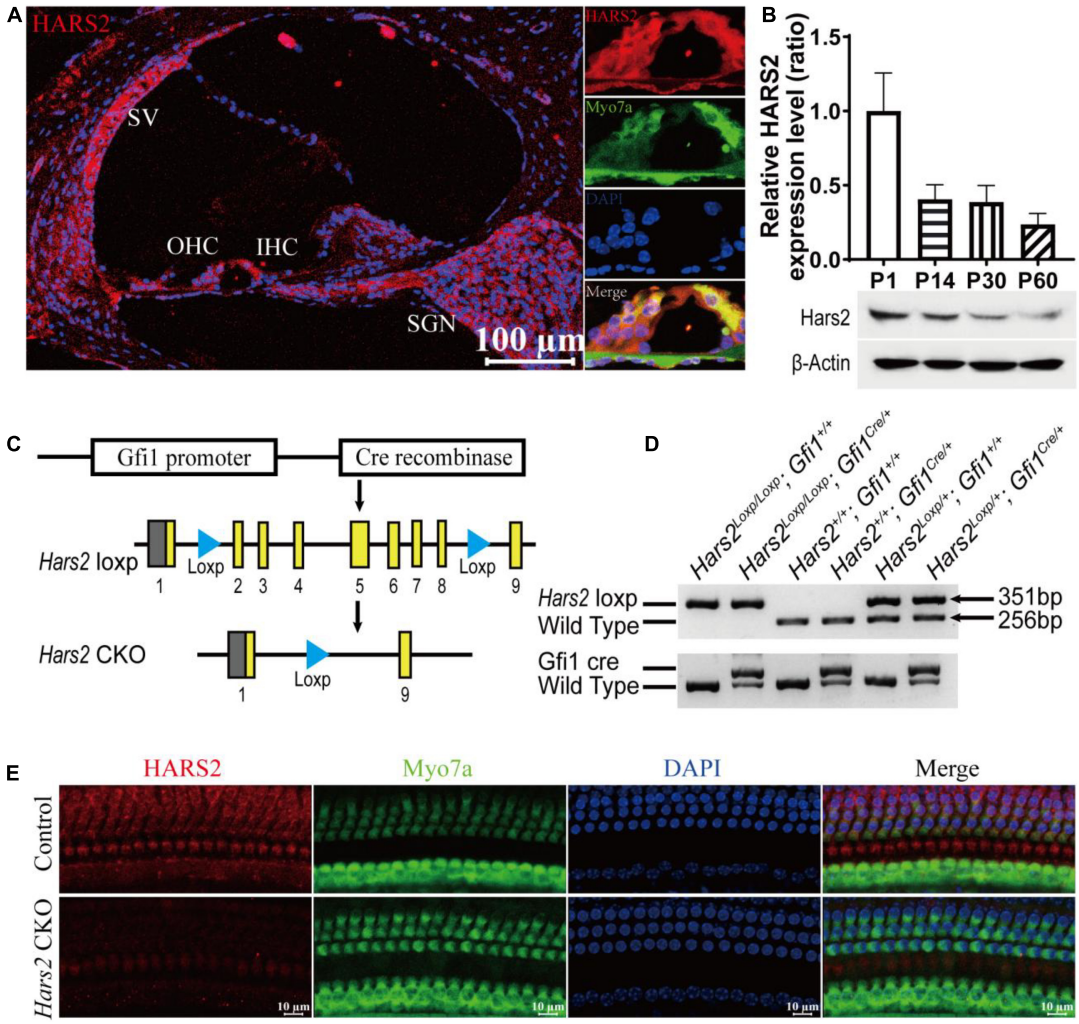

FIGURE 1 | Cochlear expression of HARS2 in the wild-type and *Hars2* CKO mice. **(A)** Immunofluorescence staining of HARS2 in cochlea (left) and organ of corti (right) of the wild-type mice at P30 using anti-HARS2 (red) and anti-Myo7a (green, labeling hair cells) antibodies and DAPI (blue). Scale bar = 100 μm. OHC, outer hair cell; IHC, inner hair cell; SGN, spiral ganglion neuron; SV, stria vascularis. **(B)** Relative protein expression levels of HARS2 at different ages by Western blotting, which was normalized by endogenous β-actin expression. **(C)** Generation of the hair cell-specific *Hars2* CKO mice with the Loxp sites inserted into intron 1 and 8 of mouse *Hars2* and crossed with the *Gfi1*^{Cre}. **(D)** Verification of targeted genomic deletion of the *Hars2*-Loxp allele by PCR amplification. **(E)** Immunofluorescence staining of HARS2 in the cochleae of P30 control and *Hars2* CKO mice, showing the successful knockout of *Hars2* in hair cells. Scale bars = 10 μm.

previously described protocol with minor modification (Zheng et al., 1999; Liu et al., 2019a), hearing thresholds at sound frequencies 4, 5.6, 8, 11.3, 16, 22.6, and 32 kHz were assessed in TDT system 3 (Tucker-Davies Technologies, United States). Briefly, Animals were deeply anesthetized with an intraperitoneal injection of 0.01 g/ml pentobarbital sodium (100 mg/kg), and body temperature was kept on 37°C in the recording process using a Homeothermic Monitoring System (Harvard Apparatus) in a soundproof chamber. ABR was recorded with three subcutaneously implanted stainless needle electrodes. The active electrode was positioned at the vertex, the reference at the right mastoid region, and the ground at the left shoulder. Before ABR analysis was conducted, mice with normal external auditory canal and tympanic membrane were examined using an otoscope. Pure tone bursts were produced by the RZ6 workstation (Tucker-Davis Technologies, United States). Free-field acoustic stimulation was performed through an MF1 speaker (Tucker-Davis Technologies, United States), located 10 cm from the vertex. The evoked potentials were filtered with a bandpass filter from 100 to 3000 Hz and averaged 400 times. For each analyzed frequency, the sound level was reduced from 90 to 0 dB SPL in 5 dB steps. ABR thresholds were determined by minimal stimulus level that evoked any visible recording of waveforms at each frequency. If the hearing threshold could not be measured at 90 dB SPL, the result was noted as threshold of 100 dB SPL for statistical analysis. All amplitudes and latencies of ABR peak I were measured and analyzed using BioSigRZ software (Tucker-Davis Technologies, United States) as previously described (Scimemi et al., 2014; McKay et al., 2015). Amplitude was calculated from the average value of $\triangle V$ on both sides of peak I, and

latency referred to the time from the beginning of the stimulus signal to peak I.

Immunofluorescence Staining and Confocal Imaging

After animals were deeply anesthetized and sacrificed, cochleae were quickly harvested from dissected temporal bones in cold 4% paraformaldehyde (PFA). A small hole was punctured at the top of cochlea and then 4% PFA was slowly perfused through the small hole, oval window and round window. The cochleae were kept in this fixation overnight at 4°C. The next day, after decalcified in 10% EDTA for 2–24 h at room temperature according to postnatal age, the organ of corti was dissected and cut into three turns (apex, middle, and base) for immunofluorescent staining (Akil and Lustig, 2013). For frozen cochlear sections, after making sure the cochleae were soft enough after decalcification, the samples were dehydrated through the 15% and 30% sucrose solution successively for 24 h, immerged into the OCT compound (Sakura Finetek United States, Inc., 4583) and hardened at −20°C. Slices with thickness of 10 μm were cut through the modiolus by a freezing microtome (Leica Biosystems Inc., CM3050S). Slices containing 3–4 organs of corti were collected on glass slides.

For immunofluorescent staining, all samples were first permeabilized with 1% Triton X-100 for 1 h and immersed in blocking solution containing 10% goat serum, 1% bovine serum albumin, and 1% Triton X-100 in PBS (pH 7.2) for 2 h at room temperature. The samples were then incubated with primary antibodies including mouse monoclonal anti-Myo7a (Developmental Studies Hybridoma Bank, MYO7A 138-1), rabbit polyclonal anti-Myo7a (Thermo Fisher Scientific, PA1-936), rabbit polyclonal anti-HARS2 (Abcam, 46545), mouse monoclonal anti-3-nitrotyrosine (3-NT) (Sigma-Aldrich, N5538), rabbit polyclonal anti-4-hydroxynonenal (4-HNE) (Abcam, 46545), and mouse monoclonal anti-CtBP2 (BD Biosciences, 612044) at 1:200 dilution at 4°C overnight. Next day, after three 10-min washing with PBS, the samples were incubated with appropriate secondary antibodies at 1:400 dilution for 2 h at room temperature in darkness, which include Alexa Fluor 488-conjugated goat anti-mouse (CST, 4408S), Alexa Fluor 594-conjugated goat anti-rabbit (CST, 8889S), and Alexa Fluor 488-conjugated goat anti-rabbit (Thermo Fisher Scientific, A32731). According to immunofluorescence staining requirement, the samples were incubated with Alexa-Fluor 647-phalloidin (Thermo Fisher Scientific, A22287) for 1 h at room temperature in darkness. After three final washes with PBS, all immunolabeling samples were mounted on a slide with anti-fade reagent (Invitrogen, P10144). Immunofluorescence images were captured by Zeiss LSM 880 laser confocal microscope (Carl Zeiss Microscopy, Germany).

Semi-Quantification of the Immunofluorescence Images

Immunofluorescence images for 3-NT and 4-HNE were semi-quantified from original confocal images as previously described (Wu et al., 2020). Briefly, samples were processed in parallel under identical immunofluorescence staining conditions, and confocal microscope images were acquired with the same parameter settings. Using the ImageJ software (NIH, United States), the immunofluorescence images of hair cells were converted into 16-bit grayscale images for further measurement. After subtraction of the background intensity, the averaged grayscale intensity per cell was analyzed. For each repetition, the relative grayscale value was determined by normalizing the ratio to controls.

Transmission Electron Microscopy

Cochleae were quickly immersed and dissected in 2.5% glutaraldehyde (Sigma-Aldrich, G7651) in phosphate buffer (PB) solution. After fixed with 2.5% glutaraldehyde at 4°C overnight, the basilar membranes were fixed with 1% osmium tetroxide for 2 h at room temperature. The samples were dehydrated through an ethanol and acetone gradient and gradually embedded in Epon-812 (Sigma-Aldrich, 45345). Ultrathin sections were made by a diamond knife on a PowerTome-PC ultramicrotome (RMC, United States) and then placed on copper mesh, sequentially post-stained with uranyl acetate and lead citrate. The samples were imaged with a JEM-1230 transmission electron microscope (JEOL, Japan).

qPCR Analysis

Cochleae RNA extraction and qPCR analysis were performed as previous described (Vikhe Patil et al., 2015). Briefly, total RNA was extracted from sensory epithelia (without spiral ganglion neurons) of three mice for each genotype group using the TRIzol reagent (Invitrogen, 15596018). cDNA was reverse transcribed by applying RevertAid First Strand cDNA synthesis Kit (Invitrogen, K1622). The primers are listed in **Supplementary Table 1**. The qPCR was performed on a Roche 480II Real Time PCR System (Roche, United States) using the QuantiNova SYBR Green PCR Kit (QIAGEN, 208052). The mRNA relative expression levels were normalized to the endogenous control *Gapdh*. Each reaction was performed at least in triplicate, and the results were analyzed using the $2^{--\Delta\Delta CT}$ method (Schmittgen and Livak, 2008).

Western Blotting Analysis

Five mice (10 cochleae) were sacrificed for each genotype group. The cochleae were rapidly dissected in ice-cold PBS. Tissues of sensory epithelia (without spiral ganglion neurons) were gathered in tubes and mixed with ice-cold RIPA lysis buffer plus protease inhibitor cocktail and phosphatase inhibitors. The samples were homogenized and centrifuged at 10000 × *g* at 4°C for 20 min. The supernatants were collected and the protein concentration was measured using the BCA Protein Assay Kit (Beyotime, P0010). With 5 × SDS sample loading buffer added, the samples were boiled for 5 min and centrifuged at 3000 × *g* for 1 min. A total of 20 μg of each protein sample was separated by polyacrylamide gel electrophoresis (PAGE) and transferred onto a Polyvinylidene Fluoride (PVDF) membrane. The membranes were blocked with 5% non-fat milk for 2 h at room temperature and then incubated overnight at 4°C with the primary antibodies including anti-cleaved caspase-3 Rabbit mAb (CST, 9664) at 1:700, anti-Bcl2 Rabbit mAb (CST, 3498) at 1:700, anti-Cytochrome C Rabbit mAb (CST, 11940) at 1:700, anti-cleaved caspase-9 (CST, 9509) at 1:700, and anti-HARS2 (proteintech, 11301-1-AP) at 1:1000.

The membranes were washed three times in TBS with Tween 20 buffer and then incubated with secondary antibody conjugated with horseradish peroxidase for 2 h at room temperature. The immunoreactive bands were detected using a Tanon-4600 Chemiluminescent Imaging System (Tanon, China). The ImageJ software was used to calculate the relative density of probe protein. For HARS2 protein expression analysis, the relative protein expression was determined by normalizing the ratio to P1 HARS2 protein expression.

Whole-Cell Patch Clamp Recordings

The apical turn of the basilar membrane of the mouse cochlea was micro dissected in the extracellular solution. Whole-cell Patch clamp recordings were performed using the EPC10/2 amplifier (HEKA Electronics, Germany) with the Patchmaster software (HEKA Electronics, Germany) as described in our previous studies (Lin et al., 2019; Liu et al., 2019a; Zhao et al., 2020). Current-voltage relationships of Ca^{2+} influx in inner hair cells (IHCs) were obtained from current responses to ramp depolarization from -90 to 60 mV, and fitted to the following equation:

$$I(V) = (V - V_{rev}) \times \frac{G_{max}}{1 + \exp\left(-(V - V_{half})/K_{slope}\right)}$$

where V is the command membrane potential, V_{rev} is the reversal potential, G_{max} is the maximum conductance, V_{half} is the half activation potential, and the K_{slope} is steepness of voltage dependence in current activation.

Inner hair cell capacitance measurement (C_m) were performed with the lock-in feature and the "Sine + DC" method in the software Patchmaster (Liu et al., 2019b). Briefly, a 1 kHz sine wave and 70 mV peak-to-peak magnitude was superposed on the IHC holding potential of –90 mV. The averaged capacitances change before and after the depolarization were calculated to monitor exocytosis from IHCs: $\triangle C_m$ = C_m (response) – C_m (baseline). Ca^{2+} current charge (Q_{ca}) was calculated by taking the integral of the leak-subtracted current during depolarization.

In situ Apoptosis Staining

Hair cell apoptosis in the cochlea was evaluated using a terminal deoxynucleotidyl transferase-mediated deoxyuridine triphosphate nick-end labeling (TUNEL) staining kit (*in situ* cell death detection kit, Roche). After hair cells were labeled with anti-Myo7a antibody, the cochlear tissues were incubated with freshly prepared TUNEL working solution at 37°C for 1 h in a humidified chamber away from light. After rinsing in PBS three times, Nuclei were counterstained with a 4′, 6-diamidino-2-phenylindole (DAPI) staining solution (Beyotime, P0131). Nuclei of TUNEL positive cells intensely labeled by green were identified as apoptotic cells. Images were captured on a Zeiss LSM 880 laser confocal scanning microscopy (Carl Zeiss Microscopy, Germany).

Date Processing and Statistical Analysis

Imaging data processing and statistical analyses were carried out with GraphPad Prism 8.0 and Adobe Illustrator CC 2018. A two-tailed, unpaired Student's *t*-test with Welch's correction was used for comparisons between the *Hars2* CKO and control mice. For multiple comparison which involves sound level, frequency and cochlear turn, statistical analysis was performed using two-way ANOVA followed by Bonferroni *post-hoc* test. Data were expressed as mean ± SEM. For all statistical analysis, values were considered statistically significant when $P < 0.05$. In Figures, NS represents $P > 0.05$, * represents $P < 0.05$, ** represents $P < 0.01$, *** represents $P < 0.001$.

RESULTS

HARS2 Is Robustly Expressed in Postnatal Mouse Cochlea

To explore the role of HARS2 in hearing function, we first examined the expression pattern of HARS2 in the mouse cochlea. As shown in **Figure 1A**, cryosection immunostaining of the P30 WT mice indicated that HARS2 is widely expressed in the cochlea including inner (IHC) and outer hair cells (OHC), spiral ganglia neurons, stria vascularis, and supporting cells. Western blot analysis in cochleae of different postnatal ages showed that the expression of HARS2 is highest at P1 and gradually decreases at P14, P30, and P60 (**Figure 1B**).

The *Hars2* Conditional Knockout Mice Have Rapidly Progressive Hearing Loss

The $Hars2^{Loxp/Loxp}$;$ACTB^{Cre}$ full-body KO mice died perinatally, hindering further investigation of *Hars2* in auditory function. To overcome this obstacle, we generated a $Hars2^{Loxp/Loxp}$;$Gfi1^{Cre}$ CKO mouse line (**Figures 1C,D**). The specifical knockout of *Hars2* in cochlear hair cells was confirmed by immunofluorescence staining (**Figure 1E**). The *Hars2* CKO mice has apparently normal development. ABR thresholds of the *Hars2* CKO mice were initially indistinguishable from that of the littermate $Hars2^{+/+}$; $Gfi1^{Cre}$ controls at P21 (**Figure 2A**), but gradually elevated at P30 and P45 and rapidly reached profoundly deaf before P60 (**Figures 2B–D**). At P30 but not P21, the *Hars2* CKO mice also showed decreased supra-threshold amplitude and prolonged latency of the ABR wave I at sound frequencies 8, 16, and 22.6 kHz (**Figures 2E,F** and **Supplementary Figure 1**), which indicates abnormal IHC synaptic transmission, synchronization and auditory nerve conduction (McKay et al., 2015).

The *Hars2* Conditional Knockout Mice Have Progressive Hair Cell Loss

Immunostaining of the cochlear hair cells showed that the *Hars2* CKO mice have normal OHC and IHC numbers as the wild-type at P21 and P30 (**Figures 3A,B**). At P45, mild hair cell loss, more notable in OHCs than IHCs, can be observed at the basal turns of the *Hars2* CKO cochleae (**Figure 3C**). The hair cell loss proceeds rapidly and extends from the basal turn to the middle and apical. At P60, most OHCs of the *Hars2* CKO mice are lost, especially in the middle and basal turns, while the IHC loss is relatively less severe (**Figure 3D**).

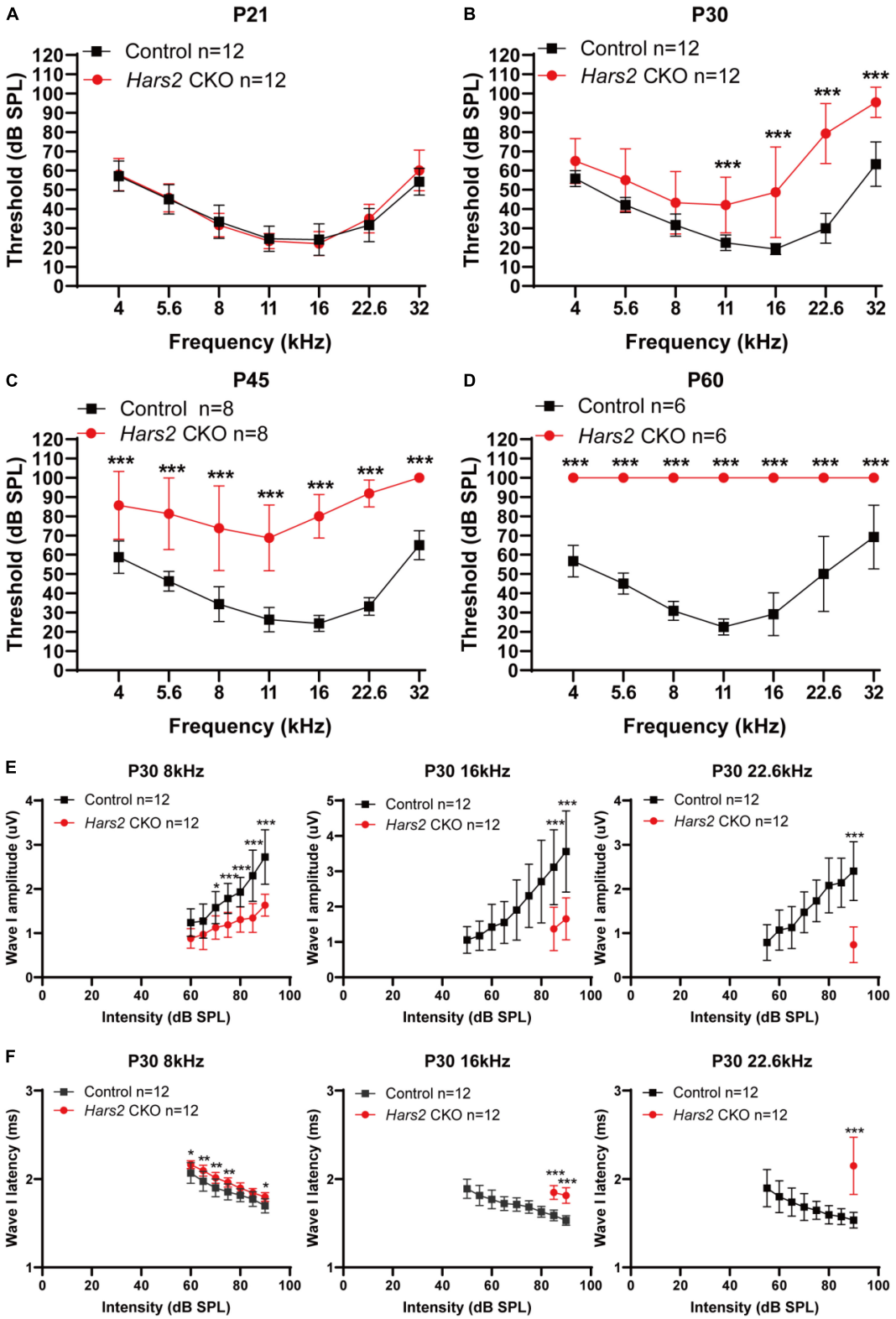

FIGURE 2 | Auditory brainstem response threshold and Wave-I analysis of the *Hars2* CKO mice. **(A)** Indistinguishable ABR thresholds of the *Hars2* CKO and control mice at P21. **(B)** Significantly elevated ABR thresholds at frequencies of 11–32 kHz at P30. **(C)** Further elevated ABR thresholds at all frequencies at P45. **(D)** Profound hearing loss at P60. **(E)** Significantly reduced ABR suprathreshold wave-I amplitudes at frequencies of 8, 16, and 22.6 kHz at P30. **(F)** Significantly prolonged ABR suprathreshold wave-I latencies at frequencies of 8, 16, and 22.6 kHz at P30. * represents $P < 0.05$, ** represents $P < 0.01$, *** represents $P < 0.001$.

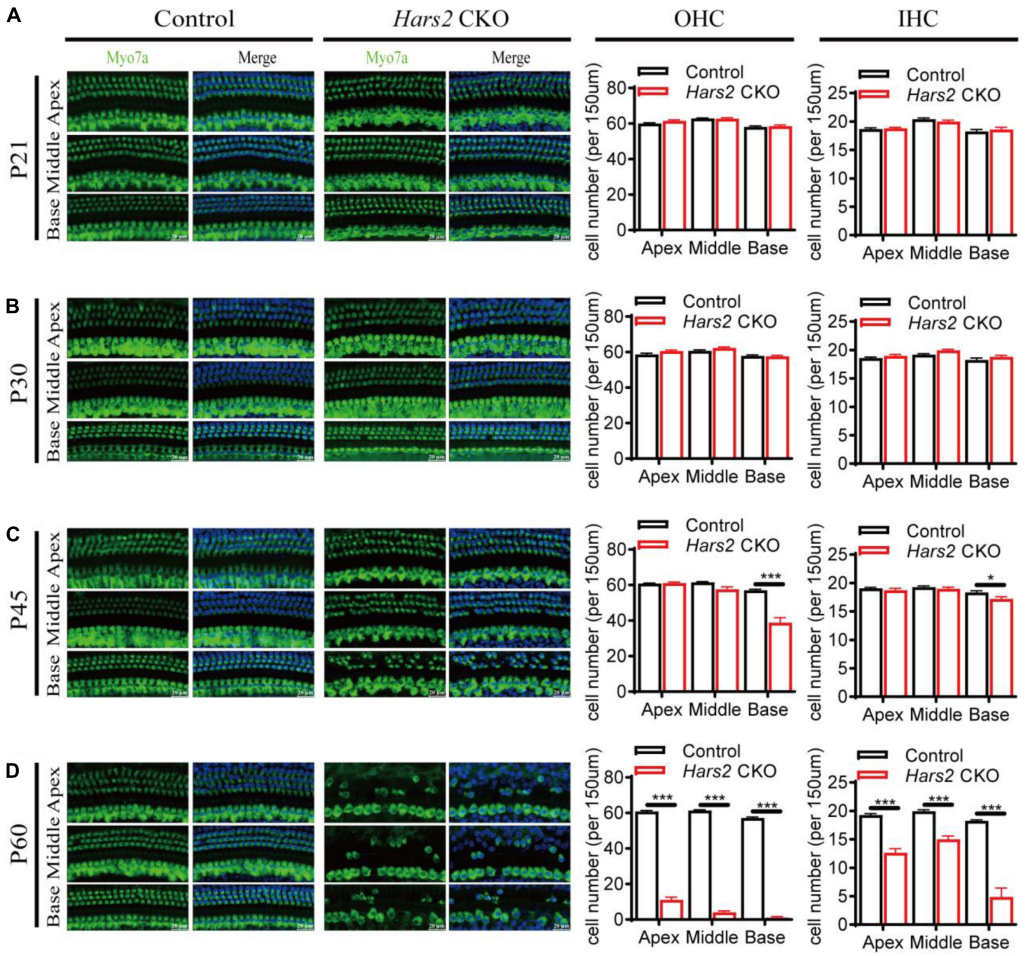

FIGURE 3 | Hair cell loss in the *Hars2* CKO mice. **(A,B)** No significant hair cell loss at P21 and P30. **(C)** Partial loss of hair cells at the basal turn at P45. **(D)** Severe hair cell loss in all turns at P60. Left panels: Whole-mount cochleae were immunostained with anti-Myo7a antibody (green) and DAPI (blue). Right panels: Quantification of the numbers of OHCs (left) and IHCs (right). control: $n = 5$; *Hars2* CKO: $n = 5$. Scale bars = 20 μm. * represents $P < 0.05$, *** represents $P < 0.001$.

Hars2 Knockout Activates Mitochondrial Apoptosis Pathway in Hair Cells

We next investigated that whether hair cell loss of the *Hars2* CKO mice is due to apoptosis. The TUNEL assay was used to label nuclear DNA fragmentation, a key feature of apoptosis (Majtnerová and Roušar, 2018). At P30, all hair cells remain TUNEL-negative (**Supplementary Figure 2**). At P45, TUNEL-positive OHCs can be observed in all three turns of the *Hars2* CKO cochleae, while TUNEL-positive IHCs are present in the basal turn only (**Figures 4A,B**). Expression of multiple pro-apoptotic proteins caspase-3, caspase-9, and cytochrome C are significantly up-regulated in the *Hars2* CKO cochleae, while the anti-apoptotic protein BCL-2 is down-regulated (**Figures 4C,D**).

Hars2 Knockout Elevates Reactive Oxygen Species in Hair Cells

Since mitochondrial ROS has pivotal role in triggering hair cell apoptosis and hearing loss (Wu et al., 2020; Fu et al., 2021b), we then assessed the level of ROS in the *Hars2* CKO cochleae. Increased immunolabeling of the ROS markers 3-NT and 4-HNE can be observed as early as P30 in most turns of cochleae (**Figures 5A–D**). Quantitative reversed transcribed PCR also showed decreased mRNA expression of several antioxidant enzymes xCT, Nqo1, Sod2, and Gsr, and increased expression of the oxidant enzyme Lpo in the *Hars2* CKO cochleae (**Figure 5E**). These results suggested that increased ROS in cochlear hair cells is likely the initiating cause for hearing loss in the *Hars2* CKO mice.

Hars2 Knockout Disrupts Inner Hair Cell Synaptic Transmission

Since the *Hars2* CKO mice has significant hearing loss at P30 without apparent hair cell loss (**Figures 2B**, **3B**), we further investigated the IHC functions of the *Hars2* CKO mice at this age. Whole-mount immunostaining showed that the *Hars2* CKO mice has normal IHC ribbon synapse counts as the controls (**Supplementary Figure 3**). Whole-cell patch-clamp recording in IHCs, however, recorded a significantly smaller Ca^{2+} current

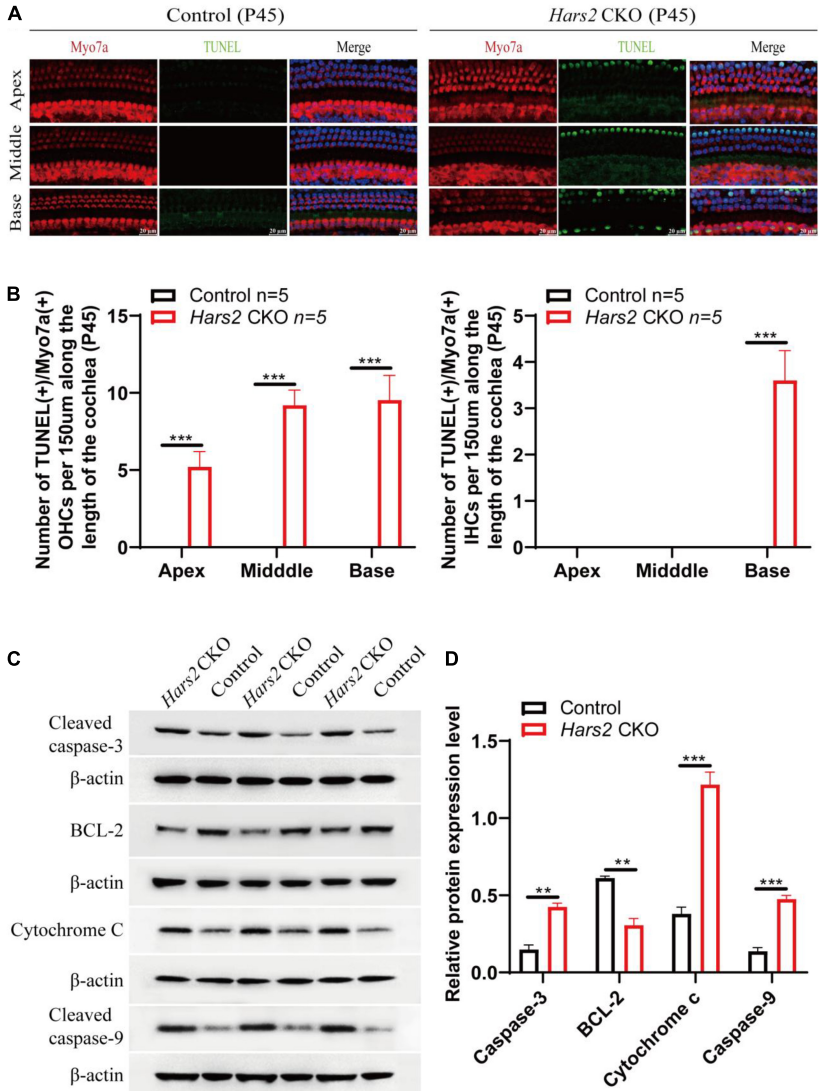

FIGURE 4 | Apoptosis analysis by TUNEL and Western blot in the cochleae of the *Hars2* CKO mice at P45. **(A)** TUNEL (green) and anti-Myo7a (red), DAPI (blue) staining of whole-mount cochlea in the *Hars2* CKO and control mice. Scale bars = 20 μm. **(B)** Quantification of the number of TUNEL positive OHCs and IHCs at the apical, middle, and basal turns of cochlea. **(C)** Protein expression of cleaved caspase-3, BCL-2, cytochrome C, and cleaved caspase-9 detected by Western blotting. **(D)** Relative protein expression levels after normalization against endogenous β-actin. All experiments were replicated in triplets. ** represents $P < 0.01$, *** represents $P < 0.001$.

with lower current amplitude (I_{Ca}), reversal potential (V_{rev}) and half activation potential (V_{half}), and normal steepness of voltage dependence (k_{slope}) for the *Hars2* CKO mice at physiological conditions (**Figures 6A–E**). Membrane capacitance change (ΔC_m), which measures synaptic vesicle release, is normal under short (20 ms) stimulation but significantly reduced under prolonged (200 ms) stimulation (**Figures 6F–J**). The Ca^{2+} efficiency triggering exocytosis, quantified as the ratio of $\Delta C_m/Q_{Ca}$, remain unaltered for both short and prolonged stimulations (**Figures 6H,K**). Taken together, these results suggested that the *Hars2* CKO mice have disrupted IHC synaptic transmission due to reduced calcium influx, which likely contributes to the hearing loss at P30 and is consistent with the decreased supra-threshold amplitude and prolonged latency of the ABR wave I (**Figures 2E,F**).

Hars2 Knockout Causes Accumulation of Morphologically Abnormal Mitochondria in Hair Cells

We finally evaluated the proportion of morphologically abnormal mitochondria, defined by swelling, deformation, loss of cristae, and emergence of large intrinsic vacuoles, in IHCs (**Figure 7**) and OHCs (**Figure 8**) of the *Hars2* CKO mice by Transmission Electron Microscopy (TEM). At P7, the number and distribution of mitochondria in both IHCs and OHCs of the *Hars2* CKO

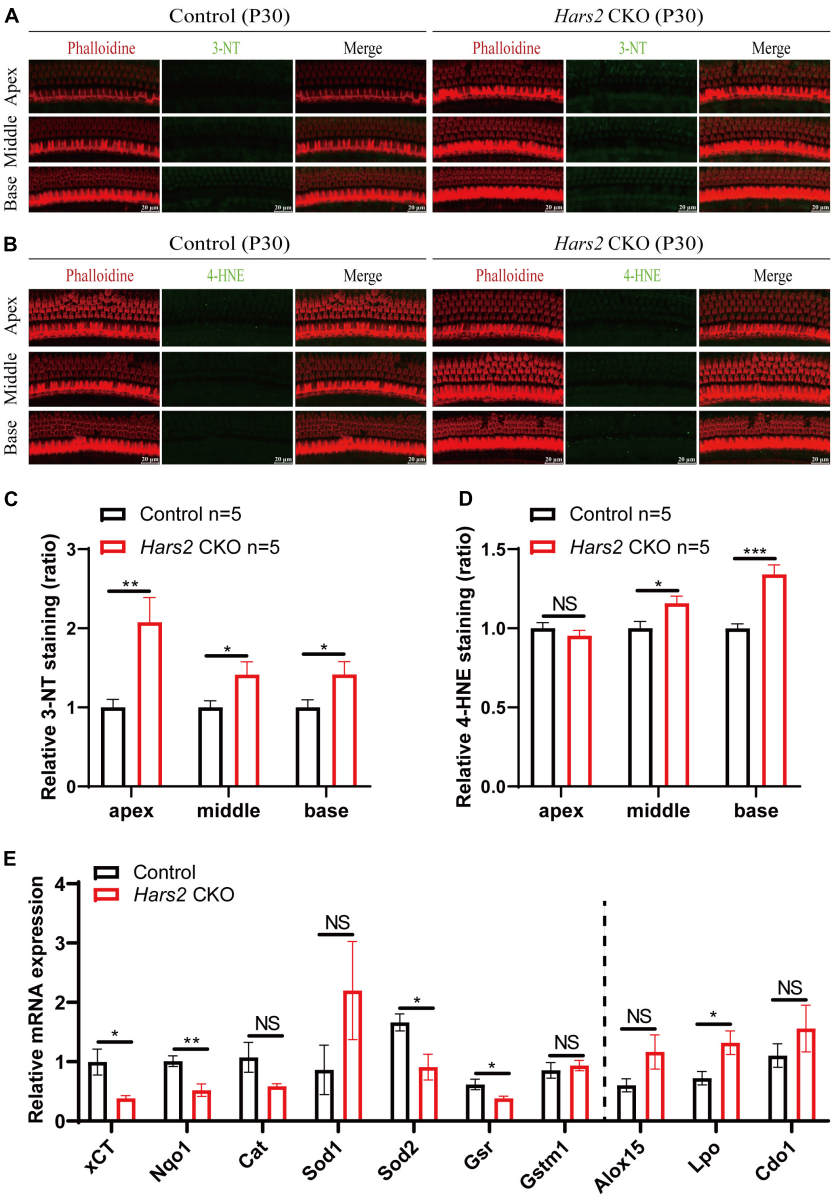

FIGURE 5 | ROS analysis in the cochleae of the *Hars2* CKO mice at P30. **(A,B)** Immunostaining of whole-mount cochleae using anti-3-NT or anti-4-HNE antibodies (green), Phalloidin (red), and DAPI (blue). Scale bars = 20 μm. **(C,D)** Quantification of the 3-NT or 4-HNE immunolabeling in hair cells. **(E)** qPCR analysis of sensory epithelia (without spiral ganglion neurons) showing significantly decreased expression of the antioxidant factors xCT, Nqo1, Sod2, and Gsr and increased expression of pro-oxidant factor Lpo ($n = 6$). NS represents $P > 0.05$, * represents $P < 0.05$, ** represents $P < 0.01$, *** represents $P < 0.001$.

mice are normal, and the ultrastructure of the mitochondria is mostly indistinguishable from the control mice with clearly visible cristae. From P14, a series of abnormal mitochondria can be observed in hair cells of the *Hars2* CKO mice (**Figures 7A**, **8A**), which represents reduced inner membrane surface together with low-density mitochondrial mass. The proportion of morphological abnormal mitochondria appears to increase with age and is larger in IHCs than in OHCs (**Figures 7B**, **8B**). In addition, cristae surface area, positively correlated with the amount of ATP produced by oxidative phosphorylation (van der Laan et al., 2012; Wollweber et al., 2017), significantly decreases in the *Hars2* CKO mice, again more prominently in IHCs than in OHCs (**Figures 7C**, **8C**).

DISCUSSION

The functions of deafness genes play an essential role on the morphology and development of hair cells (Liu et al., 2019d; Qi et al., 2019, 2020; Chen et al., 2021a), synaptic transmission of spiral ganglion neurons (Guo et al., 2020; Guo R. et al., 2021; Hu et al., 2021; Wei et al., 2021), and many other important

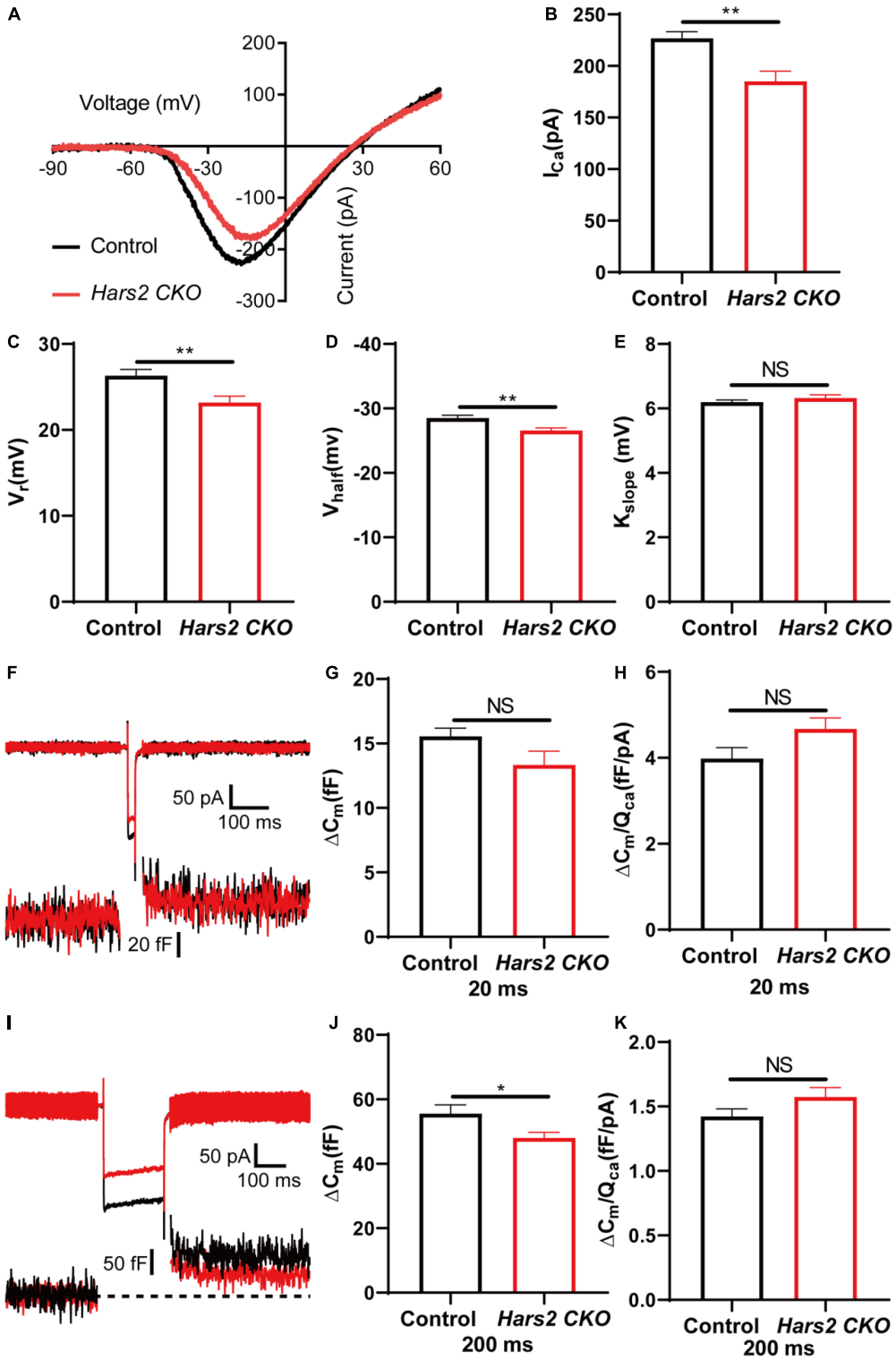

FIGURE 6 | Inner hair cell patch-clamp recording in the *Hars2* CKO mice. **(A)** Representative of the Ca^{2+} current in IHCs of the *Hars2* CKO and control mice. The current response was induced by a voltage ramp from –90 to 60 mV and then leak subtracted. **(B,C)** The Ca^{2+} current amplitude (I_{Ca}) and reversal potential (V_{rev}) are significantly reduced. **(D)** The half activation potential (V_{half}) of calcium current is less negative. **(E)** Slope of activation (k_{slope}) is normal. **(F)** Representative traces of Ca^{2+} current (top) and capacitance (bottom) upon 20 ms step depolarization. **(G)** The membrane capacitance change (ΔC_m) is comparable for stimulations of 20 ms. **(H)** The Ca^{2+} efficiency of exocytosis triggering, quantified as the ratio of $\Delta C_m/Q_{Ca}$, is comparable for stimulation of 20 ms. **(I)** Representative traces of Ca^{2+} current (top) and capacitance (bottom) upon 200 ms step depolarization. **(J)** The ΔC_m is significantly reduced for stimulations of 200 ms. **(K)** The $\Delta C_m/Q_{Ca}$ is comparable for stimulation of 200 ms (control: $n = 5$; *Hars2* CKO: $n = 5$). NS represents $P > 0.05$, * represents $P < 0.05$, ** represents $P < 0.01$.

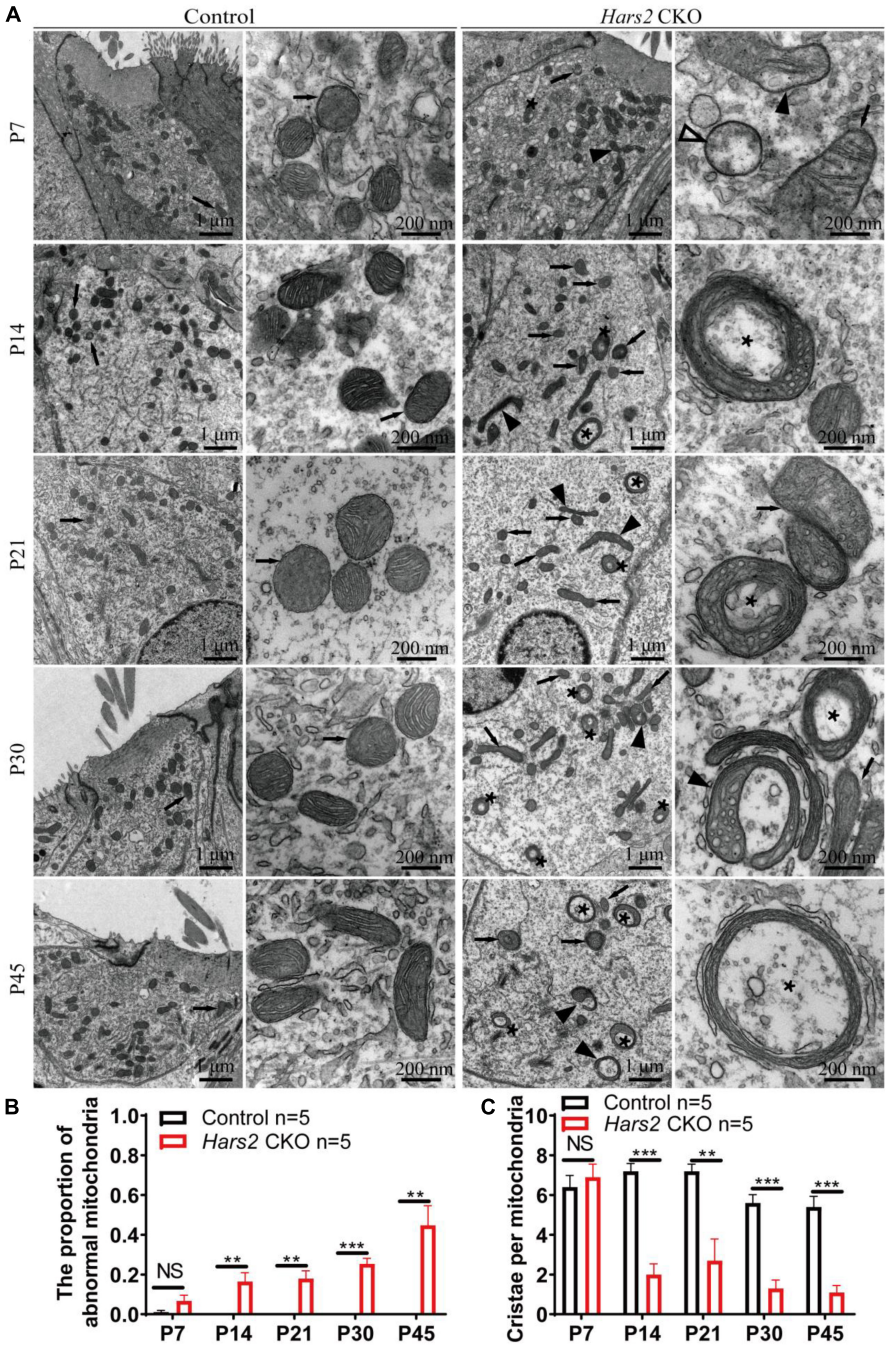

FIGURE 7 | Inner hair cell transmission electron microscopy of the *Hars2* CKO mice between P7 and P45. **(A)** IHCs of the control mice at different ages contains abundant mitochondria with easily-identifiable cristae, whereas various morphologically abnormal mitochondria be observed in IHCs of the *Hars2* CKO mice including swollen (open arrowhead), deformed (black arrowhead) mitochondria, mitochondria with deformed cristae (black arrows), or intrinsic vacuole (black asterisk). **(B)** Quantified proportion of abnormal mitochondria in IHCs. **(C)** Quantified number of mitochondrial cristae per mitochondria in IHCs. NS represents $P > 0.05$, ** represents $P < 0.01$, *** represents $P < 0.001$.

components of the inner ear, including supporting cells, greater epithelial ridge cells and lesser epithelial ridge cells (Ding et al., 2020; Zhang et al., 2020; Chen et al., 2021b). In this study, we generated a *Hars2* conditional knockout mice to investigate the function of HARS2 in hearing and its pathogenic mechanism for deafness. Previous studies have shown that missense mutations in *HARS2*, which account for the majority of reported mutations in humans, lead to significantly decreased protein function (Yu et al., 2020), similar to the loss of function effect in this mouse model. Though HARS2 was found to be widely expressed in

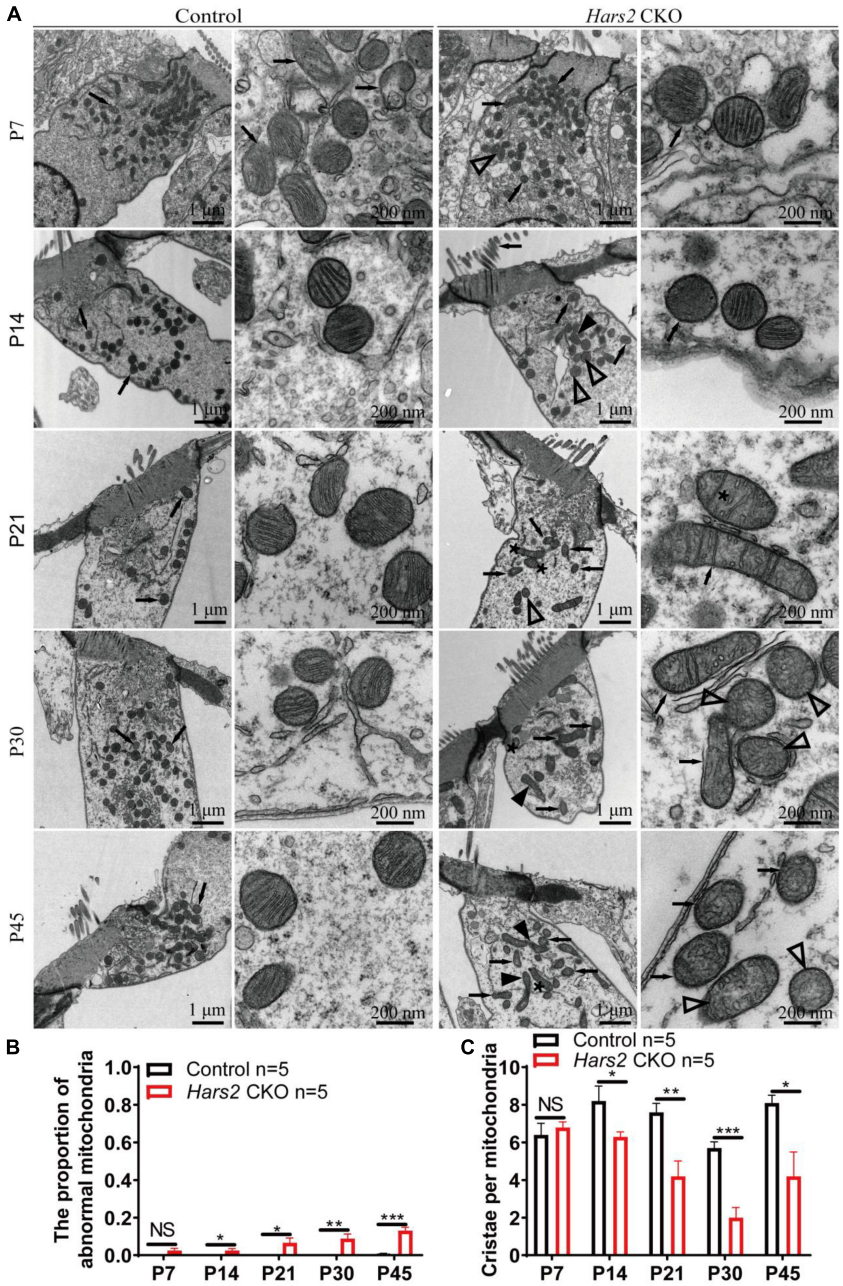

FIGURE 8 | Outer hair cell transmission electron microscopy of the *Hars2* CKO mice between P7-P45. **(A)** OHCs of the control mice at different ages contains abundant mitochondria with easily-identifiable cristae, whereas various morphologically abnormal mitochondria be observed in OHCs of the *Hars2* CKO mice including swollen (open arrowhead), deformed (black arrowhead) mitochondria, mitochondria with deformed cristae (black arrows), or intrinsic vacuole (black asterisk). **(B)** Quantified proportion of abnormal mitochondria in OHCs. **(C)** Quantified number of mitochondrial cristae per mitochondria in OHCs. NS represents $P > 0.05$, * represents $P < 0.05$, ** represents $P < 0.01$, *** represents $P < 0.001$.

many cell types of mouse cochlea (**Figure 1**), the current study chose to focus on cochlear hair cells that have an essential role in converting mechanical sound stimulus into neural electrical signals (Schwander et al., 2010). Notably, our hair cell-specific *Hars2* CKO mice display delayed-onset, rapidly progressive hearing loss (**Figure 2**), which is very similar to the human hearing phenotype associated with the *HARS2* mutations (Yu et al., 2020), supporting our hypothesis that hair cell is among the primary targets for *Hars2*-related pathogenesis in cochlea. At the same time, we acknowledge that the function of HARS2 in other inner ear cell types, such as spiral ganglion neurons and supporting cells, remain to be further studied.

Underlying increasingly elevated ABR hearing thresholds in postnatal *Hars2* CKO mice (**Figure 2**), we observed rapidly

progressive hair cell loss due to increased ROS level and activated apoptosis pathway (**Figures 3**, **4**, **5**). These results are consistent with previous studies on HEK293T cells, which show that the mtARSs are essential in mitochondrial protein synthesis and oxidative phosphorylation (OXPHOS) (Fine et al., 2019; Yu et al., 2020). Reduction of OXPHOS electron transport chain activity may lead to elevated ROS, which in turn can induce opening of mitochondrial permeability transition pore and reduce of mitochondrial membrane potential, triggering mitochondrial apoptotic pathways (Kamogashira et al., 2015).

The hearing loss of the *Hars2* CKO mice, however, cannot be entirely attributed to loss of hair cells, as it already occurs at as early as P30 without apparent hair cell loss (**Figures 2B**, **3B**). In hair cells, neurotransmission of the sound signal relies on rapid and sustained vesicle release of the ribbon synapses, which is an energy demanding process relying heavily on mitochondria (Safieddine et al., 2012). Patch-clamp recordings in acute brainstem slices have demonstrated that energy limitations can negatively affect synaptic transmission (Nagase et al., 2014), with similar results also reported in hippocampal slices (Liotta et al., 2012). In this study, by TEM we observed morphological degeneration of mitochondria, which indicate mitochondrial dysfunction in *Hars2* CKO hearing cells at different postnatal periods including P14. In mammalian hair cells, Ca^{2+} influx current triggers both rapid and sustained exocytosis, which releases the readily releasable pool of synaptic vesicles and ensures their efficient recycling (Meyer et al., 2009; Graydon et al., 2011). Besides energy supply, mitochondria also contributes to maintaining of intracellular calcium homeostasis and influx in hair cells (Wang et al., 2019) and is associated with the susceptibility to noise-induced hearing loss (Liu et al., 2020). Although the number of ribbon synapses in IHCs of the *Hars2* CKO mice is unaltered at P30 (**Supplementary Figure 3**), our IHC patch-clamp recording showed that the IHC Ca^{2+} influx current is significantly reduced at physiological conditions (**Figure 6**). Consistently, while the rapid exocytosis and the efficiency of Ca^{2+} triggering exocytosis remains normal, the sustained exocytosis is also reduced in IHCs of the *Hars2* CKO mice. These results are in agreement with previous studies showing that partial block of evoked mitochondria-Ca^{2+} uptake in mature zebrafish hair cells was sufficient to impair presynaptic-Ca^{2+} influx current, especially during sustained stimuli (Castellano-Muñoz and Ricci, 2014; Wong et al., 2019). Overall, our results suggested that *Hars2* deficiency leads to mitochondrial dysfunction, reduced presynaptic Ca^{2+} influx current and compromised sustained exocytosis, which in combination likely contributes to the hearing loss of the *Hars2* CKO mice prior to the hair cell loss.

Our TEM study revealed the progressive morphological abnormalities of mitochondria in hair cells of the *Hars2* CKO mice (**Figures 7**, **8**). Mitochondria is a dynamic organelle whose morphology directly reflects its functional status (Friedman and Nunnari, 2014). Here we calculated the proportion of morphologically abnormal mitochondria and the number of mitochondrial cristae per mitochondria to quantify the mitochondrial dysfunction. Interestingly, the distortion and corruption of mitochondria is far more severe in IHCs than in OHCs of the *Hars2* CKO mice. This is in agreement with previous studies on cisplatin-induced hearing loss and noise-induced hearing loss, which showed similar trends for differential mitochondrial damages between IHCs and OHCs (Hill et al., 2016; Chen et al., 2019). However, both previous and our current studies (**Figure 3**) showed that OHCs encounter greater cell loss than IHCs under ROS stress (Choung et al., 2009), suggesting that these two hair cell types perceive the mitochondrial damage differently.

Overall, our study revealed a progressive, rapidly deteriorating course for hair cell mitochondrial damage and hearing loss in the

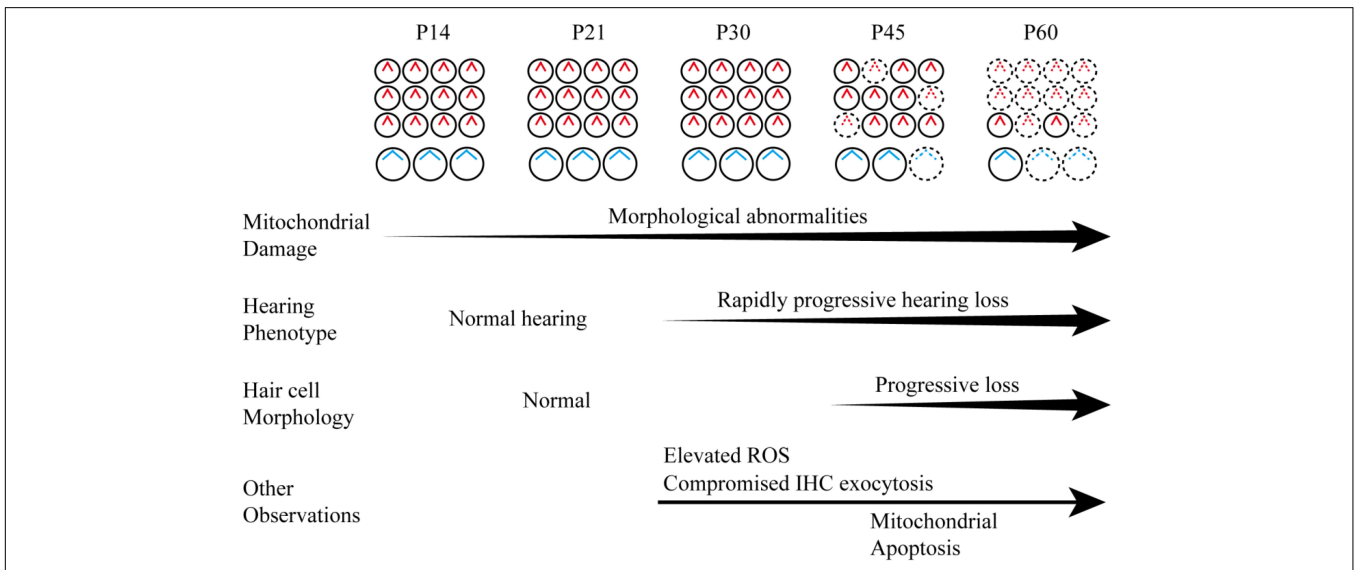

FIGURE 9 | Schematic diagram of the hearing phenotype and hair cell maintenance of the *Hars2* CKO mice between P14 and P60 based on the current morphological and functional studies.

Hars2 CKO mice, accompanied with elevated ROS, compromised IHC sustained exocytosis and eventual hair cell loss (**Figure 9**). As antioxidant drugs targeting mitochondrial ROS pathway have been proven effective to relieve hearing loss associated with noise, ototoxic-drug, and aging (Fetoni et al., 2013; Kamogashira et al., 2015; Kim et al., 2019), HARS2 and other mtARSs may present interesting targets for future therapeutic studies.

CONCLUSION

Our study suggested that *Hars2* is critically required for hair cell survival and maintenance of appropriate function. Mutations in *Hars2* may lead to progressive, rapidly deteriorating hearing loss by hair cell synaptopathy and mitochondrial apoptosis, which are triggered by accumulating mitochondrial damage and elevated ROS stress.

DATA AVAILABILITY STATEMENT

The datasets presented in this study can be found in online repositories. The names of the repository/repositories and accession number(s) can be found in the article/ **Supplementary Material**.

ETHICS STATEMENT

The animal study was reviewed and approved by The Committee of Laboratory Animals of the Ninth People's Hospital, Shanghai Jiao Tong University School of Medicine.

AUTHOR CONTRIBUTIONS

TY and HW designed and supervised the whole project. PX, LW, and XP designed, conducted experiments, and analyzed data. HP helped with confocal imaging and TEM observation. HuL and HoL carried out the IHC patch clamp recordings and analyzed data. QY, YL, and JX assisted in generating *Hars2* CKO mice, performed qPCR and WB analysis. XP, TY, and HW acquired funding. PX, XP, and TY wrote and reviewed the manuscript. All authors contributed to the article and approved the submitted version.

FUNDING

This work was supported by grants from National Science Foundation of China (81700920 to XP, 81970894 to TY, and 81730028 to HW), Natural Science Foundation of Jiangsu Province (BK20191229 to XP), the Fifth "333 Project" Scientific Research Foundation of Jiangsu Province (BRA2019192 to XP), Shanghai Key Laboratory of Translational Medicine on Ear and Nose Diseases (14DZ2260300 to HW), and Shanghai Municipal Education Commission-Gaofeng Clinical Medicine Grant (20152519 to TY).

ACKNOWLEDGMENTS

We would like to thank Yu Kong, Xu Wang, Lijun Pan, and Xue Xu (Electron Microscopy Facilities of Center for Excellence in Brain Science and Technology, Chinese Academy of Sciences) for assistance with TEM sample preparation and analysis of TEM images.

SUPPLEMENTARY MATERIAL

The Supplementary Material for this article can be found online at: https://www.frontiersin.org/articles/10.3389/fncel.2021.804345/full#supplementary-material

REFERENCES

Agnew, T., Goldsworthy, M., Aguilar, C., Morgan, A., Simon, M., Hilton, H., et al. (2018). A Wars2 Mutant Mouse Model Displays OXPHOS Deficiencies and Activation of Tissue-Specific Stress Response Pathways. *Cell Rep.* 25, 3315.e–3328.e. doi: 10.1016/j.celrep.2018.11.080

Akil, O., and Lustig, L. R. (2013). Mouse Cochlear Whole Mount Immunofluorescence. *Bio Protoc.* 3:5. doi: 10.21769/bioprotoc.332

Bock, F. J., and Tait, S. W. G. (2020). Mitochondria as multifaceted regulators of cell death. *Nat. Rev. Mol. Cell Biol.* 21, 85–100. doi: 10.1038/s41580-019-0173-8

Castellano-Muñoz, M., and Ricci, A. J. (2014). Role of intracellular calcium stores in hair-cell ribbon synapse. *Front. Cell Neurosci.* 8:162. doi: 10.3389/fncel.2014.00162

Chen, Y., Gu, J., Liu, J., Tong, L., Shi, F., Wang, X., et al. (2019). Dexamethasone-loaded injectable silk-polyethylene glycol hydrogel alleviates cisplatin-induced ototoxicity. *Int. J. Nanomed.* 14, 4211–4227. doi: 10.2147/IJN.S195336

Chen, Y., Gu, Y., Li, Y., Li, G. L., Chai, R., Li, W., et al. (2021a). Generation of mature and functional hair cells by co-expression of Gfi1, Pou4f3, and Atoh1 in the postnatal mouse cochlea. *Cell Rep.* 35:109016. doi: 10.1016/j.celrep.2021.109016

Chen, Y., Qiang, R., Zhang, Y., Cao, W., Wu, L., Jiang, P., et al. (2021b). The Expression and Roles of the Super Elongation Complex in Mouse Cochlear Lgr5+ Progenitor Cells. *Front. Cell Neurosci.* 15:735723. doi: 10.3389/fncel.2021.735723

Cheng, C., Hou, Y., Zhang, Z., Wang, Y., Lu, L., Zhang, L., et al. (2021). Disruption of the autism-related gene Pak1 causes stereocilia disorganization, hair cell loss, and deafness in mice. *J. Genet. Genomics* 2021:10. doi: 10.1016/j.jgg.2021.03.010

Cheng, C., Wang, Y., Guo, L., Lu, X., Zhu, W., Muhammad, W., et al. (2019). Age-related transcriptome changes in Sox2+ supporting cells in the mouse cochlea. *Stem Cell Res. Ther.* 10:365. doi: 10.1186/s13287-019-1437-0

Choung, Y., Taura, A., Pak, K., Choi, S., Masuda, M., and Ryan, A. (2009). Generation of highly-reactive oxygen species is closely related to hair cell damage in rat organ of Corti treated with gentamicin. *Neuroscience* 161, 214–226. doi: 10.1016/j.neuroscience.2009.02.085

Davis, A. C., and Hoffman, H. J. (2019). Hearing loss: rising prevalence and impact. *Bull World Health Organ.* 97, 646a–646a. doi: 10.2471/blt.19.224683

Dehne, N., Rauen, U., de Groot, H., and Lautermann, J. (2002). Involvement of the mitochondrial permeability transition in gentamicin ototoxicity. *Hear. Res.* 169, 47–55. doi: 10.1016/S0378-5955(02)00338-6

Ding, Y., Meng, W., Kong, W., He, Z., and Chai, R. (2020). The Role of FoxG1 in the Inner Ear. *Front. Cell Dev. Biol.* 8:614954. doi: 10.3389/fcell.2020.614954

Dogan, S. A., Pujol, C., Maiti, P., Kukat, A., Wang, S., Hermans, S., et al. (2014). Tissue-specific loss of DARS2 activates stress responses independently

of respiratory chain deficiency in the heart. *Cell Metab.* 19, 458–469. doi: 10.1016/j.cmet.2014.02.004

Du, Z., Yang, Y., Hu, Y., Sun, Y., Zhang, S., Peng, W., et al. (2012). A long-term high-fat diet increases oxidative stress, mitochondrial damage and apoptosis in the inner ear of D-galactose-induced aging rats. *Hear. Res.* 287, 15–24. doi: 10.1016/j.heares.2012.04.012

Fetoni, A. R., De Bartolo, P., Eramo, S. L. M., Rolesi, R., Paciello, F., Bergamini, C., et al. (2013). Noise-Induced Hearing Loss (NIHL) as a Target of Oxidative Stress-Mediated Damage: Cochlear and Cortical Responses after an Increase in Antioxidant Defense. *J. Neurosci.* 33, 4011–4023. doi: 10.1523/jneurosci.2282-12.2013

Figuccia, S., Degiorgi, A., Ceccatelli Berti, C., Baruffini, E., Dallabona, C., and Goffrini, P. (2021). Mitochondrial Aminoacyl-tRNA Synthetase and Disease: The Yeast Contribution for Functional Analysis of Novel Variants. *Int. J. Mol. Sci.* 22:9. doi: 10.3390/ijms22094524

Fine, A. S., Nemeth, C. L., Kaufman, M. L., and Fatemi, A. (2019). Mitochondrial aminoacyl-tRNA synthetase disorders: an emerging group of developmental disorders of myelination. *J. Neurodev. Disord* 11:29. doi: 10.1186/s11689-019-9292-y

Fischel-Ghodsian, N., Kopke, R. D., and Ge, X. (2004). Mitochondrial dysfunction in hearing loss. *Mitochondrion* 4, 675–694. doi: 10.1016/j.mito.2004.07.040

Friedman, J. R., and Nunnari, J. (2014). Mitochondrial form and function. *Nature* 505, 335–343. doi: 10.1038/nature12985

Fu, X., An, Y., Wang, H., Li, P., Lin, J., Yuan, J., et al. (2021a). Deficiency of Klc2 Induces Low-Frequency Sensorineural Hearing Loss in C57BL/6 J Mice and Human. *Mol. Neurobiol.* 2021:2422. doi: 10.1007/s12035-021-02422-w

Fu, X., Wan, P., Li, P., Wang, J., Guo, S., Zhang, Y., et al. (2021b). Mechanism and Prevention of Ototoxicity Induced by Aminoglycosides. *Front. Cell. Neurosci.* 15:692762. doi: 10.3389/fncel.2021.692762

Gong, S. S., Wang, X. Q., Meng, F. L., Cui, L. M., Yi, Q. Z., Zhao, Q., et al. (2020). Overexpression of mitochondrial histidyl-tRNA synthetase restores mitochondrial dysfunction caused by a deafness-associated tRNA(His) mutation. *J. Biol. Chem.* 295, 940–954. doi: 10.1074/jbc.RA119.010998

Graydon, C. W., Cho, S., Li, G. L., Kachar, B., and von Gersdorff, H. (2011). Sharp Ca^{2+} nanodomains beneath the ribbon promote highly synchronous multivesicular release at hair cell synapses. *J. Neurosci.* 31, 16637–16650. doi: 10.1523/jneurosci.1866-11.2011

Guo, L., Cao, W., Niu, Y., He, S., Chai, R., and Yang, J. (2021). Autophagy Regulates the Survival of Hair Cells and Spiral Ganglion Neurons in Cases of Noise, Ototoxic Drug, and Age-Induced Sensorineural Hearing Loss. *Front. Cell Neurosci.* 15:760422. doi: 10.3389/fncel.2021.760422

Guo, R., Li, J., Chen, C., Xiao, M., Liao, M., Hu, Y., et al. (2021). Biomimetic 3D bacterial cellulose-graphene foam hybrid scaffold regulates neural stem cell proliferation and differentiation. *Coll. Surf. B Biointerf.* 200:111590. doi: 10.1016/j.colsurfb.2021.111590

Guo, R., Xiao, M., Zhao, W., Zhou, S., Hu, Y., Liao, M., et al. (2020). 2D Ti(3)C(2)T(x)MXene couples electrical stimulation to promote proliferation and neural differentiation of neural stem cells. *Acta Biomater* 2020:35. doi: 10.1016/j.actbio.2020.12.035

Han, S., Xu, Y., Sun, J., Liu, Y., Zhao, Y., Tao, W., et al. (2020). Isolation and analysis of extracellular vesicles in a Morpho butterfly wing-integrated microvortex biochip. *Biosens Bioelect.* 154:112073. doi: 10.1016/j.bios.2020.112073

He, Z., Fang, Q., Li, H., Shao, B., Zhang, Y., Zhang, Y., et al. (2019). The role of FOXG1 in the postnatal development and survival of mouse cochlear hair cells. *Neuropharmacology* 144, 43–57. doi: 10.1016/j.neuropharm.2018.10.021

He, Z., Guo, L., Shu, Y., Fang, Q., Zhou, H., Liu, Y., et al. (2017). Autophagy protects auditory hair cells against neomycin-induced damage. *Autophagy* 13, 1884–1904. doi: 10.1080/15548627.2017.1359449

He, Z. H., Li, M., Fang, Q. J., Liao, F. L., Zou, S. Y., Wu, X., et al. (2021). FOXG1 promotes aging inner ear hair cell survival through activation of the autophagy pathway. *Autophagy* 2021, 1–22. doi: 10.1080/15548627.2021.1916194

He, Z. H., Zou, S. Y., Li, M., Liao, F. L., Wu, X., Sun, H. Y., et al. (2020). The nuclear transcription factor FoxG1 affects the sensitivity of mimetic aging hair cells to inflammation by regulating autophagy pathways. *Redox Biol.* 28:101364. doi: 10.1016/j.redox.2019.101364

Hill, K., Yuan, H., Wang, X., and Sha, S. (2016). Noise-Induced Loss of Hair Cells and Cochlear Synaptopathy Are Mediated by the Activation of AMPK. *J. Neurosci.* 36, 7497–7510. doi: 10.1523/jneurosci.0782-16.2016

Hu, Y., Li, D., Wei, H., Zhou, S., Chen, W., Yan, X., et al. (2021). Neurite Extension and Orientation of Spiral Ganglion Neurons Can Be Directed by Superparamagnetic Iron Oxide Nanoparticles in a Magnetic Field. *Int. J. Nanomed.* 16, 4515–4526. doi: 10.2147/ijn.S313673

Kamogashira, T., Fujimoto, C., and Yamasoba, T. (2015). Reactive oxygen species, apoptosis, and mitochondrial dysfunction in hearing loss. *BioMed. Res. Internat.* 2015:617207. doi: 10.1155/2015/617207

Kim, Y. R., Baek, J. I., Kim, S. H., Kim, M. A., Lee, B., Ryu, N., et al. (2019). Therapeutic potential of the mitochondria-targeted antioxidant MitoQ in mitochondrial-ROS induced sensorineural hearing loss caused by Idh2 deficiency. *Redox Biol.* 20, 544–555. doi: 10.1016/j.redox.2018.11.013

Konovalova, S., and Tyynismaa, H. (2013). Mitochondrial aminoacyl-tRNA synthetases in human disease. *Mol. Genet. Metab.* 108, 206–211. doi: 10.1016/j.ymgme.2013.01.010

Li, A., You, D., Li, W., Cui, Y., He, Y., Li, W., et al. (2018). Novel compounds protect auditory hair cells against gentamycin-induced apoptosis by maintaining the expression level of H3K4me2. *Drug Deliv.* 25, 1033–1043. doi: 10.1080/10717544.2018.1461277

Lin, X., Li, G., Zhang, Y., Zhao, J., Lu, J., Gao, Y., et al. (2019). Hearing consequences in Gjb2 knock-in mice: implications for human p.V37I mutation. *Aging* 11, 7416–7441. doi: 10.18632/aging.102246

Liotta, A., Rösner, J., Huchzermeyer, C., Wojtowicz, A., Kann, O., Schmitz, D., et al. (2012). Energy demand of synaptic transmission at the hippocampal Schaffer-collateral synapse. *J. Cereb. Blood Flow Metab.* 32, 2076–2083. doi: 10.1038/jcbfm.2012.116

Liu, H., Li, G., Lu, J., Gao, Y. G., Song, L., Li, G. L., et al. (2019a). Cellular Differences in the Cochlea of CBA and B6 Mice May Underlie Their Difference in Susceptibility to Hearing Loss. *Front. Cell Neurosci.* 13:60. doi: 10.3389/fncel.2019.00060

Liu, H., Lu, J., Wang, Z., Song, L., Wang, X., Li, G. L., et al. (2019b). Functional alteration of ribbon synapses in inner hair cells by noise exposure causing hidden hearing loss. *Neurosci. Lett.* 707:134268. doi: 10.1016/j.neulet.2019.05.022

Liu, H., Peng, H., Wang, L., Xu, P., Wang, Z., Liu, H., et al. (2020). Differences in Calcium Clearance at Inner Hair Cell Active Zones May Underlie the Difference in Susceptibility to Noise-Induced Cochlea Synaptopathy of C57BL/6J and CBA/CaJ Mice. *Front. Cell Dev. Biol.* 8:635201. doi: 10.3389/fcell.2020.635201

Liu, W., Xu, L., Wang, X., Zhang, D., Sun, G., Wang, M., et al. (2021). PRDX1 activates autophagy via the PTEN-AKT signaling pathway to protect against cisplatin-induced spiral ganglion neuron damage. *Autophagy* 2021, 1–23. doi: 10.1080/15548627.2021.1905466

Liu, W., Xu, X., Fan, Z., Sun, G., Han, Y., Zhang, D., et al. (2019c). Wnt Signaling Activates TP53-Induced Glycolysis and Apoptosis Regulator and Protects Against Cisplatin-Induced Spiral Ganglion Neuron Damage in the Mouse Cochlea. *Antioxid Redox Signal* 30, 1389–1410. doi: 10.1089/ars.2017.7288

Liu, Y., Qi, J., Chen, X., Tang, M., Chu, C., Zhu, W., et al. (2019d). Critical role of spectrin in hearing development and deafness. *Sci. Adv.* 5:eaav7803. doi: 10.1126/sciadv.aav7803

Lv, J., Fu, X., Li, Y., Hong, G., Li, P., Lin, J., et al. (2021). Deletion of Kcnj16 in Mice Does Not Alter Auditory Function. *Front. Cell Dev. Biol.* 9:630361. doi: 10.3389/fcell.2021.630361

Majtnerová, P., and Roušar, T. (2018). An overview of apoptosis assays detecting DNA fragmentation. *Mol. Biol. Rep.* 45, 1469–1478. doi: 10.1007/s11033-018-4258-9

Matern, M., Vijayakumar, S., Margulies, Z., Milon, B., Song, Y., Elkon, R., et al. (2017). Gfi1(Cre) mice have early onset progressive hearing loss and induce recombination in numerous inner ear non-hair cells. *Sci. Rep.* 7:42079. doi: 10.1038/srep42079

McKay, S. E., Yan, W., Nouws, J., Thormann, M. J., Raimundo, N., Khan, A., et al. (2015). Auditory Pathology in a Transgenic mtTFB1 Mouse Model of Mitochondrial Deafness. *Am. J. Pathol.* 185, 3132–3140. doi: 10.1016/j.ajpath.2015.08.014

Meyer, A. C., Frank, T., Khimich, D., Hoch, G., Riedel, D., Chapochnikov, N. M., et al. (2009). Tuning of synapse number, structure and function in the cochlea. *Nat. Neurosci.* 12, 444–453. doi: 10.1038/nn.2293

Nagase, M., Takahashi, Y., Watabe, A. M., Kubo, Y., and Kato, F. (2014). On-site energy supply at synapses through monocarboxylate transporters maintains

excitatory synaptic transmission. *J. Neurosci.* 34, 2605–2617. doi: 10.1523/jneurosci.4687-12.2014

Natarajan, V., Chawla, R., Mah, T., Vivekanandan, R., Tan, S. Y., Sato, P. Y., et al. (2020). Mitochondrial Dysfunction in Age-Related Metabolic Disorders. *Proteomics* 20:e1800404. doi: 10.1002/pmic.201800404

Nemeth, C. L., Tomlinson, S. N., Rosen, M., O'Brien, B. M., Larraza, O., Jain, M., et al. (2020). Neuronal ablation of mt-AspRS in mice induces immune pathway activation prior to severe and progressive cortical and behavioral disruption. *Exp. Neurol.* 326:113164. doi: 10.1016/j.expneurol.2019.113164

Oprescu, S. N., Griffin, L. B., Beg, A. A., and Antonellis, A. (2017). Predicting the pathogenicity of aminoacyl-tRNA synthetase mutations. *Methods* 113, 139–151. doi: 10.1016/j.ymeth.2016.11.013

Pierce, S. B., Chisholm, K. M., Lynch, E. D., Lee, M. K., Walsh, T., Opitz, J. M., et al. (2011). Mutations in mitochondrial histidyl tRNA synthetase HARS2 cause ovarian dysgenesis and sensorineural hearing loss of Perrault syndrome. *Proc. Natl. Acad. Sci. U S A* 108, 6543–6548. doi: 10.1073/pnas.1103471108

Qi, J., Liu, Y., Chu, C., Chen, X., Zhu, W., Shu, Y., et al. (2019). A cytoskeleton structure revealed by super-resolution fluorescence imaging in inner ear hair cells. *Cell Discov.* 5:12. doi: 10.1038/s41421-018-0076-4

Qi, J., Zhang, L., Tan, F., Liu, Y., Chu, C., Zhu, W., et al. (2020). Espin distribution as revealed by super-resolution microscopy of stereocilia. *Am. J. Transl. Res.* 12, 130–141.

Qian, F., Wang, X., Yin, Z., Xie, G., Yuan, H., Liu, D., et al. (2020). The slc4a2b gene is required for hair cell development in zebrafish. *Aging*12, 18804–18821. doi: 10.18632/aging.103840

Safieddine, S., El-Amraoui, A., and Petit, C. (2012). The auditory hair cell ribbon synapse: from assembly to function. *Ann. Rev. Neurosci.* 35, 509–528. doi: 10.1146/annurev-neuro-061010-113705

Schmittgen, T. D., and Livak, K. J. (2008). Analyzing real-time PCR data by the comparative C(T) method. *Nat. Protoc.* 3, 1101–1108. doi: 10.1038/nprot.2008.73

Schwander, M., Kachar, B., and Müller, U. (2010). Review series: The cell biology of hearing. *J Cell Biol.* 190, 9–20. doi: 10.1083/jcb.201001138

Scimemi, P., Santarelli, R., Selmo, A., and Mammano, F. (2014). Auditory brainstem responses to clicks and tone bursts in C57 BL/6J mice. *Acta Otorhinolaryngol. Ital.* 34, 264–271.

Sheffield, A. M., and Smith, R. J. H. (2019). The Epidemiology of Deafness. *Cold Spr. Harb. Perspect. Med.* 9:33258. doi: 10.1101/cshperspect.a033258

Spoendlin, H. (1971). Primary structural changes in the organ of Corti after acoustic overstimulation. *Acta Otolaryngol.* 71, 166–176. doi: 10.3109/00016487109125346

van der Laan, M., Bohnert, M., Wiedemann, N., and Pfanner, N. (2012). Role of MINOS in mitochondrial membrane architecture and biogenesis. *Trends Cell Biol.* 22, 185–192. doi: 10.1016/j.tcb.2012.01.004

Vikhe Patil, K., Canlon, B., and Cederroth, C. R. (2015). High quality RNA extraction of the mammalian cochlea for qRT-PCR and transcriptome analyses. *Hear Res* 325, 42–48. doi: 10.1016/j.heares.2015.03.008

Wang, M., Sips, P., Khin, E., Rotival, M., Sun, X., Ahmed, R., et al. (2016). Wars2 is a determinant of angiogenesis. *Nat. Commun.* 7:12061. doi: 10.1038/ncomms12061

Wang, X., Zhu, Y., Long, H., Pan, S., Xiong, H., Fang, Q., et al. (2019). Mitochondrial Calcium Transporters Mediate Sensitivity to Noise-Induced Losses of Hair Cells and Cochlear Synapses. *Front. Mole. Neurosci.* 11:469. doi: 10.3389/fnmol.2018.00469

Wang, Y., Zhou, J. B., Zeng, Q. Y., Wu, S., Xue, M. Q., Fang, P., et al. (2020). Hearing impairment-associated KARS mutations lead to defects in aminoacylation of both cytoplasmic and mitochondrial tRNA(Lys). *Sci. China Life Sci.* 2020:1619. doi: 10.1007/s11427-019-1619-x

Wei, H., Chen, Z., Hu, Y., Cao, W., Ma, X., Zhang, C., et al. (2021). Topographically Conductive Butterfly Wing Substrates for Directed Spiral Ganglion Neuron Growth. *Small* 17:e2102062. doi: 10.1002/smll.202102062

Wollweber, F., von der Malsburg, K., and van der Laan, M. (2017). Mitochondrial contact site and cristae organizing system: A central player in membrane shaping and crosstalk. *Biochim. Biophys. Acta Mol. Cell Res.* 1864, 1481–1489. doi: 10.1016/j.bbamcr.2017.05.004

Wong, H. C., Zhang, Q., Beirl, A. J., Petralia, R. S., Wang, Y. X., and Kindt, K. (2019). Synaptic mitochondria regulate hair-cell synapse size and function. *Elife* 8:48914. doi: 10.7554/eLife.48914

Wu, F., Xiong, H., and Sha, S. (2020). Noise-induced loss of sensory hair cells is mediated by ROS/AMPKα pathway. *Redox Biol.* 29:101406. doi: 10.1016/j.redox.2019.101406

Yang, H., Gan, J., Xie, X., Deng, M., Feng, L., Chen, X., et al. (2010). Gfi1-Cre knock-in mouse line: A tool for inner ear hair cell-specific gene deletion. *Genesis* 48, 400–406. doi: 10.1002/dvg.20632

Yu, J., Jiang, W., Cao, L., Na, X., and Yang, J. (2020). Two novel likely pathogenic variants of HARS2 identified in a Chinese family with sensorineural hearing loss. *Hereditas* 157:47. doi: 10.1186/s41065-020-00157-7

Yu, J., Wang, Y., Liu, P., Li, Q., Sun, Y., and Kong, W. (2014). Mitochondrial DNA common deletion increases susceptibility to noise-induced hearing loss in a mimetic aging rat model. *Biochem. Biophys. Res. Commun.* 453, 515–520. doi: 10.1016/j.bbrc.2014.09.118

Zhang, L., Du, Z., and Gong, S. (2021). Mitochondrial Dysfunction and Sirtuins: Important Targets in Hearing Loss. *Neural. Plasticity* 2021:5520794. doi: 10.1155/2021/5520794

Zhang, S., Dong, Y., Qiang, R., Zhang, Y., Zhang, X., Chen, Y., et al. (2021). Characterization of Strip1 Expression in Mouse Cochlear Hair Cells. *Front. Genet.* 12:625867. doi: 10.3389/fgene.2021.625867

Zhang, S., Zhang, Y., Dong, Y., Guo, L., Zhang, Z., Shao, B., et al. (2020). Knockdown of Foxg1 in supporting cells increases the trans-differentiation of supporting cells into hair cells in the neonatal mouse cochlea. *Cell Mol. Life Sci.* 77, 1401–1419. doi: 10.1007/s00018-019-03291-2

Zhang, Y., Li, Y., Fu, X., Wang, P., Wang, Q., Meng, W., et al. (2021). The Detrimental and Beneficial Functions of Macrophages After Cochlear Injury. *Front. Cell Dev. Biol.* 9:631904. doi: 10.3389/fcell.2021.631904

Zhao, J., Li, G., Zhao, X., Lin, X., Gao, Y., Raimundo, N., et al. (2020). Down-regulation of AMPK signaling pathway rescues hearing loss in TFB1 transgenic mice and delays age-related hearing loss. *Aging* 12, 5590–5611. doi: 10.18632/aging.102977

Zheng, Q. Y., Johnson, K. R., and Erway, L. C. (1999). Assessment of hearing in 80 inbred strains of mice by ABR threshold analyses. *Hear. Res.* 130, 94–107. doi: 10.1016/s0378-5955(99)00003-9

Zhong, Z., Fu, X., Li, H., Chen, J., Wang, M., Gao, S., et al. (2020). Citicoline Protects Auditory Hair Cells Against Neomycin-Induced Damage. *Front. Cell Dev. Biol.* 8:712. doi: 10.3389/fcell.2020.00712

Zhou, H., Qian, X., Xu, N., Zhang, S., Zhu, G., Zhang, Y., et al. (2020). Disruption of Atg7-dependent autophagy causes electromotility disturbances, outer hair cell loss, and deafness in mice. *Cell Death Dis.* 11:913. doi: 10.1038/s41419-020-03110-8

Conflict of Interest: The authors declare that the research was conducted in the absence of any commercial or financial relationships that could be construed as a potential conflict of interest.

Publisher's Note: All claims expressed in this article are solely those of the authors and do not necessarily represent those of their affiliated organizations, or those of the publisher, the editors and the reviewers. Any product that may be evaluated in this article, or claim that may be made by its manufacturer, is not guaranteed or endorsed by the publisher.

frontiers in Cellular Neuroscience

REVIEW
published: 05 January 2022
doi: 10.3389/fncel.2021.814891

Mechanism and Prevention of Spiral Ganglion Neuron Degeneration in the Cochlea

*Li Zhang[1], Sen Chen[1] and Yu Sun[1,2]**

[1] Department of Otorhinolaryngology, Union Hospital, Tongji Medical College, Huazhong University of Science and Technology, Wuhan, China, [2] Institute of Otorhinolaryngology, Tongji Medical College, Huazhong University of Science and Technology, Wuhan, China

Sensorineural hearing loss (SNHL) is one of the most prevalent sensory deficits in humans, and approximately 360 million people worldwide are affected. The current treatment option for severe to profound hearing loss is cochlear implantation (CI), but its treatment efficacy is related to the survival of spiral ganglion neurons (SGNs). SGNs are the primary sensory neurons, transmitting complex acoustic information from hair cells to second-order sensory neurons in the cochlear nucleus. In mammals, SGNs have very limited regeneration ability, and SGN loss causes irreversible hearing loss. In most cases of SNHL, SGN damage is the dominant pathogenesis, and it could be caused by noise exposure, ototoxic drugs, hereditary defects, presbycusis, etc. Tremendous efforts have been made to identify novel treatments to prevent or reverse the damage to SGNs, including gene therapy and stem cell therapy. This review summarizes the major causes and the corresponding mechanisms of SGN loss and the current protection strategies, especially gene therapy and stem cell therapy, to promote the development of new therapeutic methods.

Keywords: spiral ganglion neuron, sensorineural hearing loss, gene therapy, stem cell therapy, cochlea

OPEN ACCESS

Edited by:
Zuhong He,
Wuhan University, China

Reviewed by:
Ke Liu,
Capital Medical University, China
Wenwen Liu,
Shandong University, China

****Correspondence:***
Yu Sun
sunyu@hust.edu.cn

Specialty section:
This article was submitted to Cellular Neuropathology, a section of the journal Frontiers in Cellular Neuroscience

Received: *14 November 2021*
Accepted: *09 December 2021*
Published: *05 January 2022*

Citation:
Zhang L, Chen S and Sun Y (2022) Mechanism and Prevention of Spiral Ganglion Neuron Degeneration in the Cochlea. Front. Cell. Neurosci. 15:814891. doi: 10.3389/fncel.2021.814891

INTRODUCTION

Hearing loss is one of the major health problems worldwide, affecting over 5% of the population of the world or approximately 466 million people[1]. Children with hearing loss have difficulties in language and cognitive development, thus affecting their school performance, ability to integrate into mainstream job markets, and overall quality of life (Wake et al., 2004; Borton et al., 2010). Hearing loss in the elderly may increase the risk of dementia and Alzheimer's disease (Lin et al., 2011). Based on the affected cochlear sites, hearing loss is generally categorized into conductive and sensorineural hearing loss (SNHL). SNHL is usually caused by irreversible damage to cells along the auditory pathway, including spiral ganglion neurons (SGNs). The major causes of SGN loss include harmful extrinsic (noise, ototoxic drugs, etc.) and intrinsic causes (genetic factors, aging, etc.). The mature sensorineural tissues of the cochlea in mammals, including hair cells (HCs) and SGNs, have very limited repair capacity and do not regenerate, so this damage is usually permanent.

The somata of SGNs reside in Rosenthal's spiral canal. Each cell body of SGNs gives rise to a peripheral process that extends toward the organ of Corti and a central process that connects

[1]https://www.who.int/news-room/fact-sheets/detail/deafness-and-hearing-loss

together to form the auditory nerve emitting into the brain, thus establishing a point-to-point communication between the cochlear HCs and the cochlear nucleus. Human SGNs are divided into two types: type I and type II afferent neurons. Ninety-five percent of the neuron population in the spiral ganglion consists of type I afferent neurons, which are myelinated and connect inner hair cells (IHC) with the cochlear nuclei of the brainstem (Eybalin, 1993). Each dendrite of type I afferent neurons innervates only one IHC, while each IHC receives contacts from 10 to 20 dendrites from type I afferent neurons (Eybalin, 1993). Type II afferent neurons account for only 5–10% of the neuron population (Spoendlin, 1972; Ruggero et al., 1982) and they are pseudounipolar and non-myelinated neurons (Berglund and Ryugo, 1986, 1991). Each type II afferent neuron innervates approximately 15 to 20 outer hair cells (OHCs), which are from the same row, while each OHC receives only one contact from one type II afferent neuron.

Until recently, the only treatments for SNHL have been hearing aids and cochlear implants, both of which are highly unnatural compared with normal sound stimulation, and they perform poorly in noisy environments. Cochlear implants are the standard therapy for severe to profound hearing loss, and their performance is variable, which is likely related to the number of residual SGNs (Seyyedi et al., 2014). No clinical therapies existed to rescue the dying SGNs or regenerate these cells once lost. Fortunately, great progress has been made in new biological therapies, such as gene therapy and stem cell therapy, providing promising perspectives for the future restoration of hearing in deaf people. This review summarizes the major causes and the related mechanisms leading to the degeneration of SGNs and discusses recent therapeutic strategies in gene therapy and stem cell therapy research to reverse SGN damage.

MAJOR CAUSES AND CORRESPONDING MECHANISMS OF SPIRAL GANGLION NEURONS LOSS

Noise Exposure

Exposure to excessive levels of sound leads to a temporary threshold shift (TTS) that can fully recover to normal or a permanent threshold shift (PTS) that fails to return to pre-exposure levels. The loss of afferent ribbon synapses and the degeneration of SGNs can be triggered by noise exposure (Fernandez et al., 2015). After mild noise exposure with TTS, swelling of afferent endings and the primary degeneration of SGNs were observed in a mouse model (Puel et al., 1998; Kujawa and Liberman, 2009). During the early stage of noise exposure, the quantity and quality of the ribbon synapses significantly deceased without total recovery even after several days when the hearing was fully recovered (Shi et al., 2015). This form of damage is thought to contribute to hearing difficulties in noisy environments, tinnitus, and other auditory dysfunctions (Kujawa and Liberman, 2009). However, high-intensity exposure (>100 dB sound pressure level, SPL) or repeated overstimulation leads to PTSs (Spoendlin, 1985). After overexposure, hair cell damage can be visible within minutes, while the death of SGNs is delayed by months to years (Johnsson, 1974).

Excitotoxicity is a complex process triggered by the overactivation of glutamate receptors that results in degenerative neuronal cell death (Lai et al., 2014). Type I SGNs are activated by glutamate, and excessive release of the excitatory neurotransmitter (glutamate) from IHC could lead to the death of SGNs. Excitotoxicity is thought to play an essential role in noise-induced hearing loss. SGN afferent synapse swelling after noise exposure is likely due to glutamate toxicity (Robertson, 1983; Puel et al., 1998). Excessive glutamate release after noise overstimulation leads to the overactivation of glutamate receptors on the postsynaptic membrane of SGNs. Such overactivation leads to an influx of cations such as Na^+ and Ca^{2+}. Then, Cl^- and water molecules passively cross the plasma membrane, leading to edema and even death of the SGNs (Pujol and Puel, 1999; Wang et al., 2002). Administration of exogenous glutamate receptor agonists, including AMPA and kainite, to the cochlea could mimic this process (Ruel et al., 2000; Le Prell et al., 2004), while swelling of the afferent synapse could be prevented by treatment with a glutamate antagonist (Puel et al., 1998). These results suggest a contribution of excitotoxicity to SGN damage induced by noise exposure. In addition, an influx of Ca^{2+} into the afferent nerves of the cochlea leads to calcium-dependent caspase-mediated apoptosis by the intrinsic (mitochondria-mediated) pathway (Puel et al., 1998; Pujol and Puel, 1999; Ruel et al., 2007).

Toxic Drugs

Certain therapeutic agents could cause functional impairment and cellular degeneration of SGNs. More than 130 drugs have been found to be ototoxic (Liu et al., 2011, 2012; Lanvers-Kaminsky et al., 2017). Two important classes are aminoglycoside antibiotics (Jeong et al., 2010; Wang et al., 2021) and platinum-based antineoplastic agents (Tsukasaki et al., 2000; Liu et al., 2019b, 2021), which could cause permanent hearing loss. Cisplatin, the most commonly used platinum-based antineoplastic agent and the most ototoxic drug in frequent use in the clinic (Muggia et al., 2015), results in OHC loss in a basal to apical gradient and SGN and cell loss in the stria vascularis (Schacht et al., 2012). Degeneration of SGNs caused by toxic drugs is frequently observed secondary to hair cell loss. However, Wang et al. (2003) found that the neurotoxic effects after carboplatin treatment occurred approximately 1 day before the IHCs were injured. A unique case showed that the benefit of cochlear implantation (CI) was lost due to the use of cisplatin (Harris et al., 2011). These results indicate that SGNs are the primary injury sites after treatment with platinum-based antineoplastic agents, and they are not limited to hair cell loss. However, the mechanisms of SGN damage induced by cisplatin have not been fully explained. One of these mechanisms is thought to be mediated through ROS generation, subsequently inducing calcium influx and apoptosis (Kawai et al., 2006; Mohan et al., 2014). Cisplatin also activates apoptosis by increasing the release of cytochrome c (Garcia-Berrocal et al., 2007; Jeong et al., 2007). The expression of JNK, phospho-JNK, c-Jun, and phospho-c-Jun are also increased (Jeong et al., 2010), indicating that activation of the c-Jun N-terminal kinase signaling pathway

is involved in SGN apoptosis in response to oxidative stress. Liu et al. (2019b) found that Wnt signaling activated TIGAR, protecting SGNs against cisplatin-induced damage through the suppression of oxidative stress and apoptosis. Autophagic flux was found to be activated by PRDX1 *via* the PTEN/AKT signaling pathway in SGNs after cisplatin damage, attenuating ROS accumulation to mediate protective effects (Liu et al., 2021).

Infections

Infection with some viruses or bacteria, such as cytomegalovirus (CMV) and *Streptococcus pneumoniae*, leads to SNHL due to the degeneration of SGNs. CMV is the leading cause of congenital virus infection, and it affects around0.5–1% of all live births worldwide, with approximately 10% of infected infants developing hearing loss (Lombardi et al., 2010; Plosa et al., 2012). A histopathological study of the human temporal bone showed that the total number of SGNs was significantly reduced in ears with congenital infectious diseases compared to normal ears (Miura et al., 2002). However, the mechanisms of the pathogenesis are still unclear. Mouse models of CMV-induced profound SNHL have shown that SGNs are preferentially infected by CMV and that the number of SGNs dramatically decreases (Juanjuan et al., 2011; Schachtele et al., 2011; Bradford et al., 2015; Ikuta et al., 2015). These results indicate that a reduction in the number of SGNs may be the major cause of congenital CMV infection-induced SNHL. Increased numbers of macrophages and CD3 + mononuclear cells were detected in the SGNs of infected mice with hearing loss (Schachtele et al., 2011; Bradford et al., 2015). High levels of ROS were found to be involved in CMV-induced profound SNHL (Schachtele et al., 2011; Zhuang et al., 2018). Multiple proinflammatory molecules, including tumor necrosis factor-α, interleukin-6, CCL8, CXCL9, and CXCL10 were increased in CMV infection-induced SNHL (Teissier et al., 2011; Gabrielli et al., 2013; Melnick and Jaskoll, 2013; Bradford et al., 2015). Li et al. (2016) demonstrated that SGN apoptosis has an important relationship with SNHL induced by CMV infection. In addition to CMV, *Streptococcus pneumonia* and *Mycobacterium tuberculosis* infection-induced SNHL also led to a markedly decreased density of SGNs (Klein et al., 2003; Kuan et al., 2007; Perny et al., 2016).

Genetic Factors

Genetic factors play a crucial role in SNHL, including congenital and later-onset hearing loss. More than 150 genes have been identified to be directly associated with SNHL. Among the genes identified are those encoding transcription factors (*POU3F4*), ion channels (*KCNQ1* and *KCNE1*), extracellular matrix components (*COCH*), cytoskeletal proteins (several unconventional myosins), and proteins of unknown function (*DFNA5*). Mutations in these genes result in either primary and/or secondary SGN damage. Primary SGN degeneration is more likely to be observed with mutations of genes that play an important role in neuronal survival and the regulation of synaptic transmission, such as *POU3F4*, *SLC17A8*, and *PJVK* (Ruel et al., 2008; Brooks et al., 2020; Cheng et al., 2020). Mutations in *POU3F4*/*Pou3f4*, the encoding of a transcription factor, and POU-domain protein cause deafness in humans and mice (Kandpal et al., 1996; Minowa et al., 1999). *Pou3f4*$^{-/-}$ mice showed disrupted radial bundle fasciculation and synapse formation (Coate et al., 2012) and degeneration of SGNs (Coate et al., 2012; Brooks et al., 2020). The hair cells and supporting cells in the *Pou3f4*$^{-/-}$ mice appeared normal, indicating that the degeneration of SGNs is primary in this mouse model. Secondary SGN degeneration often occurs due to mutations in genes affecting hair cells or supporting cells. Mutations in the *GJB2* gene, expressed in supporting cells, are the most common cause of hereditary hearing loss. Conditional Cx26-null mice exhibit secondary SGN degeneration resulting from the degeneration of hair cells and supporting cells (Wang et al., 2009; Takada et al., 2014). Degeneration of SGNs was observed in mice with mutations in other deafness genes, such as *KCNQ1* and *KCNE1* (Vetter et al., 1996; Eugene et al., 2009). In addition, hundreds of genes, including mitochondrial genes and antioxidant defense-related genes, are thought to predispose people to noise-induced, drug-induced and age-related hearing loss by aggravating SGN damage (Wang and Puel, 2018).

Aging

Age-related hearing loss (ARHL) is the third most prevalent chronic medical condition affecting the elderly (Lethbridge-Cejku et al., 2004), and it is characterized by difficulties in speech discrimination and sound detection and localization, particularly in the presence of background noise. It is symmetric, progressive, and sensorineural, and it begins in the high-frequency region and spreads toward the low-frequency regions as age advances. SGNs are frequently lost during aging secondary to the loss of HCs (Schacht and Hawkins, 2005) as hair cells and supporting cells provide neurotrophic support, including neurotrophin-3 (NT3), brain-derived neurotrophic factor (BDNF), and glial cell line-derived neurotrophic factor (GDNF) for SGN survival (Ernfors et al., 1995; Fritzsch et al., 1997; Takeno et al., 1998). However, SGN degeneration without HC loss is common among mammals during aging. The loss of SGNs is probably independent of the age-related loss of HCs. Primary and secondary degeneration of SGNs may coincide in the same cochlea (Hequembourg and Liberman, 2001). It may be impossible to separate the primary and secondary degeneration of SGNs during the early degeneration stages of aging. Oxidative metabolism is involved in age-related SGN loss. Significant age-related loss of SGN fibers has been observed prior to HC in mice lacking copper/zinc superoxide dismutase, the first-line defense against oxidative damage caused by ROS (Keithley et al., 2005). Mitochondria play a key role in ROS generation. It has been shown that age-related loss of SGNs in mice with mitochondrial dysfunction is more severe than in control mice (Niu et al., 2007; Yamasoba et al., 2007). In addition to ROS generation, mitochondria may also promote ARHL *via* apoptosis and calcium signaling pathways.

Signaling pathways that impact the aging of the whole organism could influence age-related SGN loss, as age is the most important predictor of SGN survival. Two key molecular pathways, the insulin/insulin-like growth factor-1 (IGF-1) pathway and the lipophilic/steroid hormone pathway, are closely related to the survival of SGNs. Caloric restriction

(CR) can effectively modulate the IGF-1 pathway to prevent age-related neuronal loss of the enteric nervous system (Cowen, 2002; Thrasivoulou et al., 2006). CR was found to delay auditor brainstem response (ABR) threshold shifts during aging and ameliorate SGN degeneration in mice (Park et al., 1990; Willott et al., 1995; Someya et al., 2007; Yamasoba et al., 2007). Glucocorticoids, lipophilic/steroid hormones, have been shown to have detrimental effects on neuronal function during aging (Sapolsky et al., 1986; Miller and O'Callaghan, 2005; Landfield et al., 2007). In mice lacking the β2 subunit of the nicotinic acetylcholine receptor, SGN loss was accelerated (Bao et al., 2005) and serum corticosterone (a major glucocorticoid) increased (Zoli et al., 1999) during ageing. Acceleration of age-related SGN loss was also found in mice lacking NF-κB (Lang et al., 2006) whose translocation in SGNs appears to be controlled by glucocorticoids (Tahera et al., 2006).

PROTECTION AND REGENERATION OF SPIRAL GANGLION NEURONS

Currently, there are no clinical therapies to prevent SGN degeneration or to regenerate these cells once lost. Numerous efforts have been made to explore potential therapies that could ameliorate the degeneration of SGNs. It is not surprising that agents that could interfere with the progression of SGN degeneration are promising candidates for SNHL. These pharmacological therapies include mitochondrial metabolic regulators, autophagy modulators, antioxidants or inhibitors of kinases, and apoptosis. However, there are no known drugs specifically approved by the FDA to prevent SGN degeneration or promote SGN repair. Although osmotic pumps containing neurotrophic factors (NTs) have been used to treat deaf animal models and have shown promising results, concerns about infection and the duration of efficacy restrict their widespread clinical application (Ma et al., 2019). More recent studies have focused on gene therapy and stem cell therapy, which could possibly provide long-term treatment efficacy (Liu et al., 2019a).

Gene Therapy

Gene therapy is a method that introduces a target foreign gene or gene regulatory element into target cells to replace or fix defective genes (Mulligan, 1993). Factors including vector types, administration routes, administration time, etc., have a vital role in the treatment effect. Currently, transfer vectors include viral and non-viral vectors. The most commonly used and most promising vectors in cochlear gene therapy are adenovirus (Ad)-based and vector adeno-associated virus (AAV)-based vectors, as both have effective transduction of many cochlear cell types (Kesser and Lalwani, 2009; Ruan et al., 2010). The capacity of Ad vectors is large (26–45 kb), which greatly expands the number of target genes, while AAV vectors have limited capacity (4–5 kb). AAV vectors are not associated with any known human disease, making them unique among viral vectors. In addition to choosing a proper vector, a safe and efficient administration route is required for inner ear gene therapies. The most commonly used routes for introducing delivery vectors into the inner ear of neonatal and adult animals are through the scala media, scala tympani, and the semicircular canal (Kilpatrick et al., 2011; Gassner et al., 2012; Chien et al., 2015). Some studies also delivered viral vectors *in utero* (Bedrosian et al., 2006; Gubbels et al., 2008). Gene therapy goals for SGNs include preventing the degeneration of SGNs and promoting the regeneration of SGNs. The most studied gene therapies in animal models to protect the SGN are NTs, such as BDNF and NT3 (Wan et al., 2014; Budenz et al., 2015; Pfingst et al., 2017). Neurotrophins regulate neuronal differentiation and survival during cochlear development (Fritzsch et al., 1999; Farinas et al., 2001; Rubel and Fritzsch, 2002; Yang et al., 2011). BDNF and NT3, mainly provided by supporting cells of the organ of Corti, have important roles in the development and maintenance of SGNs (Schecterson and Bothwell, 1994; Fritzsch et al., 1999; Stankovic et al., 2004). Loss of BDNF and NT3 support leads to the gradual degeneration of SGNs (Fritzsch et al., 1999; Alam et al., 2007).

Exogenous NT (BDNF, GDNF, NT3, CNTF, and others) administration into the cochlea can prevent precipitous SGN loss (Gillespie et al., 2003) and also promote long-term survival of SGNs (Shepherd et al., 2008; Agterberg et al., 2009; Leake et al., 2011), especially when combined with electrical stimulation (Shepherd et al., 2005; Leake et al., 2013). Several studies in deaf animal models, including guinea pigs, mice (Fukui et al., 2012), rats (Wu et al., 2011) and cats, have reported improved SGN survival with virally mediated NT expression compared to controls after acoustic trauma (**Table 1**). Staecker et al. (1998) reported that an HSV-1 vector containing *BDNF* could almost completely rescue the damaged SGNs caused by neomycin despite the destruction of all HCs. Another study demonstrated that enhanced SGN survival was observed for up to 4 weeks in aminoglycoside/diuretic-induced deafened guinea pigs with the administration of Ad-mediated transfection of *GDNF* compared to the controls (Yagi et al., 2000). Ad-mediated gene transfer of *BDNF* and *NT3* also prevented SGN degeneration after aminoglycoside-induced deafness in guinea pigs (Wise et al., 2010). HSV1-mediated NT3 expression protected SGNs from degeneration caused by cisplatin-induced ototoxicity in aged mice (Bowers et al., 2002). In addition to SGN protection, gene therapy with NTs could also improve the survival and resprouting of the radial nerve fibers of SGNs (Shibata et al., 2010; Wise et al., 2010; Atkinson et al., 2012, 2014; Fukui et al., 2012; Chen et al., 2018).

Noise-induced synapse loss could be prevented with inner ear gene therapy with NTs. SGN degeneration and hearing loss in rats exposed to blast waves were prevented by gene therapy with Ad-mediated human beta-nerve growth factor gene transfer (Wu et al., 2011). Synapse damage caused by noise exposure could be prevented by *Ntf3* overexpression *via* gene therapy (Wan et al., 2014). AAV-mediated *NT3* overexpression prevented and repaired noise-induced synaptopathy (Chen et al., 2018; Hashimoto et al., 2019). Pfingst et al. (2017) also demonstrated that AAV-mediated *NT3* gene therapy could prevent SGN degeneration in deafened, implanted guinea pigs.

A proper administration approach is important for SGN gene therapy. Wise et al. (2010) demonstrated that injection of vectors into the scala media resulted in more localized gene

TABLE 1 | Studies of gene therapy for SGNs rescue in deafened animals.

Animal	Damage model	Administration route	Viral vectors	Morphological protection	References
CBA/6J mice	Neomycin	scala tympani	HSV1-*BDNF*	significantly improved SGNs survival	Staecker et al., 1998
Guinea pig	Kanamycin + ethacrynic acid	scala tympani	Ad5-*GDNF*	significantly enhanced SGNs survival	Yagi et al., 2000
Guinea pig	Kanamycin + ethacrynic acid	Scala media	AAV-*BDNF*	significantly enhanced SGNs survival	Lalwani et al., 2002
CBA/CaJ aging mice	cisplatin	scala tympani	HSV1-*NT3*	significantly improved SGNs survival	Bowers et al., 2002
Guinea pig	Kanamycin + ethacrynic acid	scala tympani	Ad-*BDNF* Ad-*CNTF*	*BDNF* alone and the combined *BDNF* and *CNTF* treatment significantly enhanced SGN survival. *CNTF* did not enhance the protective effect of *BDNF*.	Nakaizumi et al., 2004
Guinea pig	Kanamycin + ethacrynic acid	scala tympani	Ad-*BDNF*	significantly preserved SGNs in the basal turns	Rejali et al., 2007
Guinea pig	Neomycin	scala tympani	Ad-*BDNF*	higher SGNs survival and lower CI thresholds	Chikar et al., 2008
Rat	Kanamycin	scala tympani	AAV1-*GDNF*	Significantly reduced SGNs damage and improved auditory function	Liu et al., 2008
Guinea pig	Kanamycin + furosemide	scala tympani scala media	Ad5-*BDNF* Ad5-*NT3*	significant preservation of SGNs and radial nerve fiber survival	Wise et al., 2010
Rat	Noise exposure	scala tympani	Ad-*hNGF*β	Significant greater number of SGNs and smaller ABR threshold shift	Wu et al., 2011
Guinea pig	Kanamycin + furosemide	scala media	Ad5-*BDNF* or Ad5-*NT3*	Significant SGNs protection in the entire basal turn for the 1 week deaf group, in the lower basal turn for the 4 week deaf group and no protection for the 8 week deaf group	Wise et al., 2011
Mutant mice	*Pou4f3* mutant	scala media	Ad-*BDNF*	Enhanced preservation of SGNs and pronounced sprouting of nerve fiber	Fukui et al., 2012
Guinea pigs	Kanamycin + furosemide	scala media	Ad5-*BDNF* Ad5-*NT3*	Sustain protection of SGNs and directed peripheral fiber regrowth (4–11 weeks)	Atkinson et al., 2012
Guinea pigs	Kanamycin + furosemide	scala tympani	Plasmid-*BDNF*	Regeneration of SGNs neurites	Pinyon et al., 2014
Guinea pigs	Kanamycin + furosemide	scala media	Ad5-*BDNF* Ad5-*NT3*	Long term protection of SGNs (6 months)	Atkinson et al., 2014
Guinea pigs	Neomycin or Kanamycin + furosemide	scala tympani	AAV-*BDNF* AAV-*NT3*	A transient elevation in NT levels can sustain the cochlear neural substrate in the long term; BDNF was more effective than NT3 in preserving SGNs	Budenz et al., 2015
Guinea pigs	Neomycin	scala tympani	AAV2-*NT3*	Long term protection of SGNs (5–14 months)	Pfingst et al., 2017
Guinea pigs	Noise exposure	scala tympani	AAV8-*NT3*	Significant SGNs synaptic protection	Chen et al., 2018
Cat	Neomycin	scala tympani	AAV2-hBDNF AAV5-GDNF	Improved SGNs and radial nerve fiber survival	Leake et al., 2019

SGNs, spiral ganglion neurons; HSV1, Herpes simplex virus type 1; Ad, adenovirus; AAV, adeno-associated virus; BDNF, brain-derived neurotrophic factor; GDNF, glial cell line-derived neurotrophic factor; NT3, neurotrophin-3; CNTF, ciliary neurotrophic factor.

expression, greater neuron survival, and more localized fiber responses than scala tympani injection. This result indicates that vector injection into the scala media may be a better method for gene therapy of SGNs. Another important factor to consider with gene therapy is the acute treatment window. Andrew et al. showed that the efficacy of SGNs protection of viral-mediated NT expression diminished with an increasing duration of deafness, which indicates that there is a treatment window of gene therapy (Wise et al., 2011). Interestingly, Budenz et al. (2015) reported that BDNF was more effective in preventing SGN degeneration after deafness, while NT3 had a greater effect in eliciting the regrowth of radial nerve fibers. These results suggest that combining the overexpression of *BDNF* and *NT3* may have a better effect on SGN protection.

Although great progress has been made in gene therapy for protecting SGNs, there are some problems that need to be solved. NT overexpression has been reported to have detrimental effects on hearing. A recent study showed that overexpression of *Ntf3* in normal guinea pig cochleae led to disruption of synapses in the cochlea and hearing loss (Lee et al., 2016). Another study also found that overexpression of human *GDNF* in normal mice caused severe neurological symptoms and hearing loss (Akil et al., 2019). These findings indicate that extremely high levels of transgene NT expression should be avoided. Another obstacle for gene therapy application is that the gene therapy effect gradually disappears due to degeneration of the transduced cell (Atkinson et al., 2014). A long-term study on NT gene therapy showed that the efficacy of one-time injection could only last for up to 11 weeks (Atkinson et al., 2012). At 3 months after gene therapy with *BDNF* or *NT3*, peripheral auditory fibers still showed considerable regrowth in the basilar membrane area compared to the controls, although the neurotrophin levels were not significantly elevated in the cochlear fluids (Budenz et al., 2015). Finally, an important limitation blocking the

TABLE 2 | Studies of stem cell in animal models for SGN regeneration.

Animals	Damages	Type of cells	Delivery site of transplantation	Morphology change	Hearing outcome	References
Mouse	Cisplatin	mNSCs	Modiolus	Robust survival of transplant-derived cells in the modiolus of the cochlea, but the majority of grafted NSCs differentiated into glial cells	Not mentioned	Tamura et al., 2004
Guinea pig	Kanamycin and ethacrynic acid	mESCs	Modiolus	Transplanted cell was found in cochlea and project neurites toward peripheral and central nervous systems.	Significant improvement in the ABR thresholds	Okano et al., 2005
Guinea pig	Neomycin	mESCs	Scala tympani	Transplanted cells were found close both to the sensory epithelium, and the SGNs with peripheral dendritic processes projecting to the organ of Corti. Co-transplantation with mDRGs increased SGNs survival.	Not mentioned	Hu et al., 2005a
Rat	NA	mDRGs	Scala tympani	A significant difference was identified in the number of DRG neurons between the NGF and non-NGF groups. Extensive neurite projections from DRGs were found penetrating the osseous modiolus toward the spiral ganglion.	Not mentioned	Hu et al., 2005b
Guinea pig	Neomycin	mNSCs	Scala tympani	Transplanted cells expressed the neuronal marker and were found close to the sensory epithelium and adjacent to the SGNs and their peripheral processes.	Not mentioned	Hu et al., 2005c
Guinea pig	Kanamycin and frusemide	mESCs	Scala tympani	Small numbers of MESCs were detected in the scala tympani for up to 4 weeks and a proportion of these cells retained expression of neurofilament protein.	Not mentioned	Coleman et al., 2006
Gerbil	Ouabain	mESCs	cochlear nerve trunk	SGNs and neuronal processes near the sensory epithelium increased	Not mentioned	Corrales et al., 2006
Gerbil	Ouabain	BM-MSCs	Scala tympani or Modiolus	Transplanted cells were able to survive in the modiolus.	Not mentioned	Matsuoka et al., 2007
Mice and guinea pig	Noise	NSC	Scala tympani	Transplanted cells showed characteristic of both neuron tissues and the cells of the organ of Corti. SGNs increased.	Not mentioned	Parker et al., 2007
Gerbil	Ouabain	mESCs	Perilymph or endolymph	ESCs introduced into perilymph most differentiated into glia-like cells. ESCs transplanted into endolymph survived poorly.	Not mentioned	Lang et al., 2008
Guinea pig	Kanamycin and ethacrynic acid	mESCs	Scala tympani	50–75% of transplanted cells express markers of early neurons, and a majority of these cells had a glutamatergic phenotype.	Not mentioned	Reyes et al., 2008
Mouse	NA	miPSCs	Scala tympani	Neurons derived from iPS cells projected neurites toward cochlear hair cells.	Not mentioned	Nishimura et al., 2009
Rat	β-bungarotoxin	mESCs	Modiolus or internal auditory meatus	Transplanted cells were found in the scala tympani, the modiolus, the auditory never trunk. BDNF increased cell survival and neuronal differentiation.	Not mentioned	Ganat et al., 2012
Rat	Noise Neomycin	hBM-MSCs	Intravenous administration	Delivered hMSCs were largely entrapped in the lungs; Recruitment of hMSCs was limited to the spiral ganglion area	No improvement	Choi B. Y. et al., 2012
Guinea pig	Neomycin and Ouabain	hUC-MSCs	Intravenous administration	Increase in spiral ganglion and hair cells	Significant improvement in the ABR thresholds	Choi M. Y. et al., 2012
Gerbil	Ouabain	hESCs	Modiolus	Forming an ectopic spiral ganglion	improvement in the ABR thresholds	Chen et al., 2012
Rat	Ouabain	oe-NSCs	Cochlear lateral wall	NSCs migrated into RC with a high efficiency and differentiated into neurons in a degenerated SGN	Not mentioned	Zhang et al., 2013
Rat	Ouabain	mNSCs	Scala tympani	Transplanted mNSCs were more likely to differentiate into neurons in SGN-degenerated cochleae than in control cochleae	Not mentioned	He et al., 2014

(Continued)

TABLE 2 | (Continued)

Animals	Damages	Type of cells	Delivery site of transplantation	Morphology change	Hearing outcome	References
Guinea pig	Neomycin	hMSCs	Scala tympani	Significant SGN increase	Not mentioned	Jang et al., 2015
Congenital deaf albino pig	Hereditary	hUC-MSCs	subarachnoid cavity	UMSC cells were detected in SGNs, basal membrane and Stria Vescularis	Detectible wave change of ABR	Ma et al., 2016
Guinea pig	Neomycin and Ouabain	hPD-MSCs	Intravenous administration	Significant SGN increase	improvement in the ABR and DOPAE thresholds	Kil et al., 2016
Rat	Noise	oe-NSCs	retroauricular approach	Oe-NSC survived and migrated around the SGNs in RC	Hearing loss was restored	Xu et al., 2016
Mouse	Neomycin	miPSCs	Scala tympani	miPSC could differentiate into hair cell-like cells and spiral ganglion-like cells	No improvement	Chen et al., 2017
Guinea pig	NA	hiPSCs	Scala tympani	The survival of transplant-derived neurons was achieved when inflammatory responses were appropriately controlled	Not mentioned	Ishikawa et al., 2017
Guinea pig	Ouabain	hESCs	Internal auditory meatus	Transplanted cells survival was poor	Partially recovered of ABR	Hackelberg et al., 2017
Mouse	NA	miPSCs	Scala tympani	Transplanted cells were observed in the cochlear perilymph, endolymph, and modiolus, and some cells expressed neural cell markers.	No improvement	Zhu et al., 2018
Guinea pig	Kanamycin and furosemide	hMSCs	Scala tympani	In deafened animals, the alginate-MSC coating of the CI significantly prevented SGN from degeneration, but the injection of alginate-MSCs only did not.	No improvement	Scheper et al., 2019a
DTR mice	DT	hESCs	Scala tympani	Transplanted hESC-derived ONP spheroids survived and neuronally differentiated into otic neuronal lineages and also extended neurites toward the bony wall of the cochlea	Not mentioned	Chang et al., 2020

SGNs, spiral ganglion neurons; RC, Rosenthal's canal; NA, Not Applied; mNSCs, mouse neural stem cells; mDRGs, mouse embryonic dorsal root ganglion cells; NGF, nerve growth factor; hMB-MSCs, Human mesenchymal stem cells from bone marrow; hESCs, human embryonic stem cells; rESCs, rat embryonic stem cells; mESCs, murine embryonic stem cells; hUC-MSCs, human umbilical cord mesenchymal stem cells; hPD-MSCs, human placenta mesenchymal stem cells; miPSCs, mouse induced pluripotent stem cells; oe-NSCs, olfactory epithelium neural stem cells; hPSCs, human pluripotent stem cells.

transition into clinical practice is the lack of diagnostic tools to detect synaptopathy.

Stem Cell Therapy

Cell therapy refers to the use of live cells to repair damaged cells or to replace lost cells. Stem cells and differentiated cells can be used for these purposes (Parker, 2011). Stem cells, including embryonic stem cells (ESCs), adult stem cells (ASCs), and induced pluripotent stem cells (iPSCs), are involved in the regeneration of SGNs. There are two strategies for stem cell-based therapy: to stimulate resident stem cells within the organ of Corti to differentiate into SGNs and to supply exogenous stem cells (stem cell transplantation) into the inner ear. Theoretically, the first approach is supposed to be the best strategy for repairing or replacing damaged SGNs. Unfortunately, there is an insufficient number of resident stem cells in the adult cochlea, and they are not capable of restoring hearing.

Consequently, recent studies (**Table 2**) have focused on the second approach (Maharajan et al., 2021). Stem cell therapy includes stem cell differentiation into target cells *in vitro* and differentiated cell transplantation into the cochlea. Gunewardene et al. (2012) proposed the stepwise differentiation of ESCs and iPSCs into otic or neuronal precursors. In our opinion, the major challenge in stem cell therapy is cell transplantation, as the environment in the cochlea is hostile to the survival of foreign stem cells. Strategies to introduce exogenous neural stem cells into the cochlea include administration *via* the perilymph and endolymph (Lang et al., 2008) into the modiolus or the cochlear nerve (Corrales et al., 2006; Ogita et al., 2009) and into the lateral wall (Zhang et al., 2013). Although transplantation into the modiolus has shown a higher cell survival rate and increased populations of exogenous cells in Rosenthal's canal compared to transplantation into the perilymph and endolymph (Matsuoka et al., 2007; Lang et al., 2008), the transplantation process may cause hearing damage (Corrales et al., 2006; Ogita et al., 2009). The transplantation of stem cells into the sidewall of the cochlea achieved efficient results and temporary relief of auditory impairment (Zhang et al., 2013). This method may be a better choice for transplantation. Lee et al. (2017) preconditioned the scala media to reduce the potassium concentration before transplantation, thus increasing the survival of transplanted cells. However, some stem cells lose their pluripotency and differentiation ability.

Embryonic stem cells (ESCs) are pluripotent stem cells and have limitless potential to proliferate and differentiate. Studies have demonstrated that human ESCs (hESCs) are able to differentiate into otic neuronal progenitors (ONPs) and SGN-like cells. Newly differentiated SGN-like cells have genotypic and

phenotypic SGN-specific features, and their neurites extend toward the cochlear nucleus (Matsuoka et al., 2017). Hyakumura et al. (2019) recently found that human pluripotent stem cells (hPSCs) could be derived from sensory neuronal cells, which formed synaptic connections with hair cells and cochlear nuclei in organotypic coculture. ESC-derived mouse neural progenitor cells were transplanted *via* a round window membrane into ouabain-deafened gerbils, and they successfully engrafted into the modiolus and formed ectopic ganglia with differentiated neuronal-type cells that projected to sensory cells in the organ of Corti (Corrales et al., 2006). Chen et al. (2012) demonstrated that transplantation of neural progenitors into adult ouabain-deafened animals rescued the auditory function of the deafened animals. Although hESCs have high proliferative capacity, ethical concerns, immunological rejection, difficulty in procurement, and tumorigenic potential limit their utilization.

ASCs are thought to be a promising resource for SGN regeneration from both ethical and patient compatibility perspectives. Some cell markers of stem cells in the olfactory epithelium are the same as some cells in the auditory epithelium, and they have good regenerative capacity in adults, making them a good source of SGNs (Graziadei and Graziadei, 1979; Roisen et al., 2001). Olfactory stem cells can survive and migrate to Rosenthal's canal after transplantation (Zhang et al., 2013; Xu et al., 2016), ameliorating noise-induced hearing impairment (Xu et al., 2016). Bone marrow stromal stem cells (Naito et al., 2004) and a purified subpopulation of glial cells expressing Sox2 isolated from the auditory nerve also showed efficient cell migration and differentiation ability (Lang et al., 2015). However, ASCs showed far less differentiation ability than ESCs, which limited their application.

In recent years, much attention has been given to iPSCs with the development of reprogramming technology. iPSCs are adult differentiated cells that are genetically reprogrammed to form pluripotent stem cells. iPSCs can easily be obtained from the somatic cells of the patient. Thus, there is no concern about immunological rejection and fewer ethical problems. A research group demonstrated that hiPSC-derived neurons could form presynaptic connections with HCs in the *in vitro* coculture system (Gunewardene et al., 2016). iPSCs also have some disadvantages, such as a low proliferation rate, the tendency to differentiate into the original somatic tissue, and tumorigenicity (Nishimura et al., 2012). One main concern in regards to their tumorigenicity is the use of viral vectors during reprogramming. A recent study described a specific stepwise neural induction method for hiPSCs to eliminate undifferentiated cells from transplants, allowing the use of only terminally differentiated neurons, thus reducing the probability of tumorigenicity. First, a neural induction method was established on Matrigel-coated plates. Then, hiPSCs were differentiated into neurons on a 3D collagen matrix, and the neuron subtypes were examined. Finally, the cultured neurons were transplanted into the guinea pig cochlea (Ishikawa et al., 2017). Boddy et al. (2020) found that human-induced pluripotent cell lines are capable of differentiating into otic cell types, including hair cells and neuronal lineages, using the non-integration approach. This technology lacks genetic integration problems, making it highly attractive in the field of regenerative medicine.

CONCLUSION AND FUTURE PROSPECTS

Different approaches are being developed for the treatment of deafness. Great progress has been made in gene therapy and stem cell therapy over the last decade. There are some problems that need to be solved, including viral safety and long-term treatment effects. Ad and AAV are widely used in cochlear gene therapy, and their safety has been confirmed in animal models. Additional research should be conducted to assess the safety and efficiency of treating humans. The treatment efficacy gradually decreases over time, so a second or even regular repeated treatments may be a solution. With regard to stem cell therapy, iPSC technology is thought to be promising. As a transplant source, autologous neurons from patient-derived iPSCs are ideal for the replacement of neurons in the injured cochlea. However, some challenges need to be overcome before application to humans, such as tumorigenesis and controlled growth of transplanted cells. Future therapies to rescue auditory function must consider multiple targets.

Combining several therapeutic strategies, for instance, stem cell delivery, gene therapy and cochlear implants, may achieve better performance. The treatment effect of cochlear implants relies at least partially on the number of surviving SGNs (Yagi et al., 2000). It is not surprising that gene therapy or stem cell therapy combined with cochlear implants could enhance the performance of cochlear implants, as gene therapy and stem cell therapy could prevent SGN degeneration. Guinea pigs treated with Ad-*BDNF* had a lower CI threshold and higher survival of SGNs, indicating that the combination of Ad-*BDNF* inoculation and electrical stimulation improved the functional measures of cochlear implant performance (Chikar et al., 2008). Scheper et al. (2019a) also showed that the alginate-MSC coating of CI significantly prevented SGN degeneration. A study demonstrated that coculture with Wnt1-expressing Schwann cells enhanced the neuronal differentiation of transplanted neural stem cells (He et al., 2014). This result reminds us that cotransplantation modified cells expressing specific cytokines along with stem cells may help us overcome the barrier of a low transplant survival rate. Genetically modified hMSCs overexpressing BDNF protect neurons significantly better from degeneration than native MSCs (Scheper et al., 2019b), which indicates that genetic modification prior to stem cell transplantation may provide a better effect. Efforts should continue toward the development of gene therapy and stem cell therapy for treating deafness.

AUTHOR CONTRIBUTIONS

YS conceived and designed the manuscript. SC and LZ wrote the manuscript. All authors contributed to the article and approved the submitted version.

FUNDING

This work was financially supported by the National Natural Science Foundation of China (Nos. 81771003 and 82071508).

REFERENCES

Agterberg, M. J., Versnel, H., van Dijk, L. M., de Groot, J. C., and Klis, S. F. (2009). Enhanced survival of spiral ganglion cells after cessation of treatment with brain-derived neurotrophic factor in deafened guinea pigs. *J. Assoc. Res. Otolaryngol.* 10, 355–367. doi: 10.1007/s10162-009-0170-2

Akil, O., Blits, B., Lustig, L. R., and Leake, P. A. (2019). Virally mediated overexpression of glial-derived neurotrophic factor elicits age- and dose-dependent neuronal toxicity and hearing loss. *Hum. Gene Ther.* 30, 88–105. doi: 10.1089/hum.2018.028

Alam, S. A., Robinson, B. K., Huang, J., and Green, S. H. (2007). Prosurvival and proapoptotic intracellular signaling in rat spiral ganglion neurons *in vivo* after the loss of hair cells. *J. Comp. Neurol.* 503, 832–852. doi: 10.1002/cne.21430

Atkinson, P. J., Wise, A. K., Flynn, B. O., Nayagam, B. A., and Richardson, R. T. (2014). Viability of long-term gene therapy in the cochlea. *Sci. Rep.* 4:4733. doi: 10.1038/srep04733

Atkinson, P. J., Wise, A. K., Flynn, B. O., Nayagam, B. A., Hume, C. R., O'Leary, S. J., et al. (2012). Neurotrophin gene therapy for sustained neural preservation after deafness. *PLoS One* 7:e52338. doi: 10.1371/journal.pone.0052338

Bao, J., Lei, D., Du, Y., Ohlemiller, K. K., Beaudet, A. L., and Role, L. W. (2005). Requirement of nicotinic acetylcholine receptor subunit beta2 in the maintenance of spiral ganglion neurons during aging. *J. Neurosci.* 25, 3041–3045. doi: 10.1523/JNEUROSCI.5277-04.2005

Bedrosian, J. C., Gratton, M. A., Brigande, J. V., Tang, W., Landau, J., and Bennett, J. (2006). *In vivo* delivery of recombinant viruses to the fetal murine cochlea: transduction characteristics and long-term effects on auditory function. *Mol. Ther.* 14, 328–335. doi: 10.1016/j.ymthe.2006.04.003

Berglund, A. M., and Ryugo, D. K. (1986). A monoclonal antibody labels type II neurons of the spiral ganglion. *Brain Res.* 383, 327–332. doi: 10.1016/0006-8993(86)90034-x

Berglund, A. M., and Ryugo, D. K. (1991). Neurofilament antibodies and spiral ganglion neurons of the mammalian cochlea. *J. Comp. Neurol.* 306, 393–408. doi: 10.1002/cne.903060304

Boddy, S. L., Romero-Guevara, R., Ji, A. R., Unger, C., Corns, L., Marcotti, W., et al. (2020). Generation of otic lineages from integration-free human-induced pluripotent stem cells reprogrammed by mRNAs. *Stem Cells Int.* 2020:3692937. doi: 10.1155/2020/3692937

Borton, S. A., Mauze, E., and Lieu, J. E. (2010). Quality of life in children with unilateral hearing loss: a pilot study. *Am. J. Audiol.* 19, 61–72. doi: 10.1044/1059-0889(2010/07-0043)

Bowers, W. J., Chen, X., Guo, H., Frisina, D. R., Federoff, H. J., and Frisina, R. D. (2002). Neurotrophin-3 transduction attenuates cisplatin spiral ganglion neuron ototoxicity in the cochlea. *Mol. Ther.* 6, 12–18. doi: 10.1006/mthe.2002.0627

Bradford, R. D., Yoo, Y. G., Golemac, M., Pugel, E. P., Jonjic, S., and Britt, W. J. (2015). Murine CMV-induced hearing loss is associated with inner ear inflammation and loss of spiral ganglia neurons. *PLoS Pathog.* 11:e1004774. doi: 10.1371/journal.ppat.1004774

Brooks, P. M., Rose, K. P., MacRae, M. L., Rangoussis, K. M., Gurjar, M., Hertzano, R., et al. (2020). Pou3f4-expressing otic mesenchyme cells promote spiral ganglion neuron survival in the postnatal mouse cochlea. *J. Comp. Neurol.* 528, 1967–1985. doi: 10.1002/cne.24867

Budenz, C. L., Wong, H. T., Swiderski, D. L., Shibata, S. B., Pfingst, B. E., and Raphael, Y. (2015). Differential effects of AAV.BDNF and AAV.Ntf3 in the deafened adult guinea pig ear. *Sci. Rep.* 5:8619. doi: 10.1038/srep08619

Chang, H. T., Heuer, R. A., Oleksijew, A. M., Coots, K. S., Roque, C. B., Nella, K. T., et al. (2020). An engineered three-dimensional stem cell niche in the inner ear by applying a nanofibrillar cellulose hydrogel with a sustained-release neurotrophic factor delivery system. *Acta Biomater.* 108, 111–127. doi: 10.1016/j.actbio.2020.03.007

Chen, H., Xing, Y., Xia, L., Chen, Z., Yin, S., and Wang, J. (2018). AAV-mediated NT-3 overexpression protects cochleae against noise-induced synaptopathy. *Gene Ther.* 25, 251–259. doi: 10.1038/s41434-018-0012-0

Chen, J., Guan, L., Zhu, H., Xiong, S., Zeng, L., and Jiang, H. (2017). Transplantation of mouse-induced pluripotent stem cells into the cochlea for the treatment of sensorineural hearing loss. *Acta Otolaryngol.* 137, 1136–1142. doi: 10.1080/00016489.2017.1342045

Chen, W., Jongkamonwiwat, N., Abbas, L., Eshtan, S. J., Johnson, S. L., Kuhn, S., et al. (2012). Restoration of auditory evoked responses by human ES-cell-derived otic progenitors. *Nature* 490, 278–282. doi: 10.1038/nature11415

Cheng, Y. F., Tsai, Y. H., Huang, C. Y., Lee, Y. S., Chang, P. C., Lu, Y. C., et al. (2020). Generation and pathological characterization of a transgenic mouse model carrying a missense PJVK mutation. *Biochem. Biophys. Res. Commun.* 532, 675–681. doi: 10.1016/j.bbrc.2020.07.101

Chien, W. W., McDougald, D. S., Roy, S., Fitzgerald, T. S., and Cunningham, L. L. (2015). Cochlear gene transfer mediated by adeno-associated virus: comparison of two surgical approaches. *Laryngoscope* 125, 2557–2564. doi: 10.1002/lary.25317

Chikar, J. A., Colesa, D. J., Swiderski, D. L., Di Polo, A., Raphael, Y., and Pfingst, B. E. (2008). Over-expression of BDNF by adenovirus with concurrent electrical stimulation improves cochlear implant thresholds and survival of auditory neurons. *Hear. Res.* 245, 24–34. doi: 10.1016/j.heares.2008.08.005

Choi, B. Y., Song, J. J., Chang, S. O., Kim, S. U., and Oh, S. H. (2012). Intravenous administration of human mesenchymal stem cells after noise- or drug-induced hearing loss in rats. *Acta Otolaryngol.* 132(Suppl. 1), S94–S102. doi: 10.3109/00016489.2012.660731

Choi, M. Y., Yeo, S. W., and Park, K. H. (2012). Hearing restoration in a deaf animal model with intravenous transplantation of mesenchymal stem cells derived from human umbilical cord blood. *Biochem. Biophys. Res. Commun.* 427, 629–636. doi: 10.1016/j.bbrc.2012.09.111

Coate, T. M., Raft, S., Zhao, X., Ryan, A. K., Crenshaw, E. B. III, and Kelley, M. W. (2012). Otic mesenchyme cells regulate spiral ganglion axon fasciculation through a Pou3f4/EphA4 signaling pathway. *Neuron* 73, 49–63. doi: 10.1016/j.neuron.2011.10.029

Coleman, B., Hardman, J., Coco, A., Epp, S., de Silva, M., Crook, J., et al. (2006). Fate of embryonic stem cells transplanted into the deafened mammalian cochlea. *Cell Transplant.* 15, 369–380. doi: 10.3727/000000006783981819

Corrales, C. E., Pan, L., Li, H., Liberman, M. C., Heller, S., and Edge, A. S. (2006). Engraftment and differentiation of embryonic stem cell-derived neural progenitor cells in the cochlear nerve trunk: growth of processes into the organ of Corti. *J. Neurobiol.* 66, 1489–1500. doi: 10.1002/neu.20310

Cowen, T. (2002). Selective vulnerability in adult and ageing mammalian neurons. *Auton. Neurosci.* 96, 20–24. doi: 10.1016/s1566-0702(01)00376-9

Ernfors, P., Van De Water, T., Loring, J., and Jaenisch, R. (1995). Complementary roles of BDNF and NT-3 in vestibular and auditory development. *Neuron* 14, 1153–1164. doi: 10.1016/0896-6273(95)90263-5

Eugene, D., Deforges, S., Vibert, N., and Vidal, P. P. (2009). Vestibular critical period, maturation of central vestibular neurons, and locomotor control. *Ann. N. Y. Acad. Sci.* 1164, 180–187. doi: 10.1111/j.1749-6632.2008.03727.x

Eybalin, M. (1993). Neurotransmitters and neuromodulators of the mammalian cochlea. *Physiol. Rev.* 73, 309–373. doi: 10.1152/physrev.1993.73.2.309

Farinas, I., Jones, K. R., Tessarollo, L., Vigers, A. J., Huang, E., Kirstein, M., et al. (2001). Spatial shaping of cochlear innervation by temporally regulated neurotrophin expression. *J. Neurosci.* 21, 6170–6180.

Fernandez, K. A., Jeffers, P. W., Lall, K., Liberman, M. C., and Kujawa, S. G. (2015). Aging after noise exposure: acceleration of cochlear synaptopathy in "recovered" ears. *J. Neurosci.* 35, 7509–7520. doi: 10.1523/JNEUROSCI.5138-14.2015

Fritzsch, B. I, Silos-Santiago, I., Bianchi, L. M., and Farinas, I. I. (1997). Effects of neurotrophin and neurotrophin receptor disruption on the afferent inner ear innervation. *Semin. Cell Dev. Biol.* 8, 277–284.

Fritzsch, B., Pirvola, U., and Ylikoski, J. (1999). Making and breaking the innervation of the ear: neurotrophic support during ear development and its clinical implications. *Cell Tissue Res.* 295, 369–382. doi: 10.1007/s004410051244

Fukui, H., Wong, H. T., Beyer, L. A., Case, B. G., Swiderski, D. L., Di Polo, A., et al. (2012). BDNF gene therapy induces auditory nerve survival and fiber sprouting in deaf Pou4f3 mutant mice. *Sci. Rep.* 2:838. doi: 10.1038/srep00838

Gabrielli, L., Bonasoni, M. P., Santini, D., Piccirilli, G., Chiereghin, A., Guerra, B., et al. (2013). Human fetal inner ear involvement in congenital cytomegalovirus infection. *Acta Neuropathol. Commun.* 1:63. doi: 10.1186/2051-5960-1-63

Ganat, Y. M., Calder, E. L., Kriks, S., Nelander, J., Tu, E. Y., Jia, F., et al. (2012). Identification of embryonic stem cell-derived midbrain dopaminergic neurons for engraftment. *J. Clin. Invest.* 122, 2928–2939. doi: 10.1172/JCI58767

Garcia-Berrocal, J. R., Nevado, J., Ramirez-Camacho, R., Sanz, R., Gonzalez-Garcia, J. A., Sanchez-Rodriguez, C., et al. (2007). The anticancer drug cisplatin

induces an intrinsic apoptotic pathway inside the inner ear. *Br. J. Pharmacol.* 152, 1012–1020. doi: 10.1038/sj.bjp.0707405

Gassner, D., Durham, D., Pfannenstiel, S. C., Brough, D. E., and Staecker, H. (2012). Canalostomy as a surgical approach for cochlear gene therapy in the rat. *Anat. Rec. (Hoboken)* 295, 1830–1836. doi: 10.1002/ar.22593

Gillespie, L. N., Clark, G. M., Bartlett, P. F., and Marzella, P. L. (2003). BDNF-induced survival of auditory neurons *in vivo*: cessation of treatment leads to accelerated loss of survival effects. *J. Neurosci. Res.* 71, 785–790. doi: 10.1002/jnr.10542

Graziadei, P. P., and Graziadei, G. A. (1979). Neurogenesis and neuron regeneration in the olfactory system of mammals. I. Morphological aspects of differentiation and structural organization of the olfactory sensory neurons. *J. Neurocytol.* 8, 1–18. doi: 10.1007/BF01206454

Gubbels, S. P., Woessner, D. W., Mitchell, J. C., Ricci, A. J., and Brigande, J. V. (2008). Functional auditory hair cells produced in the mammalian cochlea by in utero gene transfer. *Nature* 455, 537–541. doi: 10.1038/nature07265

Gunewardene, N., Crombie, D., Dottori, M., and Nayagam, B. A. (2016). Innervation of cochlear hair cells by human induced pluripotent stem cell-derived neurons *in vitro*. *Stem Cells Int.* 2016:1781202. doi: 10.1155/2016/1781202

Gunewardene, N., Dottori, M., and Nayagam, B. A. (2012). The convergence of cochlear implantation with induced pluripotent stem cell therapy. *Stem Cell Rev. Rep.* 8, 741–754. doi: 10.1007/s12015-011-9320-0

Hackelberg, S., Tuck, S. J., He, L., Rastogi, A., White, C., Liu, L., et al. (2017). Nanofibrous scaffolds for the guidance of stem cell-derived neurons for auditory nerve regeneration. *PLoS One* 12:e0180427. doi: 10.1371/journal.pone.0180427

Harris, M. S., Gilbert, J. L., Lormore, K. A., Musunuru, S. A., and Fritsch, M. H. (2011). Cisplatin ototoxicity affecting cochlear implant benefit. *Otol. Neurotol.* 32, 969–972. doi: 10.1097/MAO.0b013e3182255893

Hashimoto, K., Hickman, T. T., Suzuki, J., Ji, L., Kohrman, D. C., Corfas, G., et al. (2019). Protection from noise-induced cochlear synaptopathy by virally mediated overexpression of NT3. *Sci. Rep.* 9:15362. doi: 10.1038/s41598-019-51724-6

He, Y., Zhang, P. Z., Sun, D., Mi, W. J., Zhang, X. Y., Cui, Y., et al. (2014). Wnt1 from cochlear schwann cells enhances neuronal differentiation of transplanted neural stem cells in a rat spiral ganglion neuron degeneration model. *Cell Transplant.* 23, 747–760. doi: 10.3727/096368913X669761

Hequembourg, S., and Liberman, M. C. (2001). Spiral ligament pathology: a major aspect of age-related cochlear degeneration in C57BL/6 mice. *J. Assoc. Res. Otolaryngol.* 2, 118–129. doi: 10.1007/s101620010075

Hu, Z., Andang, M., Ni, D., and Ulfendahl, M. (2005a). Neural cograft stimulates the survival and differentiation of embryonic stem cells in the adult mammalian auditory system. *Brain Res.* 1051, 137–144. doi: 10.1016/j.brainres.2005.06.016

Hu, Z., Ulfendahl, M., and Olivius, N. P. (2005b). NGF stimulates extensive neurite outgrowth from implanted dorsal root ganglion neurons following transplantation into the adult rat inner ear. *Neurobiol. Dis.* 18, 184–192. doi: 10.1016/j.nbd.2004.09.010

Hu, Z., Wei, D., Johansson, C. B., Holmstrom, N., Duan, M., Frisen, J., et al. (2005c). Survival and neural differentiation of adult neural stem cells transplanted into the mature inner ear. *Exp. Cell Res.* 302, 40–47. doi: 10.1016/j.yexcr.2004.08.023

Hyakumura, T., McDougall, S., Finch, S., Needham, K., Dottori, M., and Nayagam, B. A. (2019). Organotypic cocultures of human pluripotent stem cell derived-neurons with mammalian inner ear hair cells and cochlear nucleus slices. *Stem Cells Int.* 2019:8419493. doi: 10.1155/2019/8419493

Ikuta, K., Ogawa, H., Hashimoto, H., Okano, W., Tani, A., Sato, E., et al. (2015). Restricted infection of murine cytomegalovirus (MCMV) in neonatal mice with MCMV-induced sensorineural hearing loss. *J. Clin. Virol.* 69, 138–145. doi: 10.1016/j.jcv.2015.06.083

Ishikawa, M., Ohnishi, H., Skerleva, D., Sakamoto, T., Yamamoto, N., Hotta, A., et al. (2017). Transplantation of neurons derived from human iPS cells cultured on collagen matrix into guinea-pig cochleae. *J. Tissue Eng. Regen. Med.* 11, 1766–1778. doi: 10.1002/term.2072

Jang, S., Cho, H. H., Kim, S. H., Lee, K. H., Jun, J. Y., Park, J. S., et al. (2015). Neural-induced human mesenchymal stem cells promote cochlear cell regeneration in deaf Guinea pigs. *Clin. Exp. Otorhinolaryngol.* 8, 83–91. doi: 10.3342/ceo.2015.8.2.83

Jeong, H. J., Kim, S. J., Moon, P. D., Kim, N. H., Kim, J. S., Park, R. K., et al. (2007). Antiapoptotic mechanism of cannabinoid receptor 2 agonist on cisplatin-induced apoptosis in the HEI-OC1 auditory cell line. *J. Neurosci. Res.* 85, 896–905. doi: 10.1002/jnr.21168

Jeong, S. W., Kim, L. S., Hur, D., Bae, W. Y., Kim, J. R., and Lee, J. H. (2010). Gentamicin-induced spiral ganglion cell death: apoptosis mediated by ROS and the JNK signaling pathway. *Acta Otolaryngol.* 130, 670–678. doi: 10.3109/00016480903428200

Johnsson, L. G. (1974). Sequence of degeneration of Corti's organ and its first-order neurons. *Ann. Otol. Rhinol. Laryngol.* 83, 294–303. doi: 10.1177/000348947408300303

Juanjuan, C., Yan, F., Li, C., Haizhi, L., Ling, W., Xinrong, W., et al. (2011). Murine model for congenital CMV infection and hearing impairment. *Virol. J.* 8:70. doi: 10.1186/1743-422X-8-70

Kandpal, G., Jacob, A. N., and Kandpal, R. P. (1996). Transcribed sequences encoded in the region involved in contiguous deletion syndrome that comprises X-linked stapes fixation and deafness. *Somat. Cell Mol. Genet.* 22, 511–517. doi: 10.1007/BF02369442

Kawai, Y., Nakao, T., Kunimura, N., Kohda, Y., and Gemba, M. (2006). Relationship of intracellular calcium and oxygen radicals to Cisplatin-related renal cell injury. *J. Pharmacol. Sci.* 100, 65–72. doi: 10.1254/jphs.fp0050661

Keithley, E. M., Canto, C., Zheng, Q. Y., Wang, X., Fischel-Ghodsian, N., and Johnson, K. R. (2005). Cu/Zn superoxide dismutase and age-related hearing loss. *Hear. Res.* 209, 76–85. doi: 10.1016/j.heares.2005.06.009

Kesser, B. W., and Lalwani, A. K. (2009). Gene therapy and stem cell transplantation: strategies for hearing restoration. *Adv. Otorhinolaryngol.* 66, 64–86. doi: 10.1159/000218208

Kil, K., Choi, M. Y., Kong, J. S., Kim, W. J., and Park, K. H. (2016). Regenerative efficacy of mesenchymal stromal cells from human placenta in sensorineural hearing loss. *Int. J. Pediatr. Otorhinolaryngol.* 91, 72–81. doi: 10.1016/j.ijporl.2016.10.010

Kilpatrick, L. A., Li, Q., Yang, J., Goddard, J. C., Fekete, D. M., and Lang, H. (2011). Adeno-associated virus-mediated gene delivery into the scala media of the normal and deafened adult mouse ear. *Gene Ther.* 18, 569–578. doi: 10.1038/gt.2010.175

Klein, M., Koedel, U., Pfister, H. W., and Kastenbauer, S. (2003). Morphological correlates of acute and permanent hearing loss during experimental pneumococcal meningitis. *Brain Pathol.* 13, 123–132. doi: 10.1111/j.1750-3639.2003.tb00012.x

Kuan, C. C., Kaga, K., and Tsuzuku, T. (2007). Tuberculous meningitis-induced unilateral sensorineural hearing loss: a temporal bone study. *Acta Otolaryngol.* 127, 553–557. doi: 10.1080/00016480600951418

Kujawa, S. G., and Liberman, M. C. (2009). Adding insult to injury: cochlear nerve degeneration after "temporary" noise-induced hearing loss. *J. Neurosci.* 29, 14077–14085. doi: 10.1523/JNEUROSCI.2845-09.2009

Lai, T. W., Zhang, S., and Wang, Y. T. (2014). Excitotoxicity and stroke: identifying novel targets for neuroprotection. *Prog. Neurobiol.* 115, 157–188. doi: 10.1016/j.pneurobio.2013.11.006

Lalwani, A. K., Han, J. J., Castelein, C. M., Carvalho, G. J., and Mhatre, A. N. (2002). *In vitro* and *in vivo* assessment of the ability of adeno-associated virus-brain-derived neurotrophic factor to enhance spiral ganglion cell survival following ototoxic insult. *Laryngoscope* 112, 1325–1334. doi: 10.1097/00005537-200208000-00001

Landfield, P. W., Blalock, E. M., Chen, K. C., and Porter, N. M. (2007). A new glucocorticoid hypothesis of brain aging: implications for Alzheimer's disease. *Curr. Alzheimer Res.* 4, 205–212. doi: 10.2174/156720507780362083

Lang, H., Schulte, B. A., Goddard, J. C., Hedrick, M., Schulte, J. B., Wei, L., et al. (2008). Transplantation of mouse embryonic stem cells into the cochlea of an auditory-neuropathy animal model: effects of timing after injury. *J. Assoc. Res. Otolaryngol.* 9, 225–240. doi: 10.1007/s10162-008-0119-x

Lang, H., Schulte, B. A., Zhou, D., Smythe, N., Spicer, S. S., and Schmiedt, R. A. (2006). Nuclear factor kappaB deficiency is associated with auditory nerve degeneration and increased noise-induced hearing loss. *J. Neurosci.* 26, 3541–3550. doi: 10.1523/JNEUROSCI.2488-05.2006

Lang, H., Xing, Y., Brown, L. N., Samuvel, D. J., Panganiban, C. H., Havens, L. T., et al. (2015). Neural stem/progenitor cell properties of glial cells in the adult mouse auditory nerve. *Sci. Rep.* 5:13383. doi: 10.1038/srep13383

Lanvers-Kaminsky, C., Zehnhoff-Dinnesen, A. A., Parfitt, R., and Ciarimboli, G. (2017). Drug-induced ototoxicity: mechanisms, Pharmacogenetics, and protective strategies. *Clin. Pharmacol. Ther.* 101, 491–500. doi: 10.1002/cpt.603

Le Prell, C. G., Yagi, M., Kawamoto, K., Beyer, L. A., Atkin, G., Raphael, Y., et al. (2004). Chronic excitotoxicity in the guinea pig cochlea induces temporary functional deficits without disrupting otoacoustic emissions. *J. Acoust. Soc. Am.* 116, 1044–1056. doi: 10.1121/1.1772395

Leake, P. A., Hradek, G. T., Hetherington, A. M., and Stakhovskaya, O. (2011). Brain-derived neurotrophic factor promotes cochlear spiral ganglion cell survival and function in deafened, developing cats. *J. Comp. Neurol.* 519, 1526–1545. doi: 10.1002/cne.22582

Leake, P. A., Rebscher, S. J., Dore, C., and Akil, O. (2019). AAV-Mediated neurotrophin gene therapy promotes improved survival of cochlear spiral ganglion neurons in neonatally deafened cats: comparison of AAV2-hBDNF and AAV5-hGDNF. *J. Assoc. Res. Otolaryngol.* 20, 341–361. doi: 10.1007/s10162-019-00723-5

Leake, P. A., Stakhovskaya, O., Hetherington, A., Rebscher, S. J., and Bonham, B. (2013). Effects of brain-derived neurotrophic factor (BDNF) and electrical stimulation on survival and function of cochlear spiral ganglion neurons in deafened, developing cats. *J. Assoc. Res. Otolaryngol.* 14, 187–211. doi: 10.1007/s10162-013-0372-5

Lee, M. Y., Hackelberg, S., Green, K. L., Lunghamer, K. G., Kurioka, T., Loomis, B. R., et al. (2017). Survival of human embryonic stem cells implanted in the guinea pig auditory epithelium. *Sci. Rep.* 7:46058. doi: 10.1038/srep46058

Lee, M. Y., Kurioka, T., Nelson, M. M., Prieskorn, D. M., Swiderski, D. L., Takada, Y., et al. (2016). Viral-mediated Ntf3 overexpression disrupts innervation and hearing in nondeafened guinea pig cochleae. *Mol. Ther. Methods Clin. Dev.* 3:16052. doi: 10.1038/mtm.2016.52

Lethbridge-Cejku, M., Schiller, J. S., and Bernadel, L. (2004). Summary health statistics for U.S. adults: national health interview survey, 2002. *Vital Health Stat.* 10, 1–151.

Li, X., Shi, X., Wang, C., Niu, H., Zeng, L., and Qiao, Y. (2016). Cochlear spiral ganglion neuron apoptosis in neonatal mice with murine cytomegalovirus-induced sensorineural hearing loss. *J. Am. Acad. Audiol.* 27, 345–353. doi: 10.3766/jaaa.15061

Lin, F. R., Metter, E. J., O'Brien, R. J., Resnick, S. M., Zonderman, A. B., and Ferrucci, L. (2011). Hearing loss and incident dementia. *Arch. Neurol.* 68, 214–220.

Liu, W., Fan, Z., Han, Y., Lu, S., Zhang, D., Bai, X., et al. (2011). Curcumin attenuates peroxynitrite-induced neurotoxicity in spiral ganglion neurons. *Neurotoxicology* 32, 150–157. doi: 10.1016/j.neuro.2010.09.003

Liu, W., Fan, Z., Han, Y., Zhang, D., Li, J., and Wang, H. (2012). Intranuclear localization of apoptosis-inducing factor and endonuclease G involves in peroxynitrite-induced apoptosis of spiral ganglion neurons. *Neurol. Res.* 34, 915–922. doi: 10.1179/1743132812Y.0000000098

Liu, W., Xu, X., Fan, Z., Sun, G., Han, Y., Zhang, D., et al. (2019b). Wnt signaling activates TP53-induced glycolysis and apoptosis regulator and protects against Cisplatin-induced spiral ganglion neuron damage in the mouse cochlea. *Antioxid. Redox Signal.* 30, 1389–1410. doi: 10.1089/ars.2017.7288

Liu, W., Wang, X., Wang, M., and Wang, H. (2019a). Protection of spiral ganglion neurons and prevention of auditory neuropathy. *Adv. Exp. Med. Biol.* 1130, 93–107. doi: 10.1007/978-981-13-6123-4_6

Liu, W., Xu, L., Wang, X., Zhang, D., Sun, G., Wang, M., et al. (2021). PRDX1 activates autophagy *via* the PTEN-AKT signaling pathway to protect against cisplatin-induced spiral ganglion neuron damage. *Autophagy* 1–23. doi: 10.1080/15548627.2021.1905466

Liu, Y., Okada, T., Shimazaki, K., Sheykholeslami, K., Nomoto, T., Muramatsu, S. I., et al. (2008). Protection against aminoglycoside-induced ototoxicity by regulated AAV vector-mediated GDNF gene transfer into the cochlea. *Mol. Ther.* 16, 474–480.

Lombardi, G., Garofoli, F., and Stronati, M. (2010). Congenital cytomegalovirus infection: treatment, sequelae and follow-up. *J. Matern. Fetal Neonatal Med.* 23(Suppl. 3), 45–48. doi: 10.3109/14767058.2010.506753

Ma, Y., Guo, W., Yi, H., Ren, L., Zhao, L., Zhang, Y., et al. (2016). Transplantation of human umbilical cord mesenchymal stem cells in cochlea to repair sensorineural hearing. *Am. J. Transl. Res.* 8, 5235–5245.

Ma, Y., Wise, A. K., Shepherd, R. K., and Richardson, R. T. (2019). New molecular therapies for the treatment of hearing loss. *Pharmacol. Ther.* 200, 190–209. doi: 10.1016/j.pharmthera.2019.05.003

Maharajan, N., Cho, G. W., and Jang, C. H. (2021). Therapeutic application of mesenchymal stem cells for cochlear regeneration. *In Vivo* 35, 13–22. doi: 10.21873/invivo.12227

Matsuoka, A. J., Kondo, T., Miyamoto, R. T., and Hashino, E. (2007). Enhanced survival of bone-marrow-derived pluripotent stem cells in an animal model of auditory neuropathy. *Laryngoscope* 117, 1629–1635. doi: 10.1097/MLG.0b013e31806bf282

Matsuoka, A. J., Morrissey, Z. D., Zhang, C., Homma, K., Belmadani, A., Miller, C. A., et al. (2017). Directed differentiation of human embryonic stem cells toward placode-derived spiral ganglion-like sensory neurons. *Stem Cells Transl. Med.* 6, 923–936. doi: 10.1002/sctm.16-0032

Melnick, M., and Jaskoll, T. (2013). An *in vitro* mouse model of congenital cytomegalovirus-induced pathogenesis of the inner ear cochlea. *Birth Defects Res. A Clin. Mol. Teratol.* 97, 69–78. doi: 10.1002/bdra.23105

Miller, D. B., and O'Callaghan, J. P. (2005). Aging, stress and the hippocampus. *Ageing Res. Rev.* 4, 123–140. doi: 10.1016/j.arr.2005.03.002

Minowa, O., Ikeda, K., Sugitani, Y., Oshima, T., Nakai, S., Katori, Y., et al. (1999). Altered cochlear fibrocytes in a mouse model of DFN3 nonsyndromic deafness. *Science* 285, 1408–1411. doi: 10.1126/science.285.5432.1408

Miura, M., Sando, I., Hirsch, B. E., and Orita, Y. (2002). Analysis of spiral ganglion cell populations in children with normal and pathological ears. *Ann. Otol. Rhinol. Laryngol.* 111, 1059–1065. doi: 10.1177/000348940211101201

Mohan, S., Smyth, B. J., Namin, A., Phillips, G., and Gratton, M. A. (2014). Targeted amelioration of cisplatin-induced ototoxicity in guinea pigs. *Otolaryngol. Head Neck Surg.* 151, 836–839. doi: 10.1177/0194599814544877

Muggia, F. M., Bonetti, A., Hoeschele, J. D., Rozencweig, M., and Howell, S. B. (2015). Platinum antitumor complexes: 50 years since barnett rosenberg's discovery. *J. Clin. Oncol.* 33, 4219–4226. doi: 10.1200/JCO.2015.60.7481

Mulligan, R. C. (1993). The basic science of gene therapy. *Science* 260, 926–932.

Naito, Y., Nakamura, T., Nakagawa, T., Iguchi, F., Endo, T., Fujino, K., et al. (2004). Transplantation of bone marrow stromal cells into the cochlea of chinchillas. *Neuroreport* 15, 1–4. doi: 10.1097/00001756-200401190-00001

Nakaizumi, T., Kawamoto, K., Minoda, R., and Raphael, Y. (2004). Adenovirus-mediated expression of brain-derived neurotrophic factor protects spiral ganglion neurons from ototoxic damage. *Audiol. Neurootol.* 9, 135–143. doi: 10.1159/000077264

Nishimura, K., Nakagawa, T., Ono, K., Ogita, H., Sakamoto, T., Yamamoto, N., et al. (2009). Transplantation of mouse induced pluripotent stem cells into the cochlea. *Neuroreport* 20, 1250–1254.

Nishimura, K., Nakagawa, T., Sakamoto, T., and Ito, J. (2012). Fates of murine pluripotent stem cell-derived neural progenitors following transplantation into mouse cochleae. *Cell Transplant.* 21, 763–771. doi: 10.3727/096368911X623907

Niu, X., Trifunovic, A., Larsson, N. G., and Canlon, B. (2007). Somatic mtDNA mutations cause progressive hearing loss in the mouse. *Exp. Cell Res.* 313, 3924–3934. doi: 10.1016/j.yexcr.2007.05.029

Ogita, H., Nakagawa, T., Lee, K. Y., Inaoka, T., Okano, T., Kikkawa, Y. S., et al. (2009). Surgical invasiveness of cell transplantation into the guinea pig cochlear modiolus. *ORL J. Otorhinolaryngol. Relat. Spec.* 71, 32–39. doi: 10.1159/000165915

Okano, T., Nakagawa, T., Endo, T., Kim, T. S., Kita, T., Tamura, T., et al. (2005). Engraftment of embryonic stem cell-derived neurons into the cochlear modiolus. *Neuroreport* 16, 1919–1922. doi: 10.1097/01.wnr.0000187628.38010.5b

Park, J. C., Cook, K. C., and Verde, E. A. (1990). Dietary restriction slows the abnormally rapid loss of spiral ganglion neurons in C57BL/6 mice. *Hear. Res.* 48, 275–279. doi: 10.1016/0378-5955(90)90067-y

Parker, M. A. (2011). Biotechnology in the treatment of sensorineural hearing loss: foundations and future of hair cell regeneration. *J. Speech Lang. Hear. Res.* 54, 1709–1731. doi: 10.1044/1092-4388(2011/10-0149)

Parker, M. A., Corliss, D. A., Gray, B., Anderson, J. K., Bobbin, R. P., Snyder, E. Y., et al. (2007). Neural stem cells injected into the sound-damaged cochlea migrate throughout the cochlea and express markers of hair cells, supporting cells, and spiral ganglion cells. *Hear. Res.* 232, 29–43. doi: 10.1016/j.heares.2007.06.007

Perny, M., Roccio, M., Grandgirard, D., Solyga, M., Senn, P., and Leib, S. L. (2016). The severity of infection determines the localization of damage and

extent of sensorineural hearing loss in experimental pneumococcal meningitis. *J. Neurosci.* 36, 7740–7749. doi: 10.1523/JNEUROSCI.0554-16.2016

Pfingst, B. E., Colesa, D. J., Swiderski, D. L., Hughes, A. P., Strahl, S. B., Sinan, M., et al. (2017). Neurotrophin gene therapy in deafened ears with cochlear implants: long-term effects on nerve survival and functional measures. *J. Assoc. Res. Otolaryngol.* 18, 731–750. doi: 10.1007/s10162-017-0633-9

Pinyon, J. L., Tadros, S. F., Froud, K. E., Wong, Y. A. C., Tompson, I. T., Crawford, E. N., et al. (2014). Close-field electroporation gene delivery using the cochlear implant electrode array enhances the bionic ear. *Sci. Transl. Med.* 6:233ra54.

Plosa, E. J., Esbenshade, J. C., Fuller, M. P., and Weitkamp, J. H. (2012). Cytomegalovirus infection. *Pediatr. Rev.* 33, 156–163; quiz 63.

Puel, J. L., Ruel, J., Gervais d'Aldin, C., and Pujol, R. (1998). Excitotoxicity and repair of cochlear synapses after noise-trauma induced hearing loss. *Neuroreport* 9, 2109–2114. doi: 10.1097/00001756-199806220-00037

Pujol, R., and Puel, J. L. (1999). Excitotoxicity, synaptic repair, and functional recovery in the mammalian cochlea: a review of recent findings. *Ann. N. Y. Acad. Sci.* 884, 249–254. doi: 10.1111/j.1749-6632.1999.tb08646.x

Rejali, D., Lee, V. A., Abrashkin, K. A., Humayun, N., Swiderski, D. L., and Raphael, Y. (2007). Cochlear implants and ex vivo BDNF gene therapy protect spiral ganglion neurons. *Hear. Res.* 228, 180–187. doi: 10.1016/j.heares.2007.02.010

Reyes, J. H., O'Shea, K. S., Wys, N. L., Velkey, J. M., Prieskorn, D. M., Wesolowski, K., et al. (2008). Glutamatergic neuronal differentiation of mouse embryonic stem cells after transient expression of neurogenin 1 and treatment with BDNF and GDNF: *in vitro* and *in vivo* studies. *J. Neurosci.* 28, 12622–12631. doi: 10.1523/JNEUROSCI.0563-08.2008

Robertson, D. (1983). Functional significance of dendritic swelling after loud sounds in the guinea pig cochlea. *Hear. Res.* 9, 263–278. doi: 10.1016/0378-5955(83)90031-x

Roisen, F. J., Klueber, K. M., Lu, C. L., Hatcher, L. M., Dozier, A., Shields, C. B., et al. (2001). Adult human olfactory stem cells. *Brain Res.* 890, 11–22.

Ruan, Q., Chen, D., Wang, Z., Chi, F., He, J., Wang, J., et al. (2010). Effects of Kir2.1 gene transfection in cochlear hair cells and application of neurotrophic factors on survival and neurite growth of co-cultured cochlear spiral ganglion neurons. *Mol. Cell. Neurosci.* 43, 326–339. doi: 10.1016/j.mcn.2009.12.006

Rubel, E. W., and Fritzsch, B. (2002). Auditory system development: primary auditory neurons and their targets. *Annu. Rev. Neurosci.* 25, 51–101. doi: 10.1146/annurev.neuro.25.112701.142849

Ruel, J., Bobbin, R. P., Vidal, D., Pujol, R., and Puel, J. L. (2000). The selective AMPA receptor antagonist GYKI 53784 blocks action potential generation and excitotoxicity in the guinea pig cochlea. *Neuropharmacology* 39, 1959–1973. doi: 10.1016/s0028-3908(00)00069-1

Ruel, J., Emery, S., Nouvian, R., Bersot, T., Amilhon, B., Van Rybroek, J. M., et al. (2008). Impairment of SLC17A8 encoding vesicular glutamate transporter-3, VGLUT3, underlies nonsyndromic deafness DFNA25 and inner hair cell dysfunction in null mice. *Am. J. Hum. Genet.* 83, 278–292. doi: 10.1016/j.ajhg.2008.07.008

Ruel, J., Wang, J., Rebillard, G., Eybalin, M., Lloyd, R., Pujol, R., et al. (2007). Physiology, pharmacology and plasticity at the inner hair cell synaptic complex. *Hear. Res.* 227, 19–27. doi: 10.1016/j.heares.2006.08.017

Ruggero, M. A., Santi, P. A., and Rich, N. C. (1982). Type II cochlear ganglion cells in the chinchilla. *Hear. Res.* 8, 339–356. doi: 10.1016/0378-5955(82)90023-5

Sapolsky, R. M., Krey, L. C., and McEwen, B. S. (1986). The neuroendocrinology of stress and aging: the glucocorticoid cascade hypothesis. *Endocr. Rev.* 7, 284–301. doi: 10.1210/edrv-7-3-284

Schacht, J., and Hawkins, J. E. (2005). Sketches of otohistory. Part 9: presby[a]cusis. *Audiol. Neurootol.* 10, 243–247. doi: 10.1159/000086524

Schacht, J., Talaska, A. E., and Rybak, L. P. (2012). Cisplatin and aminoglycoside antibiotics: hearing loss and its prevention. *Anat. Rec. (Hoboken)* 295, 1837–1850. doi: 10.1002/ar.22578

Schachtele, S. J., Mutnal, M. B., Schleiss, M. R., and Lokensgard, J. R. (2011). Cytomegalovirus-induced sensorineural hearing loss with persistent cochlear inflammation in neonatal mice. *J. Neurovirol.* 17, 201–211. doi: 10.1007/s13365-011-0024-7

Schecterson, L. C., and Bothwell, M. (1994). Neurotrophin and neurotrophin receptor mRNA expression in developing inner ear. *Hear. Res.* 73, 92–100. doi: 10.1016/0378-5955(94)90286-0

Scheper, V., Hoffmann, A., Gepp, M. M., Schulz, A., Hamm, A., Pannier, C., et al. (2019a). Stem cell based drug delivery for protection of auditory neurons in a guinea pig model of cochlear implantation. *Front. Cell. Neurosci.* 13:177. doi: 10.3389/fncel.2019.00177

Scheper, V., Schwieger, J., Hamm, A., Lenarz, T., and Hoffmann, A. (2019b). BDNF-overexpressing human mesenchymal stem cells mediate increased neuronal protection in vitro. *J. Neurosci. Res.* 97, 1414–1429. doi: 10.1002/jnr.24488

Seyyedi, M., Viana, L. M., and Nadol, J. B. Jr. (2014). Within-subject comparison of word recognition and spiral ganglion cell count in bilateral cochlear implant recipients. *Otol. Neurotol.* 35, 1446–1450. doi: 10.1097/MAO.0000000000000443

Shepherd, R. K., Coco, A., and Epp, S. B. (2008). Neurotrophins and electrical stimulation for protection and repair of spiral ganglion neurons following sensorineural hearing loss. *Hear. Res.* 242, 100–109. doi: 10.1016/j.heares.2007.12.005

Shepherd, R. K., Coco, A., Epp, S. B., and Crook, J. M. (2005). Chronic depolarization enhances the trophic effects of brain-derived neurotrophic factor in rescuing auditory neurons following a sensorineural hearing loss. *J. Comp. Neurol.* 486, 145–158. doi: 10.1002/cne.20564

Shi, L., Liu, K., Wang, H., Zhang, Y., Hong, Z., Wang, M., et al. (2015). Noise induced reversible changes of cochlear ribbon synapses contribute to temporary hearing loss in mice. *Acta Otolaryngol.* 135, 1093–1102. doi: 10.3109/00016489.2015.1061699

Shibata, S. B., Cortez, S. R., Beyer, L. A., Wiler, J. A., Di Polo, A., Pfingst, B. E., et al. (2010). Transgenic BDNF induces nerve fiber regrowth into the auditory epithelium in deaf cochleae. *Exp. Neurol.* 223, 464–472. doi: 10.1016/j.expneurol.2010.01.011

Someya, S., Yamasoba, T., Weindruch, R., Prolla, T. A., and Tanokura, M. (2007). Caloric restriction suppresses apoptotic cell death in the mammalian cochlea and leads to prevention of presbycusis. *Neurobiol. Aging* 28, 1613–1622. doi: 10.1016/j.neurobiolaging.2006.06.024

Spoendlin, H. (1972). Innervation densities of the cochlea. *Acta Otolaryngol.* 73, 235–248.

Spoendlin, H. (1985). Histopathology of noise deafness. *J. Otolaryngol.* 14, 282–286.

Staecker, H., Gabaizadeh, R., Federoff, H., and Van De Water, T. R. (1998). Brain-derived neurotrophic factor gene therapy prevents spiral ganglion degeneration after hair cell loss. *Otolaryngol. Head Neck Surg.* 119, 7–13. doi: 10.1016/S0194-5998(98)70194-9

Stankovic, K., Rio, C., Xia, A., Sugawara, M., Adams, J. C., Liberman, M. C., et al. (2004). Survival of adult spiral ganglion neurons requires erbB receptor signaling in the inner ear. *J. Neurosci.* 24, 8651–8661. doi: 10.1523/JNEUROSCI.0733-04.2004

Tahera, Y., Meltser, I., Johansson, P., Bian, Z., Stierna, P., Hansson, A. C., et al. (2006). NF-kappaB mediated glucocorticoid response in the inner ear after acoustic trauma. *J. Neurosci. Res.* 83, 1066–1076. doi: 10.1002/jnr.20795

Takada, Y., Beyer, L. A., Swiderski, D. L., O'Neal, A. L., Prieskorn, D. M., Shivatzki, S., et al. (2014). Connexin 26 null mice exhibit spiral ganglion degeneration that can be blocked by BDNF gene therapy. *Hear. Res.* 309, 124–135. doi: 10.1016/j.heares.2013.11.009

Takeno, S., Wake, M., Mount, R. J., and Harrison, R. V. (1998). Degeneration of spiral ganglion cells in the chinchilla after inner hair cell loss induced by carboplatin. *Audiol. Neurootol.* 3, 281–290. doi: 10.1159/000013800

Tamura, T., Nakagawa, T., Iguchi, F., Tateya, I., Endo, T., Kim, T. S., et al. (2004). Transplantation of neural stem cells into the modiolus of mouse cochleae injured by cisplatin. *Acta Otolaryngol. Suppl.* 124, 65–68. doi: 10.1080/03655230310016780

Teissier, N., Delezoide, A. L., Mas, A. E., Khung-Savatovsky, S., Bessieres, B., Nardelli, J., et al. (2011). Inner ear lesions in congenital cytomegalovirus infection of human fetuses. *Acta Neuropathol.* 122, 763–774. doi: 10.1007/s00401-011-0895-y

Thrasivoulou, C., Soubeyre, V., Ridha, H., Giuliani, D., Giaroni, C., Michael, G. J., et al. (2006). Reactive oxygen species, dietary restriction and neurotrophic factors in age-related loss of myenteric neurons. *Aging Cell* 5, 247–257. doi: 10.1111/j.1474-9726.2006.00214.x

Tsukasaki, N., Whitworth, C. A., and Rybak, L. P. (2000). Acute changes in cochlear potentials due to cisplatin. *Hear. Res.* 149, 189–198. doi: 10.1016/s0378-5955(00)00182-9

Vetter, D. E., Mann, J. R., Wangemann, P., Liu, J., McLaughlin, K. J., Lesage, F., et al. (1996). Inner ear defects induced by null mutation of the isk gene. *Neuron* 17, 1251–1264. doi: 10.1016/s0896-6273(00)80255-x

Wake, M., Hughes, E. K., Poulakis, Z., Collins, C., and Rickards, F. W. (2004). Outcomes of children with mild-profound congenital hearing loss at 7 to 8 years: a population study. *Ear Hear.* 25, 1–8. doi: 10.1097/01.AUD.0000111262.12219.2F

Wan, G., Gomez-Casati, M. E., Gigliello, A. R., Liberman, M. C., and Corfas, G. (2014). Neurotrophin-3 regulates ribbon synapse density in the cochlea and induces synapse regeneration after acoustic trauma. *Elife* 3:e03564. doi: 10.7554/eLife.03564

Wang, J., and Puel, J. L. (2018). Toward cochlear therapies. *Physiol. Rev.* 98, 2477–2522.

Wang, J., Ding, D., and Salvi, R. J. (2003). Carboplatin-induced early cochlear lesion in chinchillas. *Hear. Res.* 181, 65–72. doi: 10.1016/s0378-5955(03)00176-x

Wang, M., Han, Y., Wang, X., Liang, S., Bo, C., Zhang, Z., et al. (2021). Characterization of EGR-1 expression in the auditory cortex following kanamycin-induced hearing loss in mice. *J. Mol. Neurosci.* 71, 2260–2274. doi: 10.1007/s12031-021-01791-0

Wang, Y., Chang, Q., Tang, W., Sun, Y., Zhou, B., Li, H., et al. (2009). Targeted connexin26 ablation arrests postnatal development of the organ of Corti. *Biochem. Biophys. Res. Commun.* 385, 33–37. doi: 10.1016/j.bbrc.2009.05.023

Wang, Y., Hirose, K., and Liberman, M. C. (2002). Dynamics of noise-induced cellular injury and repair in the mouse cochlea. *J. Assoc. Res. Otolaryngol.* 3, 248–268. doi: 10.1007/s101620020028

Willott, J. F., Erway, L. C., Archer, J. R., and Harrison, D. E. (1995). Genetics of age-related hearing loss in mice. II. Strain differences and effects of caloric restriction on cochlear pathology and evoked response thresholds. *Hear. Res.* 88, 143–155. doi: 10.1016/0378-5955(95)00107-f

Wise, A. K., Hume, C. R., Flynn, B. O., Jeelall, Y. S., Suhr, C. L., Sgro, B. E., et al. (2010). Effects of localized neurotrophin gene expression on spiral ganglion neuron resprouting in the deafened cochlea. *Mol. Ther.* 18, 1111–1122. doi: 10.1038/mt.2010.28

Wise, A. K., Tu, T., Atkinson, P. J., Flynn, B. O., Sgro, B. E., Hume, C., et al. (2011). The effect of deafness duration on neurotrophin gene therapy for spiral ganglion neuron protection. *Hear. Res.* 278, 69–76. doi: 10.1016/j.heares.2011.04.010

Wu, J., Liu, B., Fan, J., Zhu, Q., and Wu, J. (2011). Study of protective effect on rat cochlear spiral ganglion after blast exposure by adenovirus-mediated human beta-nerve growth factor gene. *Am. J. Otolaryngol.* 32, 8–12. doi: 10.1016/j.amjoto.2009.08.012

Xu, Y. P., Shan, X. D., Liu, Y. Y., Pu, Y., Wang, C. Y., Tao, Q. L., et al. (2016). Olfactory epithelium neural stem cell implantation restores noise-induced hearing loss in rats. *Neurosci. Lett.* 616, 19–25. doi: 10.1016/j.neulet.2016.01.016

Yagi, M., Kanzaki, S., Kawamoto, K., Shin, B., Shah, P. P., Magal, E., et al. (2000). Spiral ganglion neurons are protected from degeneration by GDNF gene therapy. *J. Assoc. Res. Otolaryngol.* 1, 315–325. doi: 10.1007/s101620010011

Yamasoba, T., Someya, S., Yamada, C., Weindruch, R., Prolla, T. A., and Tanokura, M. (2007). Role of mitochondrial dysfunction and mitochondrial DNA mutations in age-related hearing loss. *Hear. Res.* 226, 185–193. doi: 10.1016/j.heares.2006.06.004

Yang, T., Kersigo, J., Jahan, I., Pan, N., and Fritzsch, B. (2011). The molecular basis of making spiral ganglion neurons and connecting them to hair cells of the organ of Corti. *Hear. Res.* 278, 21–33. doi: 10.1016/j.heares.2011.03.002

Zhang, P. Z., He, Y., Jiang, X. W., Chen, F. Q., Chen, Y., Shi, L., et al. (2013). Stem cell transplantation *via* the cochlear lateral wall for replacement of degenerated spiral ganglion neurons. *Hear. Res.* 298, 1–9.

Zhu, H., Chen, J., Guan, L., Xiong, S., and Jiang, H. (2018). The transplantation of induced pluripotent stem cells into the cochleae of mature mice. *Int. J. Clin. Exp. Pathol.* 11, 4423–4430.

Zhuang, W., Wang, C., Shi, X., Qiu, S., Zhang, S., Xu, B., et al. (2018). MCMV triggers ROS/NLRP3-associated inflammasome activation in the inner ear of mice and cultured spiral ganglion neurons, contributing to sensorineural hearing loss. *Int. J. Mol. Med.* 41, 3448–3456. doi: 10.3892/ijmm.2018.3539

Zoli, M., Picciotto, M. R., Ferrari, R., Cocchi, D., and Changeux, J. P. (1999). Increased neurodegeneration during ageing in mice lacking high-affinity nicotine receptors. *EMBO J.* 18, 1235–1244. doi: 10.1093/emboj/18.5.1235

Conflict of Interest: The authors declare that the research was conducted in the absence of any commercial or financial relationships that could be construed as a potential conflict of interest.

Publisher's Note: All claims expressed in this article are solely those of the authors and do not necessarily represent those of their affiliated organizations, or those of the publisher, the editors and the reviewers. Any product that may be evaluated in this article, or claim that may be made by its manufacturer, is not guaranteed or endorsed by the publisher.

frontiers in Cellular Neuroscience

ORIGINAL RESEARCH
published: 17 January 2022
doi: 10.3389/fncel.2021.819194

Connexin30-Deficiency Causes Mild Hearing Loss With the Reduction of Endocochlear Potential and ATP Release

Junmin Chen[1,2,3†], *Penghui Chen*[1,2,3†], *Baihui He*[1,2,3†], *Tianyu Gong*[1,2,3], *Yue Li*[1,2,3], *Jifang Zhang*[1,2,3], *Jingrong Lv*[1,2,3], *Fabio Mammano*[4,5], *Shule Hou*[1,2,3]* *and Jun Yang*[1,2,3]*

[1]*Department of Otorhinolaryngology—Head & Neck Surgery, Xinhua Hospital, Shanghai Jiaotong University School of Medicine, Shanghai, China,* [2]*Ear Institute, Shanghai Jiaotong University School of Medicine, Shanghai, China,* [3]*Shanghai Key Laboratory of Translational Medicine on Ear and Nose Diseases, Shanghai, China,* [4]*Department of Physics and Astronomy "G. Galilei", University of Padua, Padua, Italy,* [5]*Department of Biomedical Sciences, Institute of Cell Biology and Neurobiology, Italian National Research Council, Monterotondo, Italy*

OPEN ACCESS

Edited by:
Zuhong He,
Wuhan University, China

Reviewed by:
Renjie Chai,
Southeast University, China
Cheng Cheng,
Nanjing Drum Tower Hospital, China

***Correspondence:**
Shule Hou
houshule8562@xinhuamed.com.cn
Jun Yang
yangjun@xinhuamed.com.cn

[†]*These authors have contributed equally to this work*

Specialty section:
This article was submitted to Cellular Neuropathology, a section of the journal Frontiers in Cellular Neuroscience

Received: *21 November 2021*
Accepted: *22 December 2021*
Published: *17 January 2022*

Citation:
Chen J, Chen P, He B, Gong T, Li Y, Zhang J, Lv J, Mammano F, Hou S and Yang J (2022) Connexin30-Deficiency Causes Mild Hearing Loss With the Reduction of Endocochlear Potential and ATP Release. Front. Cell. Neurosci. 15:819194. doi: 10.3389/fncel.2021.819194

GJB2 and *GJB6* are adjacent genes encoding connexin 26 (Cx26) and connexin 30 (Cx30), respectively, with overlapping expressions in the inner ear. Both genes are associated with the commonest monogenic hearing disorder, recessive isolated deafness DFNB1. Cx26 plays an important role in auditory development, while the role of Cx30 in hearing remains controversial. Previous studies found that Cx30 knockout mice had severe hearing loss along with a 90% reduction in Cx26, while another Cx30 knockout mouse model showed normal hearing with nearly half of Cx26 preserved. In this study, we used CRISPR/Cas9 technology to establish a new Cx30 knockout mouse model ($Cx30^{-/-}$), which preserves approximately 70% of Cx26. We found that the 1, 3, and 6-month-old $Cx30^{-/-}$ mice showed mild hearing loss at full frequency. Immunofluorescence and HE staining suggested no significant differences in microstructure of the cochlea between $Cx30^{-/-}$ mice and wild-type mice. However, transmission electron microscopy showed slight cavity-like damage in the stria vascularis of $Cx30^{-/-}$ mice. And Cx30 deficiency reduced the production of endocochlear potential (EP) and the release of ATP, which may have induced hearing loss. Taken together, this study showed that lack of Cx30 can lead to hearing loss with an approximately 30% reduction of Cx26 in the present Cx30 knockout model. Hence, Cx30 may play an important rather than redundant role in hearing development.

Keywords: connexin30, hearing loss, connexin26, stria vascularis, endocochlear potential

INTRODUCTION

Hearing loss is a major global health problem, which can be caused by continued excessive noise (Guo et al., 2021), ototoxic drugs (Breglio et al., 2020), aging (Guo et al., 2021), genetic factors (Fu et al., 2021), and infections (Zhang et al., 2021), among which genetic factors caused 50% of the hearing loss. *GJB2* and *GJB6* are two adjacent genes encoding connexin 26 (Cx26) and connexin 30 (Cx30) respectively which form gap junctions (GJs) between supporting cells (SCs) or exist as the hemichannels at the surface of the SCs in the cochlea (Mammano, 2019).

There are two independent GJ networks identified in the inner ear: the epithelial gap junctional network in the organ of Corti and the connective tissue gap junctional network in the cochlear lateral wall (Kikuchi et al., 1995).

Auditory development depends not only on the functional maturation of cochlear hair cells (HCs) but also on the normal differentiation and organization of nonsensory SCs. SCs are coupled through Cx26 and/or Cx30 GJ channels or hemichannels to form a supporting cell network, transmit ATP, ions, signals, and nutrient molecules (Bruzzone et al., 1996; Jagger and Forge, 2015; Verselis, 2019), and the microenvironment of surrounding HCs (Chen et al., 2018). ATP triggers cytosolic Ca^{2+} concentration oscillations and propagation of intercellular Ca^{2+} waves, which appear to play a crucial role in the normal development of the cochlear sensory epithelium, hearing acquisition and the functional maturation of HCs (Johnson et al., 2017; Mammano and Bortolozzi, 2018; Mazzarda et al., 2020). Chai et al. (He et al., 2017; Zhang et al., 2020a,b; Zhang Y. et al., 2020) further confirmed that regenerating HCs cannot achieve functional maturity in the absence of a normal and stable microenvironment by SCs.

GJB2 and *GJB6* mutations account for up to 50% of all nonsyndromic hearing loss cases (Denoyelle et al., 1997; Estivill et al., 1998; Mishra et al., 2018). Homozygous Cx26 and Cx30 deletions lead to severe hearing loss in animal models (Kelsell et al., 1997; del Castillo et al., 2002). It has been reported that Cx26 and Cx30 are both important for hearing development (Adadey et al., 2020). Notably, Cx30 knockout mice displayed severe hearing loss in the absence of endocochlear potential, accompanied by a 90% reduction in Cx26 (Teubner et al., 2003; Boulay et al., 2013). Over-expression of Cx26 in Cx30 knockout mice rescued hearing (Ahmad et al., 2007), but not *vice versa* (Qu et al., 2012). These results indicated that Cx26 is critical for hearing development since it could not be substituted by Cx30 in early cochlear development. Cx30-deficient mice with nearly 50% Cx26 expression showed normal hearing (Boulay et al., 2013). Therefore, the role of Cx30 in the cochlea remains controversial.

In this study, we used CRISPR/Cas9 technology to establish a novel Cx30 knockout mouse model ($Cx30^{-/-}$), which preserved approximately 70% of Cx26 expression in the cochlea and displayed mild hearing loss under full frequency. This new genotype model showed different morphological and functional phenotypes from the past. We believe that this model is of significant importance to explore the mechanism of hearing loss caused by Cx30 deletion.

MATERIALS AND METHODS

Creation and Genotyping of Cx30 Knockout Mice

Cx30 knockout mice ($Cx30^{-/-}$) maintained on a pure C57BL/6 background were purchased from the Shanghai Model Organisms. CRISPR/Cas9 technology was used to repair the mutation introduced by non-homologous recombination, resulting in the shift of the protein reading frame of the *Gjb6* Exon3 gene and loss of function. The mouse genotyping was identified by PCR amplification with the following primers: *Gjb6* primer 1 (P1) 5′-CTAGTGCAACAGCACCCGTA-3′, *Gjb6* P2 5′-CTAGTGCTGAAGGTGTGGGG-3′,*Gjb6* P3 5′-TGGCATTGTTTCACCGTAGT-3′, *Gjb6* P4 5′-AGGTCATGTGAATCTGTCTC-3′, Wild type (WT): *Gjb6* P1 and P2 PCR to obtain a single 2369 bp band; *Gjb6* P3 and P4 can obtain a 512 bp band; Heterozygous (HE): *Gjb6* P1 and P2 PCR to obtain both 527 bp and 2,369 bp bands; *Gjb6* P3 and P4 to obtain 512 bp band; Homozygous (HO): *Gjb6* P1 and P2 PCR obtained a single 527 bp band; *Gjb6* P3 and P4 could not obtain a band. The WT littermates served as controls in the experiment. The experimental procedures were approved by the Shanghai Xinhua Hospital's Animal Center and conducted according to the standards of the NIH Guidelines for the Care and Use of Laboratory Animals.

Assessment of Hearing Loss

Auditory brainstem response (ABR) reflects the electrical response of the cochlear ganglion neurons and the nuclei of the central auditory pathway to sound stimulation. Their threshold assesses the cochlear sensitivity and it is visually measured according to the occurrence of Wave II in a series of repeatable ABR responses obtained at various sound intensities. After 1, 3, and 6-month-old littermates were anesthetized with ketamine (80 mg/kg) and xylazine (10 mg/kg), they were subjected to sudden tones of various frequencies from 4 to 32 kHz (duration of 10 ms, rising -The fall time is 0.5 ms). The sound is generated by Tucker-Davis System II hardware and software (Tucker-Davis Technologies, Alachua, FL).

Quantitative PCR Analyses

Total RNA was extracted from the whole dissected cochlea, the basemental membrane (BM), or the stria vascularis (SV) of postnatal day 5 (P5, where P0 is the date of birth) and 1-month-old mice using the Takara MiniBEST Universal RNA Extraction Kit (Takara, 9767, Japan). Reverse transcription was performed using 1 μg of RNA. Quantitative PCR (qPCR) was conducted on cDNAs using. The primers used are as follows:

Cx30 primers: Forward 5′-AAGACCTGGAGGACATCAAACG-3′ and

Reverse 5′-CGAAATGAAGCAGTCCACGAG-3′

Cx26 primers: Foward 5′-TCACAGAGCTGTGCTATTTG-3′ and

Reverse 5′-ACTGGTCTTTTGGACTTTCC-3′

Actin primers: Foward 5′-GAGAGGGAAATCGTGCGTGA-3′ and

Reverse 5′-ACATCTGCTGGAAGGTGGAC-3′),

using TB Green® Premix Ex Taq™ (Takara, RR420B, Japan). Samples were analyzed in triplicate on Applied Biosystems 7500 (ThermoFisher). The expression levels of mRNAs were calculated by the $2^{-\Delta\Delta CT}$ method.

Western Blot Analysis

Proteins were extracted from the whole dissected cochlea, the BM, or the SV of P5 and 1-month-old mice. The proteins were separated by SDS-PAGE and transferred to PVDF membranes (Millipore, Billerica, MA, USA). The membranes were blocked with 5% skim milk (Beyotime, Shanghai, China)

at room temperature for 1 h and then incubated with primary antibodies against Tublin (Zen Bioscience, 330628, 1:1,000, China), Cx30 antibody (Invitrogen, 71-2800, 1:200, USA), and Cx26 antibody (Invitrogen, 33-5800, 1:200, USA) at 4°C overnight. After three times of washing with PBS-0.01% Tween 20 (PBS-T), the membranes were incubated with a secondary antibody, anti-rabbit IgG, or antimouse IgG (Beyotime; 1:1,000, China), for 2 h at 37°C. After washing the membranes, and adding freshly prepared chemiluminescence solution (Millipore; A:B = 1:1), the immunoreactive bands were imaged under the Bio-Rad ChemiDoc XRS+ (Bio-Rad Co., Hercules, CA, USA). Semiquantitative densitometric analysis was performed with ImageJ software.

Immunohistochemistry and Confocal Imaging

Cochleas of P5 and 1-month-old mice were fixed with 4% paraformaldehyde, decalcified, frozen, and cut by a cryostat. The tissue sections were directly mounted onto glass slides for staining and storage. The cochlear section was incubated in a blocking solution (10% goat serum and 1% BSA in the PBS) with 0.1% Triton X-100 for 1 h at room temperature. Then, the section was incubated with rabbit anti-Cx30 antibody (Invitrogen, 71-2800, 1:200, USA), the rabbit anti-Cx26 antibody (Invitrogen, 51-2800, 1:200, USA), or the mouse anti-Cx26 antibody (Invitrogen, 33-5800, 1:200, USA) in the blocking solution at 4°C overnight, following reaction with corresponding Alexa Fluor 488-, 458- or 647- secondary antibodies (Invitrogen, 1:500, USA) for 2 h at room temperature (23°C). The sections were further stained by 1% 40, 6-diamidino-2-phenylindole (DAPI, Invitrogen, 1:200, USA) for ∼10 min or AlexaFluor 568 phalloidin (Servicebio, G1041, 1:500) for ∼15 min following the 2nd antibody incubation to visualize cell nuclei or F–Actin. After washout, the sections were mounted and observed under a microscope.

ATP Release Measurement

The P5 mouse temporal bone was micro-dissected in ice-cold HBSS (Thermo Fisher Scientific). The inner ear was opened from its apex to base. After removal of the bone, the exposed BM and SV were dissected separately and put into an incubation chamber. For testing ATP release, the isolated BM and SV was incubated in a zero Ca^{2+} solution (ZCS) containing (in mM): 137 NaCl, 5.36 KCl, 0.44 KH2PO4, 0.18 Na2HPO4, 0.1 EGTA, 25 HEPES, and 5.55 Dextrose (pH 7.3). To quantify ATP release, the BM and SV were incubated in ZCS for 20 min at 37°C, 5% CO2. The collected incubation solutions were kept on ice. The amount of ATP was measured by a bioluminescence method with a luciferin-luciferase assay kit (FL-ASC, Sigma, USA) using a black 96-well plate to avoid optical cross-talk. The bioluminescence was read by a Biotek Synergy 4 Hybrid Microplate Reader (Biotek Instruments Inc, Winooski, VT, USA). All bioluminescence measurements reported in this article fell within the linearity range of the ATP standard curve generated according to the manufacturer's instructions.

Measurement of Endocochlear Potential

The endocochlear potential was recorded under general anesthesia on $Cx30^{-/-}$ (n = 6) mice and Wt (n = 6) mice at 1-month-old. Mice were anesthetized with ketamine (150 mg/kg, IP) and xylazine (6 mg/kg, IP). Body temperature was maintained at 37°C on a heating operating table (Harvard Apparatus, 73-3771). A mouse head holding adaptor (MA-6N, Narishige, Tokyo, Japan) was used to maintain a supine position. A tracheotomy was performed, followed by opening the auditory bulla through a ventral approach to expose the basal turn of the cochlea. A silver chloride reference electrode was placed under the skin. Access to the scala media of the basal turn was obtained by thinning the bone over the spiral ligament and making a small opening with a pick. A micropipette electrode (∼2 μm) filled with 150 mM KCl was advanced through the bony aperture into the spiral ligament. Entry of the electrode tip into the endolymph is characterized by transients in recorded potentials. The electrode was advanced until a stable potential was observed. The signal was amplified through a patch-Clamp Amplifier (HEKA EPC 10 USB double, Germany). The DC potentials were recorded *via* an A-D converter (HEKA EPC 10 USB PROBE 1, Germany).

Transmission Electron Microscope Observation

After the cochlea of P5 mice was dissected, it was fixed in 2.5% glutaraldehyde for 24 h and decalcified with 10% EDTA for several days. The samples were fixed in 1% osmic acid for 2 h, dehydrated with acetone, and embedded in 812 resin. After staining the ultrathin sections with alkaline lead citrate and uranyl acetate, the structure of each cochlea under a Hitachi HF5000 transmission electron microscope (Hitachi, Tokyo, Japan) was observed.

Statistics

Several statistical methods were used to analyze the data. The Kolmogorov-Smirnov test was used to analyze the normality of the distribution. The Student t-test compared statistical means. The Mann-Whitney U test was used for non-normal distributions or distributions with different variances. All statistical analyses were performed using SPSS v19.0 (SPSS Inc. Chicago, IL). Mean values are quoted ± standard error of the mean (s.e.m.) where $p < 0.05$ was assumed as statistically significant.

RESULTS

Deletion of Cx30 in the Cochlea

In our model, CRISPR/Cas9 technology was used to repair the mutation introduced by non-homologous recombination, resulting in a shift of the protein reading frame of the *Gjb6* exon 3 gene and loss of function (**Figures 1A,B**). To test for Cx30 inactivation, we measured Cx30 expression in the inner ear by qPCR (**Figure 1C**). As expected, no Cx30 transcript was detected in $Cx30^{-/-}$ mice, whereas $Cx30^{+/-}$ mice displayed a 57.6% reduction in expression of Cx30 mRNA compared to $Cx30^{+/+}$ (WT) control mice. Consistent with the mRNA results, Western

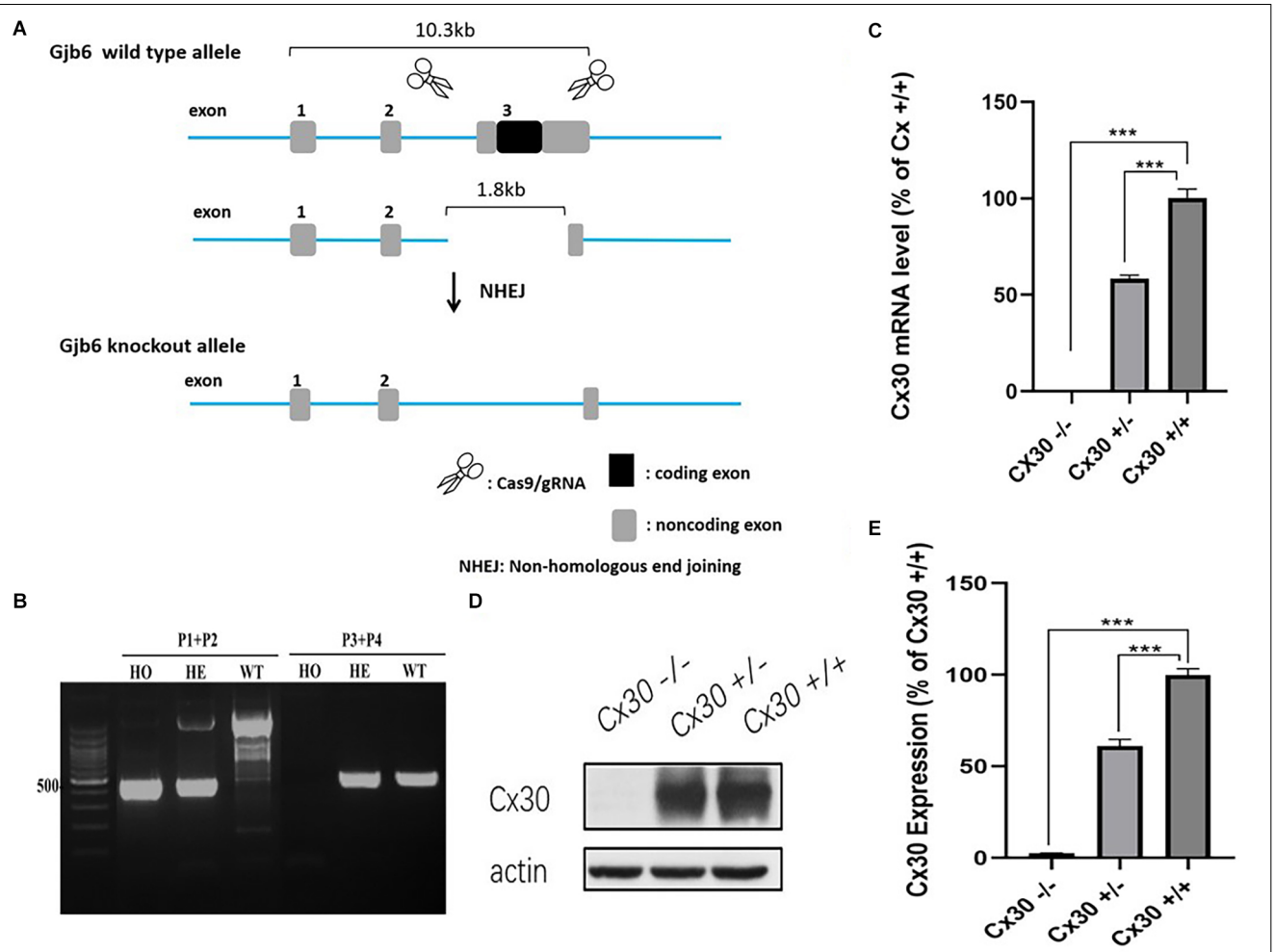

FIGURE 1 | Cx30$^{-/-}$ mice model. **(A)** CRISPR/Cas9 technology was used to repair the mutation introduced by non-homologous recombination, resulting in the shift of the protein reading frame of the *Gjb6* Exon3 gene. **(B)** PCR genotyping: Wild type (WT): *Gjb6* primer 1 (P1) and P2 PCR to obtain a single 2,369 bp band; *Gjb6* P3 and P4 can obtain a 512 bp band; Heterozygous (HE): *Gjb6* P1 and P2 PCR to obtain both 527 bp and 2,369 bp bands; *Gjb6* P3 and P4 to obtain 512 bp band; Homozygous (HO): *Gjb6* P1 and P2 PCR obtained a single 527 bp band; *Gjb6* P3 and P4 could not obtain a band. **(C–E)** Cx30 expression was quantified by qPCR **(C)** and western blot **(D,E)** in the whole cochlea. Data presented as Mean ± SEM; three independent experiments; three mice of each genotype per experiment; *t*-test. ***$p < 0.001$.

blot analysis of protein levels in the inner ear of Cx30 +/- mice showed a 61.1% reduction compared to WT mice, while it was undetectable in Cx30 $^{-/-}$ mice (**Figures 1D,E**).

Hearing Loss in Cx30$^{-/-}$ Mice

One-month-old, 3-month-old and 6-month-old Cx30$^{-/-}$ mice displayed mild hearing loss at the full frequency (**Figure 2**). Compared with WT mice, the ABR thresholds in 1-month-old Cx30$^{-/-}$ mice at 4, 8, 11, 16, 22, 32, and 40 kHz were elevated by 22.7 ± 2.1 ($p < 0.001$), 20 ± 4.2 ($p < 0.01$), 15 ± 5.9, 11.3 ± 3.8 ($p < 0.01$), 15.3 ± 4.2 ($p < 0.05$), and 6.8 ± 4.4 dB SPL, respectively. Compared with WT mice, the ABR thresholds in 3-month-old Cx30$^{-/-}$ mice at 4, 8, 11, 16, 22, 32, and 40 kHz were elevated by 21.8 ± 2.62 ($p < 0.001$), 17 ± 2.9 ($p < 0.001$), 18.6 ± 3.4 ($p < 0.001$), 14.3 ± 2.9 ($p < 0.001$), 15 ± 4.5 ($p < 0.01$), and 25.5 ± 3.9 ($p < 0.001$) dB SPL, respectively. Compared with WT mice, the ABR thresholds in 6-month-old Cx30$^{-/-}$ mice at 4, 8, 11, 16, 22, 32, and 40 kHz were elevated by 17.5 ± 2.9 ($p < 0.01$), 35 ± 2.9 ($p < 0.001$), 32.1 ± 1.7 ($p < 0.001$), 33.3 ± 1.7 ($p < 0.001$), 18.3 ± 4.4, and −2.5 ± 2.9 dB SPL, respectively. At 6-months of age, the high-frequency hearing thresholds in Cx30$^{-/-}$ mice and WT mice were nearly identical.

Normal Cochlea Microstructure in Cx30$^{-/-}$ Mice

Cx30$^{-/-}$ mice had no cochlear developmental disorders (**Figure 3**). Whole-mounting of the apical, middle, and basal turns of the cochlear sensory epithelium of 1-month-old Cx30$^{-/-}$ mice and WT mice showed no apparent hair cell loss (**Figures 3A,E**). HE staining of cochlear frozen sections in Cx30$^{-/-}$ mice and WT mice showed no difference in the number of SGNs and the thickness of SV (**Figures 3B–D**).

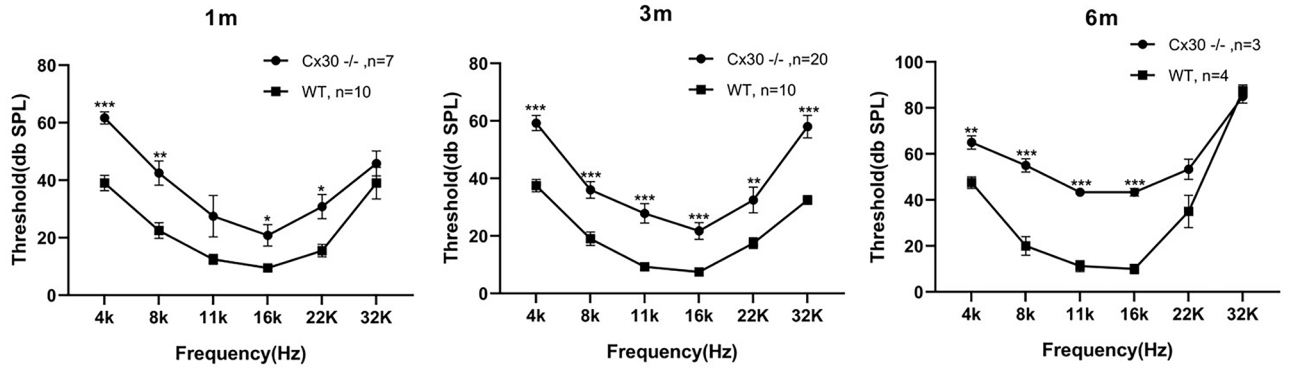

FIGURE 2 | Mild hearing loss in Cx30$^{-/-}$ mice. ABR waveforms were recorded from Cx30$^{-/-}$ and WT littermate mice at 1 m, 3 m, 6 m. 1 m: 1-month-old; 3 m: 3-month-old; 6 m: 6-month-old. Data presented as Mean ± SEM; $n > 3$ in each group. *t*-test. $^{*}p < 0.05$, $^{**}p < 0.01$, $^{***}p < 0.001$. ABR, Auditory brainstem response.

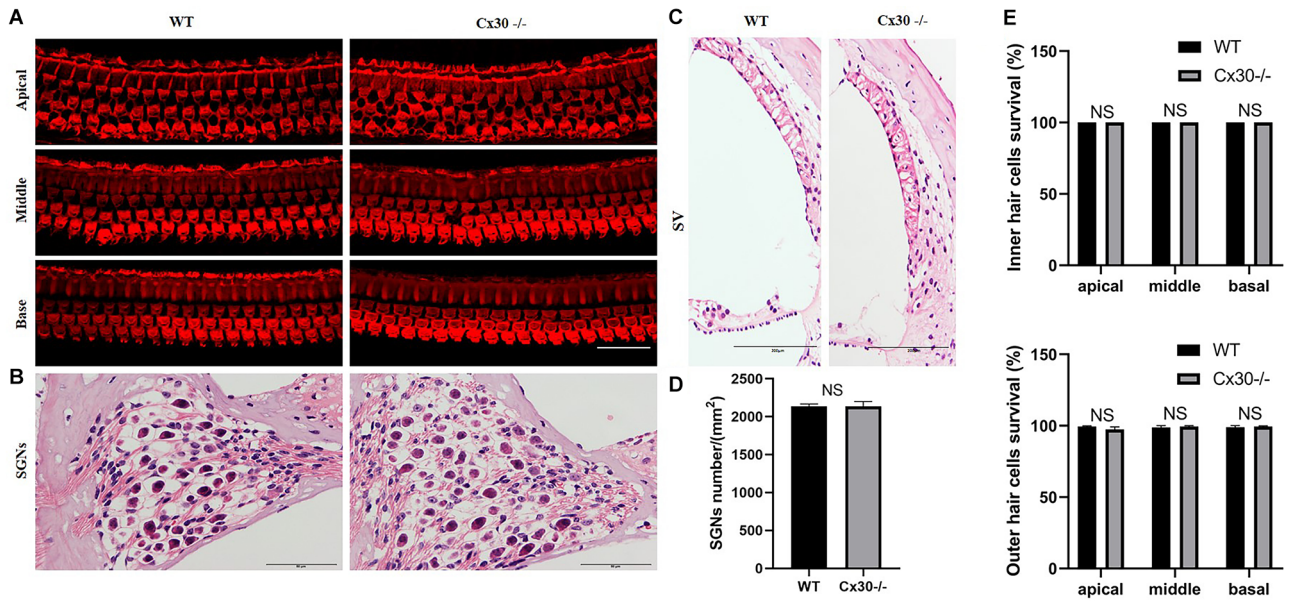

FIGURE 3 | The microscopic structure of cochlea in Cx30$^{-/-}$ mice. **(A,E)** Whole-mountings of the apical, middle and basal turns of cochlear sensory epithelium in 1-month-old Cx30$^{-/-}$ mice and WT mice were obtained by maximal intensity back-projection of 15 confocal optical sections from a 0.8 μm step through—focus sequence (z-stack); actin filaments were stained with phalloidin (red); scale bar: 50 μm. **(B,D)** HE staining of frozen sections of the cochlea in Cx30$^{-/-}$ mice and WT mice showed no difference in the number of spiral ganglions (SGNs). Scale bar: 50 μm. **(C)** HE staining of frozen sections of the cochlea in Cx30$^{-/-}$ mice and WT mice showed no difference in the thickness of SV. SV, stria vascularis. Scale bar: 50 μm. NS, not statistically significant. Data presented as Mean ± SEM. *t*-test.

Cx26 Expression in Cx30$^{-/-}$ Mice

Immunofluorescence showed that Cx26 expression in the BM of Cx30$^{-/-}$ mice was stronger than that of WT mice, and Cx26 expression in the vascular stripe of Cx30$^{-/-}$ mice was significantly lower than that of WT mice both in 1-mouth-old and P5 (**Figures 4A,B**).The mRNA and protein levels of Cx26 in the cochlea of Cx30$^{-/-}$ mice relative to that of WT mice were quantified (**Figures 4C,D**). qPCR analysis showed that the whole cochlear Cx26 mRNA levels of 1-month-old Cx30$^{-/-}$ mice decreased by 41.8% compared with WT mice; whole cochlear mRNA levels in Cx30$^{-/-}$ mice decreased by 28% compared with WT mice at P5; cochlear BM Cx26 mRNA levels in Cx30$^{-/-}$ mice increased by 36.7% compared with WT mice at P5; cochlear SV Cx26 mRNA levels in Cx30$^{-/-}$ mice decreased by 56.6% compared with WT mice in P5 (**Figure 4D**). Western blot showed that the whole cochlear Cx26 protein levels in 1-month-old Cx30$^{-/-}$ mice decreased by 25.9% compared with WT mice; whole cochlear Cx26 protein levels of Cx30$^{-/-}$ mice reduced by 9.84% compared with WT mice at P5; cochlear BM Cx26 protein levels of Cx30$^{-/-}$ mice increased by 19.8% compared with WT mice at P5; cochlear SV Cx26 protein level of Cx30$^{-/-}$ mice decreased by 25.6% compared with WT mice in P5 (**Figure 4C**).

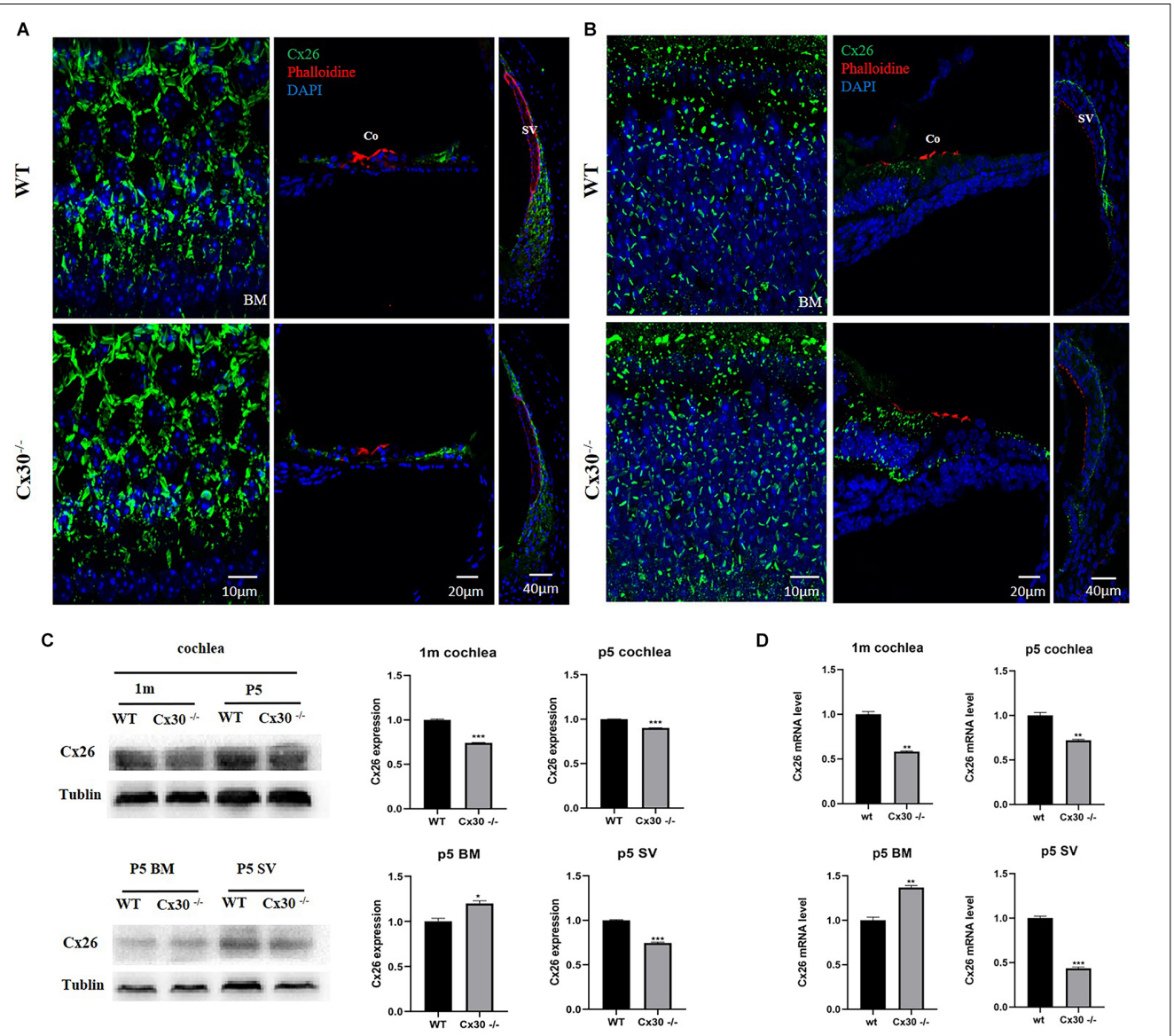

FIGURE 4 | Cx26 expression in Cx30$^{-/-}$ mice. **(A)** Immunofluorescence analysis of frozen sections and BM in the cochlea of 1-month-old mouse. **(B)** Immunofluorescence analysis of frozen sections and BM in the cochlea at P5. Both in 1-month-old and P5, Cx26 expression in the BM of Cx30$^{-/-}$ mice was stronger than that of WT mice, and Cx26 expression in the vascular stripe of Cx30$^{-/-}$ mice was significantly lower than that of WT mice. Cx26: Green, Phalloidin: Red, DAPI: Blue (for cell nuclei); scale bar: 10 μm, 20 μm, 40 μm. **(C)** Western blot analysis of the cochlea, BM, and SV in 1-month-old and P5 mice. Whole cochlear Cx26 protein levels in 1-month-old Cx30$^{-/-}$ mice showed a 25.9% decrease compared with WT mice; whole cochlear Cx26 protein levels of Cx30$^{-/-}$ mice showed 9.84% reduction compared with WT mice at P5; cochlear BM Cx26 protein levels of Cx30$^{-/-}$ mice increased by 19.8% compared with WT mice at P5; Cx26 protein level in SV of the cochlea in Cx30$^{-/-}$ mice decreased by 25.6% compared with WT mice in P5. **(D)** qPCR analysis of the cochlea, BM, and SV in 1-month-old and P5 mice. Whole cochlear Cx26 mRNA levels of 1-month-old Cx30$^{-/-}$ mice declined by 41.8% compared with WT mice; whole cochlear mRNA levels of Cx30$^{-/-}$ mice decreased by 28% compared with WT mice at P5; cochlear BM Cx26 mRNA levels in Cx30$^{-/-}$ mice increased by 36.7% compared with WT mice at P5; cochlear SV Cx26 mRNA levels in Cx30$^{-/-}$ mice reduced by 56.6% compared with WT mice at P5. Data presented as Mean ± SEM. *t*-test. $^{*}p < 0.05$, $^{**}p < 0.01$, $^{***}p < 0.001$. BM, basemental membrane; SV, stria vascularis; Co, Corti's organ.

Mild Damaged Stria Vascularis Submicroscopic Structure in Cx30$^{-/-}$ Mice

Figure 5 shows the transmission electron microscopy images of the submicroscopic structure of the SV in Cx30$^{-/-}$ mice. There was some visible vacuolar injury in the SV of Cx30$^{-/-}$ mice compared with WT mice, which suggested that Cx30 deletion might cause mild damage to the SV.

Reduction of Endocochlear Potential in Cx30$^{-/-}$ Mice

Figure 6 shows a reduction of EP in 1-month-old Cx30$^{-/-}$ mice compared with the WT mice. EPs in Cx30$^{-/-}$ mice and WT mice were 80.1 ± 2.6 mV and 104.6 ± 1.9 mV, respectively (**Figure 6B**). EP in Cx30$^{-/-}$ mice was significantly reduced by 23.4% ($p < 0.001$) relative to WT mice.

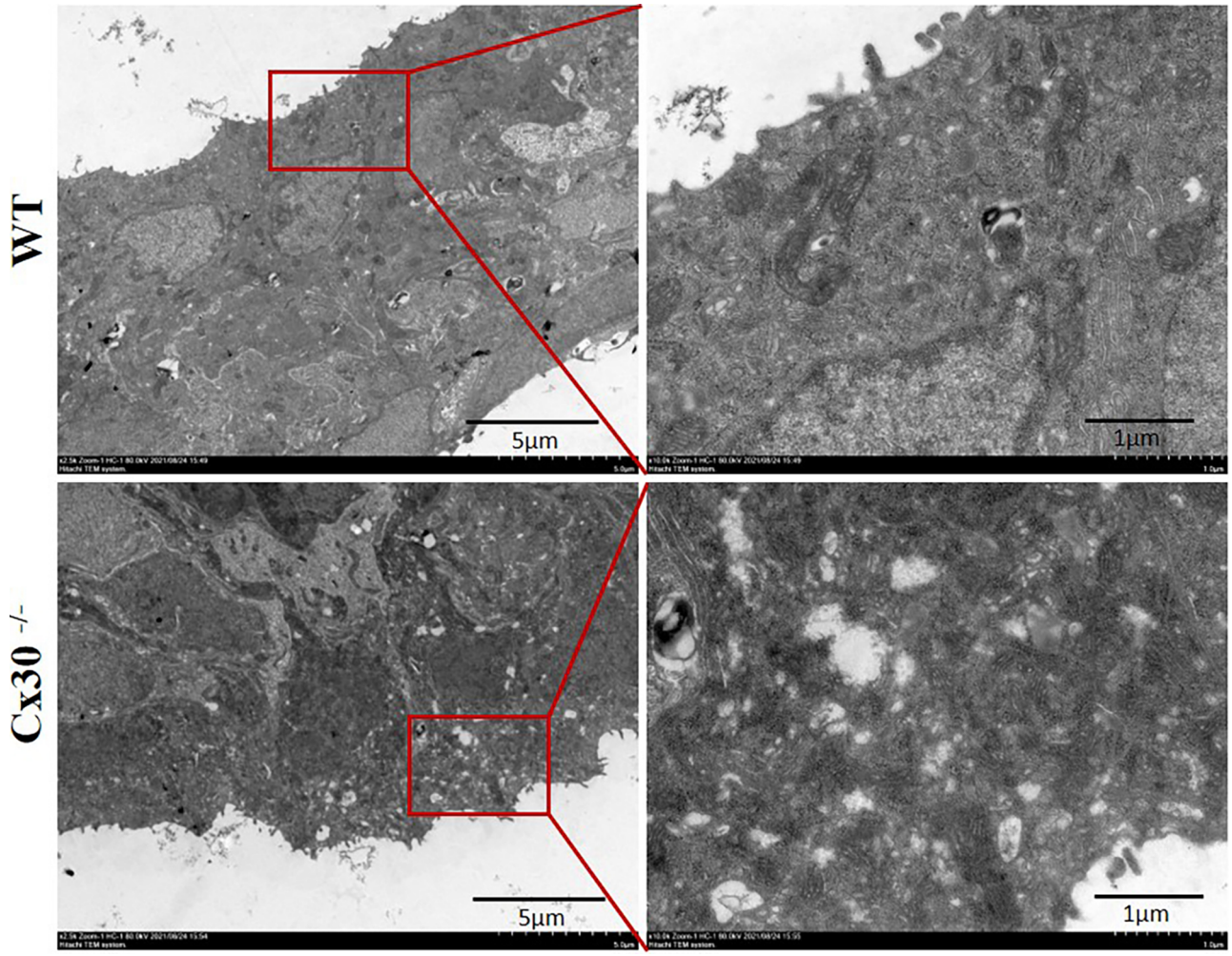

FIGURE 5 | Transmission electron microscopy of the submicroscopic structure of the stria vascularis in Cx30$^{-/-}$ mice. Visible cavity-like damage in the SV of Cx30$^{-/-}$ mice compared with WT mice. Scale bar: 5 μm, 1 μm.

Reduction of ATP Release in Cx30$^{-/-}$ Mice

Figure 7 shows reductions in ATP release of Cx30$^{-/-}$ mice relative to WT mice, both in BM and SV at P5. Compared with WT mice, ATP release in Cx30$^{-/-}$ mice was significantly reduced by 14.2% ($p < 0.05$) in BM and 37.9% ($p < 0.01$) in SV, respectively. ATP release of SV decreased more significantly than that of BM.

DISCUSSION

Seven large genomic deletions of *GJB6* have been previously reported, including >920 kb deletion (Feldmann et al., 2009), 179 kb deletion (Tayoun et al., 2016), 131 kb deletion (Wilch et al., 2010), del(*GJB6*-D13S175), del(*GJB6*-D13S1830), del(*GJB6*-D13S1854; Bliznetz et al., 2017) and del(*GJB6*-D13S1834; Pandya et al., 2020). Homozygous deletion of *GJB6* results in severe to profound hearing loss in humans, similar to the mouse model (Teubner et al., 2003; Mei et al., 2017; Pandya et al., 2020). In many cases, the large deletions of *GJB6* disrupt a 50 cis-acting element upstream of both genes, which abolishes the expression of *GJB2*, and hence is responsible for the phenotype (Rodriguez-Paris and Schrijver, 2009). A recent study reported the del (*GJB6*-D13S1830) deletion in 16.35% of all *GJB2* heterozygotes, which causes more profound hearing loss than those with bi-allelic change in *GJB2* (Pandya et al., 2003, 2020; Snoeckx et al., 2005). The more severe audiological findings in digenic probands cannot be explained by the sole theory of a putative cis-regulatory element in the deleted region (Pandya et al., 2020), suggesting that both *GJB6* and *GJB2* products may contribute to the hearing loss.

The Corti's organ is the core in the auditory system, which is composed of HCs and SCs. SCs release ATP via connexin which triggers intercellular Ca^{2+} wave propagation and might be critical for the functional maturation of HCs (Johnson et al., 2017). The function of HCs is to transduce the sound mechanical stimulation into the primary acoustic signals (Abeytunge et al., 2021), while the spiral ganglion neurons (SGNs) transmit primary acoustic information from HCs in the organ of Corti to the higher auditory centers

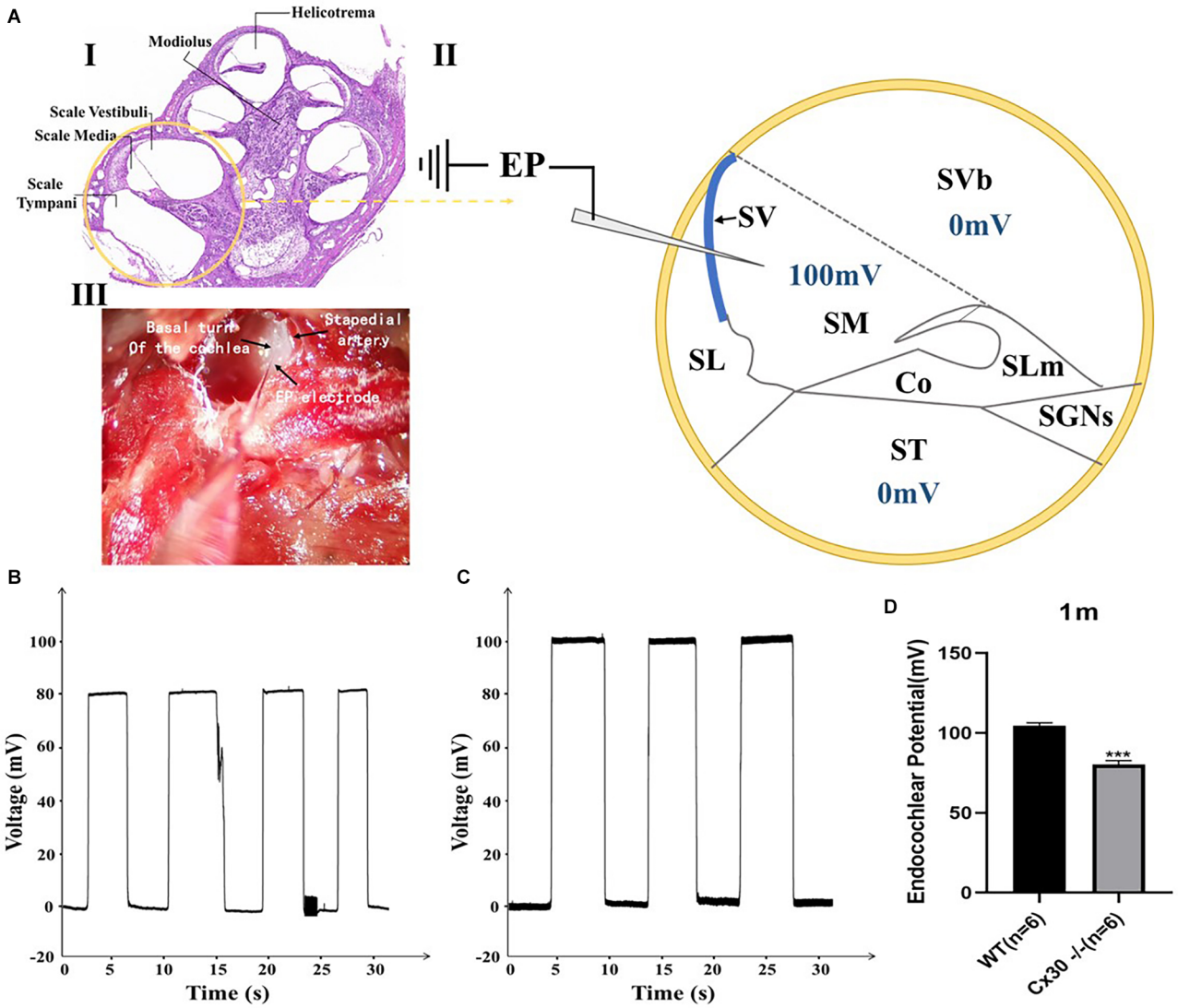

FIGURE 6 | Endocochlear potential (EP) measurements in WT and Cx30 KO mice. **(A)** (I) Cross-section of a cochlea. (II) Schematic diagram of the cross-section of the basal cochlear turn illustrating the method of EP measurement. A microelectrode filled with 3 M KCl was inserted into the endolymph-filled scala media (100 mV in a WT mouse) to record EP. (III) Photograph of a surgically exposed cochlea before EP measurement showing the location of the stapedial artery and the insertion site of the microelectrode. **(B,C)** Representative EP recordings from 1-month-old WT and Cx30 KO mice. The traces showed the voltage (mV) of the scala media as a function of time (s). **(D)** The graph illustrates a significant 23.4% reduction in the EP in 1-month-old Cx30 KO mice (80.1 ± 2.6 mV) compared with age-matched WT mice (104.6 ± 1.9 mV). Data presented as Mean ± SEM ($n = 6$). *t*-test. ***$p < 0.001$. Co, Corti's organ; SGNs, spinal ganglion neurons; SL, spiral ligament; SLm, spiral limbus; SM, scala media; ST, scala tympani; SV, stria vascularis; SVb, scala vestibuli.

of the central nervous system (Wei et al., 2021). *GJB6* and *GJB2* are located on the same chromosome (13q12.11) in the human genome. Due to the relative proximity of these two genes, their expressions might be controlled by the same set of regulatory elements (Wilch et al., 2006). Homozygous deletion mutations of either Cx26 or Cx30 could cause deafness in humans (Kelsell et al., 1997; del Castillo et al., 2002). Cx26 plays a critical role in auditory function and its deficiency leads to significant hearing loss in the animal model (Cohen-Salmon et al., 2002; Chen et al., 2014). Cx26 deficiency in the cochlea could cause pathological changes, including cochlear developmental disorders (Wang et al., 2009; Liang et al., 2012), HCs and SGNs degeneration (Cohen-Salmon et al., 2002; Sun et al., 2009; Wang et al., 2009), EP reduction (Chen et al., 2014), and impairment of active cochlear amplification (Zhu et al., 2013, 2015). HCs and SGNs degeneration was detected around P14 in Cx26-deficient mice (Sun et al., 2009; Wang et al., 2009). However, severe hearing loss precedes substantial hair cell loss after the deletion of Cx26 (Liang et al., 2012). Nevertheless, EP remained normal after targeted deletion of Cx26 expression in Deiters SCs and outer pillar SCs, which are located around OHCs in the cochlear sensory epithelium (Zhu et al., 2013). This indicates that impairment of the cochlear sensory GJ network may not affect EP generation in the inner

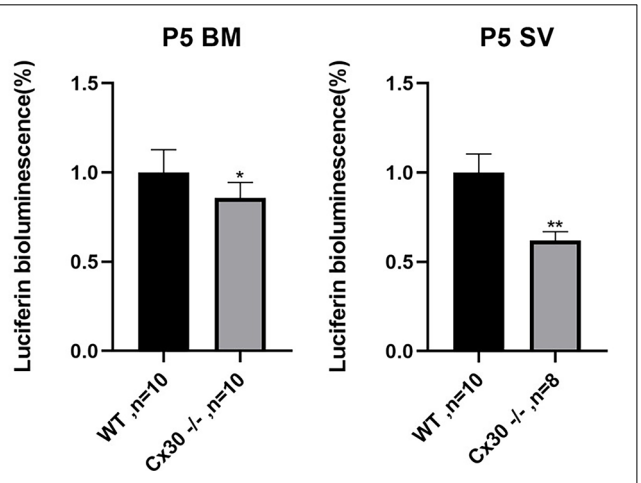

FIGURE 7 | Reduction of ATP release in the cochlea in $Cx30^{-/-}$ mice. ATP release is reduced in $Cx30^{-/-}$ mice in BM and SV at P5. Data presented as Mean ± SEM. *t*-test. $^{*}p < 0.05$, $^{**}p < 0.01$. BM, basemental membrane; SV, stria vascularis.

ear (Zhu et al., 2013; Chen and Zhao, 2014; Chen et al., 2015). However, Cx26 deficiency in the cochlear SCs can affect OHC electromotility and active cochlear amplification, since distortion product otoacoustic emission (DPOAE) was reduced (Yu and Zhao, 2009; Zhu et al., 2013, 2015). On the other hand, the cochlear tunnel opens from P5 (Kraus and Aulbach-Kraus, 1981). Cx26 deficiency before P5 can lead to occlusion of the cochlear tunnel and induce cochlear developmental disorders with congenital deafness (Chen et al., 2014). Nevertheless, cochlear development proceeded normally, the cochlear tunnel opened normally, and hearing remained normal at a young age after deletion of Cx26 after P5 (Chen et al., 2014). These findings suggest that Cx26 expression in the cochlea at the early postnatal development stage is critical for cochlear postnatal development and maturation.

Teubner et al. (2003) found that Cx30 knockout mice display severe hearing loss with the absence of EP. Whether the Cx30 deficiency itself or the accompanying significant decrease of Cx26 (approximately 90%) leads to hearing loss in this model remains unknown. Restoration of Cx26 protein level in the cochlea completely rescues hearing in Cx30 knockout mice, whereas hearing loss in the conditional Cx26 (cCx26) null mice could not be rescued by genetically over-expressing Cx30 (Ahmad et al., 2007; Qu et al., 2012). Cx26 protein expression preceded that of Cx30, and Cx26 is the only and essential GJ protein detected by immunolabeling in the organ of Corti during the early postnatal period (Qu et al., 2012). During the postnatal development, the lack of GJs in the Corti's organ leads to obstacles in intercellular material transport and communication, and failure of Corti's organ to mature, leading to hearing loss. However, the Cx26 expression of BM increased in $Cx30^{-/-}$ mice at the early postnatal period (P5) in the present study.

Boulay et al. (2013) established $Cx30^{fl/fl}$ mice, and found no significant difference in hearing between $Cx30^{fl/fl}$ mice and WT mice, however, Cx26 was decreased to 35% and Cx30 was reduced to 64%. Normal EP and DPOAE were observed in this kind of mice (Boulay et al., 2013). Crossing $Cx30^{fl/fl}$ mice with Pgk-Cre mice generated $Cx30^{\Delta/\Delta}$ mice to delete Cx30, which exhibited no hearing loss, while Cx26 was decreased to 52% (Boulay et al., 2013). The threshold level of Cx26 decline in Cx30-deficient mice that causes hearing loss remains unclear. The $Cx30^{-/-}$ mice established in this study exhibited only mild hearing loss, while cochlear Cx26 decreased to 74%. Since Cx26 did not show any major decrease through Cx30 knockout, the mechanism of hearing loss needs to be further explored.

The high positive potential of EP is critical for animal hearing and develops rapidly in the days before the onset of hearing (P4–P11; Chen et al., 2015). EP (+100–110 mV) is the driving force for the generation of auditory receptor currents and potentials by K^+ ions through transduction channels in the HCs, which are formed by a complex process in the SV of the cochlea. The widely accepted "two-cell" model suggests that EP production begins in the fibroblasts of the spiral ligament. Type II fibroblasts depolarize the cells to ∼5 mV *via* Na^+/K^+ - ATPase and Na^+, K^+, $2Cl^-$ cotransport proteins. The intermediate cells of the SV are subsequently coupled by Cx26 and Cx30 *via* GJs. Thereafter, the ATP-dependent Kir4.1 K^+ channel on the apical membrane of intermediate cells (Ando and Takeuchi, 1999; Liu and Zhao, 2008; Nin et al., 2008) generates a 105–110 mV transmembrane potential (Nernst's K^+ balance potential) between the intracellular space and the intrastriatal space. This positive intrastriatal potential eventually leads to EP positivity in the middle-grade endolymph. The network of two GJs composed of Cx26 and Cx30 forms a pathway through which K^+ ions that pass through sensory cells during mechanosensory transmission can be recirculated into the endolymphatic space such that they re-enter sensory cells (Wangemann, 2002). GJs deficiency may lead to the obstruction of K^+ circulation, thus affecting the formation of EP and hearing. ATP is necessary for EP generation and K^+ recycling (Zhu and Zhao, 2010; Chen et al., 2015). The perfusion of ATP into the cochlea can significantly increase EP (Sueta et al., 2003). As described above, depolarization of fibroblasts by co-activation of Na^+/K^+ - ATPase and Na^+, K^+, $2Cl^-$-cotransporters is the first step in EP production. Although Na^+/K^+ - ATPase is primarily driven by intracellular ATP, extracellular ATP can stimulate Na^+/K^+ - ATPase activity by activating purinergic receptor and Src family kinase (SFK) as well (Shahidullah et al., 2012). In addition, the function of the primary active Na^+/K^+ - ATPase requires K-channel coupling to recycle K^+ (Muto et al., 2003). This "pump coupling" was proposed in 1958, and was subsequently confirmed by experimental data (Koefoed-Johnsen and Ussing, 1958; Dawson and Richards, 1990; Tsuchiya et al., 1992). Recently, it was found that extracellular ATP can also activate ATP-sensitive (KIR) K channels in hippocampal CA3 pyramidal neurons and lung epithelial cells, which cooperate with Na^+/K^+ - ATPase activity. ATP may initially activate the P2X receptor and subsequently activate the KIR potassium channel and Na^+/K^+ - ATPase (Telang et al., 2010; Jiang et al., 2013; Schmid and Evans, 2019).

In this study, we established a novel Cx30 complete knockout mouse model, with a mild full-frequency hearing loss as indicated

by ABR. The protein level of Cx26 was decreased by less than 30% in the cochlea of these mice, which was significantly different from the previous Cx30-deficient mouse model. Moreover, both EP and ATP release showed a decreasing trend in the present mouse model. These results suggest that Cx30 may play an important role in hearing development, however, further investigation on the underlying mechanism is needed in the future.

DATA AVAILABILITY STATEMENT

The original contributions presented in the study are included in the article, further inquiries can be directed to the corresponding author/s.

ETHICS STATEMENT

The animal study was reviewed and approved by the Ethics Committee of Xin Hua Hospital Affiliated to Shanghai Jiao Tong University School of Medicine (XHEC-2021-636).

AUTHOR CONTRIBUTIONS

JC: experimental implementation, data quality control, and wrote the manuscript. PC: immunohistochemical staining and statistical data analysis. BH: western blot and qPCR. TG: qPCR experiments. YL: collection of cochlear samples for TEM experiments. JZ: collection of cochlear samples for H&E experiments. JL: collection of cochlear samples for TEM experiments. FM: EP experiments. SH: research conception and experimental supervision. JY: research conception, manuscript review and revision. All authors contributed to the article and approved the submitted version.

FUNDING

This work was sponsored by grants from the National Natural Science Foundation of China-China Academy of General Technology Joint Fund for Basic Research (81873698, 82000977) and Shanghai Sailing Program (20YF1428900).

REFERENCES

Abeytunge, S., Gianoli, F., Hudspeth, A. J., and Kozlov, A. S. (2021). Rapid mechanical stimulation of inner-ear hair cells by photonic pressure. *eLife* 10:e65930. doi: 10.7554/eLife.65930

Adadey, S. M., Wonkam-Tingang, E., Twumasi Aboagye, E., Nayo-Gyan, D. W., Boatemaa Ansong, M., Quaye, O., et al. (2020). Connexin genes variants associated with non-syndromic hearing impairment: a systematic review of the global burden. *Life (Basel)* 10:258. doi: 10.3390/life10110258

Ahmad, S., Tang, W., Chang, Q., Qu, Y., Hibshman, J., Li, Y., et al. (2007). Restoration of connexin26 protein level in the cochlea completely rescues hearing in a mouse model of human connexin30-linked deafness. *Proc. Natl. Acad. Sci. U S A* 104, 1337–1341. doi: 10.1073/pnas.0606855104

Ando, M., and Takeuchi, S. (1999). Immunological identification of an inward rectifier K+ channel (Kir4. 1) in the intermediate cell (melanocyte) of the cochlear stria vascularis of gerbils and rats. *Cell Tissue Res.* 298, 179–183. doi: 10.1007/s004419900066

Bliznetz, E. A., Lalayants, M. R., Markova, T. G., Balanovsky, O. P., Balanovska, E. V., Skhalyakho, R. A., et al. (2017). Update of the GJB2/DFNB1 mutation spectrum in Russia: a founder Ingush mutation del(GJB2–D13S175) is the most frequent among other large deletions. *J. Hum. Genet.* 62, 789–795. doi: 10.1038/jhg.2017.42

Boulay, A. C., del Castillo, F. J., Giraudet, F., Hamard, G., Giaume, C., Petit, C., et al. (2013). Hearing is normal without connexin30. *J. Neurosci.* 33, 430–434. doi: 10.1523/JNEUROSCI.4240-12.2013

Breglio, A. M., May, L. A., Barzik, M., Welsh, N. C., Francis, S. P., Costain, T. Q., et al. (2020). Exosomes mediate sensory hair cell protection in the inner ear. *J. Clin. Invest.* 130, 2657–2672. doi: 10.1172/JCI128867

Bruzzone, R., White, T. W., and Paul, D. L. (1996). Connections with connexins: the molecular basis of direct intercellular signaling. *Eur. J. Biochem.* 238, 1–27. doi: 10.1111/j.1432-1033.1996.0001q.x

Chen, J., Chen, J., Zhu, Y., Liang, C., and Zhao, H. B. (2014). Deafness induced by Connexin 26 (GJB2) deficiency is not determined by endocochlear potential (EP) reduction but is associated with cochlear developmental disorders. *Biochem. Biophys. Res. Commun.* 448, 28–32. doi: 10.1016/j.bbrc.2014.04.016

Chen, S., Xu, K., Xie, L., Cao, H.-Y., Wu, X., Du, A.-N., et al. (2018). The spatial distribution pattern of Connexin26 expression in supporting cells and its role in outer hair cell survival. *Cell Death Dis.* 9:1180. doi: 10.1038/s41419-018-1238-x

Chen, J., and Zhao, H. B. (2014). The role of an inwardly rectifying K(+) channel (Kir4.1) in the inner ear and hearing loss. *Neuroscience* 265, 137–146. doi: 10.1016/j.neuroscience.2014.01.036

Chen, J., Zhu, Y., Liang, C., Chen, J., and Zhao, H.-B. (2015). Pannexin1 channels dominate ATP release in the cochlea ensuring endocochlear potential and auditory receptor potential generation and hearing. *Sci. Rep.* 5:10762. doi: 10.1038/srep10762S

Cohen-Salmon, M., Ott, T., Michel, V., Hardelin, J. P., Perfettini, I., Eybalin, M., et al. (2002). Targeted ablation of connexin26 in the inner ear epithelial gap junction network causes hearing impairment and cell death. *Curr. Biol.* 12, 1106–1111. doi: 10.1016/s0960-9822(02)00904-1

Dawson, D. C., and Richards, N. W. (1990). Basolateral K conductance: role in regulation of NaCl absorption and secretion. *Am. J. Physiol.* 259, C181–C195. doi: 10.1152/ajpcell.1990.259.2.C181

del Castillo, I., Villamar, M., Moreno-Pelayo, M. A., del Castillo, F. J., Alvarez, A., Telleria, D., et al. (2002). A deletion involving the connexin 30 gene in nonsyndromic hearing impairment. *N. Engl. J. Med.* 346, 243–249. doi: 10.1056/NEJMoa012052

Denoyelle, F., Weil, D., Maw, M. A., Wilcox, S. A., Lench, N. J., Allen-Powell, D. R., et al. (1997). Prelingual deafness: high prevalence of a 30delG mutation in the connexin 26 gene. *Hum. Mol. Genet.* 6, 2173–2177. doi: 10.1093/hmg/6.12.2173

Estivill, X., Fortina, P., Surrey, S., Rabionet, R., Melchionda, S., D'Agruma, L., et al. (1998). Connexin-26 mutations in sporadic and inherited sensorineural deafness. *Lancet* 351, 394–398. doi: 10.1016/S0140-6736(97)11124-2

Feldmann, D., Le Marechal, C., Jonard, L., Thierry, P., Czajka, C., Couderc, R., et al. (2009). A new large deletion in the DFNB1 locus causes nonsyndromic hearing loss. *Eur. J. Med. Genet.* 52, 195–200. doi: 10.1016/j.ejmg.2008.11.006

Fu, X., An, Y., Wang, H., Li, P., Lin, J., Yuan, J., et al. (2021). Deficiency of Klc2 induces low-frequency sensorineural hearing loss in C57BL/6 J mice and human. *Mol. Neurobiol.* 58, 4376–4391. doi: 10.1007/s12035-021-02422-w

Guo, L., Cao, W., Niu, Y., He, S., Chai, R., and Yang, J. (2021). Autophagy regulates the survival of hair cells and spiral ganglion neurons in cases of noise, ototoxic drug and age-induced sensorineural hearing loss. *Front. Cell. Neurosci.* 15:760422. doi: 10.3389/fncel.2021.760422

He, Z., Guo, L., Shu, Y., Fang, Q., Zhou, H., Liu, Y., et al. (2017). Autophagy protects auditory hair cells against neomycin-induced damage. *Autophagy* 13, 1884–1904. doi: 10.1080/15548627.2017.1359449

Jagger, D. J., and Forge, A. (2015). Connexins and gap junctions in the inner ear-it's not just about K+ recycling. *Cell Tissue Res.* 360, 633–644. doi: 10.1007/s00441-014-2029-z

Jiang, R., Taly, A., and Grutter, T. (2013). Moving through the gate in ATP-activated P2X receptors. *Trends Biochem. Sci.* 38, 20–29. doi: 10.1016/j.tibs.2012.10.006

Johnson, S.L., Ceriani, F., Houston, O., Polishchuk, R., Polishchuk, E., Crispino, G., et al. (2017). Connexin-mediated signaling in nonsensory cells is crucial for the development of sensory inner hair cells in the mouse cochlea. *J. Neurosci.* 37, 258–268. doi: 10.1523/jneurosci.2251-16.2016

Kelsell, D. P., Dunlop, J., Stevens, H. P., Lench, N. J., Liang, J., Parry, G., et al. (1997). Connexin 26 mutations in hereditary non-syndromic sensorineural deafness. *Nature* 387, 80–83. doi: 10.1038/387080a0

Kikuchi, T., Kimura, R.S., Paul, D.L., and Adams, J.C. (1995). Gap junctions in the rat cochlea: immunsohistochemical and ultrastructural analysis. *Anat. Embryol. (Berl)* 191, 101–118. doi: 10.1007/BF00186783

Koefoed-Johnsen, V., and Ussing, H. H. (1958). The nature of the frog skin potential. *Acta Physiol. Scand.* 42, 298–308. doi: 10.1111/j.1748-1716.1958.tb01563.x

Kraus, H. J., and Aulbach-Kraus, K. (1981). Morphological changes in the cochlea of the mouse after the onset of hearing. *Hear. Res.* 4, 89–102. doi: 10.1016/0378-5955(81)90038-1

Liang, C., Zhu, Y., Zong, L., Lu, G. J., and Zhao, H. B. (2012). Cell degeneration is not a primary causer for Connexin26 (GJB2) deficiency associated hearing loss. *Neurosci. Lett.* 528, 36–41. doi: 10.1016/j.neulet.2012.08.085

Liu, Y.-P., and Zhao, H.-B. (2008). Cellular characterization of Connexin26 and Connnexin30 expression in the cochlear lateral wall. *Cell Tissue Res.* 333, 395–403. doi: 10.1007/s00441-008-0641-5

Mammano, F. (2019). Inner ear connexin channels: roles in development and maintenance of cochlear function. *Cold Spring Harb. Perspect. Med.* 9:a033233. doi: 10.1101/cshperspect.a033233

Mammano, F., and Bortolozzi, M. (2018). $Ca^{(2+)}$ signaling, apoptosis and autophagy in the developing cochlea: milestones to hearing acquisition. *Cell Calcium* 70, 117–126. doi: 10.1016/j.ceca.2017.05.006

Mazzarda, F., D'Elia, A., Massari, R., De Ninno, A., Bertani, F.R., and Businaro, L. (2020). Organ-on-chip model shows that ATP release through connexin hemichannels drives spontaneous $Ca^{(2+)}$ signaling in non-sensory cells of the greater epithelial ridge in the developing cochlea. *Lab Chip.* 20, 3011–3023. doi: 10.10.1039/d0lc00427h

Mei, L., Chen, J., Zong, L., Zhu, Y., Liang, C., Jones, R. O., et al. (2017). A deafness mechanism of digenic Cx26 (GJB2) and Cx30 (GJB6) mutations: reduction of endocochlear potential by impairment of heterogeneous gap junctional function in the cochlear lateral wall. *Neurobiol. Dis.* 108, 195–203. doi: 10.1016/j.nbd.2017.08.002

Mishra, S., Pandey, H., Srivastava, P., Mandal, K., and Phadke, S. R. (2018). Connexin 26 (GJB2) mutations associated with non-syndromic hearing loss (NSHL). *Indian J. Pediatr.* 85, 1061–1066. doi: 10.1007/s12098-018-2654-8

Muto, S., Asano, Y., Wang, W., Seldin, D., and Giebisch, G. (2003). Activity of the basolateral K+ channels is coupled to the Na+-K+-ATPase in the cortical collecting duct. *Am. J. Physiol. Renal. Physiol.* 285, F945–F954. doi: 10.1152/ajprenal.00081.2003

Nin, F., Hibino, H., Doi, K., Suzuki, T., Hisa, Y., and Kurachi, Y. (2008). The endocochlear potential depends on two K+ diffusion potentials and an electrical barrier in the stria vascularis of the inner ear. *Proc. Natl. Acad. Sci. U S A* 105, 1751–1756. doi: 10.1073/pnas.0711463105

Pandya, A., Arnos, K. S., Xia, X. J., Welch, K. O., Blanton, S. H., Friedman, T. B., et al. (2003). Frequency and distribution of GJB2 (connexin 26) and GJB6 (connexin 30) mutations in a large North American repository of deaf probands. *Genet. Med.* 5, 295–303. doi: 10.1097/01.GIM.0000078026.01140.68

Pandya, A., O'Brien, A., Kovasala, M., Bademci, G., Tekin, M., and Arnos, K. S. (2020). Analyses of del(GJB6–D13S1830) and del(GJB6–D13S1834) deletions in a large cohort with hearing loss: caveats to interpretation of molecular test results in multiplex families. *Mol. Genet. Genomic. Med.* 8:e1171. doi: 10.1002/mgg3.1171

Qu, Y., Tang, W., Zhou, B., Ahmad, S., Chang, Q., Li, X., et al. (2012). Early developmental expression of connexin26 in the cochlea contributes to its dominate functional role in the cochlear gap junctions. *Biochem. Biophys. Res. Commun.* 417, 245–250. doi: 10.1016/j.bbrc.2011.11.093

Rodriguez-Paris, J., and Schrijver, I. (2009). The digenic hypothesis unraveled: the GJB6 del(GJB6–D13S1830) mutation causes allele-specific loss of GJB2 expression in cis. *Biochem. Biophys. Res. Commun.* 389, 354–359. doi: 10.1016/j.bbrc.2009.08.152

Schmid, R., and Evans, R. J. (2019). ATP-gated P2X receptor channels: molecular insights into functional roles. *Annu. Rev. Physiol.* 81, 43–62. doi: 10.1146/annurev-physiol-020518-114259

Shahidullah, M., Mandal, A., Beimgraben, C., and Delamere, N. (2012). Hyposmotic stress causes ATP release and stimulates Na, K-ATPase activity in porcine lens. *J. Cell. Physiol.* 227, 1428–1437. doi: 10.1002/jcp.22858

Snoeckx, R. L., Huygen, P. L., Feldmann, D., Marlin, S., Denoyelle, F., Waligora, J., et al. (2005). GJB2 mutations and degree of hearing loss: a multicenter study. *Am. J. Hum. Genet.* 77, 945–957. doi: 10.1086/497996

Sueta, T., Paki, B., Everett, A., and Robertson, D. (2003). Purinergic receptors in auditory neurotransmission. *Hear. Res.* 183, 97–108. doi: 10.1016/s0378-5955(03)00221-1

Sun, Y., Tang, W., Chang, Q., Wang, Y., Kong, W., and Lin, X. (2009). Connexin30 null and conditional connexin26 null mice display distinct pattern and time course of cellular degeneration in the cochlea. *J. Comp. Neurol.* 516, 569–579. doi: 10.1002/cne.22117

Tayoun, A. N., Mason-Suares, H., Frisella, A. L., Bowser, M., Duffy, E., Mahanta, L., et al. (2016). Targeted droplet-digital PCR as a tool for novel deletion discovery at the DFNB1 locus. *Hum. Mutat.* 37, 119–126. doi: 10.1002/humu.22912

Telang, R. S., Paramananthasivam, V., Vlajkovic, S. M., Munoz, D. J., Housley, G. D., and Thorne, P. R. (2010). Reduced P2x 2 receptor-mediated regulation of endocochlear potential in the ageing mouse cochlea. *Purinergic Signal.* 6, 263–272. doi: 10.1007/s11302-010-9195-6

Teubner, B., Michel, V., Pesch, J., Lautermann, J., Cohen-Salmon, M., Sohl, G., et al. (2003). Connexin30 (Gjb6)-deficiency causes severe hearing impairment and lack of endocochlear potential. *Hum. Mol. Genet.* 12, 13–21. doi: 10.1093/hmg/ddg001

Tsuchiya, K., Wang, W., Giebisch, G., and Welling, P. (1992). ATP is a coupling modulator of parallel Na, K-ATPase-K-channel activity in the renal proximal tubule. *Proc. Natl. Acad. Sci. U S A* 89, 6418–6422. doi: 10.1073/pnas.89.14.6418

Verselis, V. K. (2019). Connexin hemichannels and cochlear function. *Neurosci. Lett.* 695, 40–45. doi: 10.1016/j.neulet.2017.09.020

Wang, Y., Chang, Q., Tang, W., Sun, Y., Zhou, B., Li, H., et al. (2009). Targeted connexin26 ablation arrests postnatal development of the organ of corti. *Biochem. Biophys. Res. Commun.* 385, 33–37. doi: 10.1016/j.bbrc.2009.05.023

Wangemann, P. (2002). K+ cycling and its regulation in the cochlea and the vestibular labyrinth. *Audiol. Neurotol.* 7, 199–205. doi: 10.1159/000063736

Wei, H., Chen, Z., Hu, Y., Cao, W., Ma, X., Zhang, C., et al. (2021). Topographically conductive butterfly wing substrates for directed spiral ganglion neuron growth. *Small* 17:e2102062. doi: 10.1002/smll.202102062

Wilch, E., Azaiez, H., Fisher, R. A., Elfenbein, J., Murgia, A., Birkenhager, R., et al. (2010). A novel DFNB1 deletion allele supports the existence of a distant cis-regulatory region that controls GJB2 and GJB6 expression. *Clin. Genet.* 78, 267–274. doi: 10.1111/j.1399-0004.2010.01387.x

Wilch, E., Zhu, M., Burkhart, K. B., Regier, M., Elfenbein, J. L., Fisher, R. A., et al. (2006). Expression of GJB2 and GJB6 is reduced in a novel DFNB1 allele. *Am. J. Hum. Gen.* 79, 174–179. doi: 10.1086/505333

Yu, N., and Zhao, H. B. (2009). Modulation of outer hair cell electromotility by cochlear supporting cells and gap junctions. *PLoS One* 4:e7923. doi: 10.1371/journal.pone.0007923

Zhang, Y., Li, Y., Fu, X., Wang, P., Wang, Q., Meng, W., et al. (2021). The detrimental and beneficial functions of macrophages after cochlear injury. *Front. Cell Dev. Biol.* 9:631904. doi: 10.3389/fcell.2021.631904

Zhang, S., Qiang, R., Dong, Y., Zhang, Y., Chen, Y., Zhou, H., et al. (2020a). Hair cell regeneration from inner ear progenitors in the mammalian cochlea. *Am. J. Stem Cells* 9, 25–35.

Zhang, S., Zhang, Y., Dong, Y., Guo, L., Zhang, Z., Shao, B., et al. (2020b). Knockdown of foxg1 in supporting cells increases the trans-differentiation of supporting cells into hair cells in the neonatal mouse cochlea. *Cell. Mol. Life Sci.* 77, 1401–1419. doi: 10.1007/s00018-019-03291-2

Zhang, Y., Zhang, S., Zhang, Z., Dong, Y., Ma, X., Qiang, R., et al. (2020). Knockdown of Foxg1 in Sox9+ supporting cells increases the trans-differentiation of supporting cells into hair cells in the neonatal mouse utricle. *Aging (Albany NY)* 12, 19834–19851. doi: 10.18632/aging.104009

Zhu, Y., Chen, J., Liang, C., Zong, L., Chen, J., Jones, R. O., et al. (2015). Connexin26 (GJB2) deficiency reduces active cochlear amplification leading to late-onset hearing loss. *Neuroscience* 284, 719–729. doi: 10.1016/j.neuroscience.2014.10.061

Zhu, Y., Liang, C., Chen, J., Zong, L., Chen, G. D., and Zhao, H. B. (2013). Active cochlear amplification is dependent on supporting cell gap junctions. *Nat. Commun.* 4:1786. doi: 10.1038/ncomms2806

Zhu, Y., and Zhao, H.-B. (2010). ATP-mediated potassium recycling in the cochlear supporting cells. *Purinergic Signal.* 6, 221–229. doi: 10.1007/s11302-010-9184-9

Conflict of Interest: The authors declare that the research was conducted in the absence of any commercial or financial relationships that could be construed as a potential conflict of interest.

Publisher's Note: All claims expressed in this article are solely those of the authors and do not necessarily represent those of their affiliated organizations, or those of the publisher, the editors and the reviewers. Any product that may be evaluated in this article, or claim that may be made by its manufacturer, is not guaranteed or endorsed by the publisher.

frontiers in Cellular Neuroscience

ORIGINAL RESEARCH
published: 28 January 2022
doi: 10.3389/fncel.2021.753369

Autophagy Contributes to the Rapamycin-Induced Improvement of Otitis Media

Daoli Xie[1†], Tong Zhao[1†], Xiaolin Zhang[2†], Lihong Kui[1], Qin Wang[1], Yuancheng Wu[1], Tihua Zheng[1], Peng Ma[3], Yan Zhang[4], Helen Molteni[5], Ruishuang Geng[1], Ying Yang[1], Bo Li[1]* and Qing Yin Zheng[5]*

[1] Hearing and Speech Rehabilitation Institute, College of Special Education, Binzhou Medical University, Yantai, China, [2] Department of Otolaryngology-Head and Neck Surgery, Binzhou Medical University Hospital, Binzhou, China, [3] Department of Genetics, School of Pharmacy, Binzhou Medical University, Yantai, China, [4] Department of Otolaryngology, Head and Neck Surgery, Second Affiliated Hospital, Xi'an Jiaotong University School of Medicine, Xi'an, China, [5] Department of Otolaryngology, Head and Neck Surgery, Case Western Reserve University, Cleveland, OH, United States

OPEN ACCESS

Edited by:
Wei-Jia Kong, Huazhong University of Science and Technology, China

Reviewed by:
A. Raquel Esteves, University of Coimbra, Portugal
Mark J. Ranek, Johns Hopkins University, United States

***Correspondence:**
Bo Li
liboyjt@163.com
Ying Yang
yang_yingzi@163.com

† These authors have contributed equally to this work and share first authorship

Specialty section:
This article was submitted to Cellular Neuropathology, a section of the journal Frontiers in Cellular Neuroscience

Received: *04 August 2021*
Accepted: *31 December 2021*
Published: *28 January 2022*

Citation:
Xie D, Zhao T, Zhang X, Kui L, Wang Q, Wu Y, Zheng T, Ma P, Zhang Y, Molteni H, Geng R, Yang Y, Li B and Zheng QY (2022) Autophagy Contributes to the Rapamycin-Induced Improvement of Otitis Media. Front. Cell. Neurosci. 15:753369. doi: 10.3389/fncel.2021.753369

Otitis media (OM) is a pervasive disease that involves hearing loss and severe complications. In our previous study, we successfully established a mouse model of human OM using *Tlr2tm1Kir* (TLR2$^{-/-}$) mice with middle ear (ME) inoculation of streptococcal peptidoglycan-polysaccharide (PGPS). In this study, we found that hearing loss and OM infections in OM mice were significantly alleviated after treatment with rapamycin (RPM), a widely used mechanistic target of RPM complex 1 (mTORC1) inhibitor and autophagy inducer. First of all, we tested the activity of mTORC1 by evaluating p-S6, Raptor, and mTOR protein expression. The data suggested that the protein expression level of p-S6, Raptor and mTOR are decreased in TLR2$^{-/-}$ mice after the injection of PGPS. Furthermore, our data showed that both the autophagosome protein LC3-II, Beclin-1, ATG7, and autophagy substrate protein p62 accumulated at higher levels in mice with OM than in OM-negative mice. The expression of lysosomal-associated proteins LAMP1, Cathepsin B, and Cathepsin D increased in the OM mice compared with OM-negative mice. Rab7 and Syntaxin 17, which is necessary for the fusion of autophagosomes with lysosomes, are reduced in the OM mice. In addition, data also described that the protein expression level of p-S6, mTOR and Raptor are lower than PGPS group after RPM treatment. The accumulation of LC3-II, Beclin-1, and ATG7 are decreased, and the expression of Rab7 and Syntaxin 17 are increased significantly after RPM treatment. Our results suggest that autophagy impairment is involved in PGPS-induced OM and that RPM improves OM at least partly by relieving autophagy impairment. Modulating autophagic activity by RPM may be a possible effective treatment strategy for OM.

Keywords: otitis media, TLR2, autophagy, PGPS, rapamycin

INTRODUCTION

OM (otitis media), one of the most common childhood infections (Rovers et al., 2004; Monasta et al., 2012), is associated with the potential burden of hearing loss and leads to excessive antibiotic consumption and severe complications (Vergison et al., 2010). The pathogenesis of OM is associated with many factors, including immune system dysfunction, genetic susceptibility,

pathogen exposure, and middle ear (ME) damage (Rovers et al., 2004). ME is part of a functional system composed of the nasopharynx and eustachian tube anteriorly and the mastoid air cells posteriorly (Bluestone and Doyle, 1988). The tympanic membrane serves as the boundary between the ME and the outer ear. OM is a common inflammatory response in diseases of the auditory system (Harmes et al., 2013). Toll receptors (TLR) play a role in the innate immune response in mammals and TLR2 recognizes components from a variety of microbial pathogens (Takeda and Akira, 2015). Previously, we successfully established a mouse model of OM using *Tlr2tm1Kir* (TLR2$^{-/-}$) mice. TLR2$^{-/-}$ mice were inoculated with streptococcal peptidoglycan-polysaccharide (PGPS) into their ME by tympanic membrane puncture (Zhang et al., 2015). Our results demonstrated that compared with wild-type (WT) C57BL/6J mice, TLR2$^{-/-}$ mice inoculated with PGPS exhibited severe and long-lasting inflammation and tissue damage.

Recently, autophagy was found to be involved in immunological and inflammatory diseases. Autophagy provides a source of peptides for antigen presentation and is involved in the engulfment and degradation of intracellular pathogens, and it is also a key regulator of inflammatory cytokines (Harris et al., 2017). Autophagy plays an important role in inflammasome activation and in the release of interleukin-1 (IL-1) family cytokines, which are an essential part of innate and adaptive immune responses (Garlanda et al., 2013). Autophagy is a lysosome-dependent intracellular degradation pathway unique to eukaryotes. It is considered to have several stages: autophagy induction, autophagosome formation, the fusion of autophagosomes and lysosomes and substrate degradation (Mizushima, 2007; Glick et al., 2010). The lipidated form of microtubule-associated protein 1A/1B-light chain 3 (LC3), LC3-II, and the accumulation of the cargo receptor of autophagosomes, sequestosome 1 (SQSTM1/p62), have been used as markers for active autophagy (Tanida et al., 2004; Sou et al., 2006). In recent years, researchers have discovered that the expression of mRNA associated with autophagy, like *LC3-II* and *Beclin-1* in the ME fluid samples of patients with OM increased (Jung et al., 2020a,b), but the mechanism of autophagy involved in OM has not been clarified. Therefore, our experiment would like to verify whether autophagy is involved in OM and explore the role of autophagy in OM.

Rapamycin (RPM), an autophagy inducer, activates autophagy by repressing the mechanistic target of RPM complex 1 (mTORC1) (Sekiguchi et al., 2012). It has been used in some clinical trials, such as allograft rejection, cancer and lymphangioleiomyomatosis (Bissler et al., 2008; Li et al., 2014; Franz et al., 2016; Koenig et al., 2018; Mandrioli et al., 2018). Topical RPM appears effective and safe for treatment of tuberous sclerosis complex -related facial angiofibromas. To date, RPM has been also shown to be effective in a variety of inflammatory diseases in animal model. It relieved inflammation in experimental autoimmune encephalomyelitis in a mouse model (Li et al., 2019a,b). It also suppressed airway inflammation and inflammatory molecules in retinal inflammation (Okamoto et al., 2016; Joean et al., 2017). In addition, it was shown to protect cartilage endplates from chronic inflammation-induced degeneration (Zuo et al., 2019). However, previous studies have not determined whether RPM treatment has an otoprotective effect in OM. We speculate that autophagy may be involved in the process of OM, and RPM may have a protective effect on OM. Therefore, we also want to find out whether RPM could relieves the OM caused by PGPS and identify the possible mechanism of this process.

We have confirmed that the ME inflammation of TLR2$^{-/-}$ mice injected with PGPS was more severe than that of WT mice through the electric otoscope image and the hematoxylin-eosin (H&E) staining firstly (**Supplementary Figures 1A,B**). In addition, we found that the protein expressions of LC3-II and p62 were increased obviously from the ME tissues injected by PGPS in TLR2$^{-/-}$ mice but not in WT mice, which suggested that the autophagy impairment may be involved in PGPS-induced OM in TLR2$^{-/-}$ mice (**Supplementary Figure 1C**). PGPS induces relatively stable OM in TLR2$^{-/-}$ mice, which provides a longer time window for drug screening and studying mechanisms of prevention and treatment. Based on the above reasons, we chose TLR2$^{-/-}$ mice as our OM model. In this study, TLR2$^{-/-}$ mice with PGPS-induced OM are called "OM mice."

In this study, we observed the therapeutic effect of RPM against PGPS-induced OM and investigated the role of autophagy in this process. Our results suggested that RPM alleviates hearing loss and inflammation in the OM mice and that normal autophagy contributes to this process. We hope that our study will help improve the clinical treatment of OM.

MATERIALS AND METHODS

Animals

Both male and female *Tlr2tm1Kir* (TLR2$^{-/-}$) mice and WT mice aged 6–8 weeks were obtained from the Jackson Laboratory (Bar Harbor, ME, United States) and housed in a pathogen-free facility. The experimental protocol was approved by the Animal Use and Care Committee of Binzhou Medical University.

Drug Treatment

Mice were treated with normal saline (NS), PGPS, NS + DMSO, or PGPS + rapamycin (RPM). Individual mice were intraperitoneally anesthetized with 4% chloral hydrate (0.01 ml/g; Biotopped Life Sciences, Beijing, China). All the mice received treatment in their right ears. The mice in the NS group received intratympanic (IT) injections of 10 μl of saline. The mice in the PGPS group received IT injections of 60 μg PGPS (100P, BD Bioscience, San Jose, CA, United States) freshly prepared in 10 μl of NS as described previously (Zhang et al., 2015). Purified (purity 99%) PGPS was extracted from the *Streptococcus pneumoniae* cell wall (Fulghum and Brown, 1998; Komori et al., 2011). RPM (Selleck, S1039, Shanghai, China) for IT injections was dissolved in 100% dimethyl sulfoxide (DMSO) to make 22 mM stock solutions and diluted with a PGPS solution immediately before injection for a final dose of either 0.35 or 0.7 μM in a 10 μl PGPS solution. 0.7 μM RPM and 0.35 μM

are obtained from 22 mM stock solutions diluted with PBS. The mice in the vehicle group received IT injections of equal volumes of DMSO or NS. The mouse tympanic membranes were examined on day 3 post-injection using an otoscopic digital imaging system (MedRx VetScope System, Largo, FL, United States).

Auditory Brainstem Response and Tympanometry Procedure

The Auditory brainstem response (ABR) and tympanometry of individual experimental mice were assessed on day 3 post-injection. A computer-aided evoked potential system (IHS3.30 Intelligent Hearing Systems, Miami, FL, United States) was used for ABR measurements as described previously (Hu et al., 2016). Briefly, click, 8, 16, and 32 kHz tone burst frequencies were channeled through an earphone inserted into the right ear. The ABR threshold was identified as the lowest stimulus level at which clear and repeatable waveforms were recognized. Tympanometry measurements were performed using an MT 10 tympanometer (Interacoustics, Assens, Denmark).

Histological Analysis of the Middle Ear

The experimental mice were sacrificed on day 3 post-injection, and their right auditory bullae (including both the middle and inner ear) were dissected and subjected to pathological examination as described previously (Zhang et al., 2015). The bullae tissues were fixed with 4% paraformaldehyde for 24 h at 4°C, decalcified with a 10% EDTA solution for 5 days, and embedded in paraffin. The paraffin sections were stained with H&E and examined under a light microscope (Leica DMI4000 B, Germany).

Immunohistochemistry

The right bullae from experimental mice were fixed in 4% paraformaldehyde and decalcified before they were embedded in paraffin. The bullae tissues were sectioned at 5–7 μm. After deparaffinization, rehydration, and antigen retrieval, the sections were immunohistochemically stained with an anti-p62 antibody (Abcam, ab56416, Cambridge, England, United Kingdom), anti-Beclin-1 antibody (Abcam, ab210498), anti-ATG7 antibody (Proteintech, 10088-2-AP), anti-Cathepsin B Rabbit Polyclonal Antibody (Proteintech, 12216-1-AP), anti-Cathepsin D antibody (Proteintech, 21327-1-AP), anti-Rab7 antibody (Abcam, ab137029), anti-p-S6 antibody (Ser235/236) (Cell Signaling Technology, #4858), anti-mTOR antibody (Proteintech, 20657-1-AP), and anti-Raptor antibody (Affinity, #DF7527). The sample slides were observed under a light microscope and imaged by LAS X software (Leica DM4500 B, Leica Microsystems Inc., Buffalo Grove, IL, United States).

Immunofluorescence

After deparaffinization, rehydration, and antigen retrieval, the sections were stained with an anti-LC3B antibody (Novus Biologicals, NB100-2220, Co., United States), anti-TNF-α antibody (Proteintech, 17590-1-AP), anti-LAMP1 antibody (Abcam, ab24170), anti-Syntaxin 17 antibody (Proteintech, 17815-1-AP) and DAPI (Invitrogen, Carlsbad, United States). The stained tissues were imaged using a confocal microscope (LSM 880, Zeiss, Oberkochen, Germany).

Terminal Deoxynucleotidyl Transferase-Mediated dUTP-Biotin Nick End Labeling Staining

Paraffin sections from bullae tissues obtained from the mice were stained using a TUNEL Kit (*In Situ* Cell Death Detection Kit, Fluorescein, 11684795910; Roche Diagnostics) and following the manufacturer's protocol. The samples were then viewed under a fluorescence microscope (Leica DM4500 B, Leica Microsystems Inc., Buffalo Grove, IL, United States).

Statistical Analysis

Each experiment was repeated at least three times. All the data are presented as the mean ± SEM. Data analyses were conducted using Microsoft Excel and GraphPad Prism 9 software (GraphPad, San Diego, CA, United States). Unpaired Student's *t*-tests were used to determine the statistical significance when comparing two groups, and one-way ANOVA was used when comparing more than two groups. The value of $P < 0.05$ was considered statistically significant.

RESULTS

PGPS Induces Severe Otitis Media

TLR2$^{-/-}$ mice were inoculated with 10 μl of 60 μg PGPS or NS solution. Images of the mouse ears under an otoscope showed that hyperemia and hydrotympanum (white arrowhead) were present in the ears of the PGPS group (**Figure 1A**). Histological examination revealed excessive inflammatory infiltrations in the tympanic cavity and severe tissue damage in the PGPS group compared with the NS group (**Figure 1B**). The inflammatory areas in the ME of PGPS-treated mice were significantly larger than those of NS-treated mice (**Figure 1D**). Tumor Necrosis Factor α (TNF-α), an inflammatory cytokine, is responsible for a diverse range of signaling events within cells, leading to necrosis or apoptosis (Idriss and Naismith, 2000). The immunofluorescence staining revealed that expression levels of TNF-α increased in the PGPS group (**Figures 1C,E**). Taken together, these data confirmed that PGPS induced severe inflammation in the mouse ME.

Next, we investigated the hearing function of the OM mice. The average ABR thresholds and tympanometry values were measured after inoculation. Representative images of ABR waveforms for click stimuli are shown in **Figure 1F**. The mean ABR thresholds in the PGPS group were significantly higher than those in the NS solution group at click, 8 kHz and 32 kHz stimulus frequencies (**Figure 1G**). The latency of ABR wave I at click stimuli (80 dB SPL) increased in PGPS-injected mice compared with NS-injected mice (**Figure 1H**). There were significant differences in tympanometry value, compliance, and pressure between the NS and PGPS groups (**Figure 1I**).

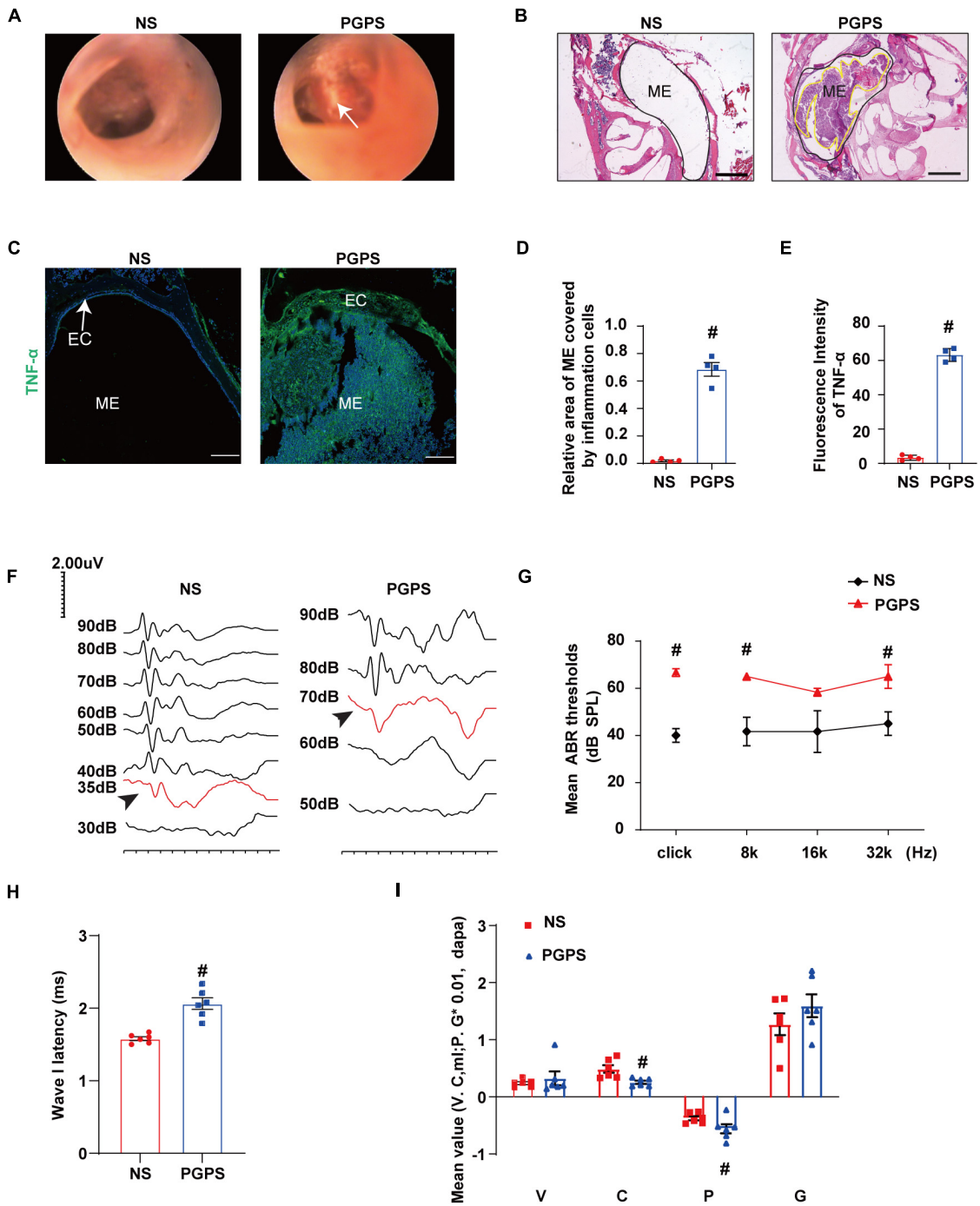

FIGURE 1 | Inoculation with PGPS induces ME inflammation and hearing loss. **(A)** Otoscopic images of ears from the NS and PGPS groups are shown. Hyperemia and hydrotympanum (white arrow) were detected in PGPS group. **(B)** H&E histology showing the structures and pathology of the ME. **(C)** Mice were inoculated with NS or PGPS for 3 days. Representative immunostaining for TNF-α expression in ME. **(D)** Quantification of the relative area of ME covered by inflammatory cells is shown in the bar graph. $n = 4$ per group **(E)** Quantification of the fluorescence intensity of TNF-α is shown in the bar graph. $n = 4$ per group **(F)** Representative images of ABR waveforms at click stimuli are shown. The red lines and arrowheads represent threshold waveforms. **(G)** Mice were inoculated with PGPS for 3 days, and the ABR thresholds were measured at the stimuli frequencies of click, 8 kHz, 16 kHz, and 32 kHz. The mean ABR thresholds in PGPS-injected mice were compared with those in NS-injected mice. The data is presented as the mean ± SEM. $n = 10$ per group **(H)** The latency of ABR wave I at click stimuli (80 dB SPL) in PGPS-injected mice compared with that in NS-injected mice is shown. Horizontal bars are mean values. $n = 10$ per group. **(I)** The tympanometry values in PGPS-injected mice compared with those in NS-injected mice are shown. The data are presented as the mean ± SEM. $n = 10$ per group. V represents the mean value of volume, C represents compliance in tympanometry parameters, G represents the gradient, and P represents the pressure. $^{\#}P < 0.05$ vs. NS group, Student's *t*-test. Scales bar, 100 μm **(B,C)**.

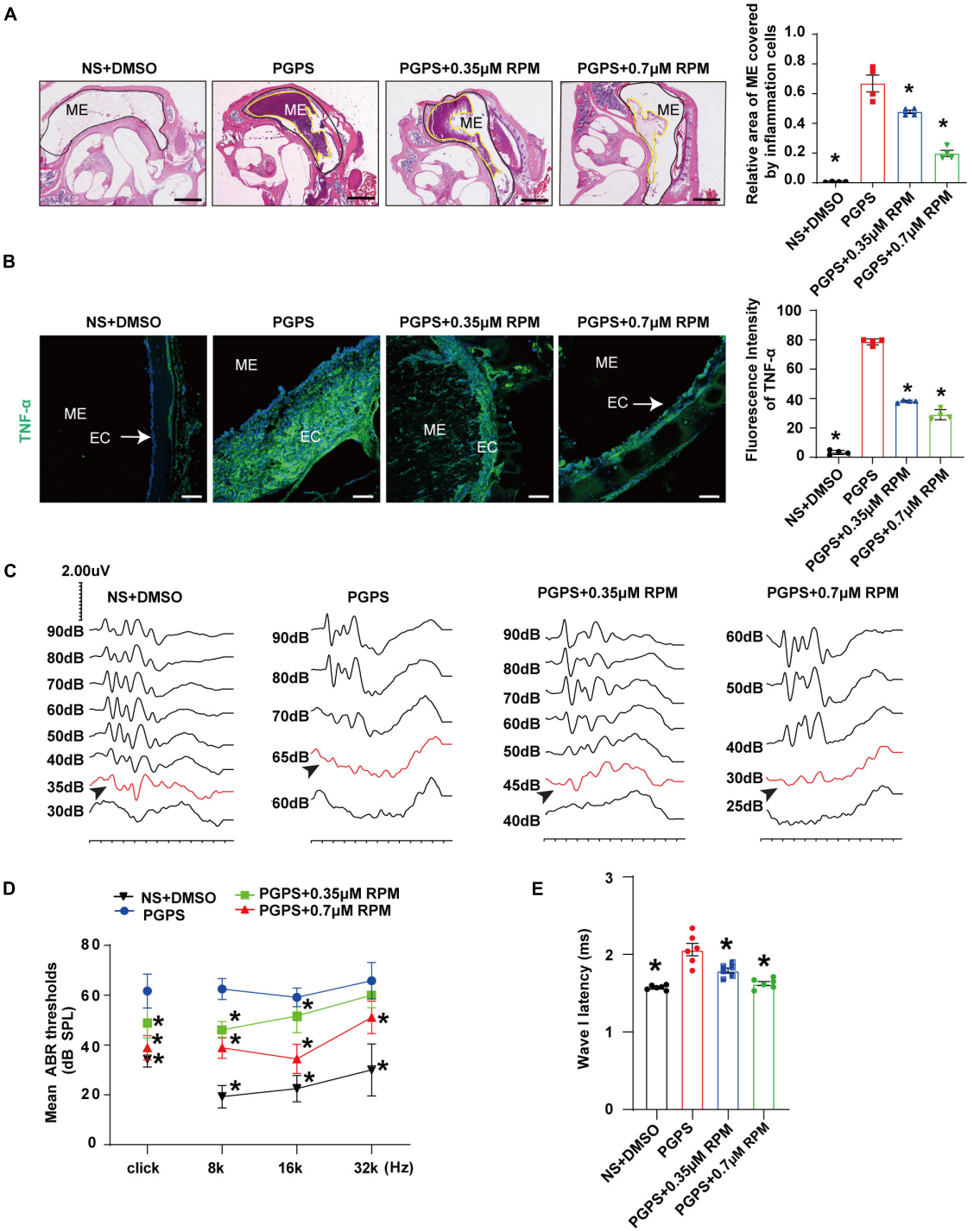

FIGURE 2 | Rapamycin treatment inhibits PGPS-induced inflammation and improves hearing function in PGPS-inoculated OM mice. **(A)** H&E histological images showing the structures and pathology of the ME. Quantification of the relative area of ME covered by inflammatory cells is shown in the bar graph. $n = 4$ per group. **(B)** Representative immunostaining for TNF-α expression in the ME. Quantification of the fluorescence intensity of TNF-α is shown in the bar graph. $n = 4$ per group. **(C)** Representative images of ABR waveforms at click stimuli are shown. The red lines and arrowheads represent threshold waveforms. **(D)** Mice were inoculated with PGPS or a combination of PGPS and either 0.35 or 0.7 μM RPM. The ABR thresholds were measured at the stimuli frequencies of click, 8, 16, and 32 kHz. The mean ABR thresholds in the NS + DMSO, PGPS + 0.35 μM RPM, and PGPS + 0.7 μM RPM groups were compared with those in the PGPS group. The data is presented as the mean ± SEM. $n = 10$ per group. **(E)** The latency of ABR wave I at click stimuli (80 dB SPL) in the NS + DMSO, PGPS + RPM combination treatment groups were compared with that in the PGPS group. Horizontal bars are mean values. $n = 10$ per group. *$P < 0.05$ vs. the PGPS group, one-way ANOVA, Scale bar, 100 μm **(A)**, 50 μm **(B)**.

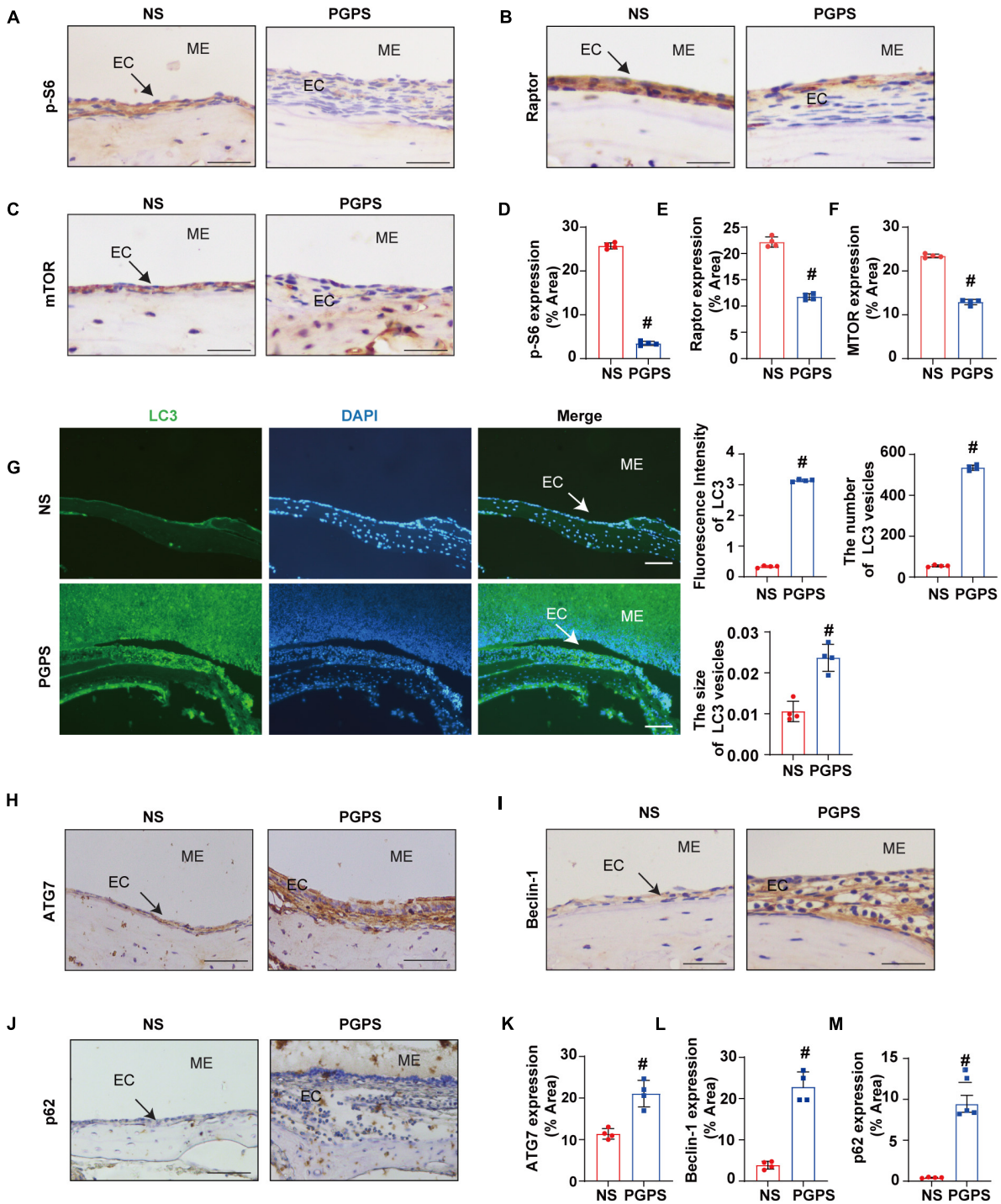

FIGURE 3 | Peptidoglycan-polysaccharide induces autophagy impairment in OM mice. Mice were inoculated with NS or PGPS for 3 days. Paraffin-embedded sections of ME tissues were immunostained with antibodies. **(A)** The representative images of p-S6 expression in ME tissues. **(B)** The representative images of Raptor expression in ME tissues. **(C)** The representative images of mTOR expression in ME tissues. **(D)** The quantification of p-S6 expression in ME tissues. **(E)** The quantification of Raptor expression in ME tissues. **(F)** The quantification of mTOR expression in ME tissues. **(G)** The representative images of LC3 expression, as well as quantitative images of the fluorescence intensity of LC3 protein expression and quantitative images of the size and number of LC3 vesicles. **(H)** The representative images of ATG7 expression in ME tissues. **(I)** The representative images of Beclin-1 expression in ME tissues. **(J)** The representative images and quantification of p62 expression in ME tissues. **(K)** The quantification of ATG7 expression in ME tissues. **(L)** The quantification of Beclin-1 expression in ME tissues. **(M)** The quantification of p-62 expression in ME tissues. $^{\#}P < 0.05$ vs. NS group, $n = 4$ per group, Student's t-test. ME represents the middle ear; EC represents epithelial cells. Scale bar = 25 μm.

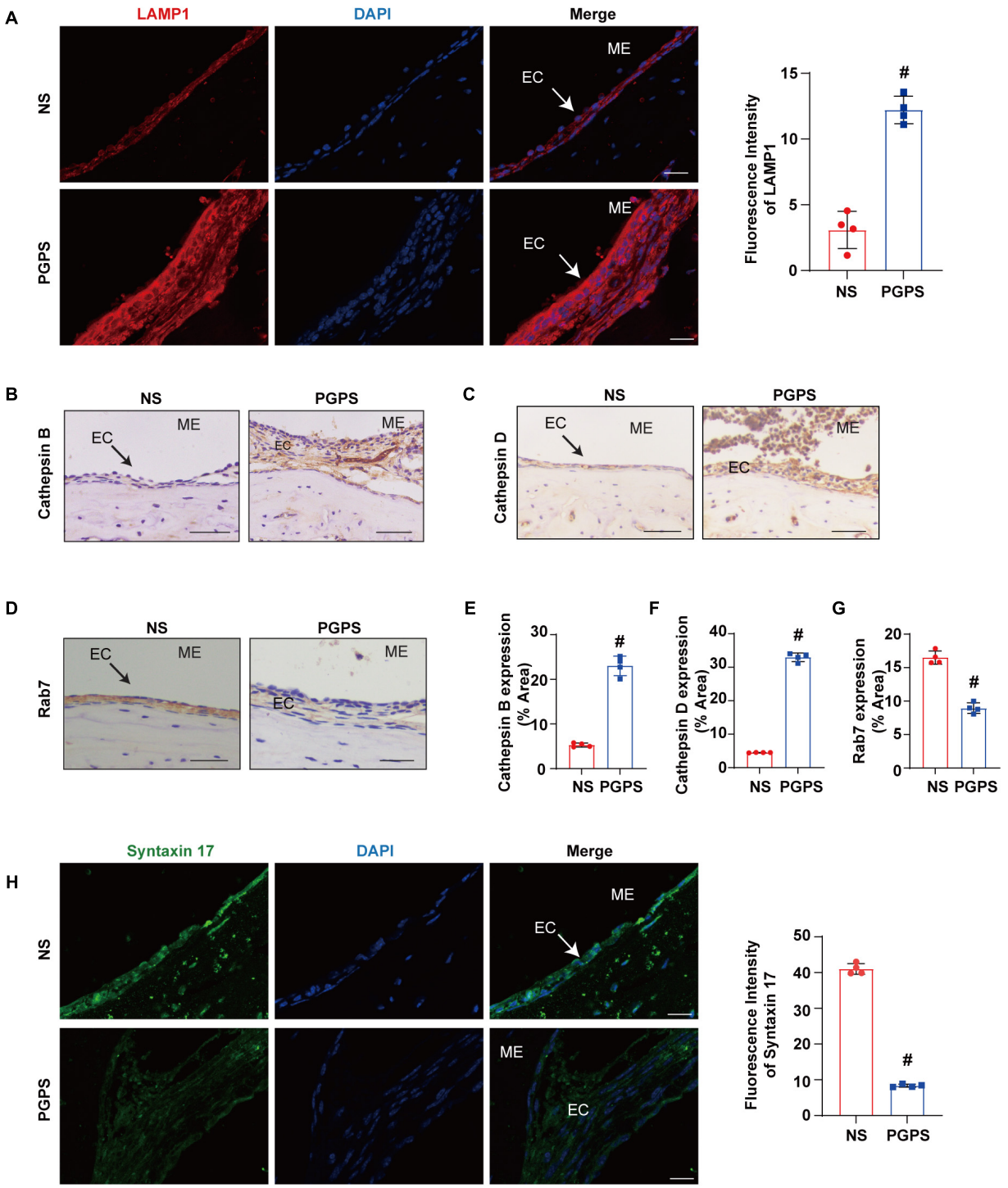

FIGURE 4 | Peptidoglycan-polysaccharide induces obstacles to the fusion of autophagosomes and lysosomes in OM mice. Mice were inoculated with NS or PGPS for 3 days. Paraffin-embedded sections of ME tissues were immunostained with antibodies. **(A)** The representative images and quantification of LAMP1 expression in ME tissues. **(B)** The representative images of Cathepsin B expression in ME tissues. **(C)** The representative images of Cathepsin D expression in ME tissues. **(D)** The representative images of Rab7 expression in ME tissues. **(E)** The quantification of Cathepsin B expression in ME tissues. **(F)** The quantification of Cathepsin D expression in ME tissues. **(G)** The quantification of Rab7 expression in ME tissues. **(H)** The representative images and quantification of Syntaxin 17 expression in ME tissues. $^{\#}P < 0.05$ vs. NS group, $n = 4$ per group, Student's t-test. ME represents the middle ear; EC represents epithelial cells. Scale bar = 25 μm.

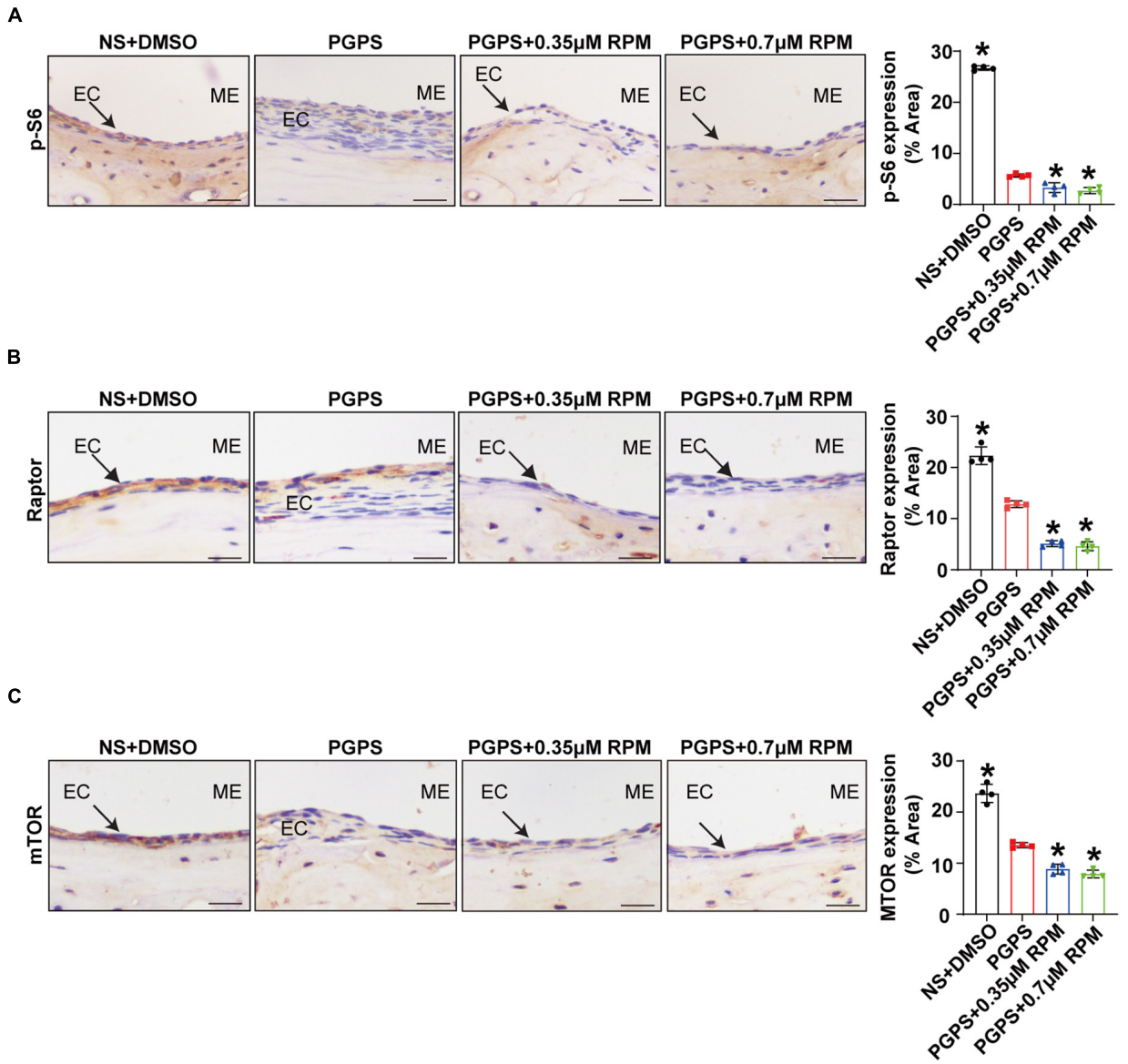

FIGURE 5 | Rapamycin treatment inhibits mTORC1 activity. Mice were inoculated with PGPS or a combination of PGPS and either 0.35 or 0.7 μM RPM. Paraffin-embedded sections of ME tissues were immunostained antibodies. **(A)** The representative images and quantification of p-S6 expression in ME tissues. **(B)** The representative images and quantification of Raptor expression in ME tissues. **(A)** The representative images and quantification of p-S6 expression in ME tissues. **(C)** The representative images and quantification of mTOR expression in ME tissues. $n = 4$ per group. ME represents the middle ear; EC represents epithelial cells. *$P < 0.05$ vs. the PGPS group, one-way ANOVA, Scale bar = 25 μm.

These data indicated that the OM mice developed severe hearing impairment.

Rapamycin Treatments Alleviate the Severity of Otitis Media Induced by PGPS

Previous studies have shown that RPM improves inflammation in organs such as the airway and retina. Thus, we investigated whether RPM has a protective effect in PGPS-induced OM mice. Histomorphological examination showed that after RPM treatment, the ME inflammation was reduced, and the inflammation area of ME in RPM-treated mice was significantly smaller than that of PGPS-treated mice (**Figure 2A**). In addition, the immunofluorescence staining revealed that the expression of TNF-α decreased more in the RPM-treated mice than in the PGPS-treated mice (**Figure 2B**). These results showed that RPM could reduce the inflammatory infiltrates in the tympanic cavity and the expression level of TNF-α. Representative images of ABR waveforms at click stimuli are shown in **Figure 2C**. The mean ABR thresholds decreased more in the PGPS + 0.35 μM RPM group and the PGPS + 0.7 μM RPM group than in the PGPS-treated group at click, 8 and 16 kHz stimulus frequencies

(**Figure 2D**). The latency of ABR wave I at click stimuli (80 dB SPL) decreased in the PGPS + 0.7 μM RPM group compared to the PGPS-treated group (**Figure 2E**). These data suggested that RPM may ease hearing loss by attenuating PGPS-induced inflammation in OM mice.

Taking into account the complexity of RPM signaling pathways, we also injected the mice with 0.35 and 0.7 μM RPM separately. Compared with the PGPS group, the two groups of mice injected with RPM alone had normal morphology and no obvious inflammatory cells (**Supplementary Figure 2A**). The results of immunofluorescence demonstrated that the expression of TNF-α was almost invisible after the RPM injection alone (**Supplementary Figure 2B**). Compared with the PGPS group, the area of ME covered by inflammatory cells and TNF-α expression level were significantly lower in the RPM injection alone group. Compared with the NS group, there was no statistical significance. The experimental results showed that there was no obvious inflammation caused by RPM injection alone.

We also investigated the hearing function in RPM single treatment group by ABR, and the representative images of ABR waveforms at click stimuli are shown in **Supplementary Figure 2C**. Compared with the PGPS group, the average ABR thresholds of the NS group, 0.35 and 0.7 μM RPM group at click, 8, 16, and 32 kHz stimulation frequencies were lower than those in the PGPS group, and were statistically significant (**Supplementary Figure 2D**). In addition, the latency of ABR wave I in the PGPS group under the click stimulus (80 dB SPL) was longer than that of the other three groups (**Supplementary Figure 2E**). Compared with NS group, the hearing threshold and the wave I latency in RPM treatment alone group is basically no statistical significance. These data showed that after injection of RPM alone, there is almost no effect on the hearing of mice.

Autophagy Impairment Is Involved in PGPS-Induced Otitis Media

Rapamycin, an autophagy inducer, activates autophagy by repressing the mTORC1 (Sekiguchi et al., 2012). S6 ribosomal protein (S6) phosphorylation was shown to be a critical downstream component of mTOR signaling (Ruvinsky et al., 2005). mTORC1 contains mTOR, which is the catalytic subunit of the complex (Laplante and Sabatini, 2009). It also contains the large protein Raptor, which is the regulatory-associated protein of mTOR (Thoreen et al., 2009). To find out whether mTORC1 signaling is involved in PGPS-induced autophagy impairment, we examined the phosphorylation of mTORC1 substrate, S6 phosphorylation at 235/236 (p-S6) and mTORC1 components, mTOR and Raptor. PGPS treatment resulted in a significant decrease in the levels of p-S6, Raptor and mTOR compared with NS group (**Figures 3A–F**), suggesting an inhibition of mTORC1 activity. In this study, we found that the fluorescence intensity of LC3 in PGPS-treated OM mice was higher than that in NS-treated mice. Quantification of the size and number of LC3 vesicles also increased in PGPS-treated OM mice (**Figure 3G**). These results suggested that OM mice are activated at the initial stage of autophagy, but it may also be due to the accumulation of LC3 caused by the blocked autophagy flux.

In addition, we also tested the expressions of ATG7 and Beclin-1. ATG7 is considered to be essential molecules for the induction of autophagy (Arakawa et al., 2017), and Beclin-1 initiates the nucleation step of autophagy to begin autophagic flux (Liang et al., 1999; Matsunaga et al., 2009). The results of immunohistochemistry showed that compared with the NS group, the expression of ATG7 and Beclin-1 were increased in OM mice (**Figures 3H,I,K,L**). These results suggested that after the injection of PGPS, the activity of mTORC1 was inhibited and the initial stage of autophagy was activated. We speculate that autophagy may act as an instinctive stress response to resist external stimuli by PGPS. However, p62 protein accumulation in the ME epithelial cells of OM mice was higher after PGPS treatment than after NS treatment (**Figures 3J,M**). These data indicated that PGPS could induce the initiation of autophagy, but at the same time cause impairment in the degradation of stage autophagy.

PGPS Induces Dysfunction of Autophagosome and Lysosome Fusion

The dysfunction of autophagy degradation may be due to the impairment of lysosomal function or dysfunction in the fusion stage of autophagosomes and lysosomes. Firstly, we test lysosomal function. Lysosomal activity is important for the autophagy degradation process (Tai et al., 2017). In order to investigate whether the autophagy impairment mechanism induced by PGPS is related to the dysfunction of lysosome, we examined the protein expression level of key lysosome enzymes like LAMP-1, Cathepsin B and Cathepsin D to evaluate the lysosomal function. Lysosome associated membrane protein-1 (LAMP-1) is a major protein component of the lysosomal membrane (Eskelinen, 2006). Cathepsin B, a member of the cysteine cathepsin family, involved in regulating the bioavailability of lysosomes and autophagosomes (Man and Kanneganti, 2016). Cathepsin D is one of the major lysosomal proteases indispensable for the maintenance of cellular proteostasis (Marques et al., 2020). Immunofluorescence results showed that compared with NS group, the expression of LAMP1 protein increased in the PGPS group (**Figure 4A**). The immunohistochemical results of Cathepsin B and Cathepsin D also showed a consistent increase in PGPS group (**Figures 4B,C,E,F**). These data showed that lysosome function maybe is not impaired.

Considering that lysosome function does not seem to be impaired, we examined the process of autophagosome and lysosome fusion by evaluating expression of Rab7 and Syntaxin 17 protein. Rab7 is a member of the Rab family, involved in transport to late endosomes and in the biogenesis of the perinuclear lysosome compartment (Gutierrez et al., 2004; Guerra and Bucci, 2016). It plays a critical role in the final maturation of late autophagic vacuoles (autophagosome and lysosome fusion) (Jager et al., 2004; He et al., 2019). Syntaxin 17 is also required for fusion between the autophagosome and

lysosome (Itakura et al., 2012; Shen et al., 2021). Our results showed that Rab7 and Syntaxin 17 expression decreased in the PGPS group compared with the NS group (**Figures 4D,G,H**). These results suggested that PGPS may block the autophagy degradation stage mainly due to the impairment of the autophagosome and lysosome fusion stage. And PGPS may impair the fusion of autophagosomes with lysosomes by decreasing the expression of Rab7 and Syntaxin 17.

Rapamycin Treatment Enhances Autophagy in PGPS-Treated Otitis Media Mice

Immunohistochemical staining showed that after injection of PGPS + 0.35/0.7 μM RPM, p-S6, Raptor and mTOR exhibited lower protein levels than the PGPS group (**Figures 5A–C**). These results suggested that RPM may enhance autophagic initiation by inhibiting mTORC1 activity. LC3 staining in ME epithelial cells revealed lower expression of LC3 and lower numbers of LC3 vesicles in RPM-treated mice than in PGPS-treated mice, the size of LC3 vesicles did not show a significant difference (**Figure 6A**). These results suggested that there may be a certain accumulation of LC3 after injection of PGPS, and after the treatment of RPM, the autophagy flux may became smooth. Immunohistochemical staining showed that after injection of PGPS + 0.35/0.7 μM RPM, ATG7 and Beclin-1 exhibited lower protein levels than the PGPS group (**Figures 6B–C**).

In order to understand the role of RPM, we injected RPM alone in TLR2$^{-/-}$ mice. The results showed that the expression of LC3 and the number of LC3 vesicles in RPM injection group was lower than that of the PGPS group, but it was higher than that of the NS group (**Supplementary Figures 3A,B,D**). There was almost no statistical difference in the size of LC3 vesicles among the groups (**Supplementary Figures 3A,C**). These results suggested that after the injection of PGPS, the mouse ME epithelial cells activated the initiation of autophagy to resist the toxicity by PGPS. However, obstacle may occur in the autophagy degradation stage, which led to the accumulation of LC3 protein. Moreover, RPM may promote the degradation stage of autophagy.

In addition, there was less p62 protein accumulation in the RPM-treated mice than in the PGPS-treated mice (**Figure 6D**). After injection of RPM alone, the expression level of p62 was significantly lower compared with the PGPS group, and there was almost no difference compared with the NS group (**Supplementary Figure 3E**). These results indicated that degradation function may be improved after RPM treatment.

Similarly, we tested lysosome function and the fusion function of autophagosome and lysosome after RPM treatment alone. The results showed that the expression of LAMP1, Cathepsin B and Cathepsin D (**Figures 7A–C**) in the RPM-treated mice was relatively weaker than that in the PGPS group. After RPM injection alone, we found that the expression level of Cathepsin B protein was lower than that of the PGPS group, but higher than that of the NS group (**Supplementary Figure 3F**). We further speculate that the increased activity of lysosomal after PGPS injection may be a response to external stimuli by PGPS, so the expression level of Cathepsin B is higher than that of the RPM injection group. We speculate that RPM may promote lysosome function, thus the expression level of Cathepsin B in RPM injection alone group is higher than that of NS group. In addition, the expression of Rab7 and Syntaxin 17 protein increased in the PGPS + RPM-treated mice (**Figures 8A,B**), thus RPM may promote the process of autophagosome and lysosome fusion. TUNEL staining showed that there were less apoptotic cells in the ME after RPM treatment (**Figure 9**). In addition, we did not find obvious apoptotic cells in the RPM alone group (**Supplementary Figure 4**). These data indicated that RPM may enhance the autophagic activity of OM mice by inhibiting the activity of mTORC1, increasing the fusion of autophagosomes with lysosomes and relieving ME epithelial cell apoptosis.

DISCUSSION

Otitis media, a general term for inflammatory changes in the ME cavity, is one of the most common childhood conditions (Mittal et al., 2014; Venekamp et al., 2017). The pathogenic mechanism of OM is not yet clear and excessive antibiotic treatment has also brought a heavy burden to society, so it is particularly important to explore the mechanism of OM and find suitable drug treatments (Vergison et al., 2010). In recent years, the autophagy pathway has played a certain role in inflammation, but the research on the relationship between autophagy and OM has not been in-depth. It was found that the expression of *LC3-II* was significantly increased in the inflammatory ME tissues in human (Jung et al., 2020b). Studies have shown that in the ME fluid of patients with OM, the mRNA level of autophagy initiation-related genes such as *Beclin-1*, is increased in OM patients with cholesteatom (Jung et al., 2020a). Our study aims to explore the role of autophagy in the pathogenesis of OM by TLR2$^{-/-}$ mice model, and treat OM mice by RPM, aiming to provide a theoretical basis and new treatment strategies for the treatment of clinical OM.

The mTOR is involved in the induction and initiation of autophagy (Cayo et al., 2021). We tested the expression of p-S6, Raptor and mTOR after injection of PGPS, and found that the mTORC1 activity of mice in the PGPS group was weakened. These results indicated that autophagy may be activated in the mice in the PGPS group, which seems to be consistent with the increase in the expression of proteins related to autophagy initiation like LC3, ATG7 and Beclin-1. Among them, the expressions of LC3, ATG7 and Beclin-1 in the PGPS group all showed increased compared with NS group. We speculate that autophagy may act as an instinctive stress response to resist external stimuli by PGPS. RPM + PGPS combination treatment groups showed that the protein expression of LC3, ATG7 and Beclin-1 were reduced compared with the PGPS group. Considering the complexity of the RPM pathway, we also injected RPM alone in TLR2$^{-/-}$ mice. The results suggested that the expression of LC3, ATG7, and Beclin-1 in RPM injection alone group was also lower than PGPS group, but was higher than NS group. These results indicated that the PGPS group does not seem to be impaired during the initiation of autophagy.

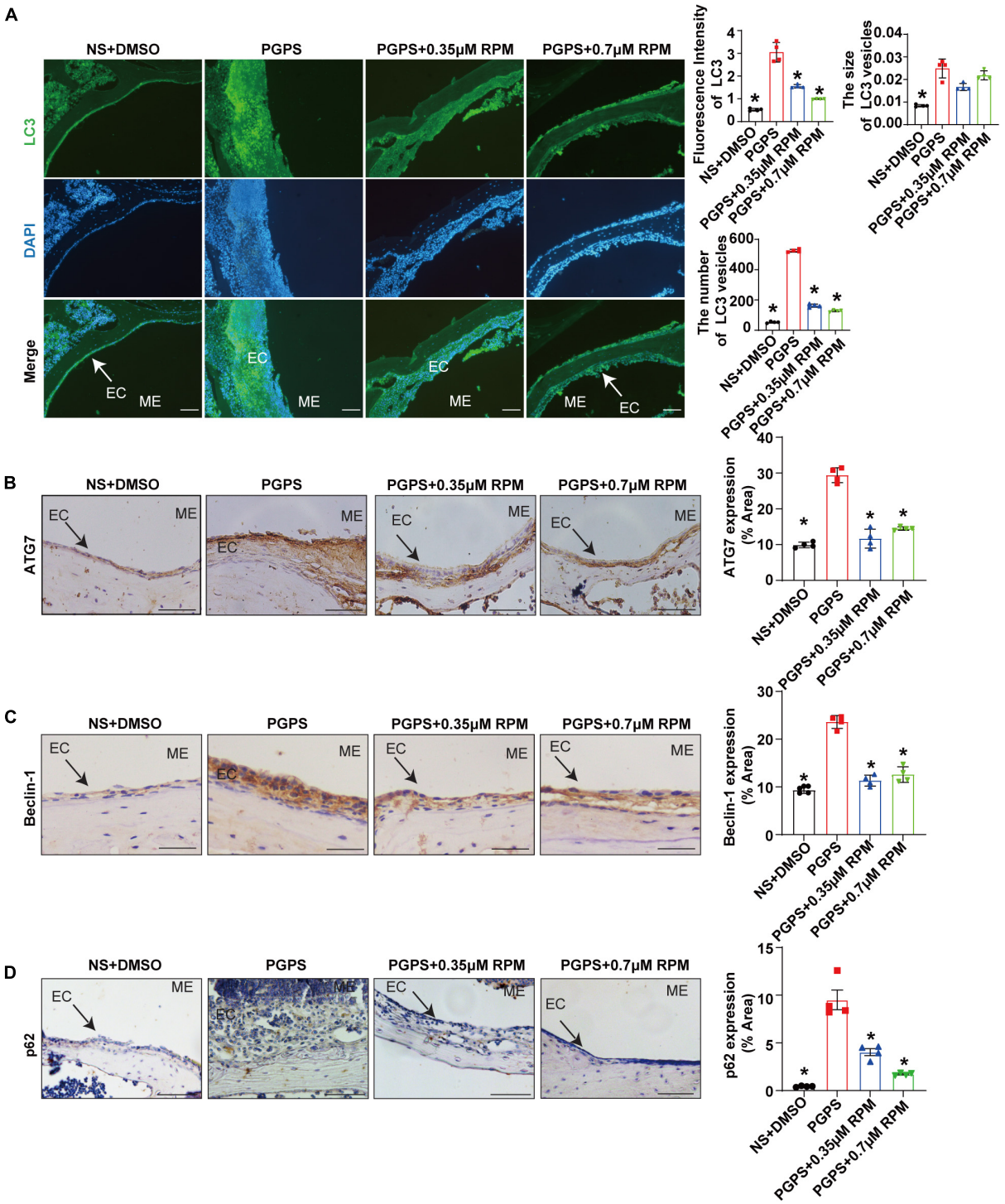

FIGURE 6 | Rapamycin treatment enhances autophagy in PGPS-treated OM mice. Mice were inoculated with PGPS or a combination of PGPS and either 0.35 or 0.7 μM RPM. Paraffin-embedded sections of ME tissues were immunostained antibodies. **(A)** The representative images of LC3 expression, as well as quantitative images of the fluorescence intensity of LC3 protein expression and quantitative images of the size and number of LC3 vesicles. *n* = 4 per group. **(B)** The representative images and quantification of ATG7 expression in ME tissues. *n* = 4 per group. **(C)** The representative images and quantification of Beclin-1 expression in ME tissues. *n* = 4 per group. **(D)** The representative images and quantification of p62 expression in ME tissues. *n* = 4 per group. ME represents the middle ear; EC represents epithelial cells. **P* < 0.05 vs. the PGPS group, one-way ANOVA, Scale bar = 25 μm.

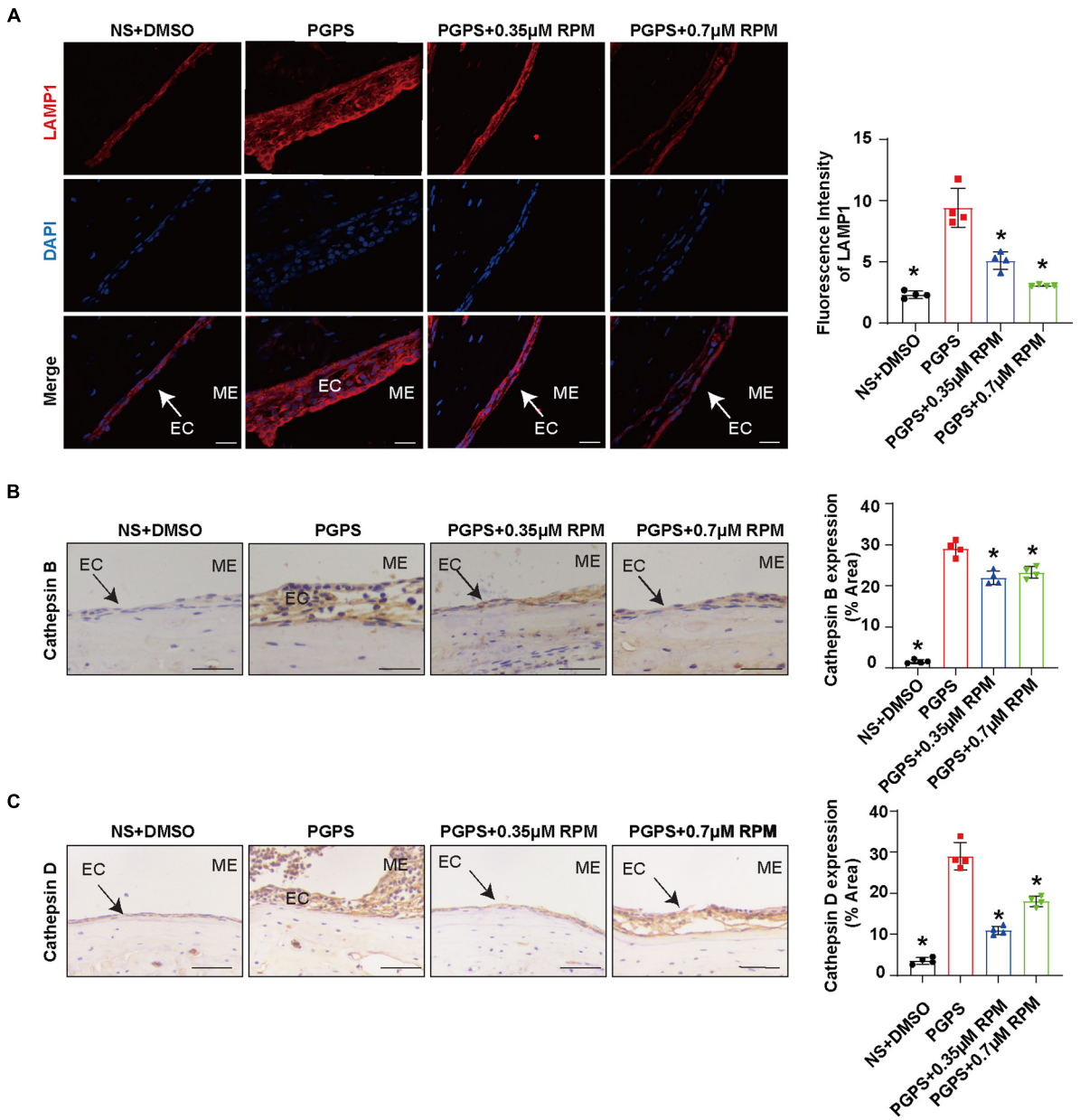

FIGURE 7 | Lysosome function may not be impaired after PGPS injection Mice were inoculated with PGPS or a combination of PGPS and either 0.35 or 0.7 μM RPM. Paraffin-embedded sections of ME tissues were immunostained antibodies. **(A)** The representative images and quantification of LAMP1 expression in ME tissues. **(B)** The representative images and quantification of Cathepsin B expression in ME tissues. **(C)** The representative images and quantification of Cathepsin D expression in ME tissues. $n = 4$ per group, ME represents the middle ear; EC represents epithelial cells. *$P < 0.05$ vs. the PGPS group, one-way ANOVA, Scale bar = 25 μm.

We speculated that there may be obstacles in the degradation stage of autophagy, resulting in accumulation of LC3 protein in PGPS group. The expression of p62 in PGPS group is more increasing than NS group, and after the injection of PGPS + RPM combination, the level of p62 decreased, which demonstrated that PGPS may induce autophagy impairment in the autophagy degradation stage and RPM may promote the degradation stage of autophagy.

Both the function of lysosome and the fusion of autophagosomes and lysosomes affect the autophagic degradation. We first evaluated the lysosomal function. Lysosome-related proteins such as LAMP1, Cathepsin B and Cathepsin D play an important role in the normal function of lysosomes (Eskelinen, 2006; Man and Kanneganti, 2016; Marques et al., 2020). In our experiment, compared with the NS group, the expression of the three proteins increased in

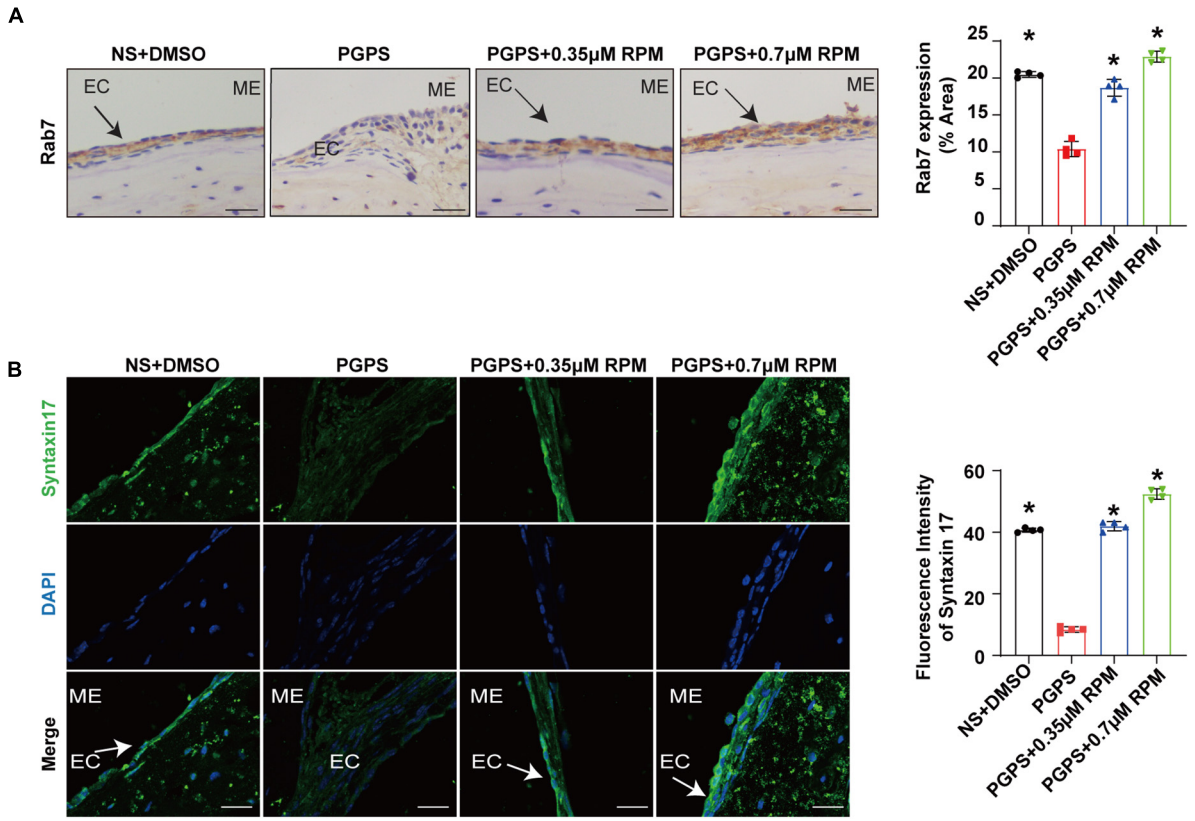

FIGURE 8 | Rapamycin treatment increases the fusion of autophagosomes and lysosomes in OM mice. Mice were inoculated with PGPS or a combination of PGPS and either 0.35 or 0.7 μM RPM. Paraffin-embedded sections of ME tissues were immunostained antibodies. **(A)** The representative images and quantification of Rab7 expression in ME tissues. **(B)** The representative images and quantification of Syntaxin 17 expression in ME tissues. $n = 4$ per group, ME represents the middle ear; EC represents epithelial cells. *$P < 0.05$ vs. the PGPS group, one-way ANOVA, Scale bar = 25 μm.

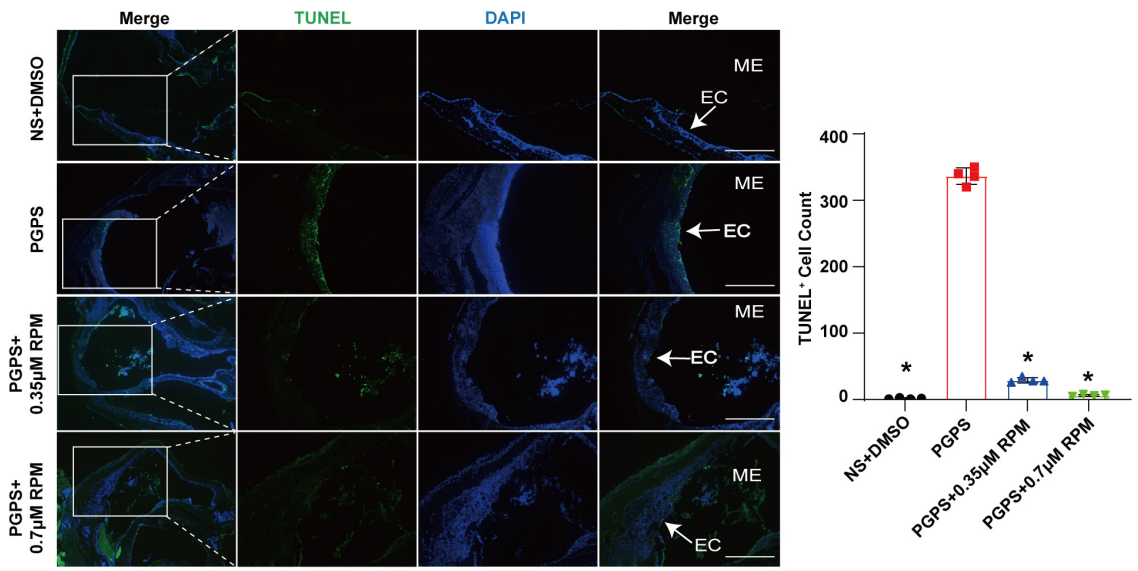

FIGURE 9 | Rapamycin treatment relieved ME epithelial cell apoptosis. Apoptotic cells in the MEs were examined by TUNEL staining. The quantitative image of apoptotic cells was shown in Figure B. The PGPS + 0.7 μM RPM group showed fewer TUNEL-positive epithelial cells than the PGPS group. ME represents the middle ear; EC represents epithelial cells. *$P < 0.05$ vs. the PGPS group, $n = 4$ per group, Scale bar = 500 μm, one-way ANOVA.

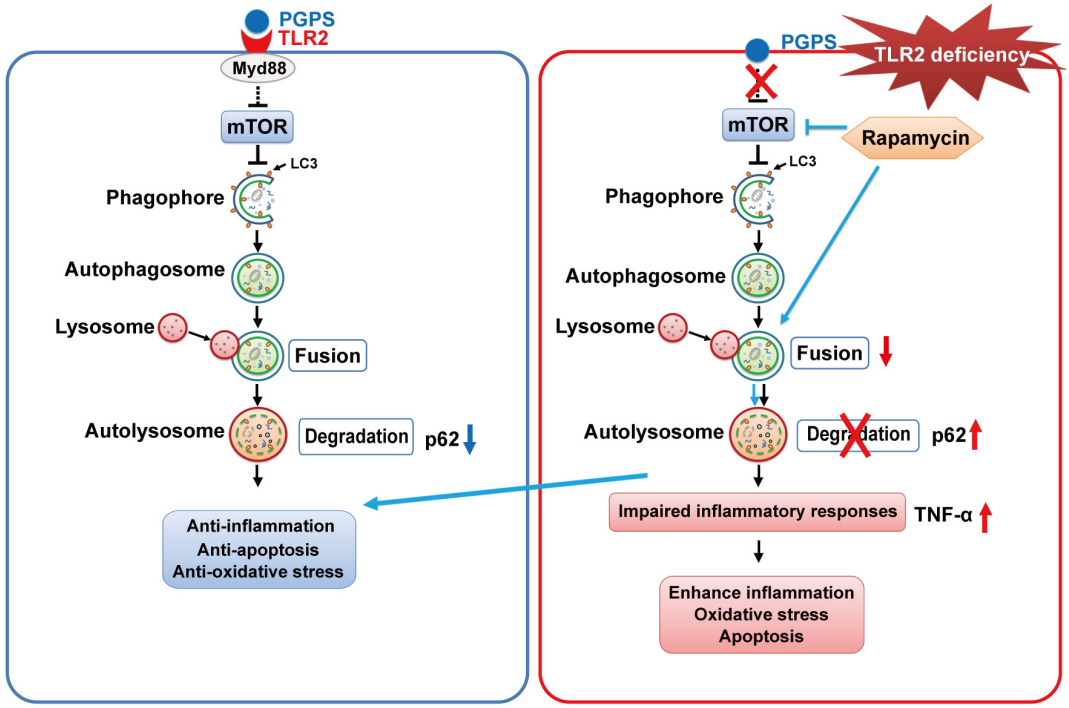

FIGURE 10 | The proposed mechanism for RPM-enhanced autophagy protects against PGPS-induced OM in TLR2$^{-/-}$ mice. TLR2 deficiency may inhibit fusion between autophagosomes and lysosomes, leading to the accumulation of p62. It may also induce inflammation and apoptosis. RPM treatment may improve the autophagic clearance ability and have a protective effect against OM injury.

the PGPS group. The expression level of the three proteins in the RPM + PGPS combination treatment group was lower than that of the PGPS group. After injection of RPM alone, the expression of Cathepsin B also decreased compared with PGPS group, but was higher than NS group. These results seemed to demonstrate that the lysosomes of OM mice are not impaired. On the contrary, increased lysosomal function may be a stress response after PGPS injection.

Based on the above experimental results, we tested the fusion stage of autophagosomes and lysosomes by evaluating the protein expression of Rab7 and Syntaxin 17. Our results showed that after PGPS injection, the expression of Rab7 and Syntaxin 17 decreased, and co-treatment with RPM, the expression of Rab7 and Syntaxin 17 increased. These results suggested that after injection of PGPS, the fusion of autophagosome and lysosome is impaired, leading to autophagy impairment. RPM treatment may stimulate the fusion of autophagosomes and lysosomes, making the autophagy pathway smoothly. Previous study also found that RPM could promote the fusion of lysosomes and autophagosomes (Choi et al., 2016). In addition, we also found that after PGPS and RPM combination treatment, the expression of p-S6, mTOR and Raptor was lower than that of PGPS alone. Therefore, we speculate that when TLR2$^{-/-}$ mice injected with PGPS, autophagy acts as an instinctive stress response to resist external stimuli. But, there may be an obstacle when autophagosomes fuse with lysosomes, which leads to obstacles in the degradation stage of autophagy and causes protein accumulation. This may produce proteotoxic stress, and autophagy is insufficient to resist proteotoxic stress during OM. After RPM treatment, mTORC1 could be further inhibited, thereby promoting the initial stage of autophagy. At the same time, our experimental results also found that RPM may promote the degradation stage of autophagy. In summary, RPM may play a positive role in both stages, so as to exert its therapeutic effect.

In this study, we verify again that PGPS injection could cause OM in TLR2$^{-/-}$ mice, which leads to hearing loss. In addition, we demonstrated that inflammation in OM mice may be due to the impairment of autophagy pathway, mainly due to impairment in the process of autophagosome fusing to lysosomes, which is manifested by the decrease of Rab7 and Syntaxin 17 expression in the PGPS group. We also found that after injection of RPM, it could inhibit the activity of mTORC1, increase the expression level of Rab7 and Syntaxin 17 and promote autophagy flux. RPM treatment also reduce the inflammatory response of ME epithelial cells, reduce cell apoptosis, and thereby alleviate hearing loss in OM mice. Therefore, these data suggested that autophagy impairment may be involved in the development of OM and that RPM could effectively improve OM conditions, most likely by alleviating autophagy impairment. A general scheme showing that RPM-enhanced autophagy protects against PGPS-induced OM in TLR2$^{-/-}$ mice is shown in **Figure 10**.

Autophagy is a bulk degradation system that delivers cytoplasmic constituents to autolysosomes for recycling and maintaining cell homeostasis. In addition, autophagy has

critical functions in cell-autonomous defense in immunity (Matsuzawa-Ishimoto et al., 2018). Many studies found autophagy impairment could mediate susceptibility to infectious and inflammatory diseases like Crohn's disease and chronic obstructive pulmonary disease (Lupfer et al., 2013; Lassen et al., 2014; Murthy et al., 2014). In this study, we found for the first time that autophagy was involved in OM and that RPM significantly alleviated autophagy impairment and improved ME inflammatory conditions.

To date, RPM has been used in some clinical trials like tuberous sclerosis complex-related facial angiofibromas (Koenig et al., 2018). It has been also shown to be effective in a variety of inflammatory diseases like autoimmune encephalomyelitis and retinal inflammation (Okamoto et al., 2016; Joean et al., 2017; Li et al., 2019a,b). In this study, we showed that RPM significantly alleviated autophagy impairment and improved ME inflammatory conditions. Some researchers also found that RPM could promote the fusion of lysosomes and autophagosomes (Choi et al., 2016; Cheng et al., 2021). Therefore, we speculate that RPM may play a positive role in the treatment of OM. Due to the complexity of RPM signaling pathways, we do not rule out the possibility that the protective effect of RPM on the OM may also involve other branches of RPM signaling in addition to autophagy. Nonetheless, our data suggest that modulating autophagy activity may be possible intervention for OM. Our study provides a theoretical basis for the clinical application of RPM in the treatment of OM. However, it has been reported that RPM has immunosuppressive side effects. Several new RPM analogs have demonstrated reduced side effects, and these new drugs may be safer and less immunosuppressive than RPM (Fu et al., 2018). Perhaps the ability of these analogs to prevent OM should be tested.

In summary, our research shows that autophagy impairment is related to OM, and impairment to the fusion of autophagosomes and lysosomes is an important factor leading to the occurrence of PGPS-induced otitis media. RPM treatment could alleviate hearing loss to a certain extent. These findings highlight the potential of specific autophagosome-to-lysosome fusion activators in reducing PGPS-induced OM. Considering that increasing autophagic clearance may be useful as a new therapeutic strategy against severe OM damage, autophagosome and lysosome fusing dysfunction may be a candidate target for therapeutic intervention. Therefore, extensive pharmaceutical studies should be performed in the near future. Future research is necessary to better explain the mechanism underlying the protective role of the normal autophagy process against the pathogenesis of OM, and then design and test potential therapeutic methods to prevent or treat OM.

DATA AVAILABILITY STATEMENT

The original contributions presented in the study are included in the article/**Supplementary Material**, further inquiries can be directed to the corresponding authors.

ETHICS STATEMENT

The animal study was reviewed and approved by the Animal Use and Care Committee of Binzhou Medical University.

AUTHOR CONTRIBUTIONS

DX, ToZ, XZ, LK, QW, and YW performed the experiments. BL and DX wrote the manuscript. ToZ and BL analyzed the data. RG, YY, PM, XZ, and YZ participated in discussion of the project. BL and QZ designed the study. YW, TiZ, HM, and QZ revised the manuscript. All authors reviewed and approved the manuscript.

FUNDING

This work was supported by grants from the National Natural Science Foundation of China (81873697, 81530030, 81500797, and 81700902); the National Institutes of Health of United States (R01DC015111 and R21DC005846); the Shandong Provincial Natural Science Foundation of China (ZR2019PH062, ZR2020KH025, and ZR2021MC052); the Humanities and Social Sciences Youth Foundation, Ministry of Education of the People's Republic of China (18YJC740128); and the Taishan Scholars Program Foundation.

ACKNOWLEDGMENTS

We would like to express the most sincere thanks to Maria Hatzoglou from Case Western Reserve University for comments and advice on the article.

SUPPLEMENTARY MATERIAL

The Supplementary Material for this article can be found online at: https://www.frontiersin.org/articles/10.3389/fncel.2021.753369/full#supplementary-material

REFERENCES

Arakawa, S., Honda, S., Yamaguchi, H., and Shimizu, S. (2017). Molecular mechanisms and physiological roles of Atg5/Atg7-independent alternative autophagy. *Proc. Jpn. Acad. Ser. B Phys. Biol. Sci.* 93, 378–385. doi: 10.2183/pjab.93.023

Bissler, J. J., McCormack, F. X., Young, L. R., Elwing, J. M., Chuck, G., Leonard, J. M., et al. (2008). Sirolimus for angiomyolipoma in tuberous sclerosis complex or lymphangioleiomyomatosis. *N. Engl. J. Med.* 358, 140–151.

Bluestone, C. D., and Doyle, W. J. (1988). Anatomy and physiology of eustachian tube and middle ear related to otitis media. *J. Allergy Clin. Immunol.* 81, 997–1003. doi: 10.1016/0091-6749(88)90168-6

Cayo, A., Segovia, R., Venturini, W., Moore-Carrasco, R., Valenzuela, C., and Brown, N. (2021). mTOR activity and autophagy in senescent cells, a complex partnership. *Int. J. Mol. Sci.* 22:8149. doi: 10.3390/ijms22158149

Cheng, J. T., Liu, P. F., Yang, H. C., Huang, S. J., Griffith, M., Morgan, P., et al. (2021). Tumor Susceptibility gene 101 facilitates rapamycin-induced autophagic flux in neuron cells. *Biomed. Pharmacother.* 134:111106. doi: 10.1016/j.biopha.2020.111106

Choi, J. Y., Won, N. H., Park, J. D., Jang, S., Eom, C. Y., Choi, Y., et al. (2016). From the cover: ethylmercury-induced oxidative and endoplasmic reticulum stress-mediated autophagic cell death: involvement of autophagosome-lysosome fusion arrest. *Toxicol. Sci.* 154, 27–42. doi: 10.1093/toxsci/kfw155

Eskelinen, E. L. (2006). Roles of LAMP-1 and LAMP-2 in lysosome biogenesis and autophagy. *Mol. Aspects Med.* 27, 495–502. doi: 10.1016/j.mam.2006.08.005

Franz, D. N., Belousova, E., Sparagana, S., Bebin, E. M., Frost, M. D., Kuperman, R., et al. (2016). Long-term use of everolimus in patients with tuberous sclerosis complex: final results from the EXIST-1 study. *PLoS One* 11:e0158476. doi: 10.1371/journal.pone.0158476

Fu, X., Sun, X., Zhang, L., Jin, Y., Chai, R., Yang, L., et al. (2018). Tuberous sclerosis complex-mediated mTORC1 overactivation promotes age-related hearing loss. *J. Clin. Invest.* 128, 4938–4955. doi: 10.1172/JCI98058

Fulghum, R. S., and Brown, R. R. (1998). Purified streptococcal cell wall (PG-APS) causes experimental otitis media. *Auris Nasus Larynx* 25, 5–11. doi: 10.1016/s0385-8146(97)10025-6

Garlanda, C., Dinarello, C. A., and Mantovani, A. (2013). The interleukin-1 family: back to the future. *Immunity* 39, 1003–1018. doi: 10.1016/j.immuni.2013.11.010

Glick, D., Barth, S., and Macleod, K. F. (2010). Autophagy: cellular and molecular mechanisms. *J. Pathol.* 221, 3–12. doi: 10.1002/path.2697

Guerra, F., and Bucci, C. (2016). Multiple Roles of the Small GTPase Rab7. *Cells* 5:34. doi: 10.3390/cells5030034

Gutierrez, M. G., Munafo, D. B., Beron, W., and Colombo, M. I. (2004). Rab7 is required for the normal progression of the autophagic pathway in mammalian cells. *J. Cell Sci.* 117, 2687–2697. doi: 10.1242/jcs.01114

Harmes, K. M., Blackwood, R. A., Burrows, H. L., Cooke, J. M., Harrison, R. V., and Passamani, P. P. (2013). Otitis media: diagnosis and treatment. *Am. Fam. Phys.* 88, 435–440.

Harris, J., Lang, T., Thomas, J. P. W., Sukkar, M. B., Nabar, N. R., and Kehrl, J. H. (2017). Autophagy and inflammasomes. *Mol. Immunol.* 86, 10–15.

He, K., Sun, H., Zhang, J., Zheng, R., Gu, J., Luo, M., et al. (2019). Rab7mediated autophagy regulates phenotypic transformation and behavior of smooth muscle cells via the Ras/Raf/MEK/ERK signaling pathway in human aortic dissection. *Mol. Med. Rep.* 19, 3105–3113. doi: 10.3892/mmr.2019.9955

Hu, J., Li, B., Apisa, L., Yu, H., Entenman, S., Xu, M., et al. (2016). ER stress inhibitor attenuates hearing loss and hair cell death in Cdh23(erl/erl) mutant mice. *Cell Death Dis.* 7:e2485. doi: 10.1038/cddis.2016.386

Idriss, H. T., and Naismith, J. H. (2000). TNF alpha and the TNF receptor superfamily: structure-function relationship(s). *Microsc. Res. Tech.* 50, 184–195. doi: 10.1002/1097-0029(20000801)50:3<184::AID-JEMT2>3.0.CO;2-H

Itakura, E., Kishi-Itakura, C., and Mizushima, N. (2012). The hairpin-type tail-anchored SNARE syntaxin 17 targets to autophagosomes for fusion with endosomes/lysosomes. *Cell* 151, 1256–1269. doi: 10.1016/j.cell.2012.11.001

Jager, S., Bucci, C., Tanida, I., Ueno, T., Kominami, E., Saftig, P., et al. (2004). Role for Rab7 in maturation of late autophagic vacuoles. *J. Cell Sci.* 117, 4837–4848. doi: 10.1242/jcs.01370

Joean, O., Hueber, A., Feller, F., Jirmo, A. C., Lochner, M., Dittrich, A. M., et al. (2017). Suppression of Th17-polarized airway inflammation by rapamycin. *Sci. Rep.* 7:15336. doi: 10.1038/s41598-017-15750-6

Jung, J., Jung, S. Y., Kim, M. G., Kim, Y. I., Kim, S. H., and Yeo, S. G. (2020a). Comparison of autophagy mRNA expression between chronic otitis media with and without cholesteatoma. *J. Audiol. Otol.* 24, 191–197. doi: 10.7874/jao.2020.00108

Jung, J., Park, D. C., Kim, Y. I., Lee, E. H., Park, M. J., Kim, S. H., et al. (2020b). Decreased expression of autophagy markers in culture-positive patients with chronic otitis media. *J. Int. Med. Res.* 48:300060520936174. doi: 10.1177/0300060520936174

Koenig, M. K., Bell, C. S., Hebert, A. A., Roberson, J., Samuels, J. A., Slopis, J. M., et al. (2018). Efficacy and safety of topical rapamycin in patients with facial angiofibromas secondary to tuberous sclerosis complex: the treatment randomized clinical trial. *JAMA Dermatol.* 154, 773–780. doi: 10.1001/jamadermatol.2018.0464

Komori, M., Nakamura, Y., Ping, J., Feng, L., Toyama, K., Kim, Y., et al. (2011). Pneumococcal peptidoglycan-polysaccharides regulate Toll-like receptor 2 in the mouse middle ear epithelial cells. *Pediatr. Res.* 69, 101–105. doi: 10.1203/PDR.0b013e3182055237

Laplante, M., and Sabatini, D. M. (2009). mTOR signaling at a glance. *J. Cell Sci.* 122, 3589–3594. doi: 10.1242/jcs.051011

Lassen, K. G., Kuballa, P., Conway, K. L., Patel, K. K., Becker, C. E., Peloquin, J. M., et al. (2014). Atg16L1 T300A variant decreases selective autophagy resulting in altered cytokine signaling and decreased antibacterial defense. *Proc. Natl. Acad. Sci. U.S.A.* 111, 7741–7746. doi: 10.1073/pnas.1407001111

Li, J., Kim, S. G., and Blenis, J. (2014). Rapamycin: one drug, many effects. *Cell Metab.* 19, 373–379. doi: 10.1016/j.cmet.2014.01.001

Li, Z., Nie, L., Chen, L., Sun, Y., and Guo, L. (2019a). [Rapamycin alleviates inflammation by up-regulating TGF-beta/Smad signaling in a mouse model of autoimmune encephalomyelitis]. *Nan Fang Yi Ke Da Xue Xue Bao* 39, 35–42. doi: 10.12122/j.issn.1673-4254.2019.01.06

Li, Z., Nie, L., Chen, L., Sun, Y., and Li, G. (2019b). Rapamycin relieves inflammation of experimental autoimmune encephalomyelitis by altering the balance of Treg/Th17 in a mouse model. *Neurosci. Lett.* 705, 39–45. doi: 10.1016/j.neulet.2019.04.035

Liang, X. H., Jackson, S., Seaman, M., Brown, K., Kempkes, B., Hibshoosh, H., et al. (1999). Induction of autophagy and inhibition of tumorigenesis by beclin 1. *Nature* 402, 672–676. doi: 10.1038/45257

Lupfer, C., Thomas, P. G., Anand, P. K., Vogel, P., Milasta, S., Martinez, J., et al. (2013). Receptor interacting protein kinase 2-mediated mitophagy regulates inflammasome activation during virus infection. *Nat. Immunol.* 14, 480–488. doi: 10.1038/ni.2563

Man, S. M., and Kanneganti, T. D. (2016). Regulation of lysosomal dynamics and autophagy by CTSB/cathepsin B. *Autophagy* 12, 2504–2505. doi: 10.1080/15548627.2016.1239679

Mandrioli, J., D'Amico, R., Zucchi, E., Gessani, A., Fini, N., Fasano, A., et al. (2018). Rapamycin treatment for amyotrophic lateral sclerosis: protocol for a phase II randomized, double-blind, placebo-controlled, multicenter, clinical trial (RAP-ALS trial). *Medicine (Baltimore)* 97:e11119. doi: 10.1097/MD.0000000000011119

Marques, A. R. A., Di Spiezio, A., Thiessen, N., Schmidt, L., Grotzinger, J., Lullmann-Rauch, R., et al. (2020). Enzyme replacement therapy with recombinant pro-CTSD (cathepsin D) corrects defective proteolysis and autophagy in neuronal ceroid lipofuscinosis. *Autophagy* 16, 811–825. doi: 10.1080/15548627.2019.1637200

Matsunaga, K., Saitoh, T., Tabata, K., Omori, H., Satoh, T., Kurotori, N., et al. (2009). Two Beclin 1-binding proteins, Atg14L and Rubicon, reciprocally regulate autophagy at different stages. *Nat. Cell Biol.* 11, 385–396. doi: 10.1038/ncb1846

Matsuzawa-Ishimoto, Y., Hwang, S., and Cadwell, K. (2018). Autophagy and Inflammation. *Annu. Rev. Immunol.* 36, 73–101.

Mittal, R., Kodiyan, J., Gerring, R., Mathee, K., Li, J. D., Grati, M., et al. (2014). Role of innate immunity in the pathogenesis of otitis media. *Int. J. Infect. Dis.* 29, 259–267. doi: 10.1016/j.ijid.2014.10.015

Mizushima, N. (2007). Autophagy: process and function. *Genes Dev.* 21, 2861–2873. doi: 10.1101/gad.1599207

Monasta, L., Ronfani, L., Marchetti, F., Montico, M., Vecchi Brumatti, L., Bavcar, A., et al. (2012). Burden of disease caused by otitis media: systematic review and global estimates. *PLoS One* 7:e36226. doi: 10.1371/journal.pone.0036226

Murthy, A., Li, Y., Peng, I., Reichelt, M., Katakam, A. K., Noubade, R., et al. (2014). A Crohn's disease variant in Atg16l1 enhances its degradation by caspase 3. *Nature* 506, 456–462. doi: 10.1038/nature13044

Okamoto, T., Ozawa, Y., Kamoshita, M., Osada, H., Toda, E., Kurihara, T., et al. (2016). The neuroprotective effect of rapamycin as a modulator of the mTOR-NF-kappaB axis during retinal inflammation. *PLoS One* 11:e0146517. doi: 10.1371/journal.pone.0146517

Rovers, M. M., Schilder, A. G., Zielhuis, G. A., and Rosenfeld, R. M. (2004). Otitis media. *Lancet* 363, 465–473.

Ruvinsky, I., Sharon, N., Lerer, T., Cohen, H., Stolovich-Rain, M., Nir, T., et al. (2005). Ribosomal protein S6 phosphorylation is a determinant of cell size and glucose homeostasis. *Genes Dev.* 19, 2199–2211. doi: 10.1101/gad.351605

Sekiguchi, A., Kanno, H., Ozawa, H., Yamaya, S., and Itoi, E. (2012). Rapamycin promotes autophagy and reduces neural tissue damage and locomotor impairment after spinal cord injury in mice. *J. Neurotrauma* 29, 946–956.

Shen, Q., Shi, Y., Liu, J., Su, H., Huang, J., Zhang, Y., et al. (2021). Acetylation of STX17 (syntaxin 17) controls autophagosome maturation. *Autophagy* 17, 1157–1169. doi: 10.1080/15548627.2020.1752471

Sou, Y. S., Tanida, I., Komatsu, M., Ueno, T., and Kominami, E. (2006). Phosphatidylserine in addition to phosphatidylethanolamine is an in vitro target of the mammalian Atg8 modifiers, LC3, GABARAP, and GATE-16. *J. Biol. Chem.* 281, 3017–3024. doi: 10.1074/jbc.M505888200

Tai, H., Wang, Z., Gong, H., Han, X., Zhou, J., Wang, X., et al. (2017). Autophagy impairment with lysosomal and mitochondrial dysfunction is an important characteristic of oxidative stress-induced senescence. *Autophagy* 13, 99–113. doi: 10.1080/15548627.2016.1247143

Takeda, K., and Akira, S. (2015). Toll-like receptors. *Curr. Protoc. Immunol.* 109, 14.12.1–14.12.10.

Tanida, I., Ueno, T., and Kominami, E. (2004). LC3 conjugation system in mammalian autophagy. *Int. J. Biochem. Cell Biol.* 36, 2503–2518. doi: 10.1016/j.biocel.2004.05.009

Thoreen, C. C., Kang, S. A., Chang, J. W., Liu, Q., Zhang, J., Gao, Y., et al. (2009). An ATP-competitive mammalian target of rapamycin inhibitor reveals rapamycin-resistant functions of mTORC1. *J. Biol. Chem.* 284, 8023–8032. doi: 10.1074/jbc.m900301200

Venekamp, R. P., Damoiseaux, R. A., and Schilder, A. G. (2017). Acute Otitis Media in Children. *Am Fam. Phys.* 95, 109–110.

Vergison, A., Dagan, R., Arguedas, A., Bonhoeffer, J., Cohen, R., Dhooge, I., et al. (2010). Otitis media and its consequences: beyond the earache. *Lancet Infect. Dis.* 10, 195–203. doi: 10.1016/S1473-3099(10)70012-8

Zhang, X., Zheng, T., Sang, L., Apisa, L., Zhao, H., Fu, F., et al. (2015). Otitis media induced by peptidoglycan-polysaccharide (PGPS) in TLR2-deficient (Tlr2(-/-)) mice for developing drug therapy. *Infect. Genet. Evol.* 35, 194–203. doi: 10.1016/j.meegid.2015.08.019

Zuo, R., Wang, Y., Li, J., Wu, J., Wang, W., Li, B., et al. (2019). Rapamycin induced autophagy inhibits inflammation-mediated endplate degeneration by enhancing Nrf2/Keap1 signaling of cartilage endplate stem cells. *Stem Cells* 37, 828–840. doi: 10.1002/stem.2999

Conflict of Interest: The authors declare that the research was conducted in the absence of any commercial or financial relationships that could be construed as a potential conflict of interest.

Publisher's Note: All claims expressed in this article are solely those of the authors and do not necessarily represent those of their affiliated organizations, or those of the publisher, the editors and the reviewers. Any product that may be evaluated in this article, or claim that may be made by its manufacturer, is not guaranteed or endorsed by the publisher.

frontiers in Cellular Neuroscience

REVIEW
published: 31 January 2022
doi: 10.3389/fncel.2021.831591

Application of New Materials in Auditory Disease Treatment

*Ming Li, Yurong Mu, Hua Cai, Han Wu and Yanyan Ding**

Department of Otorhinolaryngology, Union Hospital, Tongji Medical College, Huazhong University of Science and Technology, Wuhan, China

Auditory diseases are disabling public health problems that afflict a significant number of people worldwide, and they remain largely incurable until now. Driven by continuous innovation in the fields of chemistry, physics, and materials science, novel materials that can be applied to hearing diseases are constantly emerging. In contrast to conventional materials, new materials are easily accessible, inexpensive, non-invasive, with better acoustic therapy effects and weaker immune rejection after implantation. When new materials are used to treat auditory diseases, the wound healing, infection prevention, disease recurrence, hair cell regeneration, functional recovery, and other aspects have been significantly improved. Despite these advances, clinical success has been limited, largely due to issues regarding a lack of effectiveness and safety. With ever-developing scientific research, more novel materials will be facilitated into clinical use in the future.

Keywords: new materials, auditory diseases, conductive hearing loss, sensorineural hearing loss, therapy

OPEN ACCESS

Edited by:
Zuhong He,
Wuhan University, China

Reviewed by:
Fuping Qian,
Nantong University, China
Ling Lu,
Nanjing Drum Tower Hospital, China

***Correspondence:**
Yanyan Ding
dingyanyande@163.com

Specialty section:
This article was submitted to Cellular Neuropathology, a section of the journal Frontiers in Cellular Neuroscience

Received: *08 December 2021*
Accepted: *22 December 2021*
Published: *31 January 2022*

Citation:
Li M, Mu Y, Cai H, Wu H and Ding Y (2022) Application of New Materials in Auditory Disease Treatment. Front. Cell. Neurosci. 15:831591. doi: 10.3389/fncel.2021.831591

INTRODUCTION

According to the latest World Health Organization estimates, 466 million people around the world (over 5% of the world population) experience disabling hearing loss. By 2050, this number is projected to rise to approximately 900 million, and nearly 2.5 billion people are at risk of contracting auditory diseases (World Health Organization [WHO], 2021). The early detection, vaccination, accurate management, and timely treatment of auditory diseases can help improve clinical outcome. Nevertheless, therapeutic modalities and prevention strategies for the occurrence and development of auditory diseases are still limited currently. Hearing impairment caused by auditory diseases is categorized into three clinical types: conductive (CHL), sensorineural (SNHL), and mixed (MHL) hearing loss. CHL is known to result primarily from structural damage, blockage, and sclerosis of the outer and middle ear, eventually leading to aberrant signaling to the inner ear. Disruption of the inner ear, auditory nerve, central auditory nuclei, or cortex are classified as SNHL, with an elaborate pathology that includes loss of sensory hair cells, spiral ganglion neurons (SGNs), and stria vascularis cells in the inner ear, ultimately leading to the failure of auditory perception (Ma et al., 2019). The established therapy for patients suffering from conductive deafness focuses on middle-ear infection, otosclerosis, etc. Research on curative therapies for sensorineural hearing loss mainly focuses on the repair and regeneration of hair cells, stria vascularis, and nerve synapses.

The practical application of new materials is continuously undergoing considerable advancements, and substantial success has been achieved in some aspects. Whereas the new materials are being applied to treat auditory diseases, the abundant advances made in the fields of diabetes, cardiovascular disease, and neuromuscular disease using new materials are progressing. Recently, the Food and Drug Administration (FDA) approved the first RNA interference-based gene silencing technology drug—Patisiran—which regulates gene expression by the delivery of RNA to target cells, improving the prognosis of patients with rare cardiac and neurologic disease (Adams et al., 2018). For another example, with a fundamental role in the future repair or

replacement of tissues defects (Zakrzewski et al., 2019), stem cells differentiate into insulin-producing cells after being implanted into the body, bringing considerable improvements to the prognosis of type 1 diabetes (Shahjalal et al., 2018). Regarding to stem cell therapy, graphene, with remarkable biocompatible and bioadhesive properties, can be fabricated as scaffolds for the proliferation and direct differentiation of stem cells (Kenry Lee et al., 2018). Some scholars even propose stem cell engraftment as a highly feasible and fundamental curing method for sensorineural deafness (Nakagawa and Ito, 2005; Cheng et al., 2019). Many prostheses formed out of new materials were reported to induce fewer immune responses and had a better overall prognosis than conventional materials after implantation (Diken Turksayar et al., 2019; Nappi et al., 2021). This review will focus on the research progress of the novel materials employed for the treatment of CHL and SNHL (see **Figure 1**).

TREATMENT ORIENTATION OF HEARING LOSS

Hearing loss is attributable to genetic factors, specific viral infections, chronic ear infections, birth complications, exposure to excessive noise, aging, and ototoxic drugs. CHL may occur as middle-ear effusion, tympanic membrane perforation, physical external trauma, infection, canal stenosis, cholesteatoma, otitis media, otosclerosis, ossicular erosions, and so on (Ontario Health, 2020). At present, treatment for CHL primarily involves surgery and drugs. Primary research directions for novel therapies are focused on new pharmaceuticals, materials, artificial auditory implantation, and other aspects. The artificial auditory implantation comprises middle-ear implant (MEI) and implantable bone-conduction devices (Chen et al., 2014). The current widespread adoption of artificial auditory implantation includes bone-anchored hearing aids (BAHAs), subcutaneous bone bridges (BBs), vibrant sound bridges (VSBs), and semi-implantable middle-ear transducers. However, due to the pathway for bone conduction being more complex than air conduction, the following areas must be considered: percutaneous attenuation of high-frequency sound after the implantation of bone-conduction hearing aid devices; the susceptibility to infection of surgical sites after BAHA implantation; vibrator displacement after MEI implantation; ossicular necrosis; the wide fluctuation of postoperative gain, and so on. Therefore, further research aimed at bone-conduction audiology and more development of audiological assist devices are still required (Ghoncheh et al., 2016).

Diseases that could contribute to SNHL are age-related hearing loss (ARHL), inherited hearing impairments, Meniere's disease (endolymphatic hydrops), autoimmune inner-ear disease, ear infection, drug-induced deafness, ear trauma, and idiopathic SNHL (Merchant and Nadol, 2001; Kanzaki et al., 2020). In addressing sudden sensorineural hearing loss (SSNHL), current SSNHL management guidelines recommend glucocorticoids, psychotherapy, and intravenous agents that can improve microcirculation and neurotrophy, besides which numerous attempts for novel therapies have been reported. For instance, Vanwijck et al. (2019) summarized the efficacy of intratympanic injections of corticosteroids with a Silverstein tube to treat refractory SSNHL. They found that the topical application of corticosteroids with such a tube to the inner ear through the round window membrane can improve the hearing and clarity of patients who have failed in previous conventional therapies. However, therapies for SNHL remain clinically limited thus far, and the therapeutic effects remain less than satisfactory. Owing to the natural anatomical and physiological barriers of the cochlea, the supply and absorption of drugs reaching the targeting cochlea cells have been severely hindered (Zou et al., 2016; Yuan and Qi, 2018). An example is that the cochlea, surrounded by bones and located in a relatively closed environment, is difficult for drugs to access from the blood due to the presence of the blood labyrinth barrier (BLB). For local drug delivery to the cochlea, drug penetration through the oval window (OW) and round window membrane (RWM) becomes difficult due to their permselectivity. In addition, some of the drugs have a short half-life, and inter-individual differences in metabolism are marked, therefore limiting the benefits of drugs administered using traditional approaches.

In recent years, a range of new signaling pathways and genes playing essential roles in hair cell development and differentiation have been discovered that target therapies against SNHL (Diensthuber and Stover, 2018). For example, overexpressing Atoh1 can potentially reprogram supporting cells to become hair cells, subsequently promoting mammalian hair cell regeneration (Richardson and Atkinson, 2015). In cell cycle regulation, the absence of p27Kip1 drives the enhanced proliferation of supporting cells in adult mice, and inactivation of the retinoblastoma 1 (RB1) gene leads to the acquisition of newly generated hair cells originated from highly differentiated hair cells (Sage et al., 2005). For other signaling pathways, the activator of the Wnt signal pathway—β-catenin, the overexpression of which triggers Lgr5-positive cell growth and mitosis—elevates hair cell regeneration (Shi et al., 2013). When β-catenin and Atoh1 are co-expressed, the differentiation of Lg5-positive hair cells in neonatal mice is significantly advanced (Kuo et al., 2015). Furthermore, inhibition of the Notch pathway *via* γ-secretase inhibitors enables mice to regenerate hair cells in response to noise-induced damage, simultaneously gaining an improvement in their hearing level (Mizutari et al., 2013). Furthermore, there is crosstalk between Notch and Wnt signaling (Li et al., 2015; Ding et al., 2020). Hence, various predictions can be hypothesized based on these theories; that is, gene targets that can be selectively modulated using small molecules or related drugs might drive the regeneration of hair cells.

APPLICATION OF NOVEL MATERIALS IN HEARING LOSS

Treatment of New Materials in Conductive Hearing Loss

In auricle-related disorders, the microtia is a congenital craniofacial malformation, ranking only second to cleft lip

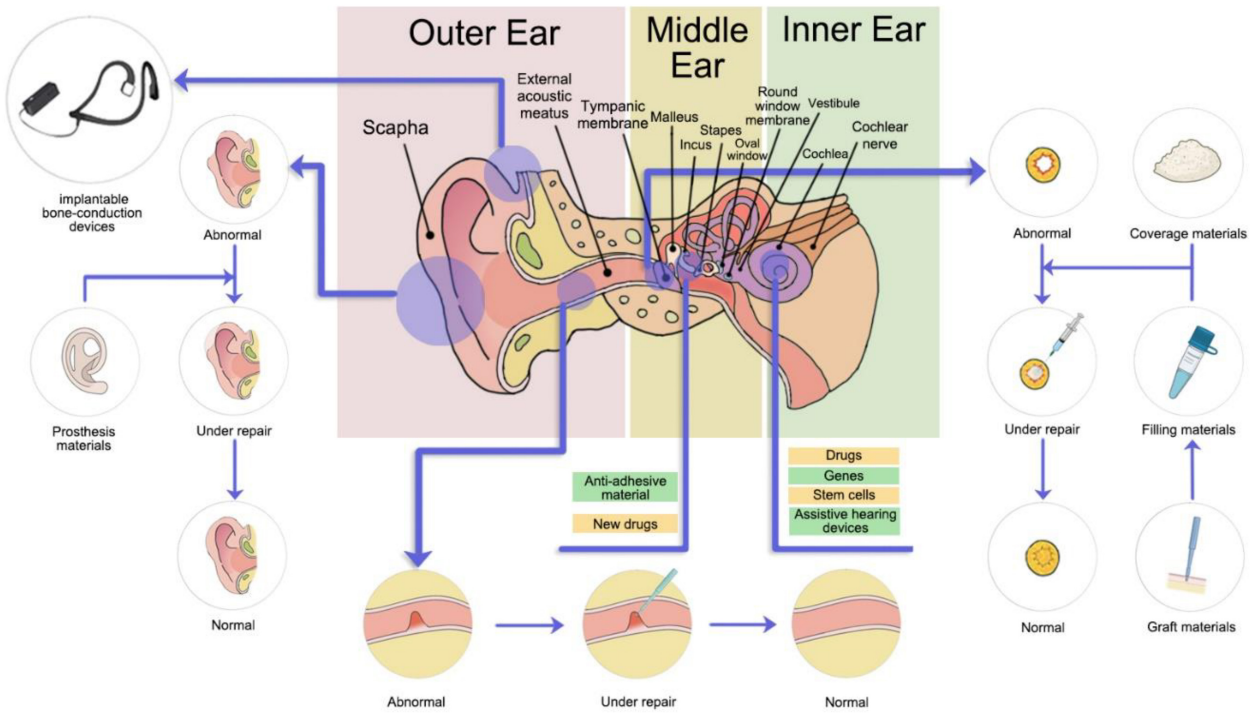

FIGURE 1 | Treatment sites of new materials for auditory diseases.

(Jiao and Zhang, 2001). Traditional healing strategies employ autologous cartilage as conventional grafts (Bichara et al., 2012). Shang et al. (2016) used 3D printing technology and medical silicone to fabricate an auricular scaffold, and they found the scaffolds were implanted *in vivo* smoothly, with excellent bio-compatibility, affordable cost, and a simple preparation process. Presently, besides adipose-derived stem cell (ADSC) application for cartilage regeneration, cartilage stem/progenitor cells (CSPCs) have also been used for the successful ear reconstruction and modeling the pathogenesis of auricular deformities (Zhou G. et al., 2018; Zucchelli et al., 2020).

In tympanic-associated disorders, tympanic membrane perforation (TMP) is a commonly seen disease in otorhinolaryngology. Although the preferred autograft materials, such as temporal muscle, cartilage, and fat, have a variety of applications, they have also been reported to be highly susceptible to infection and have pronounced dependence on nutrients from the surrounding tissue (Teh et al., 2013). Therefore, an increasing emphasis is being placed on new materials that can decrease the rate of inflammation, foster tympanic membrane regeneration, and enhance the proliferation and migration of the epithelium. The current methods for tympanic membrane repair combine autologous tissue and novel materials, the latter including platelet-rich plasma (PRP), platelet-rich fibrin (PRF), hyaluronic acid (HA), epidermal growth factor (EGF), and basic fibroblast growth factor (bFGF). Among them, PRP and PRF have gained particular interest because they are enriched in growth factors, which are effective in inducing tissue regeneration and with a lower prevalence of infections (Gur et al., 2016; Stavrakas et al., 2016; Huang et al., 2021). Moreover, a study by Lin et al. (2013) found that recombinant human epidermal growth factor (rhEGF) in conjunction with a gelatin-based sponge scaffold can remarkably enhance the wound healing rate of chronic TMP, reduce improvement time, further improve hearing level, and has no toxic side effects on inner-ear function. Similar multiple studies have been performed for combining new materials into clinical practice, and correspondingly, an increased likelihood of TMP healing has been reported (Gisselsson-Solen et al., 2020). For example, heparin-binding epidermal growth factor (EGF)-like growth factor (Santa Maria et al., 2015), EGF-released nanofibrous patches (Seonwoo et al., 2019b), bacterial cellulose (Mandour et al., 2019), chitosan patch scaffolds incorporated with insulin-like growth factor-binding protein 2 (Seonwoo et al., 2019a), and a fibroblast growth factor (FGF)-infiltrated gelatin sponge (Omae et al., 2017; Kanemaru et al., 2018) have been documented to accelerate tympanic membrane (TM) perforation healing. As a type of novel material, Maharajan et al. (2020) have also reported that mesenchymal stem cells (MSCs) are promising candidates for therapy to treat TMP. Either separate engraftment of multipotent MSCs or a combination of these cells with biological materials and growth factors (GFs) can achieve faster TMP healing *via* increasing the activation of epidermal stem cell markers and stimulating the proliferation and migration of keratinocytes. MSCs, scaffolds, and GFs have a synergistic role in TM regeneration. The recent advancement of 3D- and 4D-printing technology has driven the development of a precise MSC-attached scaffold designed for the physical structure of patients. The direction of

physical and chemical engineering may be incorporated in this advancement, further boosting the degree and rate of the target tissue regeneration (Maharajan et al., 2020). The introduction of a cobalt-chromium (Co-Cr) coronary stent into the eustachian tube potentiates middle-ear ventilation, as validated in sheep (Pohl et al., 2018). A new class of tympanostomy stent made of nickel and titanium with a TiO2 coating has previously been shown to reduce *Pseudomonas aeruginosa* biofilm formation, resulting in a lower incidence of postoperative complications, such as deafness and catheter blockage after tympanotomy tube insertion (Joe and Seo, 2018).

Tympanoplasty exerts significant actions on the treatment of auditory diseases such as chronic otitis mastoidea, tympanosclerosis, cholesteatomatous chronic otitis media, and middle-ear sound transmission defect caused by trauma. Adhesive otitis patients often require surgical interventions when they present with concomitant middle-ear atelectasis, structural adhesion in the tympanic chamber, sound transmission disorder, recurrent infection, and persistent otorrhea (Larem et al., 2016). To avoid postoperative adhesion and to clean effusion, the filler materials are required for adhesion prevention after removal of tympanic sclerotic foci and middle-ear blockage caused by pathological factors; these materials can be divided into two categories: absorbable and non-absorbable. The most recent anti-adhesive materials include chitosan hydrogel within absorbable materials (Unsaler et al., 2016) and natural polymeric biomaterials–Naso Pore (Huang et al., 2011). These two ingredients are otherwise used for nasal surgery and are of low ototoxicity, inflammatory response, and have strong anti-adhesion effects (Chen and Li, 2020). In the medical management of middle-ear cholesteatoma, traditional surgery combined with novel materials has been found to have superior efficacy. For mastoid postoperative tamponade, synthetic materials have clear advantages of easy accessibility, short procedure time, being less prone to contamination and so on, compared with traditional autologous materials, which are less accessible and unstable. Common filling synthetic materials in mastoid disorders include bioactive glass, hydroxyapatite, titanium, and silicon, with bioactive glass being most frequently used (Lee H. B. et al., 2013; Sorour et al., 2018). Tympanoplasty necessitates the use of transplanted materials, but classically employed autogenous materials are with high risk of shift, complete absorption, and residual cholesteatoma. Bartel et al. (2018) determined that total (TORP) and partial (PORP) ossicular replacement prostheses can be biosynthesized and are stiff, safe, and stable. Compared with traditional materials, the hearing improvement after ossicular chain reconstruction is almost equivalent to using biosynthesizing materials, and the curative effect of myringoplasty is even superior to that of traditional autologous grafting materials (Bartel et al., 2018; Li et al., 2021).

The ear is one of the predilection sites for keloids, frequently following trauma, surgery, burns, and ear piercing. Due to the high rate of recurrence, the search for excellent postoperative coverage materials and preventing recurrence has become a particular research hotspot in the treatment of keloids (Du and Zhu, 2015). Park et al. proposed that employing hydrocolloid dressing as a wound coverage and pressurizing with a magnet during the early postoperative period, compared with traditional dressings used to cover wounds, could protect the wound tissue, facilitate the healing process, and reduce the water content inside the wound tissue (Park and Chang, 2013). Besides, more coverage materials to promote wound healing and reduce inflammation will become available in the coming years. For patients with CHL but normal hearing function of the inner ear, other assistive hearing devices are increasingly promising in addition to the aforementioned BAHA, BB, vibrant sound-bridge (VSB), and middle-ear transducers, such as ADHEAR–a new non-invasive bone-conduction hearing-assistive device, which uses a cohesive adaptor affixed to the skin surface behind the ear and applies no pressure to the skin (Brill et al., 2019).

Treatment of New Materials in Sensorineural Hearing Loss

The loss of outer hair cells and spiral ganglion cell degeneration are major causes of sensorineural hearing loss (Wong and Ryan, 2015). The loss of hair cells, spiral ganglion cells, and auditory nerve fibers in the adult ear is irreversible, leading to permanent SNHL. The surgical implantation of a cochlear implant (CI) is envisaged as one of means to restore hearing, but the function of artificial cochlea is highly reliant on residue numbers of spiral ganglion cells. A recent study has found that superparamagnetic iron oxide (SPIO) nanoparticles can direct spiral ganglion neurites to orient to a CI electrode under the application of magnetic field modulation and maintain the survival of SGNs, producing a positive CI treatment effect (Hu et al., 2021). Various other *in vitro* experiments have newly demonstrated that the cGMP-dependent atrial natriuretic peptide (ANP) and the permissive environment created by novel silicon micro-pillar substrates (MPS) could facilitate the survival and growth of SGNs (Mattotti et al., 2015; Sun et al., 2020). Through *in vivo* experiments, mesenchymal stem cells (Maharajan et al., 2021), valproic acid (VPA; 2-propylpentanoic acid) with growth factors (Wakizono et al., 2021), as well as neural stem cells (He et al., 2021) have been found to be beneficial for SGN growth.

Additionally, to achieve more SGNs and hair cell regeneration, researchers have been studying drug delivery systems (DDSs), gene therapy, and cell therapy from different perspectives (Ma et al., 2019) (see **Figure 2**).

The clinical advancement of DDS has been hindered by a short biological half-life, poor pharmacokinetics, and low permeability through the biological barriers of nerve growth factor (NGF). Hence, developing highly efficient and inexpensive materials is of substantial importance (Bartus, 2012; Khalin et al., 2015). Currently, the nanotechnology-based ongoing development of novel NGF delivery systems covers nanogels, hydrogels, micelles, microspheres, electrospun nanofibers, nanoparticles, and supraparticles. NGF could be immobilized in nanomaterials *via* physical trapping, adsorption, or electrostatic interactions, then the sustained release can be obtained using diffusion of NGF and/or degradation of carriers, with the aim of local, sustained drug release (Ma et al., 2019). One such nanoscaled drug delivery system could be used in targeted drug delivery. By constructing degradable and non-toxic nanoparticle loading

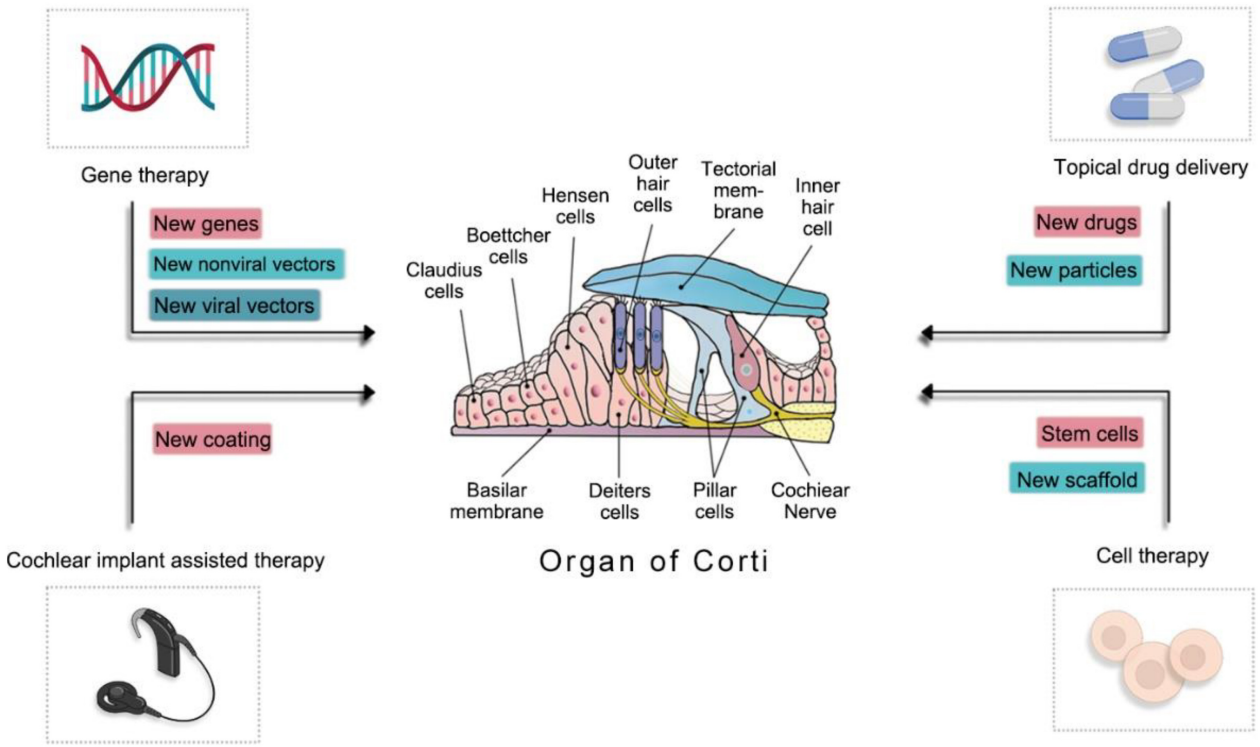

FIGURE 2 | The mechanism of novel materials involved in inner-ear regeneration.

drugs, ligands for the specific recognition and delivery into targeted organs or tissues, nanoscaled drug delivery systems show the stability and property of sustained release (Ding et al., 2019; An and Zha, 2020). Moreover, supraparticles have increased volume in comparison to nano-onions, which have yet to be fully translated into clinical practice. The supraparticles have a larger capacity for the delivery of drugs and provide sustained drug release, concurrently spreading to particular targeted areas (Ma et al., 2018). However, several challenges persist for the clinical application of nanoparticle drug delivery systems, such as drug delivery risk assessments through the RWM or OW routes and the implementation of controlled release and targeted nano-drug delivery. For example, intratympanic medication injection or nanoparticle delivery may access the inner ear more through the RWM approach (Du et al., 2013; Liu et al., 2013), but OW shows higher permeability than RWM (King et al., 2011, 2013; Zou et al., 2012). Chen et al. also found similar results in that fluorescence traceable chitosan nanoparticles (CS-NPs) were more quickly transported into the inner ear through OW, with less damage exhibited (Ding et al., 2019), but further validation regarding nanomaterials and loaded drugs for optimum routes of delivery is still necessary. In gene therapy, the introgressed gene in the inner ear typically involves the basic helix-loop-helix (bHLH) family transcription factor (Shou et al., 2003) as well as neurotrophic (Sun et al., 2011), anti-apoptotic (Chan et al., 2007; Pfannenstiel et al., 2009), antioxidant (Kawamoto et al., 2004), connexin (Birkenhager et al., 2006; Sun et al., 2009), cochlear protein-related, interleukin, and other (Zhuo et al., 2008) genes. To cross the BBB and blood labyrinth barrier successfully and transfer functional genes into the mammalian inner ear, both viral and non-viral vectors are the most common tools for transgene delivery. Viral vectors consist of adenovirus (AV), adeno-associated virus (AAV), herpes simplex virus type I, vaccinia virus, and so on. Non-viral vectors can be categorized into liposomes, cationic polymers, peptide-based nanoparticles, and other synthetic vectors (Sun and Wu, 2013). Other vectors, such as viral and non-viral composite carriers, as well as bacterial vectors, are being studied (Akin et al., 2007). AAV2/Anc80L65, a recently discovered synthetic viral vector, targets the inner and outer hair cells of the cochlea with high efficiency and elicits only a weak immune response when compared to other viral vectors with low transfection ability (Zinn et al., 2015). Tan et al. designed a variant of AAV—AAV-inner ear (AAV-ie). The variant not only achieved 90% successful transfection to supporting cells but also expanded the number of mice hair cells *via* carrying the Atoh1 gene, which did not affect the numbers of hair cells or hearing level (Tan et al., 2019). MicroRNA regulates gene expression *in vivo* by means of inhibiting protein translation and promoting mRNA degradation, the primary function of which is to play a suppressor role post-transcriptionally (Wu et al., 2020). Luo et al. constructed MicroRNA-146a (miR-146a) lentiviral recombinant vectors and found that miR-146a could significantly mitigate inflammatory injury and auditory dysfunctions of the inner ear after being injected into the inner ear through the scala tympani (Luo et al., 2016). A single microRNA can regulate hundreds of different transcription processes, by which the

regeneration of damaged hair cells in the inner ear and treating hearing loss are major focuses of much recent research (Zhou W. et al., 2018). Autoimmune inner ear disease (AIED) is an independent disorder, the main clinical manifestation of which is bilateral, rapidly progressive sensorineural hearing loss. Distinct from conventional systemic glucocorticoid treatment, Cai et al. injected adenoviral-mediated interleukin-10 (IL-10) through the RWM. The authors found that adenoviral carrying IL-10 can be imported into the inner ear of guinea pigs and express the gene products, consequently attenuating inflammatory injury and impairment in the auditory function of the inner ear to some extent (Cai and Tan, 2015). Therapies for sensorineural hearing loss by replacement of damaged or lost cells and secreting neurotrophic factors, cytokines, immunoregulatory protein, etc., with the transplanted cells hold promise in a wide variety of fields (Mehrabani et al., 2016; Kanzaki, 2018). Mesenchymal (MSCs), embryonic (ESCs), and induced pluripotent (iPSCs) stem cells are the most frequently used sources for regenerative medicine in the field of otology. Nevertheless, in contrast, the potential tumorigenicity and immune rejection response caused by ESCs and iPSCs, MSCs have a higher safety profile, anti-apoptotic properties, and characteristics of easy amplification; hence, MSCs have become a particular focus of regenerative medicine research (Kaboodkhani et al., 2021). The application of MSCs promotes BDNF secretion and increases the expression of connexin26 and connexin30, contributing to the alleviation of inflammation, oxidative stress, and apoptosis, the recovery of cell-cell junctions, an increased number of SGNs differentiated into neural progenitor cells and specific lineages of neurons, and significantly decreased hearing threshold and improved audial function (Matsuoka et al., 2007; Jang et al., 2015; Young et al., 2018; Mittal et al., 2020). In regenerative medicine, scaffolds are essential for cell growth and could provide a three-dimensional structure for cell differentiation and migration to restore the normal function of damaged organs (Khodakaram-Tafti et al., 2017). The preparation of scaffolds can be accomplished with various source materials, including decellularizing tissue (Hashemi et al., 2018), 3D printing technologies (Wang and Yang, 2021), tailored hydrogels (Slaughter et al., 2009), and electrospinning (Malik et al., 2021). Recent studies have used biological scaffolds comprising 3D graphene and artificial photonic crystals for stem cell culture. Scaffolds mimicking the microenvironment of cell growth *in vivo* can positively regulate stem cell growth, proliferation, and differentiation (Yang et al., 2013; Ankam et al., 2015; Fang et al., 2019). Other novel materials yielding similarly supportive effects for stem cells include 3D polydopamine-functionalized carbon microfibrous scaffolds (Yang et al., 2020), $Ti_3C_2T_x$Mxene membranes (Guo et al., 2020), microfluidic chip platforms (Park et al., 2014), and anisotropy inverse opals (Pettinato et al., 2015). Suggested mechanisms of the aforementioned materials include the promotion of cell growth, expansion, development and cell-cell adhesion, alignment, and connection.

In terms of hearing ancillary equipment, the application of CI for bilateral severe-to-profound SNHL has also reached maturity. However, implantation surgery can potentially cause invasive damage. Recent studies have increasingly found that degradable cell coatings for CI electrodes can increase neuronal survival by persistently releasing BDNF from cell-coated surfaces (Richardson et al., 2009). In addition, the local delivery of dexamethasone into the inner ear or coating *Cis* with dexamethasone during cochlear implantation may alleviate inflammation in the surgical sites (Farhadi et al., 2013; Lee J. et al., 2013).

OTHER NOVEL MATERIALS FOR TREATING AUDITORY-RELATED CONDITIONS

The control of tinnitus by external noise stimuli has become a therapy of particular interest. Tinnitus afflicts approximately 15% of the general population worldwide, and there is currently no cure for this disorder. Attempts have been made to ameliorate tinnitus with individually applied spectrally optimized near-threshold noise (Schilling et al., 2021), with most patients stating that subjective tinnitus loudness was suppressed during the noise stimulation.

The discovery of novel pharmaceuticals is one of the important directions for future research. Today, drug candidates with potential therapeutic applications for hearing loss include antioxidants, regulators of mitochondrial function, ion channel modulators, hair-cell protectants, and anti-inflammatory drugs (Ji et al., 2021). Other potentially effective drugs that have been experimentally validated are N-acetylcysteine (NAC) (Marie et al., 2018), melatonin (Serra et al., 2020), resveratrol (Xiong et al., 2015), mineralocorticoid aldosterone (ALD) (Campos-Banales et al., 2015; Halonen et al., 2016), teprenone (GGA) (Mikuriya et al., 2008), aspirin (Verschuur et al., 2014), and salicylic acid (Li et al., 2020) et al. One example is age-related hearing loss (ARHL); SAMP8 mice models demonstrated notably decreased auditory brainstem response (ABR) thresholds, increased distortion product otoacoustic emission (DPOAE) amplitudes, and memory improvement after the administration of NAC, suggesting that NAC has protective effects on hair cells and neurons of the central nervous system (CNS) (Li et al., 2020). Some systemic diseases are accompanied by damage to the inner ear, such as the microvascular and nerve damage caused by long-term diabetes, further leading to neurovascular injury in the cochlear. Gao et al. (2018) found resveratrol to be effective in preventing cell apoptosis and reducing diabetes damage to the inner ear by hypoglycemic activities, anti-dyslipidemic effects, and inhibiting anti-oxidative stress, ICAM-1, and VEGF expression. GGA was found to up-regulate heat-shock proteins (HSPs), and many experimental studies have demonstrated the protective effect of HSPs against cochlear damage induced by noise exposure, ototoxic drugs, and heat stress. In addition, a decline of ABR thresholds was observed in presbycusis mice (Mikuriya et al., 2008). ARHL models of DBA/2J mice were given injections of 200 mg/kg salicylic acid, and the expression of prestin, hair-cell survival, and function of the cochlea were significantly better than in saline-treated controls (Li et al., 2020). However, although antioxidants, such as resveratrol, ferulic acid (Fetoni et al., 2010), and glutathione

(Ohinata et al., 2000) are currently under active research, Sha Suhua et al. expressed caution that long-term or excessive intake of exogenous antioxidants or vitamin supplements is not only hazardous to hearing but also increases the risk of developing cancer (Sha and Schacht, 2017). Additionally, Kashio et al. (2009) and Polanski et al. identified that various antioxidants such as Ginkgo biloba extract (GBE), alpha-lipoic acid (AL), and vitamins A, E, and C do not result in hearing improvement (Polanski and Cruz, 2013). For other novel agents, bioactive peptides from Rapana venosa were found to exert an antioxidant effect, as demonstrated *via* the diminishing hair-cell uptake of gentamicin, activating Nrf2-Kcap1-ARE, up-regulation of Nrf2, and the expression of related antioxidant genes without damaging mechanoelectrical transduction channels (Yan, 2021). It has been suggested that rapamycin can slow the onset of ARHL through the inhibition of mTORC1 hyperactivation (Fu et al., 2018). Multiple previous studies have also shown that rapamycin reduces cisplatin- and gentamicin-induced nephrotoxicity (Fang and Xiao, 2014; Ebnoether et al., 2017) and alleviates noise-induced hearing loss (NIHL) by reducing oxidative stress (Yuan et al., 2015). However, rapamycin has many side effects as an immunosuppressant. New drugs can simulate the antioxidant activity of rapamycin with fewer side effects, and such classes of drugs are currently undergoing clinical experimentation. Traditional herbal medicines have been used in China for thousands of years. However, to date, the efficacy of these medicines has yet to be confirmed, and their action mechanisms remain unclear. Modern pharmacological studies have also spurred intense research programs targeting the auditory diseases. For instance, Xuan et al. (2018) demonstrated that composite Jianer formulations, mainly consisting of Puerariae Lobatae Radix (Gegen in Chinese), Scutellariae Radix (Huangqin in Chinese), and Salvia miltiorrhiza (Danshen in Chinese), reduced the level of malondialdehyde (MDA), the main product of lipid peroxidation, to exhibit an antioxidant effect in adult mice. Besides, the composite Jianer formulations ameliorated mtDNA damage and the release of Cyt-c, thereby attenuating caspase-mediated apoptosis through the mitochondrial pathway and playing a protective role against age-related decline in hair cells and spiral ganglion neurons. Furthermore, traditional Chinese herbal medicine (TCHM) seems to be associated with few adverse effects (Xuan et al., 2018). Another active ingredient extracted from traditional Chinese medicine Flos puerariae (Gehua in Chinese)—total flavonoids of Pueraria lobata—has been found to suppress the inflammatory response. The total flavonoids of Pueraria lobata reduce isoprenaline-induced damage to the inner ear of the rat *via* inhibiting the expression of TNF-α, IL-4, and Bax and up-regulating ACTH proteins, at the same time regulating auditory system homeostasis and improving the microvasculature circulation of the inner ear and the ischemia conditions of tissue cells in rats (Zhao and Liang, 2018). Thus, TCHM has substantial potential for treating auditory diseases. The development of new classes of novel antibiotics is valuable for the treatment of hearing loss. For example, for severe chronic suppurative otitis media, new antibiotics are required for effective anti-infectious therapeutics owing to the constant emergence of drug-resistant bacteria. A kind of new cephalosporin— "ceftolozane-tazobactam"—has particularly good therapeutic benefits for moderate to severe suppurative otitis media caused by multidrug- and extensively drug-resistant (MDR and XDR) *P. aeruginosa* (Saraca et al., 2019).

This study has highlighted some bottlenecks in the application of therapeutic materials for auditory diseases, such as the tumorigenicity of repair-promoting substances, immune reaction to implanted materials, high cost, and a difficult fabrication process. More research combining materials science, basic medicine, and clinical medicine is required to address these bottlenecks, with the aim of obtaining more cost-effective and safer new materials for treating hearing loss.

CONCLUSION

Presently, various deficiencies still exist regarding insufficient treatment options and their modest efficacy for auditory diseases, leading to CHL and SNHL. Nevertheless, the development and application of novel materials are gradually improving the condition. The novel materials are able to hasten perforated tympanic membrane healing, tympanoplasty of the middle ear, and repair of the microtia, as well as promote the regeneration of inner hair cells, spiral ganglion cells, and the synaptic ribbons, decrease inflammation level, and modify hearing level adjunctively. Although the efficacy and safety of novel materials in clinical application remain to be verified, with more progression of research and substantial technological innovation, these novel materials will be continuously improved, and more refined materials could be employed to treat hearing loss clinically.

AUTHOR CONTRIBUTIONS

ML conceived and wrote the manuscript. YD modified the manuscript. All authors contributed to the article and approved the submitted version.

FUNDING

This work was supported by grants from Science Foundation of Union Hospital (2021XHYN113).

ACKNOWLEDGMENTS

The authors thank Yang Zhang for his assistance in the preparation of all figures.

REFERENCES

Adams, D., Gonzalez-Duarte, A., O'Riordan, W. D., Yang, C. C., Ueda, M., Kristen, A. V., et al. (2018). Patisiran, an RNAi therapeutic, for hereditary transthyretin amyloidosis. *N. Engl. J. Med.* 379, 11–21. doi: 10.1056/NEJMoa1716153

Akin, D., Sturgis, J., Ragheb, K., Sherman, D., Burkholder, K., Robinson, J. P., et al. (2007). Bacteria-mediated delivery of nanoparticles and cargo into cells. *Nat. Nanotechnol.* 2, 441–449. doi: 10.1038/nnano.2007.149

An, X., and Zha, D. (2020). Advances in research on nanoparticle delivery systems for inner ear targeted drug delivery and therapy. *Chin. J. Otol.* 18, 409–413.

Ankam, S., Lim, C. K., and Yim, E. K. (2015). Actomyosin contractility plays a role in MAP2 expression during nanotopography-directed neuronal differentiation of human embryonic stem cells. *Biomaterials* 47, 20–28. doi: 10.1016/j.biomaterials.2015.01.003

Bartel, R., Cruellas, F., Hamdan, M., Gonzalez-Compta, X., Cisa, E., Domenech, I., et al. (2018). Hearing results after type III tympanoplasty: incus transposition versus PORP. A systematic review. *Acta Otolaryngol.* 138, 617–620. doi: 10.1080/00016489.2018.1425901

Bartus, R. T. (2012). Translating the therapeutic potential of neurotrophic factors to clinical 'proof of concept': a personal saga achieving a career-long quest. *Neurobiol. Dis.* 48, 153–178. doi: 10.1016/j.nbd.2012.04.004

Bichara, D. A., O'Sullivan, N. A., Pomerantseva, I., Zhao, X., Sundback, C. A., Vacanti, J. P., et al. (2012). The tissue-engineered auricle: past, present, and future. *Tissue Eng. Part B Rev.* 18, 51–61. doi: 10.1089/ten.TEB.2011.0326

Birkenhager, R., Zimmer, A. J., Maier, W., and Schipper, J. (2006). [Pseudodominants of two recessive connexin mutations in non-syndromic sensorineural hearing loss?]. *Laryngorhinootologie* 85, 191–196. doi: 10.1055/s-2005-870302

Brill, I. T., Brill, S., and Stark, T. (2019). [New options for rehabilitation of conductive hearing loss: tests on normal-hearing subjects with simulated hearing loss]. *HNO* 67, 698–705. doi: 10.1007/s00106-019-0685-8

Cai, W., and Tan, W. (2015). Adenovirus-mediated IL-10 gene for the treatment of autoimmune inner ear disease——an experimental study. *J. Audiol. Speech Pathol.* 23, 602–606.

Campos-Banales, E. M., Lopez-Campos, D., de Serdio-Arias, J. L., Esteban-Rodriguez, J., Garcia-Sainz, M., Munoz-Cortes, A., et al. (2015). [A comparative study on efficacy of glucocorticoids, mineralocorticoids and vasoactive drugs on reversing hearing loss in patients suffering idiopathic sensorineural cochlear hypoacusis. A preliminary clinical trial]. *Acta Otorrinolaringol. Esp.* 66, 65–73. doi: 10.1016/j.otorri.2014.05.008

Chan, D. K., Lieberman, D. M., Musatov, S., Goldfein, J. A., Selesnick, S. H., and Kaplitt, M. G. (2007). Protection against cisplatin-induced ototoxicity by adeno-associated virus-mediated delivery of the X-linked inhibitor of apoptosis protein is not dependent on caspase inhibition. *Otol. Neurotol.* 28, 417–425. doi: 10.1097/01.mao.0000247826.28893.7a

Chen, K., Dai, P., Yang, L., and Zhang, T. (2014). Progress in middle ear implants. *Progr.Biomed. Eng.* 35, 23–27.

Chen, M., and Li, S. (2020). Advances in diagnosis and treatment of adhesive otitis media. *Chin. J. Ophthalmol. Otorhinolaryngol.* 20, 493–497.

Cheng, C., Wang, Y., Guo, L., Lu, X., Zhu, W., Muhammad, W., et al. (2019). Age-related transcriptome changes in Sox2+ supporting cells in the mouse cochlea. *Stem Cell Res. Ther.* 10:365. doi: 10.1186/s13287-019-1437-0

Diensthuber, M., and Stover, T. (2018). Strategies for a regenerative therapy of hearing loss. *HNO* 66(Suppl. 1), 39–46. doi: 10.1007/s00106-017-0467-0

Diken Turksayar, A. A., Saglam, S. A., and Bulut, A. C. (2019). Retention systems used in maxillofacial prostheses: a review. *Niger. J. Clin. Pract.* 22, 1629–1634. doi: 10.4103/njcp.njcp_92_19

Ding, S., Xie, S., Chen, W., Wen, L., Wang, J., Yang, F., et al. (2019). Is oval window transport a royal gate for nanoparticle delivery to vestibule in the inner ear? *Eur. J. Pharm. Sci.* 126, 11–22. doi: 10.1016/j.ejps.2018.02.031

Ding, Y., Meng, W., Kong, W., He, Z., and Chai, R. (2020). The role of FoxG1 in the inner ear. *Front. Cell. Dev. Biol.* 8:614954. doi: 10.3389/fcell.2020.614954

Du, G., and Zhu, J. (2015). Ear keloid and clinical research progress. *J. Clin. Otorhinolaryngol. Head Neck Surg. (China)* 29, 770–772.

Du, X., Chen, K., Kuriyavar, S., Kopke, R. D., Grady, B. P., Bourne, D. H., et al. (2013). Magnetic targeted delivery of dexamethasone acetate across the round window membrane in guinea pigs. *Otol. Neurotol.* 34, 41–47. doi: 10.1097/MAO.0b013e318277a40e

Ebnoether, E., Ramseier, A., Cortada, M., Bodmer, D., and Levano-Huaman, S. (2017). Sesn2 gene ablation enhances susceptibility to gentamicin-induced hair cell death *via* modulation of AMPK/mTOR signaling. *Cell Death Discov.* 3:17024. doi: 10.1038/cddiscovery.2017.24

Fang, B., and Xiao, H. (2014). Rapamycin alleviates cisplatin-induced ototoxicity in vivo. *Biochem. Biophys. Res. Commun.* 448, 443–447. doi: 10.1016/j.bbrc.2014.04.123

Fang, Q., Zhang, Y., Chen, X., Li, H., Cheng, L., Zhu, W., et al. (2019). Three-dimensional graphene enhances neural stem cell proliferation through metabolic regulation. *Front. Bioeng. Biotechnol.* 7:436. doi: 10.3389/fbioe.2019.00436

Farhadi, M., Jalessi, M., Salehian, P., Ghavi, F. F., Emamjomeh, H., Mirzadeh, H., et al. (2013). Dexamethasone eluting cochlear implant: histological study in animal model. *Cochlear Implants Int.* 14, 45–50. doi: 10.1179/1754762811Y.0000000024

Fetoni, A. R., Mancuso, C., Eramo, S. L., Ralli, M., Piacentini, R., Barone, E., et al. (2010). In vivo protective effect of ferulic acid against noise-induced hearing loss in the guinea-pig. *Neuroscience* 169, 1575–1588. doi: 10.1016/j.neuroscience.2010.06.022

Fu, X., Sun, X., Zhang, L., Jin, Y., Chai, R., Yang, L., et al. (2018). Tuberous sclerosis complex-mediated mTORC1 overactivation promotes age-related hearing loss. *J. Clin. Invest.* 128, 4938–4955. doi: 10.1172/JCI98058

Gao, H., Qu, Y., Zhang, X., Mu, J., Zhang, P., Wang, X., et al. (2018). The protective effects and its mechanisms of resveratrol on inner ear damage in diabetes rats. *J. Audiol. Speech Pathol.* 29, 409–413.

Ghoncheh, M., Lilli, G., Lenarz, T., and Maier, H. (2016). Outer ear canal sound pressure and bone vibration measurement in SSD and CHL patients using a transcutaneous bone conduction instrument. *Hear. Res.* 340, 161–168. doi: 10.1016/j.heares.2015.12.019

Gisselsson-Solen, M., Tahtinen, P. A., Ryan, A. F., Mulay, A., Kariya, S., Schilder, A. G. M., et al. (2020). Panel 1: biotechnology, biomedical engineering and new models of otitis media. *Int. J. Pediatr. Otorhinolaryngol.* 130(Suppl. 1):109833. doi: 10.1016/j.ijporl.2019.109833

Guo, R., Xiao, M., Zhao, W., Zhou, S., Hu, Y., Liao, M., et al. (2020). 2D Ti3C2TxMXene couples electrical stimulation to promote proliferation and neural differentiation of neural stem cells. *Acta Biomater.* S1742-7061, 30749–30752. doi: 10.1016/j.actbio.2020.12.035

Gur, O. E., Ensari, N., Ozturk, M. T., Boztepe, O. F., Gun, T., Selcuk, O. T., et al. (2016). Use of a platelet-rich fibrin membrane to repair traumatic tympanic membrane perforations: a comparative study. *Acta Otolaryngol.* 136, 1017–1023. doi: 10.1080/00016489.2016.1183042

Halonen, J., Hinton, A. S., Frisina, R. D., Ding, B., Zhu, X., and Walton, J. P. (2016). Long-term treatment with aldosterone slows the progression of age-related hearing loss. *Hear. Res.* 336, 63–71. doi: 10.1016/j.heares.2016.05.001

Hashemi, S. S., Jowkar, S., Mahmoodi, M., Rafati, A. R., Mehrabani, D., Zarei, M., et al. (2018). Biochemical methods in production of three-dimensional scaffolds from human skin: a window in aesthetic surgery. *World J. Plast. Surg.* 7, 204–211.

He, Z., Ding, Y., Mu, Y., Xu, X., Kong, W., Chai, R., et al. (2021). Stem cell-based therapies in hearing loss. *Front. Cell. Dev. Biol.* 9:730042. doi: 10.3389/fcell.2021.730042

Hu, Y., Li, D., Wei, H., Zhou, S., Chen, W., Yan, X., et al. (2021). Neurite extension and orientation of spiral ganglion neurons can be directed by superparamagnetic iron oxide nanoparticles in a magnetic field. *Int. J. Nanomed.* 16, 4515–4526. doi: 10.2147/IJN.S313673

Huang, G., Chen, X., and Jiang, H. (2011). Effects of NasoPore packing in the middle ear cavity of the guinea pig. *Otolaryngol. Head Neck Surg.* 145, 131–136. doi: 10.1177/0194599811400834

Huang, J., Yuan, Z., Hu, S., Lv, C., Hu, Y., and Shen, Y. (2021). The effectiveness and research progress of platelet-rich concentrate products in tympanic membrane perforation. *Chin. J. Cell Biol.* 43, 1700–1704.

Jang, S., Cho, H. H., Kim, S. H., Lee, K. H., Jun, J. Y., Park, J. S., et al. (2015). Neural-induced human mesenchymal stem cells promote cochlear cell regeneration in

deaf Guinea pigs. *Clin. Exp. Otorhinolaryngol.* 8, 83–91. doi: 10.3342/ceo.2015.8.2.83

Ji, L., Shen, Q., and Zhao, L. (2021). Progress in treatment of presbycusis. *J. Otol.* 19, 662–665.

Jiao, T., and Zhang, F. (2001). The present situation of auricular prostheses. *Chin. J. Dent. Mater. Devices* 10, 213–215.

Joe, H., and Seo, Y. J. (2018). A newly designed tympanostomy stent with TiO2 coating to reduce *Pseudomonas aeruginosa* biofilm formation. *J. Biomater. Appl.* 33, 599–605. doi: 10.1177/0885328218802103

Kaboodkhani, R., Mehrabani, D., and Karimi-Busheri, F. (2021). Achievements and challenges in transplantation of mesenchymal stem cells in otorhinolaryngology. *J. Clin. Med.* 10:2940. doi: 10.3390/jcm10132940

Kanemaru, S. I., Kanai, R., Yoshida, M., Kitada, Y., Omae, K., and Hirano, S. (2018). Application of regenerative treatment for tympanic membrane perforation with cholesteatoma, tumor, or severe calcification. *Otol. Neurotol.* 39, 438–444. doi: 10.1097/MAO.0000000000001701

Kanzaki, S. (2018). Gene delivery into the inner ear and its clinical implications for hearing and balance. *Molecules* 23:2507. doi: 10.3390/molecules23102507

Kanzaki, S., Toyoda, M., Umezawa, A., and Ogawa, K. (2020). Application of mesenchymal stem cell therapy and inner ear regeneration for hearing loss: a review. *Int. J. Mol. Sci.* 21:5764. doi: 10.3390/ijms21165764

Kashio, A., Amano, A., Kondo, Y., Sakamoto, T., Iwamura, H., Suzuki, M., et al. (2009). Effect of vitamin C depletion on age-related hearing loss in SMP30/GNL knockout mice. *Biochem. Biophys. Res. Commun.* 390, 394–398. doi: 10.1016/j.bbrc.2009.09.003

Kawamoto, K., Sha, S. H., Minoda, R., Izumikawa, M., Kuriyama, H., Schacht, J., et al. (2004). Antioxidant gene therapy can protect hearing and hair cells from ototoxicity. *Mol. Ther.* 9, 173–181. doi: 10.1016/j.ymthe.2003.11.020

Kenry, Lee, W. C., Loh, K. P., and Lim, C. T. (2018). When stem cells meet graphene: opportunities and challenges in regenerative medicine. *Biomaterials* 155, 236–250. doi: 10.1016/j.biomaterials.2017.10.004

Khalin, I., Alyautdin, R., Kocherga, G., and Bakar, M. A. (2015). Targeted delivery of brain-derived neurotrophic factor for the treatment of blindness and deafness. *Int. J. Nanomedicine.* 10, 3245–3267. doi: 10.2147/IJN.S77480

Khodakaram-Tafti, A., Mehrabani, D., and Shaterzadeh-Yazdi, H. (2017). An overview on autologous fibrin glue in bone tissue engineering of maxillofacial surgery. *Dent. Res. J. (Isfahan)* 14, 79–86.

King, E. B., Salt, A. N., Eastwood, H. T., and O'Leary, S. J. (2011). Direct entry of gadolinium into the vestibule following intratympanic applications in Guinea pigs and the influence of cochlear implantation. *J. Assoc. Res. Otolaryngol.* 12, 741–751. doi: 10.1007/s10162-011-0280-5

King, E. B., Salt, A. N., Kel, G. E., Eastwood, H. T., and O'Leary, S. J. (2013). Gentamicin administration on the stapes footplate causes greater hearing loss and vestibulotoxicity than round window administration in guinea pigs. *Hear. Res.* 304, 159–166. doi: 10.1016/j.heares.2013.07.013

Kuo, B. R., Baldwin, E. M., Layman, W. S., Taketo, M. M., and Zuo, J. (2015). In vivo cochlear hair cell generation and survival by coactivation of beta-catenin and atoh1. *J. Neurosci.* 35, 10786–10798. doi: 10.1523/JNEUROSCI.0967-15.2015

Larem, A., Haidar, H., Alsaadi, A., Abdulkarim, H., Abdulraheem, M., Sheta, S., et al. (2016). Tympanoplasty in adhesive otitis media: a descriptive study. *Laryngoscope* 126, 2804–2810. doi: 10.1002/lary.25987

Lee, H. B., Lim, H. J., Cho, M., Yang, S. M., Park, K., Park, H. Y., et al. (2013). Clinical significance of beta-tricalcium phosphate and polyphosphate for mastoid cavity obliteration during middle ear surgery: human and animal study. *Clin. Exp. Otorhinolaryngol.* 6, 127–134. doi: 10.3342/ceo.2013.6.3.127

Lee, J., Ismail, H., Lee, J. H., Kel, G., O'Leary, J., Hampson, A., et al. (2013). Effect of both local and systemically administered dexamethasone on long-term hearing and tissue response in a Guinea pig model of cochlear implantation. *Audiol. Neurootol.* 18, 392–405. doi: 10.1159/000353582

Li, C., Wang, B., Zhang, H., Yang, S., Yang, T., Han, X., et al. (2021). Advances in the surgical treatment of cholesteatoma of the middle ear. *J. Clin. Otorhinolaryngol. Head Neck Surg. (China)* 35, 952–956.

Li, S., Wu, K., and Ji, Y. (2020). Protective effect of long-term injection of salicylic acid on presbycusis. *Chin. J. Otol.* 18, 755–762.

Li, W., Wu, J., Yang, J., Sun, S., Chai, R., Chen, Z. Y., et al. (2015). Notch inhibition induces mitotically generated hair cells in mammalian cochleae *via* activating the Wnt pathway. *Proc. Natl. Acad. Sci. U.S.A.* 112, 166–171. doi: 10.1073/pnas.1415901112

Lin, Y., Yin, F., Chen, J., Bai, Z., Liu, S., and Zhang, J. (2013). The clinical effect of recombinant human epidermal growth factor in treatment of chronic tympanic membrane perforation. *J. Kunming Med. Univ.* 34, 102–104, 109.

Liu, H., Chen, S., Zhou, Y., Che, X., Bao, Z., Li, S., et al. (2013). The effect of surface charge of glycerol monooleate-based nanoparticles on the round window membrane permeability and cochlear distribution. *J. Drug Target.* 21, 846–854. doi: 10.3109/1061186X.2013.829075

Luo, C., Li, T., Tan, C., and Huang, H. (2016). Local injection of the microRNA-146a recombinant lentiviral vector into the inner ear for immune-mediated inner ear disease in guinea pigs. *J. Med. Postgra* 29, 801–807.

Ma, Y., Bjornmalm, M., Wise, A. K., Cortez-Jugo, C., Revalor, E., Ju, Y., et al. (2018). Gel-mediated electrospray assembly of silica supraparticles for sustained drug delivery. *ACS Appl. Mater. Interfaces* 10, 31019–31031. doi: 10.1021/acsami.8b10415

Ma, Y., Wise, A. K., Shepherd, R. K., and Richardson, R. T. (2019). New molecular therapies for the treatment of hearing loss. *Pharmacol. Ther.* 200, 190–209. doi: 10.1016/j.pharmthera.2019.05.003

Maharajan, N., Cho, G. W., and Jang, C. H. (2020). Application of mesenchymal stem cell for tympanic membrane regeneration by tissue engineering approach. *Int. J. Pediatr. Otorhinolaryngol.* 133:109969. doi: 10.1016/j.ijporl.2020.109969

Maharajan, N., Cho, G. W., and Jang, C. H. (2021). Therapeutic application of mesenchymal stem cells for cochlear regeneration. *In Vivo* 35, 13–22. doi: 10.21873/invivo.12227

Malik, S., Sundarrajan, S., Hussain, T., Nazir, A., and Ramakrishna, S. (2021). Role of block copolymers in tissue engineering applications. *Cells Tissues Organs* 1–14. doi: 10.1159/000511866

Mandour, Y. M. H., Mohammed, S., and Menem, M. O. A. (2019). Bacterial cellulose graft versus fat graft in closure of tympanic membrane perforation. *Am. J. Otolaryngol.* 40, 168–172. doi: 10.1016/j.amjoto.2018.12.008

Marie, A., Meunier, J., Brun, E., Malmstrom, S., Baudoux, V., Flaszka, E., et al. (2018). N-acetylcysteine treatment reduces age-related hearing loss and memory impairment in the senescence-accelerated prone 8 (SAMP8) mouse model. *Aging Dis.* 9, 664–673. doi: 10.14336/AD.2017.0930

Matsuoka, A. J., Kondo, T., Miyamoto, R. T., and Hashino, E. (2007). Enhanced survival of bone-marrow-derived pluripotent stem cells in an animal model of auditory neuropathy. *Laryngoscope* 117, 1629–1635. doi: 10.1097/MLG.0b013e31806bf282

Mattotti, M., Micholt, L., Braeken, D., and Kovacic, D. (2015). Characterization of spiral ganglion neurons cultured on silicon micro-pillar substrates for new auditory neuro-electronic interfaces. *J. Neural Eng.* 12:026001. doi: 10.1088/1741-2560/12/2/026001

Mehrabani, D., Mojtahed Jaberi, F., Zakerinia, M., Hadianfard, M. J., Jalli, R., Tanideh, N., et al. (2016). The healing effect of bone marrow-derived stem cells in knee osteoarthritis: a case report. *World J. Plast. Surg.* 5, 168–174.

Nadol, J. B. Jr., and Merchant, S. N. (2001). Histopathology and molecular genetics of hearing loss in the human. *Int. J. Pediatr. Otorhinolaryngol.* 61, 1–15. doi: 10.1016/s0165-5876(01)00546-8

Mikuriya, T., Sugahara, K., Sugimoto, K., Fujimoto, M., Takemoto, T., Hashimoto, M., et al. (2008). Attenuation of progressive hearing loss in a model of age-related hearing loss by a heat shock protein inducer, geranylgeranylacetone. *Brain Res.* 1212, 9–17. doi: 10.1016/j.brainres.2008.03.031

Mittal, R., Ocak, E., Zhu, A., Perdomo, M. M., Pena, S. A., Mittal, J., et al. (2020). Effect of bone marrow-derived mesenchymal stem cells on cochlear function in an experimental rat model. *Anat. Rec. (Hoboken)* 303, 487–493. doi: 10.1002/ar.24065

Mizutari, K., Fujioka, M., Hosoya, M., Bramhall, N., Okano, H. J., Okano, H., et al. (2013). Notch inhibition induces cochlear hair cell regeneration and recovery of hearing after acoustic trauma. *Neuron* 77, 58–69. doi: 10.1016/j.neuron.2012.10.032

Nakagawa, T., and Ito, J. (2005). Cell therapy for inner ear diseases. *Curr. Pharm. Des.* 11, 1203–1207. doi: 10.2174/1381612053507530

Nappi, F., Iervolino, A., and Singh, S. S. A. (2021). The new challenge for heart endocarditis: from conventional prosthesis to new devices and platforms for the treatment of structural heart disease. *Biomed. Res. Int.* 2021:7302165. doi: 10.1155/2021/7302165

Ohinata, Y., Yamasoba, T., Schacht, J., and Miller, J. M. (2000). Glutathione limits noise-induced hearing loss. *Hear. Res.* 146, 28–34. doi: 10.1016/s0378-5955(00)00096-4

Omae, K., Kanemaru, S. I., Nakatani, E., Kaneda, H., Nishimura, T., Tona, R., et al. (2017). Regenerative treatment for tympanic membrane perforation using gelatin sponge with basic fibroblast growth factor. *Auris Nasus Larynx* 44, 664–671. doi: 10.1016/j.anl.2016.12.005

Ontario Health. (2020). Implantable devices for single-sided deafness and conductive or mixed hearing loss: a health technology assessment. *Ont. Health Technol. Assess. Ser.* 20, 1–165.

Park, J., Kim, S., Park, S. I., Choe, Y., Li, J., and Han, A. (2014). A microchip for quantitative analysis of CNS axon growth under localized biomolecular treatments. *J. Neurosci. Methods* 221, 166–174. doi: 10.1016/j.jneumeth.2013.09.018

Park, T. H., and Chang, C. H. (2013). Early postoperative magnet application combined with hydrocolloid dressing for the treatment of earlobe keloids. *Aesthetic Plast. Surg.* 37, 439–444. doi: 10.1007/s00266-013-0076-6

Pettinato, G., Wen, X., and Zhang, N. (2015). Engineering strategies for the formation of embryoid bodies from human pluripotent stem cells. *Stem Cells Dev.* 24, 1595–1609. doi: 10.1089/scd.2014.0427

Pfannenstiel, S. C., Praetorius, M., Plinkert, P. K., Brough, D. E., and Staecker, H. (2009). Bcl-2 gene therapy prevents aminoglycoside-induced degeneration of auditory and vestibular hair cells. *Audiol. Neurootol.* 14, 254–266. doi: 10.1159/000192953

Pohl, F., Schuon, R. A., Miller, F., Kampmann, A., Bultmann, E., Hartmann, C., et al. (2018). Stenting the eustachian tube to treat chronic otitis media - a feasibility study in sheep. *Head Face Med.* 14:8. doi: 10.1186/s13005-018-0165-5

Polanski, J. F., and Cruz, O. L. (2013). Evaluation of antioxidant treatment in presbyacusis: prospective, placebo-controlled, double-blind, randomised trial. *J. Laryngol. Otol.* 127, 134–141. doi: 10.1017/S0022215112003118

Richardson, R. T., and Atkinson, P. J. (2015). Atoh1 gene therapy in the cochlea for hair cell regeneration. *Expert Opin. Biol. Ther.* 15, 417–430. doi: 10.1517/14712598.2015.1009889

Richardson, R. T., Wise, A. K., Thompson, B. C., Flynn, B. O., Atkinson, P. J., Fretwell, N. J., et al. (2009). Polypyrrole-coated electrodes for the delivery of charge and neurotrophins to cochlear neurons. *Biomaterials* 30, 2614–2624. doi: 10.1016/j.biomaterials.2009.01.015

Sage, C., Huang, M., Karimi, K., Gutierrez, G., Vollrath, M. A., Zhang, D. S., et al. (2005). Proliferation of functional hair cells in vivo in the absence of the retinoblastoma protein. *Science* 307, 1114–1118. doi: 10.1126/science.1106642

Santa Maria, P. L., Kim, S., Varsak, Y. K., and Yang, Y. P. (2015). Heparin binding-epidermal growth factor-like growth factor for the regeneration of chronic tympanic membrane perforations in mice. *Tissue Eng. Part A* 21, 1483–1494. doi: 10.1089/ten.TEA.2014.0474

Saraca, L. M., Di Giuli, C., Sicari, F., Priante, G., Lavagna, F., and Francisci, D. (2019). Use of ceftolozane-tazobactam in patient with severe medium chronic purulent otitis by XDR *Pseudomonas aeruginosa*. *Case Rep. Infect. Dis.* 2019:2683701. doi: 10.1155/2019/2683701

Schilling, A., Krauss, P., Hannemann, R., Schulze, H., and Tziridis, K. (2021). [Reducing tinnitus intensity: pilot study to attenuate tonal tinnitus using individually spectrally optimized near-threshold noise]. *HNO* 69, 891–898. doi: 10.1007/s00106-020-00963-5

Seonwoo, H., Shin, B., Jang, K. J., Lee, M., Choo, O. S., Park, S. B., et al. (2019b). Epidermal growth factor-releasing radially aligned electrospun nanofibrous patches for the regeneration of chronic tympanic membrane perforations. *Adv. Healthc. Mater.* 8:e1801160. doi: 10.1002/adhm.201801160

Seonwoo, H., Kim, S. W., Shin, B., Jang, K. J., Lee, M., Choo, O. S., et al. (2019a). Latent stem cell-stimulating therapy for regeneration of chronic tympanic membrane perforations using IGFBP2-releasing chitosan patch scaffolds. *J. Biomater. Appl.* 34, 198–207. doi: 10.1177/0885328219845082

Serra, L. S. M., Araujo, J. G., Vieira, A. L. S., Silva, E. M. D., Andrade, R. R., Kuckelhaus, S. A. S., et al. (2020). Role of melatonin in prevention of age-related hearing loss. *PLoS One* 15:e0228943. doi: 10.1371/journal.pone.0228943

Sha, S. H., and Schacht, J. (2017). Emerging therapeutic interventions against noise-induced hearing loss. *Expert Opin. Investig. Drugs* 26, 85–96. doi: 10.1080/13543784.2017.1269171

Shahjalal, H. M., Abdal Dayem, A., Lim, K. M., Jeon, T. I., and Cho, S. G. (2018). Generation of pancreatic beta cells for treatment of diabetes: advances and challenges. *Stem Cell Res. Ther.* 9:355. doi: 10.1186/s13287-018-1099-3

Shang, J., Jiang, T., Tang, L., and Wang, Z. (2016). Key technology of transplantable human auricular scaffold based on 3D printing. *J. Natl. Univ. Defense Technol.* 38, 175–180.

Shi, F., Hu, L., and Edge, A. S. (2013). Generation of hair cells in neonatal mice by beta-catenin overexpression in Lgr5-positive cochlear progenitors. *Proc. Natl. Acad. Sci. U.S.A.* 110, 13851–13856. doi: 10.1073/pnas.1219952110

Shou, J., Zheng, J. L., and Gao, W. Q. (2003). Robust generation of new hair cells in the mature mammalian inner ear by adenoviral expression of Hath1. *Mol. Cell. Neurosci.* 23, 169–179. doi: 10.1016/s1044-7431(03)00066-6

Slaughter, B. V., Khurshid, S. S., Fisher, O. Z., Khademhosseini, A., and Peppas, N. A. (2009). Hydrogels in regenerative medicine. *Adv. Mater.* 21, 3307–3329. doi: 10.1002/adma.200802106

Sorour, S. S., Mohamed, N. N., Abdel Fattah, M. M., Elbary, M. E. A., and El-Anwar, M. W. (2018). Bioglass reconstruction of posterior meatal wall after canal wall down mastoidectomy. *Am. J. Otolaryngol.* 39, 282–285. doi: 10.1016/j.amjoto.2018.03.007

Stavrakas, M., Karkos, P. D., Markou, K., and Grigoriadis, N. (2016). Platelet-rich plasma in otolaryngology. *J. Laryngol. Otol.* 130, 1098–1102. doi: 10.1017/S0022215116009403

Sun, F., Zhou, K., Tian, K. Y., Wang, J., Qiu, J. H., and Zha, D. J. (2020). Atrial natriuretic peptide improves neurite outgrowth from spiral ganglion neurons in vitro through a cGMP-dependent manner. *Neural Plast.* 2020:8831735. doi: 10.1155/2020/8831735

Sun, H., and Wu, X. (2013). Current status and prospects of non-viral vector in inner ear gene therapy. *J. Clin. Otorhinolaryngol. Head Neck Surg. (China)* 27, 1339–1342.

Sun, H., Huang, A., and Cao, S. (2011). Current status and prospects of gene therapy for the inner ear. *Hum. Gene Ther.* 22, 1311–1322. doi: 10.1089/hum.2010.246

Sun, Y., Tang, W., Chang, Q., Wang, Y., Kong, W., and Lin, X. (2009). Connexin30 null and conditional connexin26 null mice display distinct pattern and time course of cellular degeneration in the cochlea. *J. Comp. Neurol.* 516, 569–579. doi: 10.1002/cne.22117

Tan, F., Chu, C., Qi, J., Li, W., You, D., Li, K., et al. (2019). AAV-ie enables safe and efficient gene transfer to inner ear cells. *Nat. Commun.* 10:3733. doi: 10.1038/s41467-019-11687-8

Teh, B. M., Marano, R. J., Shen, Y., Friedland, P. L., Dilley, R. J., and Atlas, M. D. (2013). Tissue engineering of the tympanic membrane. *Tissue Eng. Part B Rev.* 19, 116–132. doi: 10.1089/ten.TEB.2012.0389

Unsaler, S., Basaran, B., Ozturk Sari, S., Kara, E., Deger, K., Wormald, P. J., et al. (2016). Safety and efficacy of chitosan-dextran hydrogel in the middle ear in an animal model. *Audiol. Neurootol.* 21, 254–260. doi: 10.1159/000447623

Vanwijck, F., Rogister, F., Pierre Barriat, S., Camby, S., and Lefebvre, P. (2019). Intratympanic steroid therapy for refractory sudden sensory hearing loss: a 12-year experience with the Silverstein catheter. *Acta Otolaryngol.* 139, 111–116. doi: 10.1080/00016489.2018.1532107

Verschuur, C., Agyemang-Prempeh, A., and Newman, T. A. (2014). Inflammation is associated with a worsening of presbycusis: evidence from the MRC national study of hearing. *Int. J. Audiol.* 53, 469–475. doi: 10.3109/14992027.2014.891057

Wakizono, T., Nakashima, H., Yasui, T., Noda, T., Aoyagi, K., Okada, K., et al. (2021). Growth factors with valproic acid restore injury-impaired hearing by promoting neuronal regeneration. *JCI Insight* 6:e139171. doi: 10.1172/jci.insight.139171

Wang, Z., and Yang, Y. (2021). Application of 3D printing in implantable medical devices. *Biomed. Res. Int.* 2021:6653967. doi: 10.1155/2021/6653967

Wong, A. C., and Ryan, A. F. (2015). Mechanisms of sensorineural cell damage, death and survival in the cochlea. *Front. Aging Neurosci.* 7:58. doi: 10.3389/fnagi.2015.00058

World Health Organization [WHO] (2021). *WHO: 1 in 4 People Projected to Have Hearing Problems by 2050*. Available online at: https://www.who.int/news/item/02-03-2021-who-1-in-4-people-projected-to-have-hearing-problems-by-2050 (accessed March 2, 2021).

Wu, X., Zou, S., Wu, F., He, Z., and Kong, W. (2020). Role of microRNA in inner ear stem cells and related research progress. *Am. J. Stem Cells* 9, 16–24.

Xiong, H., Pang, J., Yang, H., Dai, M., Liu, Y., Ou, Y., et al. (2015). Activation of miR-34a/SIRT1/p53 signaling contributes to cochlear hair cell apoptosis: implications for age-related hearing loss. *Neurobiol. Aging* 36, 1692–1701. doi: 10.1016/j.neurobiolaging.2014.12.034

Xuan, Y., Ding, D., Xuan, W., Huang, L., Tang, J., Wei, Y., et al. (2018). A traditional Chinese medicine compound (Jian Er) for presbycusis in a mouse model: Reduction of apoptosis and protection of cochlear sensorineural cells and hearing. *Int. J. Herb. Med.* 6, 127–135.

Yan, G. (2021). Studies on the Protective Effects on Sensory Hair Cells of Bioactive Peptides from Rapana venosa, Vol. 10. 69. Jinan: Qilu University of Technology.

Yang, K., Jung, K., Ko, E., Kim, J., Park, K. I., Kim, J., et al. (2013). Nanotopographical manipulation of focal adhesion formation for enhanced differentiation of human neural stem cells. *ACS Appl. Mater. Interfaces* 5, 10529–10540. doi: 10.1021/am402156f

Yang, Y., Zhang, Y., Chai, R., and Gu, Z. (2020). A polydopamine-functionalized carbon microfibrous scaffold accelerates the development of neural stem cells. *Front. Bioeng. Biotechnol.* 8:616. doi: 10.3389/fbioe.2020.00616

Young, E., Westerberg, B., Yanai, A., and Gregory-Evans, K. (2018). The olfactory mucosa: a potential source of stem cells for hearing regeneration. *Regen. Med.* 13, 581–593. doi: 10.2217/rme-2018-0009

Yuan, F., and Qi, W. (2018). Development of drug delivery to inner ear. *Chin. J. Otol.* 16, 575–580.

Yuan, H., Wang, X., Hill, K., Chen, J., Lemasters, J., Yang, S. M., et al. (2015). Autophagy attenuates noise-induced hearing loss by reducing oxidative stress. *Antioxid. Redox Signal.* 22, 1308–1324. doi: 10.1089/ars.2014.6004

Zakrzewski, W., Dobrzynski, M., Szymonowicz, M., and Rybak, Z. (2019). Stem cells: past, present, and future. *Stem Cell Res. Ther.* 10:68. doi: 10.1186/s13287-019-1165-5

Zhao, J., and Liang, Y. (2018). Experimental study on the effect of total flavonoids of *Pueraria lobata* on inflammatory cytokines in rats with inner ear injury induced by iso-proterenol. *Chin. J. Clin. Pharmacol. Ther.* 23, 1003–1007.

Zhou, G., Jiang, H., Yin, Z., Liu, Y., Zhang, Q., Zhang, C., et al. (2018). In vitro regeneration of patient-specific ear-shaped cartilage and its first clinical application for auricular reconstruction. *EBioMedicine* 28, 287–302. doi: 10.1016/j.ebiom.2018.01.011

Zhou, W., Du, J., Jiang, D., Wang, X., Chen, K., Tang, H., et al. (2018). microRNA183 is involved in the differentiation and regeneration of Notch signalingprohibited hair cells from mouse cochlea. *Mol. Med. Rep.* 18, 1253–1262. doi: 10.3892/mmr.2018.9127

Zhuo, X. L., Wang, Y., Zhuo, W. L., Zhang, Y. S., Wei, Y. J., and Zhang, X. Y. (2008). Adenoviral-mediated up-regulation of Otos, a novel specific cochlear gene, decreases cisplatin-induced apoptosis of cultured spiral ligament fibrocytes *via* MAPK/mitochondrial pathway. *Toxicology* 248, 33–38. doi: 10.1016/j.tox.2008.03.004

Zinn, E., Pacouret, S., Khaychuk, V., Turunen, H. T., Carvalho, L. S., Andres-Mateos, E., et al. (2015). In silico reconstruction of the viral evolutionary lineage yields a potent gene therapy vector. *Cell Rep.* 12, 1056–1068. doi: 10.1016/j.celrep.2015.07.019

Zou, J., Poe, D., Ramadan, U. A., and Pyykko, I. (2012). Oval window transport of Gd-dOTA from rat middle ear to vestibulum and scala vestibuli visualized by in vivo magnetic resonance imaging. *Ann. Otol. Rhinol. Laryngol.* 121, 119–128. doi: 10.1177/000348941212100209

Zou, J., Pyykko, I., and Hyttinen, J. (2016). Inner ear barriers to nanomedicine-augmented drug delivery and imaging. *J. Otol.* 11, 165–177. doi: 10.1016/j.joto.2016.11.002

Zucchelli, E., Birchall, M., Bulstrode, N. W., and Ferretti, P. (2020). Modeling normal and pathological ear cartilage in vitro using somatic stem cells in three-dimensional culture. *Front. Cell. Dev. Biol.* 8:666. doi: 10.3389/fcell.2020.00666

Conflict of Interest: The authors declare that the research was conducted in the absence of any commercial or financial relationships that could be construed as a potential conflict of interest.

Publisher's Note: All claims expressed in this article are solely those of the authors and do not necessarily represent those of their affiliated organizations, or those of the publisher, the editors and the reviewers. Any product that may be evaluated in this article, or claim that may be made by its manufacturer, is not guaranteed or endorsed by the publisher.

frontiers in Cellular Neuroscience

ORIGINAL RESEARCH
published: 04 February 2022
doi: 10.3389/fncel.2021.815280

Superparamagnetic Iron Oxide Nanoparticles and Static Magnetic Field Regulate Neural Stem Cell Proliferation

Dan Li[1,2,3†], Yangnan Hu[2,3†], Hao Wei[4†], Wei Chen[2,3], Yun Liu[2,3], Xiaoqian Yan[2,3], Lingna Guo[2,3,5], Menghui Liao[2,3], Bo Chen[6], Renjie Chai[2,3] and Mingliang Tang[2,7]**

[1] School of Biology, Food and Environment, Hefei University, Hefei, China, [2] Co-innovation Center of Neuroregeneration, Nantong University, Nantong, China, [3] School of Life Sciences and Technology, Southeast University, Nanjing, China, [4] Department of Otorhinolaryngology Head and Neck Surgery, Drum Tower Clinical Medical College, Nanjing Medical University, Nanjing, China, [5] Department of Otolaryngology Head and Neck Surgery, The Second Affiliated Hospital of Anhui Medical University, Hefei, China, [6] Materials Science and Devices Institute, Suzhou University of Science and Technology, Suzhou, China, [7] Department of Cardiovascular Surgery of the First Affiliated Hospital and Institute for Cardiovascular Science, Medical College, Soochow University, Suzhou, China

OPEN ACCESS

Edited by:
Zuhong He,
Wuhan University, China

Reviewed by:
Wenli Chen,
South China Normal University, China
Fang Yang,
Southeast University, China
Xiaowei Yang,
Tongji University, China
Guangli Suo,
Suzhou Institute of Nano-Tech and Nano-Bionics, Chinese Academy of Sciences (CAS), China

***Correspondence:**
Renjie Chai
renjiec@seu.edu.cn
Mingliang Tang
mltang@suda.edu.cn

† These authors have contributed equally to this work

Specialty section:
This article was submitted to Cellular Neuropathology, a section of the journal Frontiers in Cellular Neuroscience

Received: *15 November 2021*
Accepted: *31 December 2021*
Published: *04 February 2022*

Citation:
Li D, Hu Y, Wei H, Chen W, Liu Y, Yan X, Guo L, Liao M, Chen B, Chai R and Tang M (2022) Superparamagnetic Iron Oxide Nanoparticles and Static Magnetic Field Regulate Neural Stem Cell Proliferation. Front. Cell. Neurosci. 15:815280. doi: 10.3389/fncel.2021.815280

Neural stem cells (NSCs) transplantation is a promising approach for the treatment of various neurodegenerative diseases. Superparamagnetic iron oxide nanoparticles (SPIOs) are reported to modulate stem cell behaviors and are used for medical imaging. However, the detailed effects of SPIOs under the presence of static magnetic field (SMF) on NSCs are not well elucidated. In this study, it was found that SPIOs could enter the cells within 24 h, while they were mainly distributed in the lysosomes. SPIO exhibited good adhesion and excellent biocompatibility at concentrations below 500 μg/ml. In addition, SPIOs were able to promote NSC proliferation in the absence of SMF. In contrast, the high intensity of SMF (145 ± 10 mT) inhibited the expansion ability of NSCs. Our results demonstrate that SPIOs with SMF could promote NSC proliferation, which could have profound significance for tissue engineering and regenerative medicine for SPIO applications.

Keywords: SPIO, SMF, neural stem cells, proliferation, regulation

INTRODUCTION

Neural stem cells (NSCs) act as one of the adult stem cells that are typically considered capable of giving rise to neurons and glia cell lineages (Gage, 2000). Currently, they have been widely used for spinal cord repairing and for the treatment of various neurodegenerative diseases in animal models (Gage, 2000; Madhavan and Collier, 2010; Mathieu et al., 2010; Carletti et al., 2011; Yoneyama et al., 2011; He et al., 2012; Reekmans et al., 2012). Nowadays, numerous reports have suggested that biomaterials could provide a tremendous opportunity to influence stem cell behaviors. For instance, the physicochemical properties of biomaterials, including substrate mechanical stiffness (Engler et al., 2006; Lee et al., 2013), nanometer-scale topography (Dalby et al., 2007; Yim et al., 2010; McMurray et al., 2011), and simple chemical functionality (Benoit et al., 2008; Saha et al., 2011), could regulate the stem cell fate. In particular, a previous study has shown that superparamagnetic iron oxide nanoparticles (SPIOs) promoted the proliferation of human mesenchymal stem cells (MSCs) through diminishing intracellular H_2O_2 and accelerating cell cycle progression (Huang et al., 2009). Furthermore, recent research has indicated that SPIOs promoted

osteogenic differentiation of human bone-derived mesenchymal stem cells (hBMSCs) (Wang et al., 2016). Similarly, it has also been reported that SPIOs could promote osteogenic differentiation of adipose-derived mesenchymal stem cells (ASCs) (Xiao et al., 2015). These findings suggest that SPIOs may have the potential to modulate stem cell behaviors.

Stem cell fate is determined by the complex interactions between stem cells and their surroundings, including biochemical factors, extracellular matrix components, intercellular interactions, and physical factors (Allazetta and Lutolf, 2015). A magnetic field is an effective physical factor that has been reported to modulate cell proliferation as earlier as 1999 (Fanelli et al., 1999). Meanwhile, it was reported to mediate the osteogenic differentiation of human ASCs (Kang et al., 2013) and induce MSC differentiation into osteoblasts and cartilage (Ross et al., 2015). In addition, the magnetic fields and magnetic nanomaterials were used together to induce the growth direction of neurons (Riggio et al., 2014) and facilitate drug delivery (Qiu et al., 2017). However, there is no report to explore the biological effects of SPIO under the presence of a magnetic field on NSC behaviors.

MATERIALS AND METHODS

Synthesis of Superparamagnetic Iron Oxide Nanoparticles

The SPIOs were coated by polyglucose-sorbitol-carboxymethylether (PSC) as modified in this experiment. The method to synthesize SPIOs was applied to the classic chemical coprecipitation combined with an excellent alternating-current magnetic field (ACMF)-induced internal-heat mode (Chen et al., 2016). Briefly, 40 mg PSC was dissolved in 2 ml of deionized water, then the mixture of the 6 mg $FeCl_3$ with 3 mg $FeCl_2$ dissolved in 15 ml of deionized water was added. After cooling the mixture to 5°C, 1 g 28% (w/v) ammonium hydroxide was added with stirring for over 2 min. The mixture was then heated at 80°C for 1 h, then the deionized water was purified with five cycles of ultrafiltration using a 100 kDa membrane.

Characterization of Superparamagnetic Iron Oxide Nanoparticles

The core of synthesized SPIOs was detected by transmission electron microscopy (TEM; JEOL/JEM-200CX, Japan). The size distribution was analyzed by dynamic light scattering (DLS) with a particle size analyzer (Malvern Zetasizer Nano ZS90, United Kingdom). The hysteresis loop of SPIOs was measured using a vibrating sample magnetometer (LS 7307-9309, Lakeshore Cryotronic, United States). The final concentrations of iron in the aqueous solution were measured by inductively coupled plasma mass spectrometry (ICP-MS) on an Optima 5300DV instrument.

Neural Stem Cell Culture

Neural stem cell isolation and culture were described in the previously published protocol [32]. Briefly, NSCs were cultured in mixed DMEM-F12 medium (Gibco, Grand Island, NY) containing 2% B-27 (Gibco), 100 U/ml penicillin, and 100 μg/ml streptomycin (Sigma-Aldrich, St. Louis, MO, United States) in the condition of 5% CO_2 at 37°C. NSCs were passaged every 3–5 days during culturing. For the determination of NSC proliferation, cells were seeded with a concentration of 5×10^4 cells/ml in DMEM-F12 medium with 2% B-27, 20 ng/ml EGF (R&D Systems, Minneapolis, MN, United States), and 20 ng/ml FGF-2 (R&D Systems, Minneapolis, MN, United States). For NSC differentiation assays, cells were seeded in an NSC differentiation kit (Stem Cell, Hangzhou, China). The care and use of animals in these experiments followed the guidelines and protocol approved by the Care and Use of Animals Committee of Southeast University. All efforts were made to minimize the number of animals used and their suffering.

Cellular Uptake of Superparamagnetic Iron Oxide Nanoparticles by Inductively Coupled Plasma Mass Spectrometry

Cells were seeded in 25 cm^2 flasks at the concentration of 1×10^5 to 1×10^6 per flask and incubated with SPIOs at the indicated concentrations. After 1, 2, 3, or 4 days of treatment, cells were harvested and counted. Then, the cell suspension was dissociated by hydrochloric acid with a final concentration of 60%. The concentration of iron in cell lysates was measured by ICP-MS according to PerkinElmer's operating procedures.

Cell Viability Assay

Neural stem cells were seeded in 96-well cell culture plates at the concentration of 1×10^5 cells per well ($n = 6$) and cultured overnight. The cells were then incubated with differentiation concentrations of SPIOs at indicated concentrations. After culturing for 12 or 24 h, cell viability was measured by CCK-8 assay (Beyotime, Shanghai, China) according to the manufacturer's instructions. The NSCs cultured with the ordinary medium were considered as the control.

Immunostaining

Neural stem cells were fixed with 4% paraformaldehyde for 1 h at room temperature, following treatment with blocking medium for 1 h. Next, the cells were incubated with primary antibody diluted solution overnight at 4°C. Then, each sample was washed with phosphate buffer solution [0.1% Triton X-100 in phosphate buffer solution (PBST) twice per 5 min]. The samples were further incubated with a secondary antibody for 1 h at room temperature. Finally, samples were washed with PBST, and an antifade fluorescence mounting medium (DAKO) was added. The antibodies used were Nestin (Beyotime, China). Cell proliferation was detected by Click-it EdU imaging kit (Invitrogen). All the images were captured by a Zeiss LSM 700 confocal microscope, and ImageJ (NIH) was used for image analysis.

Scanning Electron Microscope and Transmission Electron Microscopy Examination

Neural stem cells were seeded in 24-well cell culture plates at the concentration of 1×10^4 cells per well and incubated

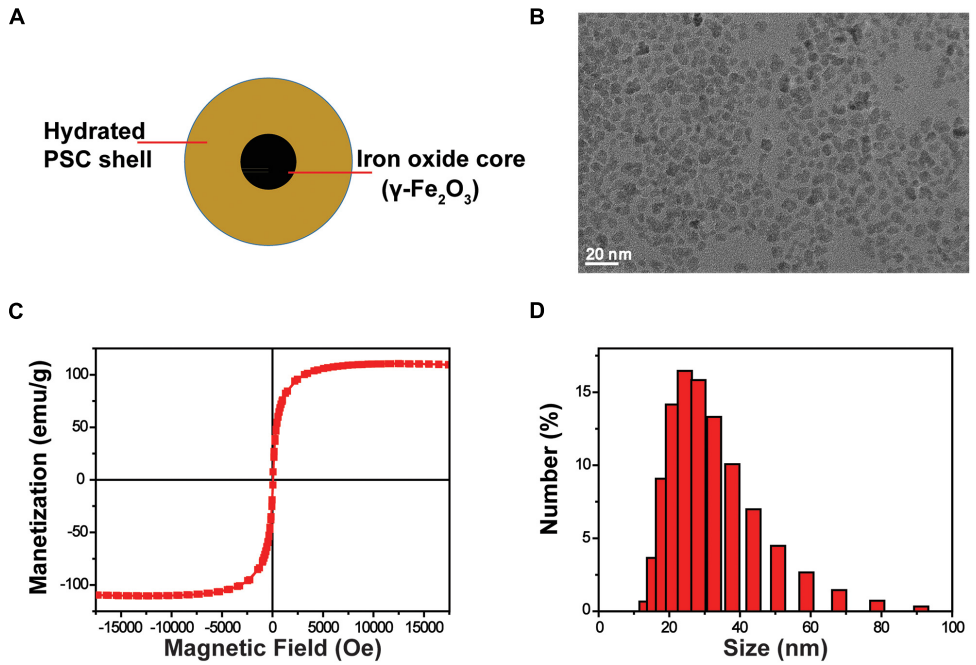

FIGURE 1 | Characterization of SPIOs. **(A)** Schematic structure of SPIOs. **(B)** TEM image of SPIOs. **(C)** Hysteresis loop of SPIOs. **(D)** Particle size distributions of the SPIOs as measured by DLS.

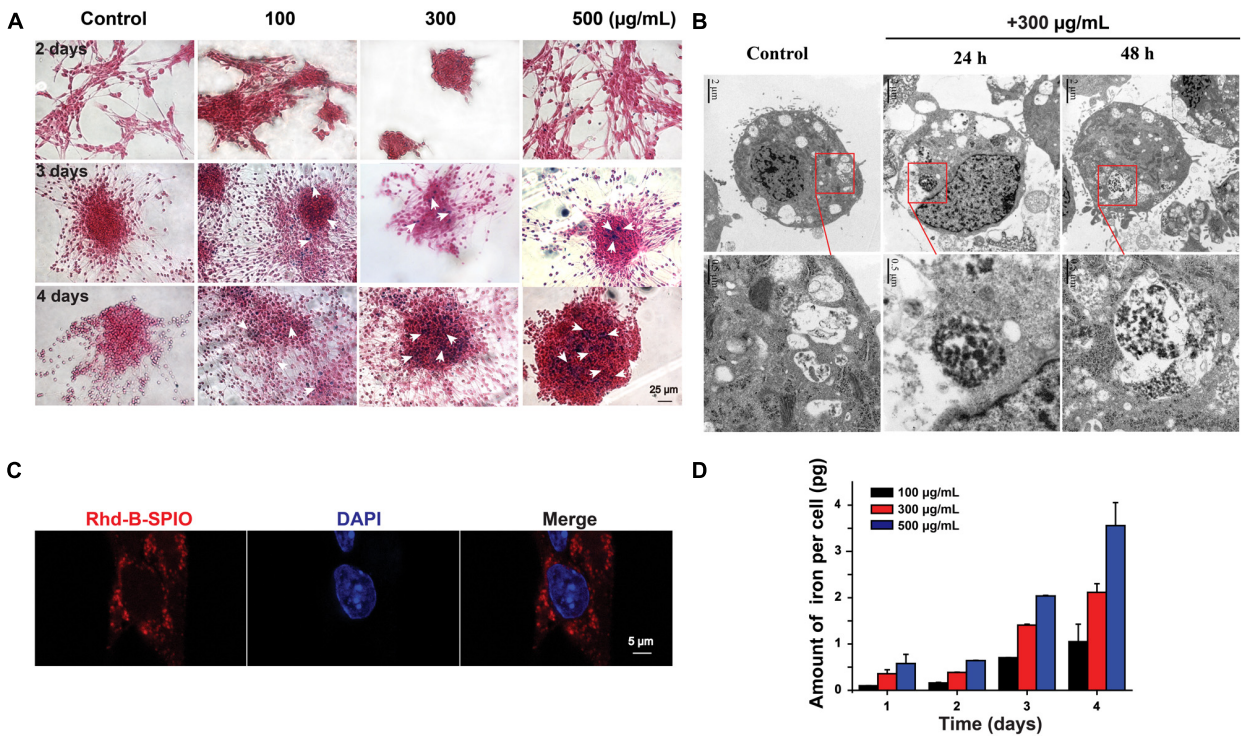

FIGURE 2 | Internalization and cellular uptake of SPIOs. **(A)** Representative Perl's blue staining images of SPIOs-treated NSCs. Scale bar = 25 μm. **(B)** TEM images of NSCs under SPIOs treatment (300 μg/ml for 24 and 48 h). A higher-magnification image of the indicated portion is shown in the inferior panel. **(C)** Laser confocal images of NSCs with Rhd-B-SPIOs treatment for 24 or 48 h. Red, Rhd-B, blue, nucleus. Scale bar = 5 μm. **(D)** The amount of intracellular iron uptake in NSCs after SPIOs treatment for different concentrations at the indicated time.

with a differentiation concentration of SPIOs at indicated concentrations. After incubation for 3 days, cells were washed two times with 1 × PBS (pH 7.4); 2.5% glutaraldehyde solution (Alfa Aesar, Tewksbury, MA, United States) was added to each sample. Cells were co-incubated for 1 h at 37°C. Then, cells were dehydrated overnight, and the cell morphology was detected by scanning electron microscope (SEM) (Ultra Plus, Zeiss, Oberkochen, Germany).

Neural stem cells were seeded in 25 cm^2 flasks at the concentration of 1 × 10^6 and incubated with SPIOs at the concentration of 100 μg/ml. After 12- or 24-h treatment, the cells were harvested and washed two times with PBS; 2.5% glutaraldehyde solution was added to each sample, and cells were co-incubated overnight at 4°C to fix the cells. Then, the samples were transferred to 1% osmium tetroxide, dehydrated in ethanol, and embedded in Epon (Sigma–Aldrich). Finally, uranyl acetate and lead citrate were used for staining of ultrathin slices (60–80 nm). The images were captured by TEM (JEOL/JEM-200CX, Tokyo, Japan).

Statistical Analysis

All data are shown as mean and SD. Statistical analyses were conducted using GraphPad Prism 6 software. For all experiments, *n* represents the number of replicates, and at least three individual experiments were conducted. One- or two-way ANOVA analysis followed by a Tukey's *post hoc* test was used to determine the statistical significance between multiple groups, and Student's *t*-test was used for comparisons between two groups. A value of $p < 0.05$ was considered to be statistically significant.

RESULTS

Synthesis and Characterization of Superparamagnetic Iron Oxide Nanoparticles

The SPIOs were composed of a γ-Fe_2O_3 core and PSC shell (**Figure 1A**). The size of the γ-Fe_2O_3 core is about 6–8 nm (**Figure 1B**). The hysteresis loop of SPIOs is about 105 emu/g (**Figure 1C**), which indicates that it has a good superparamagnetic property. The average diameter of whole SPIOs measured by DLS is about 30 nm (**Figure 1D**). These results suggest that the SPIOs synthesized by this method have a uniform particle size, stable structure, good dispersion (PDI of 0.154), and stronger magnetic properties than the conventional coprecipitation method.

Internalization and Cellular Uptake of Superparamagnetic Iron Oxide Nanoparticles

Superparamagnetic iron oxide could enter the cells after co-incubation for 1 day (**Figure 2A**). The amount of SPIO could

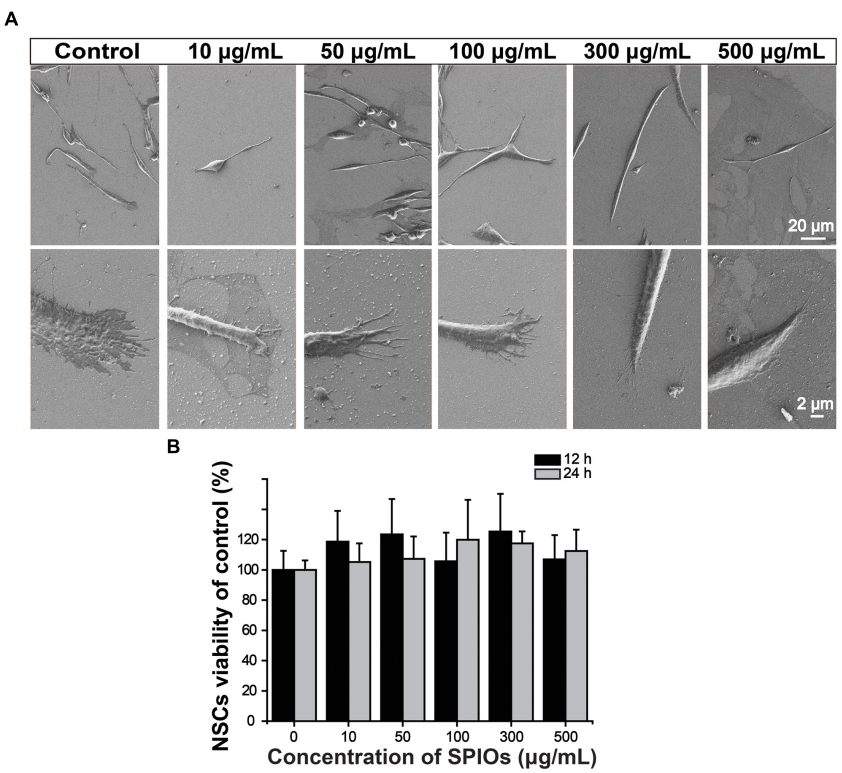

FIGURE 3 | Biocompatibility of SPIOs. **(A)** SEM images of NSCs after culturing with SPIO for 3 days at indicated concentrations. **(B)** Cell viability was detected by the CCK-8 assay. The cells were treated with SPIOs for 12–24 h at indicated concentrations. Data were normalized to the control group (no SPIOs exposure). Data are presented as mean ± SD. Student's *t*-test.

increase with time and concentrations of SPIO (**Figure 2D**). It was noticed that there was no significant difference between the 3- and 4-day groups, indicating that the uptake by a single cell was stale within 3 days. Furthermore, TEM and fluorescence imaging were employed to examine the internalization of SPIOs in NSCs. TEM results revealed that SPIOs were located in the lysosomes after 24 and 48 h of exposure (**Figure 2B**). It was further verified that SPIOs were located outside the cell nucleus after 24 h of exposure (**Figure 2C**).

The morphology of NSCs was observed by SEM after 3-day co-incubation with various concentrations of SPIOs. Cells in all groups presented normal phenotypes (**Figure 3A**). Importantly, SPIOs exposure did not affect NSC viability at concentrations up to 500 μg/ml for 24 h (**Figure 3B**), indicating the good biocompatibility of SPIOs.

Effects of Superparamagnetic Iron Oxide Nanoparticle and Static Magnetic Field on Neural Stem Cell Proliferation

Neural stem cell proliferation was first evaluated by neurosphere formation assay. NSCs from higher concentrations of SPIOs (300 and 500 μg/ml) had a significantly higher rate of neurosphere formation compared to the control group, while lower concentrations of SPIOs (10, 50, and 100 μg/ml) or 50 ± 10 mT SMF treatment had no obvious effect on the number of neurosphere formation (**Figures 4A,B**). In contrast, SPIOs at different concentrations (100, 300, and 500 μg/ml) simultaneously exposed to SMF (50 ± 10 mT) resulted in a slower rate of neurosphere formation (**Figures 4A,B**). Although more neurospheres were generated from NSCs treated with higher concentration SPIOs, there was no significant effect on the diameters of the neurospheres compared to the control group (**Figures 4A,C**). Notably, when the NSCs were simultaneously exposed to SMF, the neurospheres exhibited a larger diameter at concentrations of 100–500 μg/ml.

Since the low concentration of SPIOs (10 and 50 μg/ml) had no effect on NSC proliferation regardless of SMF presence, these two concentrations were not included in the subsequent experiments. Next, EdU^+/DAPI cells were counted to further examine NSC proliferation. NSCs treated with 100, 300, and 500 μg/ml SPIOs generated significantly more EdU^+/DAPI cells than those from the control group (control group: 38.60 ± 6.11%; 100 μg/ml: 46.61 ± 6.16; 300 μg/ml: 46.13 ± 6.62; 500 μg/ml: 53.57 ± 7.49%; $p < 0.001$) (**Figures 5A,C**). Furthermore, SMF (145 ± 10 mT) presence inhibited the ratio of EdU^+/DAPI cells when compared to the control (0 μg/ml: 71.62 ± 3.93%; SMF: 66.58 ± 4.98%; $p < 0.001$). Next, when NSCs were cultured in the presence of SPIOs (100, 300, and 500 μg/ml) plus SMF (145 ± 10 mT) for 3 days, significantly lower ratio of EdU^+/DAPI cells was observed (100 μg/ml: 54.92 ± 6.03%; 300 μg/ml: 43.79 ± 6.93%; 500 μg/ml: 38.37 ± 7.39%) (**Figures 5B,D**).

Interestingly, when the SMF intensity was reduced to 50 ± 10 mT, the exposure of SPIOs at concentrations of 100–300 μg/ml failed to reduce the ratio of EdU^+/DAPI cells (**Figures 6A,C**). However, 100 ± 10 mT SMF could significantly

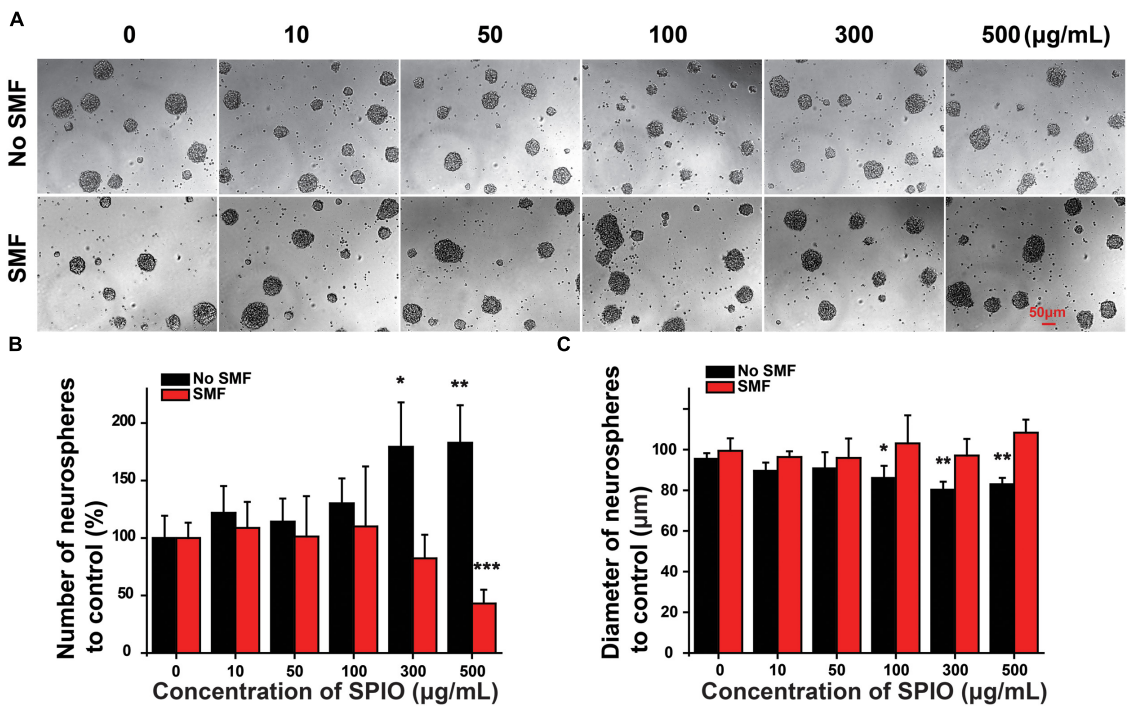

FIGURE 4 | The number and diameter of neurospheres. NSCs were cultured with indicated concentrations of SPIO (10, 50, 100, 300, and 500 μg/ml) with or without SMF for 3 days. **(A)** Representative optical images of neurospheres. **(B)** Quantification of the neurospheres number. **(C)** Quantification of the neurospheres diameter in the experimental groups. Data are presented as mean ± SD, $^*p < 0.05$, $^{**}p < 0.01$, and $^{***}p < 0.001$.

suppress NSC proliferation when SPIO concentration was more than 500 μg/ml, as evidenced by the decreased ratio of EdU^+/DAPI cells (**Figures 6B,D**).

DISCUSSION

Stem cells have a wide application prospect in the biomedical fields. NSCs have been verified for their potential in the treatment of various diseases, especially neural diseases [3–9]. The stem cell niche is the interaction between stem cells and their microenvironment which is regarded as key players in stem cell fate decisions. The niche includes several physical factors, biochemical factors, and extracellular matrix components (Allazetta and Lutolf, 2015). Many biomaterials have been proposed to modulate the stem cell niche to further regulate stem cell fate. For example, SPIOs have been reported to be able to modulate stem cell behaviors, including proliferation and differentiation (Huang et al., 2009; Xiao et al., 2015; Wang et al., 2016). Meanwhile, the magnetic field is also confirmed as one of the physical factors that affect stem cell fate decisions. In this research, we introduced SPIOs and magnetic fields together to explore whether they could affect NSC proliferation.

Some types of SPIOs have been reported to exert excellent biocompatibility, while the potential toxicity under certain conditions (e.g., surface modification) is still under debate. Numerous studies focus on SPIO cytotoxicity on different types of cells. SPIO labeling was found not to alter MSC viability and apoptosis (Schafer et al., 2009; Zhang et al., 2014; Singh et al., 2019; Xu et al., 2020). It was further revealed that SPIOs coated with unfractionated heparin did not affect MSC survival (Lee et al., 2012). Furthermore, histological examination showed that silica-coated SPIOs induced no obvious tissue impairments or abnormal inflammation and pathology in major organs (Ledda et al., 2020). Our results were consistent with the above reports that SPIOs at concentrations less than 500 μg/ml did not affect NSC adhesion or induce cell death. SPIO toxicity is believed to be highly correlated with the cores and coatings. Usually, the SPIO core should have a magnetic responsive component. Some high-magnetic materials such as nickel are easy to be oxidized, thus leading to certain toxicity

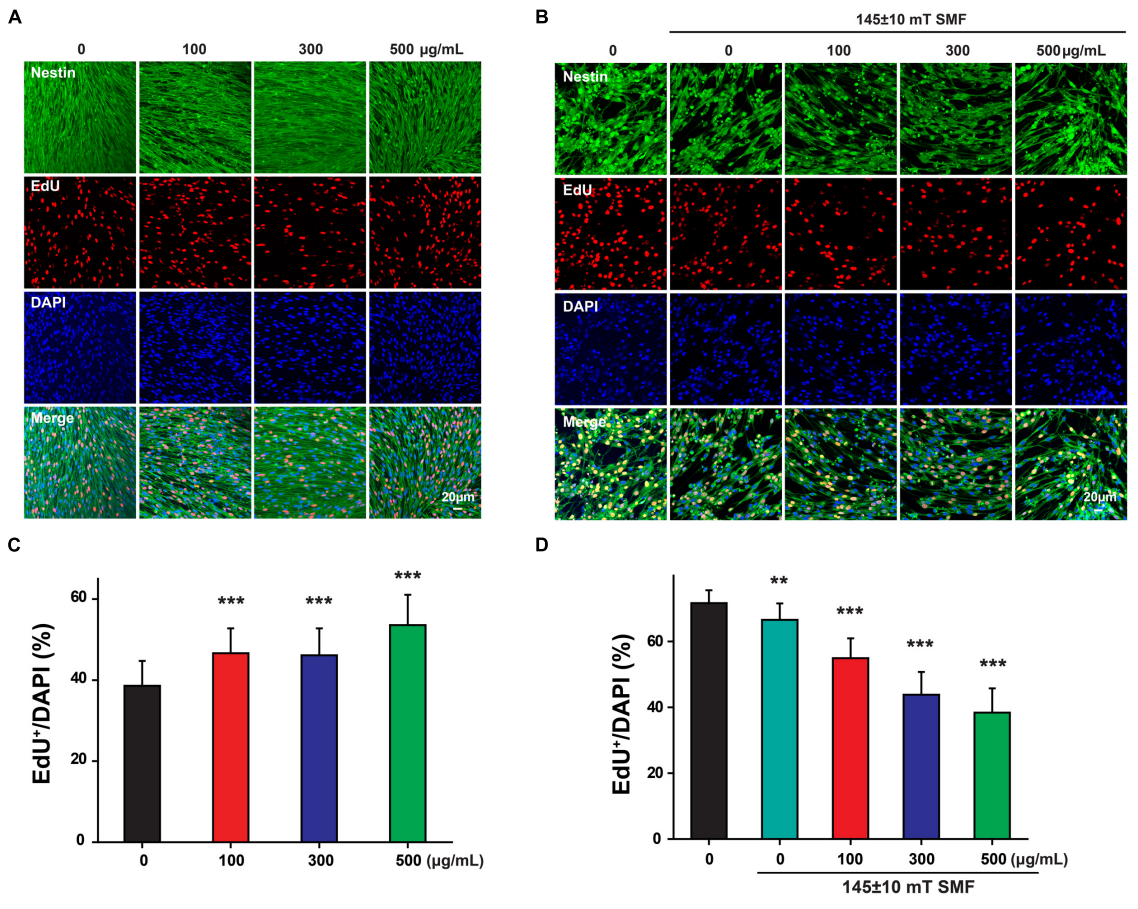

FIGURE 5 | Neural stem cells proliferation was measured by EdU labeling. NSCs were cultured with indicated concentrations of SPIO (100, 300, and 500 μg/ml) with or without 145 ± 10 SMF for 3 days. EdU was added to the culture from day 2 to day 3. Representative images for EdU staining in **(A)** control group and **(B)** 145 ± 10 mT SMF group with or without SPIO treatment at indicated concentrations (100, 300, and 500 μg/ml). The ratio of EdU + /DAPI was shown in **(C,D)**, respectively. Data are presented as mean ± SD, $^{**}p < 0.01$, $^{***}p < 0.001$.

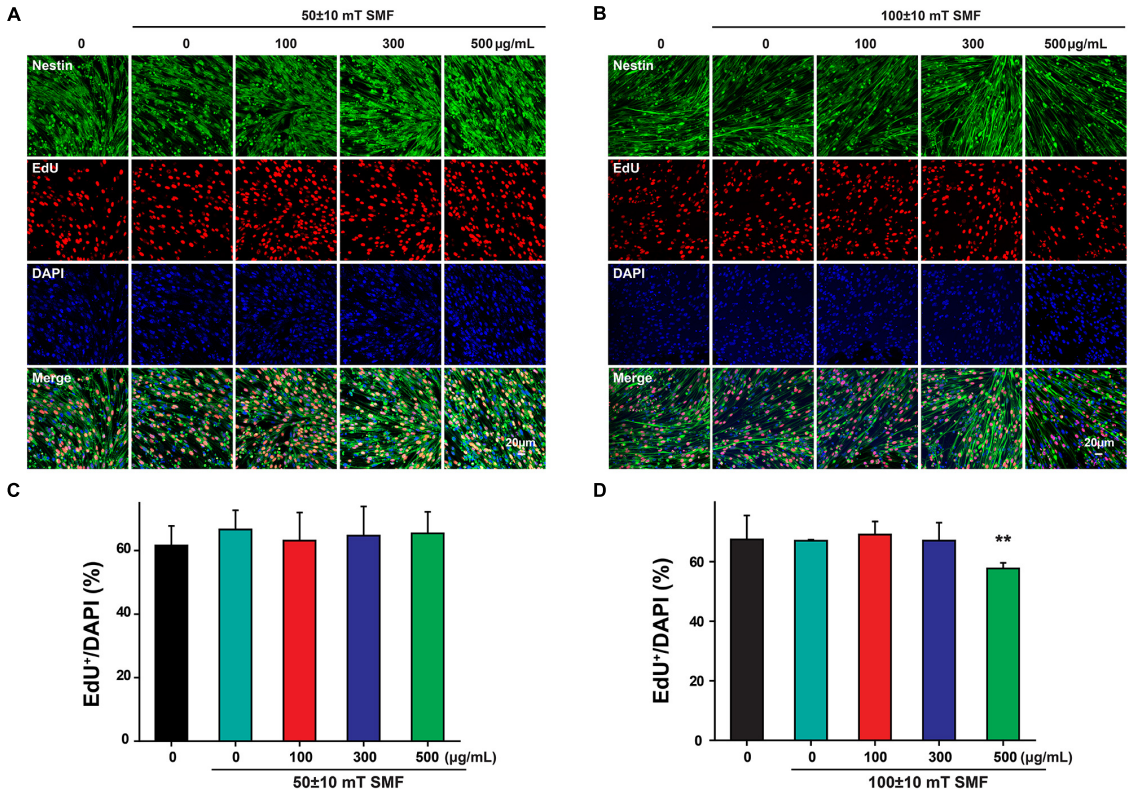

FIGURE 6 | Neural stem cells proliferation was measured by EdU labeling. NSCs were cultured with indicated concentrations of SPIO (100, 300, and 500 μg/ml) with or without SMF for 3 days. EdU was added to the culture from day 2 to day 3. Representative images for EdU staining in **(A)** 50 ± 10 mT group and **(B)** 100 ± 10 mT SMF group with or without SPIO treatment at indicated concentrations (100, 300, and 500 μg/ml). The ratio of EdU + /DAPI was shown in **(C,D)**, respectively. Data are presented as mean ± SD, $^{**}p < 0.01$.

(Tartaj and Serna, 2003; Mahmoudi et al., 2011). The main iron oxides, hematite (α-Fe_2O_3), maghemite (γ-Fe_2O_3), and magnetite (Fe_3O_4) are superparamagnetic and also have good biocompatibility. In this study, SPIOs were prepared by an alternating-current magnetic field (ACMF)-induced internal-heat mode that was described previously (Chen et al., 2016). The SPIOs synthesized in this study were composed of a γ-Fe_2O_3 core and PSC shell. This type of SPIOs has good biosafety, as evidenced by our results. In addition, size could be a critical factor to determine SPIO cytotoxicity. It is believed that SPIOs with a diameter ranging from 10 to 100 nm are considered to be optimal for the purpose of systemic administration (Wahajuddin and Arora, 2012). SPIO toxicity was also reported with a particle size within this range. In this study, the SPIO size was within 20–40 nm, and no obvious cytotoxicity was observed at this range.

In summary, we found that SPIOs are a potential regulator for NSC expansion. SPIOs at appropriate concentrations can elevate the proliferation ability of NSCs. In the meantime, our results also indicate that SMF may suppress NSC proliferation at high intensity. In the future, we will make the best effort to uncover the biological effects of SPIOs on NSC behaviors, including migration and differentiation. Also, the detailed mechanisms underlying the observed effects will be explored as well.

DATA AVAILABILITY STATEMENT

The raw data supporting the conclusions of this article will be made available by the authors, without undue reservation.

ETHICS STATEMENT

The animal study was reviewed and approved by Southeast University.

AUTHOR CONTRIBUTIONS

DL, YH, HW, WC, YL, XY, LG, ML, and BC conducted the experiments and analyzed the data. RC and MT supervised the study and acquired the funding. All authors wrote the manuscript.

FUNDING

This study was supported by grants from the Major State Basic Research Development Program of China (973 Program) (2017YFA0104303), the National Natural Science Foundation of China (No. 81970883), and the Hefei University Scientific Research and Development Fund (20ZR08ZDA).

REFERENCES

Allazetta, S., and Lutolf, M. P. (2015). Stem cell niche engineering through droplet microfluidics. *Curr. Opin. Biotechnol.* 35, 86–93. doi: 10.1016/j.copbio.2015.05.003

Benoit, D. S. W., Schwartz, M. P., Durney, A. R., and Anseth, K. S. (2008). Small functional groups for controlled differentiation of hydrogel-encapsulated human mesenchymal stem cells. *Nat. Mater.* 7, 816–823. doi: 10.1038/nmat2269

Carletti, B., Piemonte, F., and Rossi, F. (2011). Neuroprotection: the Emerging Concept of Restorative Neural Stem Cell Biology for the Treatment of Neurodegenerative Diseases. *Curr. Neuropharmacol.* 9, 313–317. doi: 10.2174/157015911795596603

Chen, B., Li, Y., Zhang, X. Q., Liu, F., Liu, Y. L., Ji, M., et al. (2016). An efficient synthesis of ferumoxytol induced by alternating-current magnetic field. *Mater. Lett.* 170, 93–96.

Dalby, M. J., Gadegaard, N., Tare, R., Andar, A., Riehle, M. O., Herzyk, P., et al. (2007). The control of human mesenchymal cell differentiation using nanoscale symmetry and disorder. *Nat. Mater.* 6, 997–1003. doi: 10.1038/nmat2013

Engler, A. J., Sen, S., Sweeney, H. L., and Discher, D. E. (2006). Matrix elasticity directs stem cell lineage specification. *Cell* 126, 677–689. doi: 10.1016/j.cell.2006.06.044

Fanelli, C., Coppola, S., Barone, R., Colussi, C., Gualandi, G., Volpe, P., et al. (1999). Magnetic fields increase cell survival by inhibiting apoptosis *via* modulation of Ca2+ influx. *FASEB J.* 13, 95–102. doi: 10.1096/fasebj.13.1.95

Gage, F. H. (2000). Mammalian neural stem cells. *Science* 287, 1433–1438. doi: 10.1126/science.287.5457.1433

He, X., Knepper, M., Ding, C., Li, J., Castro, S., Siddiqui, M., et al. (2012). Promotion of spinal cord regeneration by neural stem cell-secreted trimerized cell adhesion molecule L1. *PLoS One* 7:e46223. doi: 10.1371/journal.pone.0046223

Huang, D. M., Hsiao, J. K., Chen, Y. C., Chien, L. Y., Yao, M., Chen, Y. K., et al. (2009). The promotion of human mesenchymal stem cell proliferation by superparamagnetic iron oxide nanoparticles. *Biomaterials* 30, 3645–3651. doi: 10.1016/j.biomaterials.2009.03.032

Kang, K. S., Hong, J. M., Kang, J. A., Rhie, J. W., Jeong, Y. H., and Cho, D. W. (2013). Regulation of osteogenic differentiation of human adipose-derived stem cells by controlling electromagnetic field conditions. *Exp. Mol. Med.* 45:e6. doi: 10.1038/emm.2013.11

Ledda, M., Fioretti, D., Lolli, M. G., Papi, M., Di Gioia, C., Carletti, R., et al. (2020). Biocompatibility assessment of sub-5 nm silica-coated superparamagnetic iron oxide nanoparticles in human stem cells and in mice for potential application in nanomedicine. *Nanoscale* 12, 1759–1778. doi: 10.1039/c9nr09683c

Lee, J., Abdeen, A. A., Zhang, D., and Kilian, K. A. (2013). Directing stem cell fate on hydrogel substrates by controlling cell geometry, matrix mechanics and adhesion ligand composition. *Biomaterials* 34, 8140–8148. doi: 10.1016/j.biomaterials.2013.07.074

Lee, J. H., Jung, M. J., Hwang, Y. H., Lee, Y. J., Lee, S., Lee, D. Y., et al. (2012). Heparin-coated superparamagnetic iron oxide for *in vivo* MR imaging of human MSCs. *Biomaterials* 33, 4861–4871. doi: 10.1016/j.biomaterials.2012.03.035

Madhavan, L., and Collier, T. J. (2010). A synergistic approach for neural repair: cell transplantation and induction of endogenous precursor cell activity. *Neuropharmacology* 58, 835–844. doi: 10.1016/j.neuropharm.2009.10.005

Mahmoudi, M., Sant, S., Wang, B., Laurent, S., and Sen, T. (2011). Superparamagnetic iron oxide nanoparticles (SPIONs): development, surface modification and applications in chemotherapy. *Adv. Drug Deliv. Rev.* 63, 24–46. doi: 10.1016/j.addr.2010.05.006

Mathieu, P., Battista, D., Depino, A., Roca, V., Graciarena, M., and Pitossi, F. (2010). The more you have, the less you get: the functional role of inflammation on neuronal differentiation of endogenous and transplanted neural stem cells in the adult brain. *J. Neurochem.* 112, 1368–1385. doi: 10.1111/j.1471-4159.2009.06548.x

McMurray, R. J., Gadegaard, N., Tsimbouri, P. M., Burgess, K. V., Mcnamara, L. E., Tare, R., et al. (2011). Nanoscale surfaces for the long-term maintenance of mesenchymal stem cell phenotype and multipotency. *Nat. Mater.* 10, 637–644. doi: 10.1038/nmat3058

Qiu, Y., Tong, S., Zhang, L., Sakurai, Y., Myers, D. R., Hong, L., et al. (2017). Magnetic forces enable controlled drug delivery by disrupting endothelial cell-cell junctions. *Nat. Commun.* 8:15594. doi: 10.1038/ncomms15594

Reekmans, K., Praet, J., Daans, J., Reumers, V., Pauwels, P., Van Der Linden, A., et al. (2012). Current challenges for the advancement of neural stem cell biology and transplantation research. *Stem Cell Rev. Rep.* 8, 262–278.

Riggio, C., Calatayud, M. P., Giannaccini, M., Sanz, B., Torres, T. E., Fernandez-Pacheco, R., et al. (2014). The orientation of the neuronal growth process can be directed *via* magnetic nanoparticles under an applied magnetic field. *Nanomed. Nanotechnol. Biol. Med.* 10, 1549–1558. doi: 10.1016/j.nano.2013.12.008

Ross, C. L., Siriwardane, M., Almeida-Porada, G., Porada, C. D., Brink, P., Christ, G. J., et al. (2015). The effect of low-frequency electromagnetic field on human bone marrow stem/progenitor cell differentiation. *Stem Cell Res.* 15, 96–108. doi: 10.1016/j.scr.2015.04.009

Saha, K., Mei, Y., Reisterer, C. M., Pyzocha, N. K., Yang, J., Muffat, J., et al. (2011). Surface-engineered substrates for improved human pluripotent stem cell culture under fully defined conditions. *Proc. Natl. Acad. Sci. U. S. A.* 108, 18714–18719. doi: 10.1073/pnas.1114854108

Schafer, R., Kehlbach, R., Muller, M., Bantleon, R., Kluba, T., Ayturan, M., et al. (2009). Labeling of human mesenchymal stromal cells with superparamagnetic iron oxide leads to a decrease in migration capacity and colony formation ability. *Cytotherapy* 11, 68–78. doi: 10.1080/14653240802666043

Singh, A. V., Dad Ansari, M. H., Dayan, C. B., Giltinan, J., Wang, S., Yu, Y., et al. (2019). Multifunctional magnetic hairbot for untethered osteogenesis, ultrasound contrast imaging and drug delivery. *Biomaterials* 219:119394. doi: 10.1016/j.biomaterials.2019.119394

Tartaj, P., and Serna, C. J. (2003). Synthesis of monodisperse superparamagnetic Fe/silica nanospherical composites. *J. Am. Chem. Soc.* 125, 15754–15755.

Wahajuddin, and Arora, S. (2012). Superparamagnetic iron oxide nanoparticles: magnetic nanoplatforms as drug carriers. *Int. J. Nanomedicine* 7, 3445–3471. doi: 10.2147/IJN.S30320

Wang, Q. W., Chen, B., Cao, M., Sun, J. F., Wu, H., Zhao, P., et al. (2016). Response of MAPK pathway to iron oxide nanoparticles *in vitro* treatment promotes osteogenic differentiation of hBMSCs. *Biomaterials* 86, 11–20. doi: 10.1016/j.biomaterials.2016.02.004

Xiao, H. T., Wang, L., and Yu, B. (2015). Superparamagnetic iron oxide promotes osteogenic differentiation of rat adipose-derived stem cells. *Int. J. Clin. Exp. Med.* 8, 698–705.

Xu, L., Yuan, S., Chen, W., Ma, Y., Luo, Y., Guo, W., et al. (2020). Transplantation and Tracking of the Human Umbilical Cord Mesenchymal Stem Cell Labeled with Superparamagnetic Iron Oxide in Deaf Pigs. *Anat. Rec.* 303, 494–505. doi: 10.1002/ar.24346

Yim, E. K. F., Darling, E. M., Kulangara, K., Guilak, F., and Leong, K. W. (2010). Nanotopography-induced changes in focal adhesions, cytoskeletal organization, and mechanical properties of human mesenchymal stem cells. *Biomaterials* 31, 1299–1306. doi: 10.1016/j.biomaterials.2009.10.037

Yoneyama, M., Shiba, T., Hasebe, S., and Ogita, K. (2011). Adult Neurogenesis Is Regulated by Endogenous Factors Produced During Neurodegeneration. *J. Pharmacol. Sci.* 115, 425–432. doi: 10.1254/jphs.11r02cp

Zhang, R., Li, J., Li, J., and Xie, J. (2014). Efficient *In vitro* labeling rabbit bone marrow-derived mesenchymal stem cells with SPIO and differentiating into neural-like cells. *Mol. Cells* 37, 650–655. doi: 10.14348/molcells.2014.0010

Conflict of Interest: The authors declare that the research was conducted in the absence of any commercial or financial relationships that could be construed as a potential conflict of interest.

The reviewer FY declared a shared affiliation, with several of the authors YH, WC, YL, XY, ML, and RC to the handling editor at the time of the review.

frontiers in Cellular Neuroscience

ORIGINAL RESEARCH
published: 08 February 2022
doi: 10.3389/fncel.2022.803718

mito-TEMPO Attenuates Oxidative Stress and Mitochondrial Dysfunction in Noise-Induced Hearing Loss *via* Maintaining TFAM-mtDNA Interaction and Mitochondrial Biogenesis

Jia-Wei Chen[1†], Peng-Wei Ma[1†], Hao Yuan[1†], Wei-Long Wang[1], Pei-Heng Lu[1], Xue-Rui Ding[1], Yu-Qiang Lun[1], Qian Yang[2] and Lian-Jun Lu[1]**

[1]Department of Otolaryngology Head and Neck Surgery, Tangdu Hospital, Fourth Military Medical University, Xi'an, China, [2]Department of Experimental Surgery, Tangdu Hospital, Fourth Military Medical University, Xi'an, China

OPEN ACCESS

Edited by:
Zuhong He,
Wuhan University, China

Reviewed by:
Zheng-De Du,
Capital Medical University, China
Hangkang Chen,
Tri-Service General Hospital, Taiwan

***Correspondence:**
Lian-Jun Lu
lulianj@fmmu.edu.cn
Qian Yang
qianyang@fmmu.edu.cn

[†]These authors have contributed equally to this work

Specialty section:
This article was submitted to Cellular Neuropathology, a section of the journal Frontiers in Cellular Neuroscience

Received: *28 October 2021*
Accepted: *14 January 2022*
Published: *08 February 2022*

Citation:
Chen J-W, Ma P-W, Yuan H, Wang W-L, Lu P-H, Ding X-R, Lun Y-Q, Yang Q and Lu L-J (2022) mito-TEMPO Attenuates Oxidative Stress and Mitochondrial Dysfunction in Noise-Induced Hearing Loss via Maintaining TFAM-mtDNA Interaction and Mitochondrial Biogenesis. Front. Cell. Neurosci. 16:803718. doi: 10.3389/fncel.2022.803718

The excessive generation of reactive oxygen species (ROS) and mitochondrial damage have been widely reported in noise-induced hearing loss (NIHL). However, the specific mechanism of noise-induced mitochondrial damage remains largely unclear. In this study, we showed that acoustic trauma caused oxidative damage to mitochondrial DNA (mtDNA), leading to the reduction of mtDNA content, mitochondrial gene expression and ATP level in rat cochleae. The expression level and mtDNA-binding function of mitochondrial transcription factor A (TFAM) were impaired following acoustic trauma without affecting the upstream PGC-1α and NRF-1. The mitochondria-target antioxidant mito-TEMPO (MT) was demonstrated to enter the inner ear after the systemic administration. MT treatment significantly alleviated noise-induced auditory threshold shifts 3d and 14d after noise exposure. Furthermore, MT significantly reduced outer hair cell (OHC) loss, cochlear ribbon synapse loss, and auditory nerve fiber (ANF) degeneration after the noise exposure. In addition, we found that MT treatment effectively attenuated noise-induced cochlear oxidative stress and mtDNA damage, as indicated by DHE, 4-HNE, and 8-OHdG. MT treatment also improved mitochondrial biogenesis, ATP generation, and TFAM-mtDNA interaction in the cochlea. These findings suggest that MT has protective effects against NIHL via maintaining TFAM-mtDNA interaction and mitochondrial biogenesis based on its ROS scavenging capacity.

Keywords: noise-induced hearing loss, reactive oxygen species, mitochondrial transcription factor A, mitochondrial biogenesis, sensory hair cells, rat model

INTRODUCTION

Hearing loss is the most prevalent sensory disorder and affects more than 1.5 billion people worldwide (WHO, 2021). Common causes of acquired sensorineural hearing loss include exposure to loud noise (Sha and Schacht, 2017), aminoglycosides (He et al., 2017), platinum-based chemotherapy (Fernandez et al., 2020), heavy metals (Ding et al., 2019), and aging (He et al., 2021a). With the rapid development of modern society, noise has become one of the most common environmental pollutants in industrial and recreational settings. Exposure to high-intensity or chronic noise leads to noise-induced hearing loss (NIHL).

Moderate noise leads to temporary threshold shift (TTS) that completely recovers to normal in 1–2 weeks. However, high-intensity or chronic noise can result in permanent threshold shift (PTS), i.e., irreversible hearing loss (Kurabi et al., 2017). According to WHO, about 10% of the world's population is exposed to noise, 5.3% of whom develop NIHL (WHO, 2021). Those who experience hearing loss have difficulties in social communication, which may cause potential mental and cognitive disorders such as anxiety, depression, and dementia (Loughrey et al., 2018; Blazer and Tucci, 2019).

The cochlea is a metabolically active auditory sensory organ. Loud noise causes a dramatic increase in energy consumption of the cochlea (Chen et al., 2012). Production of reactive oxygen species (ROS) was observed in the cochlea in a few minutes following noise exposure, including superoxide (O_2·-), hydroxyl radical (·OH), and hydrogen peroxide (H_2O_2). Moreover, ROS can be generated continuously for 7–10 days after cessation of the noise exposure (Ohlemiller et al., 1999; Yamashita et al., 2004). A lower level of ROS induced by moderate noise is reported to induce autophagy which protects against NIHL (Yuan et al., 2015). However, high-intensity noise induces excess ROS and activates 5' adenosine monophosphate-activated protein kinase (AMPK), leading to hair cell death and hearing loss (Wu et al., 2020). Oxidative stress has been considered as a key factor in the mechanism of NIHL (Fetoni et al., 2019). ROS in the cochlea mainly comes from the mitochondrial metabolism of various cells. Mitochondrial pathology and dysfunction are associated with hearing loss of various etiologies (Fischel-Ghodsian et al., 2004; Böttger and Schacht, 2013). Mitochondria are essential organelles with several vital functions including energy production, maintenance of calcium homeostasis, and regulation of apoptosis (Lin and Beal, 2006). Due to the proximity to ROS production, mitochondria are also the first organelles damaged by ROS. The phenomenon of mitochondrial damage has been reported to be involved in NIHL in previous studies (Coleman et al., 2007; Park et al., 2012). However, the underlying mechanism has not been fully elucidated yet.

The mitochondrial DNA (mtDNA) is a circular double-stranded DNA located in the matrix of mitochondria, encoding 13 essential subunits of the mitochondrial respiratory chain (MRC; Scarpulla, 2008). Due to the lack of the repair mechanism and histone proteins like genomic DNA, mtDNA is more susceptible to the damage by ROS (Tsutsui et al., 2009). Mitochondrial transcription factor A (TFAM), a nucleus-encoded protein, is essential for the stabilization and maintenance of mtDNA. TFAM can bind to mtDNA in a sequence-independent manner to compact and stabilize the genome. In addition, TFAM can also bind sequence-specifically to promoter regions of mtDNA, initiating transcription and replication of mtDNA (Kang et al., 2007; Chandrasekaran et al., 2015). Previous studies have reported mitochondrial disintegration and vacuolization in hair cells (HCs) after acoustic trauma (Coleman et al., 2007; Park et al., 2012). However, the specific mechanism of noise-induced mitochondrial damage remains unclear. There are few studies on the alterations of the cochlear mtDNA content and expression level after acoustic trauma. Whether TFAM dysregulation is involved in the pathogenesis of NIHL is still unknown.

Recently, several novel antioxidants that specifically target mitochondria have been developed for the treatment of oxidative stress-related diseases (Zinovkin and Zamyatnin, 2019). 2-(2,2,6,6-tetramethylpiperidin-1-oxyl-4-ylamino)-2-oxoethyl (mito-TEMPO) is a mitochondria-target antioxidant with strong superoxide scavenging capacity and several hundred-fold accumulations in mitochondria (Shetty et al., 2019). A previous study demonstrated that mito-TEMPO (MT) can ameliorate renal fibrosis by reducing oxidative stress, mitochondrial dysfunction, and inflammation (Liu et al., 2018). In addition, recent studies have shown that MT has a protective effect against acetaminophen-induced hepatotoxicity with a wider therapeutic time window than N-acetyl-L-cysteine (NAC; Du et al., 2017; Abdullah-Al-Shoeb et al., 2020). Systemic administration of MT was able to alleviate ischemic brain damage in rats (Li et al., 2018). In addition, MT can pass through the blood-brain barrier (BBB) which is structurally similar to the blood-labyrinth barrier (BLB) in stria vascularis of the cochlea (Zhelev et al., 2013; Nyberg et al., 2019). However, whether MT has a protective effect on hearing has not been reported yet.

In the present study, we explored whether MT has a protective effect against NIHL and the underlying mechanism using an *in vivo* rat model. We first detected whether MT entered the inner ear after the systemic administration. Then we investigated the alleviation of noise-induced hearing loss, outer hair cell (OHC) loss, inner hair cell (IHC) ribbon synapse loss, and auditory nerve fiber (ANF) degeneration with systemic use of MT. We hypothesized that MT exerted the protective effect on hearing via reducing mtDNA oxidative damage, stabilizing the TFAM-mtDNA interaction, maintaining mitochondrial biogenesis and function.

MATERIALS AND METHODS

Animals

Sixty-two female adult Sprague-Dawley rats (200–250 g) were used in this study. Two rats were used for the determination of MT in the cochlea. Sixty Rats were randomly assigned to three groups (n = 20 for each group): control, noise + vehicle treatment, noise + MT treatment. All animals were kept at 22 ± 1°C under a 12 h light/12 h dark cycle with free access to water and food. All procedures of the animal experiments were approved by the Institutional Animal Care and Use Committee of Fourth Military Medical University.

Auditory Brainstem Response (ABR) Measurements

The hearing function of 18 animals (n = 6 for each group) was evaluated by auditory brainstem response (ABR) at four frequencies of 8, 16, 24, and 32 kHz. ABR measurements were carried out 2 days before (−2d), 3 days after (+3d) and 14 days after (+14d) the noise exposure to evaluate the baseline hearing function and noise-induced auditory threshold shifts. Rats were anesthetized with an intraperitoneal injection of the

cocktail anesthetic (chloral hydrate, pentobarbital sodium, and magnesium sulfate). Body temperature was maintained at near 37°C with a heating pad. Three subdermal electrodes were inserted at the vertex of the skull (active), the left mastoid (reference), and the right mastoid (ground). Tucker-Davis Technologies (TDT) RZ6 System was used to generate acoustic stimuli and record the responses. Tone pip stimuli at 8, 16, 24, and 32 kHz (5-ms-duration with 2.5-ms rise–fall time) were delivered monaurally with an earphone inserted into the external auditory canal of the left ear. Acoustic stimuli were generated from 90 dB and then attenuated in 10-dB and 5-dB steps until no ABR waves were recognizable. A total of 1,024 responses were averaged for each stimulus level. ABR wave II was used to determine ABR thresholds for each frequency. The thresholds were defined as the lowest intensity able to evoke repeatable response waves.

Drug Administration

MT (Sigma-Aldrich, SML0737) was dissolved in normal saline as a stock solution and stored at −20°C. The stock solution was diluted with normal saline at a concentration of 0.5 mg/ml before the injection. For animals in the MT treatment group, a dose of 1 mg/kg was selected based on the previous studies (Liu et al., 2018; Xing et al., 2021). For the animals to be sacrificed on day 1, MT was injected intraperitoneally (i.p.) 24 h before, 1 h before, and immediately after noise exposure. The Animals to be sacrificed on day 3 and 14 received three additional injections once daily for the following 3 days. The animals in the control group and the vehicle treatment group received three or six injections of normal saline with the same experimental procedure.

Perilymph Extraction and Sample Preparation

Two rats were injected intraperitoneally with 1 mg/kg MT. Fifteen minutes after the injection, rats were sacrificed and the cochleae were harvested. Then 2 μl of perilymph was sampled using a capillary tube from the round window of the cochlea. A total of 8 μl of perilymph was pooled and used for the determination of MT. Then 100 μl of methanol was added to the sample. After vortexing, the sample was centrifuged at 5,000×g for 10 min at 4°C. The supernatant was retained and used for liquid chromatography tandem mass spectrometry (LC-MS/MS) analysis.

Chromatographic Separation and MS/MS Detection

The LC-MS/MS analysis was performed with the Triple Quadrupole LC/MS (Agilent, 6470B, USA). Chromatographic separation was performed using an Agilent C18 column (100 × 2.1 mm i.d., 3 μm particle size). The sample injection volume was 10 μl. The column temperature was maintained at 35°C. Then a gradient of mobile phase A (0.1%(v/v) formic acid in 5 mM ammonium acetate) and mobile phase B (acetonitrile) was run at 0.3 ml/min as follows: 95% A and 5% B, 0–15 min; 20% A and 80% B, 15–17 min; 100% A, 17–20 min. The MS/MS analysis was performed in the positive electrospray ionization (ESI+) mode. The source temperature was kept at 500°C. The ion spray voltage was 4,500 V, and the curtain gas was set to 35 psi. The detection of the ions was operated in the multiple reaction monitoring (MRM) mode, monitoring transitions of m/z 474.2 → 320.1 for MT. The quantification of the MT in the perilymph was analyzed by calculating the peak area ratios using the external standard.

Acoustic Trauma

The acoustic trauma was induced by continuous noise exposure. The rats were placed separately in wire cages located in a sound-proof room. The acoustic signal of 8–16 kHz octave band noise was generated by RZ6 Noise software. Then the signal was amplified and output by the power amplifier (Crown, XLi800, China) and four loudspeakers (CHUANGMU, CP-75A, China). The level of the noise was maintained at 112 ± 1 dB SPL confirmed by the Sound Level Meter. Animals were exposed to noise for 2 h.

Immunofluorescence Histochemistry for Surface Preparations and Frozen Sections of the Cochlea

Twelve animals used for the analyses of 4-HNE, DHE, 8-OHdG level, and TFAM-mtDNA interaction were sacrificed 1 h after the noise exposure. Eighteen animals used for analyses of OHC loss, IHC ribbon synapse loss, and ANF degeneration were sacrificed 14d after the noise exposure. Rat cochleae were quickly dissected from the temporal bones following rapid decapitation. The round and oval windows were opened after removing the stapes. Then the cochleae were gently perfused with 4% paraformaldehyde (PFA) in 0.1 M phosphate-buffered saline (PBS) via the round window, and kept in the fixative overnight at 4°C. After the fixation, the cochleae were rinsed three times with PBS for 5 min and then decalcified with 10% ethylenediaminetetraacetic acid (EDTA) for 5 days at room temperature with a daily solution change. After the decalcification, the cochleae were rinsed three times with PBS for 5 min. For cochlear surface preparations, the organ of Corti (OC) was dissected in PBS by carefully removing the lateral wall, Reissner's membrane, and the tectorial membrane of the cochlea using micro-dissecting forceps and scissors under a stereomicroscope (Olympus, SZ61, Japan). Then the specimens were transferred into a 96-well plate, followed by permeabilization using 1% Triton X-100 in PBS for 15 min at room temperature. The specimens were blocked with immunol staining blocking buffer (Leagene, IH0338) for 1 h at room temperature. Then the specimens were incubated overnight at 4°C with the following primary antibodies: Myosin VIIa (Proteus Biosciences, #25-6790, 1:1,000), TFAM (Abcam, ab252432, 1:500), dsDNA (Abcam, ab27156, 1:500). After being rinsed with PBS three times, the specimens were incubated for 2 h at room temperature in darkness with following secondary antibodies: donkey anti-rabbit IgG Alexa Fluor 594 (Invitrogen, A21207, 1:200), donkey anti-mouse IgG Alexa Fluor 488 (Invitrogen, A21202, 1:200). After being rinsed with PBS three times, the specimens were incubated with Acti-Stain 670 Phalloidin (Cytoskeleton, #PHDN1-A, 1:70) or

DAPI (Roche, #10236276001, 1 μg/ml) for 30 min at room temperature.

For immunolabeling of IHC ribbon synapses, the specimens were permeabilized with 3% Triton X-100 in PBS for 30 min at room temperature. After blocking for 1 h, the specimens were incubated overnight at 37°C with following primary antibodies: Myosin VIIa (Proteus Biosciences, #25-6790, 1:1,000), CtBP2 (BD Bioscience, #612044, 1:500), GluR2 (Alomone Labs, AGC-005, 1:1,000). After being rinsed with PBS three times, the specimens were incubated for 2 h at room temperature in darkness with following secondary antibodies: goat anti-rabbit IgG Alexa Fluor 568 (Invitrogen, A11036, 1:200), goat anti-mouse IgG1 Alexa Fluor 647 (Invitrogen, A21240, 1:200), goat anti-mouse IgG2a Alexa Fluor 488 (Invitrogen, A21131, 1:200). After the final rinse with PBS, each specimen was dissected into the apex, middle and base turns. Each cochlear turn was transferred to the slide and placed in the mounting medium (Vector, H-1000). Finally, the specimen was covered with a coverslip and the edge was sealed with transparent nail polish.

For the preparation of cochlear frozen sections, the decalcified cochleae were incubated in 10% sucrose and 20% sucrose for 4 h and 30% sucrose overnight at 4°C for dehydration. Then the specimens were embedded in an optimal cutting temperature (OCT) compound. The midmodiolar cryosections at a thickness of 8 μm were prepared using a Cryostat Microtome (Leica, CM1860, Germany). The sections were permeabilized with 0.5% Triton X-100 in PBS for 15 min at room temperature, followed by blocking with immunol staining blocking buffer for 1 h at room temperature. Then the sections were incubated overnight at 4°C with following primary antibodies: Myosin VIIa (Proteus Biosciences, #25-6790, 1:1,000), Tuj1 (GeneTex, GTX631836, 1:200), 4-HNE (GeneTex, GTX17571, 1:50), 8-OHdG (Abcam, ab48508, 1:200), Tuj1(ABclonal, A17913, 1:500). After being rinsed with PBS three times, the specimens were incubated with secondary antibodies for 2 h at room temperature in darkness. For DHE staining, the permeabilized sections were incubated with 1 μM DHE solution (Beyotime, S0063) for 30 min at 37°C in darkness. After being rinsed with PBS three times, a drop of mounting medium with DAPI (Vector, H-1200) was added onto the section. Finally, the section was covered with a coverslip and the edge was sealed with transparent nail polish. Images were obtained with the Confocal Laser Scanning Microscope (CLSM; Olympus, FV1000, Japan) under identical parameter settings in each experiment.

Quantitative or Semi-quantitative Analyses of the Fluorescence Signals

The quantitative or semi-quantitative analyses of the fluorescence signals were conducted with ImageJ software (version 1.53a, USA). For the OHC counting 14d after noise exposure, cochlear surface preparations labeled with Myosin VIIa and DAPI were used. The OHC counting was measured in apex, middle and base turns of surface preparations in 0.3-mm segments. The absence of both the nucleus (DAPI) and the cell body (Myosin VIIa) was considered as the OHC loss. The mean OHC survival in each group was calculated with four specimens. The quantification of IHC ribbon synapses was analyzed in the 0.1-mm segment of the surface preparation (containing about 10 IHCs), corresponding to frequencies of 16–20 kHz. The juxtaposition of CtBP2 and GluA2 was considered as the paired synapse. The total number of paired fluorescent spots was counted and divided by the number of IHC within the image. For the analysis of ANF density, cochlear frozen sections immunolabelled with Tuj1 and Myosin VIIa were used. The intensity of Tuj1 fluorescent signals in nerve fibers in the upper-base turn of the cochlea was analyzed and considered as ANF density. For the semi-quantitative analyses of 8-OHdG and 4-HNE expression, the intensity of the fluorescent signals in SGNs, HCs, or SV region in the upper-base turn of the cochlea was analyzed. Briefly, the images were converted into 8-bit grayscale type. The intensity of the background signal was subtracted and the average grayscale intensity of SGNs, HCs or SV region was then measured. The relative grayscale values were calculated by normalizing the ratio to the control group. The quantification of TFAM-mtDNA interaction was analyzed in the 70-μm segment at the base turn of the surface preparation. Those green fluorescent spots (dsDNA) in the cytoplasm that were not colocalized with red ones (TFAM) were considered as naked mtDNA. The total naked mtDNA spots in OHCs were counted and divided by the number of OHC within the image. All quantitative and semi-quantitative analyses were performed in four specimens for each group.

Extraction of Cochlear DNA and RNA

Six animals were sacrificed on day 1 after the third injection and six animals were sacrificed on day 3 after the ABR testing. The cochleae were dissected in Hanks' balanced salt solution on ice and frozen in liquid nitrogen until use. Twelve cochleae (n = 4 for each group) of the animals sacrificed on day 1 were used for the extraction of total RNA. Twelve cochleae (n = 4 for each group) of the animals sacrificed on day 3 were used for genomic DNA (gDNA) extraction. The gDNA and total RNA were extracted using the Tissue DNA Extraction Kit (TIANGEN, DP304) and RNeasy Plus Mini Kit (QIAGEN, #74134) according to the manufacturer's instructions, respectively. The purity and concentration of the DNA and RNA products were analyzed using the microplate spectrophotometer (BioTek, Epoch, USA). Then the isolated RNA was reverse transcribed to cDNA using PrimeScript RT Master Mix (TaKaRa, RR036A). The gDNA and cDNA products were stored at −20°C until use.

Quantification of mtDNA Copy Number and Mitochondrial Nd6 mRNA Expression

The mtDNA copy number and mitochondrial Nd6 expression were quantified by real-time polymerase chain reaction (PCR) assay using Real-Time PCR Detection System (Bio-Rad, CFX96, USA). The real-time PCR reaction system was prepared using TB Green Premix Ex Taq II (TaKaRa, RR820A) according to the manufacturer's instructions. The nuclear gene β-actin was used as the internal control. For the quantification of mtDNA copy number, the gDNA was used for the template. The cycle threshold (Ct) values of 12S rRNA (mtDNA) and β-actin (nDNA) were used to determine the

relative mtDNA copy number. The following primers were designed: β-actin Forward: CTACCTCGCTGCAGGATCG, β-actin Reverse: GTCTACACCGCGGGAATACG, 12S rRNA Forward: AAGGAGAGGGCATCAAGCAC, and 12S rRNA Reverse: TATCACTGCTGAGTCCCGTG.

For the measurement of mitochondrial Nd6 mRNA expression, the cDNA was used as a template. The relative mRNA expression was estimated by the Ct values of Nd6 (mtDNA expression) and β-actin (nDNA expression). The following primers were designed: β-actin Forward: GGAGATTA CTGCCCTGGCTCCTA, β-actin Reverse: GACTCATCGTAC TCCTGCTTGCTG, Nd6 Forward: ACCCTCAAGTCTCCGG GTA, and Nd6 Reverse: GTCTAGGGTTGGCGTTGAAG. The relative levels of mtDNA copy number and mRNA expression in each group were analyzed using the $2^{-\Delta\Delta Ct}$ method.

ATP Level Measurement

Twelve animals (n = 4 for each group) in each group were sacrificed for cochlear ATP level measurement 1 h after the noise exposure. Two cochleae of an animal were quickly harvested and pooled as one sample. ATP levels in the cochlea were measured based on spectrophotometry using ATP Detection Kit (Solarbio, BC0305) according to the manufacturer's instructions. The working principle of the Kit is briefly described as follows. The Glucose and ATP are catalyzed by hexokinase to produce glucose 6-phosphate, which is further catalytically dehydrogenated to produce NADPH. The NADPH shows a characteristic absorption peak at 340 nm. The content of ATP is proportional to that of NADPH.

Extraction of Cochlear Protein and Immunoblotting

Twelve cochleae (n = 4 for each group) of six animals sacrificed on day 1 were homogenized in ice-cold RIPA lysis buffer (Beyotime, P0013B) containing protease inhibitor cocktail (Roche, #04693159001, Switzerland) using the cryogenic grinder. The tissue homogenate was placed on ice for 30 min, and then centrifuged at 12,000× g for 10 min at 4°C. The supernatant was retained and the protein concentration was determined using the BCA Determination Kit. Then the supernatant added with loading buffer was boiled for 5 min and stored at −20°C.

The protein samples (30 μg) were separated by 10–12% sodium dodecyl sulfate polyacrylamide gel electrophoresis (SDS-PAGE) electrophoresis and transferred to polyvinylidene fluoride (PVDF) membranes (Millipore, IPVH00010). After being blocked with 5% skimmed milk in TBS-T, the membranes were incubated for 1 h at room temperature on shaker and then overnight at 4°C with following primary antibodies: PGC-1α (Abcam, ab191838, 1:1,000), NRF-1 (GeneTex, GTX103179, 1:1,000), TFAM (Abcam, ab131607, 1:1,000), SOD2(GeneTex, GTX116093, 1:1,000), Bax (GeneTex, GTX109683, 1:1,000), ACTB (GeneTex, GTX109639, 1:2,000). The membranes were rinsed three times with TBS-T for 5 min, followed by incubation with HRP-linked secondary antibody (CST, #7074, 1:2,000) for 1 h at room temperature on a shaker. After being rinsed with TBS-T three times, the blots were visualized with chemiluminescent HRP substrate (Millipore, WBKLS0100) and scanned using the Chemiluminescence Imaging System (Fusion, Solo 6S, China). The band intensities were quantified using the ImageJ software (version 1.53a, USA) and normalized by using ACTB as the internal control.

Statistics

Statistical analyses were conducted using IBM SPSS software (version 25.0, USA) and GraphPad Prism software (version 8.0, USA). The group comparisons were performed using two-tailed, two-sample Student's t-test or one-way analysis of variance (ANOVA). When the difference was significant, the LSD *post hoc* test was used to identify the difference between the two groups. The p-value of <0.05 was considered statistical significance. All the data were presented as mean ± standard deviation (SD).

RESULTS

MT Entered Inner Ear After Systemic Administration

In order to investigate whether MT existed in the inner ear after the systemic administration, we analyzed the concentration of MT in the perilymph of the cochlea using LC-MS/MS. The perilymph was extracted 15 min after the injection and used for the detection and quantification of MT. As shown in **Supplementary Figures 1A–C**, the retention time of the MT in the perilymph was 3.302 min. The mass-to-charge ratio (m/z) of the parent ion was 474.2, which was consistent with the relative molecular mass of MT losing a chloride ion (**Supplementary Figure 1D**). The concentration of the MT in the perilymph of the cochlea was 18.541 μg/kg 15 min after the injection. These results indicated that MT could pass through the BLB and enter the inner ear.

Administration of MT Attenuated Noise-Induced Auditory Threshold Shift

To address whether systemic use of MT might prevent NIHL, we designed the experimental procedure as shown in **Figure 1**. The hearing function of the animals was evaluated via ABR testing 2 days before (−2d), 3 and 14 days after (+3d and +14d) noise exposure. There is no significant difference in baseline ABR threshold between groups (**Supplementary Figure 2**). Compared with saline-treated rats, MT-treated rats showed significantly decreased TTS on day 3 and PTS on day 14 at 8, 16, 24, and 32 kHz (**Figures 2A–D**). The 112dB noise exposure for 2 h resulted in about 30–40 dB threshold shift at all four frequencies on day 14 in the vehicle-treated group. However, in the MT-treated group, the threshold at 8 kHz was completely recovered and threshold shifts at 24 and 32 kHz were both within 10 dB on day 14 (**Figures 2E,F**). These data indicated that MT administration was able to attenuate noise-induced transient and permanent hearing loss.

MT Treatment Prevented OHC Loss Induced by Acoustic Trauma

We then asked if MT exhibits a protective effect on the OHC, which is one of the most vulnerable structures of the cochlea during acoustic trauma. We used the surface preparation

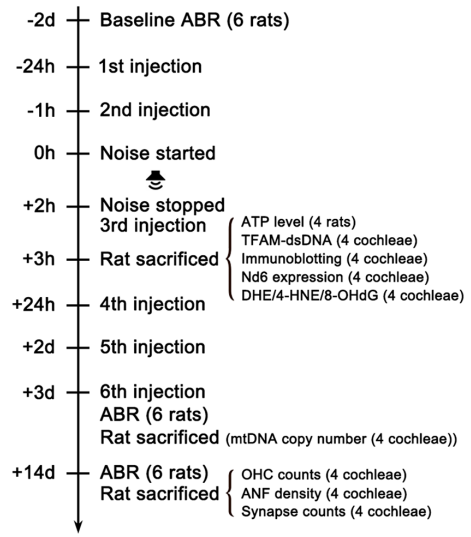

FIGURE 1 | Experimental timeline. The baseline hearing function of the rats was evaluated via ABR testing 2 days (2d) before the noise exposure. Rats were intraperitoneally injected with MT or vehicle (saline) 24 h and 1 h before the noise started. Then rats were exposed to 112dB SPL 8–16 kHz octave band noise for 2 h. The third shot was injected immediately after the noise stopped. One hour later, 12 animals in each group were sacrificed for analyses of oxidative stress level, mtDNA expression quantification, ATP measurement, immunoblotting and TFAM-mtDNA interaction. The rest of the animals received three additional injections once daily for the following 3 days. Then ABR testing were performed 3d after the noise exposure to evaluate TTS level. Then two animals in each group were sacrificed for the quantification of cochlear mtDNA copy number. After ABR testing 14d after the noise exposure for PTS level assessment, the remaining animals were sacrificed for analyses of OHC loss, IHC ribbon synapse loss and ANF degeneration. ABR, Auditory Brainstem Response.

technique to analyze the OHC loss 14 days after the noise exposure. The cochlea was divided into the apex, middle and base turns, which correspond to the low-, middle- and high-frequency regions of the cochlea. The loss of both the nucleus (DAPI) and the cell body (Myosin VIIa) was considered as the OHC loss. As shown in **Figures 3A,B**, noise overstimulation resulted in the most OHC loss at the base turn in the vehicle-treated group, showing 81.5% of the OHC survival. Compared with the vehicle-treated group, MT treatment significantly reduced noise-induced OHC loss at the base and middle turns of the cochlea. The OHC survival reached 95.2% at the base turn in the MT-treated group. These results indicated that MT was able to prevent OHC death after acoustic trauma.

MT Treatment Reduced IHC Ribbon Synapse Loss and ANF Degeneration Induced by Acoustic Trauma

Recent studies show that the loss of ribbon synapses between IHCs and spiral ganglion neurons (SGNs) is the primary pathology in NIHL, which is termed cochlear synaptopathy (Liberman and Kujawa, 2017). To explore the protective effect of MT against noise-induced IHC ribbon synapse loss, we quantified the number of paired ribbon synapses 14 days after the noise exposure. The surface preparations of the cochlea at approximately 16–20 kHz region were immunolabelled with antibodies against CtBP2 and GluA2 to manifest the pre- and post-synaptic structures. The juxtaposition of CtBP2 and GluA2 represents the functional synapses. In the vehicle-treated group, a significant decrease in the number of paired synapses was observed after noise exposure. Compared with the vehicle-treated group, treatment with MT significantly reduced the noise-induced loss of the paired ribbon synapses (**Figures 4A,B**).

In addition, NIHL is associated with the degeneration of ANFs which extend from SGNs to IHC ribbon synapses (Kujawa and Liberman, 2009). We next explored the protective effect of MT against noise-induced ANF degeneration by measuring the density of the fiber 14 days after the noise exposure. Compared with the control group, there was more than 50% degeneration of ANF in the vehicle-treated group. The remaining nerve fibers were fragmented and in a disordered arrangement. However, treatment with MT significantly recovered the density of ANF after acoustic trauma. The integrity of nerve fibers was partially restored in the MT-treated group (**Figures 4C,D**). These results indicated the neuroprotective effect of the MT against IHC ribbon synapse loss and ANF degeneration in NIHL.

MT Treatment Mitigated Oxidative Stress in the Cochlea After the Noise Exposure

Excessive ROS production is a major causative factor in noise-induced cochlear injury and hearing loss. ROS oxidizes polyunsaturated fatty acids to produce cytotoxic aldehydes. Among these, 4-hydroxynonenal (4-HNE) represents one of the major products of lipid peroxidation (Di Domenico et al., 2017). Dihydroethidium (DHE) is a fluorescent dye for detecting the level of superoxide ion (O_2·-). In the presence of O_2·-, DHE is oxidized to 2-hydroxyethidium, the fluorescence of which can be measured at an excitation and emission wavelength of 480 nm and 567 nm (Fetoni et al., 2015). In the present study, the level of cochlear oxidative stress was analyzed by 4-HNE and DHE fluorescent staining. As shown in **Figure 5A**, noise overstimulation induced a substantial increase of 4-HNE generation in the cochlea. Increased 4-HNE was mainly observed in HCs, stria vascularis (SV), and SGNs of the cochlea (**Supplementary Figure 3**). Compared with the vehicle-treated group, MT treatment significantly attenuated 4-HNE generation after the noise exposure. The DHE assay showed similar results. MT treatment remarkably reduced the DHE fluorescence induced by the noise overstimulation (**Figure 5B**). These data indicated that MT alleviated noise-induced oxidative stress in the cochlea by reducing the level of lipid peroxidation and O_2·- generation.

MT Treatment Alleviated mtDNA Oxidative Damage, and Maintained Mitochondrial Biogenesis and ATP Production After the Acoustic Trauma

The mitochondria are semi-autonomous organelles that contain their own circular genetic system. The mitochondrial genomes encode 13 essential protein subunits of the MRC complexes.

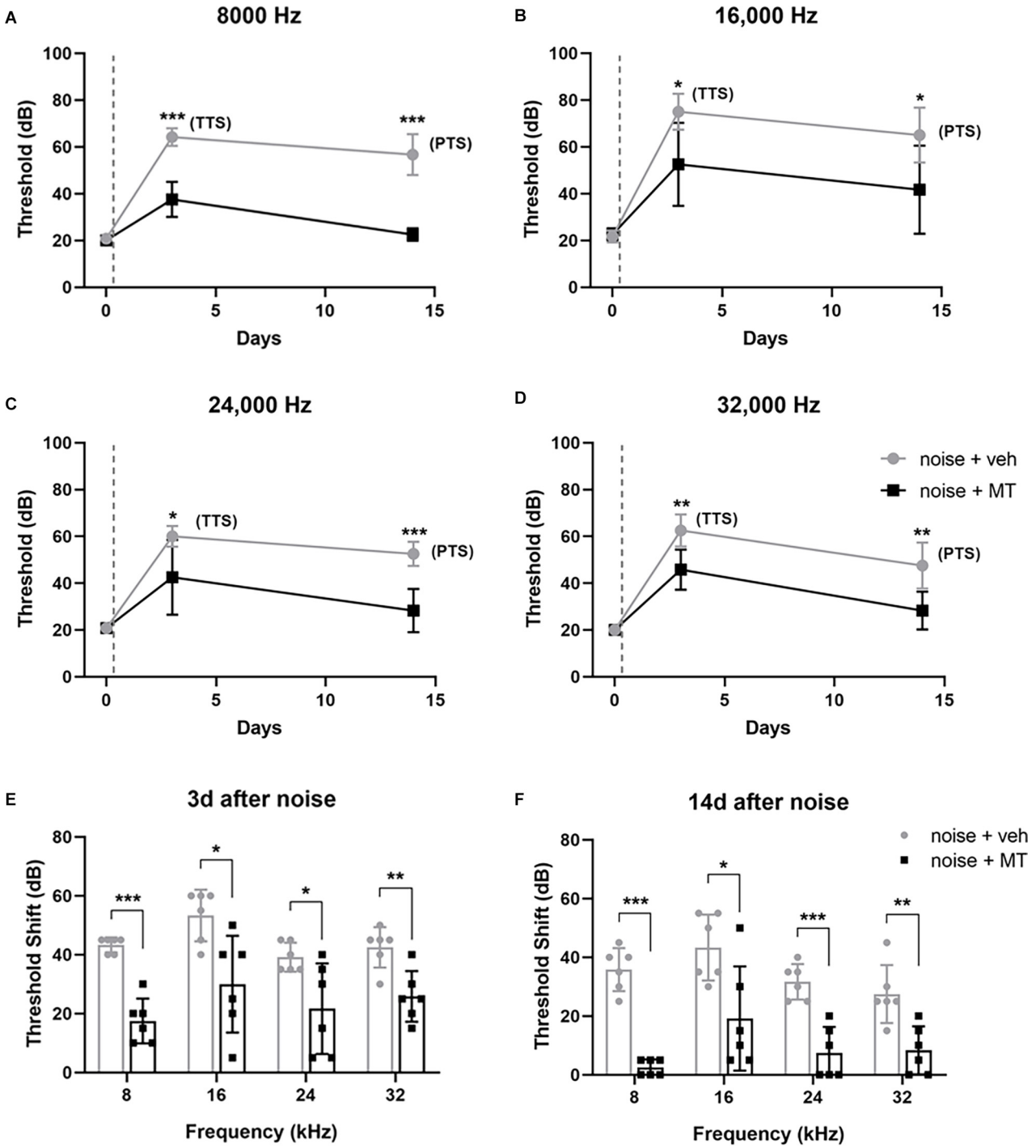

FIGURE 2 | MT treatment attenuated noise-induced auditory threshold shifts. **(A–D)** The auditory threshold alterations of the left ear of animals at 8, 16, 24 and 32 kHz over time. The baseline threshold, TTS, and PTS were evaluated before, 3d after and 14d after the noise exposure respectively. **(E,F)** The auditory threshold shifts over four frequencies on the day 3 and the day 14. The gray dotted lines indicate the time of acoustic trauma. Data are presented as means ± SD, $n = 6$ for each group, $^{*}p < 0.05$, $^{**}p < 0.01$, $^{***}p < 0.001$. MT, mito-TEMPO; TTS, temporary threshold shift; PTS, permanent threshold shift.

As is located close to the site of ROS generation, mtDNA molecules are easily damaged, resulting in decreased mtDNA content and mitochondrial dysfunction (Kang et al., 2007). 8-hydroxy-2'-deoxyguanosine (8-OHdG) is one of the most abundant oxidative adducts of DNA, reflecting the level of DNA oxidative damage (Han et al., 2020). In **Figures 6A,B**, a dramatic increase of 8-OHdG production was observed in the cytoplasm of SGNs following noise exposure. Since the DNA in cytoplasm

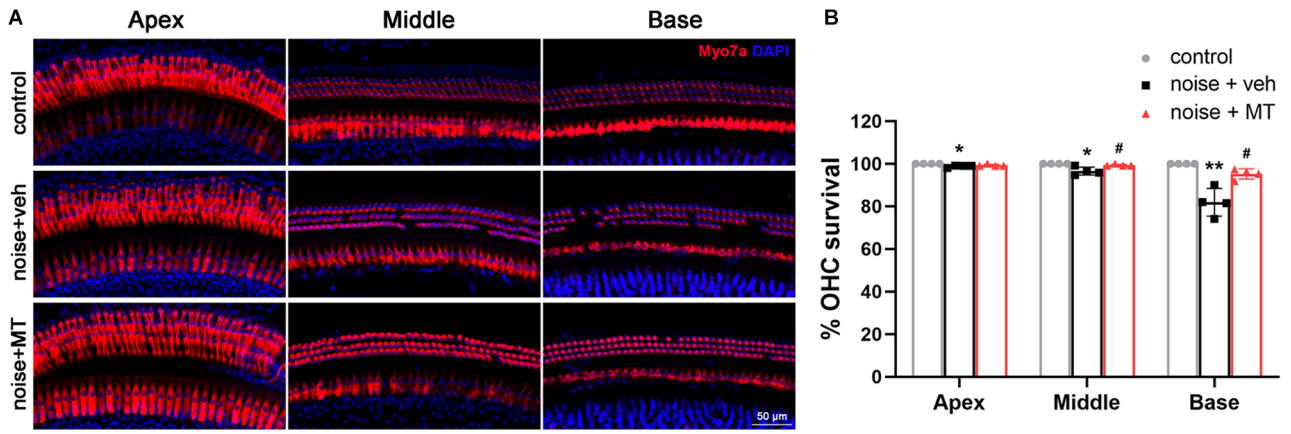

FIGURE 3 | MT treatment prevented noise-induced OHC loss. **(A)** Representative images of the apex, middle and base turn region of cochlear surface preparations 14 days after the noise exposure. HCs were indicated by Myosin VIIa (red) and DAPI (blue) fluorescent staining. **(B)** Quantification analysis of OHC survival in the apex, middle and base turn region of the cochlea 14 days after the noise exposure. Data are presented as means ± SD, $n = 4$ for each group, $^{*}p < 0.05$ vs. control group, $^{**}p < 0.01$ vs. control group, $^{\#}p < 0.05$ vs. vehicle-treated group. OHC, outer hair cell; HCs, hair cells.

refers to mtDNA, increased cytoplasmic 8-OHdG indicated that acoustic trauma-induced mtDNA oxidative damage in SGNs. Compared with the vehicle-treated group, treatment of MT significantly reduced noise-induced 8-OHdG production in SGNs.

Mitochondrial biogenesis relies on mtDNA replication and transcription to maintain mtDNA content and expression, and to produce new mitochondria. mtDNA is a multicopy genome and maintained at a relatively stable content (Scarpulla, 2008). Noise exposure resulted in a significant reduction of mtDNA content in the cochlea, reflected by the mtDNA copy number (**Figure 6C**). The mRNA level of MRC gene mt-Nd6 was also decreased after noise exposure, suggesting that the mtDNA expression in the cochlea was impaired by acoustic trauma (**Figure 6D**). In addition, ATP level in the cochlea was decreased following noise exposure, which indicated the dysfunction of the MRC (**Figure 6E**). However, treatment with MT significantly restored mtDNA content, mtDNA expression, and ATP level in the cochlea after noise exposure compared with the vehicle-treated group. These data indicated that MT was able to alleviate noise-induced mtDNA oxidative damage, maintain mitochondrial biogenesis and improve mitochondrial function of the cochlea.

MT Treatment Mitigated Noise-Induced Downregulation of TFAM and SOD2 Independent of the PGC-1α/NRF-1/TFAM Pathway

Mitochondrial biogenesis is a dynamic process of the generation of new mitochondria by synthesizing mitochondrial DNA and proteins. This activity requires several nucleus-encoded transcription factors, including peroxisome proliferator-activated receptor-gamma coactivator-1alpha (PGC-1α), nuclear respiratory factor 1 and 2 (NRF-1 and NRF-2), mitochondrial transcription factor A (TFAM), B1 (TFB1M), and B2 (TFB2M; Scarpulla, 2008). The PGC-1α/NRF-1/TFAM axis is the most studied pathway in regulating the replication and expression of mtDNA and mitochondrial biogenesis (Zhao et al., 2013; Xiong et al., 2019). In the above experiment, we found that acoustic trauma led to the decline of mtDNA content and expression level. To further explore the underlying mechanism, we next investigated the expression of PGC-1α/NRF-1/TFAM after noise exposure. As shown in **Figures 7A–D**, the expression level of PGC-1α and NRF-1 did not change following noise exposure. However, noise overstimulation resulted in a significant decrease in TFAM expression in the cochlea (**Figures 7A,E**). These results indicated that noise-induced decline of mtDNA content and expression was associated with TFAM reduction independent of PGC-1α/NRF-1/TFAM pathway. Compared with the vehicle-treated group, MT treatment attenuated TFAM expression reduction after the noise exposure.

Of the family of superoxide dismutase (SODs), only SOD2 (Mn-SOD) is located in mitochondria (Gross et al., 2014). We observed that noise exposure induced a dramatic decrease in the expression of mitochondrial SOD2 (**Figures 7A,F**). MT treatment partially improved SOD2 expression compared with the vehicle-treated group. In addition, the expression of the pro-apoptotic protein Bax was slightly upregulated following acoustic trauma and alleviated by MT treatment (**Figures 7B,G**). These data suggested that MT prevented noise-induced disruption of the mitochondrial antioxidant defense, and inhibited apoptosis activation in the inner ear.

MT Treatment Improved the Disruption of TFAM-mtDNA Interaction in the Cochlea After the Noise Exposure

TFAM binds the D-loop region of the mitochondrial genome to initiate mtDNA transcription and replication. TFAM also maintains the stability of mtDNA in a sequence-independent binding manner. We investigated the mtDNA-binding ability of TFAM by immunofluorescence colocalization analysis of TFAM and the double-stranded DNA (dsDNA) in the cytoplasm. As shown in **Figure 8A**, most mtDNA molecules were bound

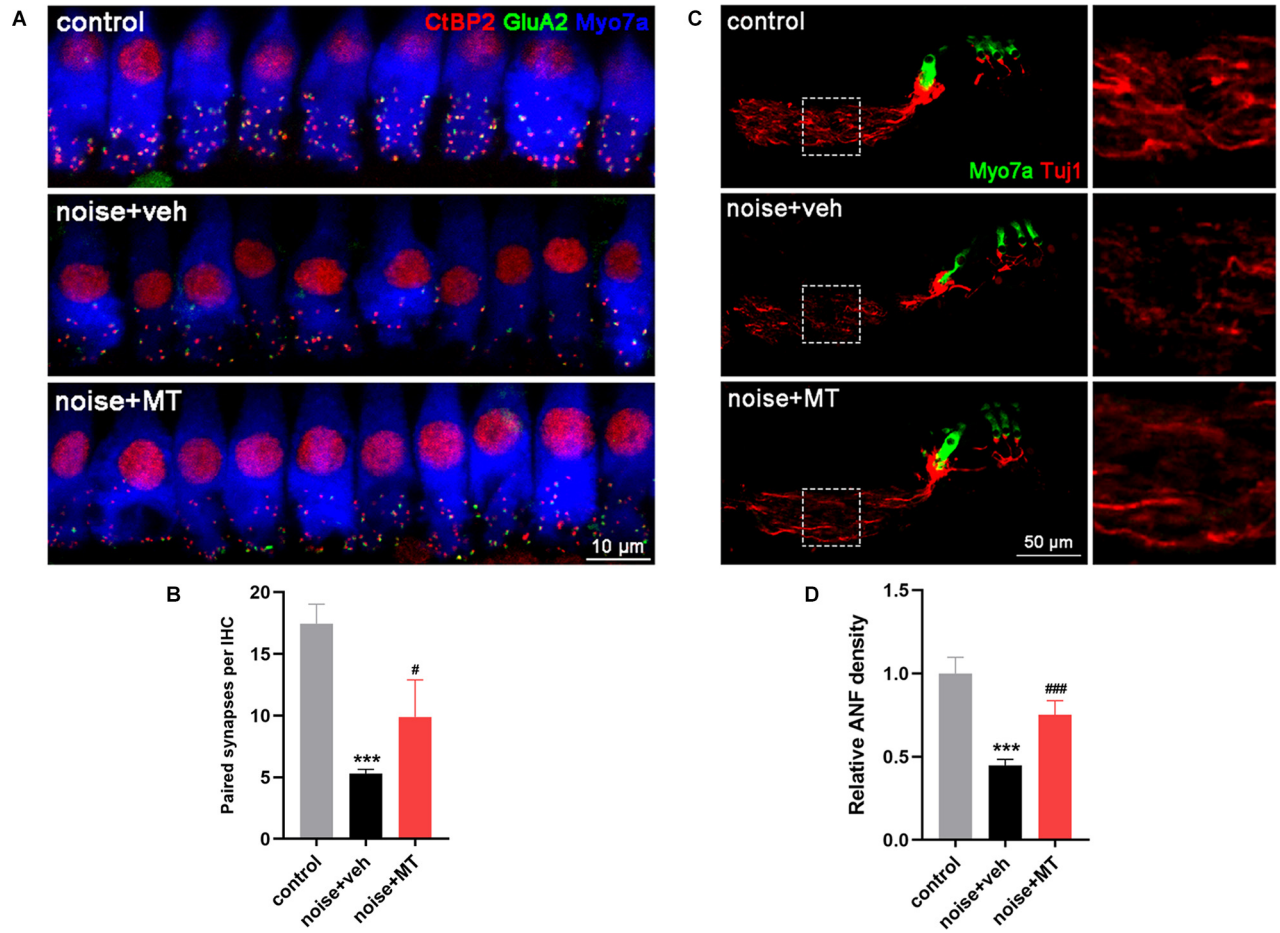

FIGURE 4 | MT treatment reduced IHC ribbon synapse loss and ANF degeneration induced by acoustic trauma. **(A)** Representative images of the IHC ribbon synapse at approximately 16–20 kHz region of the cochlea 14d after the noise exposure. Cochlear surface preparations were immunolabelled with CtBP2 (red), GluA2 (green) and Myosin VIIa (blue). **(B)** Quantification analysis of paired synapse per IHC, indicated by the juxtaposition of CtBP2 and GluA2. **(C)** Representative images of ANF and HCs in middle turn area of the midmodiolar sections 14d after the noise exposure. Cochlear sections were immunolabelled with Tuj1 (red) and Myosin VIIa (green). **(D)** Quantification analysis of ANF density 14d after the noise exposure. Data are presented as means ± SD, $n = 4$ for each group, $^{***}p < 0.001$ vs. control group, $^{\#}p < 0.05$ vs. vehicle-treated group, $^{\#\#\#}p < 0.001$ vs. vehicle-treated group. IHC, inner hair cell; ANF, auditory nerve fiber.

to TFAM (yellow arrows) within sensory hair cells labeled by Phalloidin in the control group. However, noise exposure induced a reduction of TFAM-mtDNA interaction, leading to a significant increase of naked mtDNA (white arrows) in the cytoplasm of OHCs. MT treatment partially recovered the TFAM-mtDNA interaction and significantly alleviated the increase of naked mtDNA in OHCs (**Figures 8A,B**). These data indicated that the mtDNA-binding activity of TFAM was weakened in the cochlea following acoustic trauma. MT treatment could restore the binding function of TFAM.

DISCUSSION

MT is a novelly developed mitochondria-target antioxidant with the ability to pass through the phospholipid bilayer and accumulate in mitochondria. In the present study, we investigated the protective effect of MT against NIHL and the underlying mechanism in a rat model. We found that MT reduced noise-induced threshold shift and prevented OHC loss, IHC ribbon synapse loss, and ANF degeneration after the noise exposure. We demonstrated that MT exerted its protective effect on hearing by reducing the level of oxidative stress and mtDNA damage, restoring TFAM-mtDNA interaction and mitochondrial function of the inner ear.

HCs and SGNs are two important cells responsible for the perception, mechanoelectrical transduction, and transmission of auditory signals. We found that acoustic trauma led to OHC loss while IHC remained intact. This differential vulnerability may be due to the difference in intrinsic antioxidant capacity between IHCs and OHCs (Sha et al., 2001; Rosenhall et al., 2019). However, the amount of paired ribbon synapses between IHCs and SGNs was significantly reduced after the noise exposure. ANFs are the peripheral neurites of SGNs. Noise-induced ANF degeneration was observed in our experiments. In addition, the damage of cochlear ribbon synapses and ANFs is also the pathologic change of noise-induced hidden hearing loss

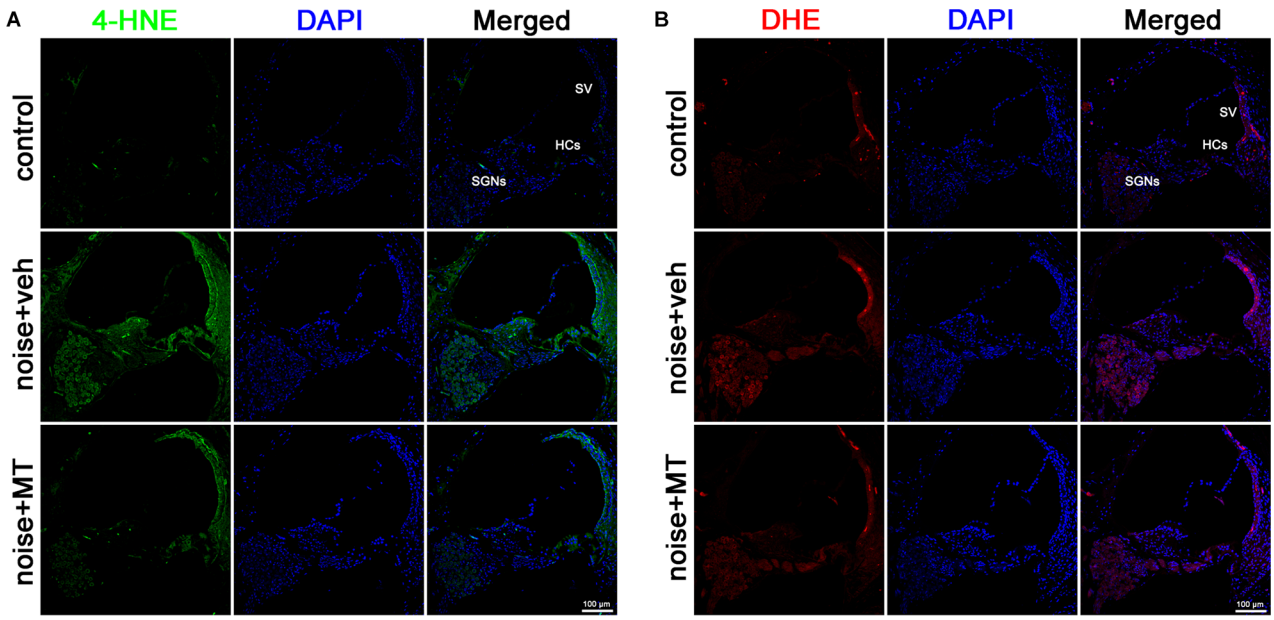

FIGURE 5 | MT treatment mitigated ROS generation in the cochlea. **(A)** Representative images of 4-HNE (green) and DAPI (blue) fluorescent staining in base turn area of the midmodiolar sections 1 h after the noise exposure. **(B)** Representative images of DHE (red) and DAPI (blue) fluorescent staining in base turn area of the midmodiolar sections 1 h after the noise exposure. Four cochleae form two animals were used in each group. HCs, hair cells; SV, stria vascularis; SGNs, spiral ganglion neurons; ROS, reactive oxygen species.

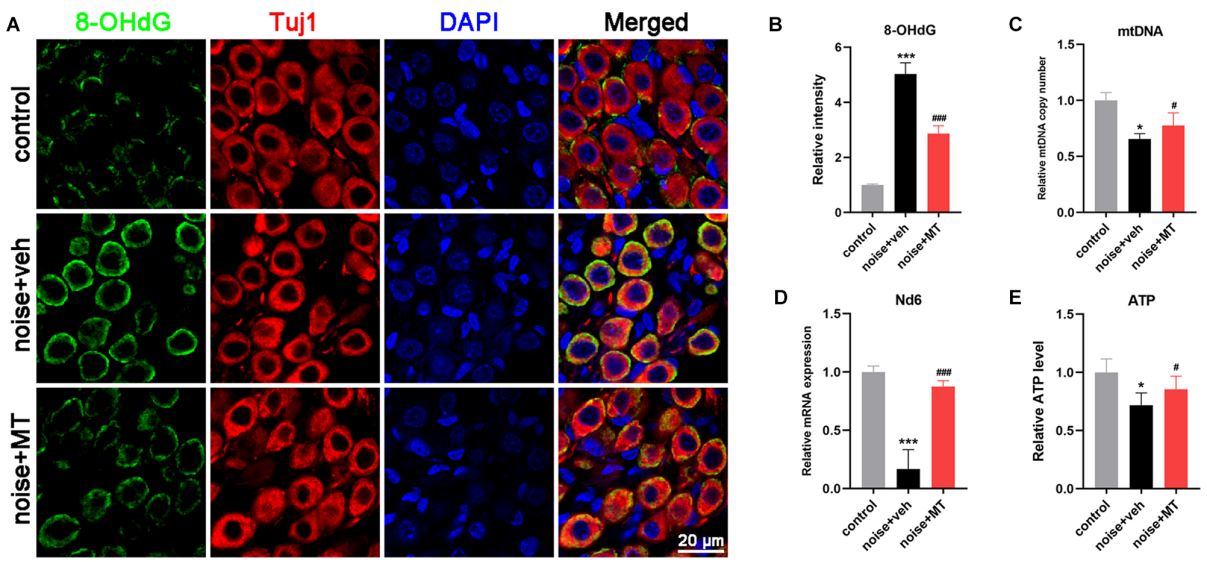

FIGURE 6 | MT treatment alleviated mtDNA oxidative damage, and maintained mitochondrial biogenesis and ATP production after the acoustic trauma. **(A)** Representative images of 8-OHdG (green), Tuj1 (red) and DAPI (blue) fluorescent staining in SGNs in frozen sections of the cochlea 1 h after the noise exposure. **(B)** Semi-quantitative analysis of the fluorescent intensity of 8-OHdG in SGNs 1 h after the noise exposure. **(C)** Real time-qPCR analysis of mtDNA copy number in the cochlea 3d after the noise exposure. **(D)** Real time-qPCR analysis of mitochondrial Nd6 expression level in the cochlear 1 h after the noise exposure. **(E)** The ATP level in the cochlea 1 h after the noise exposure. Data are presented as means ± SD, $n = 4$ for each group, $^{*}p < 0.05$ vs. control group, $^{***}p < 0.001$ vs. control group, $^{\#}p < 0.05$ vs. vehicle-treated group, $^{\#\#\#}p < 0.001$ vs. vehicle-treated group.

(NIHHL; Kujawa and Liberman, 2009; Liberman and Kujawa, 2017). The protective effect of MT on ribbon synapses and ANFs suggested its promising application to prevent NIHHL, which needs further investigations.

The present study showed increased oxidative stress indicated by cochlear 4-HNE and DHE level, which is consistent with previous studies (Park et al., 2014; Paciello et al., 2020; He et al., 2021b). We observed increased mtDNA oxidative damage

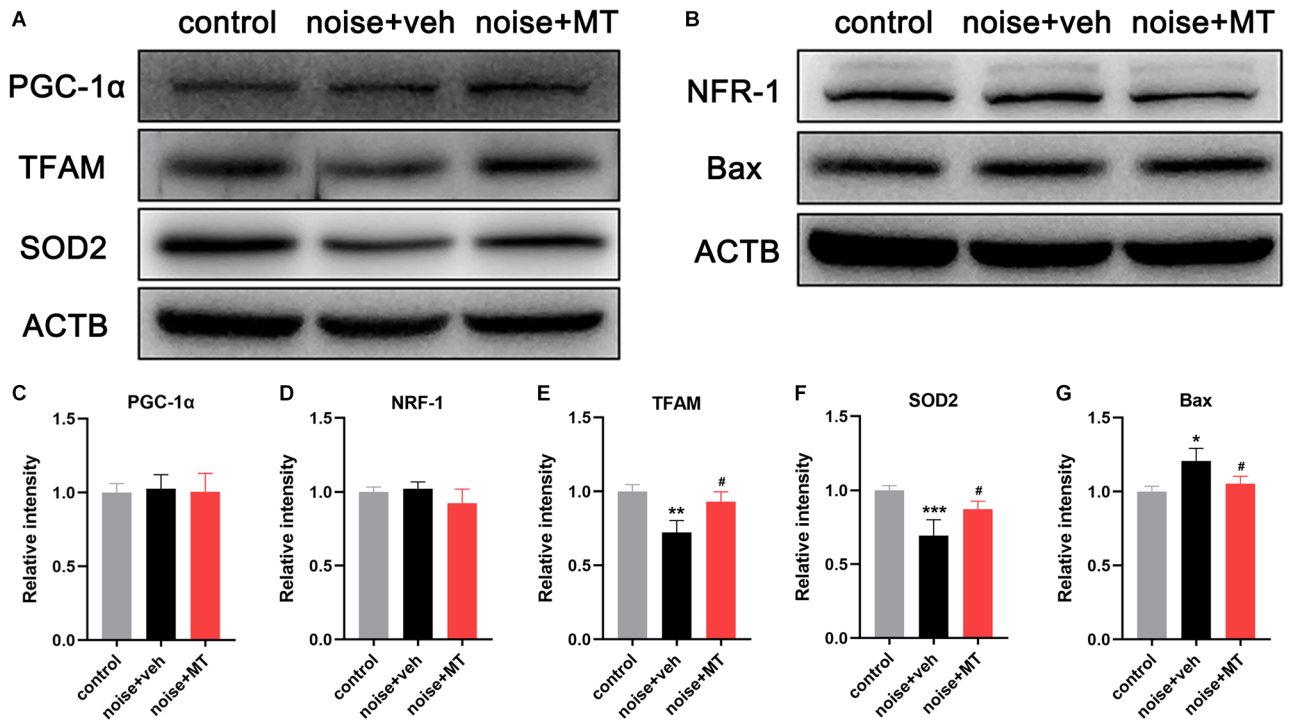

FIGURE 7 | MT treatment mitigated noise-induced downregulation of TFAM and SOD2 independent of the PGC-1α/NRF-1/TFAM pathway. **(A,B)** Immunoblotting of the PGC-1α, NRF-1, TFAM, SOD2, Bax, and ACTB protein in the cochlea 1 h after the noise exposure. **(C–G)** Quantification analysis of the optical density values of the immunoblot bands normalized by using ACTB as the internal control. Data are presented as means ± SD, $n = 4$ for each group, $^{*}p < 0.05$ vs. control group, $^{**}p < 0.01$ vs. control group, $^{***}p < 0.001$ vs. control group, $^{\#}p < 0.05$ vs. vehicle-treated group.

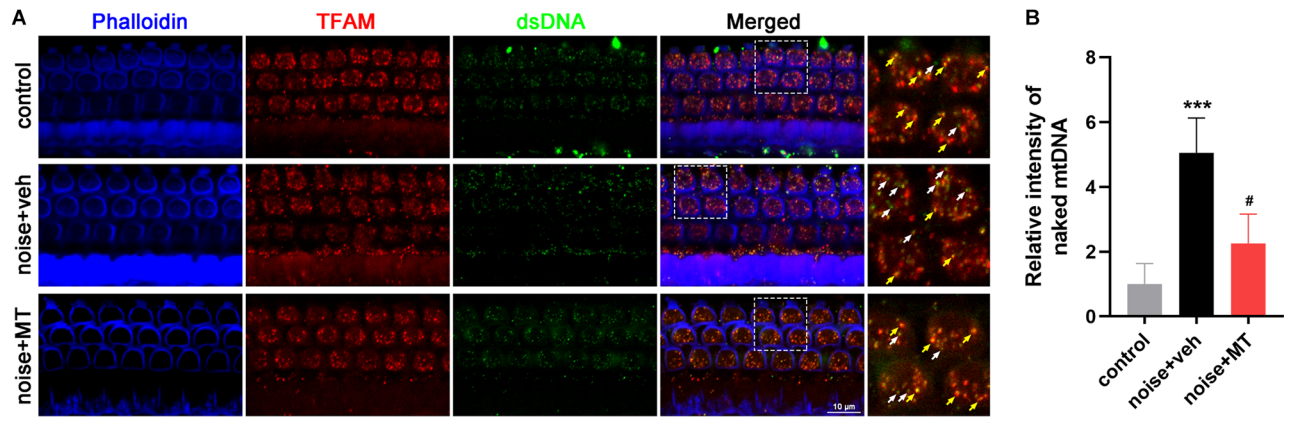

FIGURE 8 | MT treatment improved the disruption of TFAM-mtDNA interaction in the cochlea after the noise exposure. **(A)** Representative images of Phalloidin (blue), TFAM (red), and dsDNA (green) fluorescent staining in base turn area of the cochlear surface preparation 1 h after the noise exposure. Colocalized spots of TFAM and dsDNA were indicated in yellow arrows, while "orphan" dsDNA spots without colocalization of TFAM were indicated in the white arrows. **(B)** Quantification analysis of naked mtDNA in OHCs 1 h after the noise exposure. Data are presented as means ± SD, $n = 4$ for each group, $^{***}p < 0.001$ vs. control group, $^{\#}p < 0.05$ vs. vehicle-treated group.

indicated by 8-OHdG in SGNs 1 h after noise exposure. The cochlear mitochondrial function indicated by the ATP content was also impaired 1 h after the noise exposure, which is consistent with a previous study (Chen et al., 2012). Maintaining an adequate content of mtDNA copy number is important for cellular energy metabolism. Mitochondrial ROS induced by noise caused oxidative damage to mtDNA, resulting in mitochondrial dysfunction and energy insufficiency. SGNs are auditory neurons and consume a lot of energy in axoplasmic transport and electrical signal transmission. When the number

and function of the mitochondria in SGNs are impaired, the transport of cellular cargos including neurotrophin might be disrupted, resulting in the degeneration of the neurites of SGNs. Mitochondrial biogenesis is an activity to generate new mitochondria from the existing ones. This process requires the coordination of mtDNA replication and expression and is regulated by several transcription factors. The present study showed that mtDNA content and expression level were both decreased after noise exposure, which indicated the impaired mitochondrial biogenesis in the inner ear after the acoustic trauma. Yu and colleagues found mtDNA common deletion induced by D-gal increased susceptibility to NIHL in rats (Yu et al., 2014), suggesting the correlation between mtDNA integrity and the pathogenesis of NIHL. Interestingly, we found that the mtDNA expression level decreased immediately following the acoustic trauma (1 h after the noise exposure). In contrast, mtDNA copy number did not reduce until the third day after the noise exposure. The possible explanation is that DNA is more stable and has a longer half-life than RNA. It takes time for mtDNA to be degraded after oxidative stress damage. Previous studies also showed that mtDNA copy numbers decrease several days after the environmental stress (Bagul et al., 2018; Sugasawa et al., 2021).

The PGC-1α/NRF-1/TFAM axis is one of the most important pathways in regulating mitochondrial biogenesis. However, there are few studies on the alteration of the PGC-1α/NRF-1/TFAM pathway during acoustic trauma. In order to further explore the mechanism by which mtDNA content and expression are impaired in NIHL, we analyzed the expression level of this pathway. We found that the expression level of TFAM significantly decreased after the noise exposure, while the expression level of PGC-1α and NRF-1 remained unchanged. In addition, the TFAM function, as indicated by the mtDNA-binding ability, was also disrupted in OHCs after the noise exposure. These results indicate that noise-induced ROS specifically impairs the expression and function of TFAM without affecting the upstream PGC-1α and NRF-1. OHCs exhibit electromotility and mechanically amplify sound-evoked vibrations, which is an energy-consuming process. The impaired TFAM-mtDNA interaction leads to an increase of naked mtDNA molecules, which are vulnerable to oxidative damage by ROS. The abnormal mtDNA hinders the expression of mitochondrial respiratory chain proteins and ATP synthesis and might contribute to OHC dysfunction and death. A previous study showed that the phosphorylation and acetylation of TFAM within its HMG-box 1 domain reduced the DNA binding affinity, leading to TFAM-mtDNA disassembly (King et al., 2018). In addition, phosphorylation at serine 55/56 facilitated rapid degradation of TFAM by the Lon protease in mitochondria (Lu et al., 2013). Since it has been reported that acoustic trauma activates the protein kinase such as AMPK and extracellular signal-regulated protein kinase (ERK) in the inner ear (Kurioka et al., 2015; Hill et al., 2016), phosphorylation regulation might play a relevant role in the impaired expression and binding function of TFAM after the noise exposure. This speculation deserves further exploration in future studies.

Since oxidative stress plays an important role in the pathogenesis of NIHL, the antioxidants have been extensively studied in attenuating NIHL (Pak et al., 2020). A number of antioxidants show protective effects against NIHL in animal models such as glutathione, N-acetylcysteine (NAC), D-methionine, vitamin C, water-soluble coenzyme Q10, ebselen, resveratrol, and HK-2 (Ohinata et al., 2000; Seidman, 2003; Duan et al., 2004; Lynch et al., 2004; McFadden et al., 2005; Fetoni et al., 2009; Ewert et al., 2012; Chen et al., 2020), some of which have entered clinical trials (Kopke et al., 2015; Kil et al., 2017; Rosenhall et al., 2019). However, conventional antioxidants cannot remove only excess ROS without suppressing physiological ROS which are important for signal transduction. Recently, mitochondria-target antioxidants have been developed for the treatment of oxidative stress-related disease for their capacity to scavenge ROS from the source (Fujimoto and Yamasoba, 2019). MT is the antioxidant TEMPOL conjugated to the lipophilic triphenylphosphonium (TPP) cation, which can easily pass through the phospholipid bilayer and accumulate several hundred-fold into mitochondria (Trnka et al., 2008). A previous study shows that MT is BBB-penetrating and can be used as the contrast media in enhanced-magnetic resonance imaging (MRI) of the brain (Zhelev et al., 2013). In the present study, we demonstrated the existent of MT in the inner ear after the systemic administration. The lipophilic property of MT makes it easy to pass through the BLB and exert the antioxidant effects in the inner ear. MT exhibited a protective effect on hearing and cochlear cells against acoustic trauma. MT treatment reduced mitochondrial ROS production induced by noise exposure and therefore alleviated mtDNA oxidative damage and mitochondrial dysfunction. These results are consistent with a recent study (Zhao et al., 2021) which showed that MT alleviated ischemic acute kidney injury via reducing mitochondrial ROS and promoting TFAM-mediated mtDNA maintenance.

This study has several limitations. First, the methods used for hearing function evaluation were relatively simple. Four tested frequencies of the ABR covered about 50% length of the cochlea (from 30% to 80%), and may not represent well the hearing status of the animal. In future studies, we will use distortion product otoacoustic emissions (DPOAE) and compound action potential (CAP) for a comprehensive assessment of hearing function. Secondly, due to the technical difficulties, the RNA of HCs and SGNs was unable to be separately isolated. The alterations of mRNA expression of HCs and SGNs could not be analyzed respectively. Other methods such as RNA fluorescence *in situ* hybridization (FISH) will be used in our future studies. Finally, electron microscopy analysis of mitochondria was not performed in the present studies. Since mitochondrial fusion and fission are crucial processes to maintain mitochondrial homeostasis (Chan, 2020), the morphological changes of cochlear mitochondria in NIHL will be further studied in the following work.

In summary, our results first show TFAM reduction and the disruption of TFAM-mtDNA interaction in NIHL. Noise-induced ROS lead to mtDNA oxidative damage, impairing mtDNA expression and mitochondrial biogenesis. MT treatment exhibits a protective effect on hearing, OHCs,

IHC synapses, and ANFs against acoustic trauma partially by maintaining TFAM-mtDNA interaction and mitochondrial biogenesis based on its strong capacity of mitochondrial ROS scavenging.

DATA AVAILABILITY STATEMENT

The original contributions presented in the study are included in the article/**Supplementary Material**, further inquiries can be directed to the corresponding author/s.

ETHICS STATEMENT

The animal study was reviewed and approved by Institutional Animal Care and Use Committee of Fourth Military Medical University.

AUTHOR CONTRIBUTIONS

L-JL and QY designed the research. J-WC, P-WM, HY, W-LW, and P-HL performed the experiments. X-RD, Y-QL, and L-JL analyzed the data. J-WC prepared the figures. J-WC, QY, and L-JL wrote the manuscript. All authors contributed to the article and approved the submitted version.

FUNDING

This work was supported by the Military Logistics Research Project (18CXZ015).

ACKNOWLEDGMENTS

We thank Xi-Wang Hu and Ren-Feng Wang for their valuable guidance in image acquisition and ABR measurement. We also thank Qian Huo for proofreading the manuscript.

SUPPLEMENTARY MATERIALS

The Supplementary Material for this article can be found online at: https://www.frontiersin.org/articles/10.3389/fncel.2022.803718/full#supplementary-material.

REFERENCES

Abdullah-Al-Shoeb, M., Sasaki, K., Kikutani, S., Namba, N., Ueno, K., Kondo, Y., et al. (2020). The late-stage protective effect of mito-TEMPO against acetaminophen-induced hepatotoxicity in mouse and three-dimensional cell culture models. *Antioxidants (Basel)* 9:965. doi: 10.3390/antiox9100965

Bagul, P., Katare, P., Bugga, P., Dinda, A., and Banerjee, S. K. (2018). SIRT-3 modulation by resveratrol improves mitochondrial oxidative phosphorylation in diabetic heart through deacetylation of TFAM. *Cells* 7:235. doi: 10.3390/cells7120235

Blazer, D. G., and Tucci, D. L. (2019). Hearing loss and psychiatric disorders: a review. *Psychol. Med.* 49, 891–897. doi: 10.1017/S0033291718003409

Böttger, E. C., and Schacht, J. (2013). The mitochondrion: a perpetrator of acquired hearing loss. *Hear. Res.* 303, 12–19. doi: 10.1016/j.heares.2013.01.006

Chan, D. C. (2020). Mitochondrial dynamics and its involvement in disease. *Ann. Rev. Pathol.* 15, 235–259. doi: 10.1146/annurev-pathmechdis-012419-032711

Chandrasekaran, K., Anjaneyulu, M., Inoue, T., Choi, J., Sagi, A. R., Chen, C., et al. (2015). Mitochondrial transcription factor A regulation of mitochondrial degeneration in experimental diabetic neuropathy. *Am. J. Physiol. Endocrinol. Metab.* 309, E132–141. doi: 10.1152/ajpendo.00620.2014

Chen, G. D., Daszynski, D. M., Ding, D., Jiang, H., Woolman, T., Blessing, K., et al. (2020). Novel oral multifunctional antioxidant prevents noise-induced hearing loss and hair cell loss. *Hear. Res.* 388:107880. doi: 10.1016/j.heares.2019.107880

Chen, F. Q., Zheng, H. W., Hill, K., and Sha, S. H. (2012). Traumatic noise activates Rho-family GTPases through transient cellular energy depletion. *J. Neurosci.* 32, 12421–12430. doi: 10.1523/JNEUROSCI.6381-11.2012

Coleman, J. K. M., Kopke, R. D., Liu, J., Ge, X., Harper, E. A., Jones, G. E., et al. (2007). Pharmacological rescue of noise induced hearing loss using N-acetylcysteine and acetyl-l-carnitine. *Hear. Res.* 226, 104–113. doi: 10.1016/j.heares.2006.08.008

Di Domenico, F., Tramutola, A., and Butterfield, D. A. (2017). Role of 4-hydroxy-2-nonenal (HNE) in the pathogenesis of Alzheimer disease and other selected age-related neurodegenerative disorders. *Free Radic. Biol. Med.* 111, 253–261. doi: 10.1016/j.freeradbiomed.2016.10.490

Ding, X., Wang, W., Chen, J., Zhao, Q., Lu, P., and Lu, L. (2019). Salidroside protects inner ear hair cells and spiral ganglion neurons from manganese exposure by regulating ROS levels and inhibiting apoptosis. *Toxicol. Lett.* 310, 51–60. doi: 10.1016/j.toxlet.2019.04.016

Du, K., Farhood, A., and Jaeschke, H. (2017). Mitochondria-targeted antioxidant mito-tempo protects against acetaminophen hepatotoxicity. *Arch. Toxicol.* 91, 761–773. doi: 10.1007/s00204-016-1692-0

Duan, M., Qiu, J., Laurell, G., Olofsson, Å., Allen Counter, S., and Borg, E. (2004). Dose and time-dependent protection of the antioxidant N-l-acetylcysteine against impulse noise trauma. *Hear. Res.* 192, 1–9. doi: 10.1016/j.heares.2004.02.005

Ewert, D. L., Lu, J., Li, W., Du, X., Floyd, R., and Kopke, R. (2012). Antioxidant treatment reduces blast-induced cochlear damage and hearing loss. *Hear. Res.* 285, 29–39. doi: 10.1016/j.heares.2012.01.013

Fernandez, K., Spielbauer, K. K., Rusheen, A., Wang, L., Baker, T. G., Eyles, S., et al. (2020). Lovastatin protects against cisplatin-induced hearing loss in mice. *Hear. Res.* 389:107905. doi: 10.1016/j.heares.2020.107905

Fetoni, A. R., Paciello, F., Rolesi, R., Eramo, S. L., Mancuso, C., Troiani, D., et al. (2015). Rosmarinic acid up-regulates the noise-activated Nrf2/HO-1 pathway and protects against noise-induced injury in rat cochlea. *Free Radic. Biol. Med.* 85, 269–281. doi: 10.1016/j.freeradbiomed.2015.04.021

Fetoni, A. R., Paciello, F., Rolesi, R., Paludetti, G., and Troiani, D. (2019). Targeting dysregulation of redox homeostasis in noise-induced hearing loss: oxidative stress and ROS signaling. *Free Radic. Bio. Med.* 135, 46–59. doi: 10.1016/j.freeradbiomed.2019.02.022

Fetoni, A. R., Piacentini, R., Fiorita, A., Paludetti, G., and Troiani, D. (2009). Water-soluble Coenzyme Q10 formulation (Q-ter) promotes outer hair cell survival in a guinea pig model of noise induced hearing loss (NIHL). *Brain Res.* 1257, 108–116. doi: 10.1016/j.brainres.2008.12.027

Fischel-Ghodsian, N., Kopke, R. D., and Ge, X. (2004). Mitochondrial dysfunction in hearing loss. *Mitochondrion* 4, 675–694. doi: 10.1016/j.mito.2004.07.040

Fujimoto, C., and Yamasoba, T. (2019). Mitochondria-targeted antioxidants for treatment of hearing loss: a systematic review. *Antioxidants (Basel)* 8:109. doi: 10.3390/antiox8040109

Gross, J., Olze, H., and Mazurek, B. (2014). Differential expression of transcription factors and inflammation-, ROS- and cell death-related genes in organotypic cultures in the modiolus, the organ of corti and the stria vascularis of newborn rats. *Cell. Mol. Neurobiol.* 34, 523–538. doi: 10.1007/s10571-014-0036-y

Han, S., Du, Z., Liu, K., and Gong, S. (2020). Nicotinamide riboside protects noise-induced hearing loss by recovering the hair cell ribbon synapses. *Neurosci. Lett.* 725:134910. doi: 10.1016/j.neulet.2020.134910

He, Z., Guo, L., Shu, Y., Fang, Q., Zhou, H., Liu, Y., et al. (2017). Autophagy protects auditory hair cells against neomycin-induced damage. *Autophagy* 13, 1884–1904. doi: 10.1080/15548627.2017.1359449

He, Z., Li, M., Fang, Q., Liao, F., Zou, S., Wu, X., et al. (2021a). FOXG1 promotes aging inner ear hair cell survival through activation of the autophagy pathway. *Autophagy* 17, 4341–4362. doi: 10.1080/15548627.2021.1916194

He, Z., Pan, S., Zheng, H., Fang, Q., Hill, K., and Sha, S. (2021b). Treatment with calcineurin inhibitor FK506 attenuates noise-induced hearing loss. *Front. Cell Dev. Biol.* 9:648461. doi: 10.3389/fcell.2021.648461

Hill, K., Yuan, H., Wang, X., and Sha, S. H. (2016). Noise-induced loss of hair cells and cochlear synaptopathy are mediated by the activation of AMPK. *J. Neurosci.* 36, 7497–7510. doi: 10.1523/JNEUROSCI.0782-16.2016

Kang, D., Kim, S. H., and Hamasaki, N. (2007). Mitochondrial transcription factor A (TFAM): Roles in maintenance of mtDNA and cellular functions. *Mitochondrion* 7, 39–44. doi: 10.1016/j.mito.2006.11.017

Kil, J., Lobarinas, E., Spankovich, C., Griffiths, S. K., Antonelli, P. J., Lynch, E. D., et al. (2017). Safety and efficacy of ebselen for the prevention of noise-induced hearing loss: a randomised, double-blind, placebo-controlled, phase 2 trial. *Lancet* 390, 969–979. doi: 10.1016/S0140-6736(17)31791-9

King, G. A., Hashemi, S. M., Taris, K. H., Pandey, A. K., Venkatesh, S., Thilagavathi, J., et al. (2018). Acetylation and phosphorylation of human TFAM regulate TFAM-DNA interactions via contrasting mechanisms. *Nucleic Acids Res.* 46, 3633–3642. doi: 10.1093/nar/gky204

Kopke, R., Slade, M. D., Jackson, R., Hammill, T., Fausti, S., Lonsbury-Martin, B., et al. (2015). Efficacy and safety of N-acetylcysteine in prevention of noise induced hearing loss: a randomized clinical trial. *Hear. Res.* 323, 40–50. doi: 10.1016/j.heares.2015.01.002

Kujawa, S. G., and Liberman, M. C. (2009). Adding insult to injury: cochlear nerve degeneration after "temporary" noise-induced hearing loss. *J. Neurosci.* 29, 14077–14085. doi: 10.1523/JNEUROSCI.2845-09.2009

Kurabi, A., Keithley, E. M., Housley, G. D., Ryan, A. F., and Wong, A. C. Y. (2017). Cellular mechanisms of noise-induced hearing loss. *Hear. Res.* 349, 129–137. doi: 10.1016/j.heares.2016.11.013

Kurioka, T., Matsunobu, T., Satoh, Y., Niwa, K., Endo, S., Fujioka, M., et al. (2015). ERK2 mediates inner hair cell survival and decreases susceptibility to noise-induced hearing loss. *Sci. Rep.* 5:16839. doi: 10.1038/srep16839

Li, C., Sun, H., Xu, G., McCarter, K. D., Li, J., and Mayhan, W. G. (2018). Mito-tempo prevents nicotine-induced exacerbation of ischemic brain damage. *J. Appl. Physiol. (1985)* 125, 49–57. doi: 10.1152/japplphysiol.01084.2017

Liberman, M. C., and Kujawa, S. G. (2017). Cochlear synaptopathy in acquired sensorineural hearing loss: manifestations and mechanisms. *Hear. Res.* 349, 138–147. doi: 10.1016/j.heares.2017.01.003

Lin, M. T., and Beal, M. F. (2006). Mitochondrial dysfunction and oxidative stress in neurodegenerative diseases. *Nature* 443, 787–795. doi: 10.1038/nature05292

Liu, Y., Wang, Y., Ding, W., and Wang, Y. (2018). Mito-TEMPO alleviates renal fibrosis by reducing inflammation, mitochondrial dysfunction and endoplasmic reticulum stress. *Oxid. Med. Cell. Longev.* 2018:5828120. doi: 10.1155/2018/5828120

Loughrey, D. G., Kelly, M. E., Kelley, G. A., Brennan, S., and Lawlor, B. A. (2018). Association of age-related hearing loss with cognitive function, cognitive impairment and dementia: a systematic review and meta-analysis. *JAMA Otolaryngol. Head Neck Surg.* 144, 115–126. doi: 10.1001/jamaoto.2017.2513

Lu, B., Lee, J., Nie, X., Li, M., Morozov, Y. I., Venkatesh, S., et al. (2013). Phosphorylation of human TFAM in mitochondria impairs DNA binding and promotes degradation by the AAA+ lon protease. *Mol. Cell* 49, 121–132. doi: 10.1016/j.molcel.2012.10.023

Lynch, E. D., Gu, R., Pierce, C., and Kil, J. (2004). Ebselen-mediated protection from single and repeated noise exposure in rat. *Laryngoscope* 114, 333–337. doi: 10.1097/00005537-200402000-00029

McFadden, S. L., Woo, J. M., Michalak, N., and Ding, D. (2005). Dietary vitamin C supplementation reduces noise-induced hearing loss in guinea pigs. *Hear. Res.* 202, 200–208. doi: 10.1016/j.heares.2004.10.011

Nyberg, S., Abbott, N. J., Shi, X., Steyger, P. S., and Dabdoub, A. (2019). Delivery of therapeutics to the inner ear: the challenge of the blood-labyrinth barrier. *Sci. Transl. Med.* 11:eaao0935. doi: 10.1126/scitranslmed.aao0935

Ohinata, Y., Yamasoba, T., Schacht, J., and Miller, J. M. (2000). Glutathione limits noise-induced hearing loss. *Hear. Res.* 146, 28–34. doi: 10.1016/s0378-5955(00)00096-4

Ohlemiller, K. K., Wright, J. S., and Dugan, L. L. (1999). Early elevation of cochlear reactive oxygen species following noise exposure. *Audiol. Neurootol.* 4, 229–236. doi: 10.1159/000013846

Paciello, F., Di Pino, A., Rolesi, R., Troiani, D., Paludetti, G., Grassi, C., et al. (2020). Anti-oxidant and anti-inflammatory effects of caffeic acid: *in vivo* evidences in a model of noise-induced hearing loss. *Food Chem. Toxicol.* 143:111555. doi: 10.1016/j.fct.2020.111555

Pak, J. H., Kim, Y., Yi, J., and Chung, J. W. (2020). Antioxidant therapy against oxidative damage of the inner ear: protection and preconditioning. *Antioxidants (Basel)* 9:1076. doi: 10.3390/antiox9111076

Park, J., Jou, I., and Park, S. M. (2014). Attenuation of noise-induced hearing loss using methylene blue. *Cell Death Dis.* 5:e1200. doi: 10.1038/cddis.2014.170

Park, M., Lee, H. S., Song, J. J., Chang, S. O., and Oh, S. (2012). Increased activity of mitochondrial respiratory chain complex in noise-damaged rat cochlea. *Acta Otolaryngol.* 132, S134–S141. doi: 10.3109/00016489.2012.659755

Rosenhall, U., Skoog, B., and Muhr, P. (2019). Treatment of military acoustic accidents with N-Acetyl-L-cysteine (NAC). *Int. J. Audiol.* 58, 151–157. doi: 10.1080/14992027.2018.1543961

Scarpulla, R. C. (2008). Transcriptional paradigms in mammalian mitochondrial biogenesis and function. *Physiol. Rev.* 88, 611–638. doi: 10.1152/physrev.00025.2007

Seidman, M. (2003). Effects of resveratrol on acoustic trauma. *Otolaryngol. Head Neck Surg.* 129, 463–470. doi: 10.1016/s0194-5998(03)01586-9

Sha, S., and Schacht, J. (2017). Emerging therapeutic interventions against noise-induced hearing loss. *Expert Opin. Investig. Drugs.* 26, 85–96. doi: 10.1080/13543784.2017.1269171

Sha, S., Taylor, R., Forge, A., and Schacht, J. (2001). Differential vulnerability of basal and apical hair cells is based on intrinsic susceptibility to free radicals. *Hear. Res.* 155, 1–8. doi: 10.1016/s0378-5955(01)00224-6

Shetty, S., Kumar, R., and Bharati, S. (2019). Mito-TEMPO, a mitochondria-targeted antioxidant, prevents N-nitrosodiethylamine-induced hepatocarcinogenesis in mice. *Free Radic. Bio. Med.* 136, 76–86. doi: 10.1016/j.freeradbiomed.2019.03.037

Sugasawa, T., Ono, S., Yonamine, M., Fujita, S., Matsumoto, Y., Aoki, K., et al. (2021). One week of CDAHFD induces steatohepatitis and mitochondrial dysfunction with oxidative stress in liver. *Int. J. Mol. Sci.* 22:5851. doi: 10.3390/ijms22115851

Trnka, J., Blaikie, F. H., Smith, R. A. J., and Murphy, M. P. (2008). A mitochondria-targeted nitroxide is reduced to its hydroxylamine by ubiquinol in mitochondria. *Free Radic. Bio. Med.* 44, 1406–1419. doi: 10.1016/j.freeradbiomed.2007.12.036

Tsutsui, H., Kinugawa, S., and Matsushima, S. (2009). Mitochondrial oxidative stress and dysfunction in myocardial remodelling. *Cardiovasc. Res.* 81, 449–456. doi: 10.1093/cvr/cvn280

WHO. (2021). World report on hearing. Available online at: https://www.who.int/publications/i/item/world-report-on-hearing.

Wu, F., Xiong, H., and Sha, S. (2020). Noise-induced loss of sensory hair cells is mediated by ROS/AMPKα pathway. *Redox. Biol.* 29:101406. doi: 10.1016/j.redox.2019.101406

Xing, H., Zhang, Z., Shi, G., He, Y., Song, Y., Liu, Y., et al. (2021). Chronic inhibition of mROS protects against coronary endothelial dysfunction in mice with diabetes. *Front. Cell Dev. Biol.* 9:643810. doi: 10.3389/fcell.2021.643810

Xiong, H., Chen, S., Lai, L., Yang, H., Xu, Y., Pang, J., et al. (2019). Modulation of miR-34a/SIRT1 signaling protects cochlear hair cells against oxidative stress and delays age-related hearing loss through coordinated regulation of mitophagy and mitochondrial biogenesis. *Neurobiol. Aging* 79, 30–42. doi: 10.1016/j.neurobiolaging.2019.03.013

Yamashita, D., Jiang, H., Schacht, J., and Miller, J. M. (2004). Delayed production of free radicals following noise exposure. *Brain Res.* 1019, 201–209. doi: 10.1016/j.brainres.2004.05.104

Yu, J., Wang, Y., Liu, P., Li, Q., Sun, Y., and Kong, W. (2014). Mitochondrial DNA common deletion increases susceptibility to noise-induced hearing loss in a mimetic aging rat model. *Biochem. Biophys. Res. Commun.* 453, 515–520. doi: 10.1016/j.bbrc.2014.09.118

Yuan, H., Wang, X., Hill, K., Chen, J., Lemasters, J., Yang, S. M., et al. (2015). Autophagy attenuates noise-induced hearing loss by reducing oxidative stress. *Antioxid. Redox Signal.* 22, 1308–1324. doi: 10.1089/ars.2014.6004

Zhao, X., Sun, J., Hu, Y., Yang, Y., Zhang, W., Hu, Y., et al. (2013). The effect of overexpression of PGC-1α on the mtDNA4834 common deletion in a rat cochlear marginal cell senescence model. *Hear. Res.* 296, 13–24. doi: 10.1016/j.heares.2012.11.007

Zhao, M., Wang, Y., Li, L., Liu, S., Wang, C., Yuan, Y., et al. (2021). Mitochondrial ROS promote mitochondrial dysfunction and inflammation in ischemic acute kidney injury by disrupting TFAM-mediated mtDNA maintenance. *Theranostics* 11, 1845–1863. doi: 10.7150/thno.50905

Zhelev, Z., Bakalova, R., Aoki, I., Lazarova, D., and Saga, T. (2013). Imaging of superoxide generation in the dopaminergic area of the brain in Parkinson's disease, using Mito-TEMPO. *ACS Chem. Neurosci.* 4, 1439–1445. doi: 10.1021/cn400159h

Zinovkin, R. A., and Zamyatnin, A. A. (2019). Mitochondria-targeted drugs. *Curr. Mol. Pharmacol.* 12, 202–214. doi: 10.2174/1874467212666181127151059

Conflict of Interest: The authors declare that the research was conducted in the absence of any commercial or financial relationships that could be construed as a potential conflict of interest.

Publisher's Note: All claims expressed in this article are solely those of the authors and do not necessarily represent those of their affiliated organizations, or those of the publisher, the editors and the reviewers. Any product that may be evaluated in this article, or claim that may be made by its manufacturer, is not guaranteed or endorsed by the publisher.

frontiers in Cellular Neuroscience

ORIGINAL RESEARCH
published: 09 February 2022
doi: 10.3389/fncel.2022.804745

Phenotypic Profiling of People With Subjective Tinnitus and Without a Clinical Hearing Loss

Dongmei Tang[1,2†], Xiaoling Lu[1,2†], Ruonan Huang[1,2], Huiqian Yu[1,2] and Wenyan Li[1,2*]*

[1] State Key Laboratory of Medical Neurobiology and MOE Frontiers Center for Brain Science, ENT Institute and Department of Otorhinolaryngology, Eye & ENT Hospital, Fudan University, Shanghai, China, [2] NHC Key Laboratory of Hearing Medicine, Fudan University, Shanghai, China

OPEN ACCESS

Edited by:
Hai Huang,
Tulane University, United States

Reviewed by:
Lihao Ge,
National Institute of Neurological Disorders and Stroke (NINDS), United States
Jieyu Qi,
Southeast University, China

***Correspondence:**
Dongmei Tang
tang.dongm@163.com
Wenyan Li
wenyan_li2000@126.com

† These authors have contributed equally to this work and share first authorship

Specialty section:
This article was submitted to Cellular Neuropathology, a section of the journal Frontiers in Cellular Neuroscience

Received: 29 October 2021
Accepted: 04 January 2022
Published: 09 February 2022

Citation:
Tang D, Lu X, Huang R, Yu H and Li W (2022) Phenotypic Profiling of People With Subjective Tinnitus and Without a Clinical Hearing Loss. Front. Cell. Neurosci. 16:804745. doi: 10.3389/fncel.2022.804745

Our objective was to study the characteristics of patients with subjective tinnitus and normal hearing and to investigate whether the features correlated to different shapes on audiograms. In this retrospective study, 313 patients with subjective tinnitus and clinically normal hearing were enrolled from the tinnitus outpatient department of the Eye and ENT Hospital of Fudan University. The following phenotypic variables were collected: age, dominant tinnitus pitch (TP), tinnitus loudness, tinnitus duration, tinnitus severity, sex, education, hearing thresholds, tinnitus position, and tinnitus condition. The dominant TPs of patients with normal hearing were mostly high-pitched, with a mean of 4866.8 ± 2579.6 Hz; thus, we speculated that the condition is related to high-frequency hearing threshold elevations. We further divided the patients into four subgroups based on the matched TP: (i) TP $\leq$ 500 Hz (n = 34), (ii) 500 Hz $<$ TP $\leq$ 3,000 Hz (n = 15), (iii) 3,000 Hz $<$ TP $\leq$ 8,000 Hz (n = 259), and (iv) TP $>$ 8,000 Hz (n = 5). We studied the phenotypic profiling of different audiograms and found that the group with TP of $\leq$500 Hz had an average "inverted-U" shaped audiogram, and the group with TP between 500 and 3,000 Hz had a slowly ascending slope audiogram below 2,000 Hz, followed by a drastically descending slope audiogram ranging from 2,000 to 8,000 Hz; further, the high-frequency (3,000–8,000 Hz) and ultra-high-frequency ($>$8,000 Hz) groups had flat curves below 2,000 Hz and steeper slope audiograms over 2,000 Hz. Our findings confirmed a consistency ratio between the distributions of dominant TPs and the frequencies of maximum hearing thresholds in both ears. The dominant TP was positively correlated with the maximum hearing threshold elevation frequency (left ear: r = 0.277, p $<$ 0.05; right ear: r = 0.367, p $<$ 0.001). Hearing threshold elevations, especially in high frequency, might explain the appearance of dominant high-frequency TP in patients without clinically defined hearing loss. This is consistent with the causal role of high-frequency coding in the generation of tinnitus.

Keywords: tinnitus, normal hearing, audiogram, threshold elevation, high pitch

INTRODUCTION

Tinnitus is the auditory perception of sound in the absence of a corresponding external acoustic or electric stimulus. The commonly described sounds of tinnitus are chirping, buzzing, ringing, and hissing. More often, tinnitus is a tonal-like sensation, but in few cases, it sounds like a noise. Tinnitus affects 5–43% of people worldwide (McCormack et al., 2016). The risk of developing tinnitus increases with age, noise exposure, and hearing loss (Baguley et al., 2013; Langguth et al., 2013). It is widely accepted that the generation of tinnitus is often triggered by peripheral hearing damage and involves a central mechanism (Norena and Eggermont, 2003; Eggermont and Roberts, 2004). In people with hearing loss and tinnitus, the dominant tinnitus pitch (TP) is consistently associated with the region of hearing loss (Konig et al., 2006; Pan et al., 2009; Moore et al., 2010; Sereda et al., 2011, 2015; Schecklmann et al., 2012). However, clinical audiometric hearing loss does not occur in all cases of tinnitus. The percentage of tinnitus patients without clinical hearing loss is estimated at 20% (Jastreboff and Jastreboff, 2003).

One of the most frequently asked questions by patients suffering from tinnitus is "Why did I get tinnitus?," and the answer is more challenging in the presence of patients with normal hearing. A study assessing the reported lifetime noise exposure found some evidence for cochlear pathology associated with tinnitus and a normal audiogram (≤20 dB HL at 0.25–8 kHz). Guest et al. (2017) conducted a prospective study of 20 people with tinnitus and 20 controls closely matched for sex, age, and audiometric thresholds. Reported lifetime noise exposure was the only factor that differed between groups (Guest et al., 2017). Nevertheless, high-frequency hearing loss also provides some evidence for cochlear pathology associated with tinnitus and a normal audiogram (≤15 dB HL at 0.125 Hz–8 kHz). For example, by conducting a retrospective split of a sample of 75 people with tinnitus, Vielsmeier et al. (2015) found that those with hearing thresholds over 15 dB HL in at least one frequency from 10 to 16 kHz reported higher tinnitus symptom severity as measured by the Tinnitus Questionnaire (TQ) and Tinnitus Handicap Inventory (THI), compared with those with thresholds below 15 dB HL. In our previous study, we reported that extended high-frequency and average hearing thresholds across 4–16 kHz were significantly higher in the tinnitus group than in the matched volunteers without tinnitus (Song et al., 2021). In addition, some researchers have revealed that patients with normal hearing may have missed or hidden hearing loss. One study reported missed hearing loss in patients with normal audiograms when using fine frequency resolution in 1/24 octave step, suggesting that a more sophisticated pure-tone test should be considered to identify mild hearing impairment in patients with normal hearing (Xiong et al., 2019). Another study performed pure-tone audiometry (125 Hz–16 kHz), speech audiometry, transient evoked otoacoustic emissions (TEOAEs), distortion product otoacoustic emissions (DPOAEs), threshold equalizing noise (TEN) test (500 Hz–4 kHz), and electrocochleography (ECochG) for 9 individuals with tinnitus and normal hearing and 13 controls with normal hearing but no tinnitus, and the results showed that the SP/AP ratio in the ECochG test, together with the detection of dead regions in the TEN test, might be valuable in diagnosing hidden hearing loss, while the between-group differences in DPOAE and TEOAE were not significant (Kara et al., 2020).

According to this brief review of the literature, studies on tinnitus patients with normal hearing are mostly limited to detecting abnormalities of cochlear or auditory nerves; however, few studies have attempted to demonstrate the characteristics of pitch, loudness, and severity of tinnitus in patients with normal hearing (Savastano, 2008). Further, few studies have focused on the association between TP and audiogram features in patients with normal hearing. In this study, we focused on phenotypic profile of patients presenting with the primary complaint of subjective tinnitus and clinically normal hearing and confirmed that dominant TP was positively correlated with the maximum hearing threshold elevation frequency, which indicated that a more sophisticated pure-tone test, including extended high frequency, might be needed in evaluating the audiological features of dominant high-frequency TP in patients without clinically defined hearing loss.

MATERIALS AND METHODS

Participants

The study was conducted between January 2014 and October 2017 in tinnitus outpatients of the Eye and ENT Hospital of Fudan University, Shanghai. The recruited patients had a chief complaint of subjective tinnitus. We excluded patients who had pulsatile tinnitus and major health issues that impacted or prevented attendance. Patients with risk factors for tinnitus, such as noise exposure, sudden hearing loss, head or temporal trauma, tympanitis, and emotional disorders, were also identified and excluded. Finally, 313 patients with tinnitus and clinically normal hearing were identified from the database of all tinnitus patients, according to the World Health Organization [WHO] Programme for the Prevention of Deafness and Hearing Impairment (1997) definition of "the pure-tone threshold average across octave frequencies from 0.5 to 4 kHz ≤ 25 dB HL in each ear." In addition, 71 sex-matched volunteers with normal hearing and without tinnitus were also recruited in this study to compare the audiometric characteristics between the participants with and without tinnitus.

All tests were approved by the ethical committee of Fudan University. The sensitive information relevant to patient privacy was removed before analysis and all participants gave written informed consent to scientific research.

Audiometry Examination

A pre-exam otoscopic screening was performed to identify abnormalities in the external ear, including the ear canal and eardrum. Excessive or impacted cerumen was immediately cleared. All patients accepted the acoustic immittance measurement, and those with type "C" or type "B" diagram were ruled out. Pure-tone air conduction for both ears was measured between 0.25 and 8 kHz (0.25, 0.5, 1, 2, 4, and 8 kHz).

A standard Hughson-Westlake procedure (steps: 10 dB down, 5 dB up; 2 out of 3) was used to determine hearing thresholds.

Tinnitus Evaluation

A detailed tinnitus evaluation was performed on all participants (see below). We also recorded general information such as age, sex, educational background, self-reported laterality (unilateral, bilateral, or in the head), duration of tinnitus, and sound properties of tinnitus. Both intermittent and continuous tinnitus were included.

Symptom Severity

Tinnitus severity category was suggested according to the previous report (Biesinger et al., 1998). In brief, Grade I was defined as no impairment, Grade II as a mild complaint with passive emotional impact in certain defined conditions, Grade III as a permanent annoyance due to tinnitus (e.g., insomnia and anxiety), and Grade IV as severe impairment with severe negative impacts on work, study, or daily life.

To comprehensively evaluate the severity of tinnitus, three questionnaires were administered: the THI (Newman et al., 1996, 2008), Fear of Tinnitus Questionnaire (FTQ) (McCracken et al., 1992; Roelofs et al., 2007), and Athens Insomnia Scale (AIS) (Soldatos et al., 2000). The scoring criteria were as follows: (1) THI: slight (0–16), mild (18–36), moderate (38–56), and severe (58–100); (2) AIS: no insomnia (<4), suspicious insomnia (4–6), and insomnia (7–24); and (3) FTQ: 17 items in total, with 1 score per item; the higher the score, the more severe the tinnitus.

Pitch Matching

We established a "trinomial forced-choice method" for TP matching (China invention patent: ZL 201510165976.9). The first three frequencies were 2, 4, and 8 kHz, which were at least 5 dB above all the corresponding hearing thresholds, and each lasted 500 ms with a 1-s interval. Patients were instructed to identify the frequency closest to their TP and to judge whether it was higher, lower, or equal to their tinnitus. If 2 kHz was selected, then the upper limit frequency of tinnitus was 4 kHz − 1/3 octaves; if 4 kHz was selected, then the frequency of tinnitus was between 2 kHz + 1/3 octaves and 8 kHz − 1/3 octaves; and if 8 kHz was selected, then the lower limit frequency of tinnitus was 8 kHz − 1/3 octaves. In this way, the given sound range was gradually narrowed to the closest frequency by a final step of 1/3 octaves. A threefold repetition was performed to clearly distinguish between each of the three acoustic stimuli. When a final pitch match was selected, an octave confusion test was conducted to avoid selection bias. The octave confusion test conducted in the present study was 1/3 octaves above and 1/3 octaves below the selected pitch (±1 octave when below 1,000 Hz) whenever such frequencies were available. The final confirmed pitch was recorded as the dominant pitch of tinnitus. There were 15 frequencies in total for TP matching, namely, 0.25, 0.5, 1, 1.26, 1.58, 2, 2.52, 3.18, 4, 5.04, 6.35, 8, 10.08, 12.7, and 16 kHz.

Loudness Matching

The loudness matching was performed in a manner similar to that in the pitch-matching test, and the final gap difference was narrowed to the nearest 1 dB step size. The loudness of tinnitus was reflected in the sensation level (dB SL). Sensation level was defined as the loudness value above the hearing threshold at the TP.

The tinnitus testing devices for pitch and loudness were calibrated twice a year at the Shanghai Institute of Measurement and Testing Technology[1], which were authorized by the Administration of Quality Supervision, Inspection and Quarantine and accredited by the China National Accreditation Service for Conformity Assessment.

Data Analysis

The continuous variables are expressed as mean ± standard deviation, while the categorical variables are expressed as number (%). Group comparisons were performed using one-way analysis of variance and Fisher's exact test with RStudio software (version 4.0.3). Correlation analysis was performed between the dominant TP and corresponding frequency of maximum hearing threshold using the Spearman rank test. All the statistics and plotting were performed with RStudio software (version 4.0.3). The distribution of TP and frequency of maximum hearing threshold was mapped with Excel. The level of statistical significance was defined as a p-value of <0.05.

RESULTS

Clinical and Demographical Characteristics

According to the WHO grades of hearing impairment (version 1997), 313 subjects conformed to the criteria of clinically normal hearing with standard audiometry. The mean age was 40.2 ± 12.8 years, the male-to-female ratio was 54.3% (n = 170): 45.7% (n = 143), and nearly half of the patients (47.6%) had a college degree or higher. The mean dominant TP was 4866.8 ± 2579.6 Hz, demonstrating a common dominant high-frequency TP. The pitch-matching analysis showed that most of the matched frequencies (308/313) were no more than 8 kHz, while only five patients reported a dominant TP at 10.08 kHz. To further analyze the data, we divided the participants into four subgroups based on the dominant TP: low-pitched (≤500 Hz), middle-pitched (500–3,000 Hz), high-pitched (3,000–8,000 Hz), and ultra-high-pitched (>8,000 Hz). As shown in **Table 1**, the four groups were significantly different in terms of age (p = 0.037), tinnitus loudness ($p < 0.001$), and sex composition (p = 0.025). However, they were homogeneous in terms of duration (p = 0.940), severity (p = 0.965), position (p = 0.334), educational background (p = 0.166), and persistence (p = 0.089) of tinnitus. The mean duration of tinnitus was 30.7 ± 53.7 months, implying that most patients had chronic tinnitus. There was preponderance of bilateral tinnitus reported by the majority of participants (59.1% in total; 44.1, 66.7, 60.2, and 60.0% in the low, middle, high-, and ultra-high-pitched groups, respectively), with only a few reporting unilateral tinnitus (left 21.1%, right 18.2% in total; left 32.4% vs. right 23.5%, left 6.7%

[1]http://english.simt.com.cn

TABLE 1 | Demographic characteristics of patients with tinnitus and clinically normal hearing.

	Total (*n* = 313)	≤500 Hz (*n* = 34)	500–3,000 Hz (*n* = 15)	3,000–8,000 Hz (*n* = 259)	>8,000 Hz (*n* = 5)	*p*-value
Continuous variable, mean (SD)						
Age (years)	40.2 (12.8)	40.9 (13.9)	36.0 (15.4)	40.6 (12.4)	25.6 (13.1)	**0.037***
Dominant tinnitus pitch (Hz)	4866.8 (2579.6)	397.1 (124.9)	1869.3 (484.4)	5526.6 (1978.3)	1,0080 (0)	/
Tinnitus loudness (dB SL)	9.1 (5.2)	10.9 (6.1)	12.1 (9.1)	8.5 (4.6)	16.0 (6.5)	**<0.001***
Tinnitus duration (months)	30.7 (53.7)	25.8 (38.4)	32.3 (37.7)	31.4 (56.7)	24.4 (23.5)	0.940
THI score	31.0 (23.3)	30.5 (19.8)	35.1 (27.0)	31.0 (23.6)	21.2 (17.5)	0.716
AIS score	5.9 (5.3)	5.8 (5.7)	7.3 (4.7)	5.8 (5.3)	3 (3.7)	0.454
FTQ score	8.1 (4.0)	7.9 (3.5)	9.7 (4.1)	8.0 (4.0)	6.4 (4.3)	0.306
Categorical variable, n (%)						
Sex						
Male	170 (54.3%)	11 (32.4%)	7 (46.7%)	150 (57.9%)	3 (60.0%)	**0.025***
Female	143 (45.7%)	23 (67.6%)	8 (53.3%)	109 (42.1%)	2 (40.0%)	
Education						
Below high school	95 (30.4%)	15 (44.1%)	2 (13.3%)	78 (30.1%)	0 (0)	
High school or technical school	69 (22.0%)	8 (23.5%)	4 (26.7%)	55 (21.2%)	2 (40.0%)	0.166
College degree or above	149 (47.6%)	11 (32.4%)	9 (60.0%)	126 (48.7%)	3 (60.0%)	
Tinnitus position						
Left ear	66 (21.1%)	11 (32.4%)	1 (6.7%)	53 (20.5%)	1 (20.0%)	
Right ear	57 (18.2%)	8 (23.5%)	3 (20.0%)	46 (17.8%)	1 (20.0%)	0.334
Bilateral ears	185 (59.1%)	15 (44.1%)	10 (66.7%)	156 (60.2%)	3 (60.0%)	
In head	5 (1.6%)	0 (0)	1 (6.6%)	4 (1.5%)	0 (0)	
Tinnitus severity						
Grade I	5 (1.6%)	1 (2.9%)	0 (0)	4 (1.5%)	0 (0)	
Grade II	124 (39.6%)	12 (35.3%)	6 (40.0%)	103 (39.8%)	3 (60.0%)	0.965
Grade III	140 (44.7%)	17 (50.0%)	7 (46.7%)	114 (44.0%)	2 (40.0%)	
Grade IV	44 (14.1%)	4 (11.7%)	2 (13.3%)	38 (14.7%)	0 (0)	
Tinnitus condition						
Intermittent	45 (14.4%)	8 (23.5%)	4 (26.7%)	32 (12.4%)	1 (20.0%)	0.089
Continuous	268 (85.6%)	26 (76.5%)	11 (73.3%)	227 (87.6%)	4 (80.0%)	

The bold values represent the variable items compared between the four subgroups. n means number and SD means standard deviation.
**P < 0.05.*

vs. right 20.0%, left 20.5% vs. right 17.8%, and left 20.0% vs. right 20.0% in the low, middle, high-, and ultra-high-pitched groups, respectively). The overall education level of the patients varied; 47.6% had a college degree or higher, 22.0% finished high school or technical school, and 30.4% received primary education or were illiterate. Most patients (85.6%) reported continuous tinnitus, with the remaining patients reporting intermittent tinnitus (**Table 1**).

Tinnitus Loudness and Severity

The mean tinnitus loudness was 9.1 ± 5.2 dB SL above the threshold for all patients with tinnitus and normal hearing. To be visualized, the level of loudness was mid-range; hence, the tinnitus was hardly masked by the surrounding ambient sounds, causing disruption to patients' daily lives, sleep, and work. The mean loudness measured by sensation level was 10.9 ± 6.1, 12.1 ± 9.1, 8.5 ± 4.6, and 16.0 ± 6.5 in the low, middle, high-, and ultra-high-pitched groups, respectively ($p < 0.001$). According to the Biesinger classification, 1.6% of patients had no impairment (Grade I), 39.6% had slight impairment (Grade II), 44.7% had permanent annoyance (Grade III), and 14.1% had severe impairment (Grade IV), with no differences between the four subgroups. This implied that most patients with tinnitus and normal hearing were slightly or severely disturbed in private and professional areas. These findings were reconfirmed by the three questionnaire assessments: the THI global score was 31.0 ± 23.3, AIS score was 5.9 ± 5.3, and FTQ score was 8.1 ± 4.0 (**Table 1**).

Dominant Tinnitus Pitch of Clinically Normal Hearing Might Be Associated With Hearing Threshold Elevations

In previous studies, TP has been found to be consistent with the region of hearing loss (Sereda et al., 2011, 2015; Schecklmann et al., 2012). However, the cause of tinnitus without a clinical hearing loss remains unclear, especially for those who do not have any hearing deficits at all test frequencies ranging from 250 to 8,000 Hz. Among all the features of tinnitus with normal hearing, the average high-pitched-matching result was the most salient and intriguing. We speculated that the generation of tinnitus and the dominant TP in patients with normal hearing might be related to different audiogram types. We drew the average pure-tone audiograms for each ear in the low, middle, high-, and

ultra-high-pitched subgroups. As a contrast, 71 volunteers with normal hearing and without tinnitus also received the standard pure-tone audiometry in the same audiometric environment with the patients with tinnitus.

As shown in **Figure 1** and **Table 2**, the control group totally had flat audiograms both in right ears and left ears, and the average pure-tone thresholds were all less than those in patients with tinnitus from 250 to 8,000 Hz. To clearly compare the audiogram curves between tinnitus patients and the controls, the average pure-tone audiogram of volunteers without tinnitus was presented repeatedly in the four subgroups. The average pure-tone audiograms in the low-pitched (≤500 Hz) group presented an inverted-U shape in both left and right ears, indicating that dominant low-pitched tinnitus may be associated with hearing threshold elevations ranging from 250 to 500 Hz (**Figure 1A**). The inclination and intensity of threshold elevations in low frequencies were attenuated in the middle-pitched (500–3,000 Hz) subgroup when compared to the low-pitched subgroup, demonstrating a slowly ascending slope audiogram below 2,000 Hz, followed by a drastically descending slope audiogram ranging from 2,000 to 8,000 Hz (**Figure 1B**). In the high- (3,000–8,000 Hz) and ultra-high- (above 8,000 Hz) pitched subgroups, both the audiogram curves below 2,000 Hz were flat without any severe threshold elevations, while the audiograms over 2,000 Hz revealed steeper slopes in both ears (**Figures 1C,D**). Therefore, widespread threshold elevations in high frequencies (over 2,000 Hz) were found in all the four subgroups, which might contribute to reasonable explanation for our observation that the majority of patients with normal hearing had a dominant high-frequency TP. However, the threshold elevations in low frequencies (250–500 Hz) and the elevated degrees would control the final distribution of TP. The inverted-U-shaped audiogram in patients with normal hearing might indicate a low-pitched tinnitus.

We further examined the association between TP and the frequencies of hearing threshold elevation and found that TP was correlated to the frequency of maximum hearing threshold in both ears, with a coefficient of association of 0.277 in the left ears ($p = 0.015$) (**Figure 2A**) and 0.367 in the right ears ($p < 0.001$) in the high-pitched subgroup (**Figure 2B**). This finding confirmed that the dominant TP might be speculated by the different audiograms of patients, indicating that minor pure-tone threshold elevation ranging from 250 to 8,000 Hz might be responsible for the generation of tinnitus in individuals with normal hearing.

Moreover, we analyzed the distribution of dominant TP vs. the distribution of maximum threshold-elevating frequencies in both ears and found that the distributions of threshold-elevating frequencies in both ears were consistent with the distribution of dominant TP. Furthermore, of the 313 participants, 259 had high-pitched tinnitus, 251 had maximum hearing threshold in the high frequency range (3,000–8,000 Hz) in their left ears, and 249 had maximum hearing threshold in the high frequency range (3000–8000 Hz) in their right ears. These results confirmed our explanation that the matched dominant TP was mostly high-pitched in patients without clinical hearing loss (**Figure 3**). Our findings provide noteworthy links between tinnitus pitch and subclinical threshold elevations in the audiometric profile within the testing range of conventional audiometer at the first time, indicating a causal role of mild threshold elevation in the generation of tinnitus. Additionally, the pitch of tinnitus might be predicted from different types of audiograms.

DISCUSSION

It is well-known that the presence of tinnitus is strongly associated with hearing loss, and that the dominant TP is often within the region of hearing loss. However, tinnitus is not limited to individuals with a clinically measurable hearing loss. To date, only a few studies have examined the association between tinnitus and "subclinical" threshold elevations in the audiometric profile. Previous research mainly focused on discovering the existence of ultra- or extended high-frequency (above 8 kHz) hearing loss in patients with tinnitus and normal hearing, as well as the age-, sex-, and audiometry-matched controls without tinnitus; however, they failed to find a close relationship between TP and the frequency of maximum hearing loss or edge frequency. The possible reason might be partially attributed to the absence of TP-matching procedure in extended high-frequency regions. In the present study, we performed the "trinomial forced-choice method" for tinnitus matching, with 16 frequency measurement points ranging from 250 Hz to 16 kHz. Nevertheless, 308 of the 313 participants reported matched TPs no higher than 8 kHz, indicating that ultra-high frequency hearing loss might be insufficient evidence for the generation of tinnitus in patients with normal hearing and that the profiling of conventional audiometry (125 Hz–8 kHz) data should be investigated further. Hence, this study sought to verify whether minor audiometric deficits up to 8 kHz play a defining role in the phenotypic profiling of tinnitus in patients with normal hearing.

Our results found that the dominant TP of patients with clinically normal hearing was almost within the high-frequency range (especially at 4 and 8 kHz), with a mean of 4866.8 ± 2579.6 Hz. In several studies, Paglialonga et al. (2010, 2011) have established that normal hearing (with mean thresholds ≤ 20 dB HL at 0.5–4 kHz and ≤ 40 dB at 8 kHz) in patients with tinnitus does not preclude a completely normal hearing level for someone with cochlear dead regions or outer hair cell damage, particularly at high frequencies. This pattern is frequently observed when compared to controls (Paglialonga et al., 2010, 2011). In the present study, we demonstrated a more direct correspondence between TPs and the frequencies of hearing deficits according to the audiometric profiles. The participants were divided into four groups based on the pitch-matching results: low-frequency (≤500 Hz), middle-frequency (500–3,000 Hz), high-frequency (3,000–8,000 Hz), and ultra-high-frequency (>8,000 Hz). Interestingly, 82.7% of the participants had high-pitched tinnitus in the 3–8 kHz range, with audiograms characterized by dramatical threshold elevations above 2 kHz in a sharp descending slope and flat curve below 2 kHz with no obvious threshold elevations. A similar phenotypic profiling of audiograms

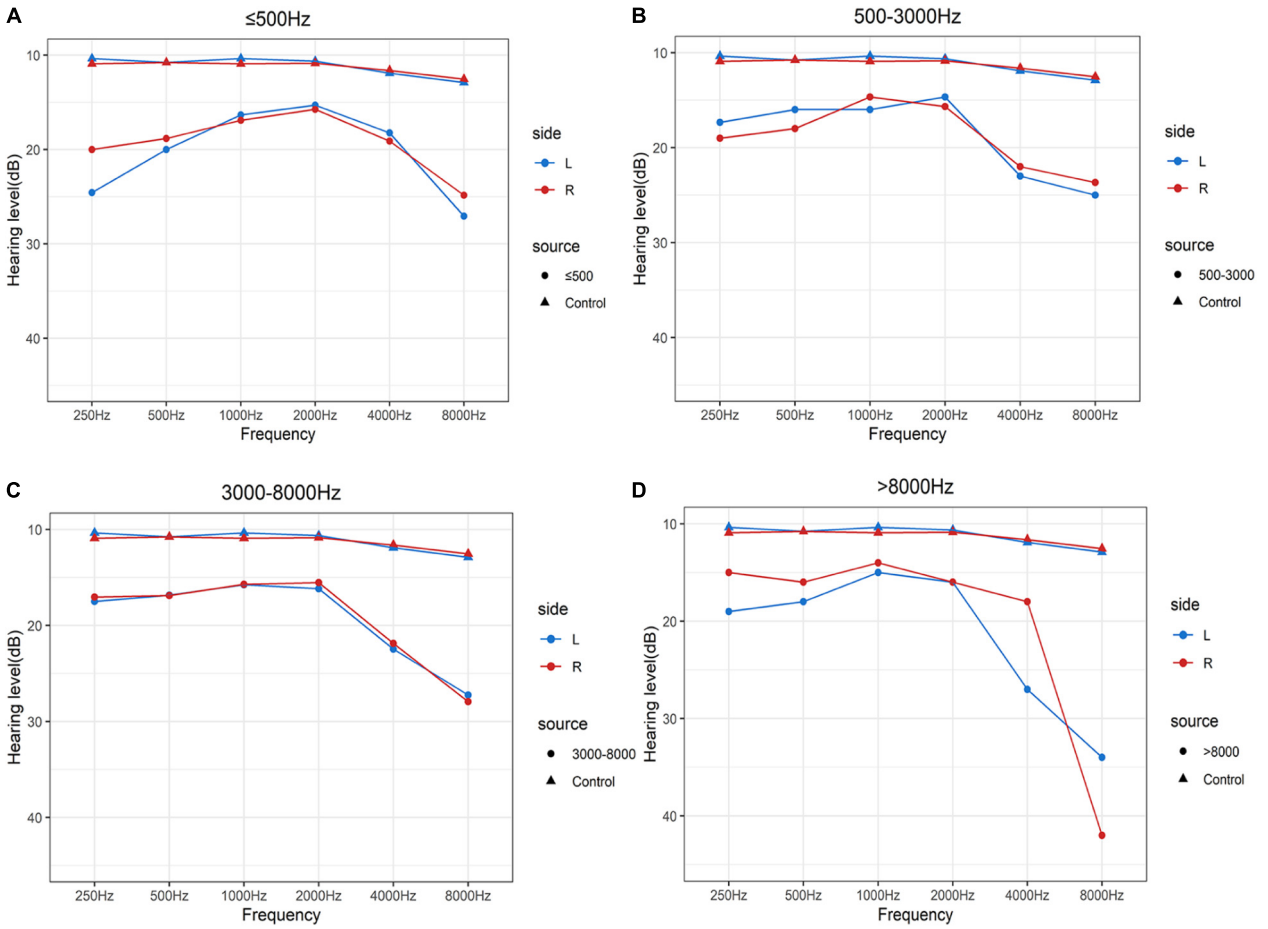

FIGURE 1 | Average pure-tone audiograms of patients with clinically normal hearing and volunteers without tinnitus using a 250–8,000 Hz conventional audiometer. **(A–D)** Mean values of average hearing thresholds for the controls with normal hearing and without tinnitus and patients with clinically normal hearing in dominant tinnitus pitch ≤500 Hz **(A)**, 500 Hz–3 kHz **(B)**, 3–8 kHz **(C)**, and >8,000 Hz **(D)**. Blue solid lines and dots represent left ears and red solid lines and dots represent right ears in patients with tinnitus. Blue solid lines and triangles represent left ears and red solid lines and triangles represent right ears in volunteers with normal hearing and without tinnitus.

TABLE 2 | The average pure tone thresholds (mean) and the corresponding standard deviations (SD) in different subgroups with tinnitus and the control group without tinnitus.

Frequency		Hearing thresholds [mean (SD), dB HL]				
		Control (*n* = 71)	≤500 Hz (*n* = 34)	500–3,000 Hz (*n* = 15)	3,000–8,000 Hz (*n* = 259)	>8,000 Hz (*n* = 5)
250 Hz	L	10.4 (4.7)	24.6 (18.4)	17.3 (3.7)	17.5 (5.1)	19.0 (7.4)
	R	10.9 (4.3)	20.0 (5.9)	19.0 (3.4)	17.0 (4.9)	15.0 (5.0)
500 Hz	L	10.8 (5.0)	20.0 (7.4)	16.0 (3.4)	16.9 (4.4)	18.0 (5.7)
	R	10.8 (3.9)	18.8 (4.8)	18.0 (3.7)	16.9 (4.3)	16.0 (4.2)
1,000 Hz	L	10.4 (3.9)	16.3 (4.3)	16.0 (7.1)	15.8 (4.1)	15.0 (3.5)
	R	10.9 (3.9)	16.9 (4.4)	14.7 (3.0)	15.7 (3.8)	14.0 (4.2)
2,000 Hz	L	10.6 (3.3)	15.3 (4.8)	14.7 (4.4)	16.2 (5.1)	16.0 (5.5)
	R	10.8 (3.4)	15.7 (5.5)	15.7 (3.7)	15.5 (4.5)	16.0 (6.5)
4,000 Hz	L	11.9 (5.4)	18.2 (6.4)	23.0 (11.9)	22.5 (10.0)	27.0 (12.5)
	R	11.6 (4.1)	19.1 (8.4)	22.0 (12.6)	21.9 (9.9)	18.0 (5.7)
8,000 Hz	L	12.9 (4.6)	27.1 (16.7)	25.0 (13.0)	27.2 (14.1)	34.0 (16.4)
	R	12.5 (4.6)	24.9 (14.0)	23.7 (11.1)	27.9 (14.9)	42.0 (29.7)

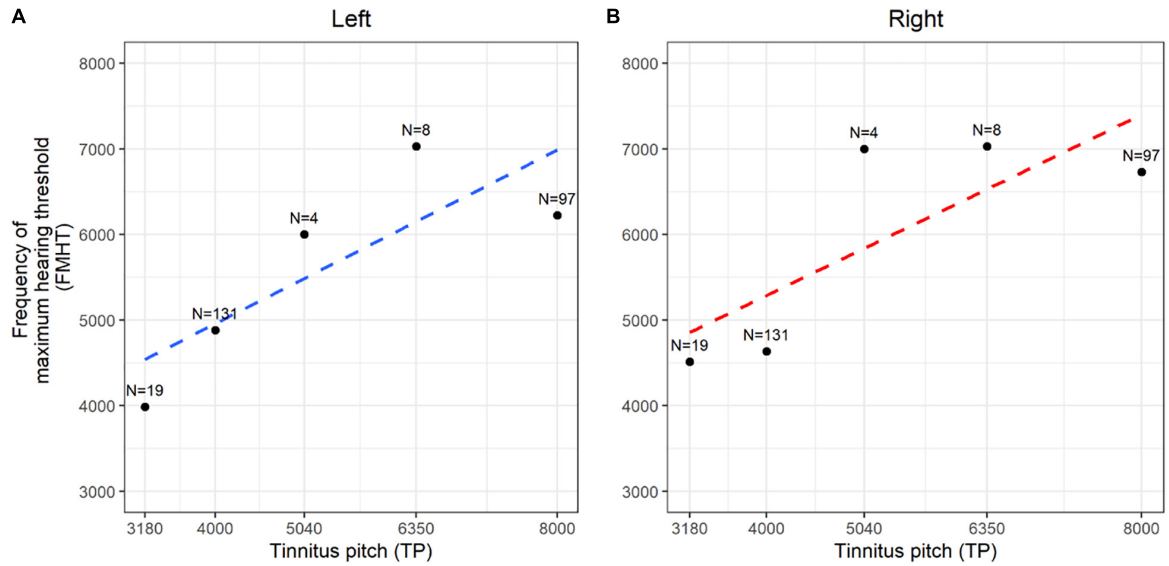

FIGURE 2 | Spearman rank correlation between dominant tinnitus pitch (TP) and frequency of maximum hearing threshold (FMHT). **(A,B)** The correlation coefficient and generalized linear regression between the matched tinnitus pitch and the frequency of maximum hearing threshold were demonstrated in the left ears (**A**, blue dotted line) and right ears (**B**, red dotted line). N means the counts of each data.

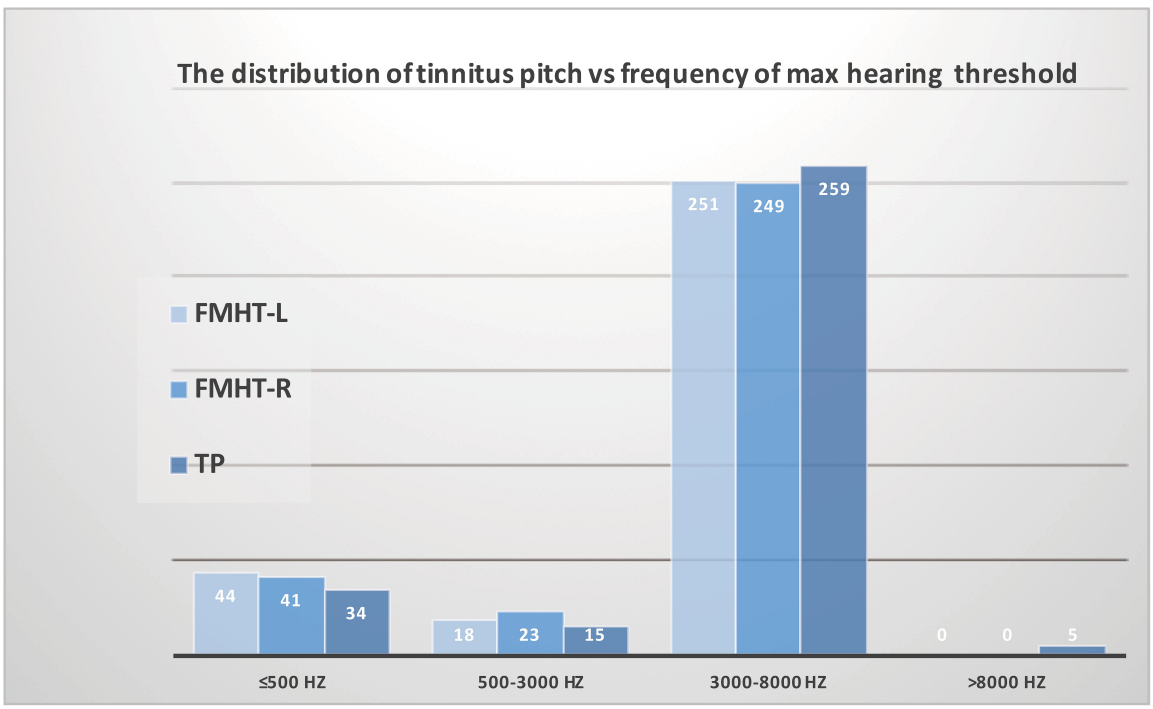

FIGURE 3 | Association between the distribution of tinnitus pitch and the distribution of maximum threshold corresponding frequency in patients with tinnitus and normal hearing. The distribution of threshold-elevated frequencies in both the left ears and right ears was consistent with the distribution of dominant tinnitus pitch.

was examined in patients with ultra-high-pitched tinnitus. Approximately 10.9% of the individuals presented low-pitched tinnitus with distinctive inverted-U-shaped audiograms in both ears, suggesting comparable threshold elevations in the low-frequency region (≤500 Hz) vs. the high-frequency region (4–8 kHz). Furthermore, we confirmed a positive correlation between TP and frequency of maximum hearing threshold in both right and left ears. Additionally, the distribution of TP was proven to be consistent with the distribution of maximum hearing threshold corresponding frequency. Therefore, our

results indicated that minor hearing deficits might be the cause of tinnitus in patients with normal hearing and that the TP might be predicted by different audiograms.

Tinnitus severity and subjective tinnitus-related discomfort are often more severe in subjects with hearing loss than in those with normal hearing. However, Yenigun et al. (2014) found that the tinnitus severity index and THI results are significantly similar between the groups with normal hearing and hearing loss. Our data did not show a significant between-group difference in THI score when the patients were divided into subgroups based on the TP ($p = 0.716$). The mean score for THI was 31.0 ± 23.3, and according to the scoring criterion for THI, the majority of patients with tinnitus and normal hearing experienced mild to moderate disturbance. The assessment of tinnitus also requires multi-dimensional psychoacoustic evaluation. Furthermore, we used AIS and FTQ to evaluate sleep disorders and fear of tinnitus in patients with normal hearing, and the results were similar to those obtained with THI, with no significant between-group difference ($p = 0.454$ for AIS and $p = 0.306$ for FTQ).

In summary, we expound the characteristics of tinnitus in patients with clinically normal hearing in terms of age, sex, education, hearing threshold, tinnitus duration, tinnitus severity, dominant TP, laterality, tinnitus loudness, multi-dimensional evaluation scales, and intermittent vs. continuous tinnitus. We discovered that the dominant TP was mostly in the high-frequency range, and that the dominant TP in patients with tinnitus and normal hearing might be related to threshold elevations up to 8 kHz. On dividing the patients into four subgroups based on the TP, we identified different types and distinctive audiograms in the low-pitched ($\leq$500 Hz), middle-pitched (500 Hz–3 kHz), high-pitched (3–8 kHz), and ultra-high-pitched subgroups. Therefore, our results suggest that the details of conventional audiogram should be well-studied in patients with tinnitus and normal hearing. We believe that our results at least partially explicit the common question "Why did I get tinnitus?" in patients with normal hearing from the aspect of audiogram. The efficacy of tinnitus management involving different subgroups in patients with normal hearing is worthy to study in the future.

DATA AVAILABILITY STATEMENT

The raw data supporting the conclusions of this article will be made available by the authors, without undue reservation.

ETHICS STATEMENT

The studies involving human participants were reviewed and approved by the Institutional Review Board (IRB) of Eye & ENT Hospital of Fudan University. Written informed consent to participate in this study was provided by the participants' legal guardian/next of kin.

AUTHOR CONTRIBUTIONS

DT and XL performed the experiments and drafted the manuscript. DT, RH, and HY analyzed the data and approved the final manuscript. DT and WL conceived and designed the study, interpreted and analyzed the data, and approved the final manuscript. All authors contributed to the article and approved the submitted version.

FUNDING

This work was supported by grants from the National Natural Science Foundation of China (No. 81800912, 81922018, 81771011, 81900931), the Program for Shanghai Hospital Development Center (SHDC12019119), and the Science and Technology Commission of Shanghai Municipality (19441900200), and the "SailingProgram" (19YF1406000).

ACKNOWLEDGMENTS

We thank Deborah Hall, University of Nottingham, for providing scientific guidance on the manuscript preparation.

REFERENCES

Baguley, D., Mcferran, D., and Hall, D. (2013). Tinnitus. *Lancet* 382, 1600–1607.

Biesinger, E., Heiden, C., Greimel, V., Lendle, T., Hoing, R., and Albegger, K. (1998). [Strategies in ambulatory treatment of tinnitus]. *HNO* 46, 157–169. doi: 10.1007/s001060050215

Eggermont, J. J., and Roberts, L. E. (2004). The neuroscience of tinnitus. *Trends Neurosci.* 27, 676–682.

Guest, H., Munro, K. J., Prendergast, G., Howe, S., and Plack, C. J. (2017). Tinnitus with a normal audiogram: relation to noise exposure but no evidence for cochlear synaptopathy. *Hear. Res.* 344, 265–274. doi: 10.1016/j.heares.2016.12.002

Jastreboff, P. J., and Jastreboff, M. M. (2003). Tinnitus retraining therapy for patients with tinnitus and decreased sound tolerance. *Otolaryngol. Clin. North Am.* 36, 321–336. doi: 10.1016/s0030-6665(02)00172-x

Kara, E., Aydın, K., Akbulut, A. A., Karakol, S. N., Durmaz, S., Yener, H. M., et al. (2020). Assessment of hidden hearing loss in normal hearing individuals with and without tinnitus. *J. Int. Adv. Otol.* 16, 87–92. doi: 10.5152/iao.2020.7062

Konig, O., Schaette, R., Kempter, R., and Gross, M. (2006). Course of hearing loss and occurrence of tinnitus. *Hear. Res.* 221, 59–64. doi: 10.1016/j.heares.2006.07.007

Langguth, B., Kreuzer, P. M., Kleinjung, T., and De Ridder, D. (2013). Tinnitus: causes and clinical management. *Lancet Neurol.* 12, 920–930. doi: 10.1016/S1474-4422(13)70160-1

McCormack, A., Edmondson-Jones, M., Somerset, S., and Hall, D. (2016). A systematic review of the reporting of tinnitus prevalence and severity. *Hear. Res.* 337, 70–79. doi: 10.1016/j.heares.2016.05.009

McCracken, L. M., Zayfert, C., and Gross, R. T. (1992). The pain anxiety symptoms scale: development and validation of a scale to measure fear of pain. *Pain* 50, 67–73. doi: 10.1016/0304-3959(92)90113-p

Moore, B. C. J., Vinay, C., and Sandhya, B. (2010). The relationship between tinnitus pitch and the edge frequency of the audiogram in individuals with hearing impairment and tonal tinnitus. *Hear. Res.* 261, 51–56. doi: 10.1016/j.heares.2010.01.003

Newman, C. W., Jacobson, G. P., and Spitzer, J. B. (1996). Development of the tinnitus handicap inventory. *Arch. Otolaryngol. Head Neck Surg.* 122, 143–148.

Newman, C. W., Sandridge, S. A., and Bolek, L. (2008). Development and psychometric adequacy of the screening version of the tinnitus handicap inventory. *Otol. Neurotol.* 29, 276–281. doi: 10.1097/MAO.0b013e31816569c4

Norena, A. J., and Eggermont, J. J. (2003). Changes in spontaneous neural activity immediately after an acoustic trauma: implications for neural correlates of tinnitus. *Hear. Res.* 183, 137–153. doi: 10.1016/s0378-5955(03)00225-9

Paglialonga, A., Del Bo, L., Ravazzani, P., and Tognola, G. (2010). Quantitative analysis of cochlear active mechanisms in tinnitus subjects with normal hearing sensitivity: multiparametric recording of evoked otoacoustic emissions and contralateral suppression. *Auris Nasus Larynx* 37, 291–298. doi: 10.1016/j.anl.2009.09.009

Paglialonga, A., Fiocchi, S., Del Bo, L., Ravazzani, P., and Tognola, G. (2011). Quantitative analysis of cochlear active mechanisms in tinnitus subjects with normal hearing sensitivity: time-frequency analysis of transient evoked otoacoustic emissions and contralateral suppression. *Auris Nasus Larynx* 38, 33–40. doi: 10.1016/j.anl.2010.04.006

Pan, T., Tyler, R. S., Ji, H., Coelho, C., Gehringer, A. K., and Gogel, S. A. (2009). The relationship between tinnitus pitch and the audiogram. *Int. J. Audiol.* 48, 277–294. doi: 10.1080/14992020802581974

Roelofs, J., Sluiter, J. K., Frings-Dresen, M. H., Goossens, M., Thibault, P., Boersma, K., et al. (2007). Fear of movement and (re)injury in chronic musculoskeletal pain: evidence for an invariant two-factor model of the Tampa Scale for Kinesiophobia across pain diagnoses and Dutch, Swedish, and Canadian samples. *Pain* 131, 181–190. doi: 10.1016/j.pain.2007.01.008

Savastano, M. (2008). Tinnitus with or without hearing loss: are its characteristics different? *Eur. Arch. Otorhinolaryngol.* 265, 1295–1300. doi: 10.1007/s00405-008-0630-z

Schecklmann, M., Vielsmeier, V., Steffens, T., Landgrebe, M., Langguth, B., and Kleinjung, T. (2012). Relationship between Audiometric slope and tinnitus pitch in tinnitus patients: insights into the mechanisms of tinnitus generation. *PLoS One* 7:e34878. doi: 10.1371/journal.pone.0034878

Sereda, M., Edmondson-Jones, M., and Hall, D. A. (2015). Relationship between tinnitus pitch and edge of hearing loss in individuals with a narrow tinnitus bandwidth. *Int. J. Audiol.* 54, 249–256. doi: 10.3109/14992027.2014.979373

Sereda, M., Hall, D. A., Bosnyak, D. J., Edmondson-Jones, M., Roberts, L. E., Adjamian, P., et al. (2011). Re-examining the relationship between audiometric profile and tinnitus pitch. *Int. J. Audiol.* 50, 303–312. doi: 10.3109/14992027.2010.551221

Soldatos, C. R., Dikeos, D. G., and Paparrigopoulos, T. J. (2000). Athens insomnia scale: validation of an instrument based on ICD-10 criteria. *J. Psychosom. Res.* 48, 555–560. doi: 10.1016/s0022-3999(00)00095-7

Song, Z., Wu, Y., Tang, D., Lu, X., Qiao, L., Wang, J., et al. (2021). Tinnitus is associated with extended high-frequency hearing loss and hidden high-frequency damage in young patients. *Otol. Neurotol.* 42, 377–383. doi: 10.1097/MAO.0000000000002983

Vielsmeier, V., Lehner, A., Strutz, J., Steffens, T., Kreuzer, P. M., Schecklmann, M., et al. (2015). The relevance of the high frequency audiometry in tinnitus patients with normal hearing in conventional pure-tone audiometry. *Biomed. Res. Int.* 2015, 302515. doi: 10.1155/2015/302515

World Health Organization [WHO] Programme for the Prevention of Deafness and Hearing Impairment (1997). *Future Programme Developments for Prevention of Deafness and Hearing Impairments: Report of the First Informal Consultation, Geneva, 23-24 January 1997*. Geneva: World Health Organization.

Xiong, B., Liu, Z., Liu, Q., Peng, Y., Wu, H., Lin, Y., et al. (2019). Missed hearing loss in tinnitus patients with normal audiograms. *Hear. Res.* 384, 107826. doi: 10.1016/j.heares.2019.107826

Yenigun, A., Dogan, R., Aksoy, F., Akyuz, S., and Dabak, H. (2014). Assessment of tinnitus with tinnitus severity index, tinnitus handicap inventory and distortion product otoacoustic emissions in patients with normal hearing and hearing loss. *Kulak Burun Bogaz Ihtis Derg.* 24, 11–16. doi: 10.5606/kbbihtisas.2014.60783

Conflict of Interest: The authors declare that the research was conducted in the absence of any commercial or financial relationships that could be construed as a potential conflict of interest.

frontiers in Cellular Neuroscience

ORIGINAL RESEARCH
published: 03 March 2022
doi: 10.3389/fncel.2022.816079

Failure Of Hearing Acquisition in Mice With Reduced Expression of Connexin 26 Correlates With the Abnormal Phasing of Apoptosis Relative to Autophagy and Defective ATP-Dependent Ca^{2+} Signaling in Kölliker's Organ

Lianhua Sun[1,2,3†], Dekun Gao[1,2,3†], Junmin Chen[1,2,3], Shule Hou[1,2,3], Yue Li[1,2,3], Yuyu Huang[1,2,3], Fabio Mammano[4,5], Jianyong Chen[1,2,3]* and Jun Yang[1,2,3]**

[1]Department of Otorhinolaryngology-Head and Neck Surgery, Xinhua Hospital, Shanghai Jiaotong University School of Medicine, Shanghai, China, [2]Ear Institute, Shanghai Jiaotong University School of Medicine, Shanghai, China, [3]Shanghai Key Laboratory of Translational Medicine on Ear and Nose Diseases, Shanghai, China, [4]Department of Physics and Astronomy "G. Galilei", University of Padua, Padua, Italy, [5]Department of Biomedical Sciences, Institute of Biochemistry and Cell Biology, Italian National Research Council, Monterotondo, Italy

Mutations in the *GJB2* gene that encodes connexin 26 (Cx26) are the predominant cause of prelingual hereditary deafness, and the most frequently encountered variants cause complete loss of protein function. To investigate how Cx26 deficiency induces deafness, we examined the levels of apoptosis and autophagy in *Gjb2*$^{loxP/loxP}$; *ROSA26*^{CreER} mice injected with tamoxifen on the day of birth. After weaning, these mice exhibited severe hearing impairment and reduced Cx26 expression in the cochlear duct. Terminal deoxynucleotidyl transferase dUTP nick end labeling (TUNEL) positive cells were observed in apical, middle, and basal turns of Kölliker's organ at postnatal (P) day 1 (P1), associated with increased expression levels of cleaved caspase 3, but decreased levels of autophagy-related proteins LC3-II, P62, and Beclin1. In Kölliker's organ cells with decreased Cx26 expression, we also found significantly reduced levels of intracellular ATP and hampered Ca^{2+} responses evoked by extracellular ATP application. These results offer novel insight into the mechanisms that prevent hearing acquisition in mouse models of non-syndromic hearing impairment due to Cx26 loss of function.

Keywords: apoptosis, ATP, autophagy, Ca^{2+}, development, deafness

OPEN ACCESS

Edited by:
Zuhong He,
Wuhan University, China

Reviewed by:
Renjie Chai,
Southeast University, China
Wenxue Tang,
Second Affiliated Hospital of Zhengzhou University, China

****Correspondence:***
Jun Yang
yangjun@xinhuamed.com.cn
Jianyong Chen
chenjianyong@xinhuamed.com.cn
Fabio Mammano
fabio.mammano@unipd.it

†These authors have contributed equally to this work

Specialty section:
This article was submitted to Cellular Neuropathology, a section of the journal Frontiers in Cellular Neuroscience

Received: *16 November 2021*
Accepted: *03 February 2022*
Published: *03 March 2022*

Citation:
Sun L, Gao D, Chen J, Hou S, Li Y, Huang Y, Mammano F, Chen J and Yang J (2022) Failure Of Hearing Acquisition in Mice With Reduced Expression of Connexin 26 Correlates With the Abnormal Phasing of Apoptosis Relative to Autophagy and Defective ATP-Dependent Ca^{2+} Signaling in Kölliker's Organ. Front. Cell. Neurosci. 16:816079. doi: 10.3389/fncel.2022.816079

Abbreviations: KO, Kölliker's organ; IHCs, inner hair cells; Cx26, gap junction protein beta-2; Cx30, gap junction protein beta-6.

INTRODUCTION

The sense of hearing originates in a portion of the cochlear sensory epithelium, the organ of Corti, which comprises two types of mechanosensory hair cells, the inner and outer hair cells (IHCs and OHCs), which do not express connexins, and at least six types of associated supporting cells, all of which express connexins. Connexin 26 (Cx26, encoded by the *GJB2* gene) and the closely related connexin 30 (Cx30, encoded by *GJB6*) are the prevailing isoforms expressed in non-sensory cells of both the epithelial and connective tissue of the developing and mature cochlea (Forge et al., 2003; Cohen-Salmon et al., 2005).

GJB2 mutations are a frequent cause of both syndromic and non-syndromic congenital deafness, with an unusually high carrier rate for truncating mutations among hearing-impaired individuals (Chan and Chang, 2014; Del Castillo and Del Castillo, 2017). Connexin proteins form large-pore hexameric plasma membrane channels, termed hemichannels, which may dock head-to-head in the extracellular space to form intercellular gap junction channels (Laird and Lampe, 2022). Interruption of the potassium ion recycling pathway *via* gap junction systems in the mammalian cochlea has been postulated as the cause of hereditary non-syndromic deafness (Kikuchi et al., 2000). However, this hypothesis lacks experimental proof and is contradicted by different studies (Beltramello et al., 2005; Jagger and Forge, 2015; Zhao, 2017). In contrast, the available evidence from mouse models points to a fundamental role played by connexins, particularly connexin hemichannels, during the crucial phases of postnatal cochlear development that lead to hearing acquisitions; reviewed in (Mammano, 2013, 2019).

In the developing rodent cochlea, the sensory epithelium is subdivided into a cellularly dense medial domain named Kölliker's organ and a less dense lateral domain, the lesser epithelial ridge (LER), separated by a central prosensory region that contains the precursors of the organ of Corti (Lim and Anniko, 1985; Lim and Rueda, 1992; Driver and Kelley, 2020). Kölliker's organ is one of the earliest structures in the inner ear, recognizable from embryonic (E) day 14 (E14) to postnatal (P) day 12–14 (P12–14, P0 indicates the day of birth), which marks the onset of hearing function that reaches adult-level auditory thresholds by the third postnatal week (Ehret, 1977).

In the pre-hearing phase of mouse cochlear development, Kölliker's organ cells release ATP periodically through connexin hemichannels (Schutz et al., 2010; Rodriguez et al., 2012; Xu et al., 2017; Zorzi et al., 2017; Mazzarda et al., 2020) to activate purinergic receptors in the surrounding cells, depolarize the hair cells and activate auditory nerve fibers (Tritsch et al., 2007; Wang and Bergles, 2015; Johnson et al., 2017; Eckrich et al., 2018; Ceriani et al., 2019). Spontaneous Ca^{2+} activity in the mouse postnatal cochlea wanes as the sensory epithelium and its innervation pattern mature, in parallel with intense remodeling which leads to the formation of the inner sulcus in place of the degenerated Kölliker's organ and outer sulcus in place of the LER (Lim and Anniko, 1985; Lim and Rueda, 1992; Driver and Kelley, 2020).

Ca^{2+} signaling, autophagic and apoptotic processes are key to this crucial remodeling phase (La Rovere et al., 2016; Bootman et al., 2018; Mammano and Bortolozzi, 2018; Zhou et al., 2020; Soundarrajan et al., 2021). Recent work examined Kölliker's organ morphological changes with autophagy and apoptosis markers between P1 and P14 and showed that: (i) autophagy is present and associated closely with the remodeling that leads to Kölliker's organ degeneration; (ii) Kölliker's organ cells are digested and absorbed by autophagy before apoptosis occurs (Hou et al., 2019). Here, we extended those studies by investigating the complex interplay between apoptosis, autophagy, ATP, and Ca^{2+} signaling in connection with the failure of hearing acquisition induced by Cx26 deficiency in a mouse model of non-syndromic deafness.

MATERIALS AND METHODS

Animals

$Gjb2^{loxP/loxP}$ mice (Cohen-Salmon et al., 2002) and $ROSA26^{CreER}$ mice (Vooijs et al., 2001) used for this study were donated by Professor Weijia Kong of the Union Hospital Affiliated to Tongji Medical College, Huazhong University of Science and Technology. All experiments were performed on animals of both sexes following the guidelines approved by the Ethics Committee of Xinhua Hospital affiliated to Shanghai Jiaotong University School of Medicine.

Breeding and Tamoxifen Injection

To achieve time-conditional Cx26 deletion, we adopted a mating scheme previously used to generate mice with targeted ablation of Cx26 in the inner ear (Crispino et al., 2011; Fetoni et al., 2018). First, $Gjb2^{loxP/loxP}$ mice were mated with $ROSA26^{CreER}$ mice, yielding $Gjb2^{loxP//wt}$; $ROSA26^{CreER}$ mice (wt = wild type *Gjb2* allele). Next, $Gjb2^{loxP//wt}$; $ROSA26^{CreER}$ mice were mated with $Gjb2^{loxP/loxP}$ mice to obtain $Gjb2^{loxP/loxP}$; $ROSA26^{CreER}$ mice. Finally, to promote deletion of the floxed alleles, P0 offspring were given a single intraperitoneal (i.p.) injection of tamoxifen (TMX, T5648-1G, Sigma–Aldrich, USA), at a dose of 100 mg/kg of body weight, as previously reported (Sun et al., 2009; Chang et al., 2015).

Mouse Genotyping

Mouse genotyping was performed as previously described (Chen et al., 2018). The primer pairs used to detect the loxP sequences were as follows:

forward 5'-CTTTCCAATGCTGGTGGAGTG-3';

reverse 5'-ACAGAAATGTGTTGGTGATGG-3'.

$Gjb2^{loxP/loxP}$ and wild-type mice generated a band of 322 bp and 288 bp, respectively.

Primer pairs used to detect the CreER sequences were as follows:

forward 5'-TATCCAGGTTACGGATATAGTTCATG-3'; and

reverse, 5'-AGCTAAACATGCTTCATCGTCGGTC-3', which generated a band of 700 bp.

Auditory Brainstem Response Test

Mice injected with tamoxifen at P0 were tested for auditory brainstem response (ABR) at P21 (Zhou et al., 2006). Six mice, three males, and three females were tested for each

group. Animals were anesthetized with ketamine (120 mg/kg, i.p.) and chlorpromazine (20 mg/kg, i.p.) and placed in a sound-attenuating chamber on a heating pad to maintain body temperature. Tone burst stimuli were generated in the free field at frequencies of 4, 8, 16, and 32 kHz and amplitudes ranging from 0 to 100 dB sound pressure level (SPL) using a system equipped with the RZ6 hardware for data acquisition and sound production, Medusa4Z amplifier and MF1 multi-field magnetic speakers (TDT, Tucker-Davis Technologies, Alachua, FL, USA). Responses were amplified and averaged 512 times using the TDT BioSigRZ software.

Immunohistochemistry

Mice injected with tamoxifen at P0 were used to obtain cochlear tissue at P21 after rapid decapitation. The cochlea was fixed with 4% paraformaldehyde overnight, decalcified with 10% EDTA, embedded in paraffin and sectioned, stained for immunohistochemistry with primary antibodies selective for Cx26 (PA518618, Invitrogen, USA) and Cx30 (700258, Invitrogen, USA), followed by incubation with HRP labeled secondary antibody (donkey anti-goat IgG, goat anti-rabbit IgG, Servicebio). Finally, samples were incubated with a DAB reaction kit (G1212-200T, Servicebio, China), which is the chromogenic substrate of HRP, and images were collected using a Nikon E100 with Nikon DS-U3 imaging system.

Analyses of Cochlear Duct and Kölliker's Organ Tissues

Mice were injected with tamoxifen at P0 and sacrificed by decapitation after 24 h to obtain cochlear duct and Kölliker's organ tissues which were processed as described hereafter.

The cochlear duct was dissected in cold phosphate-buffered saline (PBS), fixed with 4% paraformaldehyde for 30 min, embedded in paraffin, and sectioned. A TUNEL detection kit (11684817910, Roche, Switzerland) was used to detect apoptosis in paraffin-embedded cochlear tissue sections following the manufacturer's protocols.

For immunofluorescence staining, paraffin sections were incubated with primary antibodies selective for c-cas3, LC3-II, P62 (GB11009-1, Servicebio; ab192890, Abcam; GB11239-1, Servicebio) and a secondary antibody (Cy3-sheep-anti-rabbit, GB21303, Servicebio) respectively. Processed samples were observed and imaged with a fluorescence microscope (Nikon ECLIPSE CI with Nikon DS-U3 imaging system) under uniform illumination and detection conditions. The excitation wavelength was 550 nm and the emission wavelength was 570 nm.

For Western blot analyses, tissues were dissected in cold PBS and frozen in liquid nitrogen immediately after decapitation. The total protein content of the cochlea was extracted in RIPA lysis buffer (Servicebio, Wuhan, China) and quantitated following the kit instructions (BCA Protein Assay Kit, Beyotime, Haimen, China). The same amount of protein (20 μg per lane) was electrophoresed in a 15% sodium dodecyl sulfate-polyacrylamide gel and transferred to polyvinylidene difluoride (PVDF) membranes. After blocking with TBST containing 5% skimmed milk for 1 h, the sample was incubated at 4°C overnight with the primary antibodies selective for GAPDH (60004-1-lg, PTG), caspase 3 (66470-2-lg, PTG), Bcl-2 (GB13458, Servicebio), LC3 (GB11124, Servicebio), p62 (18420-1-AP, PTG), Beclin1 (GB112053, Servicebio). Next, samples were incubated at room temperature with horseradish peroxidase (HRP)-conjugated secondary antibody (GB23301, GB23303, Servicebio) for 1 h. The ECL reaction buffer (G2014, Servicebio) was added to detect the proteins in a Chemidoc XRS+ imaging system (BioRad, CA, USA).

For Luciferin–luciferase ATP bioluminescence assay, the cochlea was removed after rapid decapitation, the bony wall and the membranous labyrinth were separated from the apex to the base of the cochlea and the cochlear duct was dissected in cold phosphate-buffered saline (PBS). Next, the sensory epithelium was separated from the spiral ligament, Kölliker's organ was micro-dissected and placed in a lysis buffer (S0027, Beyotime, China) and lysed in a Polytron PT1200 homogenizer (Kinematica, Luzern, Switzerland). Finally, the total ATP concentration was measured with a luciferin-luciferase bioluminescence ATP assay kit (S0027, Beyotime, China) using the Chemidoc XRS+ imaging system. All measurements reported in this article fell within the linearity range of the ATP standard curve generated according to the manufacturer's instructions. All experiments were performed at room temperature (22–25°C).

Preparation of Kölliker's Organ Cultures From P0 Pups

For these experiments, we used pups from the same litter which was reserved for their tails for genotype identification during the experiment.

Kölliker's organ was micro-dissected in cold 1× Hank's balanced salt solution (HBSS, Thermo Fisher, 14025076, USA) as described above, transiently transferred to an Eppendorf tube containing DMEM/F12 mixed with 2% ampicillin (ST008, Beyotime, China) and then cultured as previously reported (Chen et al., 2018). Briefly, Kölliker's organ was divided into three fragments from apex to base and the fragments were placed in a 24-well plate containing a tissue culture-treated, round glass slide (14 mm diameter, WHB-24-CS, WHB) immersed in DMEM/F12 containing 1% ampicillin, 10% fetal bovine serum (10099-141, Gibco, Australia). Alternatively, for Ca^{2+} imaging experiments with fluo-4 (see below), Kölliker's organ fragments were placed on a tissue culture-treated glass-bottomed culture dish (801001, NEST, China). In either case, the culture medium was supplemented with 10 μM (Z)-4-hydroxytamoxifen (H7904, Sigma, Germany) to promote Cre recombinase-mediated *in vitro* excision of the floxed Cx26 alleles. Finally, samples were placed in an incubator (Thermo Scientific Forma Direct Heat CO_2 Incubators) and cultured at 37°C, 5% CO_2 for 12 h (Chen et al., 2018).

Visualization of ATP-Loaded Vesicles in Kölliker's Organ Cultures

Kölliker's organ cultures, prepared as described above from P0 pups, were treated with quinacrine dihydrochloride (5×10^{-6}

mol/L, orb320518, Biorbyt, UK) in 1× PBS solution for 30 min in the dark, at room temperature, washed three times with PBS, fixed with 4% paraformaldehyde for 1 h, washed three more times with PBS, incubated with cell permeabilizing solution (0.1% Triton X-100 in PBS) for 20 min and blocking solution (10% donkey serum in PBS) for 1 h, washed three times with PBS for 5 min each, and incubated overnight with an anti-LAMP1 primary antibody—lysosome marker (ab208943, Abcam). The next day, Kölliker's organ cultures were removed from the primary antibody incubation solution, washed three times with PBS for 5 min each, and incubated with a secondary antibody (donkey anti-rabbit IgG, AlexaFluor 594, R37119, Invitrogen) at room temperature for 2 h, washed three times with PBS for 5 min each, and incubated with 4', 6-diamidino-2-phenylindole (DAPI, D9542, Sigma) nuclear staining solution for 8 min. Stained cultures were mounted in an antifade mounting medium (H-1200-10, Vectorlabs, USA) and imaged with a confocal microscope (TCS-SP8, Leica, Germany). Fluorescence images of quinacrine (green), DAPI (blue), and LAMP1 (red) were obtained with a ×63 oil immersion objective (Leica) at excitation wavelengths of 488 nm, 405 nm, and 594 nm, respectively. The corresponding emission wavelengths were centered around 520 nm, 422 nm, and 617 nm, respectively.

Ca^{2+} Imaging With Fluo-4 in Kölliker's Organ Cultures

Kölliker's organ cultures, prepared as described above from P0 pups, were incubated for 20 min at 37°C in 4 μM fluo-4 AM loading solution (F14201, Thermo Fisher) containing 20% Pluronic F-127, mixed with five times volume of HBSS (14025076, Thermo Fisher) containing 1% fetal bovine serum, incubated for further 40 min at 37°C, washed with HEPES buffer (10 mM HEPES, 1 mM Na_2HPO_4, 137 mM NaCl, 5 mM KCl, 1 mM $CaCl_2$, 0.5 mM $MgCl_2$, 5 mM glucose, 0.1% BSA, pH 7.4) three times, resuspended in HEPES buffer, and incubated for another 10 min at 37°C to allow baseline Ca^{2+} levels to stabilize. Using a spinning-disk confocal microscope (Nikon CSU-W1, Japan) with excitation and emission wavelengths set at 494 nm and 516 nm, respectively, we first imaged the baseline fluorescence intensity of fluo-4 for 2 min. Thereafter, while continuing image collection, we replaced the incubation solution with a HEPES buffer supplemented with 30 μM ATP (A6559, Sigma–Aldrich, USA) to stimulate purinergic receptors of Kölliker's organ cells.

For off-line data analysis, single-pixel intensity values were background-subtracted and spatially averaged over regions of interest (ROIs) corresponding to individual cell bodies. Time-dependent fluctuations of intracellular Ca^{2+} levels were represented through the ratio F/F_0, where F is the ROI signal at time t and F_0 is the time-averaged pre-stimulus ROI intensity value (Mammano and Bortolozzi, 2010). F_{max} denotes the peak Ca^{2+}-dependent fluorescence intensity fluctuation within a given ROI during each recording period (7 min in total). Data were computed as mean ± standard deviation of $n = 30–50$ cells from three separate experiments.

Statistical Analysis

Statistical analysis of experimental data was performed with GraphPad Prism v8.0 (GraphPad Software, Inc., CA, USA) and Student's t-test. P = p-values less than 0.05 were considered statistically significant.

RESULTS

Severe Hearing Loss and Decreased Expression of Cx26 in the Cochlea of *Gjb2*$^{loxP/Loxp}$; ROSA26^{CreER} Mice Injected With Tamoxifen at P0

At P21, ABR results showed severe hearing loss in *Gjb2*$^{loxP/loxP}$; ROSA26^{CreER} mice that had been injected with tamoxifen at P0 (shortened as Cx26-cKD mice). Average hearing thresholds in these mice ($n = 6$) exceeded 80 dB at 4, 8, 16 and 32 kHz and were significantly more elevated ($P < 0.01$) than thresholds of other genotypes injected with TMX at P0 and used as controls (*Gjb2*$^{loxP/wt}$; ROSA26^{CreER}, $n = 5$; *Gjb2*$^{loxP/loxp}$, $n = 3$; *Gjb2*$^{loxP/wt}$, $n = 3$; **Figure 1A**). In addition, immunohistochemical staining revealed a collapsed organ of Corti with an almost invisible cochlear tunnel (**Figure 1B**) and a decreased expression of Cx26 in supporting cells of the organ of Corti, in epithelial cells of the inner sulcus and outer sulcus, in the spiral limbus, among fibrocytes of the lateral wall and in the basal cell region of the *stria vascularis* of Cx26-cKD mice (**Figure 1C**), whereas expression of Cx30 was increased (**Figure 1D**).

Abnormal Apoptosis and Autophagy in Kölliker's Organ of Cx26-cKD Mice

As mentioned in the introduction, prior work with mouse models indicate that Cx26 expression has a profound impact on the development of the cochlear sensory epithelium through a complex interplay between Ca^{2+} signaling, autophagy, and apoptosis; reviewed in Mammano and Bortolozzi (2018) and Mammano (2019). Therefore, we harvested the cochleae of Cx26-cKD mice at P1 and used a TUNEL assay to visualize apoptotic cells (Gorczyca et al., 1993) in 8 μm-thick transverse sections of the cochlear duct (**Figures 2A,B**). Positive cells (green) were observed exclusively in Kölliker's organ of the Cx26-cKD group, with 8 ± 1 positive cells (green) adjacent to the pro-sensory domain region in all cochlear turns, whereas no TUNEL positive cells were detected in the control group ($n = 3$). At this developmental stage, there was no sign of apoptosis in IHCs and OHCs of either Cx26-cKD or control groups.

Activated caspase-3 and -7 convert other procaspases to activated caspases, leading to the amplification of the apoptosis cascade (Slee et al., 1999; Logue and Martin, 2008). Thus, we quantified caspase 3 levels by immunofluorescence at P1 and detected significantly enhanced immunoreactivity in Kölliker's organ of all cochlear turns in the Cx26-cKD group compared to controls (**Figures 2C,D**, $P < 0.05$, $n = 3$).

LC3-II and p62 are widely used molecular markers of autophagy (Kabeya et al., 2000; Emanuele et al., 2020). At P1, we found diffused immunoreactivity against LC3-II in the sensory epithelium of the control group, with a peak in the pro-sensory

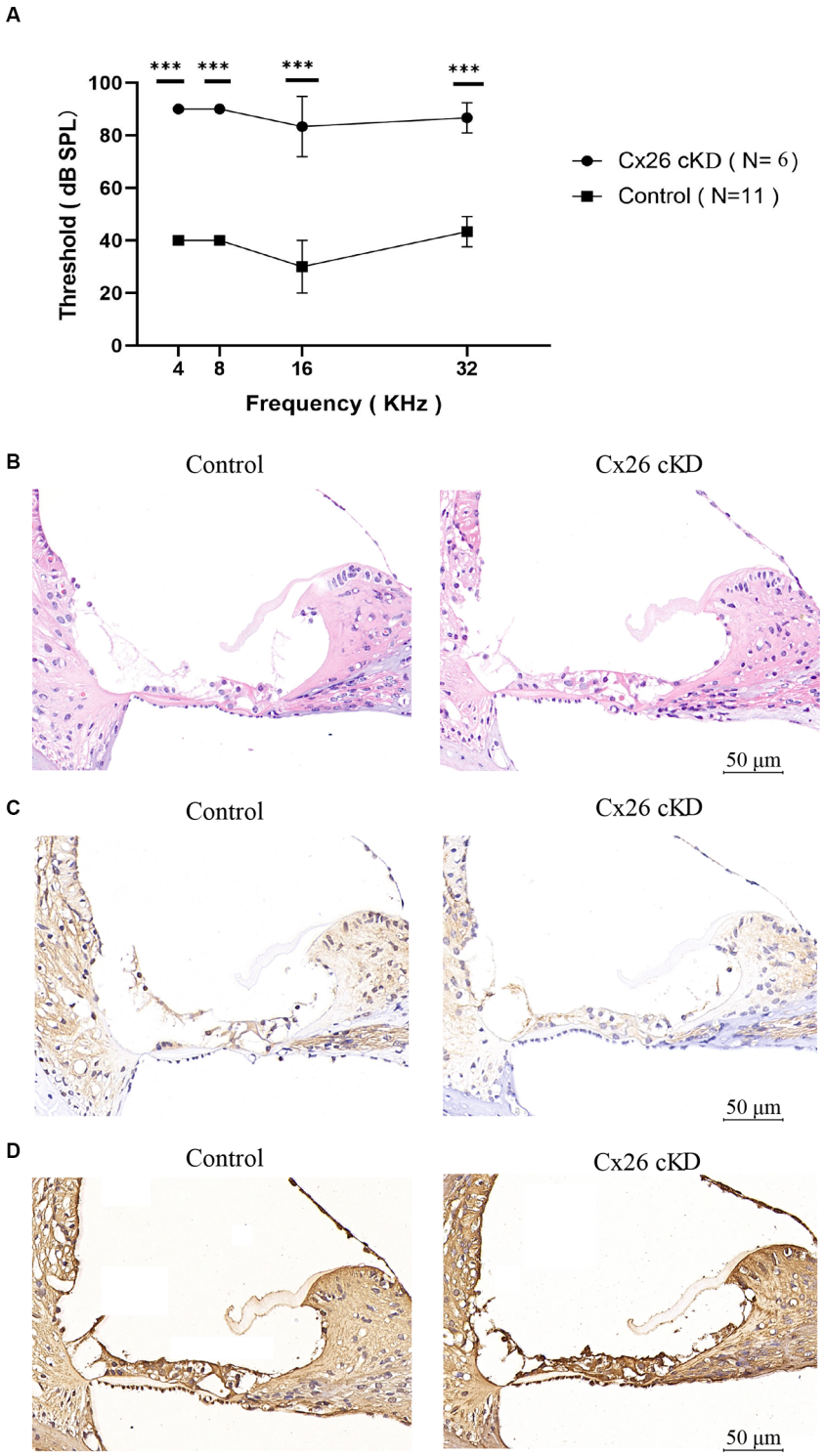

FIGURE 1 | Effect of tamoxifen injection at P0 on the auditory threshold and connexin expression at P21. **(A)** Auditory thresholds measured by pure tone ABRs vs. tone frequency; ***$p < 0.0001$. **(B–D)** Transverse sections of the cochlear duct stained with hematoxylin-eosin **(B)** or with antibodies selective for Cx26 **(C)** or Cx30 **(D)**. Scale bars = 50 μm.

region. In the Cx26-cKD group, immunoreactivity against LC3-II was significantly decreased in Kölliker's organ (**Figures 3A,B**, $P < 0.05$, $n = 3$). Likewise, we found decreased immunoreactivity against p62 in Kölliker's organ cells of the Cx26-cKD group compared to the control group (**Figures 3C,D**, $P < 0.001$, $n = 3$). Together, the results of **Figures 2**, **3** suggest that decreased

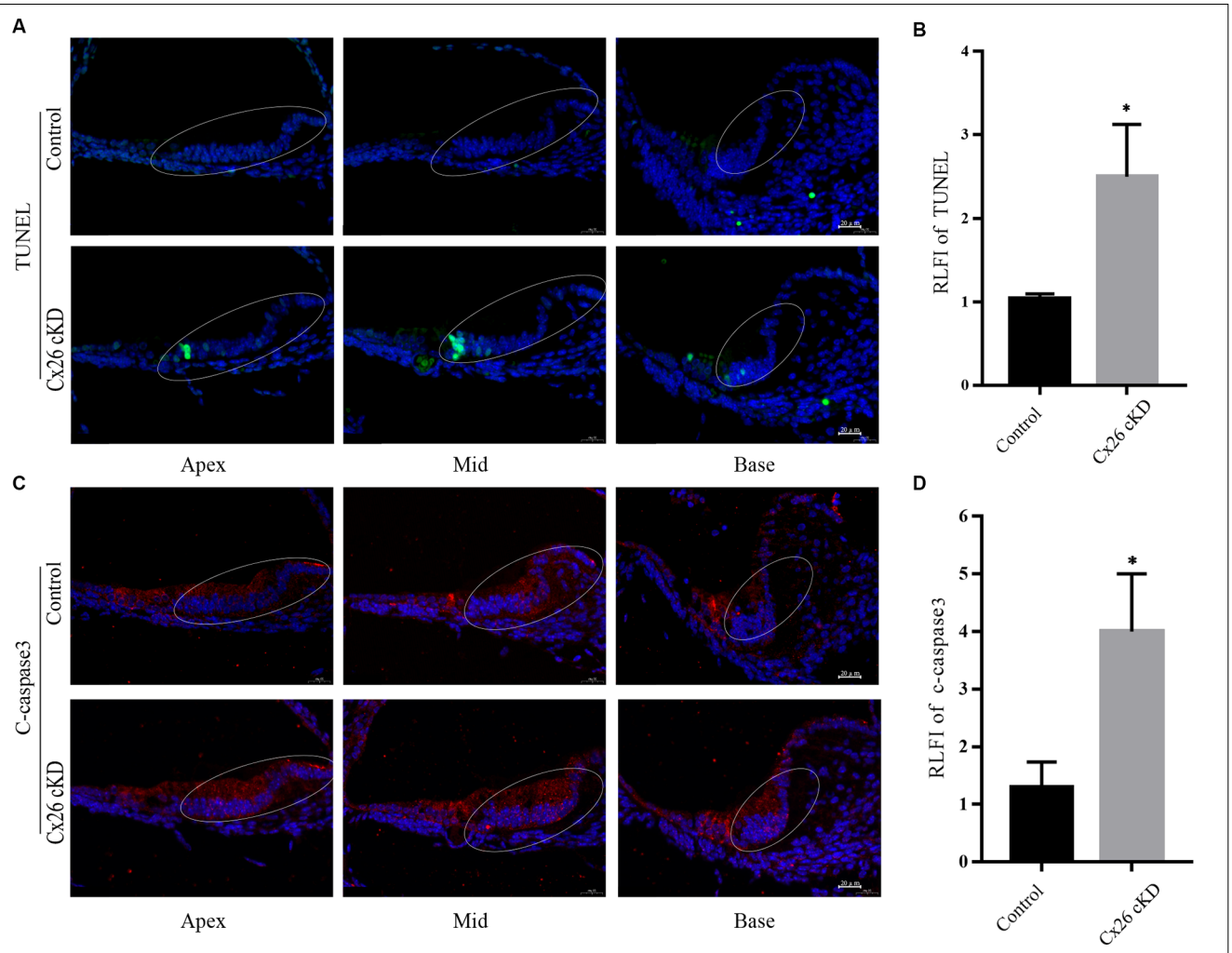

FIGURE 2 | Apoptosis of Kölliker's organ was detected by immunofluorescence staining at P1. **(A)** Representative confocal fluorescence images showing TUNEL positive cells (green) in Kölliker's organ of the Cx26-cKD group, but not in the control group. Blue signals correspond to cell nuclei stained with DAPI. Scale bars = 50 μm. **(B)** Average relative fluorescence intensity (RLFI) of TUNEL signals; * represent $p < 0.05$, $n = 3$. **(C)** Immunofluorescence staining of cleaved (c)-caspase 3 in the apical, middle, and basal turns of Kölliker's organ cells of Cx26-cKD group compared with the control group. Scale bars = 50 μm. **(D)** Average relative fluorescence intensity (RLFI) of the c-caspase 3 signal; * represents $P < 0.05$, $n = 3$.

expression of Cx26 leads to increased apoptosis and decreased autophagy in Kölliker's organ at P1.

To corroborate this conclusion, we investigated expression levels of apoptosis and autophagy markers by Western blotting (**Figure 4**). At P1, we confirmed that cleaved caspase-3 was upregulated in the Cx26-cKD group, with a significant difference compared with the control group ($P < 0.05$, $n = 5$; **Figures 4A,B**). However, these alterations did not involve the anti-apoptotic factor Bcl-2 (Vaux et al., 1992), which is expressed from the 15th day of embryonic development (E15) to P5 in the normal mouse cochlea (Ishii et al., 1996; Kamiya et al., 2001). Our Western blot analyses showed no statistically significant differences ($P > 0.05$, $n = 5$) in the expression level of Bcl-2 between the Cx26-cKD and control mice at P1 (**Figures 4A,B**).

In the normal mouse cochlea, beclin1 and other autophagy-related proteins start to be expressed in the late embryonic stage and continue to be upregulated after birth, until the inner ear achieves functional maturity of the adult stage (de Iriarte Rodriguez et al., 2015). In the Cx26-cKD group, beclin1, LC3-II/I, and p62 were significantly downregulated compared with the control group ($P < 0.05$, $n = 5$; **Figures 4C,D**). Together, these results suggest that in Kölliker's organ of Cx26-cKD mice at P1, downregulation of autophagy is accompanied by the upregulation of apoptosis independent of Bcl-2 expression.

Decreased Total ATP Content in Kölliker's Organ of Cx26-cKD Mice

Prior work showed that decreased levels of Cx26 expression in the mouse postnatal cochlea reduce gap junction coupling, limiting the transfer of nutrients, and glucose in particular, from distant blood vessels to the avascular sensory epithelium (Fetoni et al., 2018). Upon glucose deprivation, autophagy is induced to supplement the metabolic pool and provide ATP through various mechanisms (Galluzzi et al., 2014). However, this process is

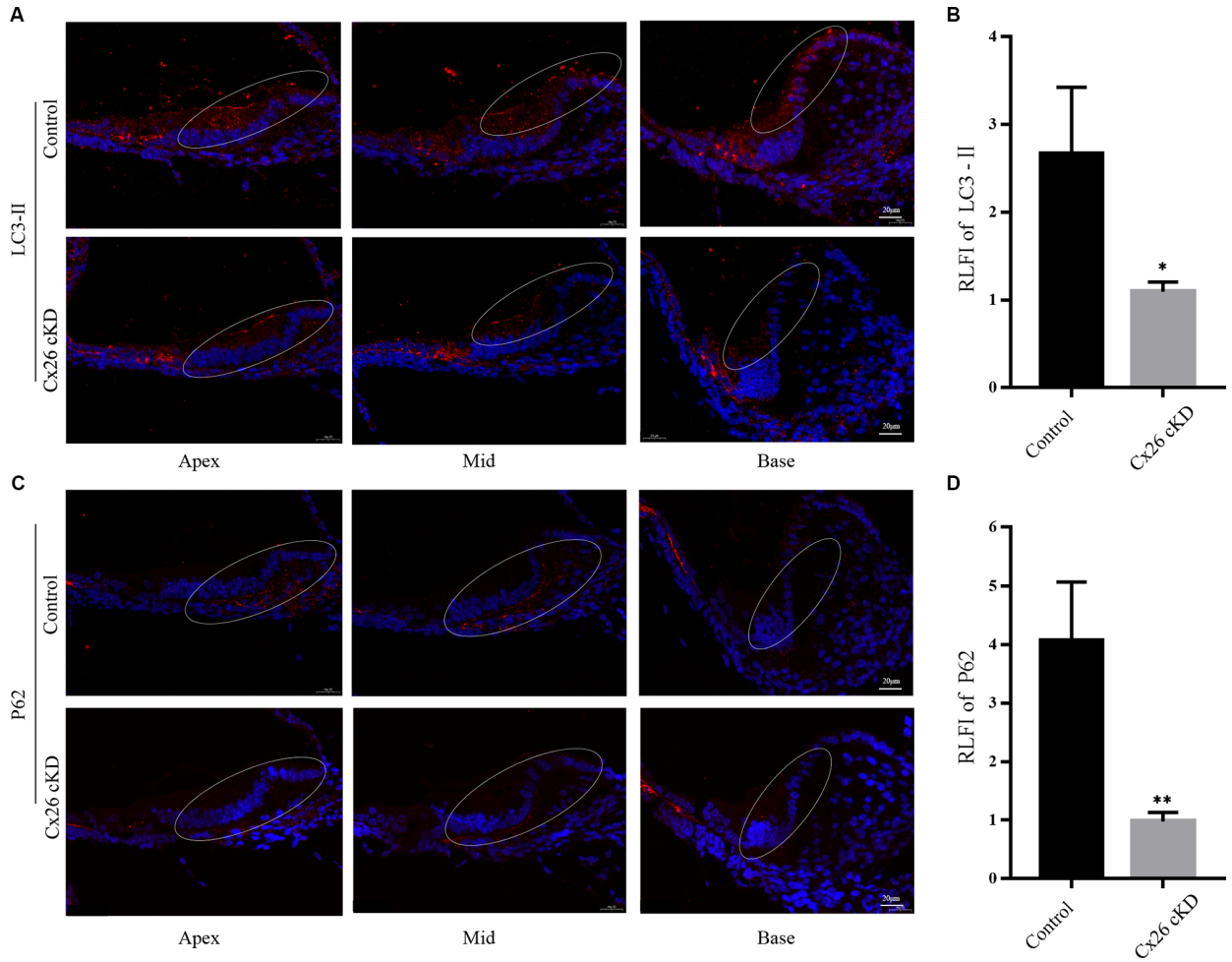

FIGURE 3 | Autophagy of Kölliker's organ was detected by immunofluorescence staining at P1. **(A)** In the apical, middle, and basal turns, immunoreactivity of LC3-II was intense in Kölliker's organ of the control group and markedly less intense in the Cx26-cKD group. Scale bars = 50 μm. **(B)** Average relative fluorescence intensity (RLFI) of LC3-II signal; * represents $P < 0.05$, $n = 3$. **(C)** Immunofluorescence staining of p62 was attenuated in Kölliker's organ cells of apical, middle, and basal turns in the Cx26-cKD group compared with the control group. Scale bars = 50 μm. **(D)** Average relative fluorescence intensity (RLFI) of p62; ** represents $P < 0.001$, $n = 3$.

hampered if autophagy is downregulated, therefore we predicted an overall reduced intracellular ATP concentration downstream of Cx26 knockdown.

To test this hypothesis, Cx26-cKD mice and their controls were sacrificed at P1. The micro-dissected Kölliker's organ was lysed and the total ATP concentration in the lysate was measured with a luciferin-luciferase bioluminescence ATP assay kit. To minimize the experimental changes, a standard curve was constructed for each experiment to estimate the corresponding ATP concentration (**Figure 5A**). ATP levels in the Cx26-cKD group were significantly reduced compared with the control group (**Figure 5B**; $P < 0.05$, $n = 4$), confirming our hypothesis.

Decreased Number of ATP-Loaded Vesicles in Kölliker's Organ of Cx26-cKD Mice

The vesicular nucleotide transporter, also known as solute carrier family 17 member 9 (SLC17A9), mediates lysosomal ATP accumulation and plays an important role in lysosomal physiology and cell viability (Cao et al., 2014). Based on the results described above, we predicted that the overall reduced ATP availability should correspond to a lower amount of ATP in the lysosomes of Kölliker's organ cells, where prior work showed ATP is accumulated (Chen et al., 2019).

To test this hypothesis, we prepared Kölliker's organ cultures from untreated P0 pups of *Gjb2*$^{loxP/loxP}$; ROSA26^{CreER} mice, and control mice. To promote Cre recombinase-mediated *in vitro* excision of Cx26 floxed alleles, cultures were exposed to 10 μM (Z)-4-hydroxytamoxifen (HTMX) and thereafter inspected by transmitted light microscopy at 10, 20, and 40× magnification (**Figure 5C**). No visible differences were noted between the HTMX and control groups. Therefore, we proceeded to stain the cultures with DAPI (to label nuclei) and quinacrine, which functions as an ATP-binding agent and acridine derivative with a very high affinity to ATP and has been used to label ATP-containing vesicles (White et al., 1995; Chen et al., 2019).

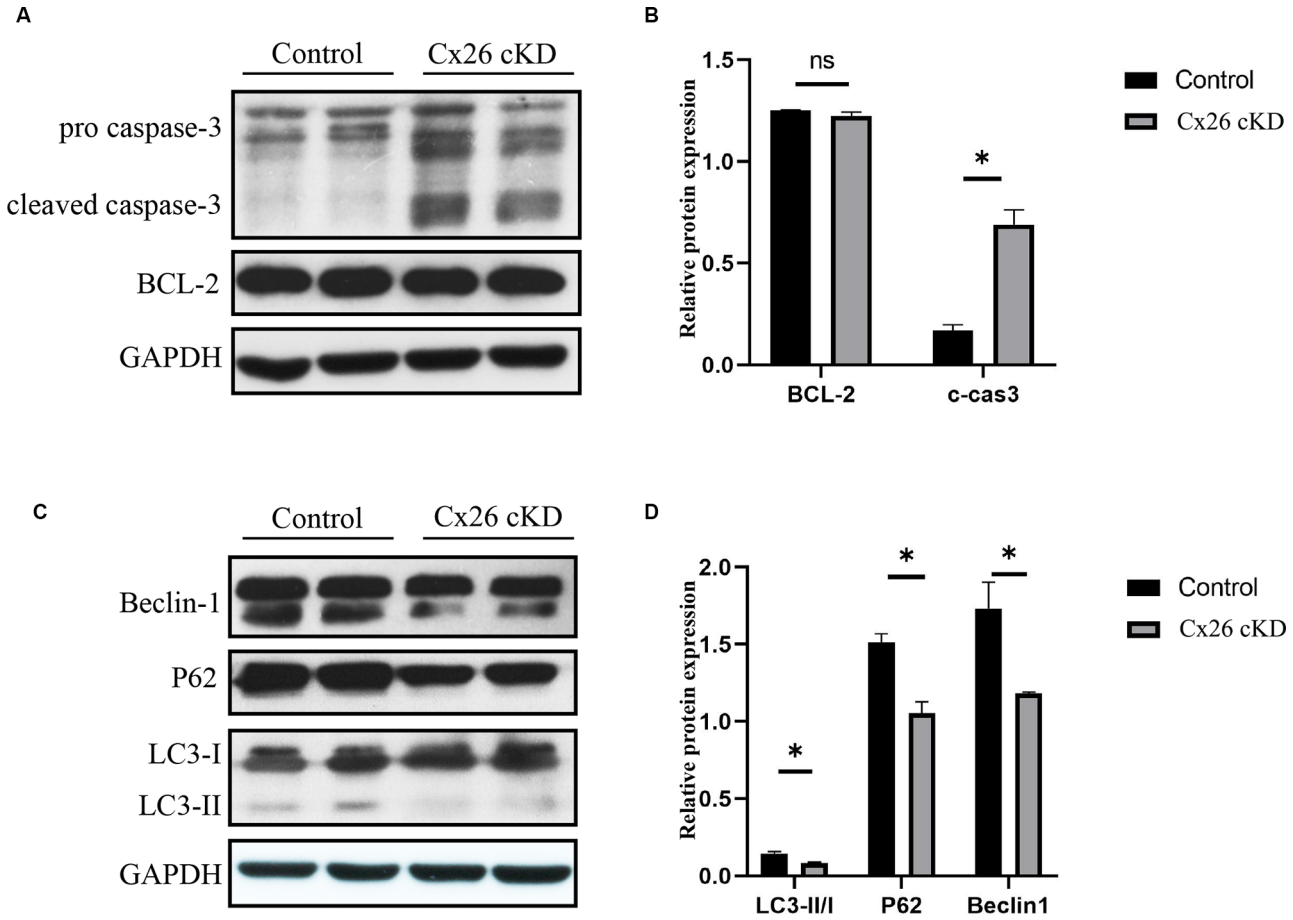

FIGURE 4 | Western blot analysis of apoptosis- and autophagy-related proteins in Kölliker's organ at P1. **(A)** Representative western blots for apoptosis-related proteins Bcl-2 and c-caspase 3. **(B)** Corresponding relative optical density; * represents $P < 0.05$, $n = 5$. **(C)** Representative western blots for autophagy-related proteins LC3-II, P62 and Beclin1. **(D)** Corresponding relative optical density; * represents $P < 0.05$, $n = 5$.

Samples were also immuno-stained with an anti-LAMP1 primary antibody (a lysosome marker) and a suitable secondary antibody (see "Materials and Methods" Section). The quinacrine signal (green) in the HTMX group was lower than in the control group, whereas LAMP1 immunoreactivity (red) was not significantly different between the two groups (**Figure 5D**). These qualitative results accord with the quantitative results of **Figure 5B** and suggest that, as a consequence of Cx26 knockdown, less ATP was accumulated in lysosomal vesicles of the Cx26-cKD group compared with the control group.

Decreased ATP-Evoked Intracellular Ca^{2+} Responses in Cx26-cKD Cochlear Cultures

To determine whether the alterations described above affect also Ca^{2+} signaling, HTMX-treated Kölliker's organ cultures were loaded with the selective Ca^{2+} indicator fluo-4 and challenged by the application of saturating amounts of exogenous ATP (30 μM, see "Materials and Methods" Section), expected to cause massive Ca^{2+} release from the ER. Ca^{2+} imaging revealed peak responses (F_{max}/F_0) in the $Gjb2^{loxP/loxP}$; $ROSA26^{CreER}$ group that were significantly downregulated compared with the control group (1.86 ± 0.37 vs. 3.13 ± 0.77, $P < 0.05$, $n = 3$; **Figure 5F**). In addition, we noted that Ca^{2+} oscillations appeared during the declining phase of the responses in the control group but were absent in the $Gjb2^{loxP/loxP}$; $ROSA26^{CreER}$ group (see "Discussion" Section, for a possible explanation). Together, the results in **Figure 5**, show that the knockdown of Cx26 affects a major ATP-dependent Ca^{2+} signaling pathway in Kölliker's organ, which is crucial for organ development and hearing acquisition as summarized in the introduction.

DISCUSSION

The organ of Corti is the core part of the auditory system, composed of hair cells and supporting cells. The hair cells function in transducing the sound mechanical stimulation into the primary acoustic signals (Liu et al., 2019), while the spiral ganglions transmit primary acoustic information from hair cells in the organ of Corti to the higher auditory centers of the central nervous system (Wei et al., 2021). Hair cells are easily injured by excessive noise exposure (Guo et al., 2021;

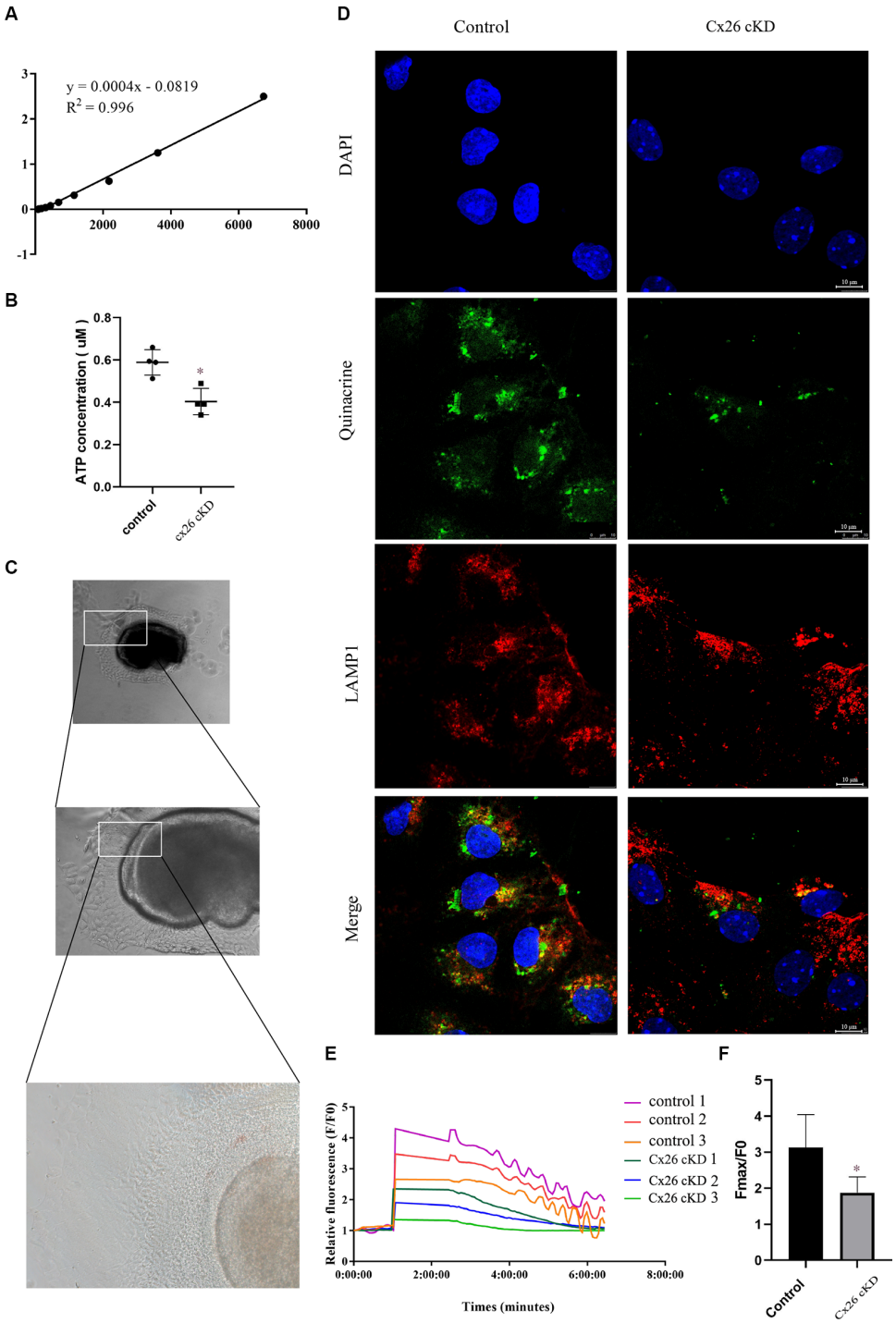

FIGURE 5 | ATP concentration and ATP-evoked Ca^{2+} signaling. **(A)** Representative standard curve used to calibrate bioluminescence signals: $Y = 0.0004X - 0.0819$, $R^2 = 0.996$. **(B)** ATP concentration estimated from luciferin-luciferase bioluminescence assay. $P < 0.05$, $n = 4$. **(C)** Representative transmitted light microscopy image of a Kölliker's organ culture viewed at 10×, 20×, and 40× magnification (from top to bottom). **(D)** Representative confocal fluorescence images of Kölliker's organ cultures labeled with quinacrine, anti-LAMP1 antibodies, and DAPI; scale bars = 10 μm. **(E)** Representative ATP-evoked Ca^{2+} responses of individual cells in Kölliker's organ cultures. **(F)** Quantification of F_{max}/F_0 signals; * represents $P < 0.05$, $n = 3$.

He et al., 2021), ototoxic drugs (He et al., 2017), aging (He et al., 2020), genetic factors (Fu et al., 2021), and infections (He et al., 2020).

Mouse models continue to provide critical insight into the functioning of the auditory system and deafness-associated genes (Bowl et al., 2017). Among these, it has long been known

that Cx26 (*Gjb2*) biallelic deletion in mice is embryonically lethal due to impaired transplacental uptake of glucose (Gabriel et al., 1998). The *Gjb2*$^{loxP/loxP}$ mice used in this study (Cohen-Salmon et al., 2002), can overcome embryonic lethality if crossed with a suitable Cre-expressing strain to achieve tissue- and/or time-conditional deletion of the floxed alleles (Orban et al., 1992; Vooijs et al., 2001). Crossing *Gjb2*$^{loxP/loxP}$ mice with the Otog-Cre strain (Cohen-Salmon et al., 2002), or the Sox10-Cre strain (Anselmi et al., 2008) resulted in mice with severe hearing loss and developmental defects in the cochlear sensory epithelium (Cohen-Salmon et al., 2002; Crispino et al., 2011). Both *Gjb2*$^{loxP/loxP}$; Otog-Cre and *Gjb2*$^{loxP/loxP}$; Sox10-Cre mice are considered models of human DFNB1 non-syndromic hearing impairment, which is frequently associated with truncating mutations that yield non-functional Cx26 proteins (Chan and Chang, 2014; Del Castillo and Del Castillo, 2017).

Results obtained from time-dependent knockdown of Cx26 in tamoxifen-induced *Gjb2*$^{loxP/loxP}$; ROSA26^{CreER} mice (Chang et al., 2015; Chen et al., 2018) lend further support to the notion that Cx26 intercellular gap junction channels and hemichannels with normal permeability to nutrients and other metabolites and signaling molecules are essential for normal development of the cochlea and normal hearing acquisition (Mammano, 2019).

Here, using tamoxifen-induced knockdown of Cx26 in *Gjb2*$^{loxP/loxP}$; ROSA26^{CreER} mice, we found decreased levels of autophagy-related proteins beclin1, LC3-II, and p62 in the cochlea, indicating that autophagy was downregulated. These alterations were accompanied by increased apoptosis in the Kölliker's organ cells, which became apoptotic as early as P1 based on TUNEL assays and upregulation of c-caspase 3 expressions. The p62 marker is particularly interesting because increasing evidence points to the N-terminal arginylated BiP (R-BiP)/Beclin-1/p62 complex as having an important role in the crosstalk between apoptosis and autophagy, which greatly affects cell death (Song et al., 2018). Recent work examined this interplay in the normal developing cochlea and concluded that autophagy precedes apoptosis in the natural postnatal degeneration of Kölliker's organ cells and their regulated replacement by cuboidal cells of the inner sulcus (Hou et al., 2019).

The accelerated apoptosis described in this article is easily explained in the light of a recent study that linked decreased Cx26 expression to apoptosis *via* impaired nutrient delivery to the sensory epithelium through gap junction channels, the reduced release of the key antioxidant glutathione through connexin hemichannels, and deregulated expression of several genes under the transcriptional control of Nrf2, a redox-sensitive transcription factor that plays a pivotal role in oxidative stress regulation (Fetoni et al., 2018; Ding et al., 2020). Thus, we conclude that impairment of Cx26 function subverts the critically timed phasing of autophagy and apoptosis in the mouse postnatal cochlea, hijacks the hearing acquisition program, and dooms animals to deafness through increased oxidative stress. This conclusion is also supported by prior studies showing that Kölliker's organ cells did not completely degenerate until 2 weeks after birth in caspase 3 knockout mice, resulting in hyperplasia of supporting cells, degeneration of hair cells, and severe hearing loss (Takahashi et al., 2001), strengthening the notion that a correctly executed postnatal apoptotic program is key to hearing acquisition in mice (Chen et al., 2020).

In non-sensory cells of the cochlear sensory epithelium, ATP binding to G protein-coupled P2Y receptors activates the production of IP_3 *via* phospholipase C (PLC), promoting Ca^{2+} release from the endoplasmic reticulum (ER) through IP_3 receptors (IP_3R) and consequent increase of the cytoplasmic free Ca^{2+} concentration (Mammano, 2013). Our Ca^{2+} imaging experiments show that the ATP/P2Y/PLC/IP_3 signal transduction cascade, which fuels Ca^{2+} signaling in Kölliker's organ, is downregulated by the knockdown of Cx26. To interpret these results, it is imperative to consider that: (i) all else held equal, the amount of Ca^{2+} released from the ER depends on the Ca^{2+} concentration in the ER; (ii) increased oxidative stress is associated with Cx26 downregulation in the developing cochlea (Fetoni et al., 2018; He et al., 2019). Thus, in our experimental conditions, SERCA pumps activity was lowered not only by the reduced availability of cytosolic ATP (this article) but also by the effect of oxidative stress (Kaplan et al., 2003). In addition, alterations in the redox state of critical thiols in the IP_3R lead to sensitization of IP_3R-mediated Ca^{2+} release associated with oxidative stress (Joseph et al., 2018), which may increase the steady-state Ca^{2+} leakage from the ER. The predicted net effect is a reduced Ca^{2+} content in the ER, hence a reduced driving force for Ca^{2+} transfer from the ER to cytosol driven by the signal transduction cascade mentioned above. This explains the reduced F_{max}/F_0 signals evoked by supramaximal exogenous ATP stimuli in Kölliker's organ cultures exposed to HTMX.

As for the issue of Ca^{2+} oscillations, data-driven computational modeling shows that they are governed by Hopf-type bifurcation and arise only within a limited range of extracellular ATP concentration through the interplay of IP_3R-mediated Ca^{2+} release from the ER and SERCA pump-mediated Ca^{2+} re-uptake into the ER (Ceriani et al., 2016). In control Kölliker's organ cultures, oscillations arose during the recovery phase from supramaximal stimulation, while the extracellular ATP concentration lowered due to diffusion and ATP hydrolysis mediated by ectonucleotidases expressed at the surface of the epithelium (Ceriani et al., 2016). As both SERCA pump activity and IP_3R are affected by oxidative stress, it comes as no surprise that Ca^{2+} oscillations were absent in Kölliker's organ cultures exposed to HTMX. This conclusion is supported also by experiments and mathematical modeling of the effects of oxidative stress on Ca^{2+} oscillation in other cellular systems (Antonucci et al., 2015).

In conclusion, our results provide further evidence for abnormal cochlear development in mice with reduced expression of Cx26, expound possible mechanisms of hearing acquisition failure, and produce novel insight, from a new perspective, for *GJB2*-related hereditary deafness.

DATA AVAILABILITY STATEMENT

The raw data supporting the conclusions of this article will be made available by the authors, without undue reservation.

ETHICS STATEMENT

The animal study was reviewed and approved by Ethics Committee of Xinhua Hospital affliated to Shanghai Jiaotong University School of Medicine.

AUTHOR CONTRIBUTIONS

LS and DG wrote the article. JuC, SH, YL, and YH analyzed the data. FM, JiC, and JY designed the study. All authors contributed to the article and approved the submitted version.

FUNDING

This study was supported by a grant from the National Natural Science Foundation of China, which was awarded to JY (Grant/Award Numbers: 81873698).

REFERENCES

Anselmi, F., Hernandez, V. H., Crispino, G., Seydel, A., Ortolano, S., Roper, S. D., et al. (2008). ATP release through connexin hemichannels and gap junction transfer of second messengers propagate Ca2+ signals across the inner ear. *Proc. Natl. Acad. Sci. U S A* 105, 18770–18775. doi: 10.1073/pnas.0800793105

Antonucci, S., Tagliavini, A., and Pedersen, M. G. (2015). Reactive oxygen and nitrogen species disturb Ca(2+) oscillations in insulin-secreting MIN6 beta-cells. *Islets* 7:e1107255. doi: 10.1080/19382014.2015.1107255

Beltramello, M., Piazza, V., Bukauskas, F. F., Pozzan, T., and Mammano, F. (2005). Impaired permeability to Ins(1,4,5)P3 in a mutant connexin underlies recessive hereditary deafness. *Nat. Cell Biol.* 7, 63–69. doi: 10.1038/ncb1205

Bootman, M. D., Chehab, T., Bultynck, G., Parys, J. B., and Rietdorf, K. (2018). The regulation of autophagy by calcium signals: do we have a consensus? *Cell Calcium* 70, 32–46. doi: 10.1016/j.ceca.2017.08.005

Bowl, M. R., Simon, M. M., Ingham, N. J., Greenaway, S., Santos, L., Cater, H., et al. (2017). A large-scale hearing loss screen reveals an extensive unexplored genetic landscape for auditory dysfunction. *Nat. Commun.* 8:886. doi: 10.1038/s41467-017-00595-4

Cao, Q., Zhao, K., Zhong, X. Z., Zou, Y., Yu, H., Huang, P., et al. (2014). SLC17A9 protein functions as a lysosomal ATP transporter and regulates cell viability. *J. Biol. Chem.* 289, 23189–23199. doi: 10.1074/jbc.M114.567107

Ceriani, F., Hendry, A., Jeng, J. Y., Johnson, S. L., Stephani, F., Olt, J., et al. (2019). Coordinated calcium signaling in cochlear sensory and non-sensory cells refines afferent innervation of outer hair cells. *EMBO J.* 38:e99839. doi: 10.15252/embj.201899839

Ceriani, F., Pozzan, T., and Mammano, F. (2016). The critical role of ATP-induced ATP release for Ca2+ signaling in nonsensory cell networks of the developing cochlea. *Proc. Natl. Acad. Sci. U S A* 113, E7194–E7201. doi: 10.1073/pnas.1616061113

Chan, D. K., and Chang, K. W. (2014). GJB2-associated hearing loss: systematic review of worldwide prevalence, genotype and auditory phenotype. *Laryngoscope* 124, E34–E53. doi: 10.1002/lary.24332

Chang, Q., Tang, W., Kim, Y., and Lin, X. (2015). Timed conditional null of connexin26 in mice reveals temporary requirements of connexin26 in key cochlear developmental events before the onset of hearing. *Neurobiol. Dis.* 73, 418–427. doi: 10.1016/j.nbd.2014.09.005

Chen, J., Hou, S., and Yang, J. (2019). ATP is stored in lysosomes of greater epithelial ridge supporting cells in newborn rat cochleae. *J. Cell. Biochem.* 120, 19469–19481. doi: 10.1002/jcb.29251

Chen, S., Xie, L., Xu, K., Cao, H.-Y., Wu, X., Xu, X.-X., et al. (2018). Developmental abnormalities in supporting cell phalangeal processes and cytoskeleton in the Gjb2 knockdown mouse model. *Dis. Model. Mech.* 11:dmm033019. doi: 10.1242/dmm.033019

Chen, B., Xu, H., Mi, Y., Jiang, W., Guo, D., Zhang, J., et al. (2020). Mechanisms of hearing loss and cell death in the cochlea of connexin mutant mice. *Am. J. Physiol. Cell Physiol.* 319, C569–C578. doi: 10.1152/ajpcell.00483.2019

Cohen-Salmon, M., del Castillo, F. J., and Petit, C. (2005). "Connexins responsiblbe for hereditary deafness - the tale unfolds," in *Gap Junctions in Development and Disease*, ed E. Winterhager (Berlin: Springer-Verlag), 111–134.

Cohen-Salmon, M., Ott, T., Michel, V., Hardelin, J. P., Perfettini, I., Eybalin, M., et al. (2002). Targeted ablation of connexin26 in the inner ear epithelial gap junction network causes hearing impairment and cell death. *Curr. Biol.* 12, 1106–1111. doi: 10.1016/s0960-9822(02)00904-1

Crispino, G., Di Pasquale, G., Scimemi, P., Rodriguez, L., Galindo Ramirez, F., De Siati, R. D., et al. (2011). BAAV mediated GJB2 gene transfer restores gap junction coupling in cochlear organotypic cultures from deaf Cx26Sox10Cre mice. *PLoS One* 6:e23279. doi: 10.1371/journal.pone.0023279

de Iriarte Rodriguez, R., Pulido, S., Rodriguez-de la Rosa, L., Magarinos, M., and Varela-Nieto, I. (2015). Age-regulated function of autophagy in the mouse inner ear. *Hear. Res.* 330, 39–50. doi: 10.1016/j.heares.2015.07.020

Del Castillo, F. J., and Del Castillo, I. (2017). DFNB1 non-syndromic hearing impairment: diversity of mutations and associated phenotypes. *Front. Mol. Neurosci.* 10:428. doi: 10.3389/fnmol.2017.00428

Ding, Y., Meng, W., Kong, W., He, Z., and Chai, R. (2020). The role of FoxG1 in the inner ear. *Front. Cell Dev. Biol.* 8:614954. doi: 10.3389/fcell.2020.614954

Driver, E. C., and Kelley, M. W. (2020). Development of the cochlea. *Development* 147:dev162263. doi: 10.1242/dev.162263

Eckrich, T., Blum, K., Milenkovic, I., and Engel, J. (2018). Fast Ca2+ transients of inner hair cells arise coupled and uncoupled to Ca2+ waves of inner supporting cells in the developing mouse cochlea. *Front. Mol. Neurosci.* 11:264. doi: 10.3389/fnmol.2018.00264

Ehret, G. (1977). Postnatal development in the acoustic system of the house mouse in the light of developing masked thresholds. *J. Acoust. Soc. Am.* 62, 143–148. doi: 10.1121/1.381496

Emanuele, S., Lauricella, M., D'Anneo, A., Carlisi, D., De Blasio, A., Di Liberto, D., et al. (2020). p62: friend or foe? Evidences for oncojanus and neurojanus roles. *Int. J. Mol. Sci.* 21:5029. doi: 10.3390/ijms21145029

Fetoni, A. R., Zorzi, V., Paciello, F., Ziraldo, G., Peres, C., Raspa, M., et al. (2018). Cx26 partial loss causes accelerated presbycusis by redox imbalance and dysregulation of Nfr2 pathway. *Redox Biol.* 19, 301–317. doi: 10.1016/j.redox.2018.08.002

Forge, A., Becker, D., Casalotti, S., Edwards, J., Marziano, N., and Nevill, G. (2003). Gap junctions in the inner ear: comparison of distribution patterns in different vertebrates and assessement of connexin composition in mammals. *J. Comp. Neurol.* 467, 207–231. doi: 10.1002/cne.10916

Fu, X., An, Y., Wang, H., Li, P., Lin, J., Yuan, J., et al. (2021). Deficiency of Klc2 induces low-frequency sensorineural hearing loss in C57BL/6J mice and human. *Mol. Neurobiol.* 58, 4376–4391. doi: 10.1007/s12035-021-02422-w

Gabriel, H. D., Jung, D., Butzler, C., Temme, A., Traub, O., Winterhager, E., et al. (1998). Transplacental uptake of glucose is decreased in embryonic lethal connexin26-deficient mice. *J. Cell Biol.* 140, 1453–1461. doi: 10.1083/jcb.140.6.1453

Galluzzi, L., Pietrocola, F., Levine, B., and Kroemer, G. (2014). Metabolic control of autophagy. *Cell* 159, 1263–1276. doi: 10.1016/j.cell.2014.11.006

Gorczyca, W., Traganos, F., Jesionowska, H., and Darzynkiewicz, Z. (1993). Presence of DNA strand breaks and increased sensitivity of DNA in situ to denaturation in abnormal human sperm cells: analogy to apoptosis of somatic cells. *Exp. Cell Res.* 207, 202–205. doi: 10.1006/excr.1993.1182

Guo, L., Cao, W., Niu, Y., He, S., Chai, R., and Yang, J. (2021). Autophagy regulates the survival of hair cells and spiral ganglion neurons in cases of noise, ototoxic drug and age-induced sensorineural hearing loss. *Front. Cell. Neurosci.* 15:760422. doi: 10.3389/fncel.2021.760422

He, Z., Fang, Q., Li, H., Shao, B., Zhang, Y., Zhang, Y., et al. (2019). The role of FOXG1 in the postnatal development and survival of mouse cochlear hair cells. *Neuropharmacology* 144, 43–57. doi: 10.1016/j.neuropharm.2018.10.021

He, Z., Guo, L., Shu, Y., Fang, Q., Zhou, H., Liu, Y., et al. (2017). Autophagy protects auditory hair cells against neomycin-induced damage. *Autophagy* 13, 1884–1904. doi: 10.1080/15548627.2017.1359449

He, Z.-H., Li, M., Fang, Q.-J., Liao, F.-L., Zou, S.-Y., Wu, X., et al. (2021). FOXG1 promotes aging inner ear hair cell survival through activation of the autophagy pathway. *Autophagy* 17, 4341–4362. doi: 10.1080/15548627.2021.1916194

He, Z.-H., Zou, S.-Y., Li, M., Liao, F.-L., Wu, X., Sun, H.-Y., et al. (2020). The nuclear transcription factor FoxG1 affects the sensitivity of mimetic aging hair cells to inflammation by regulating autophagy pathways. *Redox Biol.* 28:101364. doi: 10.1016/j.redox.2019.101364

Hou, S., Chen, J., and Yang, J. (2019). Autophagy precedes apoptosis during degeneration of the Kolliker's organ in the development of rat cochlea. *Eur. J. Histochem.* 63:3025. doi: 10.4081/ejh.2019.3025

Ishii, N., Wanaka, A., Ohno, K., Matsumoto, K., Eguchi, Y., Mori, T., et al. (1996). Localization of bcl-2, bax and bcl-x mRNAs in the developing inner ear of the mouse. *Brain Res.* 726, 123–128.

Jagger, D. J., and Forge, A. (2015). Connexins and gap junctions in the inner ear--it's not just about K(+) recycling. *Cell Tissue Res.* 360, 633–644. doi: 10.1007/s00441-014-2029-z

Johnson, S. L., Ceriani, F., Houston, O., Polishchuk, R., Polishchuk, E., Crispino, G., et al. (2017). Connexin-mediated signaling in nonsensory cells is crucial for the development of sensory inner hair cells in the mouse cochlea. *J. Neurosci.* 37, 258–268. doi: 10.1523/JNEUROSCI.2251-16.2016

Joseph, S. K., Young, M. P., Alzayady, K., Yule, D. I., Ali, M., Booth, D. M., et al. (2018). Redox regulation of type-I inositol trisphosphate receptors in intact mammalian cells. *J. Biol. Chem.* 293, 17464–17476. doi: 10.1074/jbc.RA118.005624

Kabeya, Y., Mizushima, N., Ueno, T., Yamamoto, A., Kirisako, T., Noda, T., et al. (2000). LC3, a mammalian homologue of yeast Apg8p, is localized in autophagosome membranes after processing. *EMBO J.* 19, 5720–5728. doi: 10.1093/emboj/19.21.5720

Kamiya, K., Takahashi, K., Kitamura, K., Momoi, T., and Yoshikawa, Y. (2001). Mitosis and apoptosis in postnatal auditory system of the C3H/He strain. *Brain Res.* 901, 296–302. doi: 10.1016/s0006-8993(01)02300-9

Kaplan, P., Babusikova, E., Lehotsky, J., and Dobrota, D. (2003). Free radical-induced protein modification and inhibition of Ca2+-ATPase of cardiac sarcoplasmic reticulum. *Mol. Cell. Biochem.* 248, 41–47. doi: 10.1023/a:1024145212616

Kikuchi, T., Adams, J. C., Miyabe, Y., So, E., and Kobayashi, T. (2000). Potassium ion recycling pathway *via* gap junction systems in the mammalian cochlea and its interruption in hereditary nonsyndromic deafness. *Med. Electron Microsc.* 33, 51–56. doi: 10.1007/s007950070001

La Rovere, R. M., Roest, G., Bultynck, G., and Parys, J. B. (2016). Intracellular Ca^{2+} signaling and Ca^{2+} microdomains in the control of cell survival, apoptosis and autophagy. *Cell Calcium* 60, 74–87. doi: 10.1016/j.ceca.2016.04.005

Laird, D. W., and Lampe, P. D. (2022). Cellular mechanisms of connexin-based inherited diseases. *Trends Cell Biol.* 32, 58–69. doi: 10.1016/j.tcb.2021.07.007

Lim, D. J., and Anniko, M. (1985). Developmental morphology of the mouse inner ear. A scanning electron microscopic observation. *Acta Otolaryngol. Suppl.* 422, 1–69.

Lim, D., and Rueda, J. (1992). "Structural development of the cochlea," in *Development of Auditory and Vestibular Systems - 2 (1st Edition)*, ed R. Romand (New York: Elsevier Science Publishing Co.), 33–58.

Liu, Y., Qi, J., Chen, X., Tang, M., Chu, C., Zhu, W., et al. (2019). Critical role of spectrin in hearing development and deafness. *Sci. Adv.* 5:eaav7803. doi: 10.1126/sciadv.aav7803

Logue, S. E., and Martin, S. J. (2008). Caspase activation cascades in apoptosis. *Biochem. Soc. Trans.* 36, 1–9. doi: 10.1042/BST0360001

Mammano, F. (2013). ATP-dependent intercellular Ca^{2+} signaling in the developing cochlea: facts, fantasies and perspectives. *Semin. Cell Dev. Biol.* 24, 31–39. doi: 10.1016/j.semcdb.2012.09.004

Mammano, F. (2019). Inner ear connexin channels: roles in development and maintenance of cochlear function. *Cold Spring Harb. Perspect. Med.* 9:a033233. doi: 10.1101/cshperspect.a033233

Mammano, F., and Bortolozzi, M. (2010). "Ca^{2+} imaging: principles of analysis and enhancement," in *Calcium Measurement Methods*, eds A. Verkhratsky and O. Petersen (New York: Humana Press), 57–80.

Mammano, F., and Bortolozzi, M. (2018). Ca(2+) signaling, apoptosis and autophagy in the developing cochlea: Milestones to hearing acquisition. *Cell Calcium* 70, 117–126. doi: 10.1016/j.ceca.2017.05.006

Mazzarda, F., D'Elia, A., Massari, R., De Ninno, A., Bertani, F. R., Businaro, L., et al. (2020). Organ-on-chip model shows that ATP release through connexin hemichannels drives spontaneous Ca^{2+} signaling in non-sensory cells of the greater epithelial ridge in the developing cochlea. *Lab Chip* 20, 3011–3023. doi: 10.1039/d0lc00427h

Orban, P. C., Chui, D., and Marth, J. D. (1992). Tissue- and site-specific DNA recombination in transgenic mice. *Proc. Natl. Acad. Sci. U S A* 89, 6861–6865. doi: 10.1073/pnas.89.15.6861

Rodriguez, L., Simeonato, E., Scimemi, P., Anselmi, F., Cali, B., Crispino, G., et al. (2012). Reduced phosphatidylinositol 4,5-bisphosphate synthesis impairs inner ear Ca^{2+} signaling and high-frequency hearing acquisition. *Proc. Natl. Acad. Sci. U S A* 109, 14013–14018. doi: 10.1073/pnas.1211869109

Schutz, M., Scimemi, P., Majumder, P., De Siati, R. D., Crispino, G., Rodriguez, L., et al. (2010). The human deafness-associated connexin 30 T5M mutation causes mild hearing loss and reduces biochemical coupling among cochlear non-sensory cells in knock-in mice. *Hum. Mol. Genet.* 19, 4759–4773. doi: 10.1093/hmg/ddq402

Slee, E. A., Harte, M. T., Kluck, R. M., Wolf, B. B., Casiano, C. A., Newmeyer, D. D., et al. (1999). Ordering the cytochrome c-initiated caspase cascade: hierarchical activation of caspases-2, -3, -6, -7, -8 and -10 in a caspase-9-dependent manner. *J.Cell Biol.* 144, 281–292. doi: 10.1083/jcb.144.2.281

Song, X., Lee, D. H., Dilly, A. K., Lee, Y. S., Choudry, H. A., Kwon, Y. T., et al. (2018). Crosstalk between apoptosis and autophagy is regulated by the arginylated BiP/Beclin-1/p62 complex. *Mol. Cancer Res.* 16, 1077–1091. doi: 10.1158/1541-7786.MCR-17-0685

Soundarrajan, D. K., Huizar, F. J., Paravitorghabeh, R., Robinett, T., and Zartman, J. J. (2021). From spikes to intercellular waves: tuning intercellular calcium signaling dynamics modulates organ size control. *PLoS Comput. Biol.* 17:e1009543. doi: 10.1371/journal.pcbi.1009543

Sun, Y., Tang, W., Chang, Q., Wang, Y., Kong, W., and Lin, X. (2009). Connexin30 null and conditional connexin26 null mice display distinct pattern and time course of cellular degeneration in the cochlea. *J. Comp. Neurol.* 516, 569–579. doi: 10.1002/cne.22117

Takahashi, K., Kamiya, K., Urase, K., Suga, M., Takizawa, T., Mori, H., et al. (2001). Caspase-3-deficiency induces hyperplasia of supporting cells and degeneration of sensory cells resulting in the hearing loss. *Brain Res.* 894, 359–367. doi: 10.1016/s0006-8993(01)02123-0

Tritsch, N. X., Yi, E., Gale, J. E., Glowatzki, E., and Bergles, D. E. (2007). The origin of spontaneous activity in the developing auditory system. *Nature* 450, 50–55. doi: 10.1038/nature06233

Vaux, D. L., Weissman, I. L., and Kim, S. K. (1992). Prevention of programmed cell death in Caenorhabditis elegans by human bcl-2. *Science* 258, 1955–1957. doi: 10.1126/science.1470921

Vooijs, M., Jonkers, J., and Berns, A. (2001). A highly efficient ligand-regulated Cre recombinase mouse line shows that LoxP recombination is position dependent. *EMBO Rep.* 2, 292–297. doi: 10.1093/embo-reports/kve064

Wang, H. C., and Bergles, D. E. (2015). Spontaneous activity in the developing auditory system. *Cell Tissue Res.* 361, 65–75. doi: 10.1007/s00441-014-2007-5

Wei, H., Chen, Z., Hu, Y., Cao, W., Ma, X., Zhang, C., et al. (2021). Topographically conductive butterfly wing substrates for directed spiral ganglion neuron growth. *Small* 17:2102062. doi: 10.1002/smll.202102062

White, P. N., Thorne, P. R., Housley, G. D., Mockett, B., Billett, T. E., and Burnstock, G. (1995). Quinacrine staining of marginal cells in the stria vascularis of the guinea-pig cochlea: a possible source of extracellular ATP? *Hear. Res.* 90, 97–105. doi: 10.1016/0378-5955(95)00151-1

Xu, L., Carrer, A., Zonta, F., Qu, Z., Ma, P., Li, S., et al. (2017). Design and characterization of a human monoclonal antibody that modulates mutant connexin 26 hemichannels implicated in deafness and skin disorders. *Front. Mol. Neurosci.* 10:298. doi: 10.3389/fnmol.2017.00298

Zhao, H. B. (2017). Hypothesis of K(+)-recycling defect is not a primary deafness mechanism for Cx26 (GJB2) Deficiency. *Front. Mol. Neurosci.* 10:162. doi: 10.3389/fnmol.2017.00162

Zhou, X., Jen, P. H., Seburn, K. L., Frankel, W. N., and Zheng, Q. Y. (2006). Auditory brainstem responses in 10 inbred strains of mice. *Brain Res.* 1091, 16–26. doi: 10.1016/j.brainres.2006.01.107

Zhou, H., Qian, X., Xu, N., Zhang, S., Zhu, G., Zhang, Y., et al. (2020). Disruption of Atg7-dependent autophagy causes electromotility disturbances, outer hair cell loss and deafness in mice. *Cell Death Dis.* 11:913. doi: 10.1038/s41419-020-03110-8

Zorzi, V., Paciello, F., Ziraldo, G., Peres, C., Mazzarda, F., Nardin, C., et al. (2017). Mouse Panx1 is dispensable for hearing acquisition and auditory function. *Front. Mol. Neurosci.* 10:379. doi: 10.3389/fnmol.2017.00379

Conflict of Interest: The authors declare that the research was conducted in the absence of any commercial or financial relationships that could be construed as a potential conflict of interest.

Publisher's Note: All claims expressed in this article are solely those of the authors and do not necessarily represent those of their affiliated organizations, or those of the publisher, the editors and the reviewers. Any product that may be evaluated in this article, or claim that may be made by its manufacturer, is not guaranteed or endorsed by the publisher.

frontiers in Cellular Neuroscience

ORIGINAL RESEARCH
published: 23 March 2022
doi: 10.3389/fncel.2022.841731

Glutathione Peroxidase 1 Protects Against Peroxynitrite-Induced Spiral Ganglion Neuron Damage Through Attenuating NF-κB Pathway Activation

Xue Wang[1,2†], Yuechen Han[1,2†], Fang Chen[1,2†], Man Wang[1,2], Yun Xiao[1,2], Haibo Wang[1,2], Lei Xu[1,2] and Wenwen Liu[1,2*]*

[1] Department of Otolaryngology-Head and Neck Surgery, Shandong Provincial ENT Hospital, Cheeloo College of Medicine, Shandong University, Jinan, China, [2] Shandong Institute of Otorhinolaryngology, Jinan, China

OPEN ACCESS

Edited by:
Zuhong He,
Wuhan University, China

Reviewed by:
Mingliang Tang,
Southeast University, China
Fangyi Chen,
Southern University of Science and Technology, China

***Correspondence:**
Lei Xu
sdphxl@126.com
Wenwen Liu
wenwenliu_1@yahoo.com

[†] These authors have contributed equally to this work

Specialty section:
This article was submitted to Cellular Neuropathology, a section of the journal Frontiers in Cellular Neuroscience

Received: 22 December 2021
Accepted: 22 February 2022
Published: 23 March 2022

Citation:
Wang X, Han Y, Chen F, Wang M, Xiao Y, Wang H, Xu L and Liu W (2022) Glutathione Peroxidase 1 Protects Against Peroxynitrite-Induced Spiral Ganglion Neuron Damage Through Attenuating NF-κB Pathway Activation. Front. Cell. Neurosci. 16:841731. doi: 10.3389/fncel.2022.841731

Glutathione peroxidase 1 (GPX1) is a crucial antioxidant enzyme that prevented the harmful accumulation of intra-cellular hydrogen peroxide. GPX1 might contribute in limiting cochlear damages associated with aging or acoustic overexposure, but the function of GPX1 in the inner ear remains unclear. The present study was designed to investigate the effect of GPX1 on cochlear spiral ganglion neurons (SGNs) against oxidative stress induced by peroxynitrite, a versatile oxidant generated by the reaction of superoxide anion and nitric oxide. Here, we first found that the expression of GPX1 in cultured SGNs was downregulated after peroxynitrite exposure. Then, the GPX1 mimic ebselen and the *gpx1* knockout (*gpx1*$^{-/-}$) mice were used to investigate the role of GPX1 in SGNs treated with peroxynitrite. The pretreatment with ebselen significantly increased the survived SGN numbers, inhibited the apoptosis, and enhanced the expression of 4-HNE in the cultured SGNs of peroxynitrite + ebselen group compared with the peroxynitrite-only group. On the contrary, remarkably less survived SGNs, more apoptotic SGNs, and the higher expression level of 4-HNE were detected in the peroxynitrite + *gpx1*$^{-/-}$ group compared with the peroxynitrite-only group. Furthermore, rescue experiments with antioxidant N-acetylcysteine (NAC) showed that the expression of 4-HNE and the apoptosis in SGNs were significantly decreased, while the number of surviving SGNs was increased in peroxynitrite + NAC group compared the peroxynitrite-only group and in peroxynitrite + *gpx1*$^{-/-}$ + NAC group vs. peroxynitrite + *gpx1*$^{-/-}$ group. Finally, mechanistic studies showed that the activation of nuclear factor-kappa B (NF-κB) was involved in the SGNs damage caused by peroxynitrite and that GPX1 protected SGNs against peroxynitrite-induced damage, at least in part, *via* blocking the NF-κB pathway activation. Collectively, our findings suggest that GPX1 might serve as a new target for the prevention of nitrogen radical-induced SGNs damage and hearing loss.

Keywords: glutathione peroxidase 1, spiral ganglion neuron, peroxynitrite, oxidative stress, nuclear factor-kappa B, hearing loss

INTRODUCTION

In mammals, cochlea spiral ganglion neurons (SGNs) are the primary sensory neurons on the auditory conduction pathway. SGNs transmit complex acoustic information from sensory hair cells (HCs) to the second-order sensory neurons in the cochlear nucleus for sound processing. The survival of SGNs is essential for hearing preservation and, conversely, as SGN cannot regenerate spontaneously, the impairment and irreversible loss of SGNs result in permanent sensorineural hearing loss (SNHL) (Liu et al., 2019a; Leake et al., 2020; Pavlinkova, 2020), which seriously affects the human social and cognitive development. Multiple stimuli, such as excessive noise, ototoxic drugs, hereditary defects, and aging process, can cause SGNs damage. Although the pathogenic mechanisms by which these factors lead to SGN damage are various, researches have documented that the oxidative stress is a basic mechanism involved in SGNs death (Liu et al., 2011, 2012, 2019b, 2021; Xiong et al., 2011; Yamasoba et al., 2013; Wang et al., 2019, 2021). Oxidative stress is the disturbance in the balance between the generation of free radicals, such as reactive oxygen species (ROS) and reactive nitrogen species (RNS), and antioxidant defenses, and can cause oxidative damage to diverse cellular components, such as membranes, proteins, and DNA. Among RNS molecules, peroxynitrite, a product of superoxide anion and nitric oxide, is one of the most prominent one (Liu et al., 2011, 2012; Labbe et al., 2016; Cao et al., 2017; Ramdial et al., 2017). Peroxynitrite can oxidize a wide variety of biomolecules, which, in turn, modulates cell signal transduction pathways, interferes with mitochondrial function, impairs DNA, and finally mediates necrosis and apoptosis in different cell types (Korkmaz et al., 2009). Peroxynitrite participates in the occurrence and development of the varieties of pathological conditions, but data about the effects of peroxynitrite on auditory cells in the cochlea are still very limited. In our previous studies, we found that peroxynitrite induced cytotoxicity in rat SGNs (Liu et al., 2011, 2012) and mouse cochlear HCs (Cao et al., 2017). However, the effect of peroxynitrite on SGNs has not yet been fully elucidated, and it is important to eliminate the excessive peroxynitrite so as to counteract its toxic effect to protect cells from oxidative injuries.

Studies have shown that organisms can activate a series of defense responses, such as improving the activity of antioxidant enzymes in the body and initiating lysosomal degradation pathways, to prevent oxidative damage. Glutathione peroxidase 1 (GPX1) is one of the most abundant members of the GPXs family that protects cell from oxidative damage and maintains the balance of intracellular redox systems (Brigelius-Flohé, 1999). Glutathione peroxidase 1 has been reported for its effect in modulating many pathophysiologic processes in which oxidative stress play a vital role (Lubos et al., 2011). For example, GPX1 might play a protective role in alleviating oxidative stress as a neuromodulator in neurodegenerative disorders (Sharma et al., 2021a), GPX1 is a gatekeeper restraining the oncogenic power of mitochondrial ROS generated by superoxide dismutase 2 (SOD2) (Ekoue et al., 2017), and the upregulation of the GPX1 activity allows the mitochondrial-defective cells to survive oxidative stress and cisplatin treatment (Lu et al., 2012). In the auditory system, a previous study reported that a single nucleotide polymorphism in GPX1 might be associated with the vulnerability to noise-induced hearing loss (NIHL) among the Chinese Han population (Wen et al., 2014). Kil et al. (2007) have declared that GPX1 is the dominant isoform of GPXs family and is highly expressed in HCs, supporting cells, SGNs, stria vascularis, and spiral ligament in the rat cochlea. Additionally, the mice by knockout of GPX1 are more susceptible to NIHL compared with wild type mice (Ohlemiller et al., 2000; McFadden et al., 2001). Nevertheless, the effect of GPX1 on SGNs damage induced by oxidative stress remains unclear.

Ebselen [2-phenyl-1,2-benzoisoselenazol-3(2H)-one] is a synthetic organoselenium radical scavenger compound that has GPX-like activity, and it can directly increase GPX1 activity to mimic the effect of GPX1 overproduction. Generally, ebselen is capable of reducing oxidative stress levels in various cell types potentially through a variety of mechanisms. It has been demonstrated that ebselen possesses otoprotective activity and alleviated NIHL in rat *via* preventing the loss of outer HCs and reduces the acute swelling of the stria vascularis (Kil et al., 2007), it can also attenuate cisplatin-induced ROS generation through Nrf2 activation in auditory cells (Kim et al., 2009). Besides, a phase 2 clinical trial declared the safety and efficacy of ebselen for the prevention of NIHL in human (Kil et al., 2017). Here, we used ebselen, as a GPX1 mimic, and the *gpx1* knockout ($gpx1^{-/-}$) mice to investigate the role of GPX1 in SGNs treated with peroxynitrite.

In this study, we first identified the expression change of GPX1 in mouse cochlea SGNs through the *in vitro* peroxynitrite-damaged SGNs model, then we investigated the neuroprotective effect of GPX1 against peroxynitrite-induced SGN damage. Finally, we explored the possible underlying mechanism by which GPX1 was involved in protecting SGNs against peroxynitrite damage. Our findings demonstrated that GPX1 protected against peroxynitrite-induced SGNs damage by inhibiting oxidative stress and apoptosis, at least partially, through inhibiting the activation of nuclear factor-kappa B (NF-κ B) pathway.

MATERIALS AND METHODS

Experimental Animals and Genotyping

The C57BL/6 wide type (WT) mice were purchased from the Animal Center of Shandong University (Jinan, China). The *gpx1* knockout mice ($gpx1^{-/-}$) in the C57BL/6 background (KOCMP-14775-Gpx1-B6N-VA) were constructed by Cyagen Biosciences Inc. (Suzhou, China). The genotyping for $gpx1^{-/-}$ mice with PCR was performed according to the Cyagen Biosciences recommendations. The genotyping primers are listed in **Table 1**. All animal experiments were performed according to protocols approved by the Animal Care Committee of Shandong University (No. ECAESDUSM 20123011) and were consistent with the National Institute of Health's Guide for the Care and Use of Laboratory Animals.

TABLE 1 | PCR primer sequences used in the experiments.

Gene	Forward sequence	Reverse sequence
Gpx1-WT	TTACACAATATAAGGGAGCTGTGC	ATACCTGGTGTCCGAACTGATTG
Gpx1-Mut	TTACACAATATAAGGGAGCTGTGC	TTAAGGCACTGAGTAGCAGTGTG
Bax	CGTGGTTGCCCTCTTCTACT	TTGGATCCAGACAAGCAGCC
Bcl-2	TGACTTCTCTCGTCGCTACCG	GTGAAGGGCGTCAGGTGCAG
p53	GGTGCTGACGAAGAAGAGGA	AGCCCAACTGTGATGAAGCA
Bcl-xL	GGAGCTGGTGGTTGACTTTCT	CCGGAAGAGTTCATTCACTAc
Gapdh	AGGTCGGTGTGAACGGATTTG	TGTAGACCATGTAGTTGAGGTCA

Organotypic Culture of Neonatal Mouse Cochleae Spiral Ganglion Neurons and Drug Treatments

The C57BL/6 WT mice or *gpx1*$^{-/-}$ mice were decapitated at postnatal day (P) 3, and only the middle turn segments of mouse cochleae were collected and cultured for all experiments to keep sampling consistence between groups. The tissue dissection procedure was carried out as described in our previous report (Wang et al., 2019; Liu et al., 2021). Briefly, after cutting off the temporal bones of two sides and removing the cochlear capsule and stria vascularis, the middle turn cochlear explants containing SGNs were then adhered onto 10 mm glass coverslips (Fisher Scientific, PA) pre-coated with CellTak (Corning, 354241). Isolated SGNs explants were cultured in Dulbecco's Modified Eagle Medium/F12 (DMEM/F12, Gibco, 11330032) supplemented with 10% fetal bovine serum (FBS, Gibco, 10099133C) and ampicillin (50 mg/ml, Sigma, A5354) overnight at 37°C in a 5% CO_2 atmosphere.

On the following day, samples were changed into fresh culture media containing peroxynitrite (Cayman, 81565) alone for 24 or 48 h, or with the following drugs for 48 h as indicated in the text: ebselen (30 μM, Sigma-Aldrich, E3520); NAC (2 mM, Sigma-Aldrich, A7250); BAY 11-7082 (10 μM, Med Chem Express, HY-13453). After incubation, samples were used in the immunostaining or other assays.

Cryosection

Cochleae from P3, P14, and P30 C57BL/6 WT mice were dissected out and fixed with 4% paraformaldehyde (PFA) in PBS at 4°C overnight. Tissues were then incubated in 10, 20, and 30% sucrose in 1 × PBS, embedded in OCT compound (Tissue-Tek, Sakura Finetek, 4583), snap frozen on dry ice, and then stored frozen at −80°C. Frozen sections were cut into 7 μm using a cryostat (Leica CM 1850; Leica, Germany).

Immunostaining

After organotypic culture or cryosection, the cochlear explants or tissue sections were fixed with 4% PFA, permeabilized with 1% TritonX-100 in PBS, and blocked by incubation in PBT-1 solution (0.1% Triton X-100, 8% donkey serum, 1% bovine serum albumin, and 0.02% sodium azide in PBS) at room temperature for 1 h. The samples were then incubated with the following primary antibodies: anti-Tuj 1 (1:1,000 dilution; Neuromics, MO15013), anti-GPX1 (1:500 dilution, GeneTex, GTX116040), anti-C-caspase 3 (1:400 dilution, Cell Signaling Technology, 9664), anti-NeuN (1:500, Cell Signaling Technology,12943), anti-4-HNE (1:500 dilution, Abcam, ab48506, United States), or anti-NF-κB p65 (1:500 dilution, Cell Signaling Technology, 6956) diluted in the blocking solution at 4°C overnight. The next day, samples were incubated with FITC-conjugated, TRITC-conjugated, or Cy5-conjugated (1:1000, Invitrogen, United States) secondary antibody along with 4′,6-diamidino-2-phenylindole (DAPI) (1:1000, Sigma-Aldrich, United States) at room temperature for 1 h. Then, coverslips were mounted and the samples were observed under a laser scanning confocal microscope (Leica SP8; Leica, Germany).

Western Blot

After the drug treatment, the proteins from the cultured SGNs were extracted with radioimmunoprecipitation assay buffer (RIPA) buffer (Protein Biotechnology, China). The mixture was centrifuged at 4°C and 12,000 × *g* in a refrigerated centrifuge and the supernatant was collected. A total of 30 μg of each protein sample was denatured and separated by 12% sodium dodecyl sulfate–polyacrylamide gel electrophoresis (SDS-PAGE) gels. The primary antibodies were anti-GPX1 (1:1,000 dilution, GeneTex, GTX116040), anti-C-caspase 3 (1:500 dilution, Cell Signaling Technology, 9664), anti-4-HNE (1:1000, Abcam, ab46545), anti-phosphorylated (p)-NFκB p65 (1:1,000 dilution, Cell Signaling Technology, 3033), and anti-β-actin (1:2,000 dilution, ZSGB-BIO, TA-09). The protein signals were detected using an ECL kit (Millipore, United States) and analyzed by Image J software. The relative optical density ratio was calculated by comparison to β -actin.

Real Time-Polymerase Chain Reaction

After drug treatment for 48 h, total RNA of different groups was isolated from middle turn cochlear explants using TRIzol reagent (Life Technologies, 15596026) following manufacturer's instructions. The cDNA was synthesized from each RNA sample by reverse transcription using the Revert Aid First Strand cDNA Synthesis Kit (Thermo Fisher Scientific, K1622). A SYBR Premix Ex Taq (TaKaRa Bio, RR420A) was used to quantify the mRNA levels of related genes. *Gapdh* was amplified as the housekeeping gene. All data were analyzed using an Eppendorf Realplex 2 and the relative expression levels were calculated using the $2^{-\Delta\ \Delta\ CT}$ method. PCR primers for the genes were listed in **Table 1**.

Spiral Ganglion Neuron Counting

The counting of SGNs was performed according to our previous researches (Wang et al., 2019; Liu et al., 2021). Briefly, SGNs were immunolabeled with the Tuj 1 antibody that specifically labels both SGN bodies and neurites. The images of cultured middle turn cochlear explants were taken using a Leica confocal fluorescence microscope. Spiral ganglion neurons in which the nucleus comprised 40% of the soma area were counted using the Image J software and the total number of SGNs in each spiral

ganglion explant was obtained by adding the SGN counts in all consecutive sections. The density of SGNs was then calculated per unit area (0.01 mm^2).

Statistical Analysis

All experiments were repeated at least three times and the data were presented as mean ± SEM. Two-tailed, unpaired Student's *t*-tests were used to determine statistical significance in comparisons between two groups. When comparing more than two groups, data were statistically analyzed by one-way ANOVA followed by a Dunnett multiple comparisons test. A value of $p < 0.05$ was considered to indicate a statistically significant result. Scale bars and *n* values are defined in the respective figures and legends and *n* represents the number of independent cochlear samples from each sub-group.

RESULTS

Glutathione Peroxidase 1 Expression Is Decreased in Spiral Ganglion Neurons After Peroxynitrite Injury

First, we characterized the expression of GPX1 in postnatal cochlear SGNs with mice at different ages. Immunofluorescence staining was performed on the frozen cochlear cryosections of P3, P14, and P30 C57BL/6 mouse cochleae (**Figure 1A**), and Tuj 1, a neuron-specific marker which specifically labels both the cytoplasm and neurite of SGN, was used to mark SGN. As the expression pattern of GPX1 was the same in all three turns of cochlea SGNs, the middle turn was presented as the representative sample in **Figure 1B**. The results showed that robust GPX1 labeling was observed in cochlear SGNs of P3, P14, and P30 mice, and it appeared that the expression of GPX1 was mainly in the cytoplasm but not in the nuclei of SGNs (**Figure 1B**).

Next, to determine the neurotoxic effect of peroxynitrite on cultured SGNs, the cultured SGNs were treated with different concentrations (100 or 200 μM) of peroxynitrite for 24 or 48 h, respectively (**Figure 2A**). As shown in **Figure 2B**, after the administration of peroxynitrite, the SGN morphology was disrupted and pyknotic, cells arrangement was disordered, nerve fibers were disordered, broken, or lost. Quantitative analysis showed that the numbers of survived SGNs were reduced significantly in peroxynitrite-treated groups in a dose- and time-dependent manner compared with the control group (**Figure 2B**), that is, the higher concentration of peroxynitrite and the longer processing time induced more SGNs loss. In detail, treatment with 100 μM peroxynitrite for 24 h induced minor SGN loss (75.4 ± 2.49% SGNs survived after treatment) and the higher concentration of 200 μM peroxynitrite treatment for 48 h caused approximately only 32.7 ± 1.84% SGNs survival compared with controls. The treatment of 100 μM peroxynitrite exposure for 48 h resulted in an obvious but moderate SGN loss, as there were 59.3 ± 3.71% SGNs left compared with the control group (**Figure 2B**), and it was selected as the peroxynitrite treatment condition for all subsequent experiments.

Then, the expression change of GPX1 in SGNs was analyzed after peroxynitrite damage. The cultured SGNs were exposed to 100 μM peroxynitrite for 48 h (**Figure 2C**) and immunostaining illustrated that the fluorescence intensity of GPX1 in the peroxynitrite group was significantly reduced compared with that of the control group (**Figure 2D**). Western blot showed that the protein level of GPX1 was significantly decreased in peroxynitrite group compared with the control group (**Figure 2E**). Together, these results indicated that the administration of peroxynitrite caused a reduced expression of GPX1 in cochlear SGNs, thus suggesting that GPX1 might play a role in peroxynitrite-induced SGN damage.

Glutathione Peroxidase 1 Promotes the Survival of Spiral Ganglion Neurons After Peroxynitrite Damage

To clarify the role of GPX1 in the process of SGN injury caused by peroxynitrite, we performed experiments by increasing or inhibiting the expression of GPX1 in SGNs with the GPX1 mimic ebselen or using the $gpx1^{-/-}$ mouse model. Immunofluorescence staining and western blot results verified that GPX1 expression was absent in the cochlear SGNs of $gpx1^{-/-}$ mice (**Supplementary Figures 1A,C**), and there was no significant difference in SGNs number between the $gpx1^{-/-}$ mice and WT mice (**Supplementary Figure 1B**), which indicated that the absence of GPX1 in normal SGNs would not affect the survival of SGNs. Next, we examined the effect of regulating GPX1 expression by ebselen or GPX1 deficiency on peroxynitrite-induced SGNs loss. The cultured SGNs from P3 WT mice were incubated with 100 μM peroxynitrite for 48 h with or without the pretreatment of 30 μM ebselen for 1 h, or the SGNs from $gpx1^{-/-}$ mice were cultured and exposed to 100 μM peroxynitrite for 48 h. The dose of ebselen was chosen according to our published study (Liu et al., 2021), which shows that 30 μM ebselen treatment protects against cisplatin-induced oxidative stress in SGNs. As illustrated in **Figure 3**, the protein expressions of GPX1 were significantly increased in peroxynitrite + ebselen group compared with the peroxynitrite-only group, while it was absent in the peroxynitrite + $gpx1^{-/-}$ group (**Figures 3A–C**). Immunostaining and cell counting results showed that the number of surviving SGNs was significantly increased after the pretreatment with ebselen compared with the peroxynitrite-only group, while remarkably less survived SGNs were detected in $gpx1^{-/-}$ mice group compared with WT mice after peroxynitrite treatment (**Figures 3D,E**). These results suggested that the upregulation of GPX1 promotes, while the deficiency of GPX1 suppresses, the survival of SGNs after peroxynitrite injury.

Glutathione Peroxidase 1 Inhibits Apoptosis of Spiral Ganglion Neurons After Peroxynitrite Injury

The role of GPX1 in regulating the peroxynitrite-induced apoptosis of cochlear SGNs was investigated by immunostaining and western blot. After the drug treatment (**Figure 4A**), cleaved-Caspase3 (C-CASP3) immunostaining results showed that

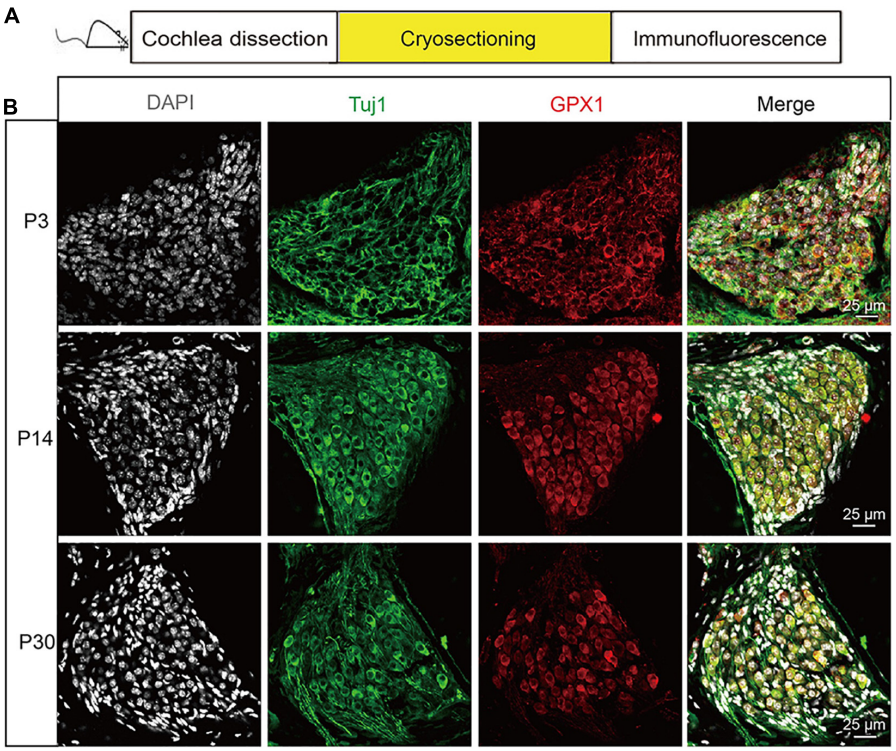

FIGURE 1 | The expression of GPX1 in postnatal cochlear spiral ganglion neurons (SGNs) with mice at different ages. **(A)** Immunofluorescence staining was performed on the frozen cochlear cryosection of P3, P14, and P30 C57BL/6 mouse cochlea. **(B)** Immunostaining images of the middle turn cochlea showed that robust GPX1 labeling was observed in cochlear SGNs of P3, P14, and P30 mice, and it appeared that the expression of GPX1 was mainly in the cytoplasm but not in the nuclei of SGNs. Scale bar = 25 μm.

distinct C-CASP3-positive SGNs were observed in peroxynitrite group, but not in the control group. The number of C-CASP3-positive SGNs was downregulated in the presence of ebselen, while it was further increased in *gpx1*$^{-/-}$ mice compared with the peroxynitrite-only group (**Figure 4B**). Western blot analysis of C-CASP3 protein was consistent with the above results, i.e., the expression level of C-CASP3 was significantly reduced in the peroxynitrite + ebselen group, while it was significantly increased in the peroxynitrite + *gpx1*$^{-/-}$ group compared with the peroxynitrite-only group (**Figure 4C**). Therefore, these results revealed that the Caspase 3-mediated apoptosis was inhibited by ebselen and was aggravated by the lack of GPX1 in SGNs after peroxynitrite injury.

Glutathione Peroxidase 1 Attenuates Peroxynitrite-Induced Oxidative Stress in Spiral Ganglion Neurons

Glutathione peroxidase 1 is known as a major intracellular peroxide-scavenging enzyme to eliminate the damage of ROS to cells, proteins, and liposomes through the reduction of glutathione. In this study, we also investigated the relationship between GPX1 and ROS generation in peroxynitrite damaged SGNs. The cultured SGN explants from WT or *gpx1*$^{-/-}$ mice were exposed to peroxynitrite with or without ebselen pretreatment, and the expression changes of 4-HNE were examined to evaluate the oxidative stress level in SGNs (**Figure 5A**). The results of immunostaining and western blot showed that an obvious increased protein expression of 4-HNE was found in peroxynitrite treated SGNs, while it was significantly decreased in peroxynitrite + ebselen group but further increased in peroxynitrite + *gpx1*$^{-/-}$ mice compared with the peroxynitrite-only group (**Figures 5B,C**).

Antioxidant Treatment Rescues the Aggravated Spiral Ganglion Neurons Loss and Apoptosis Induced by Glutathione Peroxidase 1 Deficiency After Peroxynitrite Injury

To explore whether GPX1 plays a protective role in peroxynitrite-induced SGNs damage by reducing intracellular ROS, we conducted a rescue experiment by using the antioxidant N-acetylcysteine (NAC). The cultured SGN explants from WT or *gpx1*$^{-/-}$ mice were treated with peroxynitrite and 2 mM NAC for 48 h (**Figures 6A**, **7A**). The dose of NAC was chosen according to our published studies (Liu et al., 2019b, 2021), which show that 2 mM NAC treatment successfully rescues the SGN loss from cisplatin damage. Immunostaining results illustrated that the immunofluorescence of 4-HNE was weaker in the peroxynitrite + NAC group compared

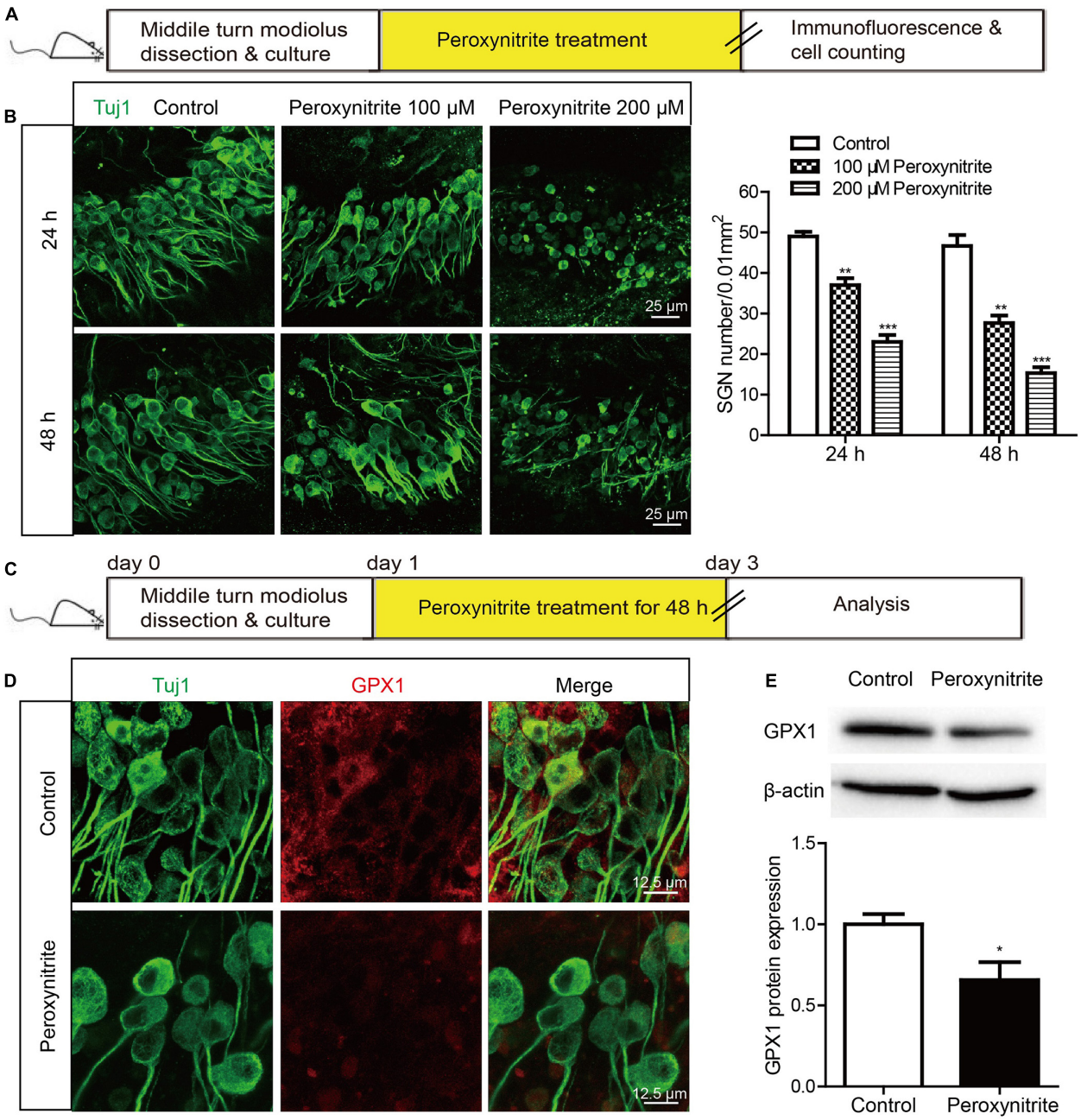

FIGURE 2 | The expression of GPX1 is decreased in cochlear SGNs after peroxynitrite injury. **(A)** The cultured SGNs from WT C57BL/6 mice were treated with different concentrations (100 or 200 μM) of peroxynitrite for 24 or 48 h, respectively. **(B)** Immunostaining images showed that the SGN morphology was disrupted, cells arrangement was disordered, and nerve fibers were disordered or lost after peroxynitrite administration. Quantitative analysis verified that the numbers of survived SGNs were reduced significantly in peroxynitrite-treated groups in a dose- and time-dependent manner compared with the control group. Scale bar = 25 μm. **(C)** The cultured SGNs were exposed to 100 μM peroxynitrite for 48 h. **(D)** Immunostaining illustrated that the fluorescence intensity of GPX1 in peroxynitrite group was significantly reduced compared with control group. Scale bar = 12.5 μm. **(E)** Western blot showed that the protein level of GPX1 was significantly decreased in peroxynitrite group compared with the control group. $^{*}p < 0.05$, $^{**}p < 0.01$, and $^{***}p < 0.001$, $n = 3$ for each group.

with the peroxynitrite-only group, and it was also lower in the peroxynitrite + *gpx1*$^{-/-}$ + NAC group compared with the peroxynitrite + *gpx1*$^{-/-}$ group (**Figure 6B**). Western blot and statistical analysis of the protein expression level of 4-HNE were consistent with the immunostaining results (**Figure 6C**). Correspondingly, we found that the NAC treatment largely increased the number of surviving SGNs in the peroxynitrite + NAC group compared with the peroxynitrite-only group, as well as in the peroxynitrite + *gpx1*$^{-/-}$ + NAC group compared with the peroxynitrite + *gpx1*$^{-/-}$ group (**Figure 6D**).

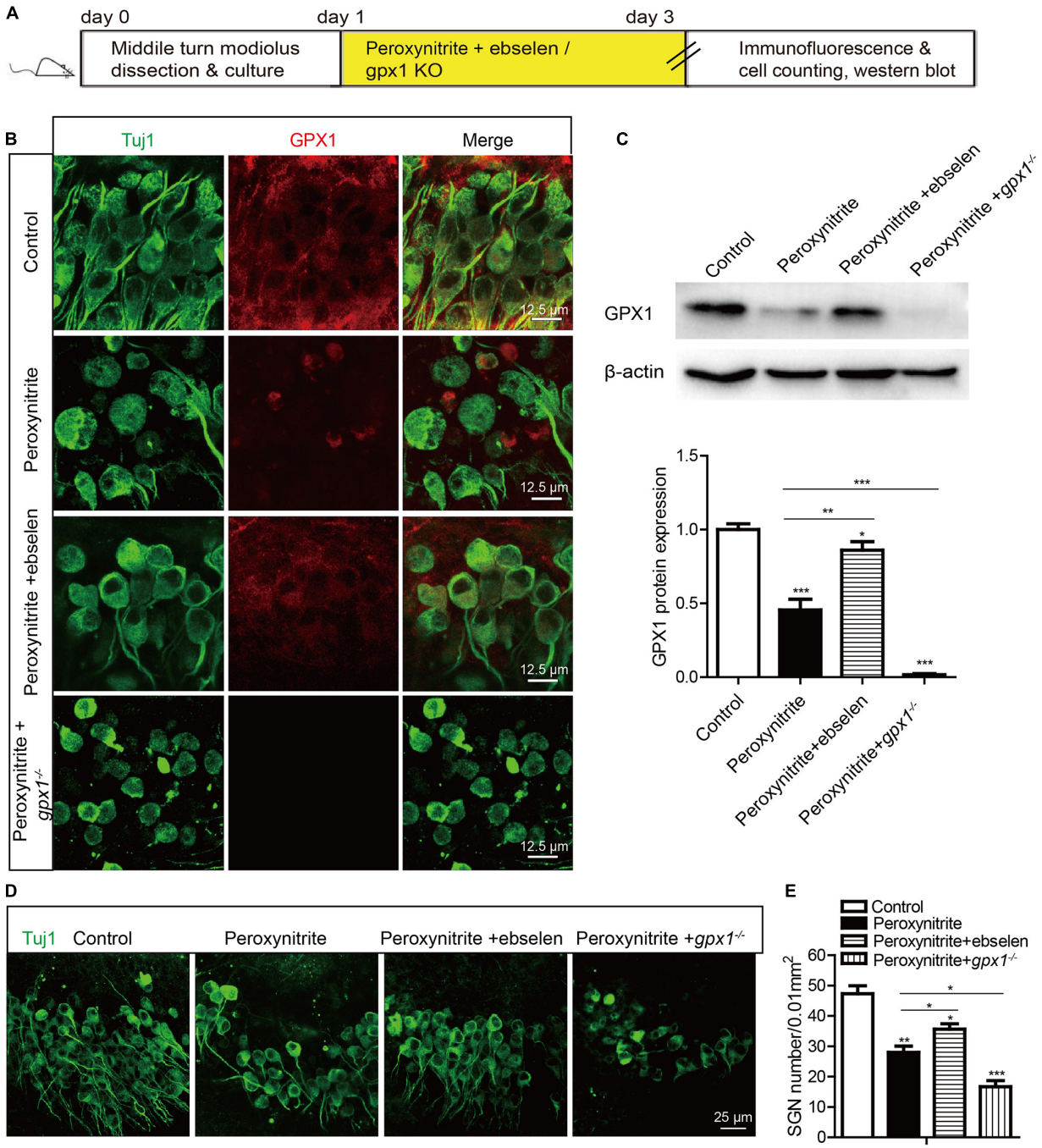

FIGURE 3 | Glutathione peroxidase promotes the survival of SGNs after peroxynitrite damage. The cultured SGNs from P3 WT mice were incubated with 100 μM peroxynitrite for 48 h with or without pretreatment of 30 μM ebselen for 1 h, or the SGNs from *gpx1*$^{-/-}$ mice were cultured and exposed to 100 μM peroxynitrite for 48 h. **(A–C)** Immunofluorescence staining and western blot results showed that the protein expressions of GPX1 were significantly increased in peroxynitrite + ebselen group compared with the peroxynitrite-only group, while it was absent in the peroxynitrite + *gpx1*$^{-/-}$ group. Scale bar = 12.5 μm. **(D,E)** Immunostaining and cell counting showed that the number of surviving SGNs was significantly increased after pretreatment with ebselen compared with the peroxynitrite-only group, while remarkably less survived SGNs were detected in *gpx1*$^{-/-}$ mice group compared with WT mice after peroxynitrite treatment. Scale bar = 25 μm. *$p < 0.05$, **$p < 0.01$, ***$p < 0.001$, and $n = 3$ for each group.

Furthermore, the apoptosis of SGNs detected by C-CASP3 immunostaining and western blot showed that there was much less C-CASP3-positive SGNs and remarkable reduction of the C-CASP3 protein levels in the NAC co-treated groups compared with the peroxynitrite-only groups, and it was also lower in the peroxynitrite + *gpx1*$^{-/-}$ + NAC group compared

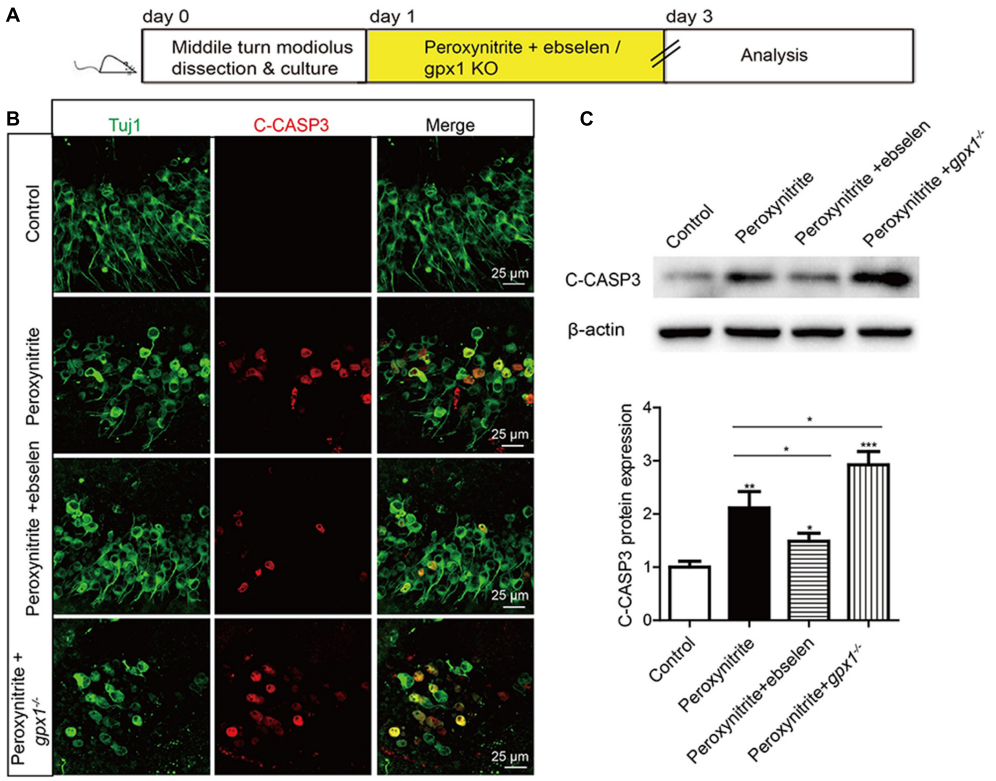

FIGURE 4 | Glutathione peroxidase inhibits the apoptosis of SGNs after peroxynitrite injury. **(A)** The cultured SGNs from P3 WT mice were incubated with 100 μM peroxynitrite for 48 h with or without the pretreatment of 30 μM ebselen for 1 h, or the SGNs from *gpx1*$^{-/-}$ mice were cultured and exposed to 100 μM peroxynitrite for 48 h. **(B)** Immunostaining results showed that distinct C-CASP3-positive SGNs were observed in the peroxynitrite group, but not in the control group. The number of C-CASP3-positive SGNs was downregulated in the presence of ebselen, while it was further increased in *gpx1*$^{-/-}$ mice compared with the peroxynitrite-only group. Scale bar = 25 μm. **(C)** The western blot analysis of C-CASP3 protein verified that the expression level of C-CASP3 was significantly reduced in the peroxynitrite + ebselen group, while it was significantly increased in the peroxynitrite + *gpx1*$^{-/-}$ group compared with the peroxynitrite-only group. $^{*}p < 0.05$, $^{**}p < 0.01$, and $^{***}p < 0.001$, $n = 3$ for each group.

with the peroxynitrite + *gpx1*$^{-/-}$ group (**Figures 7B,C**). Collectively, these findings suggest that the antioxidant NAC treatment successfully rescued the exacerbated ROS generation, SGNs loss, and apoptosis caused by GPX1-deficiency after peroxynitrite damage.

Glutathione Peroxidase 1 Inhibits the NF-κB Pathway to Protect Against Peroxynitrite-Induced Spiral Ganglion Neurons Damage

The transcription factor NF-κB plays a vital role in cellular death and survival under oxidative stress conditions (Li and Karin, 1999), and the activation of NF-κB can promote cell death (Schneider et al., 1999; Zhang et al., 2005). Recently, the correlation between GPX1 and NF-κB pathway has been declared (Koeberle et al., 2020; Sharma et al., 2021b). Therefore, to identify the role of NF-κB and the regulative mechanism between GPX1 and NF-κB in SGNs damage induced by peroxynitrite, we measured the NF-κB pathway in SGNs after peroxynitrite administration with GPX1 upregulation or deficiency (**Figure 8A**). As illustrated in **Figure 8B**, the anti-NeuN antibody was used to label the nucleus of SGN and the fluorescence of NF-κB p65 was mainly detected in the cytoplasm of SGNs in control group (**Figure 8B**). Peroxynitrite induced obvious nuclear distribution of NF-κB p65 in SGNs and pretreatment with ebselen significantly reduced it, whereas the lack of GPX1 intensified the nuclear fluorescence of NF-κB p65 in SGNs of peroxynitrite + *gpx1*$^{-/-}$ group (**Figure 8B**). Furthermore, we found that the expression of the p-NF-κB p65 protein was upregulated in peroxynitrite-exposed SGNs compared with the untreated controls, and the pretreatment with ebselen significantly reduced it while the lack of GPX1 increased it (**Figure 8C**). Besides, to further confirm peroxynitrite-mediated activation of the NF-κB pathway, we also measured the mRNA expression levels of known NF-κB p65 target genes *Bax*, *P53*, *Bcl2*, and *Bcl-xL*. Real time-PCR (RT-PCR) results revealed that peroxynitrite treatment caused significant increases in the mRNA expression of proapoptotic genes *Bax* and *P53*, and decreases in the mRNA expression of antiapoptotic genes *Bcl2* and *Bcl-xL* compared with controls (**Figure 8D**). In addition, the lower mRNA expression levels of *Bax* and *P53* and the higher expression levels of *Bcl2* and *Bcl-xL* were detected in the

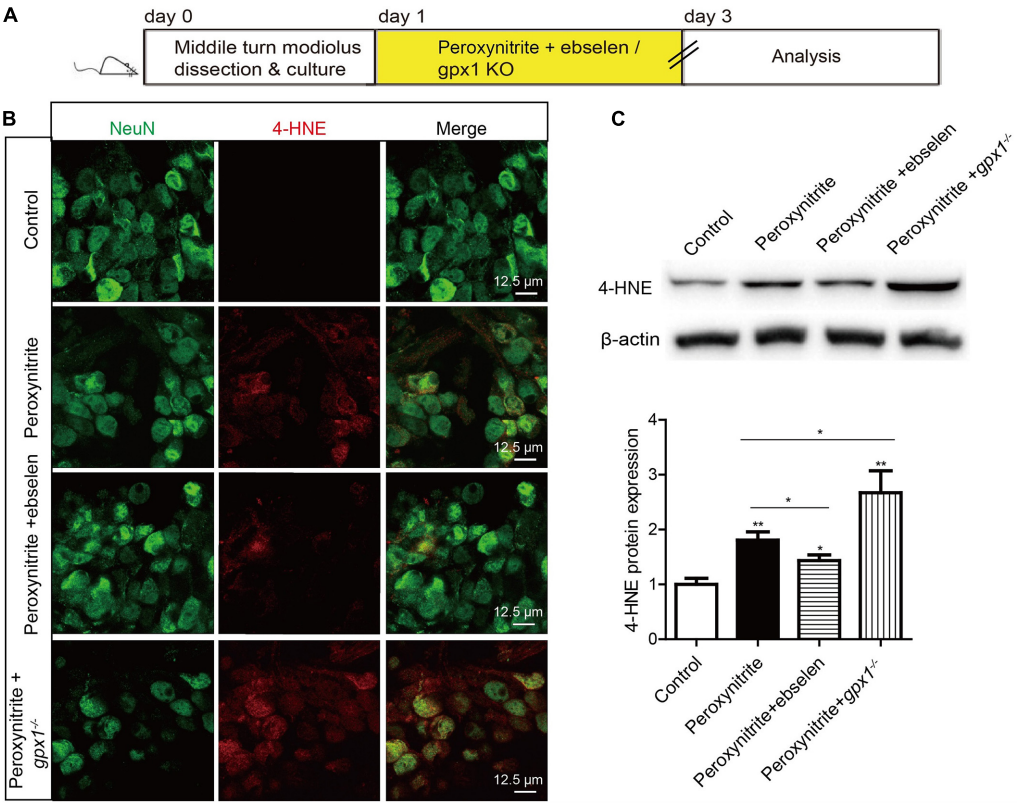

FIGURE 5 | Glutathione peroxidase attenuates peroxynitrite-induced oxidative stress in SGNs. **(A)** The cultured SGNs from P3 WT mice were incubated with 100 μM peroxynitrite for 48 h with or without the pretreatment of 30 μM ebselen for 1 h, or the SGNs from *gpx1*$^{-/-}$ mice were exposed to 100 μM peroxynitrite for 48 h. **(B,C)** Immunostaining and western blot results showed that obvious increased protein expression of 4-HNE was found in peroxynitrite treated SGNs, while it was significantly decreased in the peroxynitrite + ebselen group but further increased in the peroxynitrite + *gpx1*$^{-/-}$ mice compared with the peroxynitrite-only group. Scale bar = 12.5 μm. *$p < 0.05$, and **$p < 0.01$, $n = 3$ for each group.

peroxynitrite + ebselen group compared with the peroxynitrite-only group, while the lack of GPX1 in SGNs from *gpx1*$^{-/-}$ mice led to an opposite pattern (**Figure 8D**). These data, taken together, suggest that the NF-κB pathway is activated in SGNs after peroxynitrite treatment and GPX1 can partially block the nuclear translocation of NF-κB/p65 and inhibit the activation of the NF-κ B signaling.

Next, we used a highly potent NF-κB inhibitor, BAY 11-7082, to further verify the role of NF-κB pathway in SGNs damage induced by peroxynitrite (**Figure 9**). The cultured SGN explants from WT or *gpx1*$^{-/-}$ mice were treated with peroxynitrite and 10 μM BAY 11-7082 for 48 h. The dose of BAY11-7082 was chosen based on our preliminary results of dose response, which showed that 10 μM BAY11-7082 significantly increased the number of surviving SGNs after cisplatin damage *in vitro* (**Supplementary Figure 2**). Our results showed that 10 μM BAY 11-7082 effectively inhibited the nuclear translocation of NF-κB p65 and the mRNA expression of *Bax* and *P53*, but increased the mRNA expression of *Bcl2* and *Bcl-xL* in the peroxynitrite + BAY 11-7082 group compared with the peroxynitrite-only group, as well as in the peroxynitrite + *gpx1*$^{-/-}$ + BAY 11-7082 group compared with the peroxynitrite + *gpx1*$^{-/-}$ group (**Figures 9A–C**). Correspondingly, the inhibition of NF-κB by BAY 11-7082 significantly increased the survived SGN numbers, while decreased the C-CASP3 positive SGN numbers and the C-CASP3 expression in peroxynitrite + BAY 11-7082 group compared with the peroxynitrite group (**Figures 9D–F**). More importantly, BAY 11-7082 treatment also rescued the aggravated SGN loss and apoptosis induced by the deficiency of GPX1 after peroxynitrite injury, as the number of SGNs was added, whereas the C-CASP3 expression was reduced in the peroxynitrite + *gpx1*$^{-/-}$ + BAY 11-7082 group vs. the peroxynitrite + *gpx1*$^{-/-}$ group (**Figures 9D–F**). Therefore, these results indicate that the inhibition of NF-κB pathway contributes to promote SGNs survived from peroxynitrite injury, and that GPX1 protects SGNs against peroxynitrite-induced damage, at least in part, *via* blocking the NF-κB pathway activation.

DISCUSSION

Glutathione peroxidase is a crucial antioxidant enzyme that participate in restraining the harmful accumulation of intracellular hydrogen peroxide and is more effective than catalase at eliminating intracellular peroxides under various physiological conditions (Antunes et al., 2002; Lubos et al., 2011).

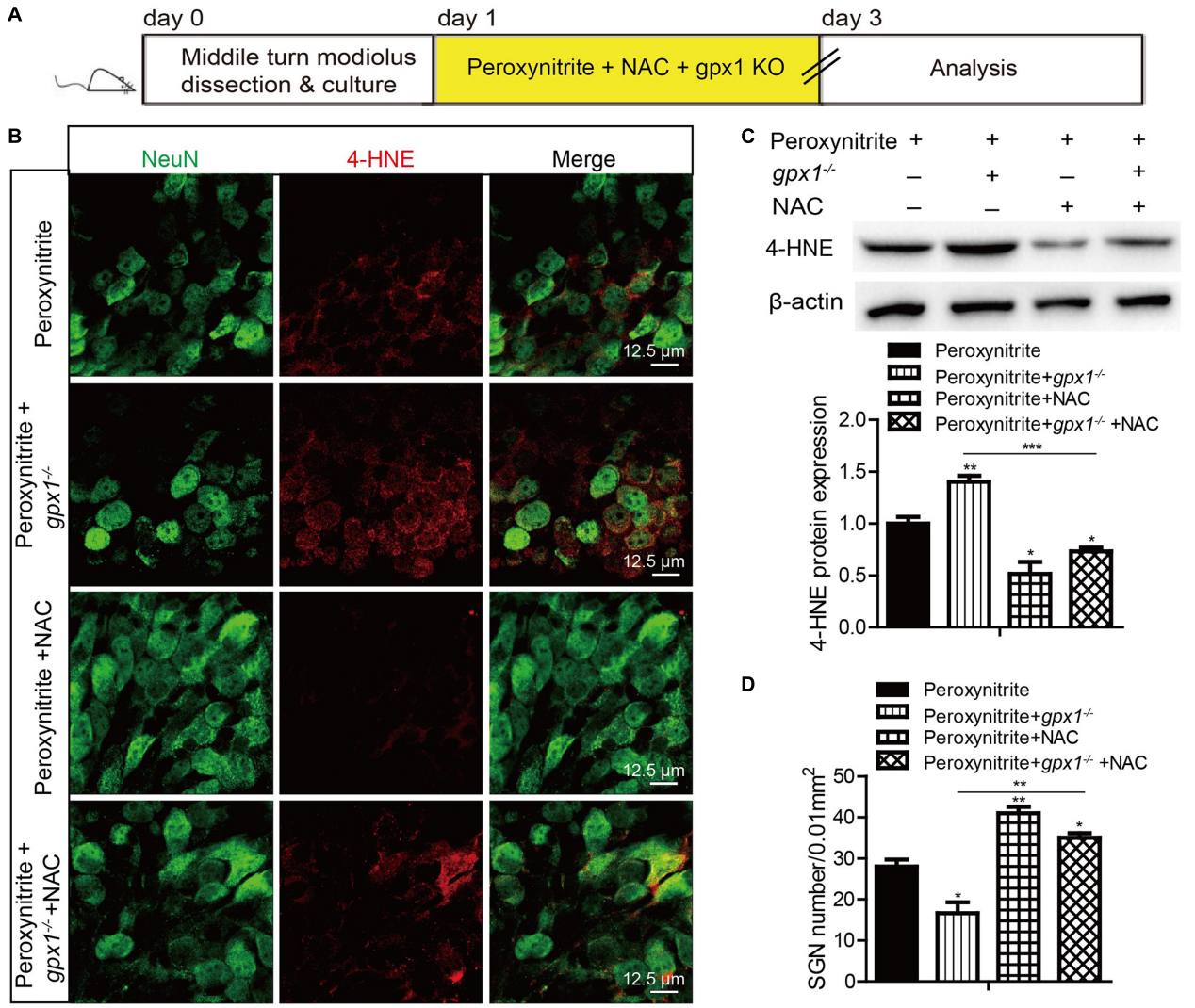

FIGURE 6 | Antioxidant treatment rescues the aggravated SGNs loss and ROS accumulation induced by GPX1 deficiency after peroxynitrite injury. **(A)** The cultured SGNs from WT or *gpx1*$^{-/-}$ mice were treated with peroxynitrite and 2 mM NAC for 48 h. **(B,C)** Immunostaining results illustrated that the immunofluorescence of 4-HNE was weaker in the peroxynitrite + NAC group compared with the peroxynitrite-only group, and it was also lower in the peroxynitrite + *gpx1*$^{-/-}$ + NAC group compared with the peroxynitrite + *gpx1*$^{-/-}$ group. Western blot results verified that the protein expression level of 4-HNE was consistent with the immunostaining results. Scale bar = 12.5 μm. **(D)** Cell counting and statistical analysis showed that the NAC treatment largely increased the number of surviving SGNs in the peroxynitrite + N-acetylcysteine (NAC) group compared with the peroxynitrite-only group, as well as in the peroxynitrite + *gpx1*$^{-/-}$ + NAC group compared with the peroxynitrite + *gpx1*$^{-/-}$ group. $^{*}p < 0.05$, $^{**}p < 0.01$, and $^{***}p < 0.001$, $n = 3$ for each group.

Here, for the first time, we reported that the expression of GPX1, which was observed robustly distributed in SGNs cytoplasm, was significantly reduced after peroxynitrite damage. Our finding is consistent with previous studies indicated that a decrease of GPX1 activity was found in mouse cochlea HCs and stria vascular after noise induced hearing loss (McFadden et al., 2001; Kil et al., 2007), and suggested that the antioxidant enzyme GPX1 might play a role in the oxidative injury of SGNs induced by peroxynitrite.

In the present study, the role of GPX1 in SGNs treated with peroxynitrite was explored *via* ebselen and GPX1 deficient mice. Ebselen was found to increase the expression of GPX1 in SGNs after peroxynitrite damage, which is consistent with the reports that ebselen can increase the expression of GPX1 in cochlea after electrical stimulation (Liang et al., 2019) and in stria vascularis after noise exposure (Kil et al., 2007). Ebselen effectively promotes SGN survival and prevents SGN apoptosis after peroxynitrite injury by reducing SGNs oxidative stress, while the absence of GPX1 in *gpx1*$^{-/-}$ mice leads to the aggravated SGN injury (cell loss and apoptosis) induced by peroxynitrite, although it might cause no effect on SGN development as SGNs presented normal morphology and cell number in *gpx1*-deficient mice. These results suggest a neuroprotective effect of GPX1 against the peroxynitrite-induced SGN damage. It is

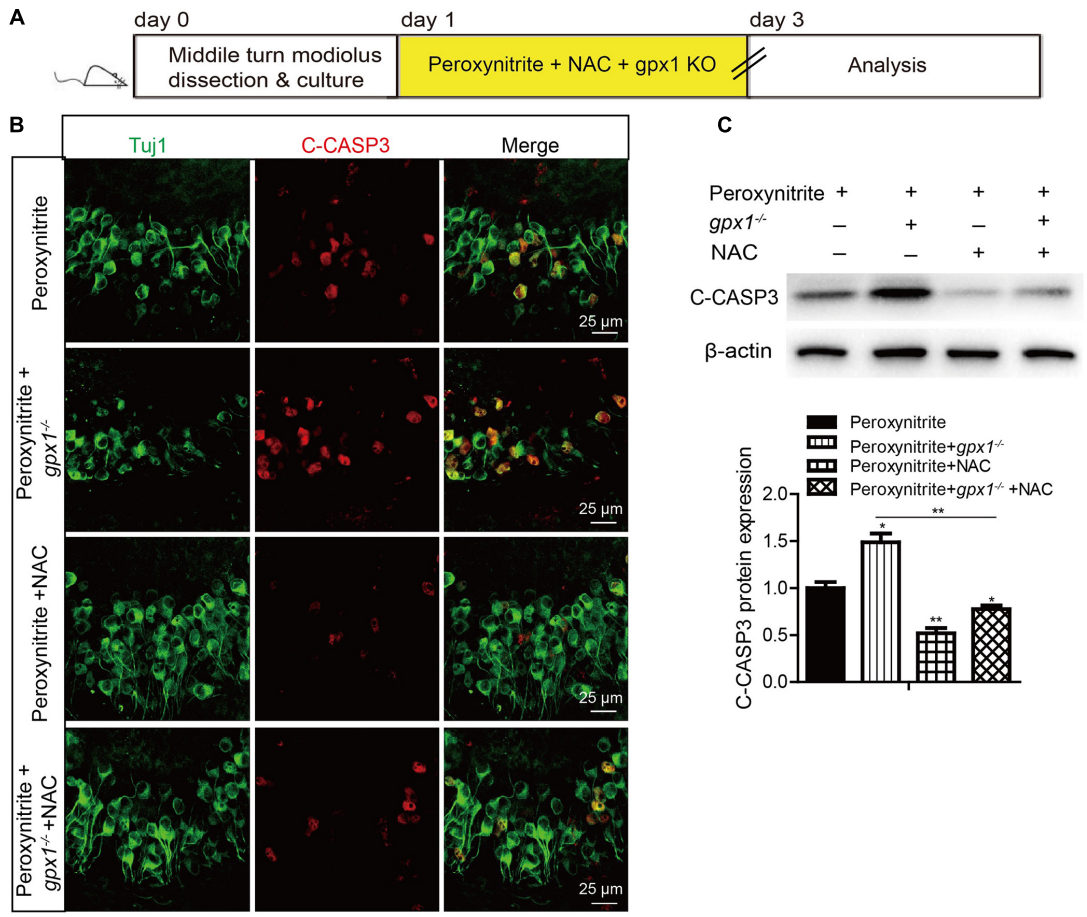

FIGURE 7 | N-acetylcysteine treatment reduced the apoptosis of SGNs in the lacking of GPX1 expression after peroxynitrite injury. **(A)** The cultured SGNs from WT or *gpx1*$^{-/-}$ mice were treated with peroxynitrite and 2 mM NAC for 48 h. **(B)** Immunostaining results illustrated that there was much less C-CASP3-positive SGNs in the peroxynitrite + NAC group compared with the peroxynitrite-only group, as well as in the peroxynitrite + *gpx1*$^{-/-}$ + NAC group compared with the peroxynitrite + *gpx1*$^{-/-}$ group. Scale bar = 12.5 μm. **(C)** Western blot results verified that the protein expression level of C-CASP3 was weaker in the peroxynitrite + NAC group compared with the peroxynitrite-only group, and it was also lower in the peroxynitrite + *gpx1*$^{-/-}$ + NAC group compared with the peroxynitrite + *gpx1*$^{-/-}$ group. *$p < 0.05$, and **$p < 0.01$, $n = 3$ for each group.

important to note that ebselen mimics the activities of all the selenium-dependent mammalian GPXs, not only to GPX1, and has other effects on redox status. Thus, its protective effects overlap those of GPX1. Other types of GPXs have been shown to be expressed in the cochlea, for instance, GPX2 protein is greatly increased in chicken utricle HC expression during HC differentiation (Zhu et al., 2019) and cisplatin injury leads to the decreased GPX2 expression in HEI-OC1 cells (Youn et al., 2017; Jo et al., 2019). It has been reported that GPX3 and GPX4 labeling are absent in the spiral ganglia, while GPX1 is the major isoform of GPXs family that highly expressed in cochlear SGNs in adult rat (Kil et al., 2007). In this study, we also examined the expression of GPX2 and GPX4 in mouse SGNs, and relative low expressions of GPX2 and GPX4 were found in mouse SGNs (**Supplementary Figure 3**). Moreover, ebselen increased the expression of GPX2 and GPX4 in SGNs after peroxynitrite injury (**Supplementary Figure 3**), which is consistent with previous studies that ebselen can increase the expression of GPX2 or GPX4 in rat stomach (Kumar et al., 2010), gastric cancer cells (Xu et al., 2018), or cochlea (Liang et al., 2019). GPX2 and GPX4 serve a distinct function in antioxidant and cellular protection in some tissues that complements that of GPX1 and experimental evidence hints that the expression of GPX2 and GPX4 is less sensitive to variations in selenium levels compared with GPX1 (Lubos et al., 2011). However, to date, studies about the specific function of GPX2 or GPX4 in SGN are still lacking. Our preliminary data suggest that they might also play a part in SGNs against oxidative stress, which is worthy to be investigated in future studies.

With regard to how GPX1 influences the apoptotic outcome, the pieces of evidence indicate that GPX1 may influence several steps in apoptotic cascades *via* regulating oxidant accumulation. For example, one study revealed that an overexpression of GPX1 inhibited the nucleus-translocation of apoptosis-inducing factor (AIF) from mitochondria in

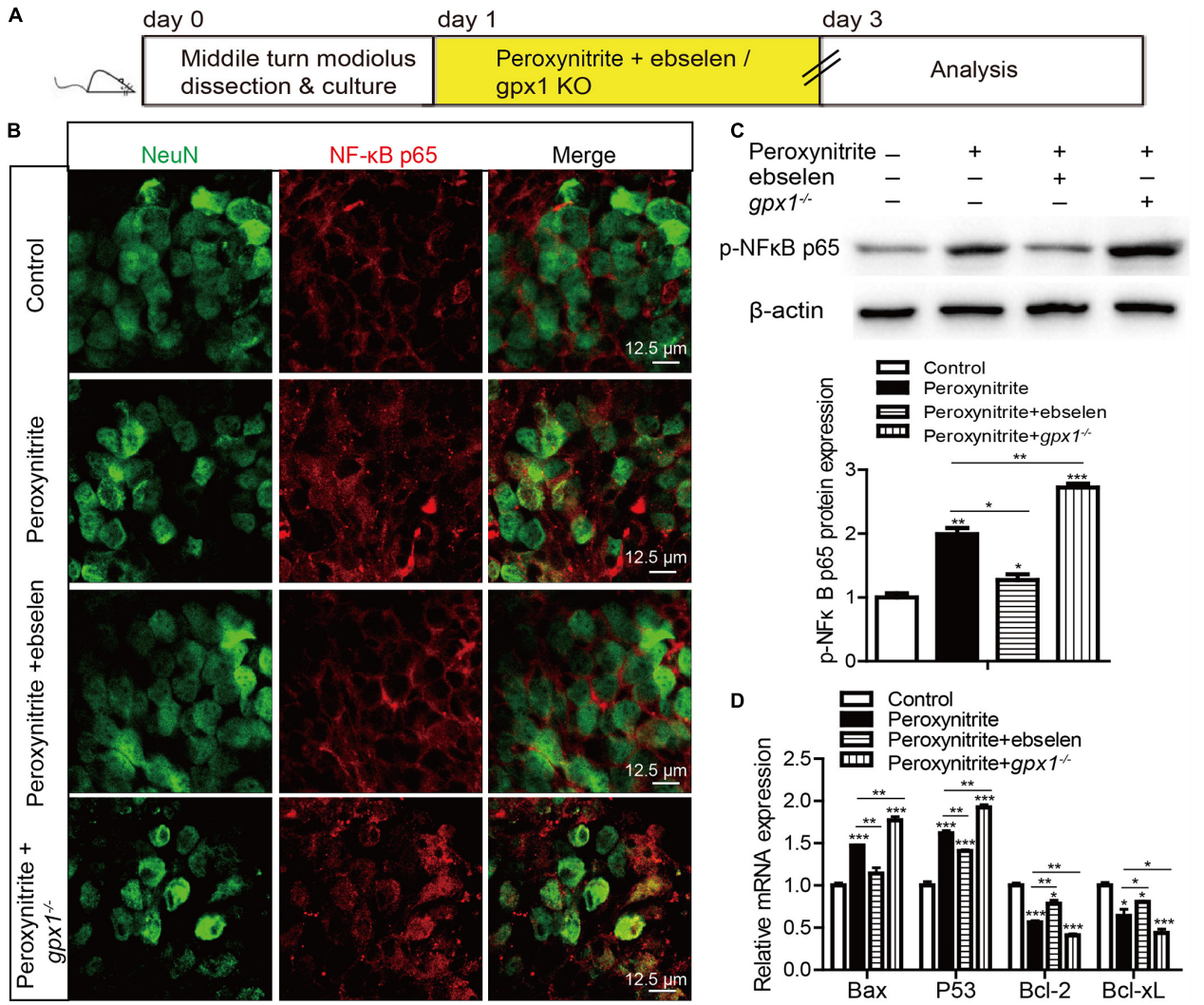

FIGURE 8 | The activated nuclear factor-kappa B (NF-κB) pathway is inhibited by GPX1 in SGNs after peroxynitrite damage. **(A)** The cultured SGNs from P3 WT mice were incubated with 100 μM peroxynitrite for 48 h with or without the pretreatment of 30 μM ebselen for 1 h, or the SGNs from *gpx1*$^{-/-}$ mice were exposed to 100 μM peroxynitrite for 48 h. **(B)** The anti-NeuN antibody was used to label the nucleus of SGN, and the immunostaining results showed that the fluorescence of NF-κB p65 was mainly detected in the cytoplasm of SGNs in the control group. Peroxynitrite induced obvious nuclear distribution of NF-κB p65 in SGNs and pretreatment with ebselen significantly reduced it, whereas the lack of GPX1 intensified the nuclear fluorescence of NF-κB p65 in SGNs of the peroxynitrite + *gpx1*$^{-/-}$ group. Scale bar = 12.5 μm. **(C)** Western blot results verified that the expression of the p-NF-kB p65 protein was upregulated in peroxynitrite-exposed SGNs compared with the untreated controls, and the pretreatment with ebselen significantly reduced it while the lack of GPX1 increased it. **(D)** Real-time PCR (RT-PCR) results revealed that peroxynitrite treatment caused significant increases in the microRNA (mRNA) expression of proapoptotic genes *Bax* and *P53*, and decreased the expression of antiapoptotic genes *Bcl2*, *Bcl-xL* compared with controls. The lower mRNA expression levels of *Bax* and *P53* and the higher expression levels of *Bcl2* and *Bcl-xL* were found in the peroxynitrite + ebselen group compared with the peroxynitrite-only group, while the lack of GPX1 in SGNs from *gpx1*$^{-/-}$ mice led to an opposite pattern. *$p < 0.05$, **$p < 0.01$, and ***$p < 0.001$, $n = 3$ for each group.

neuronal cells after ischemia-induced apoptosis (Zemlyak et al., 2009), another analysis showed that GPX1 decreased the ratio of Bax:Bcl-2 to create a more antiapoptotic environment in human endothelial cells (Faucher et al., 2005). It is known that the intrinsic pathway of apoptosis involves the mitochondria release of pro-apoptotic factors, such as AIF or cytochrome c, and these processes can be activated by ROS. Therefore, it is possible that GPX1, as an essential antioxidant enzyme, attenuates AIF release and enhances the expression of Bcl-2 to inhibit cell apoptosis, by reducing ROS level. In the current study, our results suggest that GPX1 protects against peroxynitrite-induced SGNs damage by suppressing ROS accumulation in SGNs. Interestingly, we have reported that intranuclear localization of AIF involves in the peroxynitrite-induced apoptosis of SGNs (Liu et al., 2012), whether GPX1 regulates the intranuclear localization of mitochondrial AIF to alleviate apoptosis in SGNs after peroxynitrite injury deserved further exploration.

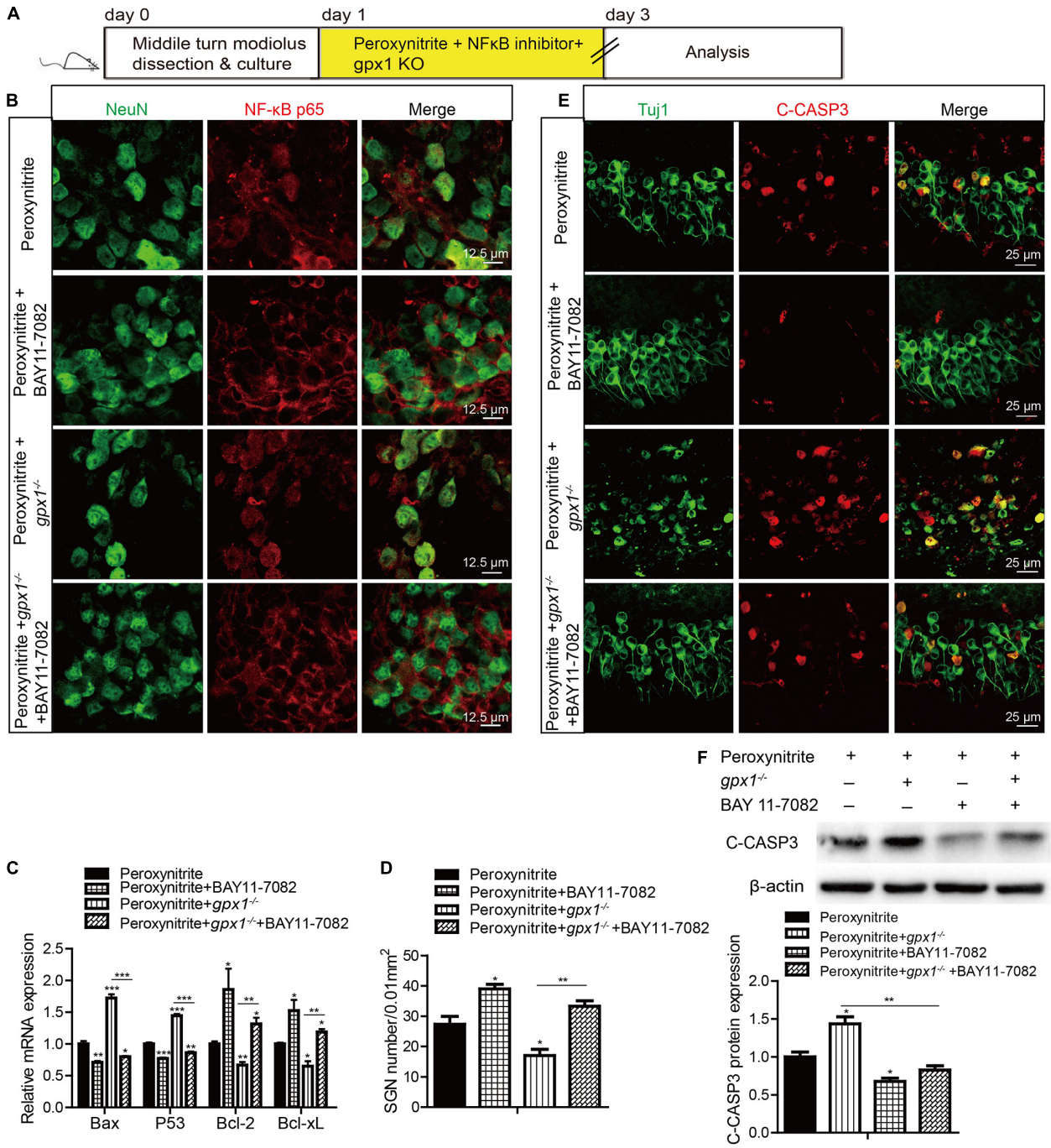

FIGURE 9 | Glutathione peroxidase inhibits the NF-κB pathway to protect against peroxynitrite-induced SGNs damage. **(A)** The cultured SGN explants from WT or *gpx1*$^{-/-}$ mice were treated with peroxynitrite and 10 μM BAY 11-7082 for 48 h. **(B,C)** Immunostaining and RT-PCR results showed that BAY 11-7082 effectively inhibited the nuclear translocation of NF-κB p65 and the mRNA expression of *Bax* and *P53*, but increased the mRNA expression of *Bcl2* and *Bcl-xL*, in the peroxynitrite + BAY 11-7082 group compared with the peroxynitrite-only group, as well as in the peroxynitrite + *gpx1*$^{-/-}$ + BAY 11-7082 group compared with the peroxynitrite + *gpx1*$^{-/-}$ group. Scale bar = 12.5 μm. **(D–F)** Immunostaining, cell counting, and western blot results showed that the inhibition of NF-κB by BAY 11-7082 significantly increased the survived SGN numbers, while decreased the C-CASP3 positive SGNs numbers and the C-CASP3 expression in the peroxynitrite + BAY 11-7082 group compared with the peroxynitrite group. Moreover, BAY 11-7082 treatment also increased the number of SGNs, whereas reduced the C-CASP3 expression in the peroxynitrite + *gpx1*$^{-/-}$ + BAY 11-7082 group vs. the peroxynitrite + *gpx1*$^{-/-}$ group. Scale bar = 25 μm. $^{*}p < 0.05$, $^{**}p < 0.01$, and $^{***}p < 0.001$, $n = 3$ for each group.

Finally, we explored the possible signaling pathways by which GPX1 was involved in protecting SGNs against peroxynitrite-induced injury. It has been shown that GPX1 can alter the activation of NF-κB (Li et al., 2001), modulate Akt pathways (Handy et al., 2009) to affect cellular proliferation and survival, and modify the ratio of Bax:Bcl-2 to create a more antiapoptotic environment (Faucher et al., 2005). NF-κB is known to be a redox-sensitive transcription factor in several cell types and involved in cellular death and survival under oxidative stress conditions (Li and Karin, 1999; Song et al., 2021). In this study, we found that the NF-κB pathway is activated in SGNs after peroxynitrite treatment and that the inhibition of NF-κB pathway contributes to promote SGNs survived from peroxynitrite injury. More importantly, we discovered that GPX1 can partially block the nuclear translocation of NF-κB p65 and inhibit the activation of the NF-κB signaling to protect SGNs against peroxynitrite damage. This observation is interesting that NF-κB activation is considered anti-apoptotic and pro-survival, partially due to augment the expression of IAPs and thus attenuating the activation of caspase. For instance, a study reported that the NF-κB signaling pathway is activated in noise-exposed cochleae to protect against inducible nitric oxide synthase-triggered oxidative stress and apoptosis (Tamura et al., 2016). We speculate the controversial effect of NF-κB pathway activation on inner ear cells, i.e., protecting or damaging cells, might rely on the cell and stimuli types. Furthermore, one possible explanation for the pro-apoptotic effect of NF-κB activation is that in the context of GPX1 deficiency, excess accumulation of cellular ROS might alter NF-κB responses. Evidence showed that excess intracellular hydrogen peroxide regulates the expression of various NF-κB component proteins, and the alterations in the composition or quantity of the NF-κB dimer can change down-stream target gene expression, and conduce to the upregulation of pro-inflammatory genes and a pro-apoptotic environment (Li et al., 2001; Oliveira-Marques et al., 2009; Lubos et al., 2011).

In summary, we investigated the role of GPX1 in protecting SGNs against oxidative stress by upregulating or inhibiting the expression of GPX1 in SGNs *via* the GPX1 mimic ebselen or the *gpx1* knockout mouse model, and further determined the mechanistic details behind the neuroprotective effect of GPX1 in SGNs against peroxynitrite injury. We found that the ebselen could significantly promote SGN survival, decrease SGN apoptosis, and reduce intracellular ROS levels after peroxynitrite exposure *in vitro*, while the deficiency of GPX1 led to opposite patterns of the above effects. Moreover, we showed that the protective mechanism of GPX1 involves inhibiting the activation of NF-κB pathway in SGNs exposed to peroxynitrite. These findings suggest that GPX1 might serve as a novel target for the prevention of oxidative stress-induced SGNs damage and hearing loss.

DATA AVAILABILITY STATEMENT

The original contributions presented in the study are included in the article/**Supplementary Material**, further inquiries can be directed to the corresponding authors.

ETHICS STATEMENT

The animal study was reviewed and approved by The Animal Care Committee of Shandong University (No. ECAESDUSM 20123011).

AUTHOR CONTRIBUTIONS

WL and LX designed and supervised the project. XW, YH, FC, MW, and YX performed the experiments and acquired the data. WL, LX, XW, FC, YX, and HW analyzed the results and performed the statistical analysis. WL, LX, and HW wrote the manuscript. All authors contributed to the article and approved the submitted version.

FUNDING

This work was supported by the Major Fundamental Research Program of the Natural Science Foundation of Shandong Province, China (ZR2020ZD39 and ZR2021ZD40), the Taishan Scholars Program of Shandong Province (Nos. tsqn201909189 and ts20130913), and the Shandong Province Science Foundation for Youths (No. ZR2020QH153).

SUPPLEMENTARY MATERIAL

The Supplementary Material for this article can be found online at: https://www.frontiersin.org/articles/10.3389/fncel.2022.841731/full#supplementary-material

Supplementary Figure 1 | GPX1 expression was absent in the cochlear SGNs of $gpx1^{-/-}$ mice. Immunofluorescence staining and western blot results verified that GPX1 expression was absent in the cochlear SGNs of $gpx1^{-/-}$ mice. Cell counting and statistical analysis showed that there was no significant difference in SGNs number between the $gpx1^{-/-}$ mice and WT mice. $^{**}p < 0.01$. Scale bar = 12.5 μm.

Supplementary Figure 2 | Dose responses of BAY11-7082 co-treated with peroxynitrite in cultured SGNs. The cultured cochlear SGNs were treated with different doses of BAY11-7082 (5 μM, 10 μM and 20 μM) and co-treated with 100 μM peroxynitrite for 48 h. **(A,B)** Immunostaining and cell counting results showed that co-treatment with 10 μM BAY11-7082 effectively increased the number of surviving SGNs after peroxynitrite damage, while the co-treatment with 5 μM or 20 μM BAY11-7082 showed no significant differences in SGN number compared to the peroxynitrite-only group. All data are presented as the mean ± SEM, $^{*}p < 0.05$, $^{**}p < 0.01$. Scale bars: 25 μm.

Supplementary Figure 3 | Effects of ebselen on expressions of GPX2 and GPX4 in SGNs after peroxynitrite injury. **(A,C)** Immunofluorescence staining was performed on cochlear frozen cryosection to determine the expression of GPX2 and GPX4 in P3 C57BL/6 mouse cochlea. The Immunofluorescence labeling of GPX2 **(A)** and GPX4 **(C)** was observed in cochlear SGNs of P3 mice. Scale bars: 25 μm. **(B,D)**The cultured middle turn cochleae were treated with peroxynitrite (100 μM) alone, or cotreated with ebselen (30 μM) for 48 h. The immunostaining result showed that the fluorescence intensity of GPX2 **(B)** and GPX4 **(D)** in the peroxynitrite group was reduced compared to that of the control group, while it was increased in the peroxynitrite + ebselen group compared with the peroxynitrite-only group. Scale bars: 12.5 μm.

REFERENCES

Antunes, F., Han, D., and Cadenas, E. (2002). Relative contributions of heart mitochondria glutathione peroxidase and catalase to H(2)O(2) detoxification in *in vivo* conditions. *Free Radic. Biol. Med.* 33, 1260–1267. doi: 10.1016/s0891-5849(02)01016-x

Brigelius-Flohé, R. (1999). Tissue-specific functions of individual glutathione peroxidases. *Free Radic. Biol. Med.* 27, 951–965. doi: 10.1016/s0891-5849(99)00173-2

Cao, Z., Yang, Q., Yin, H., Qi, Q., Li, H., Sun, G., et al. (2017). Peroxynitrite induces apoptosis of mouse cochlear hair cells *via* a Caspase-independent pathway in vitro. *Apoptosis* 22, 1419–1430. doi: 10.1007/s10495-017-1417-8

Ekoue, D. N., He, C., Diamond, A. M., and Bonini, M. G. (2017). Manganese superoxide dismutase and glutathione peroxidase-1 contribute to the rise and fall of mitochondrial reactive oxygen species which drive oncogenesis. *Biochim. Biophys. Acta Bioenerg.* 1858, 628–632. doi: 10.1016/j.bbabio.2017.01.006

Faucher, K., Rabinovitch-Chable, H., Cook-Moreau, J., Barrière, G., Sturtz, F., and Rigaud, M. (2005). Overexpression of human GPX1 modifies Bax to Bcl-2 apoptotic ratio in human endothelial cells. *Mol. Cell Biochem.* 277, 81–87. doi: 10.1007/s11010-005-5075-8

Handy, D. E., Lubos, E., Yang, Y., Galbraith, J. D., Kelly, N., Zhang, Y. Y., et al. (2009). Glutathione peroxidase-1 regulates mitochondrial function to modulate redox-dependent cellular responses. *J. Biol. Chem.* 284, 11913–11921. doi: 10.1074/jbc.M900392200

Jo, E. R., Youn, C. K., Jun, Y., and Cho, S. I. (2019). The protective role of ferulic acid against cisplatin-induced ototoxicity. *Int. J. Pediatr. Otorhinolaryngol.* 120, 30–35. doi: 10.1016/j.ijporl.2019.02.001

Kil, J., Lobarinas, E., Spankovich, C., Griffiths, S. K., Antonelli, P. J., Lynch, E. D., et al. (2017). Safety and efficacy of ebselen for the prevention of noise-induced hearing loss: a randomised, double-blind, placebo-controlled, phase 2 trial. *Lancet* 390, 969–979. doi: 10.1016/s0140-6736(17)31791-9

Kil, J., Pierce, C., Tran, H., Gu, R., and Lynch, E. D. (2007). Ebselen treatment reduces noise induced hearing loss *via* the mimicry and induction of glutathione peroxidase. *Hear Res.* 226, 44–51. doi: 10.1016/j.heares.2006.08.006

Kim, S. J., Park, C., Han, A. L., Youn, M. J., Lee, J. H., Kim, Y., et al. (2009). Ebselen attenuates cisplatin-induced ROS generation through Nrf2 activation in auditory cells. *Hear Res.* 251, 70–82. doi: 10.1016/j.heares.2009.03.003

Koeberle, S. C., Gollowitzer, A., Laoukili, J., Kranenburg, O., Werz, O., Koeberle, A., et al. (2020). Distinct and overlapping functions of glutathione peroxidases 1 and 2 in limiting NF-kappaB-driven inflammation through redox-active mechanisms. *Redox. Biol.* 28:101388. doi: 10.1016/j.redox.2019.101388

Korkmaz, A., Oter, S., Seyrek, M., and Topal, T. (2009). Molecular, genetic and epigenetic pathways of peroxynitrite-induced cellular toxicity. *Interdiscip. Toxicol.* 2, 219–228. doi: 10.2478/v10102-009-0020-4

Kumar, B. S., Tiwari, S. K., Saikant, R., Manoj, G., Kunwar, A., Sivaram, G., et al. (2010). Antibacterial and ulcer healing effects of organoselenium compounds in naproxen induced and *Helicobacter* pylori infected Wistar rat model. *J. Trace Elem. Med. Biol.* 24, 263–270. doi: 10.1016/j.jtemb.2010.04.003

Labbe, D., Bloch, W., Schick, B., and Michel, O. (2016). Hearing impairment, cochlear morphology, and peroxynitrite (ONOO(-)) formation in adult and aging NOS II knockout mice. *Acta Otolaryngol.* 136, 991–998. doi: 10.1080/00016489.2016.1183167

Leake, P. A., Akil, O., and Lang, H. (2020). Neurotrophin gene therapy to promote survival of spiral ganglion neurons after deafness. *Hear Res.* 394:107955. doi: 10.1016/j.heares.2020.107955

Li, N., and Karin, M. (1999). Is NF-kappaB the sensor of oxidative stress? *FASEB J.* 13, 1137–1143.

Li, Q., Sanlioglu, S., Li, S., Ritchie, T., Oberley, L., and Engelhardt, J. F. (2001). GPx-1 gene delivery modulates NFkappaB activation following diverse environmental injuries through a specific subunit of the IKK complex. *Antioxid. Redox. Signal.* 3, 415–432. doi: 10.1089/15230860152409068

Liang, Q., Shen, N., Lai, B., Xu, C., Sun, Z., Wang, Z., et al. (2019). Electrical Stimulation Degenerated Cochlear Synapses Through Oxidative Stress in Neonatal Cochlear Explants. *Front. Neurosci.* 13:1073. doi: 10.3389/fnins.2019.01073

Liu, W., Fan, Z., Han, Y., Lu, S., Zhang, D., Bai, X., et al. (2011). Curcumin attenuates peroxynitrite-induced neurotoxicity in spiral ganglion neurons. *Neurotoxicology* 32, 150–157. doi: 10.1016/j.neuro.2010.09.003

Liu, W., Fan, Z., Han, Y., Zhang, D., Li, J., and Wang, H. (2012). Intranuclear localization of apoptosis-inducing factor and endonuclease G involves in peroxynitrite-induced apoptosis of spiral ganglion neurons. *Neurol. Res.* 34, 915–922. doi: 10.1179/1743132812y.0000000098

Liu, W., Wang, X., Wang, M., and Wang, H. (2019a). Protection of Spiral Ganglion Neurons and Prevention of Auditory Neuropathy. *Adv. Exp. Med. Biol.* 1130, 93–107. doi: 10.1007/978-981-13-6123-4_6

Liu, W., Xu, X., Fan, Z., Sun, G., Han, Y., Zhang, D., et al. (2019b). Wnt Signaling Activates TP53-Induced Glycolysis and Apoptosis Regulator and Protects Against Cisplatin-Induced Spiral Ganglion Neuron Damage in the Mouse Cochlea. *Antioxid. Redox. Signal.* 30, 1389–1410. doi: 10.1089/ars.2017.7288

Liu, W., Xu, L., Wang, X., Zhang, D., Sun, G., Wang, M., et al. (2021). PRDX1 activates autophagy *via* the PTEN-AKT signaling pathway to protect against cisplatin-induced spiral ganglion neuron damage. *Autophagy* 17, 4159–4181. doi: 10.1080/15548627.2021.1905466

Lu, W., Chen, Z., Zhang, H., Wang, Y., Luo, Y., and Huang, P. (2012). ZNF143 transcription factor mediates cell survival through upregulation of the GPX1 activity in the mitochondrial respiratory dysfunction. *Cell Death Dis.* 3:e422. doi: 10.1038/cddis.2012.156

Lubos, E., Loscalzo, J., and Handy, D. E. (2011). Glutathione peroxidase-1 in health and disease: from molecular mechanisms to therapeutic opportunities. *Antioxid Redox. Signal.* 15, 1957–1997. doi: 10.1089/ars.2010.3586

McFadden, S. L., Ohlemiller, K. K., Ding, D., Shero, M., and Salvi, R. J. (2001). The Influence of Superoxide Dismutase and Glutathione Peroxidase Deficiencies on Noise-Induced Hearing Loss in Mice. *Noise Health* 3, 49–64.

Ohlemiller, K. K., McFadden, S. L., Ding, D. L., Lear, P. M., and Ho, Y. S. (2000). Targeted mutation of the gene for cellular glutathione peroxidase (Gpx1) increases noise-induced hearing loss in mice. *J. Assoc. Res. Otolaryngol.* 1, 243–254. doi: 10.1007/s101620010043

Oliveira-Marques, V., Marinho, H. S., Cyrne, L., and Antunes, F. (2009). Role of hydrogen peroxide in NF-kappaB activation: from inducer to modulator. *Antioxid Redox. Signal* 11, 2223–2243. doi: 10.1089/ars.2009.2601

Pavlinkova, G. (2020). Molecular Aspects of the Development and Function of Auditory Neurons. *Int. J. Mol. Sci.* 22:131. doi: 10.3390/ijms22010131

Ramdial, K., Franco, M. C., and Estevez, A. G. (2017). Cellular mechanisms of peroxynitrite-induced neuronal death. *Brain Res. Bull.* 133, 4–11. doi: 10.1016/j.brainresbull.2017.05.008

Schneider, A., Martin-Villalba, A., Weih, F., Vogel, J., Wirth, T., and Schwaninger, M. (1999). NF-kappaB is activated and promotes cell death in focal cerebral ischemia. *Nat. Med.* 5, 554–559. doi: 10.1038/8432

Sharma, G., Shin, E. J., Sharma, N., Nah, S. Y., Mai, H. N., Nguyen, B. T., et al. (2021a). Glutathione peroxidase-1 and neuromodulation: Novel potentials of an old enzyme. *Food Chem. Toxicol.* 148:111945. doi: 10.1016/j.fct.2020.111945

Sharma, N., Shin, E. J., Pham, D. T., Sharma, G., Dang, D. K., Duong, C. X., et al. (2021b). GPx-1-encoded adenoviral vector attenuates dopaminergic impairments induced by methamphetamine in GPx-1 knockout mice through modulation of NF-kappaB transcription factor. *Food Chem. Toxicol.* 154:112313. doi: 10.1016/j.fct.2021.112313

Song, Y., Wu, Z., and Zhao, P. (2021). The protective effects of activating Sirt1/NF-κB pathway for neurological disorders. *Rev. Neurosci.* [Epub Online ahead of print] doi: 10.1515/revneuro-2021-0118

Tamura, A., Matsunobu, T., Tamura, R., Kawauchi, S., Sato, S., and Shiotani, A. (2016). Photobiomodulation rescues the cochlea from noise-induced hearing loss *via* upregulating nuclear factor kappaB expression in rats. *Brain Res.* 1646, 467–474. doi: 10.1016/j.brainres.2016.06.031

Wang, M., Han, Y., Wang, X., Liang, S., Bo, C., Zhang, Z., et al. (2021). Characterization of EGR-1 Expression in the Auditory Cortex Following Kanamycin-Induced Hearing Loss in Mice. *J. Mol. Neurosci.* 71, 2260–2274. doi: 10.1007/s12031-021-01791-0

Wang, X., Han, Y., Wang, M., Bo, C., Zhang, Z., Xu, L., et al. (2019). Wnt Signaling Protects against Paclitaxel-Induced Spiral Ganglion Neuron Damage in the Mouse Cochlea In Vitro. *Biomed. Res. Int.* 2019:7878906. doi: 10.1155/2019/7878906

Wen, X., Qiu, C., Li, X., Lin, H., and Huang, Y. (2014). [Association between GPX-1 single nucleotide polymorphisms and susceptibility to noise-induced hearing loss among Chinese Han population]. *Zhonghua Lao Dong Wei Sheng Zhi Ye Bing Za Zhi.* 32, 568–572.

Xiong, M., He, Q., Lai, H., and Wang, J. (2011). Oxidative stress in spiral ganglion cells of pigmented and albino guinea pigs exposed to impulse noise. *Acta Otolaryngol.* 131, 914–920. doi: 10.3109/00016489.2011.577448

Xu, L., Gong, C., Li, G., Wei, J., Wang, T., Meng, W., et al. (2018). Ebselen suppresses inflammation induced by *Helicobacter* pylori lipopolysaccharide *via* the p38 mitogen-activated protein kinase signaling pathway. *Mol. Med. Rep.* 17, 6847–6851. doi: 10.3892/mmr.2018.8641

Yamasoba, T., Lin, F. R., Someya, S., Kashio, A., Sakamoto, T., and Kondo, K. (2013). Current concepts in age-related hearing loss: epidemiology and mechanistic pathways. *Hear Res.* 303, 30–38. doi: 10.1016/j.heares.2013.01.021

Youn, C. K., Jo, E. R., Sim, J. H., and Cho, S. I. (2017). Peanut sprout extract attenuates cisplatin-induced ototoxicity by induction of the Akt/Nrf2-mediated redox pathway. *Int. J. Pediatr. Otorhinolaryngol.* 92, 61–66. doi: 10.1016/j.ijporl.2016.11.004

Zemlyak, I., Brooke, S. M., Singh, M. H., and Sapolsky, R. M. (2009). Effects of overexpression of antioxidants on the release of cytochrome c and apoptosis-inducing factor in the model of ischemia. *Neurosci. Lett.* 453, 182–185. doi: 10.1016/j.neulet.2009.02.020

Zhang, W., Potrovita, I., Tarabin, V., Herrmann, O., Beer, V., Weih, F., et al. (2005). Neuronal activation of NF-kappaB contributes to cell death in cerebral ischemia. *J. Cereb. Blood Flow Metab.* 25, 30–40. doi: 10.1038/sj.jcbfm.9600004

Zhu, Y., Scheibinger, M., Ellwanger, D. C., Krey, J. F., Choi, D., Kelly, R. T., et al. (2019). Single-cell proteomics reveals changes in expression during hair-cell development. *Elife* 8:e50777 doi: 10.7554/eLife.50777

Conflict of Interest: The authors declare that the research was conducted in the absence of any commercial or financial relationships that could be construed as a potential conflict of interest.

Publisher's Note: All claims expressed in this article are solely those of the authors and do not necessarily represent those of their affiliated organizations, or those of the publisher, the editors and the reviewers. Any product that may be evaluated in this article, or claim that may be made by its manufacturer, is not guaranteed or endorsed by the publisher.

frontiers in Cellular Neuroscience

ORIGINAL RESEARCH
published: 23 March 2022
doi: 10.3389/fncel.2022.840143

Dual-Specificity Phosphatase 14 Regulates Zebrafish Hair Cell Formation Through Activation of p38 Signaling Pathway

Guanyun Wei[1†], Xu Zhang[1,2†], Chengyun Cai[1†], Jiajing Sheng[1†], Mengting Xu[1], Cheng Wang[1], Qiuxiang Gu[1], Chao Guo[1], Fangyi Chen[3,4], Dong Liu[1*] and Fuping Qian[1*]*

[1] Key Laboratory of Neuroregeneration of MOE, Nantong Laboratory of Development and Diseases, School of Life Sciences, Co-innovation Center of Neuroregeneration, Nantong University, Nantong, China, [2] Translational Medical Research Center, Wuxi No. 2 People's Hospital, Affiliated Wuxi Clinical College of Nantong University, Wuxi, China, [3] Department of Biomedical Engineering, Southern University of Science and Technology, Shenzhen, China, [4] Department of Biology, Brain Research Center, Southern University of Science and Technology, Shenzhen, China

OPEN ACCESS

Edited by:
Zuhong He,
Wuhan University, China

Reviewed by:
Guoqiang Wan,
Nanjing University, China
Zheng-Quan Tang,
Anhui University, China

***Correspondence:**
Fangyi Chen
chenfy@sustech.edu.cn
Dong Liu
liudongtom@gmail.com;
tom@ntu.edu.cn
Fuping Qian
qianfuping198911@163.com

[†] These authors have contributed equally to this work

Specialty section:
This article was submitted to Cellular Neuropathology, a section of the journal Frontiers in Cellular Neuroscience

Received: 20 December 2021
Accepted: 14 January 2022
Published: 23 March 2022

Citation:
Wei G, Zhang X, Cai C, Sheng J, Xu M, Wang C, Gu Q, Guo C, Chen F, Liu D and Qian F (2022) Dual-Specificity Phosphatase 14 Regulates Zebrafish Hair Cell Formation Through Activation of p38 Signaling Pathway. Front. Cell. Neurosci. 16:840143. doi: 10.3389/fncel.2022.840143

Most cases of acquired hearing loss are due to degeneration and subsequent loss of cochlear hair cells. Whereas mammalian hair cells are not replaced when lost, in zebrafish, they constantly renew and regenerate after injury. However, the molecular mechanism among this difference remains unknown. Dual-specificity phosphatase 14 (DUSP14) is an important negative modulator of mitogen-activated protein kinase (MAPK) signaling pathways. Our study was to investigate the effects of DUSP14 on supporting cell development and hair cell regeneration and explore the potential mechanism. Our results showed that *dusp14* gene is highly expressed in zebrafish developing neuromasts and otic vesicles. Behavior analysis showed that *dusp14* deficiency resulted in hearing defects in zebrafish larvae, which were reversed by *dusp14* mRNA treatment. Moreover, knockdown of *dusp14* gene caused a significant decrease in the number of neuromasts and hair cells in both neuromast and otic vesicle, mainly due to the inhibition of the proliferation of supporting cells, which results in a decrease in the number of supporting cells and ultimately in the regeneration of hair cells. We further found significant changes in a series of MAPK pathway genes through transcriptome sequencing analysis of *dusp14*-deficient zebrafish, especially *mapk12b* gene in p38 signaling. Additionally, inhibiting p38 signaling effectively rescued all phenotypes caused by *dusp14* deficiency, including hair cell and supporting cell reduction. These results suggest that DUSP14 might be a key gene to regulate supporting cell development and hair cell regeneration and is a potential target for the treatment of hearing loss.

Keywords: DUSP14, supporting cell, hair cell, zebrafish, proliferation, regeneration

INTRODUCTION

Millions of people all over the world are subjected to different degrees of hearing loss (Morton, 1991; Sun, 2021). The main causes of hearing impairment include aging, noise, genetic mutations, and exposure to ototoxic drugs, which contributed to the sensory hair cell loss in inner ear (Furness, 2015). Most cases of acquired hearing loss are due to degeneration and subsequent loss of cochlear hair cells (Vlajkovic and Thorne, 2021). However, there are no Food and Drug Administration

(FDA)-approved drugs to protect from hearing loss, which makes urgent the task of discovering new therapeutics.

The auditory epithelium located in the cochlea is composed of sensory hair cells and non-sensory supporting cells (Kelley, 2006). Although hair cells cannot regenerate in mammalian adults, regeneration of hair cells in the inner ear and lateral line is widespread in non-mammalian vertebrates, such as chicken, amphibian, and zebrafish. Additionally, those hair cells regenerate from transdifferentiating supporting cells, which aroused the interest of many auditory scientists in understanding the inner ear hair cell and supporting cell development and regeneration, with the potential to develop biologic therapies for hearing loss (Rubel et al., 2013). Therefore, it is particularly important to understand the cellular and molecular mechanisms of such striking difference between mammalian and non-mammalian vertebrates.

Dual-specificity phosphatase (DUSP) family is a group of phosphatases, which dephosphorylate of tyrosine and/or serine or threonine residues and the resulting activity regulation of their substrates (Caunt and Keyse, 2013). DUSPs are considered to be major modulators of key signaling pathways that are dysregulated in a variety of diseases (Patterson et al., 2009a; Ríos et al., 2014; An et al., 2021). DUSPs can be divided into seven subgroups with the consideration of substrate preferences: phosphatases of regenerating liver (PRL) family, cell division cycle 14 (CDC14) phosphatases, phosphatase and tensin homologs deleted on chromosome 10 (PTEN), slingshot homolog (SSH) family of phosphatases, myotubularins, mitogen-activated protein kinase phosphatases (MKPs), and atypical DUSPs (Huang and Tan, 2012). Atypical DUSPs are mostly with low molecular weight and lack the N-terminal two CDC25 homology 2 (CH2) domain. The most atypical DUSPs are localized in the cytoplasm. It is reported that some atypical DUSPs regulate MAPK, including extracellular signal-regulated kinases (ERKs), c-Jun N-terminal kinases (JNKs), and p38 kinases, which plays an important role in cell proliferation and apoptosis (Huang and Tan, 2012).

Dual-specificity phosphatase 14, an atypical member of the DUSP family of proteins, are critical modulators in various biological processes, such as apoptosis, inflammation, proliferation, and oxidative stress. Our results showed that *dusp14* gene was expressed in the inner ear and lateral line system of zebrafish, which suggest that Dusp14 may play a vital role in the regulation of hair cell fate in zebrafish.

Based on these findings, this study examined whether *dusp14* gene could regulate the hair cell fate in zebrafish, especially the behavior of supporting cell. Furthermore, we aimed to evaluate whether *dusp14* gene putative modulating hair cell actions would be related to modulation of the MAPK signaling pathway.

MATERIALS AND METHODS

Zebrafish Embryos

Zebrafish (*Danio rerio*) were reared and maintained at 28.5°C as Westerfield described (Westerfield, 1995). Two zebrafish lines were used in the study, including the wild-type AB line and the transgenic line *Tg(Brn3c:mGFP)*, where membrane-localized green fluorescent protein (GFP) is specifically expressed in the hair cells. Embryonic stages are defined as described (Kimmel et al., 1995). Embryos were collected after natural spawns. Embryos were moved to embryo medium containing 0.2 mM phenylthiourea at ∼20 h postfertilization (hpf) to prevent pigmentation. All animal procedures were performed according to protocols approved by the Animal Care and Use Committee of Nantong University and were consistent with the National Institutes of Health Guide for the Care and Use of Laboratory Animals.

Whole-Mount *in situ* Hybridization

The DNA fragments of zebrafish *dusp14* and *eya1* were amplified by PCR using the primers (**Supplementary Table 3**). Then, they were subcloned into the pGEM-T Easy Vector (Promega, United States), and a gene-specific digoxigenin-labeled RNA probe was transcribed *in vitro* using the DIG RNA Labeling Kit (SP6&T7) (Roche) following the manufacturer's instructions. The prefixed embryos were incubated with the probe overnight at 4°C. The alkaline phosphatase (AP)-conjugated antibody against digoxigenin (Roche) was used to detect the digoxigenin-labeled RNA probe. The AP-substrate NBT/BCIP solution (Roche) was added to the reaction system to stain the tissues specifically expressing *dusp14* gene or *eya1* gene in zebrafish.

Morpholino and CRISPR/Cas9 Microinjection

According to the manufacturer's instruction, morpholino antisense oligos (MOs; Gene Tools) were prepared at a stock concentration of 1 mM. We designed *dusp14* splice-modifying morpholino (*dusp14*-MO) to knockdown the expression of *dusp14* (**Supplementary Table 3**). MOs were diluted to 0.3 mM and injected into one-cell-stage embryos.

To generate the *dusp14* gene mutant zebrafish, as described in our previous work (Gong et al., 2017), 2–3 nL of solution containing specific single-guide RNA (sgRNA) and Cas9 mRNA was injected into one-cell-stage embryos (primers used are listed in **Supplementary Table 3**).

mRNA Synthesis and Phenotypic Rescue

dusp14 DNA fragments were synthesized by PCR using the primers, *dusp14-Bam*HI-F and *dusp14-Eco*RI-R (**Supplementary Table 3**). The DNA fragments were subcloned into the pCS2 + vector, and the recombinant plasmid was linearized using the restriction endonuclease *Not*I (New England Biolabs). The linearized product was purified as a template and transcribed into mRNA *in vitro* using the mMESSAGE mMACHINE High Yield Capped RNA Transcription kit (Ambion). Then, the synthesized *dusp14* mRNA was coinjected with *dusp14*-MO into one-cell-stage zebrafish embryos. The rate of rescued zebrafish after injection of *dusp14* mRNA was analyzed at 72 hpf.

RNA Extraction, Reverse Transcription, and Quantitative Real-Time PCR

Total RNAs of all samples were extracted using TRIzol reagent (Invitrogen, United States), and genomic DNA contamination

was removed by DNase I (Promega, United States). The RNA yield was determined using NanoDrop ND-2000 (Thermo Fisher Scientific, United States), and integrity was checked on a 1% agarose gel. The cDNA was synthesized using oligo-dT primers and Superscript RT-III (Takara, JP). Quantitative real-time PCR (qRT-PCR) was performed using a Plus Real-Time PCR System (Applied Biosystems, United States). SYBR Prime ScriptTM RTPCR kit (Takara, JP) was used for mRNA qRT-PCR. Data were analyzed using the relative $2^{-\Delta\Delta CT}$ method (Livak and Schmittgen, 2001; Schmittgen and Livak, 2008). The primers for qRT-PCR are listed in **Supplementary Table 3**.

Acoustic or Vibrational Startle

Acoustic or vibrational startle protocol was based on previous studies (van den Bos et al., 2017) with appropriate modifications. Larvae (6 dpf) were transferred from petri dishes to wells filled with 1 mL of E3 medium. Both the control and *dusp14*-MO zebrafish were tested. The protocol (lights on) consisted of 10-min acclimation, followed by 9 acoustic or vibrational stimuli (DanioVision intensity setting) with a 20-s interstimulus interval (ISI). Variable of interest to show the startle response was maximum velocity (mm/s) with 1-s intervals, since the startle response is a short burst of activity best captured by this parameter. When subjects did not show a clear response to the first stimulus (values lower than 15 mm/s), they were discarded from analysis.

Acoustic Startle Reflex

The acoustic startle reflex was performed as described previously (Yang et al., 2017). The larvae (5 dpf) were put in a thin layer of culture media in a petri dish attached to mini vibrator. The response of larvae to sound stimulus (a tone burst 9 dB re. m s^{-2}, 600 Hz, for 30 ms) generated by the vibrator was recorded from above by an infrared camera over a 6-s period. The mean moving distance and peak speed were used to quantify the startle response.

Immunofluorescence Staining

For immunofluorescence staining, the embryos were anesthetized and then fixed using 4% paraformaldehyde. After washing three times with PBS-T, the embryos were incubated in the antigen retrieval solution (Beyotime Biotechnology, China, #P0088) for 15 min at 98°C. Non-specific binding was then blocked with 10% donkey serum (Solarbio, China, #SL050) in PBS-T. Next, specific primary antibodies against GFP (Abcam, #ab13970) and cleaved caspase-3 (CST, #9664), 5-bromo-2′-deoxyuridine (BrdU) (Sigma, #B5002) or SOX2 (Abcam, #ab97959) were added, and secondary antibodies were used to detect the primary antibodies.

TdT-mediated dUTP nick end labeling (TUNEL) assay was performed according to the manufacturer's instructions (Alexa Fluor 640, cat#: 40308ES20, YEASEN Biotech Co. Ltd) to detect cell death in the HCs of neuromast. In brief, the embryos were anesthetized and then fixed using 4% paraformaldehyde. After washing three times with PBST, 20 μg/mL proteinase K (Roche) was used to treat the embryos. Next, Alexa Fluor 640-12-dUTP Labeling Mix was applied to label the apoptotic cells for at least 3 h. DAPI was applied to label the nucleus.

Images were taken with a Nikon confocal microscope A1R at 40× magnification and were analyzed by Nikon A1R NIS Elements. Exposure settings were adjusted to minimize oversaturation.

Drug Treatment

The p38 inhibitor (APExBIO, #C5248), with a working concentration at 50 ng/μL, was coinjected with *dusp14*-MO into the 1–2 cell-stage zebrafish embryos. Additionally, the injected zebrafish were raised at 28.5°C. The development status was recorded with a bright field microscope at about 72 hpf.

Statistical Analysis

All data were analyzed using GraphPad Prism 8.3.0. One-way ANOVA, unpaired Student's *t*-tests, and two-way ANOVA were used to determine statistical significance when comparing two groups. The value of $p < 0.05$ was considered as statistically significant. All data are presented as means with SEM, and all experiments were repeated at least three times.

RNA-Seq Analysis

To study gene expression changes after *dusp14* knockdown in zebrafish, we performed transcriptome sequencing. The wild-type zebrafish and *dusp14*-MO injected zebrafish of 3 days old were prepared, respectively. Three independent replicates of the samples were analyzed for each treatment. The total RNA was extracted using TRIzol reagent (Invitrogen, United States) following the manufacturer's procedure. The quantity and purity of total RNAs were checked using a Bioanalyzer 2100 and RNA 6000 Nano LabChip Kit (Agilent, CA, United States) with RIN value > 7.0. All RNA samples were submitted to GENEWIZ Science (Suzhou, China), and deep sequencings were performed on an Illumina Hiseq2500.

For RNA-seq data, the Cuffdiff was used to estimate differential expression between samples at the transcript level (Kim et al., 2013). The differentially expressed gene (DEG) was determined with *log2 fold change* > 1, *p-value* < 0.05. The R package Clusterprofer was used for Kyoto Encyclopedia of Genes and Genomes (KEGG) pathway and gene ontology (GO) annotation.

RESULTS

The *dusp14* Gene Is Expressed in the Otic Vesicles and Neuromasts in Zebrafish

First, to observe the conservation of DUSP14, we constructed an evolutionary tree of 14 species based on the amino acid sequence of DUSP14, including mouse, giant panda, domestic cat, human, big brown bat, Chinese horseshoe bat, sperm whale, sea lion, bottlenose dolphins, lizards, zebrafish, yeast, and nematodes (**Figure 1A**). The results showed that *dusp14* is an extensive

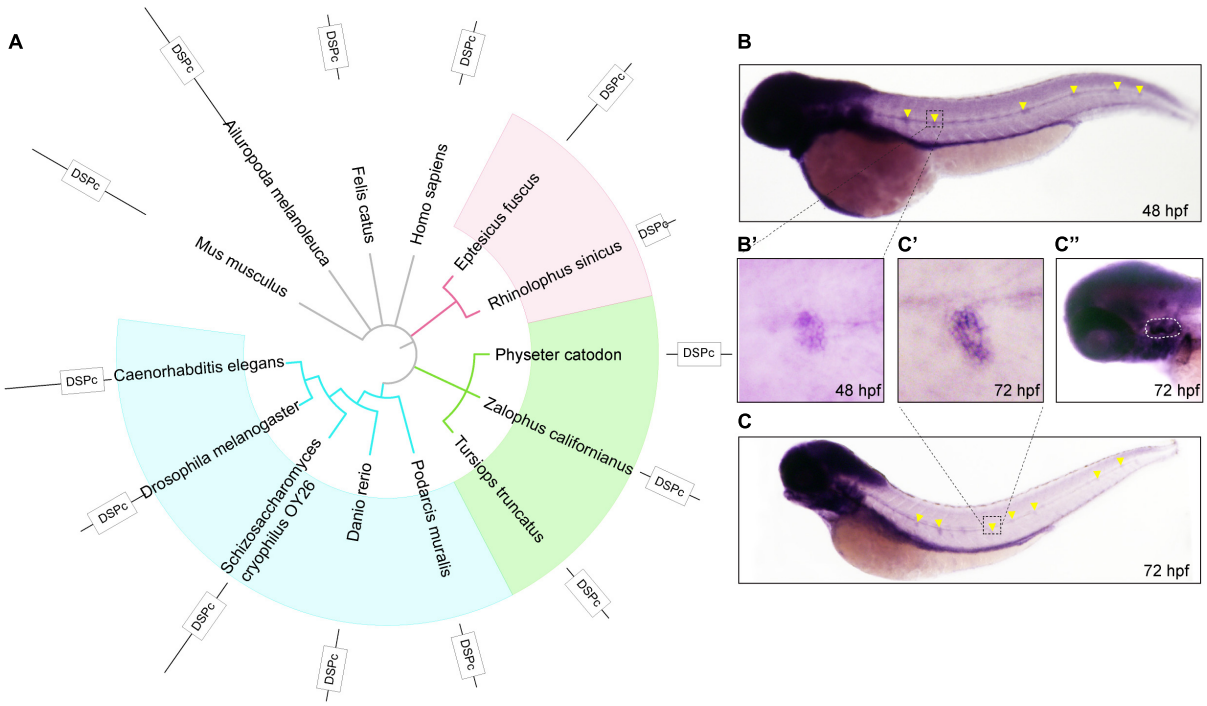

FIGURE 1 | The phylogenetic and expression analysis of zebrafish *dusp14*. **(A)** A phylogenetic tree was generated using the PhyML software base on amino acid sequences. The pictures are mouse, giant panda, domestic cat, human, big brown bat, Chinese horseshoe bat, sperm whale, sea lion, bottlenose dolphins, lizards, zebrafish, Saccharomyces cerevisiae, and nematodes. **(B,C)** WISH with the *dusp14* probe in wild-type zebrafish showed that the gene is expressed in the otic vesicle and lateral line at 48 hpf **(B)** and 72 hpf **(C)**. **(B',C',C")** Are the detailed information with higher magnification of the **(B,C)**, respectively.

conserved gene in many species with DUSP (dual-specificity phosphatases) conserved domain.

Next, to investigate the spatiotemporal expression of *dusp14* during the embryonic development, we performed the WISH using a *dusp14* antisense probe. As shown in **Figures 1B,B′**, *dusp14* is expressed in the neuromast at 48 hpf. At 72 h (**Figure 1C**), the *dusp14* gene expression is pronounced in the lateral line (**Figure 1C′**) and the otic vesicle (**Figure 1C″**). These results indicate that *dusp14* may play an important role in inner ear development.

Knockdown the *dusp14* Expression by Morpholino Leads to Hearing Defects in Zebrafish

To explore the effect of the *dusp14* gene on zebrafish behavioral response, we designed morpholino oligonucleotides to knockdown the expression of *dusp14*, and *dusp14*-MO was validated to effectively reduce *dusp14* expression (**Supplementary Figure 1**). Then, we performed acoustic or vibrational startle test after *dusp14*-MO injection at 5 dpf. The results showed that the response of *dusp14*-MO zebrafish to percussion stimuli becomes sluggish, whereas the injection of *dusp14* mRNA significantly rescued the phenotype (**Figures 2A,B**). In addition, there is no difference in movement rate among wide-type zebrafish, *dusp14*-MO zebrafish, and *dusp14*-mRNA and MO coinjected zebrafish during the total test (**Figure 2C**), which suggests that the injection did not affect locomotor activities of zebrafish.

To further investigate the effects of *dusp14*-MO on hearing dysfunction, we performed the acoustic startle reflex experiment (**Figure 2D**). The results showed that the swimming trajectory (**Figure 2E**), swimming distance (**Figure 2F**), and velocity (**Figure 2G**) of *dusp14* morphants were reduced compared to the controls, which were reversed by *dusp14*-mRNA. These results indicate that *dusp14* is necessary for hearing-related behaviors.

Knockdown *dusp14* Expression by Morpholino Decreases the Number of Hair Cells and Neuromasts in Zebrafish

It is well known that hair cells in the inner ear of zebrafish are responsible for the balance perception and hearing. Therefore, to test the underlying cellular mechanisms of *dusp14* gene on ear function, we knockdown the *dusp14* expression by morpholino in the transgenic zebrafish line *Tg*(*Brn3c:mGFP*), in which the GFP were specifically expressed in hair cells (**Figure 3A**). The results showed that the number of hair cells in three different crista hair cell clusters (anterior crista hair cells: AC; lateral crista hair cells: LC; posterior crista hair cells: PC) was reduced after *dusp14*-MO microinjection at 72 hpf (**Figures 3B,B′**), which was neutralized by *dusp14* mRNA treatment.

The hair cells in zebrafish are also present in the lateral line system containing the neuromasts that is important to perceive

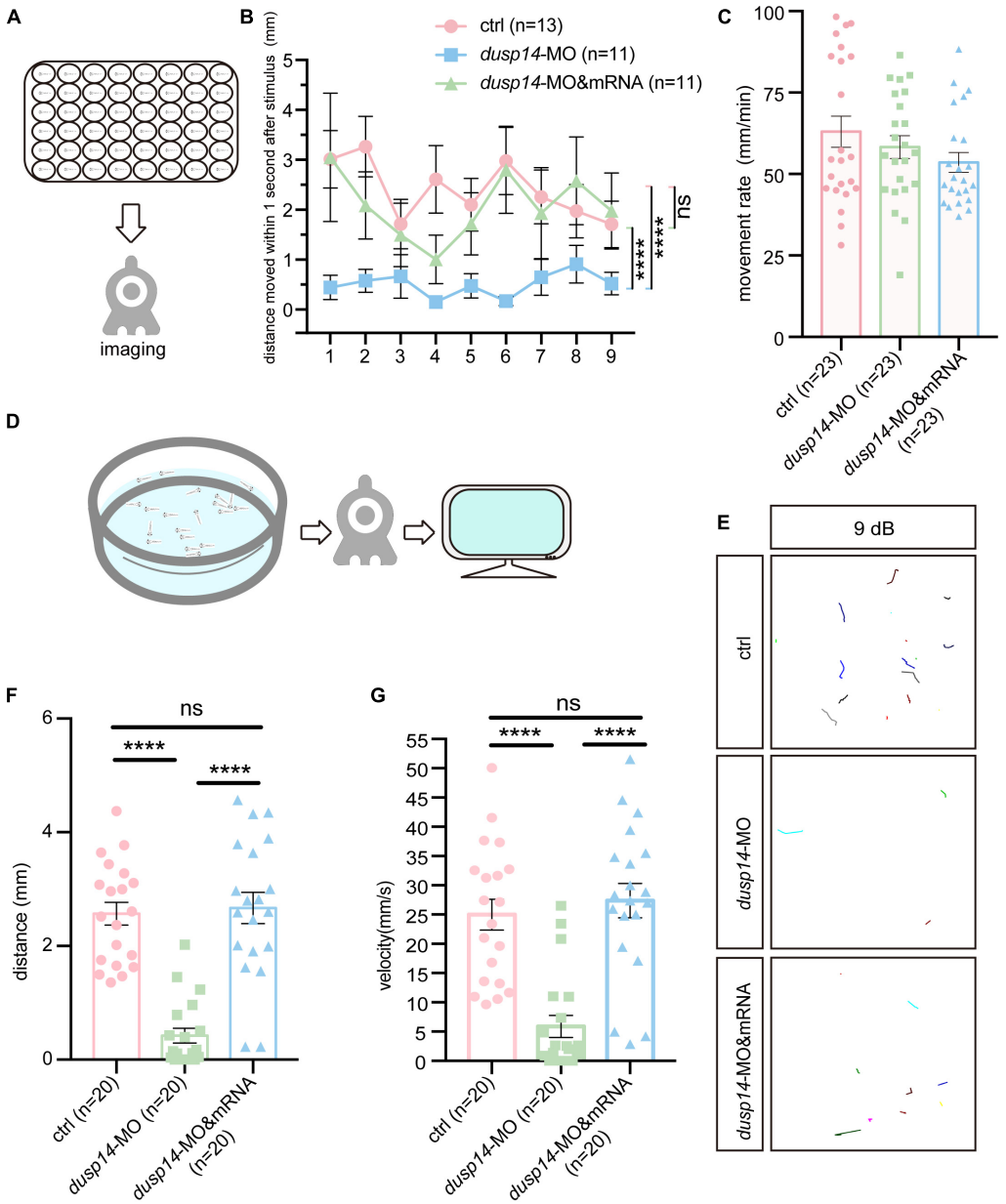

FIGURE 2 | Knockdown of *dusp14* gene affects the hearing-related behavioral response in zebrafish. **(A)** Working diagram of acoustic or vibrational startle test after *dusp14*-MO injection at 5 dpf. **(B)** The distance moved of zebrafish within 1 s after the percussion stimulation. **(C)** Statistics of the moving rate of zebrafish during the total test. **(D)** The schematic diagram shows the startle response testing equipment. **(E)** The swimming trajectory of the control, *dusp14* morphants and *dusp14*-mRNA and MO. **(F,G)** Swimming distance and peak velocity of zebrafish larvae at 5 dpf that reflected the auditory function of zebrafish larvae by examining the startle response. Values with **** above the bars are significantly different ($P < 0.0001$), ns means no significance.

changes in the surroundings. Then, we further investigate the role of *dusp14* gene on neuromast formation and found that the number of hair cell clusters in the posterior lateral line of *dusp14* morphants was significantly decreased at 72 hpf (**Figures 3C,C′**). Moreover, the number of the hair cells in the remaining neuromast L3 was also decreased (**Figures 3B,B′′**). But the *dusp14* mRNA treatment interfered these changes remarkably. In addition, we used the *eya1* gene to label the neuromast cells (Grant et al., 2005; Whitfield, 2005) in lateral line by WISH and discovered that the number of neuromasts in the posterior lateral line of *dusp14* morphants was significantly reduced (**Figures 3D,D′**). These results indicate that *dusp14* gene affects the number of hair cells in zebrafish inner ear and lateral line.

To further validate the function of *dusp14* during the hair cell development, the CRISPR/Cas9 system was utilized to knockout

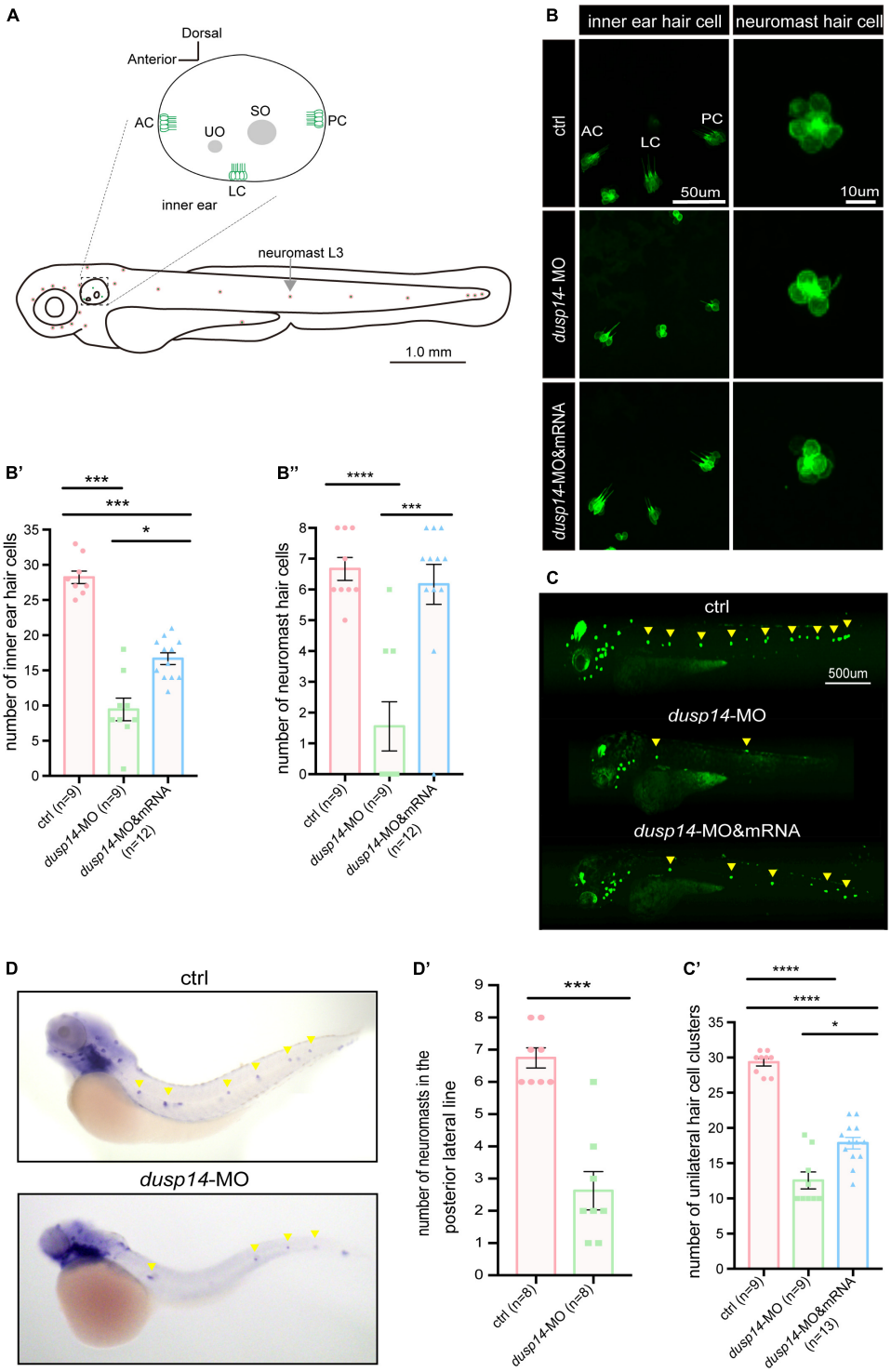

FIGURE 3 | Knockdown *dusp14* expression by morpholino decreases the number of hair cell and neuromasts in zebrafish. **(A)** Schematic diagram of zebrafish neuromast and inner ear hair cell. **(B)** Confocal imaging analysis of crista hair cells in the otic vesicle of control and *dusp14* deficiency zebrafish at 72 hpf. **(B′)** The statistical analysis of the numbers of inner ear crista hair cells in the control and *dusp14* morphants at 72 hpf. **(B′′)** The statistical analysis of the numbers of hair cells in the remaining neuromast L3 in the control and *dusp14* morphants at 72 hpf. **(C)** The imaging analysis of control and *dusp14* morphants at 72 hpf in fluorescent field. Scale bar = 500 μm. **(C′)** Quantification of the number of unilateral hair cell clusters of control and *dusp14* morphants at 72 hpf. **(D)** *in situ* hybridization of the *eya1* gene specifically expressed in the neuromasts showed that the number of neuromasts in *dusp14*-MO zebrafish was decreased. **(D′)** statistics results of D. Each bar represents the mean ± SEM. Values with *, ***, and **** above the bars are significantly different ($P < 0.05$, $P < 0.001$, and $P < 0.0001$, respectively).

dusp14 in wild-type zebrafish. As shown in **Supplementary Figure 2A**, we chose a sgRNA target site near the translation start codon in the exon1 of *dusp14* for CRISPR/Cas9-mediated mutation to abolish the protein translation. Similar to the results of the *dusp14* morphants, the number of hair cell clusters and hair cells in the posterior lateral line of the *dusp14* mutants was remarkably fewer than that of the control fish at 72 hpf, which was partially reversed by the *dusp14* mRNA injection (**Supplementary Figures 2C,C′,C′′**).

Knockdown of the *dusp14* Gene Reduces the Number of Supporting Cells and Proliferation of Supporting Cells

As we know, hair cells of the inner ear and lateral line system in zebrafish regenerate from mitotic supporting cells (Williams and Holder, 2000; Kniss et al., 2016; Thomas and Raible, 2019). Since knockdown of the *dusp14* gene caused the reduction of hair cells, we speculated that support cells, resource of hair cells, were also affected by *dusp14* morpholino injection.

To test the hypothesis, we analyzed SOX2$^+$ cells in the posterior lateral line of *dusp14* morphants by immunostaining with anti-SOX2 antibody. The results showed that SOX2$^+$ cell number was dramatically decreased after *dusp14* morpholino injection, which was substantially reserved by *dusp14* mRNA treatment (**Figures 4A,A′**). Furthermore, we performed the BrdU incorporation to measure the regeneration of supporting cells in the lateral line (**Figures 4B,B′**). Our results showed that the number of proliferating supporting cells was significantly reduced in the *dusp14* morphants. Additionally, the *dusp14* mRNA treatment partially interfered these changes. What is more, there is no difference in apoptotic signal between *dusp14* morphants and the control, which was immunostained with TUNEL and cleaved caspase 3 in zebrafish neuromasts

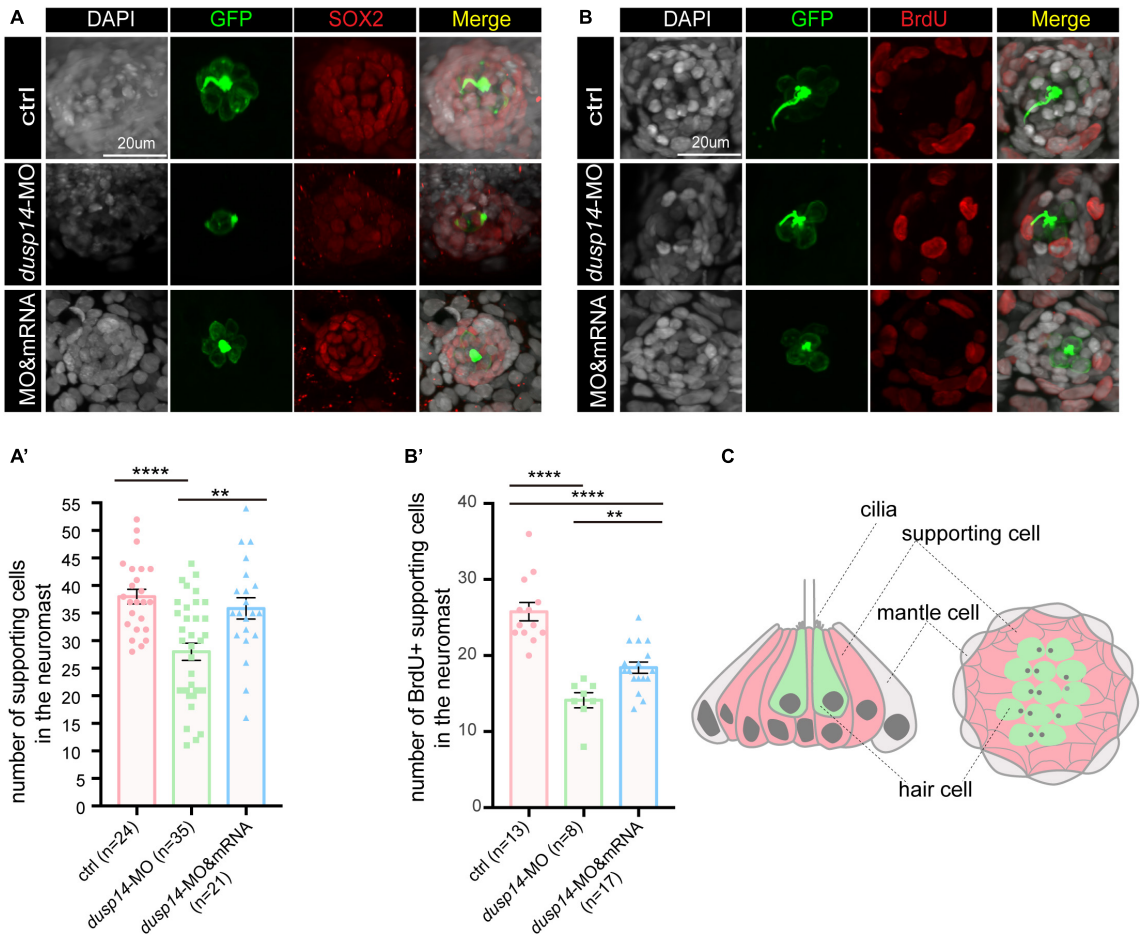

FIGURE 4 | Knockdown of the dusp14 gene reduces the number of supporting cells and proliferation of supporting cells. **(A)** The representation of SOX2 immunofluorescence images of neuromasts in the posterior lateral line of the control and *dusp14* morphants. **(A′)** Quantification of the number of supporting cells in the posterior lateral line neuromast of control and *dusp14* mutants at 72 hpf. **(B)** BrdU staining for the supporting cell in the neuromasts in the posterior lateral line of the control zebrafish and *dusp14* morphants. Scale bar = 20 μm. **(B′)** Quantification of zebrafish embryos with the BrdU$^+$ cells in the control and *dusp14* morphants. **(C)** Schematic diagram of the longitudinal structure and the plane structure of neuromast, the gray part is the mantle cell, the pink part is supporting cell, and the green represents hair cell. Experimental embryos were sampled at 72 hpf ($n > 8$). Each bar represents the mean ± SD. Values with ** and **** above the bars are significantly different ($P < 0.01$ and $P < 0.0001$, respectively).

(**Supplementary Figure 3**). Taken together, we found that *dusp14* gene may regulate the formation of hair cells and ultimately affect the hearing by modulating the proliferation of supporting cells in the zebrafish lateral line (**Figure 4C**).

Transcriptomic Sequencing Data Revealed p38 Signaling Pathways May Responsible for Regulation of *dusp14* Gene on Hearing Function

To gain a further insight into the molecular mechanism by which *dusp14* gene responsible for the regeneration of the supporting cells, we performed RNA sequencing (RNA-seq) of 72 hpf wild-type zebrafish and *dusp14*-MO zebrafish. Over 40 million valid reads per library on average were obtained after quality filtering, which was, respectively, mapped to about 90% of the zebrafish genome (**Supplementary Table 1**). The results revealed 2,418 DEGs that might be affected by the absence of *dusp14* with 1,787 upregulated DEGs and 631 downregulated DEGs (**Figure 5A** and **Supplementary Table 2**). What is more, 12 genes (*apoeb, gsta.q, pkma, meis2b, dld, prkcbb, mag, ush1ga, mkm2os.2, fbxo16, pcloa, and cyp26c1*) were randomly selected for qRT-PCR analysis to confirm the quality of RNA-seq data. Notably, the expression changes of 6 among 12 genes were consistent with the results of RNA-seq data analysis (**Supplementary Figures 4A,B**), indicating the reliability of RNA-seq analysis.

Subsequently, we performed KEGG pathway enrichment analysis on the RNA-seq data. The results showed that knockdown *dusp14* gene by morpholino mainly resulted in changes in various metabolic pathways (**Supplementary Table 2**), including carbon metabolism, tryptophan metabolism, glycine metabolism, serine metabolism, tyrosine metabolism, retinol metabolism, metabolism of xenobiotics by cytochrome P450, phenylalanine metabolism, and so on. Furthermore, the most significant GO analysis enrichment terms were oxidoreductase activity, which were assigned as molecular functions. The cell membrane was the most significant GO enrichment term assigned as cellular component, and regulation of transportation was the most significant GO enrichment term assigned as a biological process (**Figure 5B**).

The DUSP family targets to MAPK signaling pathway, which modulate diverse cellular functions, such as regeneration, differentiation, and apoptosis. Therefore, we observed the gene expression changes in p38 kinases, ERKs, and JNKs signaling

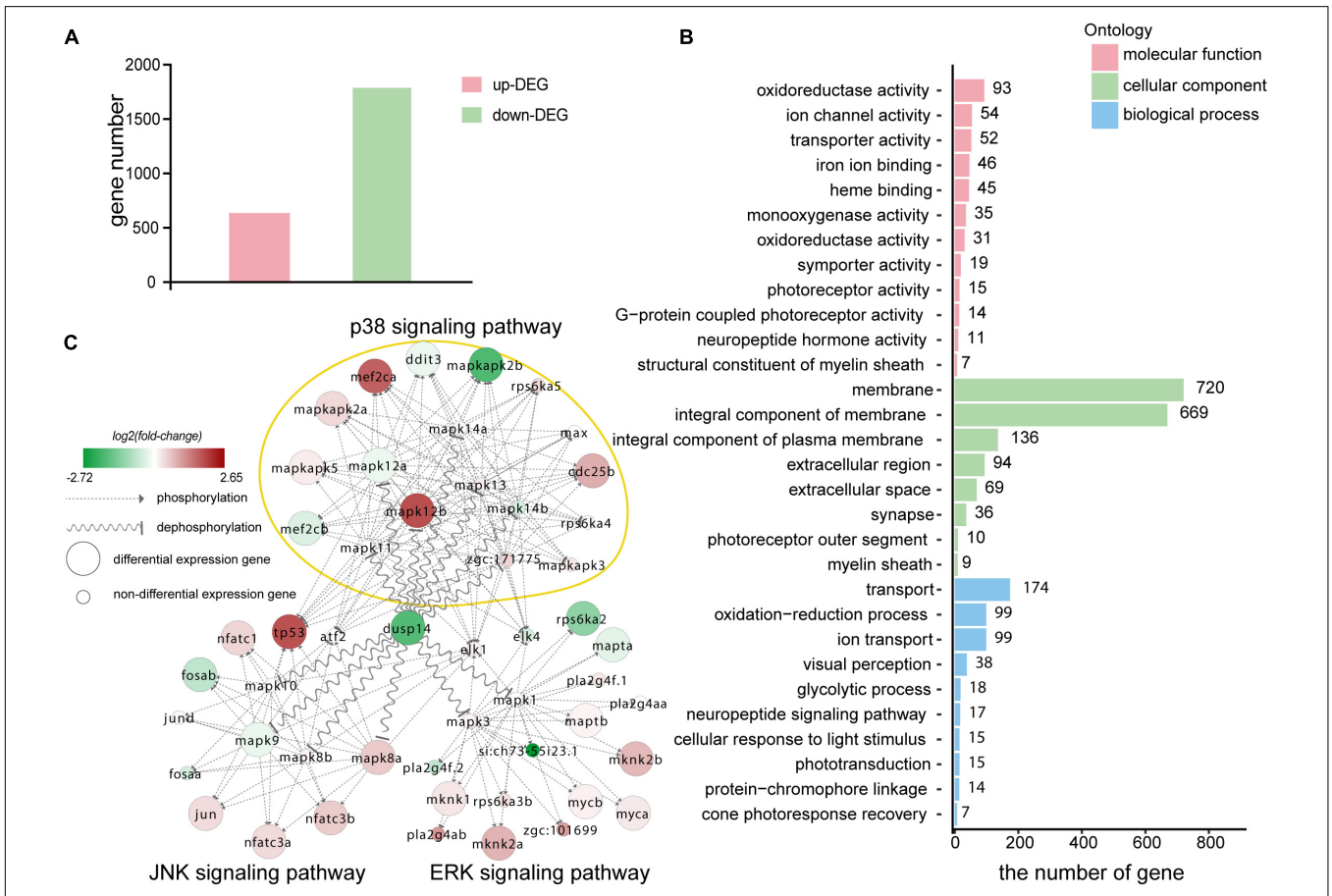

FIGURE 5 | Transcriptomic sequencing data revealed p38 signaling pathways may responsible for regulation of dusp14 gene on hearing function. **(A)** The upregulated differentially expressed genes (DEGs) and downregulated DEGs that might be affected by knockdown *dusp14* based on transcriptome data analysis. **(B)** Gene ontology (GO) annotation enrichment of DEGs. **(C)** Gene expression changes in the MAPK pathway caused by *dusp14* knockdown.

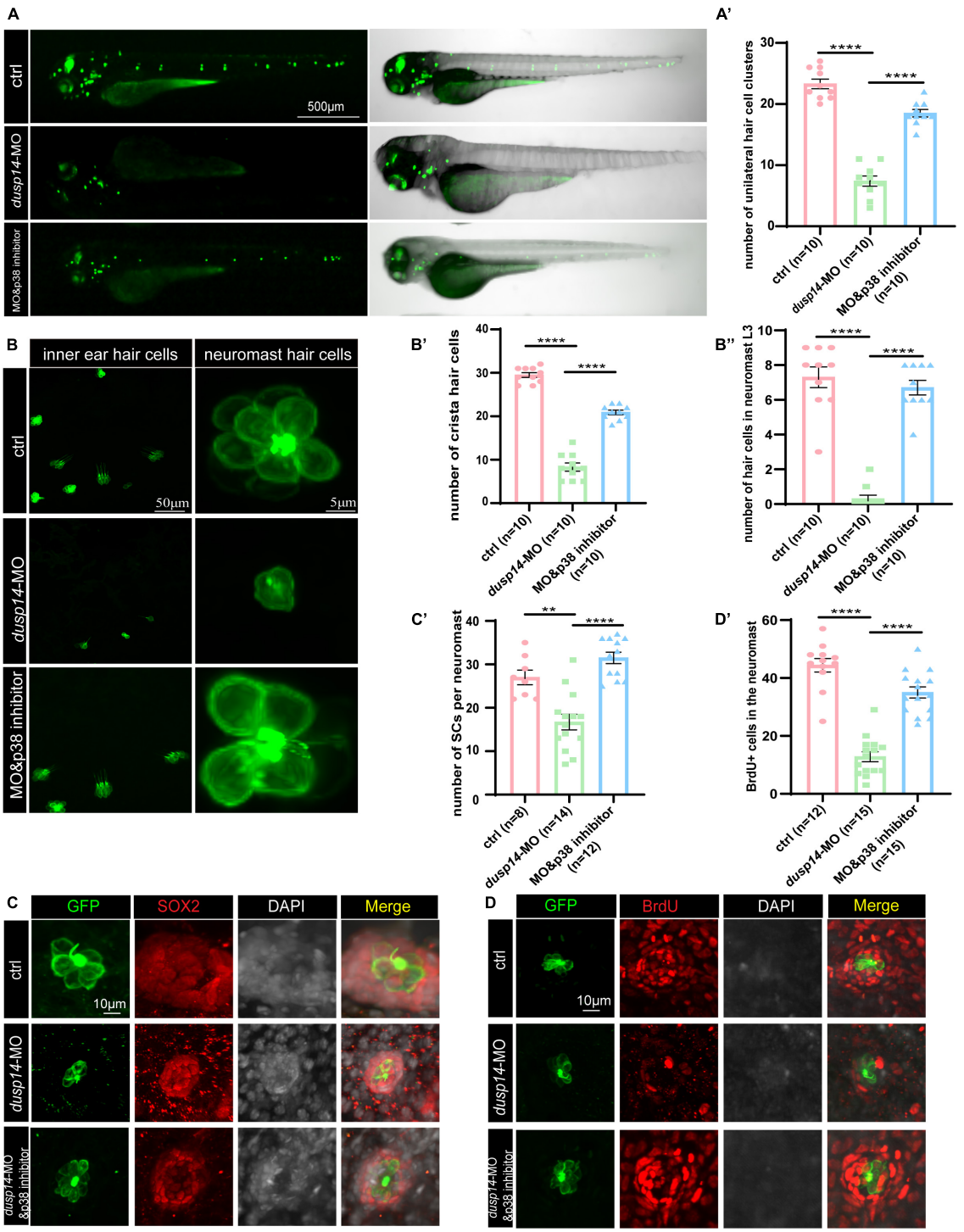

FIGURE 6 | p38 signaling pathway is involved in dusp14 regulation of inner ear hearing in zebrafish. **(A)** The imaging analysis of control and *dusp14* mutants at 72 hpf in bright field and fluorescent field. **(A′)** Quantification of the number of the unilateral hair cell clusters of control and *dusp14* mutants at 72 hpf. **(B)** Confocal imaging analysis of inner ear hair cells and lateral line neuromast hair cells of control, *dusp14* deficiency and dusp14-MO and p38 inhibitor coinjected zebrafish at 72 hpf. **(B′)** The statistical analysis of the numbers of crista hair cells for panel **(B)**. **(B″)** The statistical analysis of the numbers of hair cells in the remaining neuromast L3 for panel **(B)**. **(C)** The representation of SOX2 immunofluorescence images of neuromasts in the posterior lateral line of the control, *dusp14* morphants and dusp14-MO and p38 inhibitor coinjected zebrafish at 72 hpf. **(C′)** Quantification of the number of supporting cells per neuromast for panel **(C)**. **(D)** BrdU staining for the supporting cells in the neuromasts of the control, *dusp14* morphants and dusp14-MO and p38 inhibitor coinjected zebrafish at 72 hpf. **(D′)** Quantification of zebrafish embryos with the $BrdU^+$ cells for panel **(D)**. Experimental embryos were sampled at 72 hpf ($n > 6$). Each bar represents the mean ± SD. Values with ** and **** above the bars are significantly different ($P < 0.01$ and $P < 0.0001$, respectively).

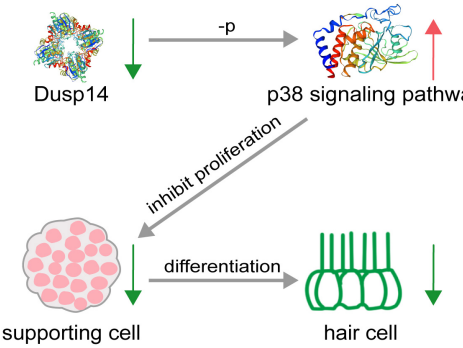

FIGURE 7 | Schematic diagram of hair cell reduction caused by *dusp14* knockdown. Knockdown of *dusp14* expression by morpholino inhibited the proliferation of supporting cells by p38 signaling pathway, resulting in a decrease in the number of hair cells and ultimately leading to abnormal hearing and balance-related behaviors in zebrafish.

pathway in RNA-seq data. As is shown in **Figure 5C**, the genes directly regulated by *dusp14* dephosphorylation include *mapk8b*, *mapk9*, *mapk12a,* and *mapk12b*, which are mainly in the JNK and p38 signaling pathways. Among them, *mapk12b* belonging to p38 signaling pathway showed the most significant difference, which suggests that p38 signaling pathway may play a vital role in *dusp14* regulation of hearing in zebrafish.

p38 Signaling Pathway Is Involved in *dusp14* Regulation of Inner Ear Hearing in Zebrafish

To further explore whether p38 signaling is responsible for *dusp14* regulation of hearing in zebrafish, the wild-type and *dusp14*-MO zebrafish were treated with p38 inhibitor. As previously shown, although knockdown *dusp14* gene expression by morpholino significantly decreased the number of hair cell clusters (**Figures 6A,A'**), the number of hair cells in inner ear cristae and neuromast L3 in the posterior lateral line, p38 inhibitor dramatically reversed these changes (**Figures 6B,B',B"**). Additionally, p38 inhibitor also blocked the effect of *dusp14*-MO on the number of supporting cell and the proliferation of supporting cells (**Figures 6C,C',D,D'**). These results indicate that p38 signaling pathway is necessary for the *dusp14* regulation of hearing.

DISCUSSION

Hearing loss in mammals mainly caused by degeneration of hair cells in the inner ear, which is an irreversible process. To date, apart from hearing aids and cochlear implants, no pharmacological therapy promoting functional recovery from hearing loss is clinically available. This study demonstrates that *dusp14*, a conserved gene between species, is highly expressed in the lateral line and otic vesicles in zebrafish. Knockdown of *dusp14* expression by morpholino inhibited the proliferation of supporting cells through p38 signaling pathway, resulting in a decrease in the number of hair cells and ultimately leading to abnormal hearing and balance-related behaviors in zebrafish (**Figure 7**).

Dual-specificity phosphatase 14, a member of the atypical DUSPs, has been implicated in inflammation, apoptosis, cancer, diabetes, cell differentiation, and proliferation (Wada and Penninger, 2004; Turjanski et al., 2007; Lountos et al., 2009; Ríos et al., 2014). Dusp14 was characterized by yeast two hybrid systems for the first time to identify a new protein interacting with T cell costimulatory CD28 (Marti et al., 2001). It is reported that DUSP14 knockout aggravated pathological processes involved in non-alcoholic fatty liver disease development, whereas DUSP14 overexpression ameliorated these pathological alterations (Wang S. et al., 2018). Moreover, hepatic ischemia–reperfusion injury reduced Dusp14 expression, which suggests that Dusp14 is a protective factor in liver damage (Wang X. et al., 2018). Suppressing DUSP14 expression exacerbated cardiac injury through activating MAPK signaling pathways (Lin et al., 2018). Cardiac-specific Dusp14 overexpression alleviated aortic banding-induced cardiac dysfunction and remodeling (Li et al., 2016). These results indicate that DUSP14 may be a positive regulator of various cellular responses. We found that *dusp14* gene is important to supporting cell proliferating in zebrafish. Highly *dusp14* expression in the lateral line and otic vesicle in zebrafish was observed, however, whether that *dusp14* gene is specific located in the supporting cell remains unclear. The more experiments are needed.

Dusp14 is a dephosphorylate regulator that mainly acts on MAPK signaling and has different MAPK pathway targets in the pathological process of various diseases. *In vitro*, GST-tagged DUSP14 can dephosphorylate p38, ERK, and JNK pathways (Patterson et al., 2009b). DUSP14 knockout mice after myocardial ischemia–reperfusion injury induce the activation of MAPKs, including elevated p-p38, p-ERK1/2, and p-JNK in heart tissues (Lin et al., 2018). However, Dusp14 deficiency after hepatic ischemia–reperfusion injury upregulated p-JNK1/2 and p-p38, but not p-ERK1/2 (Wang X. et al., 2018). The enhanced phosphorylated p38 and JNK1/2 levels, but not ERK1/2, were also observed in Dusp14 knockout mice in aortic banding-induced hypertrophic heart tissues (Wang X. et al., 2018). The phosphorylation of ERK and JNK but not p38 increased in dominant-negative Dusp14-transduced primary T cells (Galvao et al., 2018). DUSP14 negatively regulated ERK1/2 pathway in T-cell proliferation (Sun et al., 2021). Our transcriptomic sequencing analysis showed that genes mainly regulated by *dusp14* dephosphorylation belong to the JNK and p38 signaling pathways in *dusp14*-MO zebrafish. Additionally, p38 signaling, *mapk12b* gene, increased mostly in morpholino-induced *dusp14*-deficient zebrafish. In addition, p38 inhibitor significantly inhibited the effect of *dusp14*-MO on the proliferation of supporting cells and the decrease of hair cell in zebrafish. However, further experiments are needed to confirm the regulation of *mapk12b* gene on zebrafish supporting cells. Whether JNK and ERK are involved in regulating supporting cell development and how important their roles are also needed to be further investigated.

Numerous studies in non-mammalian species since the initial discoveries have elucidated that inner ear hair cell regeneration happens by two methods: supporting cells directly transdifferentiate into hair cells, supporting cells mitosis and then one of the daughter cells transdifferentiate into hair cells (Burns and Corwin, 2013; Takeda et al., 2018). However, our understanding of the molecular mechanisms that regulates supporting cell behavior is limited. Our results indicate that DUSP14 may be an important regulator of supporting cell development. Furthermore, *DUSP14* is also reported to be involved in the hepatocyte proliferation and regeneration (Wang X. et al., 2018). In the immune system, DUSP14 negatively regulates β cell proliferation and apoptosis of cancer cells (Klinger et al., 2008).

Here, we explore the molecular mechanisms that lead to hair cell regeneration in zebrafish by exploiting their ability to regenerate hair cells. To our knowledge, this study reported the important effects of *dusp14* gene on the fate of the hair cell in zebrafish for the first time, mainly through regulating proliferation of supporting cells, providing a new insight into understand the mechanism of supporting cell development and a new potential target for the treatment of hearing loss.

DATA AVAILABILITY STATEMENT

The data presented in this study are deposited in the China National GeneBank DataBase (CNGBdb), accession number: CNP0002521 (https://db.cngb.org/search/project/CNP0002521/).

ETHICS STATEMENT

The animal study was reviewed and approved by Animal Care and Use Committee of Nantong University.

AUTHOR CONTRIBUTIONS

DL and FC supervised and designed this project. GW, CC, XZ, JS, and FQ wrote the manuscript. GW, XZ, CG, and FQ analyzed the data. XZ, MX, CW, and QG performed the experiments. All authors contributed to the article and approved the submitted version.

FUNDING

This study was supported by grants from the National Natural Science Foundation of China (82001417) and Natural Science Foundation of Jiangsu Province (BK20190920, BK20180048, and BK20200966).

SUPPLEMENTARY MATERIAL

The Supplementary Material for this article can be found online at: https://www.frontiersin.org/articles/10.3389/fncel.2022.840143/full#supplementary-material

Supplementary Figure 1 | The design of *Dusp14*-Mo sequence and verification of the knockdown efficiency. **(A)** The design of *dusp14* morphant sequence. **(B)** Representative images of Dusp14^{+} cells of neuromasts in the posterior lateral line of the control and *dusp14* morphants. **(B′)** The statistical results of panel **(B)**. **(C)** *Left*: the result of *ef1α* RT-PCR of wild-type zebrafish and *dusp14* morphants. *Right*: the result of *dusp14* RT-PCR of wild-type zebrafish and *dusp14* morphants. **(C′)** The statistical results of panel **(C)**.

Supplementary Figure 2 | *Dusp14* knockout leads to a decrease in zebrafish hair cell. **(A)** The design of *dusp14* guide-RNA. **(B)** Mutations occurred in the target site of the *dusp14* gene in mutant zebrafish compared to the wild-type fish. **(C)** Confocal imaging analysis of the numbers of hair cell clusters and hair cells in the lateral line system of wild-type and *dusp14* mutants at 72 hpf. **(C′)** The statistical analysis of panel **(C)**. Experimental embryos were sampled at 72 hpf ($n > 7$). Each bar represents the mean ± SEM. Values with *, **, ***, and **** above the bars are significantly different ($p < 0.05$, $p < 0.01$, $p < 0.001$, and $p < 0.0001$, respectively).

Supplementary Figure 3 | *Dusp14* knockdown did not induce zebrafish hair cell apoptosis. **(A)** DAPI and cleaved TUNEL staining for the L3 hair cell clusters in the posterior lateral line of the control zebrafish and *dusp14* morphants. **(B)** DAPI and cleaved caspase-3 staining for the L3 hair cell clusters in the posterior lateral line of the control zebrafish and *dusp14* morphants.

Supplementary Figure 4 | qRT-PCR of different expression gene in the control and *dusp14* morphants. **(A)** Twelve DEGs were detected in transcriptome sequencing. **(B)** The results of 12 DEGs caused by *dusp14* morphants at 72 hpf ($n = 3$). Each bar represents the mean ± SEM. Values with *, **, ***, and **** above the bars are significantly different ($p < 0.05$, $p < 0.01$, $p < 0.001$, and $p < 0.0001$, respectively).

Supplementary Table 1 | Transcriptomic profiling of *dusp14*-morphant and wild-type zebrafish. The number of reads and percentage mapped to the coding genes of zebrafish genome is calculated. The 90% mapped rate presents the proportion of reads matched to the coding genes of zebrafish genome in the totally valid reads.

Supplementary Table 2 | Differentially expressed genes obtained based on transcriptome sequencing.

Supplementary Table 3 | Primer information.

REFERENCES

An, N., Bassil, K., Al Jowf, G. I., Steinbusch, H. W. M., Rothermel, M., de Nijs, L., et al. (2021). Dual-specificity phosphatases in mental and neurological disorders. *Prog. Neurobiol.* 198:101906. doi: 10.1016/j.pneurobio.2020.101906

Burns, J. C., and Corwin, J. T. (2013). A historical to present-day account of efforts to answer the question:"what puts the brakes on mammalian hair cell regeneration?". *Hear. Res.* 297, 52–67. doi: 10.1016/j.heares.2013.01.005

Caunt, C. J., and Keyse, S. M. (2013). Dual-specificity MAP kinase phosphatases (MKPs) Shaping the outcome of MAP kinase signalling. *FEBS J.* 280, 489–504. doi: 10.1111/j.1742-4658.2012.08716.x

Furness, D. N. (2015). Molecular basis of hair cell loss. *Cell Tissue Res.* 361, 387–399. doi: 10.1007/s00441-015-2113-z

Galvao, J., Iwao, K., Apara, A., Wang, Y., Ashouri, M., Shah, T. N., et al. (2018). The Krüppel-like factor gene target Dusp14 regulates axon growth and regeneration. *Invest. Ophthalmol. Vis. Sci.* 59, 2736–2747. doi: 10.1167/iovs.17-23319

Gong, J., Wang, X., Zhu, C., Dong, X., Zhang, Q., Wang, X., et al. (2017). Insm1a regulates motor neuron development in zebrafish. *Front. Mol. Neurosci.* 10:274. doi: 10.3389/fnmol.2017.00274

Grant, K. A., Raible, D. W., and Piotrowski, T. (2005). Regulation of latent sensory hair cell precursors by glia in the zebrafish lateral line. *Neuron* 45, 69–80. doi: 10.1016/j.neuron.2004.12.020

Huang, C.-Y., and Tan, T.-H. (2012). DUSPs, to MAP kinases and beyond. *Cell Biosci.* 2:24. doi: 10.1186/2045-3701-2-24

Kelley, M. W. (2006). Regulation of cell fate in the sensory epithelia of the inner ear. *Nat. Rev. Neurosci.* 7, 837–849. doi: 10.1038/nrn1987

Kim, D., Pertea, G., Trapnell, C., Pimentel, H., Kelley, R., and Salzberg, S. L. (2013). TopHat2: accurate alignment of transcriptomes in the presence of insertions, deletions and gene fusions. *Genome Biol.* 14:R36. doi: 10.1186/gb-2013-14-4-r36

Kimmel, C. B., Ballard, W. W., Kimmel, S. R., Ullmann, B., and Schilling, T. F. (1995). Stages of embryonic development of the zebrafish. *Dev. Dyn.* 203, 253–310. doi: 10.1002/aja.1002030302

Klinger, S., Poussin, C., Debril, M.-B., Dolci, W., Halban, P. A., and Thorens, B. (2008). Increasing GLP-1–induced β-cell proliferation by silencing the negative regulators of signaling cAMP response element modulator-α and DUSP14. *Diabetes* 57, 584–593. doi: 10.2337/db07-1414

Kniss, J. S., Jiang, L., and Piotrowski, T. (2016). Insights into sensory hair cell regeneration from the zebrafish lateral line. *Curr. Opin. Genet. Dev.* 40, 32–40. doi: 10.1016/j.gde.2016.05.012

Li, C.-Y., Zhou, Q., Yang, L.-C., Chen, Y.-H., Hou, J.-W., Guo, K., et al. (2016). Dual-specificity phosphatase 14 protects the heart from aortic banding-induced cardiac hypertrophy and dysfunction through inactivation of TAK1-P38MAPK/-JNK1/2 signaling pathway. *Basic Res. Cardiol.* 111:19. doi: 10.1007/s00395-016-0536-7

Lin, B., Xu, J., Feng, D.-G., Wang, F., Wang, J.-X., and Zhao, H. (2018). DUSP14 knockout accelerates cardiac ischemia reperfusion (IR) injury through activating NF-κB and MAPKs signaling pathways modulated by ROS generation. *Biochem. Biophys. Res. Commun.* 501, 24–32. doi: 10.1016/j.bbrc.2018.04.101

Livak, K. J., and Schmittgen, T. D. (2001). Analysis of relative gene expression data using real-time quantitative PCR and the 2- ΔΔCT method. *Methods* 25, 402–408. doi: 10.1006/meth.2001.1262

Lountos, G. T., Tropea, J. E., Cherry, S., and Waugh, D. S. (2009). Overproduction, purification and structure determination of human dual-specificity phosphatase 14. *Acta Crystallogr. D Biol. Crystallogr.* 65(Pt 10), 1013–1020. doi: 10.1107/s0907444909023762

Marti, F., Krause, A., Post, N. H., Lyddane, C., Dupont, B., Sadelain, M., et al. (2001). Negative-feedback regulation of CD28 costimulation by a novel mitogen-activated protein kinase phosphatase. *MKP6. J. Immunol.* 166, 197–206. doi: 10.4049/jimmunol.166.1.197

Morton, N. (1991). Genetic epidemiology of hearing impairment. *Ann. N. Y. Acad. Sci.* 630, 16–31. doi: 10.1111/j.1749-6632.1991.tb19572.x

Patterson, K. I., Brummer, T., O'Brien, P. M., and Daly, R. J. (2009a). Dual-specificity phosphatases: critical regulators with diverse cellular targets. *Biochem. J.* 418, 475–489. doi: 10.1042/bj20082234

Patterson, K. I., Brummer, T., O'brien, P. M., and Daly, R. J. (2009b). Dual-specificity phosphatases: critical regulators with diverse cellular targets. *Biochem. J.* 418, 475–489. doi: 10.1042/BJ20082234

Ríos, P., Nunes-Xavier, C. E., Tabernero, L., Köhn, M., and Pulido, R. (2014). Dual-specificity phosphatases as molecular targets for inhibition in human disease. *Antioxid. Redox Signal.* 20, 2251–2273. doi: 10.1089/ars.2013.5709

Rubel, E. W., Furrer, S. A., and Stone, J. S. (2013). A brief history of hair cell regeneration research and speculations on the future. *Hear. Res.* 297, 42–51. doi: 10.1016/j.heares.2012.12.014

Schmittgen, T. D., and Livak, K. J. (2008). Analyzing real-time PCR data by the comparative CT method. *Nat. Protoc.* 3, 1101–1108. doi: 10.1038/nprot.2008.73

Sun, F., Yue, T.-T., Yang, C.-L., Wang, F.-X., Luo, J.-H., Rong, S.-J., et al. (2021). The MAPK dual specific phosphatase (DUSP) proteins: a versatile wrestler in T cell functionality. *Int. Immunopharmacol.* 98:107906. doi: 10.1016/j.intimp.2021.107906

Sun, X. (2021). Occupational noise exposure and worker's health in China. *China CDC Weekly* 3:375. doi: 10.46234/ccdcw2021.102

Takeda, H., Dondzillo, A., Randall, J. A., and Gubbels, S. P. (2018). Challenges in cell-based therapies for the treatment of hearing loss. *Trends Neurosci.* 41, 823–837. doi: 10.1016/j.tins.2018.06.008

Thomas, E. D., and Raible, D. W. (2019). Distinct progenitor populations mediate regeneration in the zebrafish lateral line. *Elife* 8:e43736. doi: 10.7554/eLife.43736

Turjanski, A. G., Vaqué, J. P., and Gutkind, J. S. (2007). MAP kinases and the control of nuclear events. *Oncogene* 26, 3240–3253. doi: 10.1038/sj.onc.1210415

van den Bos, R., Mes, W., Galligani, P., Heil, A., Zethof, J., Flik, G., et al. (2017). Further characterisation of differences between TL and AB zebrafish (*Danio rerio*): gene expression, physiology and behaviour at day 5 of the larval stage. *PLoS One* 12:e0175420.

Vlajkovic, S. M., and Thorne, P. R. (2021). *Molecular Mechanisms of Sensorineural Hearing Loss and Development of Inner Ear Therapeutics*. Basel: Multidisciplinary Digital Publishing Institute. doi: 10.3390/ijms22115647

Wada, T., and Penninger, J. M. (2004). Mitogen-activated protein kinases in apoptosis regulation. *Oncogene* 23, 2838–2849. doi: 10.1038/sj.onc.1207556

Wang, S., Yan, Z. Z., Yang, X., An, S., Zhang, K., Qi, Y., et al. (2018). Hepatocyte DUSP14 maintains metabolic homeostasis and suppresses inflammation in the liver. *Hepatology* 67, 1320–1338. doi: 10.1002/hep.29616

Wang, X., Mao, W., Fang, C., Tian, S., Zhu, X., Yang, L., et al. (2018). Dusp14 protects against hepatic ischaemia–reperfusion injury via Tak1 suppression. *J. Hepatol.* 68, 118–129.

Westerfield, M. (1995). *The Zebrafish Book: A Guide for the Laboratory Use of Zebrafish (Brachydanio rerio)*. Eugene: University of Oregon press.

Whitfield, T. T. (2005). Lateral line: precocious phenotypes and planar polarity. *Curr. Biol.* 15, R67–R70.

Williams, J. A., and Holder, N. (2000). Cell turnover in neuromasts of zebrafish larvae. *Hear. Res.* 143, 171–181. doi: 10.1016/s0378-5955(00)00039-3

Yang, Q., Sun, P., Chen, S., Li, H., and Chen, F. (2017). Behavioral methods for the functional assessment of hair cells in zebrafish. *Front. Med.* 11:178–190. doi: 10.1007/s11684-017-0507-x

Conflict of Interest: The authors declare that the research was conducted in the absence of any commercial or financial relationships that could be construed as a potential conflict of interest.

Publisher's Note: All claims expressed in this article are solely those of the authors and do not necessarily represent those of their affiliated organizations, or those of the publisher, the editors and the reviewers. Any product that may be evaluated in this article, or claim that may be made by its manufacturer, is not guaranteed or endorsed by the publisher.

frontiers | Frontiers in Cellular Neuroscience

ORIGINAL RESEARCH
published: 06 April 2022
doi: 10.3389/fncel.2022.856124

The Risk of Hearing Impairment From Ambient Air Pollution and the Moderating Effect of a Healthy Diet: Findings From the United Kingdom Biobank

Lanlai Yuan[1†], Dankang Li[2,3†], Yaohua Tian[2,3] and Yu Sun[1]*

[1] Department of Otorhinolaryngology, Union Hospital, Tongji Medical College, Huazhong University of Science and Technology, Wuhan, China, [2] Department of Maternal and Child Health, School of Public Health, Tongji Medical College, Huazhong University of Science and Technology, Wuhan, China, [3] Ministry of Education Key Laboratory of Environment and Health, State Key Laboratory of Environmental Health (Incubating), School of Public Health, Tongji Medical College, Huazhong University of Science and Technology, Wuhan, China

The link between hearing impairment and air pollution has not been established, and the moderating effect of a healthy diet has never been investigated before. The purpose of this study was to investigate the association between air pollution and hearing impairment in British adults aged 37–73 years, and whether the association was modified by a healthy diet. We performed a cross-sectional population-based study with 158,811 participants who provided data from United Kingdom Biobank. A multivariate logistic regression model was used to investigate the link between air pollution and hearing impairment. Subgroup and effect modification analyses were carried out according to healthy diet scores, gender, and age. In the fully adjusted model, we found that exposure to PM_{10}, NO_X, and NO_2 was associated with hearing impairment [PM_{10}: odds ratio (OR) = 1.15, 95% confidence interval (95% CI) 1.02–1.30, P = 0.023; NO_X: OR = 1.02, 95% CI 1.00–1.03, P = 0.040; NO_2: OR = 1.03, 95% CI 1.01–1.06, P = 0.044], while $PM_{2.5}$ and $PM_{2.5}$ absorbance did not show similar associations. We discovered an interactive effect of age and air pollution on hearing impairment, but a healthy diet did not. The findings suggested that exposure to PM_{10}, NO_X and NO_2 was linked to hearing impairment in British adults, whereas $PM_{2.5}$ and $PM_{2.5}$ absorbance did not show similar associations. These may help researchers focus more on the impact of air pollution on hearing impairment and provide a basis for developing effective prevention strategies.

Keywords: hearing impairment, air pollution, digit triplet test (DTT), United Kingdom Biobank (UKB), healthy diet

OPEN ACCESS

Edited by:
Hai Huang,
Tulane University, United States

Reviewed by:
Zhiqiang Yan,
Fudan University, China
Hongzhe Li,
VA Loma Linda Healthcare System, United States

***Correspondence:**
Yu Sun
sunyu@hust.edu.cn

[†]These authors share first authorship

Specialty section:
This article was submitted to Cellular Neuropathology, a section of the journal Frontiers in Cellular Neuroscience

Received: *16 January 2022*
Accepted: *24 February 2022*
Published: *06 April 2022*

Citation:
Yuan L, Li D, Tian Y and Sun Y (2022) The Risk of Hearing Impairment From Ambient Air Pollution and the Moderating Effect of a Healthy Diet: Findings From the United Kingdom Biobank. Front. Cell. Neurosci. 16:856124. doi: 10.3389/fncel.2022.856124

INTRODUCTION

Hearing impairment is one of the most common age-related chronic health problems (Vos et al., 2016). The rate of clinically significant hearing impairment is doubling approximately every decade (Lin et al., 2011; Goman and Lin, 2016). Hearing impairment has been reported to be the second most prevalent disorder and the dominant cause of years lived with disability among global non-infectious diseases (Vos et al., 2016). In contrast with normal hearing adults of the same age, those with hearing impairment have a greater incidence of hospitalization (Genther et al., 2013),

death (Contrera et al., 2015), falls (Lin and Ferrucci, 2012), cardiovascular disorders (McKee et al., 2018), depression (Li et al., 2014), and dementia (Lin et al., 2013). Consequently, hearing impairment causes a huge burden on the emotional and physical wellbeing of individuals (Dawes et al., 2014b). It is predicted that one-fifth of the population of the United Kingdom will suffer from hearing impairment by 2035 (Taylor et al., 2020). Accordingly, the key is to prevent hearing impairment. Hearing impairment is caused by a combination of hereditary and environmental factors (Cunningham and Tucci, 2017). The identification of modifiable risk factors is critical to provide the basis for preventive strategies.

Global trends in urbanization and industrialization have led to a growing problem of air pollution (Landrigan, 2017), which has become the main public health issue across the world (Brunekreef and Holgate, 2002). Of note, growing evidence demonstrates that air pollution exposure is not only connected with respiratory disorders, such as lung cancer (Xing et al., 2019), but also with cardiovascular diseases (Lelieveld et al., 2019; Hayes et al., 2020), inflammatory diseases (Chang et al., 2016), diabetes (Strak et al., 2017), and neurodegenerative diseases (Chen et al., 2017). Besides, the main environmental risk factor for human death is air pollution (Gordon et al., 2014). Lately, there have been reports that air pollution may impact hearing health, but available data is limited. A recent study (Tsai et al., 2020) found that participants exposed to fine particulate matter ($PM_{2.5}$: particulate matter $\leq$ 2.5 μm in diameter) and nitrogen dioxide (NO_2) had a substantially increased risk of sudden sensorineural hearing loss (SSNHL). Another study (Chang et al., 2020) showed that increased concentrations of NO_2 were linked to a higher risk of sensorineural hearing loss, while in a nested case-control study (Choi et al., 2019), SSNHL was associated with NO_2 exposure, but particulate matter with a diameter of 10 μm or less (PM_{10}) was not associated with SSNHL. Similarly, another study (Lee et al., 2019) also found no association between PM_{10} and number of SSNHL patient. Although these studies explored the association of air pollution with sensorineural hearing loss, the results remained controversial.

A healthy diet might preserve hearing (Spankovich and Le Prell, 2013; Curhan et al., 2018, 2020), as described by their role in preventing chronic illnesses (Yevenes-Briones et al., 2021). A healthy diet includes multiple components that support antioxidant function and protect against free radical damage (Curhan et al., 2020), thereby regulating oxidative stress and delaying mitochondrial dysfunction (Yevenes-Briones et al., 2021). In addition, a healthy diet might be beneficial to hearing impairment by protecting microvascular and macrovascular damage to cochlear blood flow (Appel et al., 2006; Fung et al., 2008), providing the essential nutrients for an adequate cochlear blood supply (Yevenes-Briones et al., 2021), and reducing inflammation (Neale et al., 2016). According to previous research, dietary patterns could modify the relationship between air pollution and health-related outcomes, such as cardiovascular disease mortality risk (Lim et al., 2019) and cognitive function (Zhu et al., 2022). However, the moderating effect of a healthy diet on the link between hearing impairment and air pollution has not been investigated before. Therefore, in this cross-sectional study, we aimed to explore the link between air pollution and hearing impairment and to analyze whether a healthy diet has moderating effects on this link.

MATERIALS AND METHODS

Study Subjects

The United Kingdom Biobank is an international and accessible data resource[1] containing data on more than half a million people aged from 37 to 73 years (99.5% were between 40 and 69 years) in England, Scotland, and Wales (Collins, 2012). Adults living within a 25-mile radius of one of 22 Biobank Assessment Centers in the United Kingdom were invited by email to join the United Kingdom Biobank between 2006 and 2010, achieving a response rate of approximately 5.5% (Sudlow et al., 2015). Participants completed a computer touch screen questionnaire (which included questions on topics such as population, health, lifestyle, environment as well as medical history, etc.) and underwent physical measurements, including a hearing test. Written informed consent was signed by all the participants. The research was carried out with the general approval of the National Health Service and the National Research Ethics Service. The subjects of the current study were all those participants for whom data on both air pollution measures and hearing test results were available.

Hearing Test

The speech-in-noise hearing test (i.e., digit triplet test, DTT) of the United Kingdom Biobank provided participants with 15 groups of English monosyllabic numbers to evaluate the listening thresholds (i.e., signal-to-noise ratio) at different sound levels.[2] Each ear was examined separately, in the order that the participants were allocated at random. Participants first wore circumaural headphones and selected the most comfortable volume. Then, they started the speech-in-noise hearing test to identify and type the three numbers they had heard by touching the screen interface. The noise level of the subsequent triple would increase if the triplet was correctly recognized; otherwise, it would reduce. The speech reception threshold (SRT) was defined as the signal-to-noise ratio of correctly understanding half of the presented speech. The SRT ranged from −12 to +8 dB, with a lower score representing better performance. Based on the cutoff point established by Dawes et al. (2014b), the better performance ear was chosen for this study, and participants were divided into normal (SRT $<$ −5.5 dB) and hearing impairment (SRT $\geq$ −5.5 dB) groups.

The DTT shows a very good correlation with the pure tone hearing test (r = 0.77) (Jansen et al., 2010), so it can be considered as a measure of hearing impairment (Dawes et al., 2014b). There are some advantages to the DTT, for example, there is no need for a sound booth and the test can be delivered *via* the internet (Moore et al., 2014). The most common hearing complaint is difficulty in hearing over background noise (Pienkowski, 2017), so the speech-in-noise hearing test used to evaluate hearing

[1] www.UKbiobank.ac.UK

[2] https://biobank.ctsu.ox.ac.UK/crystal/label.cgi?id=100049

function represents an ecologically effective as well as objective hearing indicator (Couth et al., 2019).

Measures of Air Pollution

The air pollution data recorded in the United Kingdom Biobank were from the Small Area Health Statistics Unit,[3] a part of the BioShaRE-EU Environmental Determinants of Health Project.[4] The Land Use Regression model was applied to assess air pollution in 2010 by modeling at each residential address of the participants, which was developed as part of the European Study of Cohorts for Air Pollution Effects.[5] The Land Use Regression model used to calculate the spatial distribution of air pollutants was based on geographic predictors such as traffic, land use, and topography in the geographical information system. In this study, the air pollutants assessed were $PM_{2.5}$, PM_{10}, $PM_{2.5}$ absorbance, NO_X, and NO_2, of which all were annual average concentrations in $\mu g/m^3$. More details about the air pollution data used in the United Kingdom Biobank are available elsewhere.[6]

Assessment of Other Variables

Age, gender, ethnicity, educational background, employment, smoking status, and alcohol intake were utilized as baseline data. The ethnic background of participants was divided into six categories: White, Black, Asian, Chinese, Mixed, and other. The educational background was divided into six categories: higher national diploma (HND), national vocational qualification (NVQ), higher national certificate (HNC), or equivalent; A levels or AS levels (including the higher school certificate), or equivalent; O levels (including the school certificate), general certificate of secondary educations (GCSEs), or equivalent; certificate of secondary educations (CSEs), or equivalent; college or university degree; and other professional qualification. Employment status was divided into seven categories: retired; unable to work because of sickness or disability; looking after home and/or family; unemployed; in paid employment or self-employed; student (full-time or part-time); or doing unpaid or voluntary work. Smoking status (Dawes et al., 2014a) was divided into three categories: never-smokers, current and former smokers. Alcohol consumption frequency was divided into five categories: daily or almost daily; three or four times a week; once or twice a week; occasional drinking; and never. Body mass index (BMI) was categorized as obese (BMI $\geq$ 30), overweight (25 $\leq$ BMI $<$ 30), normal weight (18.5 $\leq$ BMI $<$ 25), and underweight (BMI $<$ 18.5). Evaluation of physical activity was conducted through the questions in the International Physical Activity Questionnaire, which graded activity into three degrees: low, moderate, and high.[7] A questionnaire[8] containing the usual dietary intake was completed by United Kingdom Biobank participants during the baseline assessment. The intake of fruits (fresh fruit intake and dried fruit intake), vegetables (cooked vegetable intake and salad/raw vegetable intake), fish (oily fish intake and non-oily fish intake), processed meat and unprocessed red meat (beef intake, lamb/mutton intake, and pork intake) from the United Kingdom Biobank food intake questionnaire was used to calculate the health diet scores (Wang et al., 2021): fruit intake $\geq$ three pieces per day, vegetable intake $\geq$ four tablespoons per day, fish intake $\geq$ twice per week, processed meat intake $\leq$ twice per week, unprocessed red meat intake $\leq$ twice per week. Each favorable dietary factor gave a point, so the healthy diet scores were 0–5. The serum concentrations of glycosylated hemoglobin and total cholesterol were regarded as continuous variables. Vascular problems included angina, heart attack, stroke, and high blood pressure.

Data Analysis

All analyses were performed using R version 4.0.2. The data are summarized descriptively. Continuous variables are represented as mean (standard deviation) and comparison between the two groups was performed by independent sample *t* test. The classification variables are represented as percentages (%) and the rate was compared by χ^2 test. The link between air pollution and hearing impairment was investigated using a multivariate logistic regression model with and without adjusting for other variables. Model 1 was unadjusted, Model 2 was adjusted for age and gender, and Model 3 was further adjusted for race, educational level, employment, smoking status and alcohol consumption frequency, BMI, physical activity, glycosylated hemoglobin, total cholesterol, and vascular diseases (heart attack, stroke, angina, and hypertension). Moreover, we evaluated the association between subgroups stratified by healthy diet scores (low: 0–2, and high: 3–5), gender (female and male) and age ($\leq$50, 51–60, and $>$60). The Wald test was used to test interactions among subgroups. $P < 0.05$ (two-sided test) was considered statistically significant.

RESULTS

In total, 158,811 subjects were enrolled in this study, including 18,881 (11.9%) with hearing impairment and 139,930 (88.1%) with normal hearing, 54.5% were female (n = 86,516), 91.7% were white (n = 145,633), with the mean (standard deviation) age of 56.68 (8.15) years. The distribution of baseline characteristics and air pollution in the two groups is shown in **Table 1**. Except for physical activity, other variables were significantly distributed in the two groups ($P < 0.05$). In comparison to the group of people with normal hearing, the subjects in the hearing impairment group were older on average, non-whites. In addition, they were more likely to be obese and to have cardiovascular problems. Furthermore, the hearing impairment group was exposed to higher mean annual concentrations of air pollutants than the normal hearing group (**Table 1**).

Table 2 shows the risks of several air pollutants and hearing impairment. Model 1 (without adjustment for any confounders) showed significant associations between air pollutants and hearing impairment ($P < 0.001$) [$PM_{2.5}$: odds ratio (OR) = 2.03, 95% confidence interval (95% CI) 1.73–2.40; PM_{10}: OR = 1.64, 95% CI 1.51–1.78; $PM_{2.5}$ absorbance: OR = 1.48, 95% CI 1.40–1.56; NO_X: OR = 1.06, 95% CI 1.05–1.07; NO_2: OR = 1.17,

[3]http://www.sahsu.org/

[4]http://www.bioshare.eu/

[5]http://www.escapeproject.eu/

[6]https://biobank.ndph.ox.ac.uk/showcase/ukb/docs/EnviroExposEst.pdf

[7]https://biobank.ndph.ox.ac.uk/showcase/ukb/docs/ipaq_analysis.pdf

[8]https://biobank.ndph.ox.ac.uk/showcase/label.cgi?id=100052

TABLE 1 | Characteristics of participants (*N* = 158,811).

	Normal hearing	Hearing impairment	*P*
N	139,930	18,881	
Age (years), mean (SD)	56.21 (8.13)	60.13 (7.40)	<0.001
Gender (%)			0.004
Female	76,414 (54.6)	10,102 (53.5)	
Male	63,516 (45.4)	8,779 (46.5)	
Race (%)			<0.001
White ethnicity	129,996 (93.2)	15,637 (83.3)	
Mixed ethnicity	1,053 (0.8)	137 (0.7)	
Asian ethnicity	3,541 (2.5)	1,328 (7.1)	
Black ethnicity	3,019 (2.2)	1,026 (5.5)	
Chinese ethnicity	462 (0.3)	123 (0.7)	
Other ethnicity	1,336 (1.0)	523 (2.8)	
Education (%)			<0.001
Other professional qualification	7,113 (5.9)	1,191 (8.6)	
College or university degree	48,983 (40.7)	5,098 (36.8)	
O level/GCSEs or equivalent	30,497 (25.4)	3,580 (25.9)	
CSEs or equivalent	8,280 (6.9)	845 (6.1)	
A/AS levels or equivalent	16,528 (13.7)	1,670 (12.1)	
NVQ or HND or HNC or equivalent	8,876 (7.4)	1,465 (10.6)	
Employment (%)			<0.001
Inpaid employment or self-employed	81,816 (59.0)	7,467 (40.1)	
Retired	44,969 (32.4)	9,136 (49.1)	
Looking after home and/or family	4,195 (3.0)	474 (2.5)	
Unable to work because of sickness or disability	3,575 (2.6)	883 (4.7)	
Unemployed	2,996 (2.2)	478 (2.6)	
Doing unpaid or voluntary work	678 (0.5)	115 (0.6)	
Full-time or part-time student	384 (0.3)	66 (0.4)	
BMI (%), kg/m^2			<0.001
Underweight	721 (0.5)	121 (0.6)	
Normal weight	46,225 (33.2)	5,590 (30.0)	
Overweight	58,610 (42.1)	7,817 (41.9)	
Obesity	33,548 (24.1)	5,127 (27.5)	
Smoke (%)			<0.001
Never	77,310 (55.4)	10,140 (54.0)	
Previous	48,353 (34.7)	6,572 (35.0)	
Current	13,839 (9.9)	2,054 (10.9)	
Drink frequency (%)			<0.001
Daily or almost daily	29,132 (20.8)	3,327 (17.7)	
Three or four times a week	32,246 (23.1)	3,443 (18.3)	
Once or twice a week	35,588 (25.5)	4,367 (23.2)	
Occasional drinkers	32,275 (23.1)	5,095 (27.0)	
Never	10,551 (7.5)	2,609 (13.8)	
Physical activity (%)			0.061
Low	20,316 (17.6)	2,658 (18.1)	
Moderate	46,945 (40.7)	5,839 (39.7)	
High	48,013 (41.7)	6,198 (42.2)	
HbA1c, mean (SD), mmol/mol	36.02 (6.50)	37.55 (8.10)	<0.001
TC, mean (SD), mmol/L	5.71 (1.14)	5.60 (1.20)	<0.001
Vascular problems (%)			<0.001
None	10,0638 (73.8)	11,826 (64.9)	
Hypertension	29,376 (21.5)	4,868 (26.7)	
Heart attack, angina, or stroke	3,184 (2.3)	703 (3.9)	
High blood pressure and heart attack, angina, or stroke	3,235 (2.4)	813 (4.5)	

(Continued)

TABLE 1 | Continued

	Normal	Hearing impairment	*P*
Air pollution			
$PM_{2.5}$, mean (SD), $\mu g/m^3$	9.88 (0.91)	9.94 (0.95)	<0.001
PM_{10}, mean (SD), $\mu g/m^3$	16.28 (1.82)	16.45 (1.85)	<0.001
$PM_{2.5}$ absorbance, mean (SD), per-meter	1.21 (0.27)	1.24 (0.29)	<0.001
NO_X, mean (SD), $\mu g/m^3$	43.52 (14.44)	44.92 (15.83)	<0.001
NO_2, mean (SD), $\mu g/m^3$	26.88 (7.21)	27.72 (7.70)	<0.001

Abbreviations: N, number; SD, standard deviation; GCSEs, general certificate of secondary educations; CSEs, certificate of secondary educations; NVQ, national vocational qualification; HND, higher national diploma; HNC, higher national certificate; BMI, body mass index; HbA1c, glycosylated hemoglobin; TC, total cholesterol; PM, particulate matter; NO_2, nitrogen dioxides; NO_X, nitrogen oxides.

TABLE 2 | Association of air pollution and hearing impairment.

	Model 1		Model 2		Model 3	
	OR (95% CI)	*P*	OR (95% CI)	*P*	OR (95% CI)	*P*
$PM_{2.5}$	2.03 (1.73–2.40)	<0.001	3.02 (2.56–3.57)	<0.001	1.01 (0.79–1.29)	0.970
PM_{10}	1.64 (1.51–1.78)	<0.001	1.82 (1.67–1.97)	<0.001	1.15 (1.02–1.30)	0.023
$PM_{2.5}$ absorbance	1.48 (1.40–1.56)	<0.001	1.67 (1.59–1.77)	<0.001	1.08 (0.99–1.18)	0.063
NO_X	1.06 (1.05–1.07)	<0.001	1.09 (1.08–1.10)	<0.001	1.02 (1.001–1.03)	0.040
NO_2	1.17 (1.14–1.19)	<0.001	1.24 (1.21–1.26)	<0.001	1.03 (1.01–1.06)	0.044

Abbreviations: OR, odds ratio; CI, confidence interval; PM, particulate matter; NO_2, nitrogen dioxides; NO_X, nitrogen oxides.
Model 1: unadjusted.
Model 2: adjusted for age and gender.
Model 3: adjusted for age, gender, race, education, employment, smoking, drink frequency, body mass index, physical activity, glycosylated hemoglobin, total cholesterol, and vascular disease (heart attack, stroke, angina, and hypertension).

95% CI 1.41–1.19]. After adjusting for age and gender, Model 2 showed that air pollutants were still significantly associated with hearing impairment ($P < 0.001$), and all OR values were larger than Model 1 ($PM_{2.5}$: OR = 3.02, 95% CI 2.56–3.57; PM_{10}: OR = 1.82, 95% CI 1.67–1.97; $PM_{2.5}$ absorbance: OR = 1.67, 95% CI 1.59–1.77; NO_X: OR = 1.09, 95% CI 1.08–1.10; NO_2: OR = 1.24, 95% CI 1.21–1.26). Except for $PM_{2.5}$ and $PM_{2.5}$ absorbance, which showed no significant associations with hearing impairment ($P = 0.970$ and $P = 0.063$, respectively), we observed that the associations between the other pollutants and hearing impairment remained in Model 3 after further adjusting for other confounders on the basis of Model 2 (PM_{10}: OR = 1.15, 95% CI 1.02–1.30, $P = 0.023$; NOx: OR = 1.02, 95% CI 1.00–1.03, $P = 0.040$; NO_2: OR = 1.03, 95% CI 1.01–1.06, $P = 0.044$), even though the estimates were lower than those in Models 1 and 2.

Table 3 shows the associations between several air pollutants and hearing impairment, stratified by healthy diet scores. In this study, no significant associations and moderating effects were observed. After stratification by age (**Table 4**), we found that PM_{10}, $PM_{2.5}$ absorbance, NO_X, and NO_2 were associated with hearing impairment in participants up to and including 50 years of age (PM_{10}: OR = 1.62, 95% CI 1.20–2.18, $P = 0.002$; $PM_{2.5}$ absorbance: OR = 1.32, 95% CI 1.08–1.61, $P = 0.006$; NO_X: OR = 1.04, 95% CI 1.01–1.08, $P = 0.014$; NO_2: OR = 1.09, 95% CI 1.01–1.17, $P = 0.031$). In participants aged 51 to 60 years and above 60, there was no connection between air pollution and hearing impairment. Additionally, there was a statistically significant interaction between age and air pollution with hearing impairment ($P < 0.05$). Further, after stratifying by gender (**Table 5**), we found that NO_X and NO_2 were correlated with hearing impairment in men.

DISCUSSION

In this cross-sectional study, we investigated the association between hearing impairment and air pollution (comprising $PM_{2.5}$, PM_{10}, $PM_{2.5}$ absorbance, NO_X, and NO_2) using United Kingdom Biobank data. We found that exposure to PM_{10}, NO_X, and NO_2 was linked to hearing impairment after adjusting for confounding factors, while $PM_{2.5}$ and $PM_{2.5}$ absorbance showed no similar correlations. Furthermore, there was no modification of these associations by a healthy diet. Regarding age, interaction effects were observed.

The relationship between air pollution and hearing impairment has not been fully established yet. Several studies indicated that exposure to NO_2 could be related to hearing problems. Chang et al. (2020) found that people exposed to moderate (hazard ratio, HR = 1.40, 95% CI 1.27–1.54) and high levels of NO_2 (HR = 1.63, 95% CI 1.48–1.81) were at higher risk of developing sensorineural hearing loss than those exposed to the low level. The results of Tsai et al. (2020) were similar, finding a significantly increased risk of SSNHL in those exposed to high concentrations of NO_2 (adjusted HR = 1.02, 95% CI 1.01–1.04). Likewise, Choi et al. (2019) discovered that SSNHL was associated with short-term exposure to NO_2 (14 days) (adjusted OR = 3.12, 95% CI 2.16–4.49). Consistent with previous studies, NO_2 was associated with hearing impairment

TABLE 3 | Associations of air pollution and hearing impairment in subgroups stratified by healthy diet scores.

	Low (*N* = 58324)		High (*N* = 94414)		*P*-interaction
	OR (95% CI)	*P*	OR (95% CI)	*P*	
$PM_{2.5}$	1.05 (0.69, 1.61)	0.823	0.84 (0.62, 1.14)	0.271	0.403
PM_{10}	1.20 (0.97, 1.49)	0.086	1.14 (0.98, 1.32)	0.094	0.688
$PM_{2.5}$ absorbance	1.10 (0.95, 1.27)	0.191	1.10 (0.99, 1.22)	0.060	0.902
NO_X	1.02 (0.99, 1.05)	0.147	1.01 (0.99, 1.03)	0.498	0.300
NO_2	1.04 (0.99, 1.10)	0.161	1.02 (0.98, 1.06)	0.315	0.377

Abbreviations: OR, odds ratio; CI, confidence interval; PM, particulate matter; NO_2, nitrogen dioxides; NO_X, nitrogen oxides.
All models were adjusted for age, gender, race, education, employment, smoking, drink frequency, body mass index, physical activity, glycosylated hemoglobin, total cholesterol, and vascular disease (heart attack, stroke, angina, and hypertension).
This subgroup included 152,738 participants because of the missing data of dietary information for 6,073 participants.

TABLE 4 | Associations of air pollution and hearing impairment in subgroups stratified by age.

	≤50 (*N* = 40,978)		51–60 (*N* = 53,844)		>60 (*N* = 63,989)		*P*-interaction
	OR (95% CI)	*P*	OR (95% CI)	*P*	OR (95% CI)	*P*	
$PM_{2.5}$	1.74 (0.96–3.14)	0.067	1.02 (0.66–1.59)	0.918	0.80 (0.57–1.13)	0.198	0.013
PM_{10}	1.62 (1.20–2.18)	0.002	1.15 (0.92–1.43)	0.215	1.04 (0.88–1.23)	0.647	0.005
$PM_{2.5}$ absorbance	1.32 (1.08, 1.61)	0.006	1.04 (0.89–1.21)	0.626	1.05 (0.93–1.18)	0.417	0.029
NO_X	1.04 (1.01–1.08)	0.014	1.02 (0.99–1.05)	0.247	1.00 (0.98–1.02)	0.921	0.005
NO_2	1.09 (1.01–1.17)	0.031	1.03 (0.97–1.09)	0.292	1.01 (0.97–1.06)	0.641	0.017

Abbreviations: OR, odds ratio; CI, confidence interval; PM, particulate matter; NO_2, nitrogen dioxides; NO_X, nitrogen oxides.
All models were adjusted for gender, race, education, employment, smoking, drink frequency, body mass index, physical activity, glycosylated hemoglobin, total cholesterol, and vascular disease (heart attack, stroke, angina, and hypertension).

TABLE 5 | Associations of air pollution and hearing impairment in subgroups stratified by gender.

	Female (*N* = 86516)		Male (*N* = 72295)		*P*-interaction
	OR (95% CI)	*P*	OR (95% CI)	*P*	
$PM_{2.5}$	0.86 (0.61–1.22)	0.406	1.19 (0.83–1.69)	0.346	0.191
PM_{10}	1.16 (0.98–1.38)	0.085	1.15 (0.97–1.37)	0.118	0.914
$PM_{2.5}$ absorbance	1.10 (0.98–1.23)	0.112	1.07 (0.95–1.21)	0.261	0.920
NO_X	1.01 (0.98–1.02)	0.879	1.03 (1.01–1.05)	0.011	0.061
NO_2	1.02 (0.97–1.06)	0.489	1.05 (1.00–1.09)	0.049	0.216

Abbreviations: OR, odds ratio; CI, confidence interval; PM, particulate matter; NO_2, nitrogen dioxides; NO_X, nitrogen oxides.
All models were adjusted for age, race, education, employment, smoking, drink frequency, body mass index, physical activity, glycosylated hemoglobin, total cholesterol, and vascular disease (heart attack, stroke, angina, and hypertension).

in our study. Moreover, NO_X, a term that contains several nitrogen compounds but is mainly composed of nitrogen oxide and NO_2, showed an association with hearing impairment.

In contrast to our expectations, we found a significant association between PM_{10} and hearing impairment but not $PM_{2.5}$. Conversely, previous studies (Choi et al., 2019; Lee et al., 2019) showed no correlation between PM_{10} and hearing impairment. A study reported (Tsai et al., 2020) a significantly higher risk of developing SSNHL with moderate (adjusted HR = 1.58, 95% CI 1.21–2.06) or high (adjusted HR = 1.32, 95% CI 1.00–1.74) level exposure to $PM_{2.5}$ compared to those exposed to the low level. And another study discovered a slight negative association between the maximum $PM_{2.5}$ concentration and the admission rate of SSNHL (Lee et al., 2019). In 2017, a study (Strak et al., 2017) in a large national health survey reported that oxidative potential of $PM_{2.5}$ rather than $PM_{2.5}$, was associated with diabetes prevalence, indicating that the impact of particulate matter on diabetes might vary with the compositions. According to a study (Yin and Harrison, 2008) conducted at three sites (urban roadside, central urban background, and rural) in Birmingham, United Kingdom, organics, nitrate, and sulfate accounted for a substantial amount of the overall mass for both PM_{10} and $PM_{2.5}$. This research also showed that proportions of these three major parts and other secondary compositions like iron-rich dust and sodium chloride varied in both. Although discrepancies in associations with diseases after $PM_{2.5}$ and PM_{10} exposure could be explained by different compositions of particulate matter, the evidence may still be limited. More research is required to clarify this issue in the future.

Oxidative stress and mitochondrial dysfunction play a crucial role in hearing impairment (Yamasoba et al., 2013). Air pollution might be involved in oxidative stress by producing or directly acting as reactive oxygen species (Kelly, 2003), which can then induce mitochondrial damage (Rodríguez-Martínez et al., 2013). Dysfunctional mitochondria increase reactive oxygen species generation and accumulation, reducing the mitochondrial membrane potential, activating the apoptosis pathway, and causing the death of inner ear hair cells (Park et al., 2016). What's more, air pollution might indirectly be associated with hearing impairment by causing cardiovascular diseases through pro-inflammatory pathways and the production of reactive oxygen species (Simkhovich et al., 2008; Brook et al., 2010). It has been demonstrated that cardiovascular diseases are risk factors for hearing impairment (Oron et al., 2014; Tan et al., 2018). Nonetheless, the link between air pollution and hearing impairment was still evident after adjusting for related vascular problems in Model 3, suggesting that other mechanisms may also be involved in the link between air pollution and hearing impairment.

There was evidence that a healthy diet could protect against hearing impairment by reducing vascular damage, decreasing inflammation, and inhibiting oxidative damage (Curhan et al., 2020; Yevenes-Briones et al., 2021). Based on similar mechanistic pathways, modifying the health effects of air pollution by diet may be possible. But in our study, no effect modification of diet was observed. Studies previously showed an interaction between dietary patterns and air pollution exposure on health-related outcomes. In a birth cohort in Northeast China, animal foods pattern was found to significantly modify the association between exposure to NO_2 and carbon monoxide and gestational diabetes mellitus, with higher intake related to a higher rate of gestational diabetes mellitus following exposure to air pollution (Hehua et al., 2021). A Mediterranean diet reduced cardiovascular disease mortality risk related to long-term exposure to air pollutants in a large prospective US cohort (Lim et al., 2019). A prospective cohort study of Chinese older adults reported that a plant-based dietary pattern mitigated the adverse effects of air pollution on cognitive function (Zhu et al., 2022).

It seems to be accepted that hearing impairment becomes more common with increasing age (Díaz et al., 2016). Nevertheless, the association between air pollution and hearing impairment was only found in participants younger under or equal to 50 years of age in this study. An interaction effect between age and air pollution on hearing impairment was also observed. Age is an unmodifiable risk factor for hearing impairment, which could lead to cochlear aging (Yamasoba et al., 2013). However, modifiable risk factors play a significant part in the development of hearing impairment at a relatively young age (i.e., $<$85 years old), while their effects decrease in the oldest people (i.e., $\geq$85 years old) (Zhan et al., 2010). Therefore, we speculated that air pollution, a modifiable risk factor, might have a greater impact on people younger than or equal to 50 years old compared to those over 50 years old, even if our study subjects were all under 85 years old.

Our research used data from the United Kingdom Biobank, a national cohort with good quality control. Additionally, the hearing test was based on the DTT data in the United Kingdom Biobank, which represented an ecologically effective and objective hearing indicator. We also adjusted for many confounders (including demographic information, lifestyle, and related diseases affecting hearing) to reduce their potential impact. However, our research also had some limitations. Above all, the cross-sectional design of this study was inadequate to account for the cause and effect between air pollution and hearing impairment, and further longitudinal studies are needed. Second, the sample of participants in United Kingdom Biobank was suggested to be unrepresentative of the general population because of the bias toward recruiting participants who were generally healthier and had a higher socioeconomic status (Fry et al., 2017). Hence, the subsample from United Kingdom Biobank and estimated hearing impairment rate in this study might not be representative of the general population. Third, like other epidemiological studies of air pollution, there might be potential misclassifications of air pollution exposure in this study because air pollution exposure was evaluated at the place of residence. Fourth, in the United Kingdom, where emissions regulations are strict and average pollution level is relatively low, it is not clear to what extent this study can be generalizable to other settings. Finally, in spite of adjusting for many confounders in our study, the potential effects of residual confounds of unmeasured variables could not be excluded, such as the use of ototoxic drugs, which was not considered due to lack of data.

CONCLUSION

In conclusion, we found that exposure to PM_{10}, NO_X, and NO_2 was associated with hearing impairment in British adults, while $PM_{2.5}$ and $PM_{2.5}$ absorbance did not show similar correlations. Our findings may help researchers pay more attention to the impact of air pollution on hearing impairment and provide a basis for developing effective prevention strategies.

DATA AVAILABILITY STATEMENT

The data supporting the results of this study can be found in the website of UK Biobank (www.ukbiobank.ac.uk) upon application.

ETHICS STATEMENT

The study involving human participants was carried out with the ethical approval obtained by United Kingdom Biobank from the National Health Service National Research Ethics Service.

AUTHOR CONTRIBUTIONS

YS, YT, and LY conceived the overall project and developed the methods as well as procedures throughout the study. DL and LY managed the data collection and data entry and carried out data verification and statistical analyses. LY drafted the first version of the manuscript. All authors oversaw statistical analysis, involved

in the interpretation of the results, reviewed, and approved the final manuscript.

FUNDING

This work was supported by the National Natural Science Foundation of China (Grant Number: 82071058).

ACKNOWLEDGMENTS

We are grateful to all the participants of United Kingdom Biobank. We also sincerely thank those who participated in data collection and management of United Kingdom Biobank. This study has been carried out with the use of the United Kingdom Biobank resource (application number 69741).

REFERENCES

Appel, L. J., Brands, M. W., Daniels, S. R., Karanja, N., Elmer, P. J., Sacks, F. M., et al. (2006). Dietary approaches to prevent and treat hypertension: a scientific statement from the American Heart Association. *Hypertension* 47, 296–308. doi: 10.1161/01.HYP.0000202568.01167.B6

Brook, R. D., Rajagopalan, S., Pope, C. A. III, Brook, J. R., Bhatnagar, A., Diez-Roux, A. V., et al. (2010). Particulate matter air pollution and cardiovascular disease: an update to the scientific statement from the American Heart Association. *Circulation* 121, 2331–2378. doi: 10.1161/CIR.0b013e3181dbece1

Brunekreef, B., and Holgate, S. T. (2002). Air pollution and health. *Lancet* 360, 1233–1242. doi: 10.1016/s0140-6736(02)11274-8

Chang, K. H., Hsu, C. C., Muo, C. H., Hsu, C. Y., Liu, H. C., Kao, C. H., et al. (2016). Air pollution exposure increases the risk of rheumatoid arthritis: a longitudinal and nationwide study. *Environ. Int.* 94, 495–499. doi: 10.1016/j.envint.2016.06.008

Chang, K. H., Tsai, S. C., Lee, C. Y., Chou, R. H., Fan, H. C., Lin, F. C., et al. (2020). Increased Risk of Sensorineural Hearing Loss as a Result of Exposure to Air Pollution. *Int. J. Environ. Res. Public Health* 17:1969. doi: 10.3390/ijerph17061969

Chen, C. Y., Hung, H. J., Chang, K. H., Hsu, C. Y., Muo, C. H., Tsai, C. H., et al. (2017). Long-term exposure to air pollution and the incidence of Parkinson's disease: a nested case-control study. *PLoS One* 12:e0182834. doi: 10.1371/journal.pone.0182834

Choi, H. G., Min, C., and Kim, S. Y. (2019). Air pollution increases the risk of SSNHL: a nested case-control study using meteorological data and national sample cohort data. *Sci. Rep.* 9:8270. doi: 10.1038/s41598-019-44618-0

Collins, R. (2012). What makes UK Biobank special? *Lancet* 379, 1173–1174. doi: 10.1016/s0140-6736(12)60404-8

Contrera, K. J., Betz, J., Genther, D. J., and Lin, F. R. (2015). Association of hearing impairment and mortality in the National Health and Nutrition Examination Survey. *JAMA Otolaryngol. Head Neck Surg.* 141, 944–946. doi: 10.1001/jamaoto.2015.1762

Couth, S., Mazlan, N., Moore, D. R., Munro, K. J., and Dawes, P. (2019). Hearing Difficulties and Tinnitus in Construction, Agricultural, Music, and Finance Industries: contributions of Demographic, Health, and Lifestyle Factors. *Trends Hear.* 23:2331216519885571. doi: 10.1177/2331216519885571

Cunningham, L. L., and Tucci, D. L. (2017). Hearing Loss in Adults. *N. Engl. J. Med.* 377, 2465–2473. doi: 10.1056/NEJMra1616601

Curhan, S. G., Halpin, C., Wang, M., Eavey, R. D., and Curhan, G. C. (2020). Prospective Study of Dietary Patterns and Hearing Threshold Elevation. *Am. J. Epidemiol.* 189, 204–214. doi: 10.1093/aje/kwz223

Curhan, S. G., Wang, M., Eavey, R. D., Stampfer, M. J., and Curhan, G. C. (2018). Adherence to Healthful Dietary Patterns Is Associated with Lower Risk of Hearing Loss in Women. *J. Nutr.* 148, 944–951. doi: 10.1093/jn/nxy058

Dawes, P., Fortnum, H., Moore, D. R., Emsley, R., Norman, P., Cruickshanks, K., et al. (2014b). Hearing in middle age: a population snapshot of 40- to 69-year olds in the United Kingdom. *Ear and Hearing* 35, e44–e51. doi: 10.1097/AUD.0000000000000010

Dawes, P., Cruickshanks, K. J., Moore, D. R., Edmondson-Jones, M., McCormack, A., Fortnum, H., et al. (2014a). Cigarette smoking, passive smoking, alcohol consumption, and hearing loss. *J. Assoc. .Res. Otolaryngol.* 15, 663–674. doi: 10.1007/s10162-014-0461-0

Díaz, C., Goycoolea, M., and Cardemil, F. (2016). Hipoacusia: trascendencia, Incidencia Y Prevalencia. *Revista. Médica. Clínica. Las Condes* 27, 731–739. doi: 10.1016/j.rmclc.2016.11.003

Fry, A., Littlejohns, T. J., Sudlow, C., Doherty, N., Adamska, L., Sprosen, T., et al. (2017). Comparison of Sociodemographic and Health-Related Characteristics of UK Biobank Participants With Those of the General Population. *Am. J. Epidemiol.* 186, 1026–1034. doi: 10.1093/aje/kwx246

Fung, T. T., Chiuve, S. E., McCullough, M. L., Rexrode, K. M., Logroscino, G., and Hu, F. B. (2008). Adherence to a DASH-style diet and risk of coronary heart disease and stroke in women. *Arch. Intern. Med.* 168, 713–720. doi: 10.1001/archinte.168.7.713

Genther, D. J., Frick, K. D., Chen, D., Betz, J., and Lin, F. R. (2013). Association of hearing loss with hospitalization and burden of disease in older adults. *J. Am. Med. Assoc.* 309, 2322–2324. doi: 10.1001/jama.2013.5912

Goman, A. M., and Lin, F. R. (2016). Prevalence of Hearing Loss by Severity in the United States. *Am. J. Public health* 106, 1820–1822. doi: 10.2105/ajph.2016.303299

Gordon, S. B., Bruce, N. G., Grigg, J., Hibberd, P. L., Kurmi, O. P., Lam, K. B., et al. (2014). Respiratory risks from household air pollution in low and middle income countries. *Lancet Respir. Med.* 2, 823–860. doi: 10.1016/s2213-2600(14)70168-7

Hayes, R. B., Lim, C., Zhang, Y., Cromar, K., Shao, Y., Reynolds, H. R., et al. (2020). PM2.5 air pollution and cause-specific cardiovascular disease mortality. *Int. J. Epidemiol.* 49, 25–35. doi: 10.1093/ije/dyz114

Hehua, Z., Yang, X., Qing, C., Shanyan, G., and Yuhong, Z. (2021). Dietary patterns and associations between air pollution and gestational diabetes mellitus. *Environ. Int.* 147:106347. doi: 10.1016/j.envint.2020.106347

Jansen, S., Luts, H., Wagener, K. C., Frachet, B., and Wouters, J. (2010). The French digit triplet test: a hearing screening tool for speech intelligibility in noise. *Int. J. Audiol.* 49, 378–387. doi: 10.3109/14992020903431272

Kelly, F. J. (2003). Oxidative stress: its role in air pollution and adverse health effects. *Occupat. Environ. Med.* 60, 612–616. doi: 10.1136/oem.60.8.612

Landrigan, P. J. (2017). Air pollution and health. *Lancet Public health* 2, e4–e5. doi: 10.1016/s2468-2667(16)30023-8

Lee, H. M., Kim, M. S., Kim, D. J., Uhm, T. W., Yi, S. B., Han, J. H., et al. (2019). Effects of meteorological factor and air pollution on sudden sensorineural hearing loss using the health claims data in Busan, Republic of Korea. *Am. J. Otolaryngol.* 40, 393–399. doi: 10.1016/j.amjoto.2019.02.010

Lelieveld, J., Klingmüller, K., Pozzer, A., Pöschl, U., Fnais, M., Daiber, A., et al. (2019). Cardiovascular disease burden from ambient air pollution in Europe reassessed using novel hazard ratio functions. *Eur. Heart J.* 40, 1590–1596. doi: 10.1093/eurheartj/ehz135

Li, C. M., Zhang, X., Hoffman, H. J., Cotch, M. F., Themann, C. L., and Wilson, M. R. (2014). Hearing impairment associated with depression in US adults, National Health and Nutrition Examination Survey 2005–2010. *Otolaryngol. Head Neck Surg.* 140, 293–302. doi: 10.1001/jamaoto.2014.42

Lim, C. C., Hayes, R. B., Ahn, J., Shao, Y., Silverman, D. T., Jones, R. R., et al. (2019). Mediterranean Diet and the Association Between Air Pollution and Cardiovascular Disease Mortality Risk. *Circulation* 139, 1766–1775. doi: 10.1161/CIRCULATIONAHA.118.035742

Lin, F. R., and Ferrucci, L. (2012). Hearing loss and falls among older adults in the United States. *Arch. Intern. Med.* 172, 369–371. doi: 10.1001/archinternmed.2011.728

Lin, F. R., Thorpe, R., Gordon-Salant, S., and Ferrucci, L. (2011). Hearing loss prevalence and risk factors among older adults in the United States. *J. Gerontol. Series Biol. Sci. Med. Sci.* 66, 582–590. doi: 10.1093/gerona/glr002

Lin, F. R., Yaffe, K., Xia, J., Xue, Q. L., Harris, T. B., Purchase-Helzner, E., et al. (2013). Hearing loss and cognitive decline in older adults. *JAMA Intern. Med.* 173, 293–299. doi: 10.1001/jamainternmed.2013.1868

McKee, M. M., Stransky, M. L., and Reichard, A. (2018). Hearing loss and associated medical conditions among individuals 65 years and older. *Disab. Health J.* 11, 122–125. doi: 10.1016/j.dhjo.2017.05.007

Moore, D. R., Edmondson-Jones, M., Dawes, P., Fortnum, H., McCormack, A., Pierzycki, R. H., et al. (2014). Relation between speech-in-noise threshold, hearing loss and cognition from 40-69 years of age. *PLoS One* 9:e107720. doi: 10.1371/journal.pone.0107720

Neale, E. P., Batterham, M. J., and Tapsell, L. C. (2016). Consumption of a healthy dietary pattern results in significant reductions in C-reactive protein levels in adults: a meta-analysis. *Nutr. Res.* 36, 391–401. doi: 10.1016/j.nutres.2016.02.009

Oron, Y., Elgart, K., Marom, T., and Roth, Y. (2014). Cardiovascular risk factors as causes for hearing impairment. *Audiol. Neuro-otol.* 19, 256–260. doi: 10.1159/000363215

Park, Y. H., Shin, S. H., Byun, S. W., and Kim, J. Y. (2016). Age- and Gender-Related Mean Hearing Threshold in a Highly-Screened Population: the Korean National Health and Nutrition Examination Survey 2010–2012. *PLoS One* 11:e0150783. doi: 10.1371/journal.pone.0150783

Pienkowski, M. (2017). On the Etiology of Listening Difficulties in Noise Despite Clinically Normal Audiograms. *Ear Hear.* 38, 135–148. doi: 10.1097/aud.0000000000000388

Rodríguez-Martínez, E., Martínez, F., Espinosa-García, M. T., Maldonado, P., and Rivas-Arancibia, S. (2013). Mitochondrial dysfunction in the hippocampus of rats caused by chronic oxidative stress. *Neuroscience* 252, 384–395. doi: 10.1016/j.neuroscience.2013.08.018

Simkhovich, B. Z., Kleinman, M. T., and Kloner, R. A. (2008). Air pollution and cardiovascular injury epidemiology, toxicology, and mechanisms. *J. Am. Coll. Cardiol.* 52, 719–726. doi: 10.1016/j.jacc.2008.05.029

Spankovich, C., and Le Prell, C. G. (2013). Healthy diets, healthy hearing: National Health and Nutrition Examination Survey, 1999–2002. *Int. J. Audiol.* 52, 369–376. doi: 10.3109/14992027.2013.780133

Strak, M., Janssen, N., Beelen, R., Schmitz, O., Vaartjes, I., Karssenberg, D., et al. (2017). Long-term exposure to particulate matter, NO(2) and the oxidative potential of particulates and diabetes prevalence in a large national health survey. *Environ. Int.* 108, 228–236. doi: 10.1016/j.envint.2017.08.017

Sudlow, C., Gallacher, J., Allen, N., Beral, V., Burton, P., Danesh, J., et al. (2015). UK biobank: an open access resource for identifying the causes of a wide range of complex diseases of middle and old age. *PLoS medicine* 12:e1001779. doi: 10.1371/journal.pmed.1001779

Tan, H. E., Lan, N. S. R., Knuiman, M. W., Divitini, M. L., Swanepoel, D. W., Hunter, M., et al. (2018). Associations between cardiovascular disease and its risk factors with hearing loss-A cross-sectional analysis. *Clin. Otolaryngol.* 43, 172–181. doi: 10.1111/coa.12936

Taylor, H., Shryane, N., Kapadia, D., Dawes, P., and Norman, P. (2020). Understanding ethnic inequalities in hearing health in the UK: a cross-sectional study of the link between language proficiency and performance on the Digit Triplet Test. *BMJ Open* 10:e042571. doi: 10.1136/bmjopen-2020-042571

Tsai, S. C.-S., Hsu, Y.-C., Lai, J.-N., Chou, R.-H., Fan, H.-C., Lin, F. C.-F., et al. (2020). Long-Term Exposure to Air Pollution and The Risk of Developing Sudden Sensorineural Hearing Loss. *J. Transl. Med.* doi: 10.21203/rs.3.rs-72326/v1

Vos, T., Allen, C., Arora, M., Barber, R. M., Bhutta, Z. A., Brown, A., et al. (2016). Global, regional, and national incidence, prevalence, and years lived with disability for 310 diseases and injuries, 1990–2015: a systematic analysis for the Global Burden of Disease Study 2015. *Lancet* 388, 1545–1602. doi: 10.1016/s0140-6736(16)31678-6

Wang, M., Zhou, T., Song, Y., Li, X., Ma, H., Hu, Y., et al. (2021). Joint exposure to various ambient air pollutants and incident heart failure: a prospective analysis in UK Biobank. *Eur. Heart J.* 42, 1582–1591. doi: 10.1093/eurheartj/ehaa1031

Xing, D. F., Xu, C. D., Liao, X. Y., Xing, T. Y., Cheng, S. P., Hu, M. G., et al. (2019). Spatial association between outdoor air pollution and lung cancer incidence in China. *BMC public health* 19:1377. doi: 10.1186/s12889-019-7740-y

Yamasoba, T., Lin, F. R., Someya, S., Kashio, A., Sakamoto, T., and Kondo, K. (2013). Current concepts in age-related hearing loss: epidemiology and mechanistic pathways. *Hear. Res.* 303, 30–38. doi: 10.1016/j.heares.2013.01.021

Yevenes-Briones, H., Caballero, F. F., Struijk, E. A., Machado-Fragua, M. D., Ortola, R., Rodriguez-Artalejo, F., et al. (2021). Diet Quality and the Risk of Impaired Speech Reception Threshold in Noise: the UK Biobank cohort. *Ear Hear.* doi: 10.1097/AUD.0000000000001108

Yin, J., and Harrison, R. M. (2008). Pragmatic mass closure study for PM1.0, PM2.5 and PM10 at roadside, urban background and rural sites. *Atmospher. Environ.* 42, 980–988. doi: 10.1016/j.atmosenv.2007.10.005

Zhan, W., Cruickshanks, K. J., Klein, B. E., Klein, R., Huang, G. H., Pankow, J. S., et al. (2010). Generational differences in the prevalence of hearing impairment in older adults. *Am. J. Epidemiol.* 171, 260–266. doi: 10.1093/aje/kwp370

Zhu, A., Chen, H., Shen, J., Wang, X., Li, Z., Zhao, A., et al. (2022). Interaction between plant-based dietary pattern and air pollution on cognitive function: a prospective cohort analysis of Chinese older adults. *Lancet Reg. Health West. Pac.* 20:100372. doi: 10.1016/j.lanwpc.2021.100372

Conflict of Interest: The authors declare that the research was conducted in the absence of any commercial or financial relationships that could be construed as a potential conflict of interest.

Publisher's Note: All claims expressed in this article are solely those of the authors and do not necessarily represent those of their affiliated organizations, or those of the publisher, the editors and the reviewers. Any product that may be evaluated in this article, or claim that may be made by its manufacturer, is not guaranteed or endorsed by the publisher.

frontiers | Frontiers in Cellular Neuroscience

ORIGINAL RESEARCH
published: 11 April 2022
doi: 10.3389/fncel.2022.836093

The Effect of Endolymphatic Hydrops and Mannitol Dehydration Treatment on Guinea Pigs

Shu-Qi Wang[1,2†], Chen-Long Li[1,2,3†], Jing-Qi Xu[1,2], Li-Li Chen[1,2,3], You-Zhou Xie[1,2,3], Pei-Dong Dai[1,2], Liu-Jie Ren[1,2,3], Wen-Juan Yao[4,5*] and Tian-Yu Zhang[1,2,3*]*

[1] Department of Facial Plastic Reconstruction Surgery, Eye and ENT Hospital of Fudan University, Shanghai, China, [2] ENT Institute, Eye and ENT Hospital of Fudan University, Shanghai, China, [3] Hearing Medicine Key Laboratory, National Health Commission of China, Shanghai, China, [4] School of Mechanics and Engineering Science, Shanghai University, Shanghai, China, [5] Shanghai Institute of Applied Mathematics and Mechanics, Shanghai, China

OPEN ACCESS

Edited by:
Zuhong He,
Wuhan University, China

Reviewed by:
Thomas Lenarz,
Hannover Medical School, Germany
Jeremy Hornibrook,
University of Canterbury, New Zealand
Choongheon Lee,
University of Rochester, United States

***Correspondence:**
Liu-Jie Ren
renliujie@fudan.edu.cn
Wen-Juan Yao
wjyao@shu.edu.cn
Tian-Yu Zhang
ty.zhang2006@aliyun.com

[†] These authors have contributed equally to this work

Specialty section:
This article was submitted to Cellular Neuropathology, a section of the journal Frontiers in Cellular Neuroscience

Received: 15 December 2021
Accepted: 24 February 2022
Published: 11 April 2022

Citation:
Wang S-Q, Li C-L, Xu J-Q, Chen L-L, Xie Y-Z, Dai P-D, Ren L-J, Yao W-J and Zhang T-Y (2022) The Effect of Endolymphatic Hydrops and Mannitol Dehydration Treatment on Guinea Pigs. Front. Cell. Neurosci. 16:836093. doi: 10.3389/fncel.2022.836093

Background: Endolymphatic hydrops (EH) is considered as the pathological correlate of Menière's disease (MD) and cause of hearing loss. The mechanism of EH, remaining unrevealed, poses challenges for formalized clinical trials.

Objective: This study aims to investigate the development of hearing loss, as well as the effect of dehydration treatment on EH animal models.

Methods: In this study, different severity EH animal models were created. The laser Doppler vibrometer (LDV) and auditory brainstem responses (ABR) were used to study the effects of EH and the dehydration effects of mannitol. The LDV was used to measure the vibration of the round window membrane (RWM) reflecting the changes in inner ear impedance. ABR was used to evaluate the hearing changes. Furthermore, tissue section and scanning electron microscopy (SEM) observations were used to analyze the anatomical change to the cochlea and outer hair cells.

Results: The RWM vibrations decreased with the severity of EH, indicating an increase in the cochlear impedance. The dehydration therapy lowered the impedance to restore acoustic transduction in EH 10- and 20-day animal models. Simultaneously, the ABR thresholds increased in EH models and were restored after dehydration. Moreover, a difference in the hearing was found between ABR and LDV results in severe EH animal models, and the dehydration therapy was less effective, indicating a sensorineural hearing loss (SNHL).

Conclusion: Endolymphatic hydrops causes hearing loss by increasing the cochlear impedance in all tested groups, and mannitol dehydration is an effective therapy to restore hearing. However, SNHL occurs for the EH 30-day animal models, limiting the effectiveness of dehydration. Our results suggest the use of dehydrating agents in the early stage of EH.

Keywords: endolymphatic hydrops, dehydration therapy, Ménière's disease, laser Doppler vibrometry, cochlear impedance

HIGHLIGHTS

- This study investigated the development of hearing loss on guinea pig EH models, as well as the effect of dehydration treatment. By combining analogical observations and objective measurement of hearing loss (ABR and LDV measurement of RWM vibration). The highlights of this study are:

1. EH induced hearing loss progressed with the development of EH, it starts at low frequencies, and later involves medium to high frequencies.
2. EH increases the cochlear impedance, causing conductive dysfunction. This dysfunction can be cured by dehydration treatment in early stage. But irreversible sensorineural component becomes significant for long-time EH.
3. Early dehydration treatment is suggested for reserving hearing.

- This study gives an overview of the development of hearing loss in EH, and partly revealed the mechanical basis and biological influences of EH. Moreover, the investigation of dehydration treatment may provide a reference for clinical practice.

INTRODUCTION

Menière's disease (MD) is an inner ear disorder named after Prosper Menière (Atkinson, 1961), who in 1861 described patients with episodic vertigo accompanied by fluctuating hearing, tinnitus, and aural fullness in the affected ear. Later, the correlation between MD and endolymphatic hydrops (EH) was found by Hallpike and Cairns (1938) and Yamakawa (1938). As the presence of histopathological EH was reported postmortem, the essential relationship between EH and MD were being questioned until Merchant's study found that EH and MD are associated with 100% of cases when the current definition of MD is strictly applied (Merchant et al., 2005; Gluth, 2020). Recently, the development of gadolinium chelate (GdC)-enhanced MRI demonstrated EH *in vivo* and further confirmed EH is a common pathological feature of inner ear diseases characterized by low-frequency hearing loss, including MD (Naganawa et al., 2014; Zou et al., 2020).

The physiological mechanisms of Méniere are still poorly understood, yet causative relationships between EH and disordered auditory physiology in MD have been supported by much clinical and experimental evidence. It is widely believed that the dysregulation of endolymph volume may lead to EH and cause a chain reaction. Since morphological changes such as the collapse of stereocilia of outer hair cells (Albers et al., 1987) or losing synapses in inner hair cells (Valenzuela et al., 2020) fail to explain the correlation of EH and hearing loss, potential explanations have mainly focused on the mechanical impact caused by high endolymphatic pressure on endolymph components (Oberman et al., 2017) and the function of the lymphatic sac (Swinburne et al., 2018). Among those theories, the mechanical mechanism of high pressure in the endolymphatic duct explains the clinical hearing symptoms in early and mid-stage Méniere's disease (Ichimiya and Ichimiya, 2019), prompting the dehydration therapy for patients with MD. The effectiveness of dehydration therapy has not been strictly evaluated (Quaranta et al., 2019), and a recent meta-analysis further concluded that it was unclear whether diuretics were effective (Nevoux et al., 2018), even though patients have stated subjective perception improvements (Ward et al., 2019). Whether hyperosmolar agents, such as glycerol, urea, or mannitol, can improve patient hearing and act as a diagnostic tool are still under debate (Thomsen and Vesterhauge, 1979; Angelborg et al., 1982; Van de Water et al., 1986; Sterkers et al., 1987; Magliulo et al., 2001). This apparent contradiction raises the question of why patients report relief of symptoms while most of the available studies query the effectiveness of dehydration.

As the hearing ability can be predicted by the mechanical transfer of acoustic vibration and the round window is considered as an accurate proxy for cochlear fluid displacement (Ryan et al., 2020), we propose using peak-to-peak displacement of round window membrane (RWM) to analyze the change in intra-cochlear pressure under the effects of dehydration agents on EH animal models. We chose RWM as the reflection of the inner ear transfer function because it can estimate the cochlear input impedance as a whole, so it is free from the influence of the inertia of the perilymph inside the helicontrema, thus the compliance of it can better describe the total pressure inside the cochlea (Marquardt and Hensel, 2013). As the laser Doppler vibrometer (LDV) is an established optical technique to analyze the vibration of the ossicular chain, RWM, and tympanic membranes (Zhang and Gan, 2013), we used LDV to measure the dynamic behavior of RWM to evaluate cochlear impedance and sound transmission. To better illustrate the effectiveness of dehydration therapy, we created a series of different severity EH models using guinea pigs to simulate various stages of MD, then treated with mannitol. By measuring the auditory brainstem response (ABR), the linear displacement of RWM, and observing the changes in the organ of Corti, we assessed the influence of high endolymphatic pressure and the dehydration effects of mannitol on EH models.

MATERIALS AND METHODS

Animals and Research Program

Healthy albino guinea pigs (male, weighed 250–300 g), with a positive Preyer reflex and free of tympanic membrane perforation or otitis media, were used in this study. Pre-recruiting ABR measurements (click stimuli) were conducted to exclude animals with abnormal hearing function.

Guinea pigs were classified into 10-day EH, 20-day EH, 30-day EH, and blank control groups equally (12 individuals in the blank control group and 18 animals in the EH group). For the EH group, ABR (tone burst stimuli) was conducted to evaluate the auditory responses of one-third (6 animals) of the animals, and LDV measurement was used for the other two-thirds (12 animals). For all EH groups (10, 20, and 30 days), the ABR measurements were conducted both before and after dehydration with mannitol. Bilateral ears were used in all measurements.

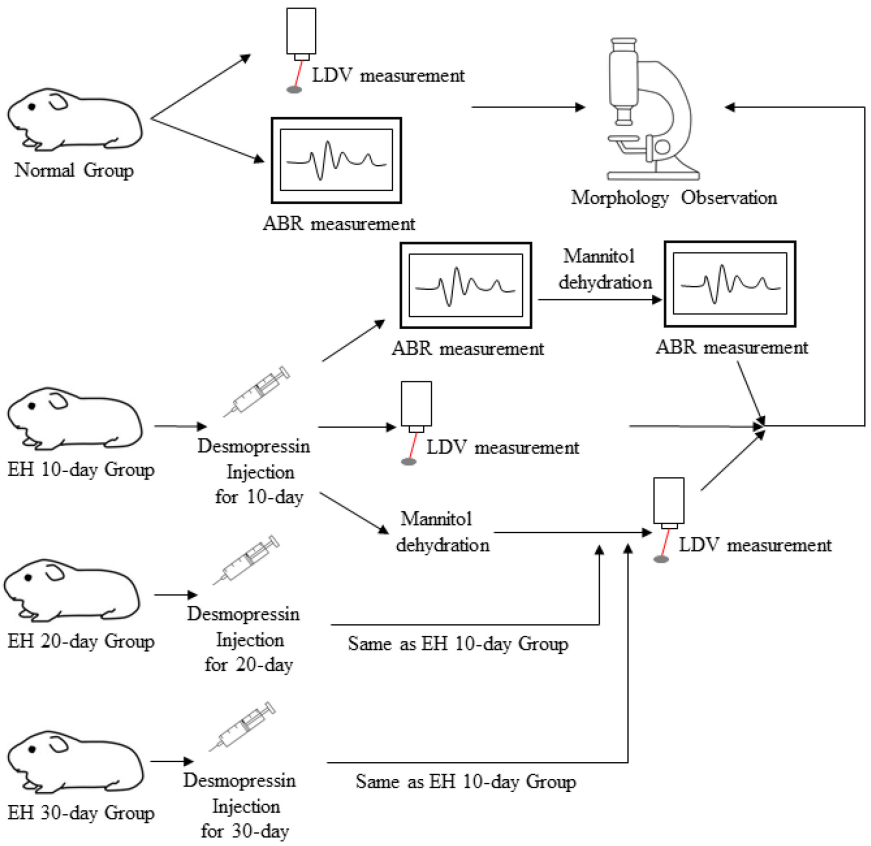

FIGURE 1 | The experimental design.

For the LDV measurements, the twelve animals in each EH group were divided into two subgroups, one for direct LDV measurement and the other for vibrometry after mannitol treatment. An operation is necessary for LDV measurement, making it hard to keep the animals healthy if further mannitol treatments are followed, which may influence the effect of dehydration. The ABR and LDV results were also obtained as baselines by the blank control groups. **Figure 1** and **Table 1** give a flowchart and roadmap of the experimental program.

After the measurements, the animals were sacrificed using an overdose of anesthetic. The cochleas were sectioned and stored in 10% polymerized formaldehyde or 2.5% glutaraldehyde for further histography.

The research program follows the principles of the guidelines for care and use of laboratory animals and was approved by the Ethics Committee of the Eye and ENT Hospital of Fudan University.

Endolymphatic Hydrops Model and Mannitol Treatment

As several studies report the importance of the endolymphatic sac and further confirm its function of regulating endolymph (Baluk et al., 2007; Swinburne et al., 2018), we used desmopressin without combining surgery to create our EH models.

The EH guinea pig model was conducted by intraperitoneal injection of desmopressin acetate (T5144, CAS: 62288-83-9, TargetMol, United States), once a day, at a dose of 8 μg/kg weight. The dose of desmopressin reported to induce EH models was variable, but there was evidence supporting increasing dosage and injection days can provide a more severe EH status in animal models at a low dose level (Takeda et al., 2000; Katagiri et al., 2014). The dose of 4–6 μg/kg weight has been widely used for EH guinea pigs modeling (Degerman et al., 2019; Jiang et al., 2019). Considering the potential for long-time medication tolerance, we increased the dose of desmopressin for our animal models (Takeda et al., 2000). To create an EH model with different levels of severity, the duration of model creation was 10, 20, and 30 days for the 10-, 20-, and 30-day EH groups, respectively.

Different kinds of hyperosmolar dehydration agents, such as glycerol, urea, isosorbide, sodium bicarbonate, and mannitol, were used to discuss their influence on the inner ears (Baldwin et al., 1992; Yazawa et al., 1998). Given the report of the rebound phenomenon of glycerol (Takeda et al., 1999) and the recent discovery of aquaporin-3 (also termed as aquaglyceroporin) in the labyrinthine membrane (Agre et al., 2002; Beitz et al., 2003), we chose mannitol as the dehydration agent applied in this study. The percentage of mannitol used in research varies from 10 to 40% (Larsen et al., 1982; Baldwin et al., 1992; Yazawa et al., 1998; Morawski et al., 2003; Le and Blakley, 2017). A high

TABLE 1 | A flowchart of the experimental procedure.

Groups	Experimental procedure		
Blank control (12 animals)	ABR (6 animals, $N = 12$)		
	LDV (6 animals, $N = 12$)		
EH 10-day (18 animals)	1st ABR (6 animals, $N = 12$)	Mannitol dehydration	2nd ABR (6 animals, $N = 12$)
	LDV (6 animals, $N = 12$)	–	–
	–	Mannitol dehydration	LDV (6 animals, $N = 12$)
EH 20-day (18 animals)	same as EH 10-day group		
EH 30-day (18 animals)	same as EH 10-day group		

dose of mannitol would cause a lethal effect, while a low dose may not ensure sufficient dehydration. In our experiment, the dehydration treatment was fulfilled by the intravenous injection of an 18% mannitol-saline solution at a safer dose of 0.5 g/kg. The dose and concentration were chosen by experience. During the dehydration process, the infusion rate was set slow, and the measurement started approximately an hour after the full dose of mannitol was given.

Auditory Brainstem Responses Measurement

Before the ABR measurement, the animals were anesthetized with an intramuscular injection of ketamine hydrochloride (40 mg/kg) and xylazine hydrochloride (10 mg/kg).

The ABR measurements were conducted in a soundproof, electromagnetically shielded room. The measurements were conducted using the RZ6/BioSigRZ system (Tucker-Davis Technologies, Alachua, FL, United States). Electrodes were inserted into the skin, one electrode at the vertex for signal recording and two electrodes at the bilateral mastoids as reference and ground. Repeated tone bursts (5 ms duration, 0.5 ms rise-fall time, Blackman envelope) were presented by a closed-field speaker at a rate of 21 stimuli/s. The test frequency points are 2, 4, 8, 16, 24, and 32 kHz. The sound-intensity level ranges from 20 to 90 dB sound pressure level (SPL) at an interval of 5 dB. ABR responses were recorded and averaged after 1,024 stimuli. The threshold for each frequency point was determined typically by the ABR I, III, and V waves.

Laser Doppler Vibrometer Measurement

The vibration of the RWM was measured to evaluate the hearing function of normal, EH-modeled, and mannitol-treated guinea pigs. The feasibility of using RWM vibration as a measure of auditory function has been previously proven (Zhang et al., 2019).

The guinea pig was anesthetized using an intramuscular injection of ketamine hydrochloride (40 mg/kg) and xylazine hydrochloride (10 mg/kg). For the duration of the surgery, the animal was placed on a heating blanket to maintain its body temperature. Bilateral auricles were partially removed, and the dorsal auditory bulla was opened to sufficiently expose the RWM (**Figure 2A**). A reflective tape (0.2×0.2 mm^2, < 0.01 mg Polytec, Germany) was carefully placed on the center of the RWM. The tympanic membrane and the ossicular chain were kept intact.

Figure 2B illustrates the setup of the LDV system. The experiment was conducted in a soundproof chamber with < 30 dB SPL noise floor. The animal was placed on a platform. An insert earphone (ER-4PT, Etymotic, United States) was inserted into the ear canal, coupled with a tiny sound pressure probe (ER-7C, Etymotic, United States). Pure tones at 85 dB SPL in the frequency range of 0.5–10 kHz (5 points/octave) were produced by the earphones, driven by a power amplifier (Type 2718, B&K, Denmark) connected with a signal generator (NI 9263, National Instruments, United States). The tip of the pressure probe was positioned approximately 2 mm from the tympanic membrane to accurately monitor the input sound pressure.

An LDV (CLV 2534-4, Polytec, Germany) was adopted to measure the vibration of the RWM. The measuring laser beam generated by the device was controlled so that the measuring angle was greater than 70°. The RWM velocity (sensitivity: 2 mm/s/V) and input sound pressure (sensitivity: 20 Pa/V) were simultaneously recorded using a four-channel data acquisition card (NI9234, sampling rate: 51.2 kHz, National Instruments, United States). Two channels were used. An in-house MATLAB code was developed for measurement control, data acquisition, and analysis. The FFT algorithm was used to obtain the velocity amplitude and sound pressure.

Histological Section

For histology, specimens (stored in 10% polymerized formaldehyde at 4°C) were decalcified in 10% ethylenediaminetetraacetic acid (EDTA), dehydrated with 15 and 30% sucrose solution, and coated with Optimum Cutting Temperature (OCT) compound. Then the cochlea was frozen and sectioned in the plane parallel to the modiolus (section thickness: 8 μm), followed by hematoxylin and eosin (H&E) stain.

For scanning electron microscopy (SEM), during specimen collection, the apical of the cochlea and RWM were opened, poured, and fixed with 2.5% glutaraldehyde at 4°C for 48 h. Then the membranous labyrinth was fully exposed. All other tissues were removed, leaving only the basement membrane, fixed in osmium tetroxide solution, and treated with tannic acid. Finally, the specimens were dehydrated with alcohol, dried, sprinkled with gold, and observed by a scanning electron microscope (SU8010, HITACHI, Toyko, Japan).

Data Processing

For sections, since the EH model is induced by desmopressin, the SAM ratio is not suitable for our case. We provided changes in the angle formed by Reissner's membrane and basilar membrane (BM) to reflect the severity of EH and response to mannitol. For LDV measured data, the RWM velocity amplitude was converted to peak-to-peak displacement according to the mathematical

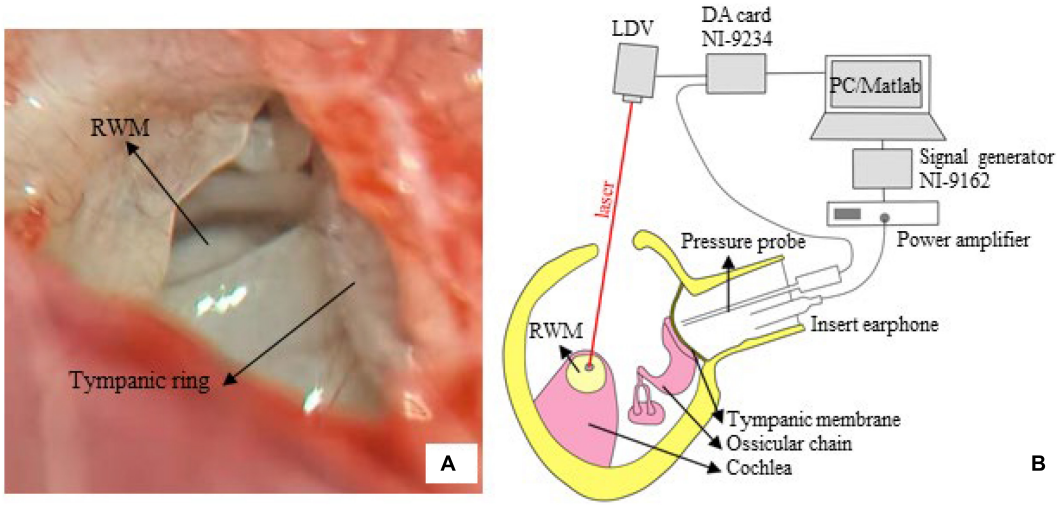

FIGURE 2 | The LDV measurement. **(A)** The surgical exposure was photographed *via* a dissecting microscope. The tympanic ring and round window membrane (RWM), with a radius of 0.5–0.6 mm, are seen from the opened middle ear cavity (right ear of tested guinea pig). **(B)** A sketch of the measurement system. The RWM velocity was measured *via* a compact LDV, and the signal was acquired by an AD card (NI-9234) and analyzed by an in-house MATLAB program.

relation: $U\text{peak-to-peak} = V/(\pi \cdot f)$ (where Upeak−to−peak is the peak-to-peak displacement, V is the velocity amplitude, and f is the frequency). Then the displacement is normalized by the sound pressure near the tympanic membrane. To statistically analyze the displacement and ABR threshold, the mean and standard deviation (SD) were calculated for each group. Two-tailed Student t-tests were used for data comparison, and p-values of < 0.05 were considered as a significant difference.

RESULTS

Observation of Tissue Sections of the Cochlea in Ears With Endolymphatic Hydrops

Figure 3 presents the H&E stained section of the cochlea for the EH groups and the blank controlled group (more section samples are presented in **Supplementary Appendix**). Turn 2 was shown. In the control group (**Figure 3A**), the Reissner's membrane (RM) did not deform so that the membrane and the BM formed a sharp angle. However, the RM bulged toward the scala vestibula (SV) in the EH groups (**Figures 3B–D**). The tissue of RM deformation became more significant with the duration of EH, indicating an increase in EH severity. These observations, consistent with the previous reports (Katagiri et al., 2014), verified our EH models.

Figures 3E–G shows turn 2 of the cochleae after dehydration. Compared with the non-dehydration results, a significant volumetric change in the scala media (SM) was shown, and in the EH 10- and 20-day groups, the RM nearly relocated to its normal location, indicating the effectiveness of mannitol treatment. Slight foldings and distortions of the RM were observed (**Figures 3E–G** and **Supplementary Figure 1**). Additionally, some cases showed the deformation of the organ of Corti (**Figures 3F,G**). The mean and SD of the angle between RM and BM were calculated and shown in **Table 2** (sections were used to calculate the mean of the angle, thus forming the sample number of 8).

Effect of Endolymphatic Hydrops and Dehydration Treatment on Auditory Brainstem Responses Measurement

Auditory brainstem response thresholds of all groups are presented in **Figure 4**. **Figure 4A** plots the ABR thresholds in the EH groups of different severity, together with the result of the control group as a baseline. In the EH 10-day group, the mean thresholds increased by approximately 10 dB, mainly at low frequencies (2, 4, and 8 kHz). In the EH 20-day group, high-frequency thresholds also increased significantly (by 10–15 dB at 16, 24, and 32 kHz, $p < 0.05$), but low-frequency thresholds were still more prominent (with an increase of 20–30 dB at 2–8 kHz, $p < 0.05$). In the EH 30-day group, the ABR thresholds increased over a broad frequency range (by approximately 30 dB at 2–32 kHz, $p < 0.05$).

The mannitol dehydration treatment effect on ABR thresholds is shown in **Figures 4B–D**, with each sub-figure corresponding to EH 10-, 20-, and 30-day groups, respectively. Compared with non-dehydration status, the ABR thresholds at the low-frequency range of EH 10-day had remarkable improvements (9.1 dB SPL at 2 kHz, 5.0 dB SPL at 4 kHz, and 5.4 dB SPL at 8 kHz; **Figure 4B**, $p < 0.05$) and almost went back to normal. In the EH 20-day group, significant improvements of approximately 10 dB ($p < 0.05$) were observed in all frequencies. The improved thresholds were still notably higher than that of the normal baseline (refer to **Figure 4C**). In the EH 30-day group, the ABR thresholds were not changed after mannitol injection (except for a slight improvement at 2 kHz), indicating the ineffectiveness of dehydration treatment (refer to **Figure 4D**).

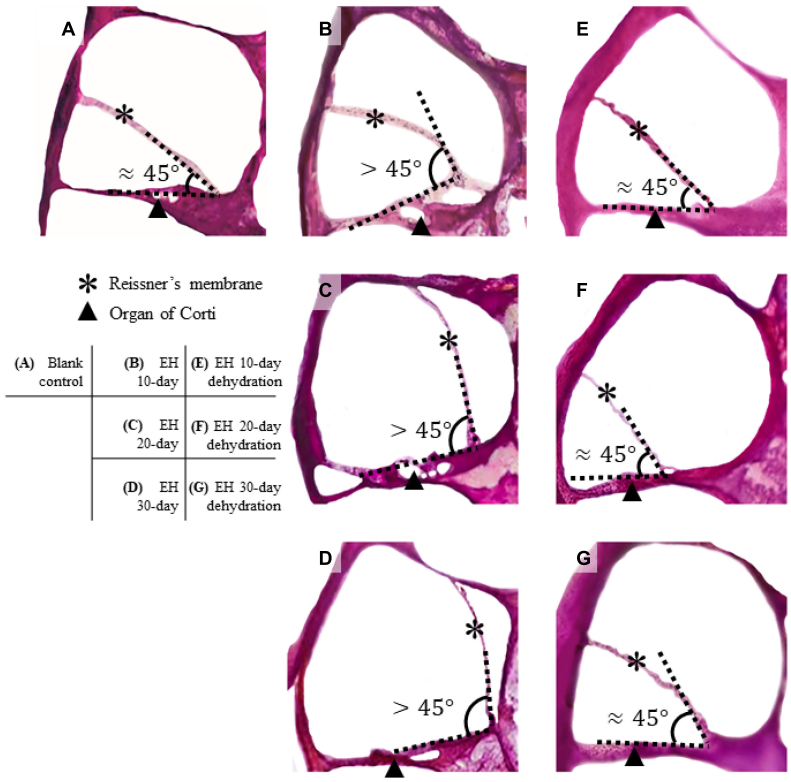

FIGURE 3 | Section of cochlear turn 2 of normal, EH-modeled, and dehydration-treated guinea pigs. In the control group **(A)**, the Reissner's membrane (RM) and the organ of Corti are in the normal position, and the RM and BM form a sharp angle (approximately 45°). In the EH groups **(B–D)**, the RM are bent, and the deformation becomes remarkable as the EH goes severe. **(E–G)** The dehydration effect where the RM is partly restored. Some distortion of the RM and the organ of Corti are shown.

Effect of Endolymphatic Hydrops and Dehydration Treatment on Round Window Membrane Vibration

Figure 5A shows the mean peak-to-peak displacement and SD of RWM in the control and EH 10-, 20-, and 30-day groups. For the normal baseline, the displacements generally decrease as frequency increases in the range of 0.5–10 kHz. The most reduction occurred at 1–5 kHz and the plateau had been reached at above 7 kHz, which coincide with the reported data (Zhang et al., 2019). In the EH 10-day group, there existed a slight reduction (approximately 10 dB) in RWM displacement at 0.5–4 kHz (11.3 dB at 0.5 kHz). For the EH 20-day group, the RWM displacement significantly decreased at the frequency range of 0.5–10 kHz (at approximately 15 dB). In the EH 30-day group, a further reduction of 15–20 dB was observed.

After dehydration treatment, the RWM vibration is shown in **Figures 5B–D**. In the EH 10-day group, the peak-to-peak displacement of RWM nearly went back to its normal range and was slightly higher than normal at 4–10 kHz (less than 4 dB, $p < 0.05$). In the EH 20-day group, the peak-to-peak displacements also showed a great improvement. However, at the range of 0.5–1 kHz, the recovery exhibited a mild reduction, compared with the normal curve (**Figure 5C**). In the EH 30-day group, the improvements were 3–8 dB, which was still 10–15 dB worse than the normal cases, suggesting the limited effect of dehydration therapy (**Figure 5D**).

Observation of Outer Hair Cells of the Cochlea in Ears With Endolymphatic Hydrops

Figure 6 shows the SEM observations of outer hair cells (OHC) in the EH 10-, 20-, and 30-day groups. Turns 2 and 3 were presented. In the EH 10-day group, the stereocilia of outer hair cells in turn 2 (**Figure 6A**) have already exhibited slight swelling and lodging, and accidental loss of stereocilia has been noticed. However, the OHC remains intact at turn

TABLE 2 | The angle between RM and BM of turn 2 in each group ($N = 8$).

Angle between RM and BM	Mean	*SD*
Normal	41.9°	3.3
EH 10-day	59.7°	4.9
EH 20-day	77.8°	7.3
EH 30-day	90.7°	8.1
EH 10-day Mannitol Tx	50.0°	5.1
EH 20-day Mannitol Tx	54.4°	3.5
EH 30-day Mannitol Tx	57.6°	4.5

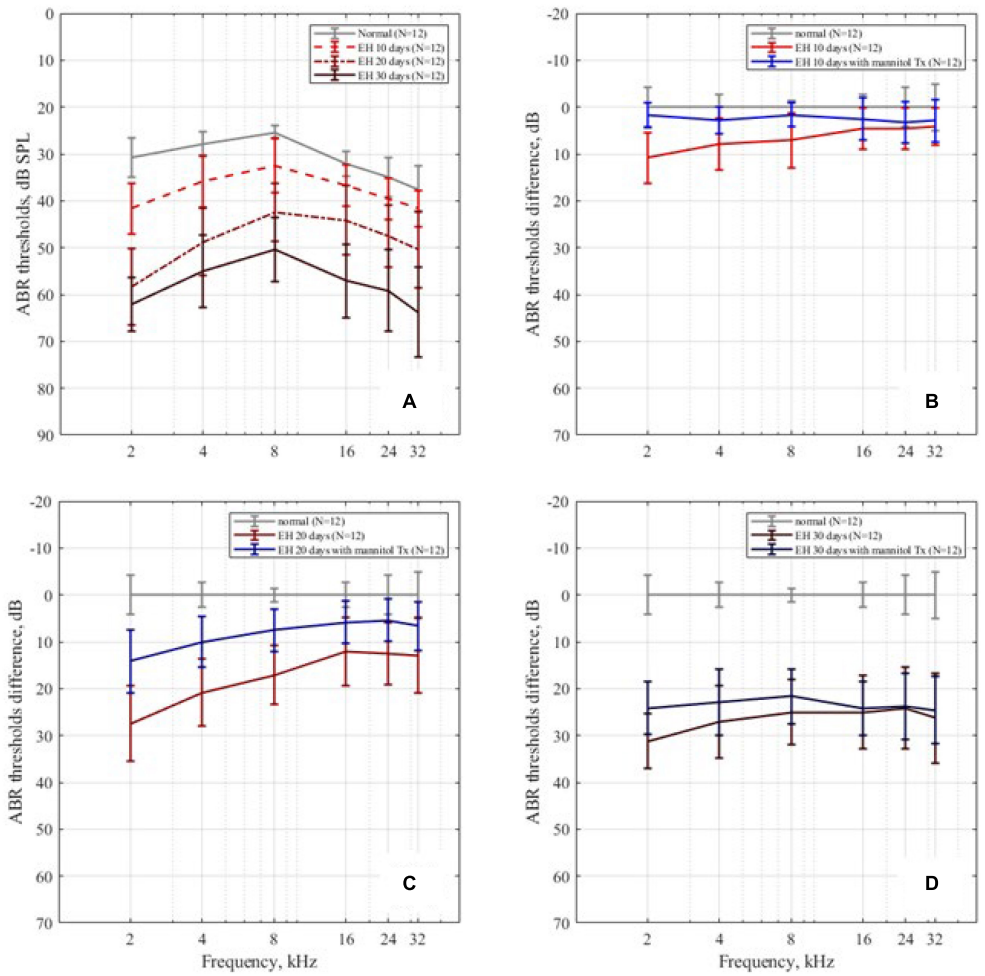

FIGURE 4 | The ABR thresholds change. **(A)** The ABR thresholds in the control, EH 10-, 20-, and 30-day groups, presenting with mean and SD; as the degree of EH became more severe, the thresholds increased. **(B–D)** The ABR threshold differences between the EH groups and the dehydration groups of 10, 20, and 30 days, compared with the control group.

3 (**Figure 6B**). In the EH 20-day group, the damage of stereocilia of OHC in turn 2 (**Figure 6C**) is very obvious, and the lodging and collapse of stereocilia have started to show up in turn 3 (**Figure 6D**). The changes in OHC were most prominent in the EH 30-day groups. The injury to OHC was more severe compared with the EH 20-day group in both turns (**Figures 6E,F**), and collapse of cilia and swelling inner hair cells (IHC) have started to appear (**Figures 6E,F**). Those finding indicating sensation dysfunction in severe EH may be the explanation of poor response to mannitol in the EH 30-day group.

DISCUSSION

The Hearing Loss in Endolymphatic Hydrops Animal Models

Animal models are commonly used in identifying and characterizing the pathophysiology of EH. Current existing animal models can resemble the dilation of SM and low-frequency hearing loss. It is widely accepted that the EH animal models, created through surgical operation, medication application, or their combination, can reproduce the chronic phase of MD (Seo and Brown, 2020).

The EH surgical model was created *via* ablation of the endolymphatic duct and endolymphatic sac by electrocauterization. It produces reliable EH models, but the permanent surgical damage and irreversible hearing loss limit its feasibility in studying the curative effect (Horner, 1991). The EH medication models are created with injections of low-dose vasopressin (VP), desmopressin, or aldosterone. In hydropic cochleae confirmed by X-ray micro-tomography (micro-CT), desmopressin influences all frequency ranges of the cochlea but is more prominent at low frequencies (Takeda et al., 2000; Chihara et al., 2013; Katagiri et al., 2014).

A similar phenomenon was observed in our EH model experiments. The ABR results showed that the hearing loss started at low frequencies (the EH 10-day group) and progressed

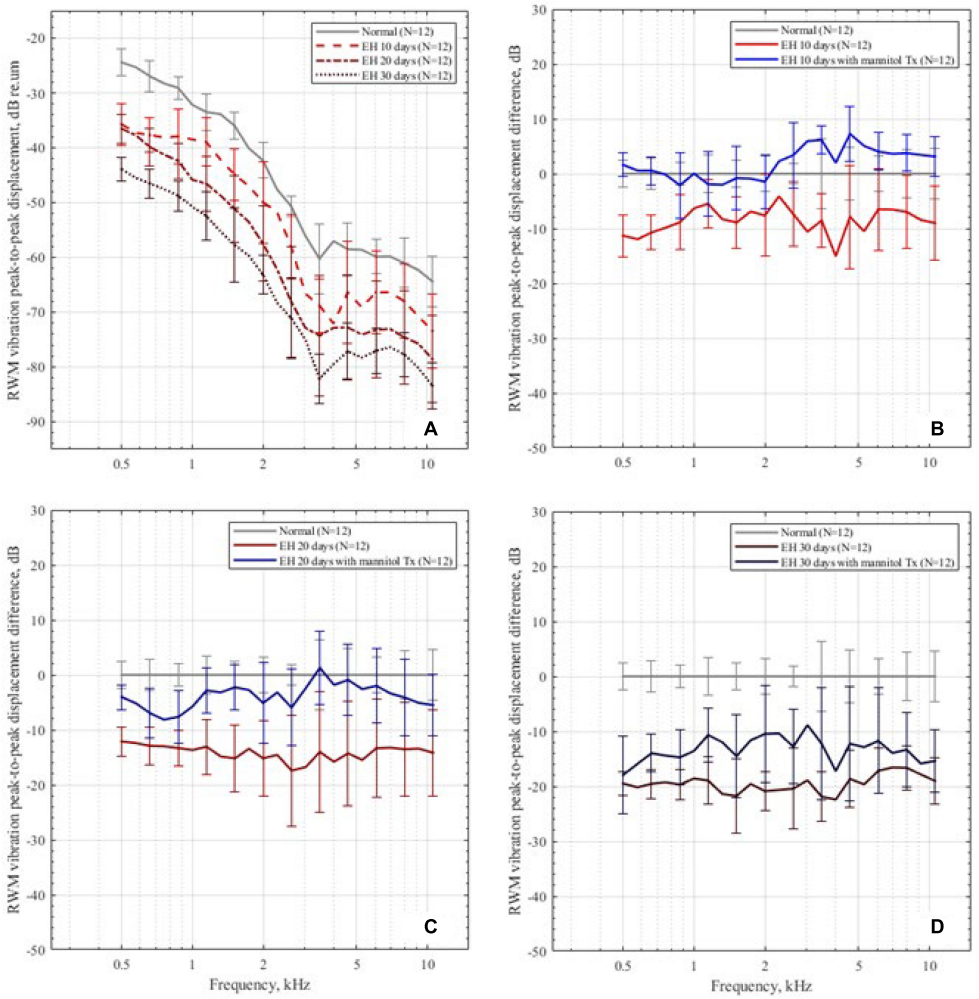

FIGURE 5 | The RWM peak-to-peak displacements in the dB scale. **(A)** The RWM peak-to-peak displacement in the control group and the EH 10-, 20-, and 30-day groups, presenting with mean and SD. The displacements are normalized by sound pressure in the ear canal. **(B–D)** The RWM peak-to-peak displacement differences in the 10-, 20-, and 30-day EH groups before and after dehydration treatment, compared with the normal baseline.

to higher frequencies (the EH 20- and 30-day groups, refer to **Figure 4A**). Note that the large variations in our ABR results may be caused by individual differences in response and the vasopressin escape phenomenon (Ecelbarger et al., 1998).

The increasing hearing losses were also reflected by the reduction of RWM vibrations (refer to **Figure 5A**). A positive correlation was found between the reduction of the RWM vibration and the severity of EH. However, the vibration reductions were not frequency-sensitive compared with the ABR results. The RWM vibration, different from ABR thresholds, is an evaluation of the mechanical influence of EH. This may cause the inconsistency between ABR and LDV results.

The Effect of Dehydration Therapy on Endolymphatic Hydrops

In clinical trials, dehydration agents (e.g., mannitol, isosorbide, and glycerol) are commonly used in the diagnosis and treatment of MD (Kakigi et al., 2004), as their influences on hearing improvement have been confirmed by clinical trials and research (Filipo et al., 1997; Degerman et al., 2019). The impacts of dehydration agents in animal models have usually been analyzed by tissue section or micro-CT. Among those studies, common morphological changes such as folding of the distended RM and deformation of the organ of Corti have been observed and reported (Egami et al., 2016). In our study, those morphological changes were also noticed (**Figures 3F,G**).

Hearing restoration after dehydration treatment was also evaluated in this study. As shown in both ABR (**Figures 4B–D**) and RWM vibration (**Figures 5B–D**) results, the hearing loss was nearly fully recovered after dehydration in the EH 10-day group and partly recovered in the EH 20-day group. In the EH 30-day group, the hearing loss was sustained. Considering the remarkable OHC injury in the EH 30-day group (**Figures 6E,F**), at that time, the causes of hearing loss may

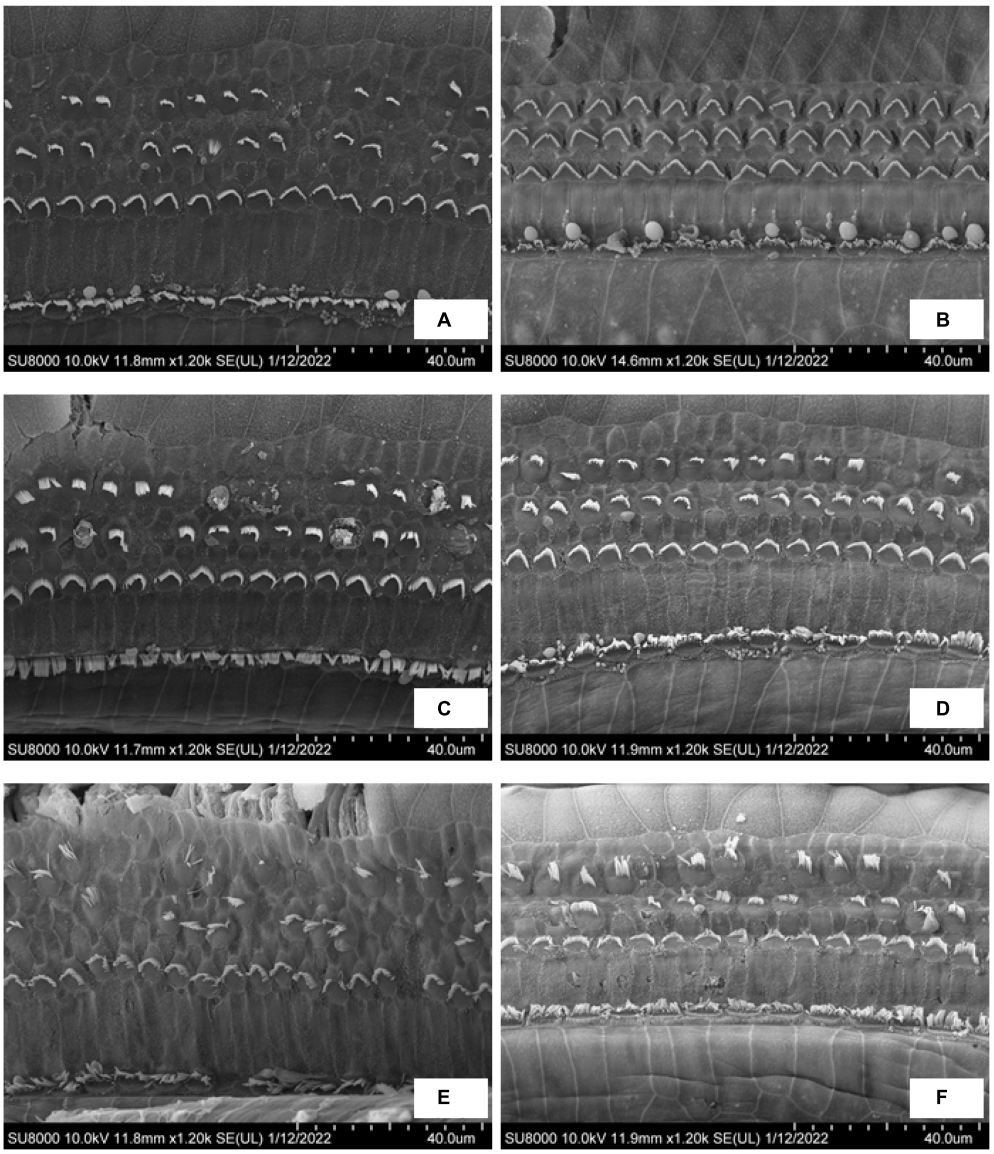

FIGURE 6 | The SEM observation of OHC in the EH 10-, 20-, and 30-day groups. **(A,C,E)** Turn 2 of the cochlea in the EH 10-, 20-, and 30-day groups. **(B,D,F)** Turn 3 of the cochlea in each group accordingly.

be transferred from conductive dysfunction to sensory impair, restoring of conductive function by dehydration is not enough to improve hearing.

Conductive and Sensorineural Hearing Loss

Typically, patients with MD experience fluctuating low-frequency hearing loss followed by medium- to high-frequency involvement. Gluth (2020) reviewed the hypothesis for MD development. The mechanical effect of high endolymphatic pressure affects cochlear conductive problems and damages the sensory hair cells, resulting in sensation dysfunction. The same damage to hair cell stereocilia in our study was also reported in many EH animal models (Momin et al., 2010; Jia et al., 2012; Ding et al., 2016).

Our results support this assumption. In the EH 10-day group, the injury stereocilia of OHC at turn 2 is minimal, and turn 3 is almost normal. The RWM vibration decreased by 7.6, 15.0, and 7.0 dB at 2,4, and 8 kHz, respectively (referring to normal range in **Figure 5B**), which were similar to ABR threshold changes (10.8, 7.9, and 7.1 dB at 2, 4, and 8 kHz, respectively, refer to **Figure 4B**). In the EH 20-day group, the hearing loss evaluated by RWM vibration was 15.2, 15.8, and 13.5 dB at 2, 4, and 8 kHz, respectively (**Figure 5C**), while the ABR threshold elevation was significantly higher (27.5, 20.8, and 17.1 dB at 2, 4, and 8 kHz, respectively, refer to **Figure 4C**). The gap was even more significant in the EH 30-day group. The ABR increases were

31.3, 27.1, and 25.0 dB, and the LDV results were 20.9, 22.4, and 16.6 dB at 2, 4, and 8 kHz, respectively (**Figures 4D**, **5D**). For long-time EH models, the hearing loss evaluated by ABR was higher than that by RWM vibration, which is consistent with OHC stereocilia injury (**Figures 6C–F**).

The RWM vibration is a measurement of cochlear impedance, representing the conductive dysfunction component in acoustic transferring, while the ABR change is a sum of the conductive and sensation dysfunction. Therefore, the gap between ABR and RWM vibration may represent the SNHL. In our study, there is no gap in the EH 10-day animal models, indicating minimal SNHL at that time. However, the gap occurs in the EH 20- and 30-day groups, suggesting an increasing sensorineural component. Therefore, the dehydration treatment shows a significant curative effect in the EH 10- and 20-day groups (**Figures 3B**, **4B**) while less effective in the EH 30-day group (**Figures 3C,D**, **4C,D**).

Endolymphatic Hydrops-Induced Cochlear Damage

Besides the dislocations of RM in EH, the BM may also deform (Xenellis et al., 2004) as shown in **Figure 3**, caused by the pressure difference between SM and scale tympani. However, the BM deformation is quite small, and sectioning observations may not be solid evidence of BM deformation since slight deformation may also be caused during the sectioning. The BM deformation in EH has been numerically calculated using finite element analysis (Lee and Koike, 2017; Areias et al., 2021). The numerical analysis also predicts a low-frequency conductive hearing loss caused by BM deformation.

There are also assumptions that the EH-induced BM deformation may damage the sensory cells and cause SNHL. Lee and Kalinec (2016) measured the deformation of the organ of Corti in acute guinea pig EH models. They observed a significant decrease in the average area and height of the organ of Corti in the apical turn. They found that the lengths of OHC and Deiters' cells in the apical turn were significantly reduced. Lee suggested that the compression and deformation of the organ of Corti may decouple the tectorial membrane and stereocilia. However, *in vivo* observations need further solid evidence. Optical coherence tomography may be a promising technique (Liu et al., 2017; Badash et al., 2021).

Limitations of This Study

The first limitation of this study is the mismatch between the frequency range in ABR and LDV measurements. The LDV measurement range was 0.5–10 kHz. Frequencies beyond this interval had not been surveyed, so the paired frequencies in ABR thresholds and RWM vibrations were restricted to 2–8 kHz. Second, mannitol injection is used in the diagnosis of MD in clinical practice instead of treatment due to severe side effects. However, it does not affect the conclusion of this study.

CONCLUSION

This study investigated the development of hearing loss in guinea pig EH models as well as the effect of dehydration treatment. By combining analogical observations (frozen section) and objective measurements of hearing loss (ABR and LDV measurement of RWM vibration), we are able to obtain an overview of the development of hearing loss in EH, both mechanically and biologically. The main conclusions of this study are as follows:

1. EH-induced hearing loss progressed with the development of EH; it starts at low frequencies and later involves medium to high frequencies.
2. EH increases the cochlear impedance, causing conductive dysfunction. This dysfunction can be cured by dehydration treatment at an early stage. But the irreversible sensorineural component becomes significant for long-time EH.
3. Early dehydration treatment is suggested for preserving hearing.

DATA AVAILABILITY STATEMENT

The original contributions presented in the study are included in the article/**Supplementary Material**, further inquiries can be directed to the corresponding author/s.

ETHICS STATEMENT

The animal study was reviewed and approved by Institutional Animal Care and Use Committee at Eye and ENT Hospital of Fudan University.

AUTHOR CONTRIBUTIONS

S-QW: methodology, formal analysis, visualization, and writing—original draft. C-LL: methodology, formal analysis, visualization, and writing—review and editing. J-QX and L-LC: methodology. Y-ZX and P-DD: writing—review and editing. L-JR: conceptualization, software, writing—review and editing, supervision, and funding acquisition. W-JY: supervision and funding acquisition. T-YZ: conceptualization, supervision, and funding acquisition. All authors contributed to the article and approved the submitted version.

FUNDING

This work was supported by the Natural Science Foundation of China [Grant/Award No: 11932010 (key projects, W-JY), 82101221 (L-JR), and 81771014 (T-YZ)] and the Shanghai Natural Science Foundation (Grant/Award No: 20ZR1409900 (T-YZ)].

SUPPLEMENTARY MATERIAL

The Supplementary Material for this article can be found online at: https://www.frontiersin.org/articles/10.3389/fncel.2022.836093/full#supplementary-material

REFERENCES

Agre, P., King, L. S., Yasui, M., Guggino, W. B., Ottersen, O. P., Fujiyoshi, Y., et al. (2002). Aquaporin water channels–from atomic structure to clinical medicine. *J. Physiol.* 542, 3–16. doi: 10.1113/jphysiol.2002.020818

Albers, F. W., Veldman, J. E., and Huizing, E. H. (1987). Early hair cell loss in experimental hydrops. *Ann. Otol. Rhinol. Laryngol.* 96, 282–285. doi: 10.1177/000348948709600309

Angelborg, C., Klockhoff, I., Larsen, H. C., and Stahle, J. (1982). Hyperosmotic solutions and hearing Meniere's disease. *Am. J. Otol.* 3, 200–202.

Areias, B., Parente, M. P. L., Gentil, F., Caroça, C., Paço, J., and Natal Jorge, R. M. (2021). A finite element model to predict the consequences of endolymphatic hydrops in the basilar membrane. *Int. J. Numer. Method Biomed. Eng.* 2021:e3541. doi: 10.1002/cnm.3541

Atkinson, M. (1961). Meniere's original papers. Reprinted with an English translation together with commentaries and biographical sketch. *Acta Otolaryngol.* 162, 1–78.

Badash, I., Applegate, B. E., and Oghalai, J. S. (2021). In vivo cochlear imaging provides a tool to study endolymphatic hydrops. *J. Vestib. Res.* 31, 269–276. doi: 10.3233/VES-200718

Baldwin, D. L., Ohlsén, K. A., Miller, J. M., and Nuttall, A. L. (1992). Cochlear blood flow and microvascular resistance changes in response to hypertonic glycerol, urea, and mannitol infusions. *Ann. Otol. Rhinol. Laryngol.* 101, 168–175. doi: 10.1177/000348949210100212

Baluk, P., Fuxe, J., Hashizume, H., Romano, T., Lashnits, E., Butz, S., et al. (2007). Functionally specialized junctions between endothelial cells of lymphatic vessels. *J. Exp. Med.* 204, 2349–2362. doi: 10.1084/jem.20062596

Beitz, E., Zenner, H. P., and Schultz, J. E. (2003). Aquaporin-mediated fluid regulation in the inner ear. *Cell Mol. Neurobiol.* 23, 315–329. doi: 10.1023/a:1023636620721

Chihara, Y., Wong, C., Curthoys, I. S., and Brown, D. J. (2013). The effect of systemic administration of desmopressin on cochlear function in guinea pigs. *Acta Otolaryngol.* 133, 676–684. doi: 10.3109/00016489.2013.771282

Degerman, E., Zandt, R., Pålbrink, A., and Magnusson, M. (2019). Endolymphatic hydrops induced by different mechanisms responds differentially to spironolactone: a rationale for understanding the diversity of treatment responses in hydropic inner ear disease. *Acta Otolaryngol.* 139, 685–691. doi: 10.1080/00016489.2019.1616819

Ding, C. R., Xu, X. D., Wang, X. W., Jia, X. H., Cheng, X., Liu, X., et al. (2016). Effect of Endolymphatic hydrops on sound transmission in live guinea pigs measured with a laser doppler vibrometer. *Neural. Plast.* 2016, 1–12. doi: 10.1155/2016/8648297

Ecelbarger, C. A., Chou, C. L., Lee, A. J., DiGiovanni, S. R., Verbalis, J. G., and Knepper, M. A. (1998). Escape from vasopressin-induced antidiuresis: role of vasopressin resistance of the collecting duct. *Am. J. Physiol.* 274, F1161–F1166. doi: 10.1152/ajprenal.1998.274.6.F1161

Egami, N., Kakigi, A., Takeda, T., and Yamasoba, T. (2016). Dehydration effects of a V2 antagonist on endolymphatic hydrops in guinea pigs. *Hear. Res.* 332, 151–159. doi: 10.1016/j.heares.2015.12.017

Filipo, R., Barbara, M., Cordier, A., Mafera, B., Romeo, R., Attanasio, G., et al. (1997). Osmotic drugs in the treatment of cochlear disorders: a clinical and experimental study. *Acta Otolaryngol.* 117, 229–231. doi: 10.3109/00016489709117777

Gluth, M. B. (2020). On the relationship between menière's disease and endolymphatic hydrops. *Otol. Neurotol.* 41, 242–249. doi: 10.1097/MAO.0000000000002502

Hallpike, C. S., and Cairns, H. (1938). Observations on the pathology of méniere's syndrome: (section of otology). *Proc. R. Soc. Med.* 31, 1317–1336.

Horner, K. C. (1991). Old theme and new reflections: hearing impairment associated with endolymphatic hydrops. *Hear. Res.* 52, 147–156. doi: 10.1016/0378-5955(91)90194-e

Ichimiya, I., and Ichimiya, H. (2019). Complex tone stimulation may induce binaural diplacusis with low-tone hearing loss. *PLoS One.* 14:e0210939. doi: 10.1371/journal.pone.0210939

Jia, X. H., Liang, Q., Chi, Z. C., Dai, P. D., Zhang, T. Y., and Wang, T. F. (2012). [Morphological changes associated with low-tone hearing loss in guinea pig models of early endolymphatic hydrops]. *Sheng Li Xue Bao* 64, 48–54.

Jiang, L. Y., He, J. J., Chen, X. X., Sun, X. J., Wang, X. Z., Zhong, S., et al. (2019). Arginine vasopressin-aquaporin-2 pathway-mediated dehydration effects of electroacupuncture in guinea pig model of AVP-induced eendolymphatic hydrops. *Chin. J. Integr. Med.* 25, 763–769. doi: 10.1007/s11655-017-2411-2

Kakigi, A., Takeda, S., Takeda, T., Sawada, S., Azuma, H., Higashiyama, K., et al. (2004). Time course of dehydrating effects of isosorbide on experimentally induced endolymphatic hydrops in guinea pigs. *ORL J. Otorhinolaryngol. Relat. Spec.* 66, 291–296. doi: 10.1159/000081884

Katagiri, Y., Takumida, M., Hirakawa, K., and Anniko, M. (2014). Long-term administration of vasopressin can cause Méniere's disease in mice. *Acta Otolaryngol.* 134, 990–1004. doi: 10.3109/00016489.2014.902989

Larsen, H. C., Angelborg, C., and Hultcrantz, E. (1982). Cochlear blood flow related to hyperosmotic solution. *Arch. Otorhinolaryngol.* 234, 145–150. doi: 10.1007/BF00453621

Le, T. N., and Blakley, B. W. (2017). Mannitol and the blood-labyrinth barrier. *J. Otolaryngol. Head Neck Surg.* 46:66. doi: 10.1186/s40463-017-0245-8

Lee, S., and Koike, T. (2017). Simulation of the basilar membrane vibration of endolymphatic hydrops. *Procedia. IUTAM* 24, 64–71. doi: 10.1016/j.piutam.2017.08.043

Lee, S. H., and Kalinec, F. (2016). Measurement of the mechanical deformation of organ of corti in a model of acute endolymphatic hydrops. *Kor. J. Otorhinolaryngol. Head Neck Surg.* 59, 110–119. doi: 10.3342/kjorl-hns.2016.59.2.110

Liu, G. S., Kim, J., Applegate, B. E., and Oghalai, J. S. (2017). Computer-aided detection and quantification of endolymphatic hydrops within the mouse cochlea in vivo using optical coherence tomography. *J. Biomed. Opt.* 22:76002. doi: 10.1117/1.JBO.22.7.076002

Magliulo, G., Cianfrone, G., Triches, L., Altissimi, G., and D'Amico, R. (2001). Distortion-product otoacoustic emissions and glycerol testing in endolymphatic hydrops. *Laryngoscope* 111, 102–109. doi: 10.1097/00005537-200101000-00018

Marquardt, T., and Hensel, J. (2013). A simple electrical lumped-element model simulates intra-cochlear sound pressures and cochlear impedance below 2 kHz. *J. Acoust. Soc. Am.* 134, 3730–3738. doi: 10.1121/1.4824154

Merchant, S. N., Adams, J. C., and Nadol, J. B. Jr. (2005). Pathophysiology of Meniere's syndrome: are symptoms caused by endolymphatic hydrops? *Otol. Neurotol.* 26, 74–81. doi: 10.1097/00129492-200501000-00013

Momin, S. R., Melki, S. J., Alagramam, K. N., and Megerian, C. A. (2010). Spiral ganglion loss outpaces inner hair cell loss in endolymphatic hydrops. *Laryngoscope.* 120, 159–165. doi: 10.1002/lary.20673

Morawski, K., Telischi, F. F., Merchant, F., Abiy, L. W., Lisowska, G., and Namyslowski, G. (2003). Role of mannitol in reducing postischemic changes in distortion-product otoacoustic emissions (DPOAEs): a rabbit model. *Laryngoscope* 113, 1615–1622. doi: 10.1097/00005537-200309000-00039

Naganawa, S., Yamazaki, M., Kawai, H., Bokura, K., Iida, T., Sone, M., et al. (2014). MR imaging of Méniere's disease after combined intratympanic and intravenous injection of gadolinium using HYDROPS2. *Magn. Reson. Med. Sci.* 13, 133–137. doi: 10.2463/mrms.2013-0061

Nevoux, J., Barbara, M., Dornhoffer, J., Gibson, W., Kitahara, T., and Darrouzet, V. (2018). International consensus (ICON) on treatment of Méniere's disease. *Eur. Ann. Otorhinolaryngol. Head Neck Dis.* 135, S29–S32. doi: 10.1016/j.anorl.2017.12.006

Oberman, B. S., Patel, V. A., Cureoglu, S., and Isildak, H. (2017). The aetiopathologies of Méniere's disease: a contemporary review. *Acta Otorhinolaryngol. Ital.* 37, 250–263. doi: 10.14639/0392-100X-793

Quaranta, N., Picciotti, P., Porro, G., Sterlicchio, B., Danesi, G., Petrone, P., et al. (2019). Therapeutic strategies in the treatment of Menière's disease: the Italian experience. *Eur. Arch. Otorhinolaryngol.* 276, 1943–1950. doi: 10.1007/s00405-019-05423-7

Ryan, M., Lally, J., Adams, J. K., Higgins, S., Ahmed, M., Aden, J., et al. (2020). Mechanical energy dissipation through the ossicular chain and inner ear using laser doppler vibrometer measurement of round window velocity. *Otol. Neurotol.* 41, e387–e391. doi: 10.1097/MAO.0000000000002509

Seo, Y. J., and Brown, D. (2020). Experimental animal models for meniere's disease: a mini-review. *J. Audiol. Otol.* 24, 53–60. doi: 10.7874/jao.2020.00115

Sterkers, O., Leriche, P., Ferrary, E., and Paquelin, F. (1987). Effets du mannitol sur les liquides de l'oreille interne. Application au traitement des surdités [Effects

of mannitol on the fluids of the internal ear. Use in the treatment of deafness]. *Ann. Otolaryngol. Chir. Cervicofac.* 104, 127–135.

Swinburne, I. A., Mosaliganti, K. R., Upadhyayula, S., Liu, T. L., Hildebrand, D. G. C., Tsai, T. Y., et al. (2018). Lamellar projections in the endolymphatic sac act as a relief valve to regulate inner ear pressure. *Elife* 7:e37131. doi: 10.7554/eLife.37131

Takeda, T., Takeda, S., Kitano, H., Okada, T., and Kakigi, A. (2000). Endolymphatic hydrops induced by chronic administration of vasopressin. *Hear Res.* 140, 1–6. doi: 10.1016/s0378-5955(99)00180-x

Takeda, T., Takeda, S., Saito, H., Hamada, M., and Sawada, S. (1999). The rebound phenomenon of glycerol-induced changes in the endolymphatic space. *Acta Otolaryngol.* 119, 341–344. doi: 10.1080/00016489950181369

Thomsen, J., and Vesterhauge, S. (1979). A critical evaluation of the glycerol test in Ménière's disease. *J. Otolaryngol.* 8, 145–150.

Valenzuela, C. V., Lee, C., Mispagel, A., Bhattacharyya, A., Lefler, S. M., Payne, S., et al. (2020). Is cochlear synapse loss an origin of low-frequency hearing loss associated with endolymphatic hydrops? *Hear Res.* 398:108099. doi: 10.1016/j.heares.2020.108099

Van de Water, S. M., Arenberg, I. K., and Balkany, T. J. (1986). Auditory dehydration testing: glycerol versus urea. *Am. J. Otol.* 7, 200–203.

Ward, B., Wettstein, V., Golding, J., Corallo, G., Nuti, D., Trabalzini, F., et al. (2019). Patient perceptions of effectiveness in treatments for menière's disease: a national survey in italy. *J. Int. Adv. Otol.* 15, 112–117. doi: 10.5152/iao.2019.5758

Xenellis, J. E., Linthicum, F. H. Jr., Webster, P., and Lopez, R. (2004). Basilar membrane displacement related to endolymphatic sac volume. *Laryngoscope* 114, 1953–1959. doi: 10.1097/01.mlg.0000147927.98766.e1

Yamakawa, K. (1938). Uber ide patholgische Veranderung bei einem Meniere-Kranken. *J. Otolaryngol. Soc. Japn.* 4, 2310–2312.

Yazawa, Y., Kitano, H., Suzuki, M., Tanaka, H., and Kitajima, K. (1998). Studies of cochlear blood flow in guinea pigs with endolymphatic hydrops. *ORL J. Otorhinolaryngol. Relat. Spec.* 60, 4–11. doi: 10.1159/000027554

Zhang, T. Y., Ren, L. J., Yang, L., Dai, P. D., Zhang, T. Y., and Liang, Q. (2019). Ethanol infiltration into the stapedio-vestibular joint reduces low-frequency vibration of the ossicular chain and round window membrane in the guinea pig. *Acta Otolaryngol.* 139, 403–408. doi: 10.1080/00016489.2019.1575521

Zhang, X., and Gan, R. Z. (2013). Dynamic properties of human round window membrane in auditory frequencies running head: dynamic properties of round window membrane. *Med. Eng. Phys.* 35, 310–318. doi: 10.1016/j.medengphy.2012.05.003

Zou, J., Wang, Z., Chen, Y., Zhang, G., Chen, L., and Lu, J. (2020). MRI detection of endolymphatic hydrops in Meniere's disease in 8 minutes using MIIRMR and a 20-channel coil after targeted gadolinium delivery. *World J. Otorhinolaryngol. Head Neck Surg.* 5, 180–187. doi: 10.1016/j.wjorl.2019.04.001

Conflict of Interest: The authors declare that the research was conducted in the absence of any commercial or financial relationships that could be construed as a potential conflict of interest.

Publisher's Note: All claims expressed in this article are solely those of the authors and do not necessarily represent those of their affiliated organizations, or those of the publisher, the editors and the reviewers. Any product that may be evaluated in this article, or claim that may be made by its manufacturer, is not guaranteed or endorsed by the publisher.

Advantages of publishing in Frontiers

OPEN ACCESS
Articles are free to read for greatest visibility and readership

FAST PUBLICATION
Around 90 days from submission to decision

HIGH QUALITY PEER-REVIEW
Rigorous, collaborative, and constructive peer-review

TRANSPARENT PEER-REVIEW
Editors and reviewers acknowledged by name on published articles

Frontiers
Avenue du Tribunal-Fédéral 34
1005 Lausanne | Switzerland

Visit us: www.frontiersin.org
Contact us: frontiersin.org/about/contact

REPRODUCIBILITY OF RESEARCH
Support open data and methods to enhance research reproducibility

DIGITAL PUBLISHING
Articles designed for optimal readership across devices

FOLLOW US
@frontiersin

IMPACT METRICS
Advanced article metrics track visibility across digital media

EXTENSIVE PROMOTION
Marketing and promotion of impactful research

LOOP RESEARCH NETWORK
Our network increases your article's readership